



UNIVERSITÀ
degli STUDI
di CATANIA



Department of Biomedical and Biotechnological Sciences

Ph.D. in Biotechnology

Curriculum in Pharmaceutical Biotechnology

XXXIII Cycle

MARIA DICHIARA

**Synthesis and preclinical evaluation of sigma receptor ligands
for cancer treatment and analgesia**

PhD Thesis

Tutor: *Prof. Emanuele Amata*

Coordinator: *Prof. Vito De Pinto*

ACADEMIC YEARS 2017/2020

Affiliation

Department of Drug and Health Sciences, University of Catania, Viale Andrea Doria 6, 95125 Catania, Italy – Professor Emanuele Amata.

Department of Chemistry and Applied Biosciences, Swiss Federal Institute of Technology (ETH Zürich), Vladimir-Prelog-Weg 4, CH-8093, Zurich, Switzerland – Professor Dario Neri (1/9/2018 – 15/3/2019).

Department of Drug Science and Technology, University of Turin, Via Pietro Giuria 9, 10125 Turin, Italy – Professor Francesca Spyraakis (9/9/2019 – 4/10/2019).

Table of Contents

Abstract	1
Sommario	2
Abbreviations	3
CHAPTER 1	
Synthesis and preclinical evaluation of sigma receptor ligands for cancer treatment and analgesia	4
1. Introduction	4
1.1 Sigma receptors	4
1.1.1 Sigma-1 receptor	6
1.1.2 Sigma-2 receptor	7
1.1.3 Pharmacological aspects of sigma receptors	8
1.2 Gasotransmitters	10
1.2.1 Biological importance of NO	10
1.2.2 Biological importance of H ₂ S	13
1.3 Blood-Brain Barrier Permeation	16
1.3.1. Physicochemical properties in BBB crossing	17
References	18
CHAPTER 2	
Small molecule ligands against human Tyrosinases	26
2. Introduction	26
2.1. DNA-Encoded Chemical Libraries	27
2.2. Human Tyrosinase and Tyrosinase-related Proteins	28
References	31
CHAPTER 3	
Aim of the thesis	33
CHAPTER 4	
Results	34
<i>Sigma Receptor Ligands Carrying a Nitric Oxide Donor Nitrate Moiety: Synthesis, In Silico, and Biological Evaluation</i>	35
<i>Synthesis and preclinical evaluation of novel H₂S-donor sigma receptor hybrids for the management of pain</i>	45
<i>Tuning Properties for Blood-Brain Barrier Permeation: A Statistics-Based Analysis</i>	61
<i>Design, synthesis and preclinical evaluation of novel sigma receptors ligands</i>	78
<i>Discovery, affinity maturation and multimerization of small molecule ligands against human Tyrosinase and Tyrosinase-Related Protein 1</i>	85

CHAPTER 5

Discussion	97
Concluding remarks	102
Supplementary information	S1
List of papers (2017–2020)	I
List of conference participations (2017–2020)	II
List of fellowships	III

Abstract

The objectives of the present PhD thesis have been pursued with the defined interest in identifying new small molecules for therapeutic purposes. The work was conducted at the Department of Drug and Health Sciences (University of Catania), and at the Department of Chemistry and Applied Biosciences (ETH Zürich).

The main approach was the establishment of new series of ligands able to bind sigma receptors (σ Rs), a class of receptor proteins accepted as valuable target for the management of different pathological states including neurological disorders, pain, and cancer. The first two series of compounds have been developed by combining selective σ R ligands endowed with specific functional profile, together with chemical donors able to release therapeutic concentrations of hydrogen sulfide (H_2S) or nitric oxide (NO), two gaseous entities known for their pharmacological capabilities. The goal was to obtain a synergistic effect when compared to the relative single entities. The compounds have been synthesized and evaluated for affinity and selectivity with competitive radioligand binding assays. Further pharmacological characterization led to dig up the precise mechanism of action and efficacy in disease models.

A third series of compounds was developed in order to identify novel pure σ R ligands for their use thereof. This chemical matter has been developed according to structure-affinity relationships approach consisting in the following steps: (i) design of new candidate ligands; (ii) in vitro radioligand binding assays; (iii) iterative compounds design based on affinity and selectivity; (iv) synthesis of the new compounds for further pharmacological evaluation.

For chemical entities that ground their therapeutic value on the effect in the central nervous system (CNS), such as in the case of tumors or central analgesia, an important issue is their ability to cross the blood-brain barrier (BBB). This diffusion barrier between the blood and the CNS represents a sophisticated protection system against pathogens and toxic compounds. In this context, a useful statistical tool supporting the identification of parameters for BBB crossing has been developed allowing defining a set of rules that would prospectively be used to tune the properties of in-house synthesized ligands.

The last stage of this PhD thesis was addressed to find out high affinity small molecules targeting the human tyrosinases TYR and TYRP1, two closely-related enzymes selectively expressed in neoplastic skin lesions. The methodologies employed included the use of DNA-encoded chemical library technology, beside to improve already known binders reported in literature.

Sommario

Gli obiettivi di questa tesi di dottorato sono stati perseguiti con lo scopo di identificare nuove molecole di sintesi con efficacia terapeutica. Il lavoro è stato condotto presso il Dipartimento di Scienze del Farmaco e della Salute (Università degli Studi di Catania) e presso il Dipartimento di Chimica e Bioscienze Applicate (ETH di Zurigo).

L'interesse principale è stato rivolto allo sviluppo di ligandi in grado di legare i recettori sigma (σ), una classe di proteine recettoriali coinvolte in diverse patologie, comprese le malattie neurologiche, il dolore e il cancro.

Le prime due serie di molecole sono state sviluppate combinando ligandi selettivi per i recettori σ , aventi specifico profilo funzionale, insieme ad entità chimiche in grado di rilasciare concentrazioni terapeutiche di acido solfidrico (H_2S) o ossido nitrico (NO), due specie gassose note per la loro azione farmacologica. L'obiettivo è stato quello di ottenere un effetto sinergico quando comparato all'effetto delle rispettive singole entità. I composti sono stati sintetizzati e la loro affinità di legame valutata attraverso saggi di binding recettoriale. Un'ulteriore caratterizzazione farmacologica ha permesso di analizzare il preciso meccanismo di azione e la loro efficacia in modelli di malattia.

Una terza serie di composti è stata sviluppata al fine di identificare ligandi selettivi per i recettori σ . Questo obiettivo è stato perseguito sulla base delle correlazioni struttura-affinità ed è consistito in diverse fasi: (i) progettazione dei nuovi ligandi; (ii) saggi di binding recettoriale in vitro; (iii) progettazione iterativa dei composti basata sui valori di affinità e di selettività; (iv) sintesi dei nuovi composti per ulteriori valutazioni farmacologiche.

Per quanto riguarda quelle entità chimiche la cui efficacia terapeutica si fonda su un'azione a livello del sistema nervoso centrale (SNC), come per esempio nel caso di tumori o analgesia centrale, un parametro importante da considerare è la loro capacità di attraversare la barriera emato-encefalica (BEE). Questa barriera, posta tra il sangue e il SNC, rappresenta un sofisticato sistema di protezione nei confronti di agenti patogeni oltre che di composti tossici. In questo contesto, è stato sviluppato un utile strumento statistico a supporto dell'identificazione di quei parametri necessari per l'attraversamento della BEE, e che consente di definire un insieme di regole che potrebbero essere utilizzate nella messa a punto delle proprietà chimico-fisiche dei ligandi sintetizzati.

L'ultima fase di questa tesi di dottorato è stata indirizzata alla scoperta di molecole con elevata affinità per le tirosinasi umane TYR e TYRP1, due enzimi strettamente correlati ed espressi selettivamente a livello delle lesioni cutanee neoplastiche. Le metodologie impiegate hanno previsto l'uso di librerie chimiche codificate dal DNA, oltre al miglioramento di ligandi noti riportati in letteratura.

Abbreviations

ADC, antibody-drug conjugate

BBB, blood-brain barrier

BiP, binding immunoglobulin protein

C_{brain} , drug in the brain

C_{blood} , drug in the blood

$C_{\text{u,brainISF}}$, unbound drug concentration in brain interstitial fluid

$C_{\text{u,plasma}}$, unbound plasma

CNS, central nervous system

CSF, cerebrospinal fluid

DECL, DNA-encoded chemical library

ER, endoplasmic reticulum

H₂S, hydrogen sulfide

HTDS, high-throughput DNA sequencing

KO, knockout

MAM, mitochondrion-associated membrane

MDRP, multidrug resistance-associated protein

NO, nitric oxide

NOD, NO donor

PGRMC1, progesterone receptor membrane component 1

P-gp, P-glycoprotein

PET, positron emission tomography

ROS, reactive oxygen species

RNS, reactive nitrogen species

σ_1 R, sigma-1 receptor

σ_2 R, sigma-2 receptor

SAfiR, structure-affinity relationships

SMDC, small molecule-drug conjugate

TMEM97, endoplasmic reticulum-resident transmembrane protein

TYR, tyrosinase

TYRP1, tyrosinase-related protein 1

TYRP2, tyrosinase-related protein 2

WT, wild type

Synthesis and preclinical evaluation of sigma receptor ligands for cancer treatment and analgesia

1. Introduction

1.1. Sigma receptors

Sigma receptors (σ Rs) represent a unique receptor class involved in several biological and pathological conditions. First introduced as subtypes of the opioid receptor, they are now recognized as a particular and unique receptor class [1]. Two subtypes are distinguished and termed sigma-1 receptor (σ_1 R) and sigma-2 receptor (σ_2 R), having different structure, biological functions, and pharmacological profile. This classification was made possible thanks to the development of [3 H](+)-pentazocine, a radioligand with high affinity and selectivity for σ_1 R [2]. Differently from σ_1 R, the σ_2 subtype does not bind dextrorotatory benzomorphans and it exhibits high affinity for ditolylguanidine (DTG) and haloperidol (Figure 1) [3].

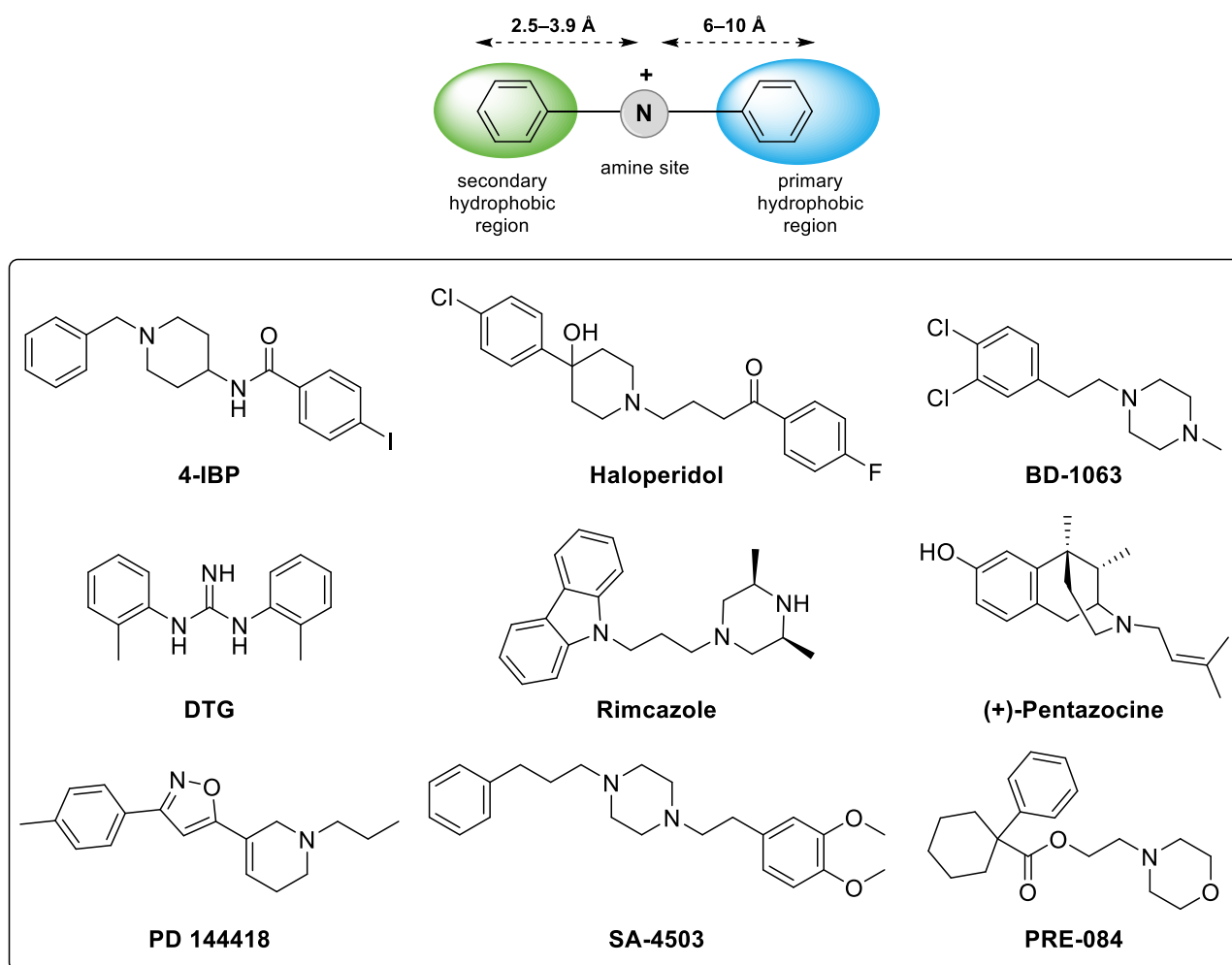


Figure 1. Structures of representative σ R ligands.

The use of [³H](+)-pentazocine also enabled the identification of some general structural features for an optimal binding to the σ_1 R. The binding site consists of a single positively charged nitrogen flanked by two hydrophobic or aromatic moieties having 6–10 Å and 2.5–3.9 Å in length. The primary hydrophobic region may bear a polar substituent even if affinity is sometimes reduced depending upon the nature and position of this substituent. The secondary hydrophobic site seems to be slightly smaller than the primary site. The amine can be secondary or tertiary, or also embedded in a cyclic structure such as a piperidine in 4-IBP (Figure 1), or piperazine in SA-4503 (Figure 1). In this last event either nitrogen atoms can bind at the amine site with different structural requirements for the binding with respect to their corresponding piperidine counterpart [4]. Several endogenous molecules (Figure 2), including steroids and notably progesterone [5, 6], sphingolipids [7], and the hallucinogen *N,N*-dimethyltryptamine (DMT) [8] bind to σ R regulating their activities. However, no endogenous ligand has been definitively identified. Recently, choline has been proposed to serve as an endogenous ligand for σ R, raising another possibility [9].

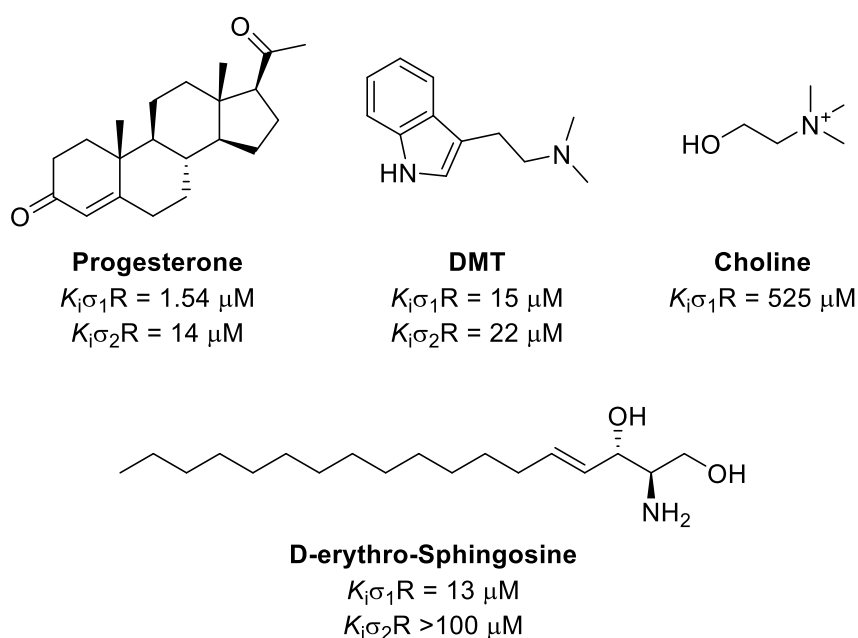


Figure 2. Structures and K_i values of σ R endogenous ligands.

The σ_1 and σ_2 subtypes can be distinguished by molecular weight (25 and 18–21.5 kDa, respectively), tissue distribution, subcellular localization, and ligand binding profile. The σ_1 R is a prospective therapeutic target for pain management, neurological disorders, and drug addiction [10-13]. Moreover, a wide number of data support the use of σ_1 R and σ_2 R ligands for the treatment as well as the imaging of cancer [14, 15].

1.1.1. Sigma-1 receptor

σ_1 R has been purified and cloned in several species and is well characterized as a chaperone protein at the mitochondrion-associated membrane (MAM) of the endoplasmic reticulum (ER) where it forms a complex with the binding immunoglobulin protein (BiP), another chaperone protein with a central role in protein folding [12]. The function of such a complex is regulated by Ca^{2+} concentrations. Indeed, at physiological Ca^{2+} concentrations (<0.5 mM), the σ_1 R-BiP complex is in a resting state, which results in a minimal chaperone activity for both. A decrease of Ca^{2+} in the ER or a stimulation by small molecules causes a rapid disassembly of the complex, with a significant chaperone activity of σ_1 R which in turn produces inositol triphosphate (IP_3) with activation and prolonged Ca^{2+} signaling into mitochondria [16, 17].

The σ_1 R overexpression in cells counteracts various forms of ER stress, whereas small interfering (si)RNA knockdown has been reported to make cells more vulnerable [18]. At the same time, the activation of σ_1 R provokes translocation to plasma membrane where it directly interacts with client proteins such as ion channels and G protein-coupled receptors [19-24]. Moreover, σ_1 R can associate with itself since it exists in multiple oligomeric states and σ_1 R ligands alter the distribution of these structures [25]. In particular, haloperidol and PD 144418 (Figure 1) bias the receptor towards multimerization, whereas (+)-pentazocine and several other ligands cause a shift to monomeric or low molecular weight species [26].

Recently, the crystal structure of the human σ_1 R in complex with different ligands has been reported. The structure reveals a trimeric architecture with a single transmembrane domain, five α helices and ten β strands. The receptor contains three hydrophobic domains and two of them are transmembrane-spanning helices with an extracellular loop in between and an intracellular C-terminus, suggesting an intimate association with the cytosolic surface of the ER membrane in cells (Figure 3).

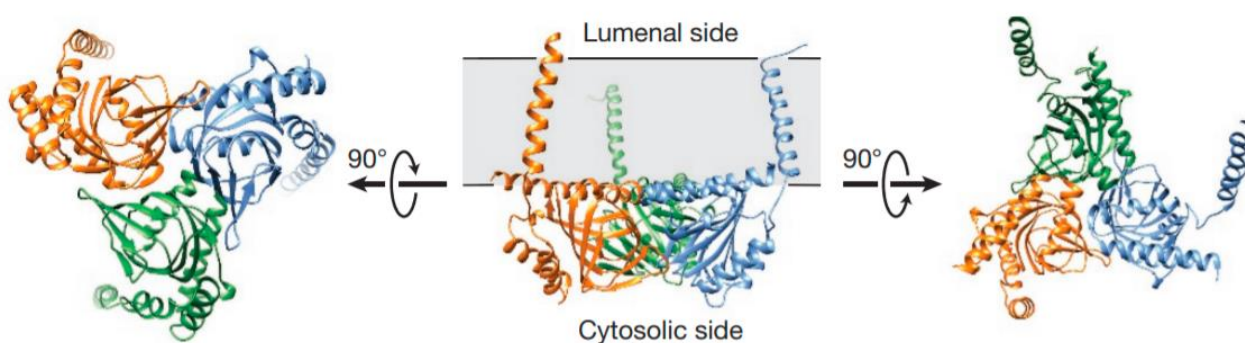


Figure 3. Crystal structure of the σ_1 R.

This domain has a cupin-like β -barrel cavity, wherein the ligand-binding site is covered, and it shows a considerable plasticity in ligand recognition and binding through a charge-charge interaction with

the highly conserved Glu172 moiety and the basic nitrogen present in most σ_1 R ligands [27]. The rest of the ligand is free to fit into the large β -barrel-like binding pocket lined with hydrophobic residues. σ_1 R ligands have historically been classified as agonists or antagonists based on their ability to mimic or not the genetic knockout (KO) of σ_1 R in animal models [11]. Ligands that mimic σ_1 R genetic KO are antagonists and they are reported to have analgesic effects in both animals and humans and to enhance the opioid mediated analgesia [28, 29]. On the contrary, σ_1 R agonists oppose the effects of antagonists, and they are associated with cytoprotective effects [30, 31]. Recently it has been shown how agonists and antagonists occupy a different region of the binding pocket [32]. Antagonists adopt a more linear pose, with the primary hydrophobic region towards the space between helices α_4 and α_5 , whereas primary hydrophobic site of agonists points towards helix α_4 (Figure 4). These small conformational changes would explain why agonists or antagonists may bias the receptor towards smaller or higher molecular weight states.

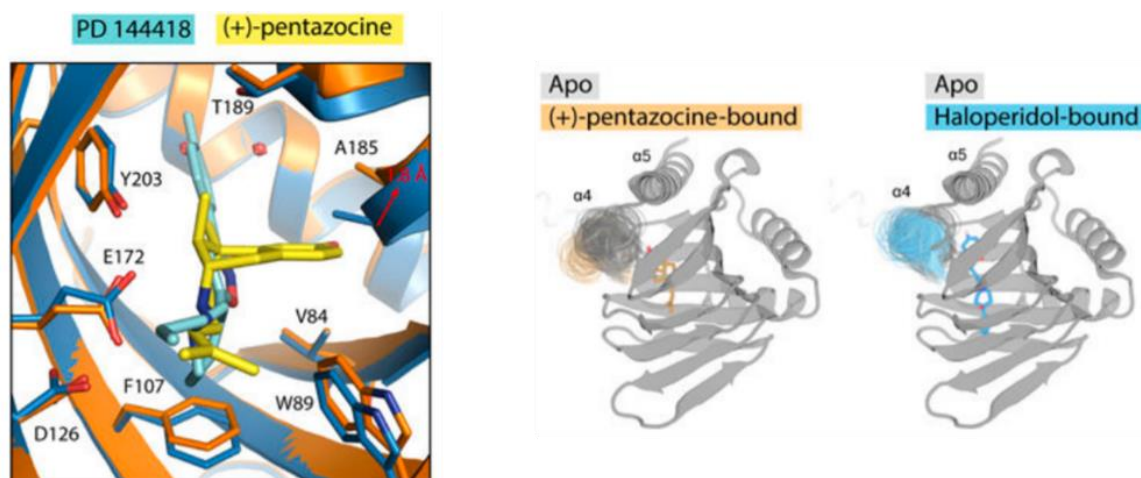


Figure 4. Alignment of (+)-pentazocine and PD 144418 in the binding pocket.

1.1.2. Sigma-2 receptor

σ_2 R is a poorly understood protein whose identification dates back to 1990 attracting considerable interest as therapeutic target for the treatment of cancer and neurological diseases [3]. For a long time its binding site has been postulated to be located in the progesterone receptor membrane component 1 (PGRMC1) [33]. However, a recent study has revealed that σ_2 R and PGRMC1 are different proteins since the presence or absence of PGRMC1 has no effect on σ_2 R binding ability in cells [33]. In 2017, σ_2 R was eventually identified as an endoplasmic reticulum-resident transmembrane protein (TMEM97) playing a role in the cholesterol homeostasis and the sterol transporter Niemann-Pick disease type C1 [34].

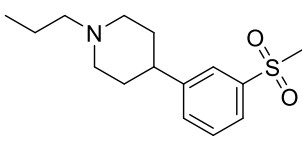
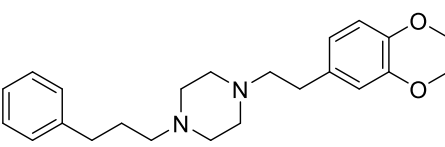
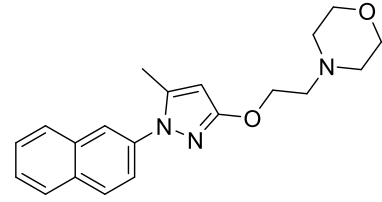
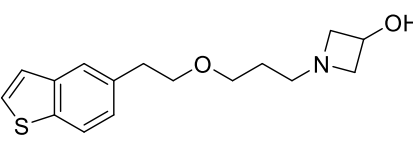
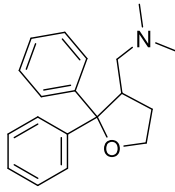
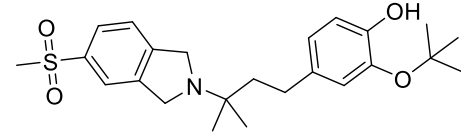
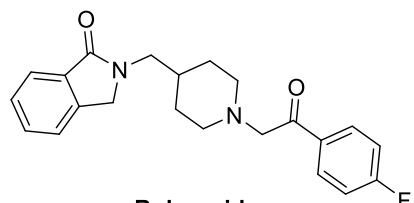
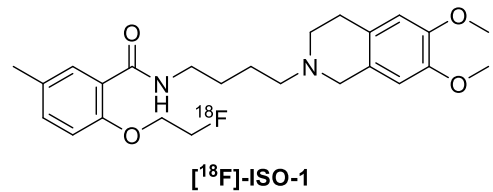
1.1.3. Pharmacological aspects of sigma receptors

The σ_1 R is highly expressed in both central and peripheral nervous system, in areas of great relevance for pain neurotransmission. In the CNS, σ_1 R has a preferential distribution in the spinal cord dorsal horn and at supraspinal levels in the periaqueductal gray matter, locus coeruleus, and rostral ventral medulla [35]. In the peripheral nervous system, σ_1 Rs are located in the soma of peripheral sensory neurons and along the nerve in Schwann cells [36, 37]. So far, four selective σ_1 R ligands have been advanced into later phase clinical studies for the treatment of neurodegenerative diseases (Table 1). Blarcamesine (ANAVEX 2-73) is a σ_1 R agonist under phase 2/3 investigation in patients with Alzheimer's disease, Rett syndrome and Parkinson's disease with dementia. Pridopidine (formerly Huntexil, ACR16, ASP2314) is in a phase 3 clinical for the early stage and symptomatic treatment of Huntington's disease, and in a phase 2 for the treatment of levodopa-induced dyskinesia in Parkinson's disease patients. Cutamesine is a selective σ_1 R agonist under phase 2 clinical trial in subjects with major depressive disorder and to restore motor function after acute ischemic stroke. The neurotropic agent Edonepic (T-817 MA) has advanced into phase 2 clinic trials in patients with mild to moderate Alzheimer's disease.

Preclinical evidences support the modulatory role of σ_1 R also in nociception, mainly based on the pain-attenuated phenotype of σ_1 R KO mice and on the antinociceptive effect exerted by σ_1 R antagonists on pain of different etiology including neuropathic, inflammatory, and visceral pain, and as adjuvants to opioid therapy [38]. The selective σ_1 R antagonist E-52862 (S1RA, Table 1) is currently undergoing phase II clinical trials for the treatment of neuropathic pain of different etiologies [39]. The systemic administration of σ_1 R antagonists enhances morphine antinociception to noxious heat stimulation (tail-flick test) [40-42]. This effect has been also described following systemic administration of other clinically relevant μ -opioids including fentanyl, oxycodone, codeine, buprenorphine and tramadol, as well as with the κ -opioid agonists U50,488, naloxone benzoylhydrazone and (-)-pentazocine [41, 43-45]. Further experiments carried out with σ_1 R KO mice and in wild type (WT) animals treated with σ_1 R antagonists showed no allodynia in both formalin- and capsaicin-induced nociception [46, 47]. Also, experiments with σ_1 R KO mice with traumatic nerve injury were consistent with results obtained with pharmacological treatments, since mutant mice did not develop signs of either cold or mechanical allodynia [48]. Both σ_1 and σ_2 subtypes are highly overexpressed in several human tumors like breast, colon, ovaries, lung and prostate. A wide number of data support the use of σ_1 R antagonists and σ_2 R agonists for the treatment of cancer due to their antiproliferative effects [49]. Rimcazole, haloperidol (Figure 1), as well as other σ_1 R antagonists have shown to inhibit cell proliferation in breast, colorectal, melanoma and glioma cancer cell lines, while having minimal effect on most non-tumor cells [50]. It has been reported that

σ_1R may activate different adaptation mechanisms as response to tumoral environmental conditions, on the basis of the client protein in a given cancer cell type [51].

Table 1. σR ligands evaluated in clinical trials.

					
Pridopidine	Cutamesine	S1RA			
					
Edonerpic	Blarcamesine	Elayta			
					
Roluperidone	[¹⁸F]-ISO-1				
Drug	Functional profile	Condition	Phase	Trial Number	
Blarcamesine	σ_1R agonist	Alzheimer's disease	II-III	03790709, 04314934	
		Parkinson's disease	II	04575259	
		Rett syndrome	II-III	03941444, 04304482	
		Pridopidine	Huntington's disease	II-III	00724048, 00665223
			Parkinson's disease	II	03922711
		Cutamesine	Depressive disorder	II	00551109
			Ischemic stroke	II	00639249
Edonerpic	Alzheimer's Disease	II	02079909, 04191486		
S1RA	σ_1R antagonist	Neuropathic pain	II	-	
Elayta	σ_2R antagonist	Alzheimer's disease	II	03493282, 03507790	
Roluperidone		Schizophrenia	III	03397134	
[¹⁸ F]-ISO-1		Imaging of σ_2R	I	03057743	

Particularly, ion channels represent one of the main client protein families for σ_1R with an involvement in the remodeling of cancer cell electrical properties and strengthening of ion channel

function associated with proliferation, cell death resistance, invasion, and angiogenesis [52]. Since high levels of the σ_2R have been found in several cancer cells and proliferating tumors, extensive data support its utility as therapeutic target for the diagnosis and treatment of cancer [15, 53, 54]. Compound [^{18}F]-ISO-1 (Table 1) is a positron emission tomography (PET) ligand evaluated in clinical trials for the imaging of σ_2R binding in primary breast cancer [55]. More recently, σ_2R has been implicated in neurological disorders including Alzheimer's disease and schizophrenia (Table 1). Elayta (CT1812), a small molecule σ_2R antagonist, is currently under phase II clinical trial in patients with mild to moderate Alzheimer's disease [56, 57]. Also, the σ_2R antagonist roluperidone (MIN-101) is in phase III clinical trials for the treatment of negative symptoms of schizophrenia [58, 59].

1.2 Gasotransmitters

Nitric oxide (NO) and hydrogen sulfide (H₂S) are two short half-life endogenous gasotransmitters involved in the modulation of the daily cellular activities as well as the cytotoxic events. NO is a Janus-faced molecule with a dichotomous role in tumor biology: μ M concentrations result in antitumor effects, while pM–nM range concentrations promote cytoprotective action [60]. Similarly, small but significant amounts of endogenous H₂S enhance nociceptive process, whereas exogenous H₂S has anti-nociceptive role at peripheral levels [61]. Based on these findings, the modulation of NO and H₂S levels might be useful in therapy, however due their reactive and unstable gaseous nature, the controlled and localized generation or administration of these gas to biological sites is greatly limited.

1.2.1 Biological importance of NO

Nitric oxide (NO) is a short-lived free radical gas engaged in the modulation of the daily cellular activities. Under physiological conditions, cells produce small but significant amount of NO which contributes to regulate anti-inflammatory and antioxidant effects [62].

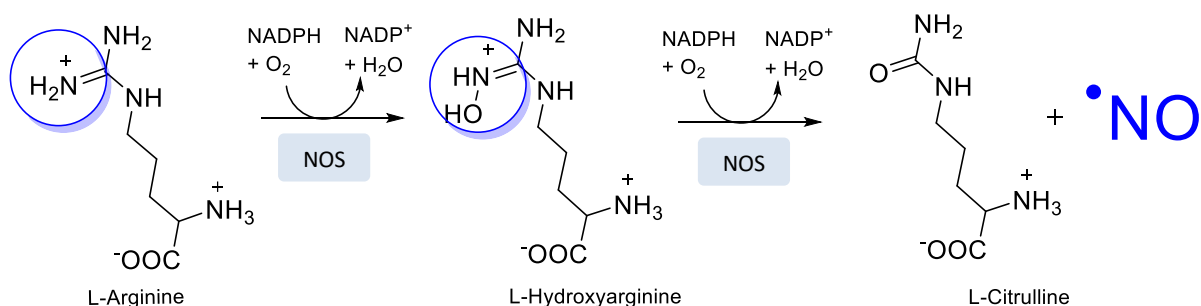
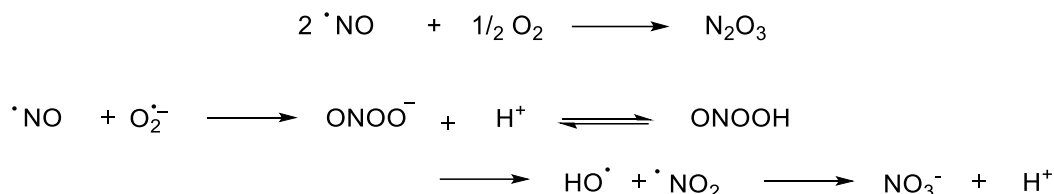


Figure 5. Biosynthesis of nitric oxide.

NO is endogenously produced by the enzyme nitric oxide synthase (NOS) that convert L-arginine into L-citrulline through oxidation of the guanidine group. This occurs in two sequential monooxygenase reactions utilizing NADPH and molecular oxygen as cofactors (Figure 5). On the other hand, an uncontrolled NO synthesis has been related to pathological conditions including cancer [63-65]. Moreover, since NO contains an unpaired electron, it rapidly reacts with superoxide ion ($O_2^{\cdot-}$) or oxygen (O_2) taking a direct part in the activation of free radical processes and reactive nitrogen species (RNS), among which dinitrogen trioxide (N_2O_3) and peroxynitrite ($ONOO^-$) [66, 67].



N_2O_3 is a potent nitrosating agent over a variety of biological targets to yield potentially carcinogenic nitrosamines and nitrosothiol derivatives. Also, $ONOO^-$ is a potent cytotoxic oxidant with a short half-life in biological systems causing DNA breaks and lipid peroxidation [68]. In turn, peroxynitrite can cause further reactive oxygen species (ROS) formation, including the reaction of interaction of peroxynitrite with protons, which can be a major source of hydroxyl radicals.

The role of NO in cancer physiopathology is certainly controversial since it is a dichotomic molecule acting as a double-edged sword with both tumoricidal as well as tumor promoting effects depending on its timing, location, and concentration [69]. However, effects of NO in the tumor mostly depend on its concentration. Low concentrations in the pM–nM range have been reported to promote genotoxic damage that may occur as a direct modification of DNA, or inhibition of reparation of nucleic acids. These mechanisms of carcinogenesis also include activation of signaling pathways stimulating cell proliferation, caspase inhibition, neovascularization, and dissemination of tumor cell [70-72]. On the contrary, high μ M concentrations have tumoricidal effects by activating caspase family proteases, up-regulation of p53 expression and acting as a proapoptotic modulator [73-75]. Based on these findings, the role of NO as valuable anticancer agent is clear. However, due to its reactive and unstable nature, controlled and localized generation of NO to cancer cells is challenging. Thus, the use of NO donors (NODs) is preferred since these agents are stable chemical compounds able to release NO under specific chemical or enzymatical conditions [76-79]. Different classes of NO donors have been investigated for their benefits in cancer treatment (Figure 6), among which organic nitrates represent the oldest class in clinical use [80].

Organic nitrates are nitric acid esters of mono- and poly-hydric alcohols with the general formula $RONO_2$. Commonly used organic nitrates include nitroglycerin (NTG), amyl nitrite, isosorbide-5-

mononitrate (ISMN), and nicorandil and pentaerythritol tetranitrate (PETN), reported to mimic NO activity with a mechanism of action not yet completely understood [81].

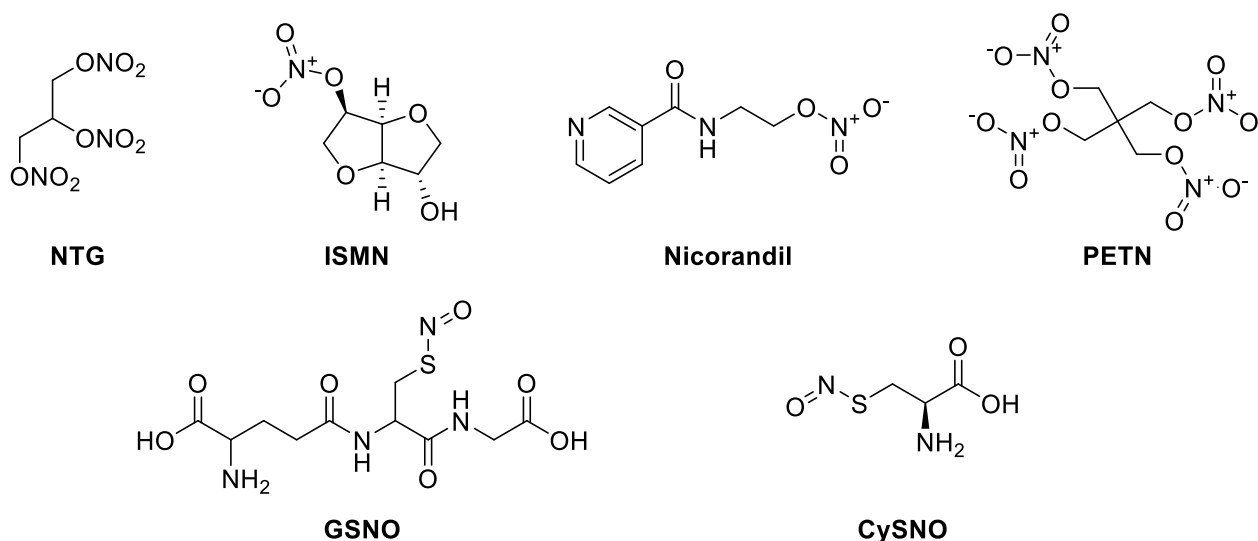


Figure 6. Structures of NO donors used for basic research.

Non-steroidal anti-inflammatory drugs such as aspirin, salicylic acid, indomethacin, ibuprofen or sulindac linked to an NO-releasing moiety (NO-NSAIDs) have been evaluated for their inhibitory properties both in colon and prostate cancer cells, and in a mouse model of early intestinal neoplasia revealing their potential role as chemopreventive agents [82-84]. *S*-nitrosothiols represent a class of NO donors performing trans-nitrosylation reactions, and they include *S*-nitroso-glutathione (GSNO), *S*-nitrosoalbumin and *S*-nitrosocysteine (CySNO), which derive from the reactions of endogenous NO with thiol groups.

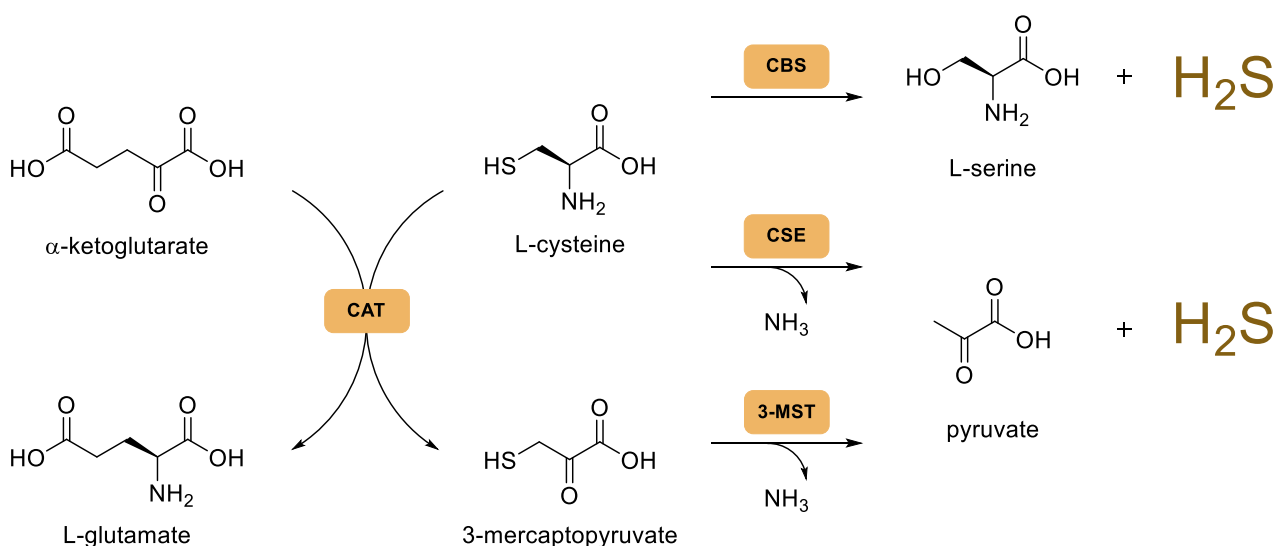
Some of these donors have reached clinical trial studies (Table 2). MK-8150 is under Phase I clinical trial for its effects on hypertension [85]. The COX-inhibiting NO donor AZD3582 is under clinical investigation for the treatment of different conditions [86-89]. 1-Bromoacetyl-3,3-dinitroazetidine (RRx-001) demonstrated good activity and tolerance without clinically significant toxic effects, moving to phase II clinical investigation in patients with advanced cancer [90].

Table 2. NO donor derivatives evaluated in clinical trials.

Drug	Condition	Phase	Trial Number
MK-8150	Hypertension	I	01656408
AZD3582	Prostate cancer	II	00383487
	Osteoarthritis	III	00542555
	Liver Disease	I	00621881
	Renal Failure	I	00674856
RRx-001	Advanced cancer	II	02452970

1.2.2 Biological importance of H₂S

Considered as a sheer toxic gas for decades, H₂S is an endogenous gasotransmitter involved in the modulation of the daily cellular activities in the central and peripheral nervous system [91, 92]. The generation of H₂S by mammalian tissues occurs slowly and constantly via the enzymatic actions of cystathionine-γ-lyase (CSE), cystathionine-β-synthase (CBS), and 3-mercapto-sulfurtransferase (3-MST) which convert cysteine or cysteine derivatives into H₂S in different tissues and organs (Figure 7) [93].

**Figure 7.** Biosynthesis of hydrogen sulfide.

Under physiological conditions, cells produce small but significant amounts of H₂S that contribute to the neuromodulation and neuroprotection of nerve cells [94]. However, the endogenous H₂S can become pronociceptive, maybe acting internally as a neurotransmitter to facilitate pain. On the contrary, exogenously administered H₂S are reported for both pronociceptive and antinociceptive effects, depending on the route of administration and doses. It has been proposed that local administration or production of H₂S may cause pain, whereas a systemic administration may result in pain attenuation [95-98]. Also, the doses of H₂S may influence pain response, with low doses contributing to pain reduction [99, 100].

One of the major limits of H₂S is the inability to handle due to its gaseous nature. Moreover, exposure is not controllable since toxic concentrations are rapidly achieved. Sodium hydrosulfide (NaSH) and sodium sulfide (Na₂S) represent the most common class of donors employed in biological studies to evaluate the exogenous H₂S delivery. Although referred as donors, sulfide salts are solid analogs of the gas, providing a quick release of the biologically relevant forms H₂S and HS⁻. All other donors class need chemical reactions to release H₂S, which can be triggered by water, light, a nucleophile such as a thiol, or other stimuli. Anyway, measuring the kinetic release of these reactions can be difficult. One common method is to use an H₂S-selective electrochemical probe which provides a real time analysis of H₂S in solution, even if this method may not reflect how donors would react in the bloodstream, where the rapid dilution would alter the release profile [101]. Another strategy is the methylene blue method, by which the reaction of sulfide species in acidic aqueous solution of *N,N*-dimethylphenylenediamine and iron (III) chloride (FeCl₃) leads to the formation of methylene blue. However, this technique is not specific since methylene blue formation also occurs in the presence of a variety of sulfur species, including thiols. Fluorescent probes are routinely used in the detection and quantification of H₂S, relying on the selective reduction of aryl or sulfonyl azides to amines in a fluorescent turn-on strategy (Figure 8) [93].

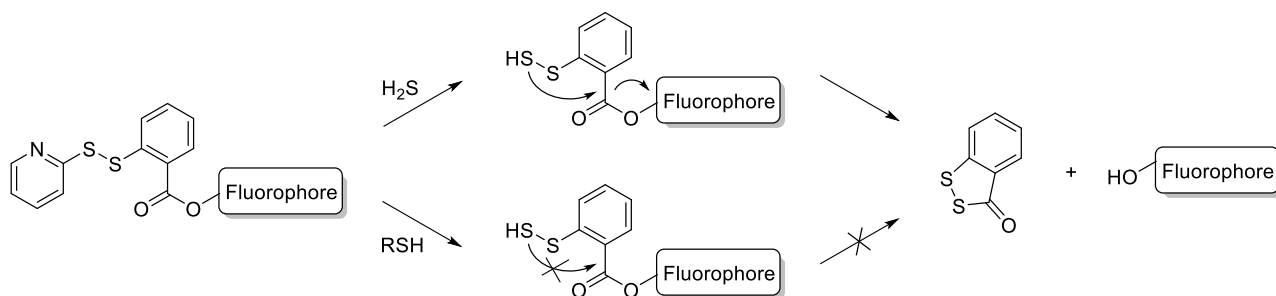


Figure 8. Fluorescent turn-on strategy in determining H₂S concentration.

An ideal H₂S donor should be water-soluble, stable under storage conditions, and have a specific and well-defined release mechanism (Figure 9). Lawesson's reagent (LR) is able to release H₂S over a

much longer period than sulfide salts. However, it is not been widely employed due to its lack of water solubility as well as a very slow H₂S release rate. The water-soluble derivative of LR, GYY4137, releases H₂S via hydrolysis and it is considered a slow releasing H₂S donor [102]. 1,2-Dithiole-3-thiones (DTTs) are a class of compounds easy to synthesize and readily attached to other molecules to make drug-DTT conjugates. It has been reported that the DTT-drug conjugates via an amide linkage are more stable to hydrolysis than the corresponding ester [103].

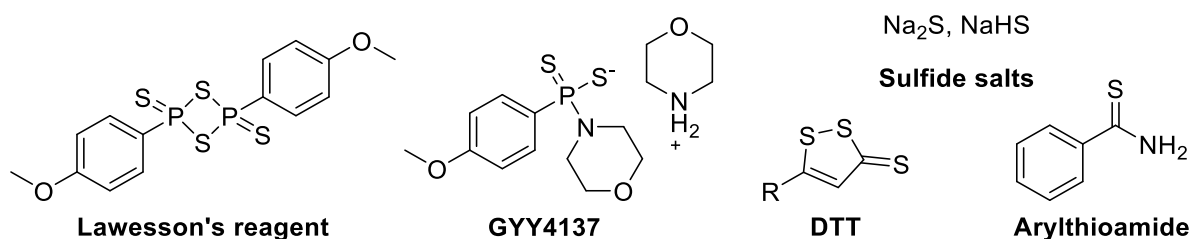


Figure 9. Structures of H₂S donors used for basic research.

Also arylthioamides are a versatile class of donors able to release H₂S under hydrolysis. In particular, the trimebutine derivative bearing a thioamide function (GIC-1001) has been reported for being able to release H₂S inducing a reduction of the nociceptive response in an animal model of colorectal distension [104].

Table 3. H₂S donor derivatives evaluated in clinical trials.

Drug	Condition	Phase	Trial Number
GIC-1001	Visceral pain	II	01926444
ATB-346	Gastric ulcer	II	03291418
SG-1002	Heart Failure	II	02278276
N-acetylcysteine	Kidney Disease	III	01232257
	Head and Neck Cancer	II	03982537
Sodium thiosulfate	Myocardial Infarction	II	02899364

Taking into consideration the in vivo efficacy and the safety in humans, GIC-1001 underwent phase II evaluation, revealing a significant pain reduction [105]. The naproxen-based H₂S donor ATB-346 is under Phase II clinical investigation for its anti-inflammatory effects [106]. Sodium polythionate (SG-1002), made of sulfur for 90%, is evaluated in Phase II clinical trial with the purpose to reduce markers of oxidative stress after heart failure [107]. In Table 3 is reported a list of H₂S donors under clinical trial investigation.

1.3. Blood-Brain Barrier Permeation

The blood-brain barrier (BBB) represents a protection system for CNS consisting of an intricate network of capillaries needed for maintaining the homeostasis and physiological environment allowing specific nutrients and hormones to selectively permeate. Besides the BBB, which separates the blood circulation from the brain's parenchyma, there is also a barrier between the blood circulation and the cerebrospinal fluid (CSF).

However, this sophisticated protection system often slows down the development of molecules active on CNS disorders. And this happens since the standard pharmacokinetic parameters such as oral bioavailability and plasma concentration are not enough to evaluate drug exposure and time course in the brain [108]. An accurate interaction between passive membrane permeability and active transport processes is also determinant for brain entry [109]. Several transporters facilitate active uptake or efflux transport of drug molecules into and out of the brain, such as the P-glycoprotein (P-gp) and the multidrug resistance-associated protein family (MRP) [110, 111]. However, certain drugs freely diffuse through the BBB by transcellular passive diffusion.

The BBB permeability can be examined both in vivo and in vitro, even if in vivo results depend on the conditions of the in situ brain perfusion method used; however this method is not suitable for routine drug discovery screening. A more popular in vivo method is to determine the amount of compound in the brain after oral or systemic administration, relating the amount of compound in the brain to the plasma exposure. However, in vitro assays have become the method of choice to assess permeability, with MDCK-MDR1 cells the most widely used although suffer some limitations.

Traditionally, an in vivo index of BBB permeability is represented by the \log_{BB} ($\log K_{p,brain}$), the logarithm of the ratio of the concentration of a drug in the brain (C_{brain}) and in the blood (C_{blood}) measured at the steady state:

$$\log_{BB} = \log \frac{C_{brain}}{C_{blood}}$$

For the determination of this parameter, mice are administered with a subcutaneous dose of drug and, after the equilibrium is reached, the drug concentration is measured in the brain and in the blood using

a chromatographic method. Although this ratio is a frequently used measure of brain penetration, high compound brain-to-plasma ratios (B/P) can often be misleading. Recently it has been highlighted the importance of the unbound portion of the total drug ($K_{p,uu,brain}$) which is free to diffuse across biological barriers and tissues eliciting pharmacodynamic effects [112]. Thus, the $K_{p,uu,brain}$ is a ratio of steady state unbound concentration of a drug in brain and plasma, defined as

$$K_{p,uu,brain} = \frac{C_{u,brainISF}}{C_{u,plasma}}$$

where, $C_{u,brainISF}$ and $C_{u,plasma}$ represent the unbound drug concentration in brain interstitial fluid (ISF) and plasma, respectively. However, few experimental $K_{p,uu,brain}$ data are currently available and at the state of the art, the output results of both methods are employed and beneficial for understanding the magnitude of BBB permeation and to some extent the CNS active dose [113-119]. This is also the result of a technology gap since experimental access to relevant compartments in the brain is often troublesome.

1.3.1. Physicochemical properties in BBB crossing

The first attempts in understanding the link between the physicochemical properties and BBB permeability of drugs were addressed to the role of lipophilicity [120]. In particular, the earliest studies on the relationship between lipophilicity and CNS drugs design were based on the octanol/water partition coefficient [121].

A significant progress in the field was done with the rise of Lipinski's rule of five based on multiple physicochemical properties to evaluate a compound's likelihood of being orally bioavailable [122, 123]. Over the years, several researchers have attempted to define the features for a successful BBB crossing, using different approaches. Particularly, based on a structure-property analysis derived from multiple ADMET assays, Gleeson has identified molecular weight and logP as important parameters in determining CNS penetration [124]. In 2016, Wager et al. realized an algorithm to optimize the druglike properties of CNS candidates using a set of six physicochemical properties rather than individual cutoffs for physicochemical properties [125].

REFERENCES

- [1] J.M. Walker, W.D. Bowen, F.O. Walker, R.R. Matsumoto, B. De Costa, K.C. Rice, Sigma receptors: biology and function, *Pharmacological reviews*, 42 (1990) 355-402.
- [2] W.D. Bowen, B.R. De Costa, S.B. Hellewell, J.M. Walker, K.C. Rice, [3H]-(+)-Pentazocine: A potent and highly selective benzomorphan-based probe for sigma-1 receptors, *Molecular Neuropharmacology*, 3 (1993) 117-126.
- [3] S.B. Hellewell, W.D. Bowen, A sigma-like binding site in rat pheochromocytoma (PC12) cells: decreased affinity for (+)-benzomorphans and lower molecular weight suggest a different sigma receptor form from that of guinea pig brain, *Brain research*, 527 (1990) 244-253.
- [4] R.A. Glennon, Pharmacophore identification for sigma-1 (sigma1) receptor binding: application of the "deconstruction-reconstruction-elaboration" approach, *Mini reviews in medicinal chemistry*, 5 (2005) 927-940.
- [5] F.P. Monnet, T. Maurice, The sigma1 protein as a target for the non-genomic effects of neuro(active)steroids: molecular, physiological, and behavioral aspects, *Journal of pharmacological sciences*, 100 (2006) 93-118.
- [6] L. Guo, J. Zhao, G. Jin, B. Zhao, G. Wang, A. Zhang, X. Zhen, SKF83959 is a potent allosteric modulator of sigma-1 receptor, *Molecular pharmacology*, 83 (2013) 577-586.
- [7] S. Ramachandran, U.B. Chu, T.A. Mavlyutov, A. Pal, S. Pyne, A.E. Ruoho, The sigma1 receptor interacts with N-alkyl amines and endogenous sphingolipids, *European journal of pharmacology*, 609 (2009) 19-26.
- [8] D. Fontanilla, M. Johannessen, A.R. Hajipour, N.V. Cozzi, M.B. Jackson, A.E. Ruoho, The hallucinogen N,N-dimethyltryptamine (DMT) is an endogenous sigma-1 receptor regulator, *Science (New York, N.Y.)*, 323 (2009) 934-937.
- [9] E. Brailoiu, S. Chakraborty, G.C. Brailoiu, P. Zhao, J.L. Barr, M.A. Ilies, E.M. Unterwald, M.E. Abood, C.W. Taylor, Choline Is an Intracellular Messenger Linking Extracellular Stimuli to IP(3)-Evoked Ca(2+) Signals through Sigma-1 Receptors, *Cell reports*, 26 (2019) 330-337.e334.
- [10] L. Romero, M. Merlos, J.M. Vela, Antinociception by Sigma-1 Receptor Antagonists: Central and Peripheral Effects, *Advances in pharmacology (San Diego, Calif.)*, 75 (2016) 179-215.
- [11] L. Nguyen, B.P. Lucke-Wold, S.A. Mookerjee, J.Z. Cavendish, M.J. Robson, A.L. Scandinaro, R.R. Matsumoto, Role of sigma-1 receptors in neurodegenerative diseases, *Journal of pharmacological sciences*, 127 (2015) 17-29.
- [12] T.Y. Weng, S.A. Tsai, T.P. Su, Roles of sigma-1 receptors on mitochondrial functions relevant to neurodegenerative diseases, *Journal of biomedical science*, 24 (2017) 74.
- [13] J.L. Katz, W.C. Hong, T. Hiranita, T.P. Su, A role for sigma receptors in stimulant self-administration and addiction, *Behavioural pharmacology*, 27 (2016) 100-115.
- [14] F.J. Kim, C.M. Maher, Sigma1 Pharmacology in the Context of Cancer, *Handbook of experimental pharmacology*, 244 (2017) 237-308.
- [15] A. van Waarde, A.A. Rybczynska, N.K. Ramakrishnan, K. Ishiwata, P.H. Elsinga, R.A. Dierckx, Potential applications for sigma receptor ligands in cancer diagnosis and therapy, *Biochimica et biophysica acta*, 1848 (2015) 2703-2714.
- [16] M. Novakova, C. Ela, W.D. Bowen, Y. Hasin, Y. Eilam, Highly selective sigma receptor ligands elevate inositol 1,4,5-trisphosphate production in rat cardiac myocytes, *European journal of pharmacology*, 353 (1998) 315-327.
- [17] T. Hayashi, T. Maurice, T.P. Su, Ca(2+) signaling via sigma(1)-receptors: novel regulatory mechanism affecting intracellular Ca(2+) concentration, *The Journal of pharmacology and experimental therapeutics*, 293 (2000) 788-798.
- [18] T. Hayashi, T.P. Su, Sigma-1 receptor chaperones at the ER-mitochondrion interface regulate Ca(2+) signaling and cell survival, *Cell*, 131 (2007) 596-610.

- [19] E. Aydar, D. Stratton, S.P. Fraser, M.B. Djamgoz, C. Palmer, Sigma-1 receptors modulate neonatal Na(v)1.5 ion channels in breast cancer cell lines, *European biophysics journal : EBJ*, 45 (2016) 671-683.
- [20] E. Aydar, C.P. Palmer, V.A. Klyachko, M.B. Jackson, The sigma receptor as a ligand-regulated auxiliary potassium channel subunit, *Neuron*, 34 (2002) 399-410.
- [21] D. Balasuriya, A.P. Stewart, J.M. Edwardson, The σ -1 receptor interacts directly with GluN1 but not GluN2A in the GluN1/GluN2A NMDA receptor, *The Journal of neuroscience : the official journal of the Society for Neuroscience*, 33 (2013) 18219-18224.
- [22] F.J. Kim, I. Kovalyshyn, M. Burgman, C. Neilan, C.C. Chien, G.W. Pasternak, Sigma 1 receptor modulation of G-protein-coupled receptor signaling: potentiation of opioid transduction independent from receptor binding, *Molecular pharmacology*, 77 (2010) 695-703.
- [23] E. Moreno, D. Moreno-Delgado, G. Navarro, H.M. Hoffmann, S. Fuentes, S. Rosell-Vilar, P. Gasperini, M. Rodríguez-Ruiz, M. Medrano, J. Mallol, A. Cortés, V. Casadó, C. Lluís, S. Ferré, J. Ortiz, E. Canela, P.J. McCormick, Cocaine disrupts histamine H3 receptor modulation of dopamine D1 receptor signaling: σ 1-D1-H3 receptor complexes as key targets for reducing cocaine's effects, *The Journal of neuroscience : the official journal of the Society for Neuroscience*, 34 (2014) 3545-3558.
- [24] G. Navarro, E. Moreno, J. Bonaventura, M. Brugarolas, D. Farré, D. Aguinaga, J. Mallol, A. Cortés, V. Casadó, C. Lluís, S. Ferré, R. Franco, E. Canela, P.J. McCormick, Cocaine inhibits dopamine D2 receptor signaling via sigma-1-D2 receptor heteromers, *PloS one*, 8 (2013) e61245.
- [25] A.K. Mishra, T. Mavlyutov, D.R. Singh, G. Biener, J. Yang, J.A. Oliver, A. Ruoho, V. Raicu, The sigma-1 receptors are present in monomeric and oligomeric forms in living cells in the presence and absence of ligands, *The Biochemical journal*, 466 (2015) 263-271.
- [26] H. Yano, A. Bonifazi, M. Xu, D.A. Guthrie, S.N. Schneck, A.M. Abramyan, A.D. Fant, W.C. Hong, A.H. Newman, L. Shi, Pharmacological profiling of sigma 1 receptor ligands by novel receptor homomer assays, *Neuropharmacology*, 133 (2018) 264-275.
- [27] H.R. Schmidt, S. Zheng, E. Gurpinar, A. Koehl, A. Manglik, A.C. Kruse, Crystal structure of the human σ 1 receptor, *Nature*, 532 (2016) 527-530.
- [28] S. Castany, G. Gris, J.M. Vela, E. Verdú, P. Boadas-Vaello, Critical role of sigma-1 receptors in central neuropathic pain-related behaviours after mild spinal cord injury in mice, *Scientific reports*, 8 (2018) 3873.
- [29] J. Bruna, S. Videla, A.A. Argyriou, R. Velasco, J. Villoria, C. Santos, C. Nadal, G. Cavaletti, P. Alberti, C. Briani, H.P. Kalofonos, D. Cortinovis, M. Sust, A. Vaqué, T. Klein, C. Plata-Salamán, Efficacy of a Novel Sigma-1 Receptor Antagonist for Oxaliplatin-Induced Neuropathy: A Randomized, Double-Blind, Placebo-Controlled Phase IIa Clinical Trial, *Neurotherapeutics : the journal of the American Society for Experimental NeuroTherapeutics*, 15 (2018) 178-189.
- [30] R. Mancuso, S. Oliván, A. Rando, C. Casas, R. Osta, X. Navarro, Sigma-1R agonist improves motor function and motoneuron survival in ALS mice, *Neurotherapeutics : the journal of the American Society for Experimental NeuroTherapeutics*, 9 (2012) 814-826.
- [31] D. Li, S.Z. Zhang, Y.H. Yao, Y. Xiang, X.Y. Ma, X.L. Wei, H.T. Yan, X.Y. Liu, Sigma-1 receptor agonist increases axon outgrowth of hippocampal neurons via voltage-gated calcium ions channels, *CNS neuroscience & therapeutics*, 23 (2017) 930-939.
- [32] H.R. Schmidt, R.M. Betz, R.O. Dror, A.C. Kruse, Structural basis for σ (1) receptor ligand recognition, *Nature structural & molecular biology*, 25 (2018) 981-987.
- [33] U.B. Chu, T.A. Mavlyutov, M.L. Chu, H. Yang, A. Schulman, C. Mesangeau, C.R. McCurdy, L.W. Guo, A.E. Ruoho, The Sigma-2 Receptor and Progesterone Receptor Membrane Component 1 are Different Binding Sites Derived From Independent Genes, *EBioMedicine*, 2 (2015) 1806-1813.
- [34] A. Alon, H.R. Schmidt, M.D. Wood, J.J. Sahn, S.F. Martin, A.C. Kruse, Identification of the gene that codes for the σ (2) receptor, *Proceedings of the National Academy of Sciences of the United States of America*, 114 (2017) 7160-7165.

- [35] G. Alonso, V. Phan, I. Guillemain, M. Saunier, A. Legrand, M. Anoa, T. Maurice, Immunocytochemical localization of the sigma(1) receptor in the adult rat central nervous system, *Neuroscience*, 97 (2000) 155-170.
- [36] M.L. Bangaru, D. Weihrauch, Q.B. Tang, V. Zoga, Q. Hogan, H.E. Wu, Sigma-1 receptor expression in sensory neurons and the effect of painful peripheral nerve injury, *Molecular pain*, 9 (2013) 47.
- [37] G. Palacios, A. Muro, E. Verdú, M. Pumarola, J.M. Vela, Immunohistochemical localization of the sigma1 receptor in Schwann cells of rat sciatic nerve, *Brain research*, 1007 (2004) 65-70.
- [38] M. Merlos, L. Romero, D. Zamanillo, C. Plata-Salamán, J.M. Vela, Sigma-1 Receptor and Pain, *Handbook of experimental pharmacology*, 244 (2017) 131-161.
- [39] L. Romero, D. Zamanillo, X. Nadal, R. Sánchez-Arroyos, I. Rivera-Arconada, A. Dordal, A. Montero, A. Muro, A. Bura, C. Segalés, M. Laloya, E. Hernández, E. Portillo-Salido, M. Escriche, X. Codony, G. Encina, J. Burgueño, M. Merlos, J.M. Baeyens, J. Giraldo, J.A. López-García, R. Maldonado, C.R. Plata-Salamán, J.M. Vela, Pharmacological properties of S1RA, a new sigma-1 receptor antagonist that inhibits neuropathic pain and activity-induced spinal sensitization, *British journal of pharmacology*, 166 (2012) 2289-2306.
- [40] C.C. Chien, G.W. Pasternak, Sigma antagonists potentiate opioid analgesia in rats, *Neuroscience letters*, 190 (1995) 137-139.
- [41] A. Vidal-Torres, B. de la Puente, M. Rocasalbas, C. Touriño, S.A. Bura, B. Fernández-Pastor, L. Romero, X. Codony, D. Zamanillo, H. Buschmann, M. Merlos, J.M. Baeyens, R. Maldonado, J.M. Vela, Sigma-1 receptor antagonism as opioid adjuvant strategy: enhancement of opioid antinociception without increasing adverse effects, *European journal of pharmacology*, 711 (2013) 63-72.
- [42] C. Sánchez-Fernández, F.R. Nieto, R. González-Cano, A. Artacho-Cordón, L. Romero, Á. Montilla-García, D. Zamanillo, J.M. Baeyens, J.M. Entrena, E.J. Cobos, Potentiation of morphine-induced mechanical antinociception by σ_1 receptor inhibition: role of peripheral σ_1 receptors, *Neuropharmacology*, 70 (2013) 348-358.
- [43] C. Sánchez-Fernández, Á. Montilla-García, R. González-Cano, F.R. Nieto, L. Romero, A. Artacho-Cordón, R. Montes, B. Fernández-Pastor, M. Merlos, J.M. Baeyens, J.M. Entrena, E.J. Cobos, Modulation of peripheral μ -opioid analgesia by σ_1 receptors, *The Journal of pharmacology and experimental therapeutics*, 348 (2014) 32-45.
- [44] C.C. Chien, G.W. Pasternak, (-)-Pentazocine analgesia in mice: interactions with a sigma receptor system, *European journal of pharmacology*, 294 (1995) 303-308.
- [45] O. Prezzavento, C. Parenti, A. Marrazzo, S. Ronsisvalle, F. Vittorio, G. Aricò, G.M. Scoto, G. Ronsisvalle, A new sigma ligand, (+/-)-PPCC, antagonizes kappa opioid receptor-mediated antinociceptive effect, *Life sciences*, 82 (2008) 549-553.
- [46] C.M. Cendán, J.M. Pujalte, E. Portillo-Salido, L. Montoliu, J.M. Baeyens, Formalin-induced pain is reduced in sigma(1) receptor knockout mice, *European journal of pharmacology*, 511 (2005) 73-74.
- [47] J.M. Entrena, E.J. Cobos, F.R. Nieto, C.M. Cendán, G. Gris, E. Del Pozo, D. Zamanillo, J.M. Baeyens, Sigma-1 receptors are essential for capsaicin-induced mechanical hypersensitivity: studies with selective sigma-1 ligands and sigma-1 knockout mice, *Pain*, 143 (2009) 252-261.
- [48] B. de la Puente, X. Nadal, E. Portillo-Salido, R. Sánchez-Arroyos, S. Ovalle, G. Palacios, A. Muro, L. Romero, J.M. Entrena, J.M. Baeyens, J.A. López-García, R. Maldonado, D. Zamanillo, J.M. Vela, Sigma-1 receptors regulate activity-induced spinal sensitization and neuropathic pain after peripheral nerve injury, *Pain*, 145 (2009) 294-303.
- [49] M. Happy, J. Dejoie, C.K. Zajac, B. Cortez, K. Chakraborty, J. Aderemi, M. Sauane, Sigma 1 Receptor antagonist potentiates the anti-cancer effect of p53 by regulating ER stress, ROS production, Bax levels, and caspase-3 activation, *Biochemical and biophysical research communications*, 456 (2015) 683-688.

- [50] B.A. Spruce, L.A. Campbell, N. McTavish, M.A. Cooper, M.V. Appleyard, M. O'Neill, J. Howie, J. Samson, S. Watt, K. Murray, D. McLean, N.R. Leslie, S.T. Safrany, M.J. Ferguson, J.A. Peters, A.R. Prescott, G. Box, A. Hayes, B. Nutley, F. Raynaud, C.P. Downes, J.J. Lambert, A.M. Thompson, S. Eccles, Small molecule antagonists of the sigma-1 receptor cause selective release of the death program in tumor and self-reliant cells and inhibit tumor growth in vitro and in vivo, *Cancer research*, 64 (2004) 4875-4886.
- [51] D. Crottès, H. Guizouarn, P. Martin, F. Borgese, O. Soriani, The sigma-1 receptor: a regulator of cancer cell electrical plasticity?, *Frontiers in physiology*, 4 (2013) 175.
- [52] D. Crottès, R. Rapetti-Mauss, F. Alcaraz-Perez, M. Tichet, G. Gariano, S. Martial, H. Guizouarn, B. Pellissier, A. Loubat, A. Popa, A. Paquet, M. Presta, S. Tartare-Deckert, M.L. Cayuela, P. Martin, F. Borgese, O. Soriani, SIGMAR1 Regulates Membrane Electrical Activity in Response to Extracellular Matrix Stimulation to Drive Cancer Cell Invasiveness, *Cancer research*, 76 (2016) 607-618.
- [53] K.W. Crawford, W.D. Bowen, Sigma-2 receptor agonists activate a novel apoptotic pathway and potentiate antineoplastic drugs in breast tumor cell lines, *Cancer research*, 62 (2002) 313-322.
- [54] C. Zeng, E.S. McDonald, R.H. Mach, Molecular Probes for Imaging the Sigma-2 Receptor: In Vitro and In Vivo Imaging Studies, *Handbook of experimental pharmacology*, 244 (2017) 309-330.
- [55] 18F ISO-1 PET/CT in Breast Cancer, in: *breast cancer*.
<https://clinicaltrials.gov/ct2/show/NCT02284919>. Oct 13, 2020
- [56] M. Grundman, R. Morgan, J.D. Lickliter, L.S. Schneider, S. DeKosky, N.J. Izzo, R. Guttendorf, M. Higgin, J. Pribyl, K. Mozzoni, H. Safferstein, S.M. Catalano, A phase 1 clinical trial of the sigma-2 receptor complex allosteric antagonist CT1812, a novel therapeutic candidate for Alzheimer's disease, *Alzheimer's & dementia (New York, N. Y.)*, 5 (2019) 20-26.
- [57] Clinical Trial of CT1812 in Mild to Moderate Alzheimer's Disease.
<https://ClinicalTrials.gov/show/NCT02907567>. Oct 13, 2020
- [58] M. Davidson, J. Saoud, C. Staner, N. Noel, E. Luthringer, S. Werner, J. Reilly, J.Y. Schaffhauser, J. Rabinowitz, M. Weiser, R. Luthringer, Efficacy and Safety of MIN-101: A 12-Week Randomized, Double-Blind, Placebo-Controlled Trial of a New Drug in Development for the Treatment of Negative Symptoms in Schizophrenia, *The American journal of psychiatry*, 174 (2017) 1195-1202.
- [59] Study to Evaluate Efficacy and Safety of Roluperidone (MIN-101) in Adult Patients With Negative Symptoms of Schizophrenia. <https://ClinicalTrials.gov/show/NCT03397134>. Oct 13, 2020
- [60] C.F. Chang, A.R. Diers, N. Hogg, Cancer cell metabolism and the modulating effects of nitric oxide, *Free radical biology & medicine*, 79 (2015) 324-336.
- [61] T.M. Cunha, D. Dal-Secco, W.A. Verri, Jr., A.T. Guerrero, G.R. Souza, S.M. Vieira, C.M. Lotufo, A.F. Neto, S.H. Ferreira, F.Q. Cunha, Dual role of hydrogen sulfide in mechanical inflammatory hypernociception, *European journal of pharmacology*, 590 (2008) 127-135.
- [62] S.K. Choudhari, M. Chaudhary, S. Bagde, A.R. Gadbail, V. Joshi, Nitric oxide and cancer: a review, *World journal of surgical oncology*, 11 (2013) 118.
- [63] S. Taysi, C. Uslu, F. Akcay, M.Y. Sutbeyaz, Malondialdehyde and nitric oxide levels in the plasma of patients with advanced laryngeal cancer, *Surgery today*, 33 (2003) 651-654.
- [64] H. Cheng, L. Wang, M. Mollica, A.T. Re, S. Wu, L. Zuo, Nitric oxide in cancer metastasis, *Cancer letters*, 353 (2014) 1-7.
- [65] D. Belgorosky, J. Girouard, Y.V. Langle, J. Hamelin-Morrisette, L. Marino, E.I. Agüero, H. Malagrino, C. Reyes-Moreno, A.M. Eiján, Relevance of iNOS expression in tumor growth and maintenance of cancer stem cells in a bladder cancer model, *Journal of molecular medicine (Berlin, Germany)*, 98 (2020) 1615-1627.
- [66] G.A. Blaise, D. Gauvin, M. Gangal, S. Authier, Nitric oxide, cell signaling and cell death, *Toxicology*, 208 (2005) 177-192.
- [67] M. Lechner, P. Lirk, J. Rieder, Inducible nitric oxide synthase (iNOS) in tumor biology: the two sides of the same coin, *Seminars in cancer biology*, 15 (2005) 277-289.

- [68] P. Pacher, J.S. Beckman, L. Liaudet, Nitric oxide and peroxynitrite in health and disease, *Physiological reviews*, 87 (2007) 315-424.
- [69] A. Ortega Mateo, A. Amaya Aleixandre de, Nitric oxide reactivity and mechanisms involved in its biological effects, *Pharmacological research*, 42 (2000) 421-427.
- [70] D.T. Hess, J.S. Stamler, Regulation by S-nitrosylation of protein post-translational modification, *The Journal of biological chemistry*, 287 (2012) 4411-4418.
- [71] E.A. Grimm, A.G. Sikora, S. Ekmekcioglu, Molecular pathways: inflammation-associated nitric-oxide production as a cancer-supporting redox mechanism and a potential therapeutic target, *Clinical cancer research : an official journal of the American Association for Cancer Research*, 19 (2013) 5557-5563.
- [72] L. Tong, C.C. Chuang, S. Wu, L. Zuo, Reactive oxygen species in redox cancer therapy, *Cancer letters*, 367 (2015) 18-25.
- [73] M. Donia, D. Maksimovic-Ivanic, S. Mijatovic, M. Mojic, D. Miljkovic, G. Timotijevic, P. Fagone, S. Caponnetto, Y. Al-Abed, J. McCubrey, S. Stosic-Grujicic, F. Nicoletti, In vitro and in vivo anticancer action of Saquinavir-NO, a novel nitric oxide-derivative of the protease inhibitor saquinavir, on hormone resistant prostate cancer cells, *Cell cycle (Georgetown, Tex.)*, 10 (2011) 492-499.
- [74] M. Mojic, S. Mijatovic, D. Maksimovic-Ivanic, D. Miljkovic, S. Stosic-Grujicic, M. Stankovic, K. Mangano, S. Travali, M. Donia, P. Fagone, M.B. Zocca, Y. Al-Abed, J.A. McCubrey, F. Nicoletti, Therapeutic potential of nitric oxide-modified drugs in colon cancer cells, *Molecular pharmacology*, 82 (2012) 700-710.
- [75] M.A. Rahat, B. Hemmerlein, Macrophage-tumor cell interactions regulate the function of nitric oxide, *Frontiers in physiology*, 4 (2013) 144.
- [76] S. Huerta, S. Chilka, B. Bonavida, Nitric oxide donors: novel cancer therapeutics (review), *International journal of oncology*, 33 (2008) 909-927.
- [77] H. Yasuda, Solid tumor physiology and hypoxia-induced chemo/radio-resistance: novel strategy for cancer therapy: nitric oxide donor as a therapeutic enhancer, *Nitric oxide : biology and chemistry*, 19 (2008) 205-216.
- [78] J.F. Jeannin, L. Leon, M. Cortier, N. Sassi, C. Paul, A. Bettaieb, Nitric oxide-induced resistance or sensitization to death in tumor cells, *Nitric oxide : biology and chemistry*, 19 (2008) 158-163.
- [79] E. Amata, M. Dichiara, E. Arena, V. Pittalà, V. Pistarà, V. Cardile, A.C.E. Graziano, A. Fraix, A. Marrazzo, S. Sortino, O. Prezzavento, Novel Sigma Receptor Ligand-Nitric Oxide Photodons: Molecular Hybrids for Double-Targeted Antiproliferative Effect, *Journal of medicinal chemistry*, 60 (2017) 9531-9544.
- [80] P.G. Wang, M. Xian, X. Tang, X. Wu, Z. Wen, T. Cai, A.J. Janczuk, Nitric oxide donors: chemical activities and biological applications, *Chemical reviews*, 102 (2002) 1091-1134.
- [81] P. Fagone, E. Mazzon, P. Bramanti, K. Bendtzen, F. Nicoletti, Gasotransmitters and the immune system: Mode of action and novel therapeutic targets, *European journal of pharmacology*, 834 (2018) 92-102.
- [82] T.R. Hundley, B. Rigas, Nitric oxide-donating aspirin inhibits colon cancer cell growth via mitogen-activated protein kinase activation, *The Journal of pharmacology and experimental therapeutics*, 316 (2006) 25-34.
- [83] J.L. Williams, K. Kashfi, N. Ouyang, P. del Soldato, L. Kopelovich, B. Rigas, NO-donating aspirin inhibits intestinal carcinogenesis in Min (APC(Min/+)) mice, *Biochemical and biophysical research communications*, 313 (2004) 784-788.
- [84] J.S. Royle, J.A. Ross, I. Ansell, P. Bollina, D.N. Tulloch, F.K. Habib, Nitric oxide donating nonsteroidal anti-inflammatory drugs induce apoptosis in human prostate cancer cell systems and human prostatic stroma via caspase-3, *The Journal of urology*, 172 (2004) 338-344.
- [85] A Multiple Dose Study to Evaluate the Safety, Tolerability, Pharmacokinetics and Pharmacodynamics of MK-8150 (MK-8150-002). <https://ClinicalTrials.gov/show/NCT01656408>. Oct 13, 2020

- [86] A Phase II Trial of Calcitriol and Naproxen in Patients With Recurrent Prostate Cancer. <https://ClinicalTrials.gov/show/NCT00383487>. Oct 13, 2020
- [87] Analgesic Efficacy and Safety Study of Naproxinod in Subjects With Osteoarthritis of the Knee. <https://ClinicalTrials.gov/show/NCT00542555>. Oct 13, 2020
- [88] A Phase 1 Study to Compare the PK and Safety of Naproxinod in Hepatic Impaired Patients and Matching Healthy Subjects. <https://ClinicalTrials.gov/show/NCT00621881>. Oct 13, 2020
- [89] A Pharmacokinetics and Safety Study of Naproxinod in Subjects With Impaired Renal Function. <https://ClinicalTrials.gov/show/NCT00674856>. Oct 13, 2020
- [90] RRx-001 in Second Line Treatment of Advanced Cholangiocarcinoma Prior to Readministration of First-Line Therapy. <https://ClinicalTrials.gov/show/NCT02452970>. Oct 13, 2020
- [91] E. Gerasimova, J. Lebedeva, A. Yakovlev, A. Zefirov, R. Giniatullin, G. Sitdikova, Mechanisms of hydrogen sulfide (H₂S) action on synaptic transmission at the mouse neuromuscular junction, *Neuroscience*, 303 (2015) 577-585.
- [92] W. Rong, H. Kimura, D. Grundy, The neurophysiology of hydrogen sulfide, *Inflammation & allergy drug targets*, 10 (2011) 109-117.
- [93] C.R. Powell, K.M. Dillon, J.B. Matson, A review of hydrogen sulfide (H₂S) donors: Chemistry and potential therapeutic applications, *Biochemical pharmacology*, 149 (2018) 110-123.
- [94] S. Panthi, H.J. Chung, J. Jung, N.Y. Jeong, Physiological Importance of Hydrogen Sulfide: Emerging Potent Neuroprotector and Neuromodulator, *Oxidative medicine and cellular longevity*, 2016 (2016) 9049782.
- [95] I.S.F. Melo, F.F. Rodrigues, S. Costa, A.V. Braga, M. Morais, J.A. Vaz, L.S. Neto, I. Galvão, L.V. Modolo, F.A. Amaral, R.B. Oliveira, Â. de Fátima, M.M. Coelho, R.R. Machado, 4-Methylbenzenecarbothioamide, a hydrogen sulfide donor, inhibits tumor necrosis factor- α and CXCL1 production and exhibits activity in models of pain and inflammation, *European journal of pharmacology*, 856 (2019) 172404.
- [96] E. Lucarini, L. Micheli, A. Martelli, L. Testai, V. Calderone, C. Ghelardini, L. Di Cesare Mannelli, Efficacy of isothiocyanate-based compounds on different forms of persistent pain, *Journal of pain research*, 11 (2018) 2905-2913.
- [97] A.T. Lee, J.J. Shah, L. Li, Y. Cheng, P.K. Moore, S. Khanna, A nociceptive-intensity-dependent role for hydrogen sulphide in the formalin model of persistent inflammatory pain, *Neuroscience*, 152 (2008) 89-96.
- [98] Y. Maeda, Y. Aoki, F. Sekiguchi, M. Matsunami, T. Takahashi, H. Nishikawa, A. Kawabata, Hyperalgesia induced by spinal and peripheral hydrogen sulfide: evidence for involvement of Cav3.2 T-type calcium channels, *Pain*, 142 (2009) 127-132.
- [99] E. Lucarini, L. Micheli, E. Trallori, V. Citi, A. Martelli, L. Testai, G.R. De Nicola, R. Iori, V. Calderone, C. Ghelardini, L. Di Cesare Mannelli, Effect of glucoraphanin and sulforaphane against chemotherapy-induced neuropathic pain: Kv7 potassium channels modulation by H₂S release in vivo, *Phytotherapy research : PTR*, 32 (2018) 2226-2234.
- [100] K. Kida, E. Marutani, R.K. Nguyen, F. Ichinose, Inhaled hydrogen sulfide prevents neuropathic pain after peripheral nerve injury in mice, *Nitric oxide : biology and chemistry*, 46 (2015) 87-92.
- [101] M.D. Brown, J.R. Hall, M.H. Schoenfisch, A direct and selective electrochemical hydrogen sulfide sensor, *Analytica chimica acta*, 1045 (2019) 67-76.
- [102] L. Li, M. Whiteman, Y.Y. Guan, K.L. Neo, Y. Cheng, S.W. Lee, Y. Zhao, R. Baskar, C.H. Tan, P.K. Moore, Characterization of a novel, water-soluble hydrogen sulfide-releasing molecule (GYY4137): new insights into the biology of hydrogen sulfide, *Circulation*, 117 (2008) 2351-2360.
- [103] M.D. Hammers, L. Singh, L.A. Montoya, A.D. Moghaddam, M.D. Pluth, Synthesis of Amino-ADT Provides Access to Hydrolytically Stable Amide-Coupled Hydrogen Sulfide Releasing Drug Targets, *Synlett : accounts and rapid communications in synthetic organic chemistry*, 27 (2016) 1349-1353.
- [104] N. Cenac, M. Castro, C. Desormeaux, P. Colin, M. Sie, M. Ranger, N. Vergnolle, A novel orally administered trimebutine compound (GIC-1001) is anti-nociceptive and features peripheral

opioid agonistic activity and Hydrogen Sulphide-releasing capacity in mice, *European journal of pain* (London, England), 20 (2016) 723-730.

[105] A Phase 2a, Proof-of-Concept Study of GIC-1001 in the Management of Visceral Pain During Sedation-Free, Full Colonoscopy. <https://ClinicalTrials.gov/show/NCT01926444>. Oct 13, 2020

[106] To Compare the Gastrointestinal Safety of a 14-Day Oral Dosing Regimen of ATB-346 to Sodium Naproxen in Healthy Subjects. <https://ClinicalTrials.gov/show/NCT03291418>. Oct 13, 2020

[107] Assessing the Safety and Bioactivity of SG1002 in Heart Failure Patients. <https://ClinicalTrials.gov/show/NCT02278276>. Oct 13, 2020

[108] L. Di, H. Rong, B. Feng, Demystifying brain penetration in central nervous system drug discovery. *Miniperspective, Journal of medicinal chemistry*, 56 (2013) 2-12.

[109] S.A. Hitchcock, L.D. Pennington, Structure-brain exposure relationships, *Journal of medicinal chemistry*, 49 (2006) 7559-7583.

[110] H. Kushihara, Y. Sugiyama, Active efflux across the blood-brain barrier: role of the solute carrier family, *NeuroRx : the journal of the American Society for Experimental NeuroTherapeutics*, 2 (2005) 73-85.

[111] S.A. Hitchcock, Structural modifications that alter the P-glycoprotein efflux properties of compounds, *Journal of medicinal chemistry*, 55 (2012) 4877-4895.

[112] Pharmacokinetics of CNS Penetration, in: *Blood-Brain Barrier in Drug Discovery*, 2015, pp. 5-41.

[113] O. Rabal, J.A. Sánchez-Arias, M. Cuadrado-Tejedor, I. de Miguel, M. Pérez-González, C. García-Barroso, A. Ugarte, A. Estella-Hermoso de Mendoza, E. Sáez, M. Espelosin, S. Ursua, T. Haizhong, W. Wei, X. Musheng, A. Garcia-Osta, J. Oyarzabal, Design, Synthesis, and Biological Evaluation of First-in-Class Dual Acting Histone Deacetylases (HDACs) and Phosphodiesterase 5 (PDE5) Inhibitors for the Treatment of Alzheimer's Disease, *Journal of medicinal chemistry*, 59 (2016) 8967-9004.

[114] J. Fiorito, J. Vendome, F. Saeed, A. Staniszewski, H. Zhang, S. Yan, S.X. Deng, O. Arancio, D.W. Landry, Identification of a Novel 1,2,3,4-Tetrahydrobenzo[b][1,6]naphthyridine Analogue as a Potent Phosphodiesterase 5 Inhibitor with Improved Aqueous Solubility for the Treatment of Alzheimer's Disease, *Journal of medicinal chemistry*, 60 (2017) 8858-8875.

[115] M.C. Frantz, L.P. Pellissier, E. Pflimlin, S. Loison, J. Gandía, C. Marsol, T. Durroux, B. Mouillac, J.A.J. Becker, J. Le Merrer, C. Valencia, P. Villa, D. Bonnet, M. Hibert, LIT-001, the First Nonpeptide Oxytocin Receptor Agonist that Improves Social Interaction in a Mouse Model of Autism, *Journal of medicinal chemistry*, 61 (2018) 8670-8692.

[116] J.A. Sánchez-Arias, O. Rabal, M. Cuadrado-Tejedor, I. de Miguel, M. Pérez-González, A. Ugarte, E. Sáez, M. Espelosin, S. Ursua, T. Haizhong, W. Wei, X. Musheng, A. Garcia-Osta, J. Oyarzabal, Impact of Scaffold Exploration on Novel Dual-Acting Histone Deacetylases and Phosphodiesterase 5 Inhibitors for the Treatment of Alzheimer's Disease, *ACS chemical neuroscience*, 8 (2017) 638-661.

[117] J. Han, H.J. Lee, K.Y. Kim, S.J.C. Lee, J.M. Suh, J. Cho, J. Chae, M.H. Lim, Tuning Structures and Properties for Developing Novel Chemical Tools toward Distinct Pathogenic Elements in Alzheimer's Disease, *ACS chemical neuroscience*, 9 (2018) 800-808.

[118] O. Rabal, J.A. Sánchez-Arias, M. Cuadrado-Tejedor, I. de Miguel, M. Pérez-González, C. García-Barroso, A. Ugarte, A. Estella-Hermoso de Mendoza, E. Sáez, M. Espelosin, S. Ursua, T. Haizhong, W. Wei, X. Musheng, A. Garcia-Osta, J. Oyarzabal, Discovery of in Vivo Chemical Probes for Treating Alzheimer's Disease: Dual Phosphodiesterase 5 (PDE5) and Class I Histone Deacetylase Selective Inhibitors, *ACS chemical neuroscience*, 10 (2019) 1765-1782.

[119] C.W. Reed, S.E. Yohn, J.P. Washecheck, H.F. Roenfanz, M.C. QUITALIG, V.B. Luscombe, M.T. Jenkins, A.L. Rodriguez, D.W. Engers, A.L. Blobaum, P.J. Conn, C.M. Niswender, C.W. Lindsley, Discovery of an Orally Bioavailable and Central Nervous System (CNS) Penetrant mGlu(7) Negative Allosteric Modulator (NAM) in Vivo Tool Compound: N-(2-(1 H-1,2,4-triazol-1-yl)-5-

- (trifluoromethoxy)phenyl)-4-(cyclopropylmethoxy)-3-methoxybenzamide (VU6012962), *Journal of medicinal chemistry*, 62 (2019) 1690-1695.
- [120] A.H. Soloway, Correlation of drug penetration of brain and chemical structure, *Science (New York, N.Y.)*, 128 (1958) 1572-1574.
- [121] C. Hansch, S.M. Anderson, The structure-activity relationship in barbiturates and its similarity to that in other narcotics, *Journal of medicinal chemistry*, 10 (1967) 745-753.
- [122] C.A. Lipinski, F. Lombardo, B.W. Dominy, P.J. Feeney, Experimental and computational approaches to estimate solubility and permeability in drug discovery and development settings, *Advanced drug delivery reviews*, 46 (2001) 3-26.
- [123] C. Lipinski, A. Hopkins, Navigating chemical space for biology and medicine, *Nature*, 432 (2004) 855-861.
- [124] M.P. Gleeson, Generation of a set of simple, interpretable ADMET rules of thumb, *Journal of medicinal chemistry*, 51 (2008) 817-834.
- [125] T.T. Wager, X. Hou, P.R. Verhoest, A. Villalobos, Central Nervous System Multiparameter Optimization Desirability: Application in Drug Discovery, *ACS chemical neuroscience*, 7 (2016) 767-775.

Small molecule ligands against human Tyrosinases

2. Introduction

The selective delivery of systemically administered chemotherapeutic drugs to neoplastic lesions remains one of the major challenges of chemotherapy [1, 2]. This issue often results in the onset of toxicity, thus preventing dose escalation to therapeutic regimens. Indeed, many anticancer drugs inhibit cells in rapid proliferation affecting also normal tissues which constantly regenerate, such as epithelial structures in the gastrointestinal tract and in the skin, hair growth, and hematopoiesis. Moreover, low molecular weight toxic drugs do not preferentially accumulate in solid tumors. An example is doxorubicin which reaches the neoplastic mass for only 5–10% of the dose which accumulates in healthy organs [3]. In an attempt to improve the pharmacokinetic properties of chemotherapeutic drugs, monoclonal antibodies and small ligands have been proposed as selective delivery vehicles at the site of disease, sparing normal organs [4].

Generally, the development of antibody-drug conjugates (ADCs, Figure 10) for cancer therapy is based on antibodies directed against an antigen on the surface of the tumor cell [5]. As a result, the antigen rapidly internalizes acting as a ‘Trojan horse’ for the delivery of a cytotoxic payload into the cell. Recently, potent activity in preclinical cancer models has been reported also for non internalizing ADCs directed against a number of targets [6]. Nine products have been approved for clinical applications and various ADCs are currently being tested in clinical trials [7]. However, one of the major limits of ADCs is the high cost and the long circulatory half-life that may cause premature drug release.

As an alternative to antibodies, small molecule-drug conjugates (SMDCs, Figure 10) have been proposed for the delivery of cytotoxics to tumors. Unlike antibodies, small organic molecules can get out of blood vessels in few seconds and in the absence of a suitable binding event, rapidly diffuse back into blood being excreted.

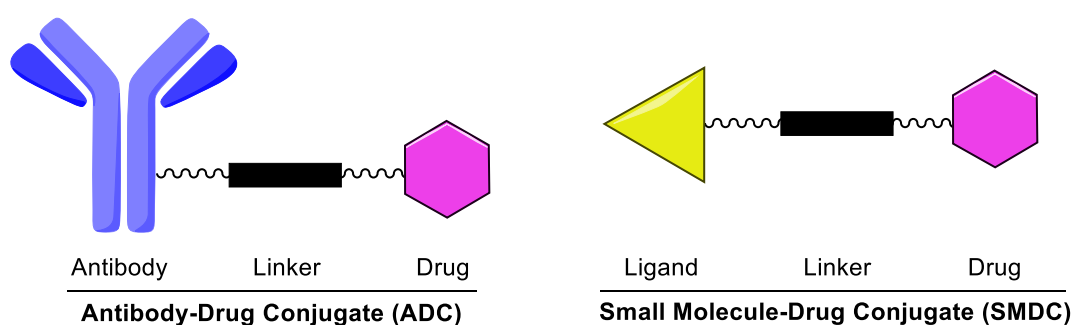


Figure 10. Schematic representation of the basic elements in ADC and SMDC.

The development of SMDCs has been limited by the availability of small organic ligands specific to tumor antigens. Suitable ligands have included folate derivatives, synthetic ligands to prostate-specific membrane antigen (PSMA) and binders to carbonic anhydrase IX (CAIX) [8-10]. However, SMDCs have been reported to accumulate more efficiently and more homogeneously in tumors compared to ADCs which are typically confined to the perivascular space [11, 12]. Small ligands are often efficiently filtered via the renal route and may display an undesired uptake in the kidney interstitium. ADCs and SMDCs exhibited a comparable therapeutic activity in mouse models of cancer, even if the SMDC biodistribution was clearly superior [11].

2.1. DNA-Encoded Chemical Libraries

DNA-encoded chemical libraries (DECLs) are collections of organic compounds individually coupled to DNA fragments, serving as unambiguous and amplifiable identification barcode [13]. The first example of DECL technology was proposed by Lerner and Brenner in 1992 to allow the construction of peptide libraries on beads containing oligonucleotide tags [14]. Over the years, the technology has been implemented without the need for beads, allowing the building of larger libraries as well as more efficient screening approaches [15, 16]. The application of this technology facilitated the identification process of small organic ligands useful for therapeutic purposes. As all compounds in the library are identified by their DNA tags, it can be mixed and used in affinity-capture experiments on target proteins of interest. Generally, the target protein is immobilized on magnetic beads and subsequently incubated with the library (Figure 11).

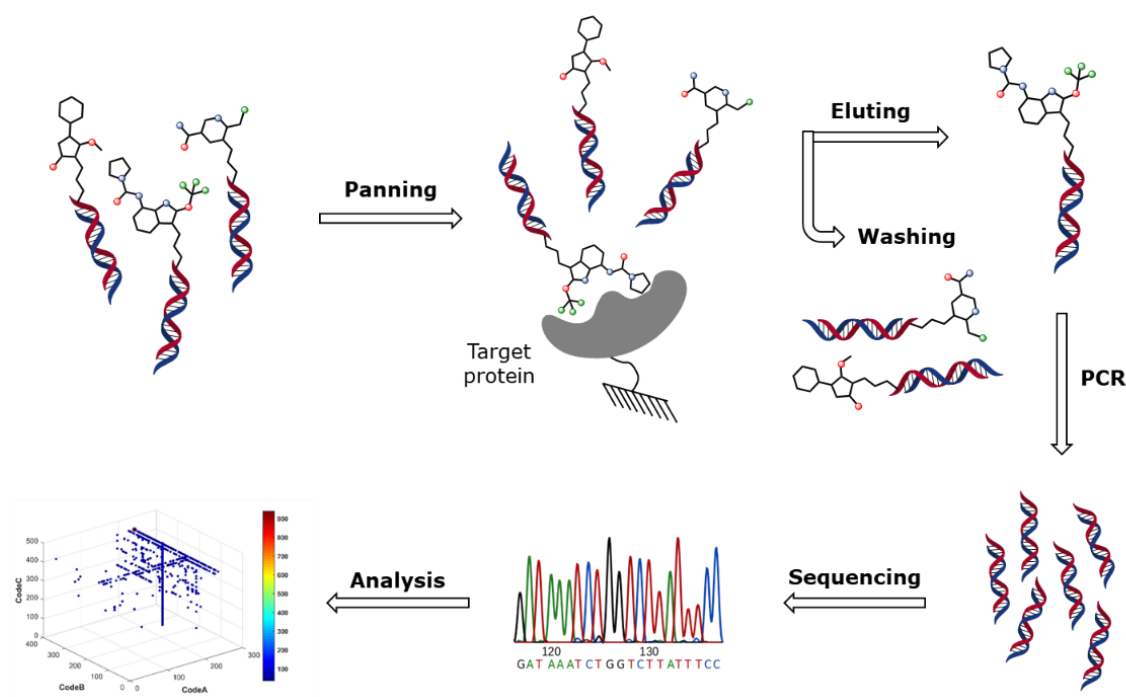


Figure 11. Screening workflow for small organic ligands using DECL.

Thus, selective binders are captured, whereas non-binding library members are removed by different washing steps. The identity and the relative quantity of individual ligands can be determined by amplification of the DNA tag in a two-steps PCR procedure, followed by decoding with high-throughput DNA sequencing (HTDS) [17]. Once the analysis of the selection results has been performed, the confirmation of hit compounds proceeds through the resynthesis of the most enriched compounds off-DNA followed by the characterization of their binding properties. Usually, it is convenient to resynthesize hit compounds with a fluorophore moiety at the position originally occupied by the DNA tag, to perform fluorescence polarization measurements in solution [18, 19].

2.2. Human Tyrosinase and Tyrosinase-related Proteins

Tyrosinases are proteins with two metal ions at the active site, abundantly expressed in melanosomes where the synthesis of melanin takes place. In mammals, tyrosinases are involved in coloring eyes, skin, and hair for protection against UV radiation and oxygen radicals. Three tyrosinase like-enzymes are involved in the biosynthesis of melanin, and specifically tyrosinase (TYR) and tyrosinase-related proteins 1 and 2 (TYRP1 and TYRP2).

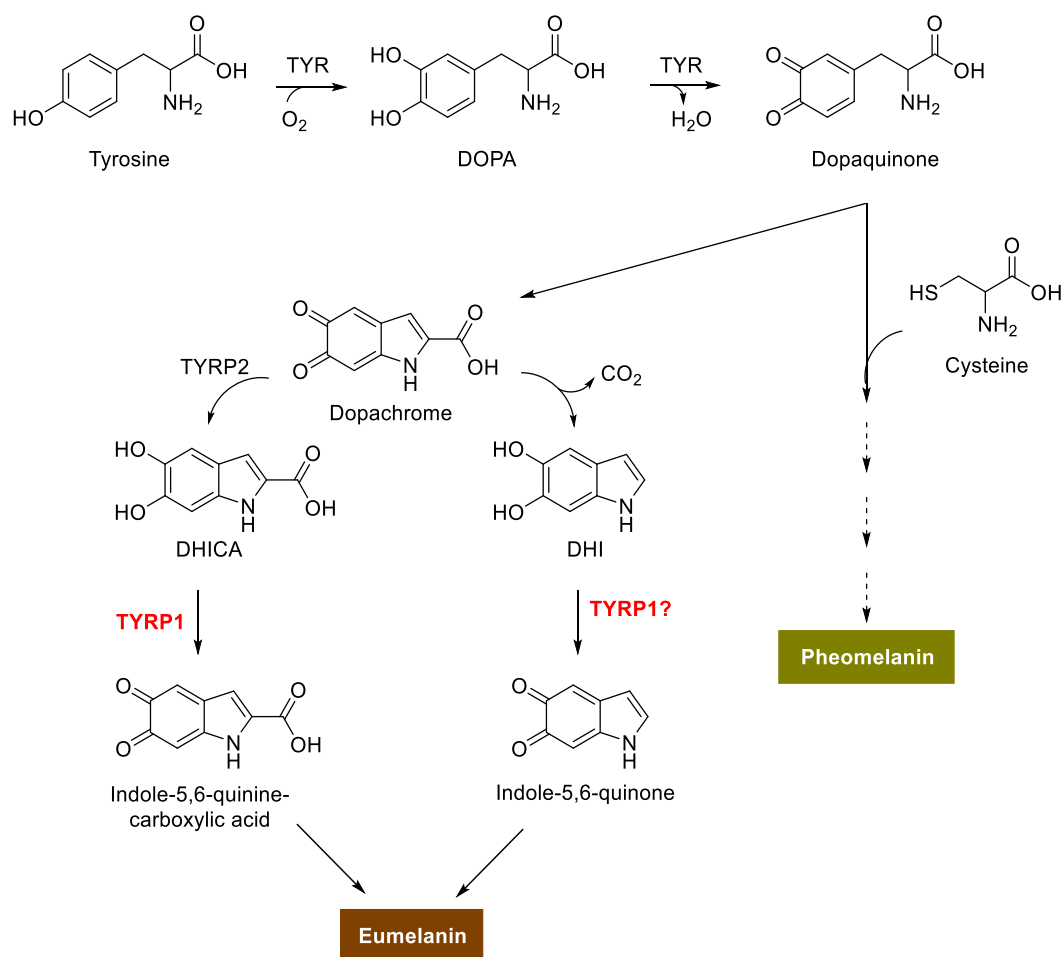


Figure 12. Melanin biosynthesis pathways.

TYR catalyzes the conversion of tyrosine into the *o*-diphenol DOPA, followed by oxidation into the corresponding *o*-quinone dopaquinone (Figure 12). TYRP2 is a tautomerase converting dopachrome into DHICA, whereas TYRP1 catalyzes the oxidation of DHICA in mice [20]. However, the process in which hTYRP1 is involved it is not clear, since for the oxidation of DHICA the hTYR seems to be sufficient. Genetic mutations of TYR and TYRP1 have been related to oculocutaneous albinism, an autosomal recessive disorder characterized by reduced production of melanin in skin, hair, and eyes. Variations of TYR and TYRP1 are associated with risk of melanoma, a malignant and aggressive tumor of the skin [21].

TYR and TYRPs are characterized by an intra-melanosomal domain containing a cysteine-rich subdomain and a catalytic tyrosinase-like subdomain with two metal ion binding sites. Whereas all TYRs bind two copper ions at the active site, human TYRPs have been shown to have two zinc ions. Despite the different metal ions, the human version of TYR, TYRP1, and TYRP2 share the same active site. Recently, the crystal structure of the human TYRP1 has been elucidated by X-ray crystallography revealing an accessible binding pocket that can be exploited for the de novo discovery of a target ligand [22]. The protein has been crystallized in complex with known TYR substrates, revealing that the ortho-hydroxyl ketone is important for the binding (Figure 13). However, no ligands have been reported so far to bind TYRP1.

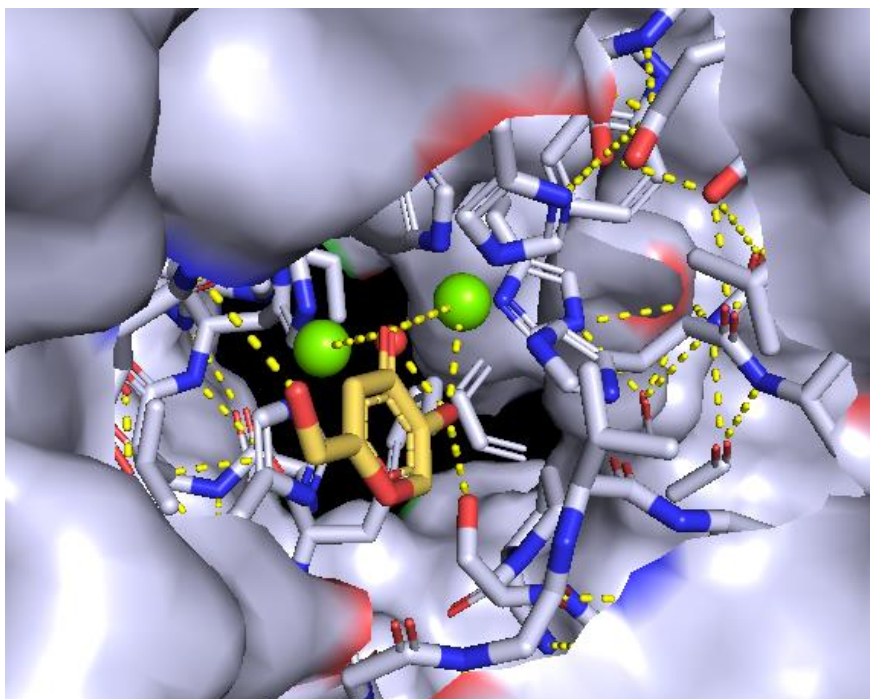


Figure 13. TYRP1 crystallized in complex with the TYR inhibitor kojic acid.

As regard TYR, its crystal structure has not been solved. Most inhibitors developed in the last decades have been developed on the base of mushroom TYR, and by computational docking using

bacterial and mushroom TYR crystal structures [20]. Thus, the lack of available crystal structures has hindered the development of drug discovery process. Recently, a radiolabeled derivative of an antibody binding to melanin has been proposed for melanoma treatment, however anti-melanoma ADC products have not yet been developed [23]. In light of these considerations, the development of high affinity small molecules for the human TYR and TYRP-1 represents a challenge for the targeted treatment of melanoma. Moreover, SMDCs against hTYR and/or hTYRP1 may be particularly suitable as the cognate antigens exhibit an extremely restricted pattern of expression in normal tissues, mainly confined to few melanocyte cells in the skin.

REFERENCES

- [1] A.A. van der Veldt, N.H. Hendrikse, E.F. Smit, M.P. Mooijer, A.Y. Rijnders, W.R. Gerritsen, J.J. van der Hoeven, A.D. Windhorst, A.A. Lammertsma, M. Lubberink, Biodistribution and radiation dosimetry of ^{11}C -labelled docetaxel in cancer patients, *European journal of nuclear medicine and molecular imaging*, 37 (2010) 1950-1958.
- [2] A.A. van der Veldt, M. Lubberink, R.H. Mathijssen, W.J. Loos, G.J. Herder, H.N. Greuter, E.F. Comans, H.B. Rutten, J. Eriksson, A.D. Windhorst, N.H. Hendrikse, P.E. Postmus, E.F. Smit, A.A. Lammertsma, Toward prediction of efficacy of chemotherapy: a proof of concept study in lung cancer patients using [^{11}C]docetaxel and positron emission tomography, *Clinical cancer research : an official journal of the American Association for Cancer Research*, 19 (2013) 4163-4173.
- [3] K. Bosslet, R. Straub, M. Blumrich, J. Czech, M. Gerken, B. Sperker, H.K. Kroemer, J.P. Gesson, M. Koch, C. Monneret, Elucidation of the mechanism enabling tumor selective prodrug monotherapy, *Cancer research*, 58 (1998) 1195-1201.
- [4] S. Cazzamalli, A.D. Corso, D. Neri, Targeted Delivery of Cytotoxic Drugs: Challenges, Opportunities and New Developments, *Chimia*, 71 (2017) 712-715.
- [5] A. Beck, L. Goetsch, C. Dumontet, N. Corvaia, Strategies and challenges for the next generation of antibody-drug conjugates, *Nature reviews. Drug discovery*, 16 (2017) 315-337.
- [6] R. Gébleux, M. Stringhini, R. Casanova, A. Soltermann, D. Neri, Non-internalizing antibody-drug conjugates display potent anti-cancer activity upon proteolytic release of monomethyl auristatin E in the subendothelial extracellular matrix, *International journal of cancer*, 140 (2017) 1670-1679.
- [7] P. Zhao, Y. Zhang, W. Li, C. Jeanty, G. Xiang, Y. Dong, Recent advances of antibody drug conjugates for clinical applications, *Acta pharmaceutica Sinica. B*, 10 (2020) 1589-1600.
- [8] G.M. van Dam, G. Themelis, L.M. Crane, N.J. Harlaar, R.G. Pleijhuis, W. Kelder, A. Sarantopoulos, J.S. de Jong, H.J. Arts, A.G. van der Zee, J. Bart, P.S. Low, V. Ntziachristos, Intraoperative tumor-specific fluorescence imaging in ovarian cancer by folate receptor- α targeting: first in-human results, *Nature medicine*, 17 (2011) 1315-1319.
- [9] J.A. Barrett, R.E. Coleman, S.J. Goldsmith, S. Vallabhajosula, N.A. Petry, S. Cho, T. Armor, J.B. Stubbs, K.P. Maresca, M.G. Stabin, J.L. Joyal, W.C. Eckelman, J.W. Babich, First-in-man evaluation of 2 high-affinity PSMA-avid small molecules for imaging prostate cancer, *Journal of nuclear medicine : official publication, Society of Nuclear Medicine*, 54 (2013) 380-387.
- [10] M. Wichert, N. Krall, W. Decurtins, R.M. Franzini, F. Pretto, P. Schneider, D. Neri, J. Scheuermann, Dual-display of small molecules enables the discovery of ligand pairs and facilitates affinity maturation, *Nature chemistry*, 7 (2015) 241-249.
- [11] S. Cazzamalli, A. Dal Corso, F. Widmayer, D. Neri, Chemically Defined Antibody- and Small Molecule-Drug Conjugates for in Vivo Tumor Targeting Applications: A Comparative Analysis, *Journal of the American Chemical Society*, 140 (2018) 1617-1621.
- [12] M.S. Dennis, H. Jin, D. Dugger, R. Yang, L. McFarland, A. Ogasawara, S. Williams, M.J. Cole, S. Ross, R. Schwall, Imaging tumors with an albumin-binding Fab, a novel tumor-targeting agent, *Cancer research*, 67 (2007) 254-261.
- [13] R.M. Franzini, D. Neri, J. Scheuermann, DNA-encoded chemical libraries: advancing beyond conventional small-molecule libraries, *Accounts of chemical research*, 47 (2014) 1247-1255.
- [14] S. Brenner, R.A. Lerner, Encoded combinatorial chemistry, *Proceedings of the National Academy of Sciences of the United States of America*, 89 (1992) 5381-5383.
- [15] Z.J. Gartner, B.N. Tse, R. Grubina, J.B. Doyon, T.M. Snyder, D.R. Liu, DNA-templated organic synthesis and selection of a library of macrocycles, *Science (New York, N.Y.)*, 305 (2004) 1601-1605.
- [16] S. Melkko, J. Scheuermann, C.E. Dumelin, D. Neri, Encoded self-assembling chemical libraries, *Nature biotechnology*, 22 (2004) 568-574.

- [17] W. Decurtins, M. Wichert, R.M. Franzini, F. Buller, M.A. Stravs, Y. Zhang, D. Neri, J. Scheuermann, Automated screening for small organic ligands using DNA-encoded chemical libraries, *Nature protocols*, 11 (2016) 764-780.
- [18] D. Neri, R.A. Lerner, DNA-Encoded Chemical Libraries: A Selection System Based on Endowing Organic Compounds with Amplifiable Information, *Annual review of biochemistry*, 87 (2018) 479-502.
- [19] G. Zimmermann, Y. Li, U. Rieder, M. Mattarella, D. Neri, J. Scheuermann, Hit-Validation Methodologies for Ligands Isolated from DNA-Encoded Chemical Libraries, *Chembiochem : a European journal of chemical biology*, 18 (2017) 853-857.
- [20] X. Lai, H.J. Wichers, M. Soler-Lopez, B.W. Dijkstra, Structure and Function of Human Tyrosinase and Tyrosinase-Related Proteins, *Chemistry (Weinheim an der Bergstrasse, Germany)*, 24 (2018) 47-55.
- [21] E. Buitrago, R. Hardré, R. Haudecoeur, H. Jamet, C. Belle, A. Boumendjel, L. Bubacco, M. Réglie, Are Human Tyrosinase and Related Proteins Suitable Targets for Melanoma Therapy?, *Current topics in medicinal chemistry*, 16 (2016) 3033-3047.
- [22] X. Lai, H.J. Wichers, M. Soler-Lopez, B.W. Dijkstra, Structure of Human Tyrosinase Related Protein 1 Reveals a Binuclear Zinc Active Site Important for Melanogenesis, *Angewandte Chemie (International ed. in English)*, 56 (2017) 9812-9815.
- [23] J.D. Nosanchuk, A. Jeyakumar, A. Ray, E. Revskaya, Z. Jiang, R.A. Bryan, K.J.H. Allen, R. Jiao, M.E. Malo, B.L. Gómez, A. Morgenstern, F. Bruchertseifer, D. Rickles, G.B. Thornton, A. Bowen, A. Casadevall, E. Dadachova, Structure-function analysis and therapeutic efficacy of antibodies to fungal melanin for melanoma radioimmunotherapy, *Scientific reports*, 8 (2018) 5466.

3. Aim of the thesis

The general objective of this thesis was to develop small molecules that could be used to treat various forms of cancer or modulate nociceptive events.

More specifically, the main aims were:

I. Development and preclinical evaluation of selective σ R ligands endowed with specific functional profile and hybridized with H₂S- or NO-donors for the management of pain condition or for the treatment of cancer, respectively. The activity of different σ R ligands is combined with the peculiar ability to generate H₂S or NO, thus obtaining a synergistic effect.

II. Create a simple set of rules that could prospectively support the development and identification of CNS, non-CNS or mixed drugs. Considering also the interest in developing σ_1 R antagonists and their benefit in treating tumor conditions including CNS tumors or for ligands with central analgesic properties, the work allows to define a set of rules that would eventually be used to tune the properties for BBB permeation of in house synthesized ligands.

III. Development of novel classes of pure σ R ligands with high affinity and selectivity based on standard structure-affinity relationships (SAfiR).

IV. Find out hTYR and hTYRP1 ligands for the selective recognition of melanoma cells in order to specifically delivery cytotoxic compounds to the tumor site. This goal has been pursued either via screening of large libraries of ligands or improving already known binders reported in literature.

4. Results

1. *Sigma Receptor Ligands Carrying a Nitric Oxide Donor Nitrate Moiety: Synthesis, In Silico, and Biological Evaluation* (ACS Med. Chem. Lett. 2020, 11, 5, 889–894)

My contributions to this work were:

1. Designing synthetic and pharmacological experiments (with Emanuele Amata and Orazio Prezzavento)
2. Synthesis and purification of compounds
3. Performing radioligand binding experiments
4. Data processing (with Emanuele Amata)

2. *Synthesis and preclinical evaluation of novel H₂S-donor sigma receptor hybrids for the management of pain* (manuscript in preparation)

My contributions to this work were:

1. Designing synthetic and pharmacological experiments (with Emanuele Amata and Enrique J. Cobos)
2. Synthesis and purification of compounds
3. Performing radioligand binding experiments
4. Performing fluorescence release experiments
5. Data processing (with Emanuele Amata)

3. *Tuning Properties for Blood-Brain Barrier Permeation: A Statistics-Based Analysis* (ACS Chem. Neurosci. 2020, 11, 1, 34–44)

My contributions to this work were:

1. Data collection for experimental in vivo logBB dataset
2. Data processing and analysis (with Emanuele Amata)

4. *Design, synthesis and preclinical evaluation of novel sigma receptors ligands* (manuscripts in preparation)

My contributions to this work were:

1. Designing synthetic and pharmacological experiments (with Emanuele Amata)
2. Synthesis and purification of compounds
3. Performing radioligand binding experiments
4. Data processing (with Emanuele Amata)

5. *Discovery, affinity maturation and multimerization of small molecule ligands against human Tyrosinase and Tyrosinase-Related Protein 1* (RSC Med. Chem., 2021, Advance Article)

My contribution to this work was the synthesis and purification of off-DNA compounds.

Sigma Receptor Ligands Carrying a Nitric Oxide Donor Nitrate Moiety: Synthesis, In Silico, and Biological Evaluation

Emanuele Amata,^{*,||} Maria Dichiara,^{||} Davide Gentile, Agostino Marrazzo, Rita Turnaturi, Emanuela Arena, Alfonsina La Mantia, Barbara Rita Tomasello, Rosaria Acquaviva, Claudia Di Giacomo, Antonio Rescifina, and Orazio Prezzavento^{*}

Department of Drug Sciences, Università degli Studi di Catania, Viale Andrea Doria 6, 95125 Catania, Italy

ACS Medicinal Chemistry Letters

Received: December 29, 2019; Accepted: April 9, 2020

ABSTRACT: We report the development of molecular hybrids in which a nitrate group serving as nitric oxide (NO) donor is covalently joined to σ receptor ligands to give candidates for double-targeted cancer therapy. The compounds have been evaluated in radioligand binding assay at both σ receptors and selected compounds tested for NO release. Compounds **9**, **15**, **18**, **19**, and **21** were subjected to MTT test. Compound **15** produced a significant reduction of MCF-7 and Caco-2 cellular viability with comparable IC_{50} as doxorubicin, being also not toxic for fibroblast HFF-1 cells. Compound **15** has shown a σ_1 receptor antagonist/ σ_2 receptor agonist profile. Two derivatives of compound **15** lacking the nitrate group did not induce a reduction of MCF-7 cellular viability, suggesting a potential synergistic effect between the σ receptors and the NO-mediated events. Overall, the combination of NO donor and σ receptors ligands provided compounds with beneficial effects for the treatment of cancer.

KEYWORDS: *Sigma receptors, nitric oxide, nitric oxide donors, cancer, bifunctional ligands*

Author Contributions

^{||}E.A. and M.D. contributed equally.

*Corresponding Authors

Orazio Prezzavento (prezzave@unict.it.)

Emanuele Amata (eamata@unict.it)

Funding

This work was financially supported by Università degli Studi di Catania, “Piano per la Ricerca 2016–2018”, Grants 57722172105 and 57722172114.

INTRODUCTION

Sigma (σ) receptors represent a unique receptor class involved in various biological and pathological conditions [1]. Two σ receptor subtypes are recognized and termed sigma-1 (σ_1) and sigma-2 (σ_2), having different structures and biological functions [2, 3]. The σ_1 receptor is a 25.3 kDa polypeptide that has been cloned in several species and recently crystallized revealing a trimeric architecture [4, 5]. The σ_1 receptor has been identified as a ligand-operated chaperone protein localized in the mitochondria-associated endoplasmic reticulum (ER) membranes (MAM). At the MAM, the σ_1 receptor forms a complex with another chaperone, the immunoglobulin heavy-chain binding protein (BiP). The σ_1 receptor-BiP complex is silent and only activated when cells are stimulated by σ_1 receptor agonists like (+)-pentazocine [(+)-PTZ] or undergo prolonged stress [6]. In contrast, haloperidol, methamphetamine, and NE-100 can preserve the σ_1 receptor-BiP complex in a silent state [7].

The σ_2 receptor is a poorly understood protein whose identification has been controversial. In 2017, Alon and coworkers identified the σ_2 receptor as an endoplasmic reticulum-resident transmembrane protein (TMEM97) playing a role in the cholesterol homeostasis and the sterol transporter Niemann-Pick disease type C1 [8]. Despite the challenges in identifying its true identity, σ_2 receptor and its ligands, as determined in radioligand binding assay using [^3H]DTG [9, 10], have earned a growing scientific interest due to its involvement in several pathological states [11, 12]. The overexpression of the σ_2 receptor has been found in several cancer cells and proliferating tumors such as lung, colorectal, and breast [13].

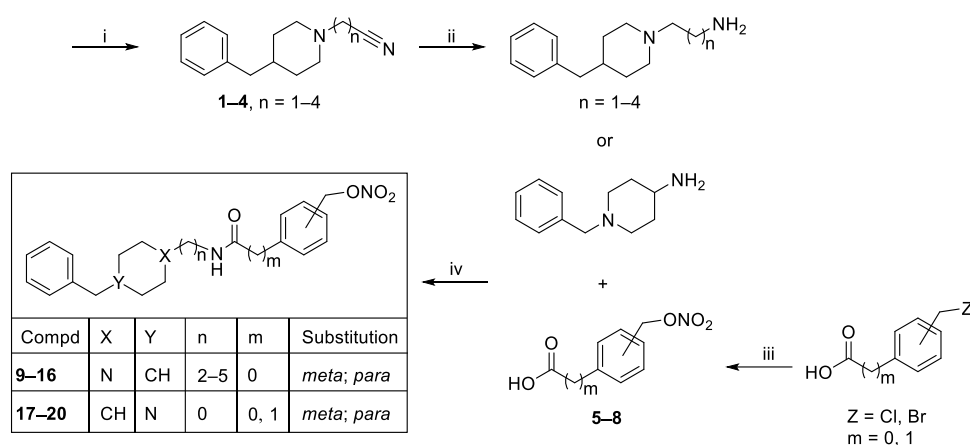
Due to a 10-fold higher density in proliferating tumor cells than in quiescent tumor cells, the σ_2 receptor also represents a significant clinical biomarker for determining the proliferative status of solid tumors [14, 15]. A vast number of data support the use of σ_1 receptor antagonists and σ_2 receptor agonists for the treatment of cancer due to their antiproliferative effects [16–20]. Rimcazole and haloperidol, as well as other σ receptors ligands endowed with opportune functional profile, have been shown to inhibit cell proliferation of several cancer cell lines [21, 22].

Nitric oxide (NO) is a short-lived gas with a dichotomous role in tumor biology. NO operates as a tumor progressor or suppressor based on its concentration, duration of exposure, and cell sensitivity [23]. For instance, μM concentrations of NO result in antitumor effects, while pM – nM concentrations promote cytoprotective effects. In this view, the modulation of NO levels seems to have benefits in the treatment of cancer. However, NO is a reactive and unstable gas; thus, the use of NO donors (NODs) is preferred since these agents are stable chemical compounds able to release NO under specific chemical or enzymatical conditions. In order to ensure a high and effective release of cytotoxic amounts of NO, the choice of the releasing agent is crucial. Among the different classes of donors, organic nitrates have been reported to release adequate amounts of NO [16, 24]. The cytotoxic activity may be carried out by NODs alone, or they may be conjugated or embedded in chemical compounds that possess additional antitumoral action for double-targeted cytotoxic activity [25, 26]. On the basis of the aforementioned, the purpose of the present work is the development, biological evaluation, and molecular modeling studies of a series of molecular hybrids where the cytotoxic activity of the NOD is conjugated with that of σ receptors for optimal effect [16].

RESULTS AND DISCUSSION

Design and Synthesis. Compounds **9–20** were synthesized according to the steps illustrated in Scheme 1. Starting from commercially available 4-benzylpiperidine, intermediates **1–4** were obtained with opportune nitrile compounds and then converted into the corresponding amine derivatives by reaction with LiAlH₄ [6, 16]. The amine intermediates underwent condensation with [(nitrooxy)methyl]benzoic acid (**5**, **6**) or para- or meta-[(nitrooxy)methyl]phenylacetic acid (**7**, **8**) previously prepared via nitration with AgNO₃ to give the final compounds **9–16**. Compounds **17–20** were obtained through condensation of 1-benzylpiperidin-4-amine with the same acids **5–8**.

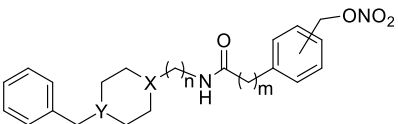
Scheme 1. Synthetic strategy for the preparation of target compounds.^a



^a*Reagents and conditions:* (i) 4-benzylpiperidine, Br[(CH₂)_{1–4}]CN, NaI, K₂CO₃, DMF, 60 °C, overnight; (ii) LiAlH₄, THF, rt, N₂; (iii) AgNO₃, CH₃CN, rt; (iv) EDC, HOBT, CH₃CN, rt, 5 h.

Radioligand Binding Assay. The synthesized compounds were evaluated for affinity at both σ_1 and σ_2 receptors through radioligand binding assay (Table 1). Within the series bearing a 4-benzylpiperidine (**9–16**), the meta-substituted compound **9** has shown a preferential σ_1 receptor affinity with K_i value of 49 nM, and 330 nM for the σ_2 receptor. The elongation to three-carbon chain (**10**) increased the σ_2 receptor affinity by more than 3-fold with $K_{i\sigma_1}$ value of 64 nM and $K_{i\sigma_2}$ of 93 nM. The increased σ_2 receptor affinity has also been maintained in compound **11** with a K_i value of 75 nM, although in the four-carbon chain, the σ_1 receptor affinity (148 nM) is reduced. Further elongation of the chain to five carbons takes back σ_1 receptor preferential affinity with a K_i value of 50 nM over the σ_2 receptor (K_i value of 142 nM).

At the same time, the para substitution of the nitrate group gives compounds with generally lower affinity with respect to both receptor subtypes. It is observed an improvement of the σ_2 receptor affinity with the linker elongation. Indeed, compound **13** has a $K_{i\sigma_2}$ of 2673 nM, while compound **16** has a $K_{i\sigma_2}$ of 70 nM. In terms of σ_1 receptor affinity, compounds **9–16** show a mixed behavior with affinity ranging from 89 nM for compound **13** to 249 nM for compound **15**. Compounds bearing the 1-benzylpiperidin-4-amine (**17–20**) have shown worthy σ_1 receptor affinities and a general lower affinity at the σ_2 receptor. In particular, compounds **17–19** have a σ_1 receptor affinity in the low double digits nM range ($K_{i\sigma_1}$ of 24, 19, and 22 nM, respectively), while only compound **17** shows σ_2 receptor affinity in the same range ($K_{i\sigma_2}$ of 19 nM). The other compounds show a lower affinity to the σ_2 receptor, which leads to a >10 times selectivity with respect to the σ_1 receptor.

Table 1. σ_1 and σ_2 binding assays for compounds **9–20**.


Compound	X	Y	n	m	Substitution	K_i (nM) \pm SD ^a	
						σ_1	σ_2
9	N	CH	2	0	meta	49.3 \pm 1.3	330.4 \pm 9.3
10	N	CH	3	0	meta	63.8 \pm 0.7	93.0 \pm 3.1
11	N	CH	4	0	meta	148.1 \pm 1.1	75.5 \pm 2.2
12	N	CH	5	0	meta	50.4 \pm 0.9	142.2 \pm 12.9
13	N	CH	2	0	para	89.0 \pm 2.1	2,673 \pm 43.6
14	N	CH	3	0	para	145.2 \pm 12.0	230.3 \pm 17.6
15	N	CH	4	0	para	249.6 \pm 9.2	89.5 \pm 1.6
16	N	CH	5	0	para	93.1 \pm 2.5	70.1 \pm 2.8
17	CH	N	0	0	meta	24.0 \pm 0.6	18.6 \pm 0.2
18	CH	N	0	1	meta	19.1 \pm 1.0	319.8 \pm 3.8
19	CH	N	0	0	para	21.8 \pm 0.8	269.7 \pm 4.6
20	CH	N	0	1	para	170.5 \pm 6.2	2,514 \pm 23.7
Haloperidol						2.5 \pm 0.40	16.0 \pm 1.60

^aEach value is the mean \pm SD of at least two experiments performed in triplicate.

Docking Studies. A docking study was conducted to identify and evaluate the key molecular interactions involved in the receptor/ligand recognition. The crystal structure of the σ_1 receptor PD144418 (PDB code 5HK1) reveals an occluded and elongated binding cavity in a similar β -barrel fashion, with the highly conserved Glu172 amino acid residue located near the center of the cavity, forming a salt bridge with the ligands. Since all compounds possess a tertiary amine, we performed the study considering the *N*-protonated structures (pH = 7.4). Therefore, the formation of the salt bridge was used as a filter for the docking poses. The calculated free binding energies (ΔG) and K_i values to the catalytic site of the σ_1 receptor for compounds **9–20** and haloperidol are reported in Table S1.

Active analysis of the site showed that the orientation changes according to the length of the ligands and the protonated *N*-position. Moreover, the position of the protonated piperidine ring is rather characteristic, being close to the carboxyl function of Glu172. The docking studies conducted upon the σ_2 receptor were performed by using its homology model previously built by us [27]. In this case, the salt bridge interactions between the ligands and the residues Asp29 and Asp56 were considered. In the 4-benzylpiperidine series with the nitrate group in the meta position (**9–12**), compound **9** showed a preferential affinity for the σ_1 receptor with a K_i value of 49 nM. Compound **9** is placed inside the receptor site with the piperidinium proton engaged in a salt bridge interaction with Glu172 and a hydrogen bond with N–H amide. The nitrate group is positioned on the opposite side helices α_4 and α_5 , showing polar interactions with the residues Asp126 and His154. The optimal position of the piperidine ring favors the π - π stacking of the hydrogen in position 4 of the piperidine system with the residue Tyr103. The benzyl group is involved in hydrophobic interactions with the Leu182 and Met93 residues. The elongation to the four-carbon chain (**11**) decreases the affinity for the σ_1 receptor

while increasing the affinity for the σ_2 receptor. Indeed, derivative **11** has an inverted orientation with respect to derivative **9**, with the nitrate group toward the helix α_5 to allow the accommodation of the aliphatic chain within the receptor pocket (Figure 1a). The para substitution of the nitrate group (**13–16**) decreases the affinity with respect to the ligands substituted in the meta position. This is probably due to a lower cation– π interaction with the His154 residue (Figure 1b). An elongation of the aliphatic portion of the ligands leads to a better affinity for the σ_2 receptor. The most similar compounds in the series (**11** and **16**) show comparable interactions within the σ_2 receptor pocket. Both form the salt bridge with the residue Asp56 while the benzyl portion in position 4 to the piperidine ring shows aliphatic interactions with the residues Leu70, Met108, Pro113, and Val146. The nitrate group establishes electrostatic interactions with the Arg36 residue, discriminating against the different affinity between the different isomers. A detailed description of the interactions with σ_2 receptor is reported in the Molecular Docking section in the Supporting Information. Compound **18** showed the preminent affinity to the σ_1 receptor. On this compound, a molecular dynamics (MD) simulation was performed (Supporting Information). An elongation of the aliphatic portion of the ligands leads to a better affinity for σ_2 receptor.

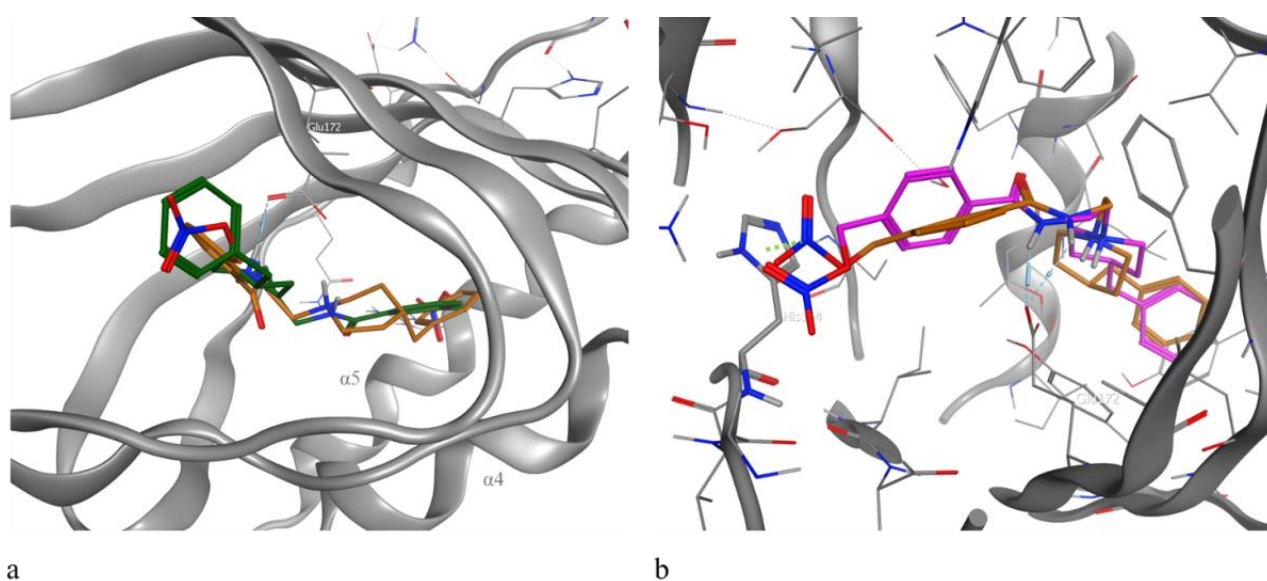


Figure 1. (a) 3D Superposition of the best-docked pose for **9** (orange) and **11** (green) bound to the σ_1 receptor orthosteric site. The different lengths of the aliphatic linker reverse the orientation of the ligand inside the receptor. (b) Top-scored docking poses for **9** (orange) and **13** (magenta) bound to the σ_1 receptor orthosteric site. The different position of the nitrate group allows better interaction with His154 (green dotted line).

Nitric Oxide Release. Once the affinity profiles of the synthesized compounds at σ receptors were evaluated, we determined the ability of these compounds to release NO. Nitrite content was measured by the Griess method incubating the compounds (100 μM), at 37 $^\circ\text{C}$, in Tris-HCl buffer for 30 min (Figure 2). For this assay, we selected the compounds based on their affinity profile against σ receptors. In particular, we evaluated compounds **9**, **11**, **15**, and **17–19**, having shown good affinity at both receptors or prevalence for one receptor subtype. Compounds **9** and **15** were able to release a significant amount of NO in the μM range (**9**, $13.0 \pm 0.5 \mu\text{M}$; **15**, $13.0 \pm 0.4 \mu\text{M}$). The amount of NO released by compound **18** was $1.3 \pm 0.2 \mu\text{M}$, while compound **19** produced $6.3 \pm 0.3 \mu\text{M}$ NO. Negligible NO amounts were detected for compounds **11** and **17** (data not shown).

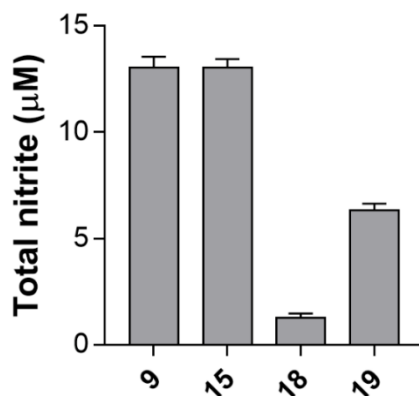


Figure 2. Total nitrite content measured using Griess reagent.

Cell Viability Assay. After having obtained the desired chemical tools, we evaluated their activity in the appropriate cell lines. We evaluated those compounds that, in previous experiments, have been demonstrated to possess the desired profile (compounds **9**, **15**, **18**, and **19**). Two cancer cell lines were selected, Caco-2 and MCF-7 cells, for their expression of both σ receptors. Although MCF-7 cells are reported to exclusively express the σ_2 subtypes, a Western blot analysis has shown the presence of the σ_1 isoform in our in-house cell line (Figure S4) [28]. The toxicity against human fibroblast HFF-1 cells was also evaluated. Doxorubicin (**21**) was used as the standard cytotoxic compound. Results showed a reduction of cellular viability on both Caco-2 and MCF-7 cell lines for compounds **9** and **15** (Table 2). These compounds were those with a higher rate of NO release. Measured IC_{50} values were better with respect to compound **21** for MCF-7 cells, with IC_{50} of 36 μ M for compound **9** and 26 μ M for compound **15**. None of the synthesized compounds, nor compound **21**, were demonstrated to be toxic for the human fibroblasts HFF-1 at the maximal tested concentration. Compounds **18** and **19** have been shown to be nontoxic for the three evaluated cell lines ($IC_{50} > 100$ μ M), probably due to the lower rate of NO release and to an unsuitable functional profile at σ receptors.

Table 3. MTT Test on MCF-7, Caco-2, and HFF-1 for compounds **21**, **9**, **15**, **18**, and **19**.

Compound	$IC_{50} \pm SD$ (μ M) ^a		
	MCF-7	Caco-2	HFF-1
21	44 \pm 0.3	21 \pm 0.3	>100 ^b
9	36 \pm 0.2	59 \pm 0.5	>100 ^b
15	26 \pm 0.4	28 \pm 0.2	>100 ^b
18	>100 ^b	>100 ^b	>100 ^b
19	>100 ^b	>100 ^b	>100 ^b

^aEach value is the mean \pm SD of at least two experiments performed in quadruplicate. ^bCell viability reduction lower than 50% at 100 μ M.

In order to determinate the precise mechanism for the reduction of cellular viability, compound **15** (IC_{50} concentration) was evaluated in combination with the σ_1 receptor agonist (+)-PTZ (1 μ M) and the σ_2 receptor antagonist 1-phenethylpiperidine (AC927, 1 μ M) by MTT [29]. Incubation of

compound **15** with (+)-PTZ or AC927 wholly restored the loss of cell viability induced by **15** alone (Figure 3). This outlines a σ_1 and σ_2 receptors involvement in the observed cellular events and a σ_1 receptor antagonist/ σ_2 receptor agonist functional profile for compound **15**.

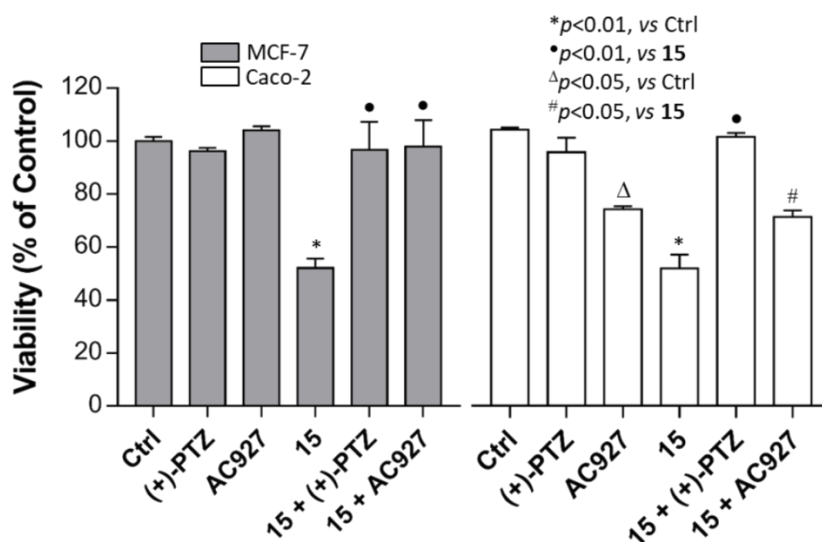
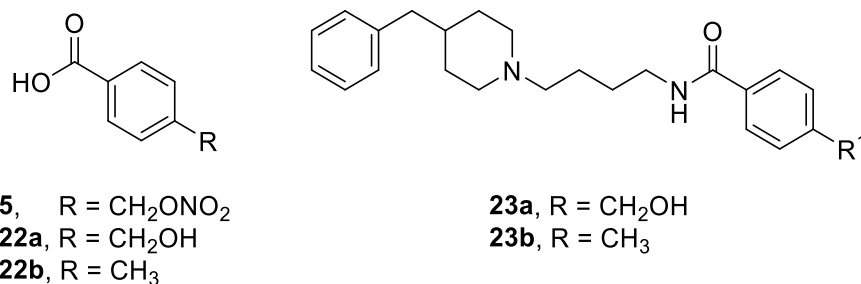


Figure 3. Effects of compound **15** in combination with the selective σ_1 receptor agonist (+)-PTZ and σ_2 receptor antagonist AC927 on MCF-7 and Caco-2 viability by MTT test.

To dig into the dual mechanism of the prepared compounds, we tested fragments **5** and **22a,b** and synthesized two derivatives of compound **15** lacking the nitrate function, compounds **23a** and **23b**, as negative control (Table 3 and Scheme S1) [30, 31].

Table 3. Binding Assays and MTT Viability Test on MCF-7 for Compounds **22a,b**, **23a,b**, and **5**.



Compound	K_i (nM) \pm SD ^a		IC ₅₀ \pm SD (μ M) ^b
	σ_1	σ_2	MCF-7
5	>10,000 ^c	>10,000 ^c	>100 ^d
22a	>10,000 ^c	>10,000 ^c	>100 ^d
22b	>10,000 ^c	>10,000 ^c	>100 ^d
23a	711 \pm 127	2,600 \pm 730	>100 ^d
23b	62 \pm 3	127 \pm 16	87 \pm 0.3

^aEach value is the mean \pm SD of at least two experiments performed in triplicate. ^bEach value is the mean \pm SD of at least two experiments performed in quadruplicate. ^cRadioligand displacement lower than 50% at 10 μ M. ^dCell viability reduction lower than 50% at 100 μ M.

The fragments **5** and **22a,b** have shown no significant viability reduction on MCF-7 and no affinity for both σ receptors. Compound **23a** showed a loss of affinity at both σ receptors, while compound **23b** retained a similar affinity profile at both σ receptors with respect to compound **9** or **15**. When evaluated on the MCF-7 cell line, compound **23a** induced lower than 50% viability reduction at 100 μ M, while compound **23b** had an IC_{50} of 87 μ M. Overall compound **23b**, while maintaining a similar profile against σ receptors, showed a lower ability in reducing MCF-7 viability, thus sustaining a possible synergistic effect between σ receptors and the NO-mediated events.

In conclusion, this contribution reports the development of novel hybrid compounds able to release NO and to bind σ receptors as candidates for double-targeted cancer therapy. The compounds have been evaluated for their affinity at σ receptors and ability to release NO. Four compounds showed the desired profile with compounds **9** and **15** also able to induce a marked loss of viability in MCF-7 and Caco-2 cell lines while not being toxic for healthy human fibroblast HFF-1. In cellular experiments involving the use of selective σ receptors agonist and antagonist, compound **15** has shown a σ_1 receptor antagonist/ σ_2 receptor agonist functional profile. The elimination of the nitrate function of compound **15** as in compounds **23a,b** determined the loss of its ability to reduce MCF-7 viability sustaining a possible synergistic effect between the σ receptors and the NO-mediated events. Molecular docking studies have shown that the length of the aliphatic linker has an essential role in the orientation of the ligands inside the receptor pocket and for σ_1/σ_2 selectivity. The nitrate group stabilizes the ligand/receptor complex to cation- π interaction with His154 residue in the σ_1 receptor, also confirmed by the MD simulation, and with Phe71 and Pro113 residues in the σ_2 receptor. Overall, the combination of NO donor and σ receptors ligands provided compounds with potential beneficial effects in the treatment of neoplastic disorders.

Notes

The authors declare no competing financial interest.

Acknowledgments

The authors thank Prof. Giuseppina Immè, Dr. Roberto Catalano, and Nunzio Giudice from the Department of Physics and Astronomy, University of Catania, for technical and instrumental support of the Beckman LS6500 liquid scintillation counter.

REFERENCES

- [1] Kim, F. J. Introduction to Sigma Proteins: Evolution of the Concept of Sigma Receptors. *Handb. Exp. Pharmacol.* 2017, 244, 1–11.
- [2] Schmidt, H. R.; Kruse, A. C. The Molecular Function of sigma Receptors: Past, Present, and Future. *Trends Pharmacol. Sci.* 2019, 40, 636–654.
- [3] Weber, F.; Wunsch, B. Medicinal Chemistry of sigma1 Receptor Ligands: Pharmacophore Models, Synthesis, Structure Affinity Relationships, and Pharmacological Applications. *Handb. Exp. Pharmacol.* 2017, 244, 51–79.
- [4] Schmidt, H. R.; Zheng, S.; Gurpinar, E.; Koehl, A.; Manglik, A.; Kruse, A. C. Crystal structure of the human sigma1 receptor. *Nature* 2016, 532, 527–530.
- [5] Kim, F. J.; Pasternak, G. W. sigma1 Receptor ligand binding: an open-and-shut case. *Nat. Struct. Mol. Biol.* 2018, 25, 992–993.

- [6] Hayashi, T.; Su, T. P. Sigma-1 receptor chaperones at the ERmitochondrion interface regulate Ca(2+) signaling and cell survival. *Cell* 2007, 131, 596–610.
- [7] Morales-Lazaro, S. L.; Gonzalez-Ramirez, R.; Rosenbaum, T. Molecular Interplay Between the Sigma-1 Receptor, Steroids, and Ion Channels. *Front. Pharmacol.* 2019, 10, 419.
- [8] Alon, A.; Schmidt, H. R.; Wood, M. D.; Sahn, J. J.; Martin, S. F.; Kruse, A. C. Identification of the gene that codes for the sigma2 receptor. *Proc. Natl. Acad. Sci. U. S. A.* 2017, 114, 7160–7165.
- [9] Nastasi, G.; Miceli, C.; Pittala, V.; Modica, M. N.; Prezzavento, O.; Romeo, G.; Rescifina, A.; Marrazzo, A.; Amata, E. S2RSLDB: a comprehensive manually curated, internet-accessible database of the sigma-2 receptor selective ligands. *J. Cheminf.* 2017, 9, 3.
- [10] Prezzavento, O.; Arena, E.; Sanchez-Fernandez, C.; Turnaturi, R.; Parenti, C.; Marrazzo, A.; Catalano, R.; Amata, E.; Pasquinucci, L.; Cobos, E. J. (+)-and (–)-Phenazocine enantiomers: Evaluation of their dual opioid agonist/sigma1 antagonist properties and antinociceptive effects. *Eur. J. Med. Chem.* 2017, 125, 603–610.
- [11] Huang, Y. S.; Lu, H. L.; Zhang, L. J.; Wu, Z. Sigma-2 receptor ligands and their perspectives in cancer diagnosis and therapy. *Med. Res. Rev.* 2014, 34, 532–566.
- [12] Crawford, K. W.; Bowen, W. D. Sigma-2 receptor agonists activate a novel apoptotic pathway and potentiate antineoplastic drugs in breast tumor cell lines. *Cancer Res.* 2002, 62, 313–322.
- [13] van Waarde, A.; Rybczynska, A. A.; Ramakrishnan, N. K.; Ishiwata, K.; Elsinga, P. H.; Dierckx, R. A. Potential applications for sigma receptor ligands in cancer diagnosis and therapy. *Biochim. Biophys. Acta, Biomembr.* 2015, 1848, 2703–2714.
- [14] Zeng, C.; McDonald, E. S.; Mach, R. H. Molecular Probes for Imaging the Sigma-2 Receptor: In Vitro and In Vivo Imaging Studies. *Handb. Exp. Pharmacol.* 2016, 244, 309–330.
- [15] McDonald, E. S.; Doot, R. K.; Young, A. J.; Schubert, E. K.; Pryma, D. A.; Farwell, M. D.; Tchou, J.; Nayak, A.; Ziober, A.; Feldman, M. D.; DeMichele, A.; Clark, A. S.; Shah, P. D.; Lee, H.; Carlin, S. D.; Mach, R. H.; Mankoff, D. A. Breast Cancer (18)F-ISO-1 Uptake as a Marker of Proliferation Status. *J. Nucl. Med.* 2019, DOI: 10.2967/jnumed.119.232363.
- [16] Amata, E.; Dichiarà, M.; Arena, E.; Pittala, V.; Pistara, V.; Cardile, V.; Graziano, A. C. E.; Fraix, A.; Marrazzo, A.; Sortino, S.; Prezzavento, O. Novel Sigma Receptor Ligand-Nitric Oxide Photodonors: Molecular Hybrids for Double-Targeted Antiproliferative Effect. *J. Med. Chem.* 2017, 60, 9531–9544.
- [17] Olivieri, M.; Amata, E.; Vinciguerra, S.; Fiorito, J.; Giurdanella, G.; Drago, F.; Caporarello, N.; Prezzavento, O.; Arena, E.; Salerno, L.; Rescifina, A.; Lupo, G.; Anfuso, C. D.; Marrazzo, A. Antiangiogenic Effect of (+/-)-Haloperidol Metabolite II Valproate Ester (+/-)-MRJF22 in Human Microvascular Retinal Endothelial Cells. *J. Med. Chem.* 2016, 59, 9960–9966.
- [18] Tesei, A.; Cortesi, M.; Zamagni, A.; Arienti, C.; Pignatta, S.; Zannoni, M.; Paolillo, M.; Curti, D.; Rui, M.; Rossi, D.; Collina, S. Sigma Receptors as Endoplasmic Reticulum Stress “Gatekeepers” and their Modulators as Emerging New Weapons in the Fight Against Cancer. *Front. Pharmacol.* 2018, 9, 711.
- [19] Floresta, G.; Dichiarà, M.; Gentile, D.; Prezzavento, O.; Marrazzo, A.; Rescifina, A.; Amata, E. Morphing of Ibogaine: A Successful Attempt into the Search for Sigma-2 Receptor Ligands. *Int. J. Mol. Sci.* 2019, 20, 488.
- [20] Amata, E.; Rescifina, A.; Prezzavento, O.; Arena, E.; Dichiarà, M.; Pittala, V.; Montilla-Garcia, A.; Punzo, F.; Merino, P.; Cobos, E. J.; Marrazzo, A. (+)-Methyl (1R,2S)-2-[[4-(4-Chlorophenyl)-4-hydroxypiperidin-1-yl]methyl-1-phenylcyclopropanecarboxylate [(+)-MR200] Derivatives as Potent

and Selective Sigma Receptor Ligands: Stereochemistry and Pharmacological Properties. *J. Med. Chem.* 2018, 61, 372–384.

[21] Happy, M.; Dejoie, J.; Zajac, C. K.; Cortez, B.; Chakraborty, K.; Aderemi, J.; Sauane, M. Sigma 1 Receptor antagonist potentiates the anti-cancer effect of p53 by regulating ER stress, ROS production, Bax levels, and caspase-3 activation. *Biochem. Biophys. Res. Commun.* 2015, 456, 683–688.

[22] Spruce, B. A.; Campbell, L. A.; McTavish, N.; Cooper, M. A.; Appleyard, M. V.; O'Neill, M.; Howie, J.; Samson, J.; Watt, S.; Murray, K.; McLean, D.; Leslie, N. R.; Safrany, S. T.; Ferguson, M. J.; Peters, J. A.; Prescott, A. R.; Box, G.; Hayes, A.; Nutley, B.; Raynaud, F.; Downes, C. P.; Lambert, J. J.; Thompson, A. M.; Eccles, S. Small molecule antagonists of the sigma-1 receptor cause selective release of the death program in tumor and self-reliant cells and inhibit tumor growth in vitro and in vivo. *Cancer Res.* 2004, 64, 4875–4886.

[23] Sakuma, S.; Ikeda, Y.; Inoue, I.; Yamaguchi, K.; Honkawa, S.; Kohda, T.; Minamino, S.; Fujimoto, Y. Nitric oxide represses the proliferation of Caco-2 cells by inducing S-G2/M cell cycle arrest. *Int. J. Physiol. Pathophysiol. Pharmacol.* 2019, 11, 205–211.

[24] Wang, P. G.; Xian, M.; Tang, X.; Wu, X.; Wen, Z.; Cai, T.; Janczuk, A. J. Nitric oxide donors: chemical activities and biological applications. *Chem. Rev.* 2002, 102, 1091–1134.

[25] Huang, Z.; Fu, J.; Zhang, Y. Nitric Oxide Donor-Based Cancer Therapy: Advances and Prospects. *J. Med. Chem.* 2017, 60, 7617–7635.

[26] Ding, Q. G.; Zang, J.; Gao, S.; Gao, Q.; Duan, W.; Li, X.; Xu, W.; Zhang, Y. Nitric oxide donor hybrid compounds as promising anticancer agents. *Drug Discoveries Ther.* 2016, 10, 276–284.

[27] Floresta, G.; Amata, E.; Barbaraci, C.; Gentile, D.; Turnaturi, R.; Marrazzo, A.; Rescifina, A. A Structure- and Ligand-Based Virtual Screening of a Database of “Small” Marine Natural Products for the Identification of “Blue” Sigma-2 Receptor Ligands. *Mar. Drugs* 2018, 16, 384.

[28] Kim, F. J.; Maher, C. M. Sigma1 Pharmacology in the Context of Cancer. *Handb. Exp. Pharmacol.* 2017, 244, 237–308.

[29] Bucolo, C.; Campana, G.; Di Toro, R.; Cacciaguerra, S.; Spampinato, S. Sigma1 recognition sites in rabbit iris-ciliary body: topical sigma1-site agonists lower intraocular pressure. *J. Pharmacol. Exp. Ther.* 1999, 289, 1362–1369.

[30] Pisani, L.; Iacobazzi, R. M.; Catto, M.; Rullo, M.; Farina, R.; Denora, N.; Cellamare, S.; Altomare, C. D. Investigating alkyl nitrates as nitric oxide releasing precursors of multitarget acetylcholinesterase monoamine oxidase B inhibitors. *Eur. J. Med. Chem.* 2019, 161, 292–309.

[31] Wold, S.; Sjöström, M.; Eriksson, L. PLS-regression: a basic tool of chemometrics. *Chemom. Intell. Lab. Syst.* 2001, 58, 109–130.

Synthesis and preclinical evaluation of novel H₂S-donor sigma receptor hybrids for the management of pain

Maria Dichiara,^a Antonia Artacho-Cordón,^b Agostino Marrazzo,^a Enrique J. Cobos,^{b,*} and Emanuele Amata^{a,*}

^a Department of Drug and Health Sciences, Medicinal Chemistry Section, Università degli Studi di Catania, Viale Andrea Doria 6, 95125 Catania, Italy

^b Department of Pharmacology, Faculty of Medicine and Institute of Neuroscience, Biomedical Research Center, University of Granada, Parque Tecnológico de Ciencias de la Salud, 18100 Armilla, Granada, Spain

Manuscript in preparation

ABSTRACT: The development of σ_1 R antagonists hybridized with H₂S-releasing moiety is here reported. The purpose is to obtain improved analgesic properties when compared to σ_1 R antagonists or H₂S-donor alone. On an in vivo model of capsaicin-induced mechanical hypersensitivity, thioamide **1a** showed analgesic properties which were synergistically enhanced when co-administered with the σ_1 R antagonist BD-1063. The selective σ_1 R agonist PRE-084 revealed a complete reversion of the effect. On the contrary, the amide analogue **1b** did not result in analgesic effects and its co-administration with BD-1063 caused no potentiation. Later, four thioamide H₂S- σ_1 R hybrids (**4–7a**) and their amide derivatives (**4–7b**) were synthesized, evaluated with radioligand binding assay over both σ Rs, tested for their ability to release H₂S and in vivo evaluated. Particularly, compound **7a** determined significant analgesia that was reversed by PRE-084, suggesting a synergistic effect between the σ_1 R and the H₂S-mediated events. The negative control **7b** showed only minimal analgesic effect at the same doses. Overall, the combination of H₂S donor and σ Rs ligands provided compounds with beneficial effects for the treatment of pain.

KEYWORDS: *Sigma receptors, hydrogen sulfide, H₂S-donors, neuropathic pain, bifunctional ligands*

*Corresponding authors

Emanuele Amata (eamata@unict.it)

Enrique J. Cobos (ejcobos@ugr.es)

INTRODUCTION

Pain is an important global health problem since millions of people suffer from chronic pain, and there is an estimated 18% of individuals in developed countries with chronic pain conditions. Current analgesics often show limited efficacy or a number of side effects which restrict their use. Moreover, pain processing implicates multiple concurrent mechanisms of nociceptive transmission and modulation. Consequently, treatments based on a single mechanism of action often lack of efficacy and targeting simultaneously with drugs from different pharmacological classes is routinely used to treat chronic pain [1-3].

Hydrogen sulfide (H_2S) is an endogenous gasotransmitter involved in the modulation of the daily cellular activities as well as the cytotoxic events, including nociceptive processes [4]. Under physiological conditions, cells produce small but significant amounts of H_2S that contribute to enhance the neutrophil/endothelium adhesion process, leading to neutrophil migration toward the inflammatory site and thus inflammatory hypernociception [5, 6]. In contrast to the pro-nociceptive role of endogenous H_2S , the systemic pretreatment of mice with an exogenous H_2S donor (NaHS) inhibited nociceptive stimuli both in a lipopolysaccharide (LPS)-induced inflammatory and in a zymosan-induced articular hypernociception model by opening ATP-sensitive potassium channels (KATP channels) [7]. The anti-nociceptive activity of exogenous H_2S has been also investigated in a rodent model of visceral pain, where H_2S inhibited colorectal distension-induced nociception via the involvement of opioid receptors [8]. Based on these findings, the combination of opioid receptor agonists with an H_2S -releasing moiety has been used to provide additive or even synergistic analgesic effect. At this regard, the trimebutine derivative GIC-1001 bearing a thioamide function has been reported for being able to release H_2S with reduction of the nociceptive response in an animal model of colorectal distension [9].

The effect of H_2S on neuropathic pain has been less investigated. A recent study has revealed the relationship between neuropathic pain and exogenous H_2S , with alleviation of chronic neuropathic pain by inhibiting the expression of cAMP response element binding (CREB), a protein involved in the development and maintenance of neuropathic pain in the spinal cord [10]. In another study of neuropathic pain induced by anticancer drugs, activation of Kv7 voltage-gated potassium channels was found to be mediated by H_2S and contribute to reduce the hypersensitivity [11].

Sigma receptors (σ Rs) are involved in several biological processes and pathological conditions. First introduced as subtypes of the opioid receptor, they are now recognized as a particular and unique receptor class. Two subtypes are currently known, denoted as sigma-1 (σ_1 R) and sigma-2 (σ_2 R), having different structure, biological function, and pharmacological profile. A wide number of data support the modulatory role of σ_1 R in nociception, mainly based on the pain-attenuated phenotype of σ_1 R knockout (KO) mice and on the antinociceptive effect exerted by σ_1 R antagonists on pain of different etiology including neuropathic, inflammatory, and visceral pain, and as adjuvants to opioid therapy [12]. The selective σ_1 R antagonist E-52862 (S1RA) is currently undergoing phase II clinical trials for the treatment of neuropathic pain of different etiologies [13]. Further experiments carried out with σ_1 R KO mice and in wild type (WT) animals treated with σ_1 R antagonists showed no allodynia in both formalin- and capsaicin-induced nociception [14, 15]. Also, experiments with σ_1 R KO mice with traumatic nerve injury were consistent with results obtained with pharmacological treatments, since mutant mice did not develop signs of either cold or mechanical allodynia [16].

With the aim to identify novel combinations of analgesic mechanisms with potential utility, here we aimed to test whether H₂S-releasing moieties acting in conjunction with σ_1 R antagonist might induce a synergistically enhanced analgesic effect when compared to σ_1 R antagonist ligand or H₂S-donor alone. We used capsaicin-induced mechanical hypersensitivity as a pain model, as it is well known that the increase in sensitivity to pain in the area surrounding capsaicin injection results from central sensitization, which is a key process in chronic pain development and maintenance [17]. Indeed, changes in capsaicin-induced mechanical hypersensitivity have been used to study the behavioral consequences of drug treatment in central sensitization in both humans and rodents [15, 18].

RESULTS AND DISCUSSION

Characterization of compounds 1a and 1b. The feasibility of the project and its proof of concept have been firstly investigated testing σ_1 R antagonism or H₂S-donor alone and the association of both mechanisms. As σ_1 R drug we selected BD-1063, as it is considered a standard and selective σ_1 R antagonist [13]. The selection of an adequate H₂S donor is more complex as the choice of the releasing agent is essential to ensure a high and effective H₂S release. Among the different classes of such donors developed to date, thioamide seems to be preferable since it has demonstrated a sufficient or higher release than other H₂S-donors. This donor is usually stable in physiological buffers, but it can release H₂S when applied to biological system via hydrolysis. For this purpose, H₂S donor thioamide **1a** was prepared starting from commercially available 4-cyanobenzoic acid by thionation with P₄S₁₀ (Scheme S1). Compound **1a** and its amide derivative **1b** as negative control were thus evaluated for their ability to release H₂S with a spectrofluorimetric method. Then compounds **1a,b**, were tested in vivo, in capsaicin-induced mechanical hypersensitivity, alone and in combination with BD-1063, a known σ_1 R antagonist.

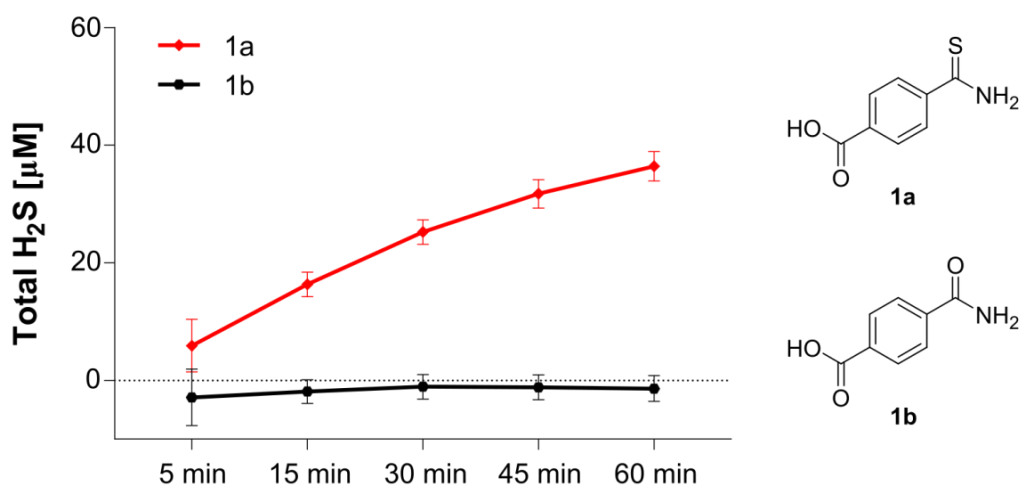


Figure 1. Chemical structures of **1a** and **1b** and H₂S release in spectrofluorimetric method.

H₂S release was assessed using a spectrofluorimetric assay based upon the reaction of H₂S with Washington State Probe-1 (WSP-1) to generate benzodithiolone and a fluorophore with excitation and emission maxima of 465 and 515 nm, respectively. The results of H₂S release in PBS buffer at regular intervals of 15 min are reported in Figure 1. Thioamide **1a** at 100 μM concentration was able to release H₂S in a significant and cumulative fashion over time. The amount of H₂S released by H₂S-donor scaffold **1a** after 1 h incubation was 34.4 μM. No H₂S release was detected for the analogue **1b** (100 μM) bearing an amide function used as negative control.

We tested the effects of these compounds and BD-1063 on capsaicin-induced mechanical hypersensitivity. The s.c. administration of BD1063 or **1a** (5–20 mg/Kg) resulted in a marked dose-dependent reduction of mechanical hypersensitivity (Figure 2, Panel A). The administration of the amide analogue **1b** showed only limited effects and at the higher doses tested (Figure 2, Panel A). The administration of PRE-084 was able to reverse the effect of BD-1063 but not the effect of **1a** (Figure 2, Panel B), indicating that σ_1 R agonism exclusively decreases the effect of σ_1 R antagonism on sensory hypersensitivity without affecting the effect induced by H₂S release.

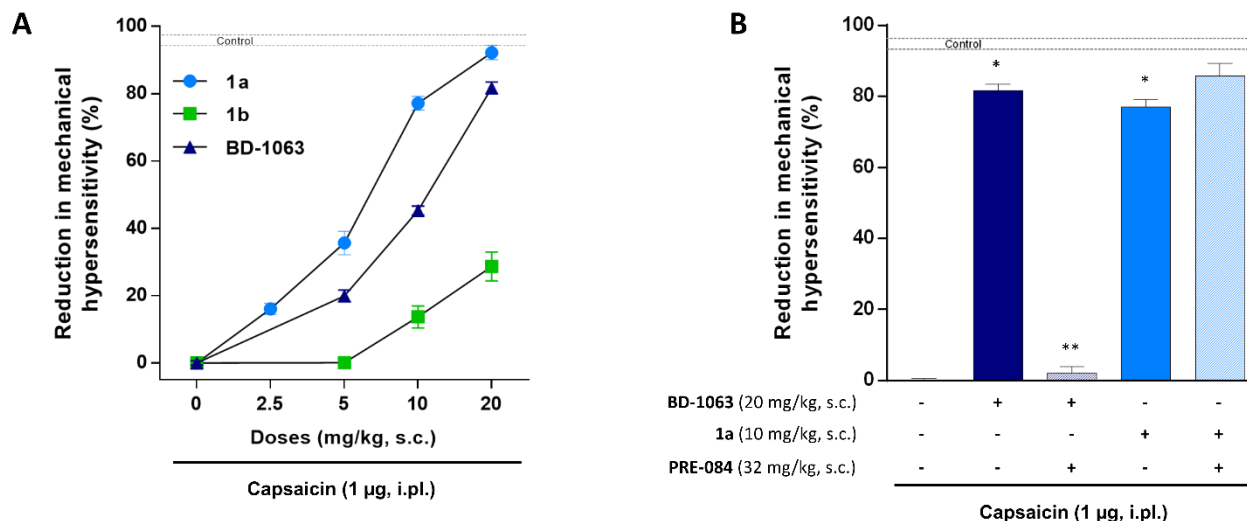


Figure 2. Mechanical antinociception induced by the systemic administration of **1a**, **1b** and BD-1063 in mice and contribution of σ_1 R to their effects. A) Dose dependency of the antinociceptive effects of the subcutaneous (s.c.) administration of **1a**, **1b** and BD-1063. B) Effects of BD-1063 and compound **1a** alone and in combination with the σ_1 R agonist PRE-084 (* p <0.01 vs Ctrl, ** p <0.01 vs BD-1063).

The concurrent administration to mice of low doses of **1a** (5 mg/Kg) and BD-1063 (5 mg/Kg) resulted in a synergistic effect in decreasing mechanical hypersensitivity (Figure 3). To test for σ_1 R involvement on the effect induced by the association of both drugs, mice were treated with the selective σ_1 R agonist PRE-084, revealing a marked reversion of the effects. These results indicate that the σ_1 R component played an important role on the pronounced effects induced by the association between BD-1063 and **1a**. Importantly, the effects of BD-1063 were not enhanced by **1b** (5 mg/Kg, Figure 3), which is lacking the H₂S release moiety. Taken together, these results suggest that both the σ_1 R and H₂S release components are needed for the marked effect on sensory hypersensitivity induced by the association of **1a** with BD-1063, and that we can control for the contribution of both mechanisms by using PRE-084 and testing analog compounds lacking the thioamide function, respectively.

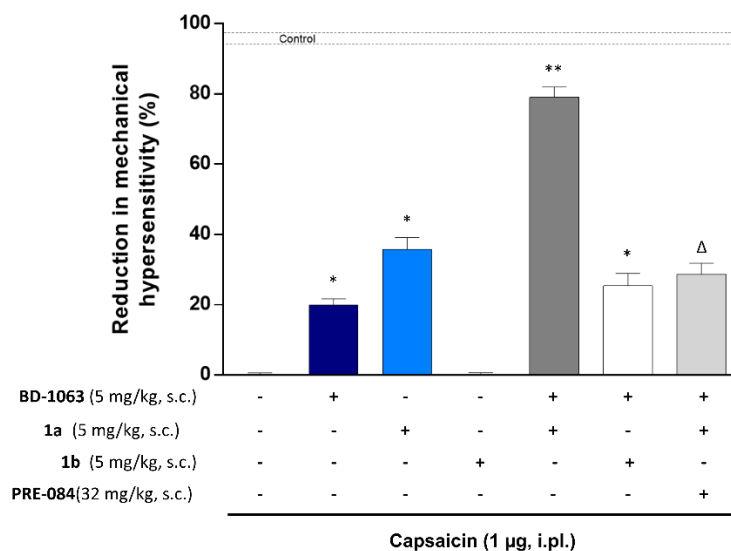
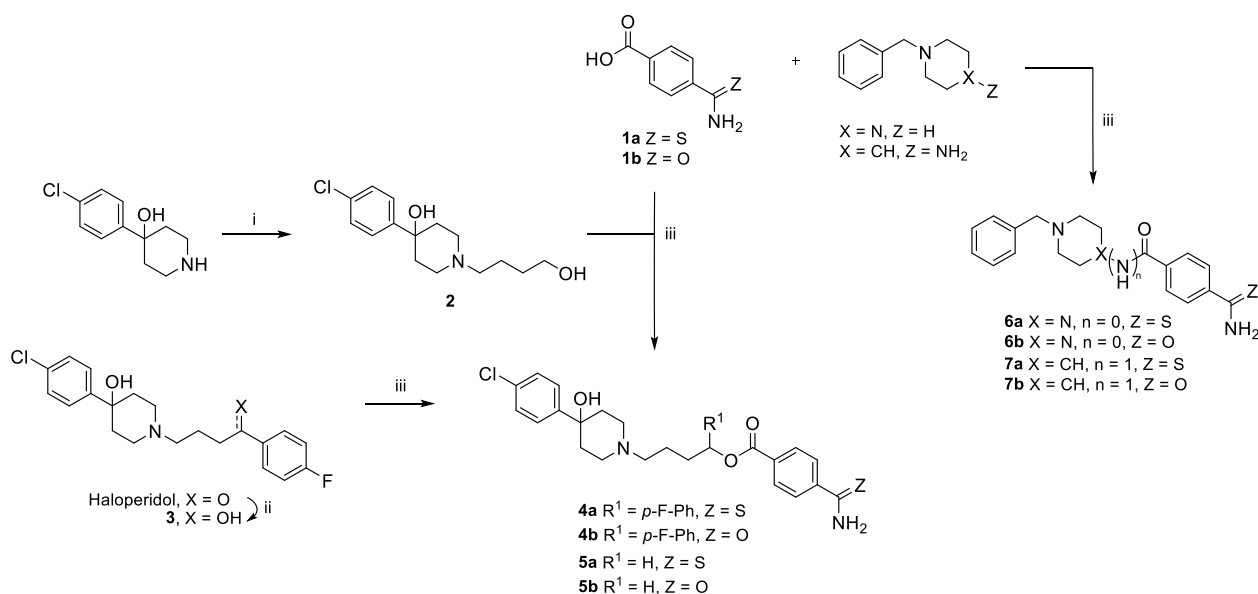


Figure 3. Mechanical antinociception induced by the systemic administration of compounds **1a** and **1b** alone and in combination with the selective σ_1 R antagonist BD-1063 and σ_1 R agonist PRE-084 in mice (* p <0.01 vs Ctrl, ** p <0.01 vs **1a**, Δp <0.01 vs **1a** + BD-1063).

Design and synthesis. Based on the preliminary pharmacological outcomes, we have designed a series of ligands in which the 4-carbamothioylbenzoic acid is covalently joined to appropriate amino moieties. However, the designed ligands **4–7a** possess as a whole the required structural elements for σ R recognition. To better dig into the precise mechanism of the synthesized compounds, derivatives **4–7b** lacking the thioamide function have also been prepared as negative control.

Scheme 1. Synthetic Strategy for the Preparation of Target Compounds.



Reagents and conditions: (i) 4-chloro-1-butanol, KHCO₃, ACN, reflux, 4 h; (ii) NaBH₄, EtOH, rt, 12 h; (iii) EDC, HOBT, DMF, rt, 6 h.

Compounds **4–7** were synthesized according to the steps illustrated in Scheme 1. The H₂S-donor scaffold **1a** has been conjugated with opportune alcohol or amine by coupling reactions to give the

final compounds **4–7a**. Negative controls **4–7b** were obtained through condensation of the same alcohols or amines with commercial 4-carbamoylbenzoic acid.

Radioligand Binding Assay. All the synthesized compounds were evaluated for affinity at both σ_1R and σ_2R through radioligand binding assay (Table 1). We have also included haloperidol, (+)-pentazocine, DTG and BD-1063 as internal controls that have been tested with the same membrane homogenates.

It is worth pointing out that **1a** and **1b** were devoid of affinity for σR s. Except for compounds **4a–b**, the sulfur atom promoted the molecular interactions involved for the σR -ligand recognition. The lack of *p*-fluorophenyl ring in **5a** increased the σ_1R affinity with respect to **4a**, together with an improved selectivity over σ_2R . Indeed, compound **5a** had a $K_i\sigma_1R$ of 58 nM vs $K_i\sigma_2R$ of 266 nM, while compound **4a** 156 nM for $K_i\sigma_1R$ vs 311 nM for $K_i\sigma_2R$. Derivatives **4b** and **5b** bearing the amide function showed lower affinity over both receptor subtypes with $K_i\sigma_1R$ of 173 nM vs $K_i\sigma_2R$ of 618 nM, and $K_i\sigma_1R$ of 126 nM vs $K_i\sigma_2R$ of 933 nM, respectively.

A worsening of the affinity for σ_1R is observed for compound **6a** having 1-benzylpiperazine moiety directly joined to the H₂S donor ($K_i\sigma_1R$ = 668 nM). Surprisingly, compound **6a** completely lost the capacity to bind σ_2R ($K_i\sigma_2R$ >10,000). Moving the nitrogen atom to an adjacent position, as in compound **7a**, restored the affinity towards σ_1R ($K_i\sigma_1R$ = 94 nM) and improved the selectivity over σ_2R ($K_i\sigma_2R$ = 1125 nM). Negative controls **6b** and **7b** had negligible or no affinity for both subtypes.

Table 1. σ_1R and σ_2R binding assays for compounds 4–7.

Compound	K_i (nM) \pm SD ^a	
	σ_1R	σ_2R
1a	>10,000	>10,000
1b	>10,000	>10,000
4a	156 \pm 41	311 \pm 75
4b	173 \pm 24	618 \pm 146
5a	58 \pm 7.0	266 \pm 73
5b	126 \pm 15	933 \pm 161
6a	668 \pm 137	>10,000
6b	>5,000	>10,000
7a	94 \pm 29	1,125 \pm 348
7b	837 \pm 125	>10,000
Haloperidol	2.6 \pm 0.4	77 \pm 18
(+)-Pentazocine	4.3 \pm 0.5	1,465 \pm 224
DTG	124 \pm 19	18 \pm 1
BD-1063	14 \pm 2.7	204 \pm 31

^aEach value is the mean \pm SD of at least two experiments performed in duplicate.

Hydrogen sulfide release. The results of H₂S release in PBS buffer at regular intervals of 15 min are reported in Figure 4. All compounds showed a good capability in releasing significant amount of H₂S in the μM range, being this an important outcome in ensuring the desired analgesic effect. Indeed, as

outlined in the design section, the releasing capability needs to be preserved after that the donor scaffold is covalently conjugated.

All the compounds synthesized and tested have shown a higher ability in releasing H₂S than compound **1a** with the maximum release recorded after 60 min of incubation. Compounds **4a** and **6a** released 51.7 and 46.7 μM of H₂S respectively, after 1h of incubation, whereas compounds **5a** and **7a** 41.8 and 38.4 μM.

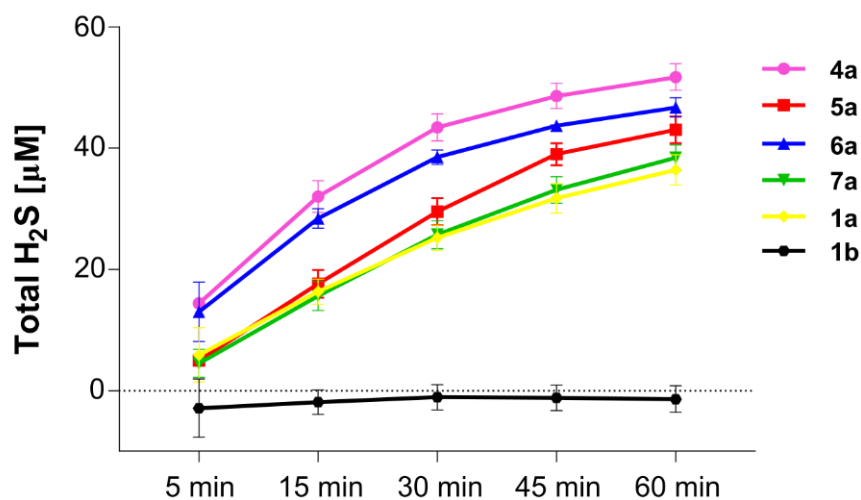


Figure 4. H₂S release evaluation at regular intervals incubation period in PBS buffer. Data are presented as mean ± SD of at least two experiments performed in triplicate.

In vivo pharmacology of compounds 4–7. After having obtained the desired chemical hybrids, we evaluated their antinociceptive effect in mice. Compound **4a**, a derivative of haloperidol bearing the thioamide function, resulted in a reversion of capsaicin-induced mechanical hypersensitivity in a dose dependent manner. However, the negative control **4b** showed to have very similar effects when tested at the same doses (Figure S9, Panel A). This result suggests that the σ R component, or additional activities, of compound **4a** are probably more pronounced compared to the analgesic activity due to the H₂S release and the synergistic effect is nullified. The derivative **5a**, lacking the *p*-F-phenyl fragment of haloperidol, was not able to completely reverse the sensitizing effect of capsaicin even at high doses (Figure S9, Panel A). Derivative **6a** was able to decrease mechanical hypersensitivity in a dose dependent manner. When PRE-084 administration was associated to **6a**, at the highest dose tested (40 mg/Kg), it resulted in a significant reversion of the effect, highlighting the involvement of σ_1 R. However, the negative control **6b** showed to have similar or even higher analgesic effects when evaluated at the same doses (Figure S9, Panel A). It must be noted that compound **6b** had no affinity at σ Rs (Table 1), and in fact its effect was not reversed by PRE-084 (Figure S9, Panel B). Thus, the observed in vivo effects induced by **6b** are related to off target activity. It may be speculated that compound **6a**, although showing a low affinity for σ_1 R ($K_i\sigma_1$ 668 nM), might provide a good analgesic in vivo activity due to the possible enhancement of the H₂S- σ_1 R antagonism combination.

Compound **7a** showed a prominent effect in vivo, markedly reducing capsaicin-induced mechanical hypersensitivity, whereas the derivative **7b** lacking the thioamide function had minimal effect. This result is a clear evidence of the H₂S contribution to the analgesic effect of **7a** (Figure 5, Panel A). The administration of the σ_1 R agonist PRE-084 nearly abolished the effect of **7a** at low doses of the later

(20 mg/Kg), but the effect of σ_1 R agonism gradually disappeared when increasing the dose of **7a**, so that at the dose of 40 mg/Kg the effect of PRE-084 was not significant (Figure 5, Panel B). It is important to note that the dose of 32 mg/Kg s.c. of PRE-084 has been previously shown to fully reverse in mice the effects of high doses (64–128 mg/Kg) of S1RA [19, 20], a high affinity and highly selective σ_1 R antagonist currently on clinical trials for pain treatment [13]. The findings of these previous studies suggest that this dose of PRE-084 is enough to fully mask the effects of σ_1 R antagonism even if the antagonist is administered at high doses. Therefore, our results showing that moderate doses of **7a** are still able to reduce mechanical hypersensitivity in spite of the administration of PRE-084 suggest that additional mechanisms, such as H₂S-mediated actions, participate on the reduction of capsaicin-induced mechanical hypersensitivity induced by this compound.

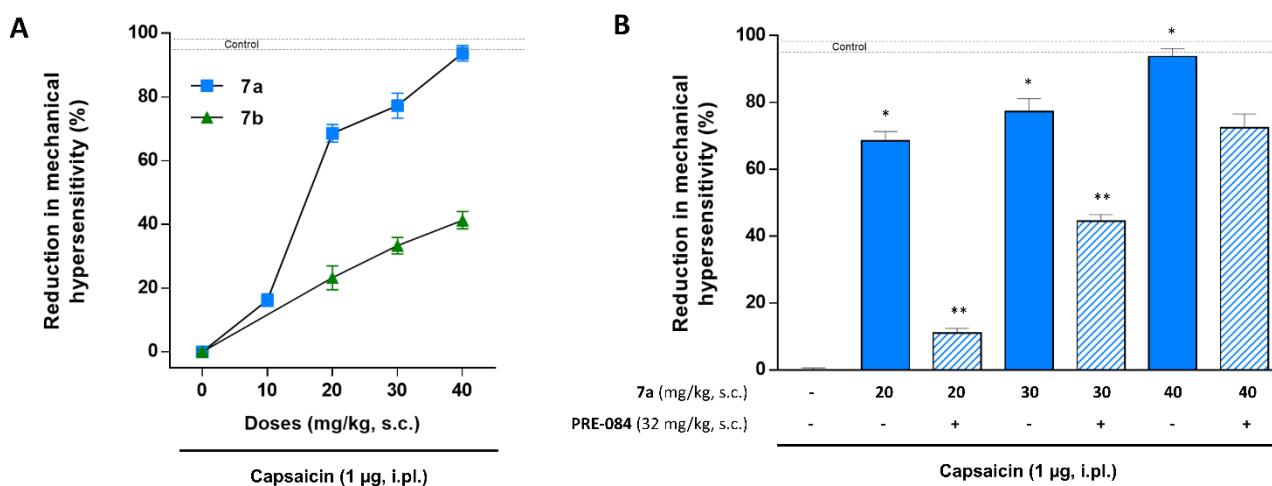


Figure 5. Mechanical antinociception induced by the systemic administration of **7a** and **7b** in mice and contribution of σ_1 R to their effects. A) Dose dependency of the antinociceptive effects of the subcutaneous (s.c.) administration of **7a** and **7b**. B) Effects of compound **7a** alone and in combination with the σ_1 R agonist PRE-084 (* p <0.01 vs Ctrl, ** p <0.01 vs **7a**).

CONCLUSION

Here we report the development of novel hybrid compounds able to release H₂S and to bind σ R as candidates for the treatment of pain conditions. The compounds have been evaluated for their affinity at σ R and ability to release H₂S. The major hurdle was to find hybrid ligands with a balanced activity when evaluated in vivo. Indeed, to have a real synergistic effect, the σ R component should not prevail on the H₂S-donor activity, and vice versa. Compound **7a** showed the desired profile, and the replacement of its thioamide function as in amide **7b** determined a substantial loss of analgesic activity. Moreover, the association of the σ_1 R agonist PRE-084 with **7a** resulted in a reversion of the effect, sustaining a clear synergistic effect between the σ_1 R and the H₂S-mediated events.

EXPERIMENTAL SECTION

General remarks. Reagent grade chemicals were purchased from Merck (Darmstadt, Germany) and were used without further purification. All reactions involving air-sensitive reagents were performed under N₂ in oven-dried glassware using the syringe-septum cap technique. Flash chromatography purification was performed on a Merck silica gel 60 (40–63 μm; 230–400 mesh) stationary phase. Nuclear magnetic resonance spectra (¹H NMR recorded at 200 and 500 MHz) were obtained on VARIAN INOVA spectrometers using CDCl₃, DMSO-d₆ or CD₃OD. TMS was used as an internal standard. Chemical shifts (δ) are given in parts per million (ppm) and coupling constants (*J*) in Hertz (Hz). The following abbreviations are used to designate the multiplicities: s = singlet, d = doublet, t = triplet, q = quartet, quint = quintet, m = multiplet, br = broad. The purity of all tested compounds, whether synthesized or purchased, reached at least 95% as determined by microanalysis (C, H, N) that was performed on a Carlo Erba instrument model E1110; all the results agreed within ± 0.4% of the theoretical values. Reactions were monitored by thin-layer chromatography (TLC) performed on 250 μm silica gel Merck 60 F₂₅₄ coated aluminum plates; the spots were visualized by UV light or iodine chamber. Compound nomenclatures were generated with ChemBioDraw Ultra version 16.0.0.82.

4-carbamothioylbenzoic acid (1a)

P₄S₁₀ (1.5 g, 6.79 mmol) was added to cold EtOH (10 mL) and the solution was stirred for 1 h at rt. Then, 4-cyanobenzoic acid (3.40 mmol, 500 mg) was added in one portion and the resulting mixture was heated under reflux for 5 h. Reaction mixture was poured into ice-water and the precipitated was filtered off. Obtained solid was solubilized in EtOAc and washed with NaHCO₃. The organic layer was removed, and the aqueous was acidified with HCl (pH 1–2) and extracted with EtOAc, brine (5 mL), and dried under anhydrous Na₂SO₄. The solvent was removed in vacuum to provide the desired product as it. Yield: 70%, yellow solid. ¹H NMR (500 MHz, DMSO-d₆) δ 12.99–13.31 (m, 1H), 10.02 (br. s., 1H), 9.63 (br. s., 1H), 7.86–8.00 (m, 4H). ¹³C NMR (500 MHz, DMSO-d₆) δ 199.4, 166.7, 143.2, 128.8, 127.3. Anal. calcd for C₈H₇NO₂S: C, 53.03; H, 3.89; N, 7.73; O, 17.66; S, 17.69. Found: C, 53.13; H, 3.90; N, 7.74; O, 17.69; S, 17.71.

4-(4-chlorophenyl)-1-(4-hydroxybutyl)piperidin-4-ol (2)

To a solution of (4-chlorophenyl)piperidin-4-ol (1.42 mmol, 300 mg) in ACN (10 mL), 4-chloro-1-butanol (1.42 mmol, 0.13 mL) and KHCO₃ (2.84 mmol, 283 mg) were added and the mixture was refluxed for 4 h. The reaction diluted with EtOAc (10 mL), washed with NaHCO₃ saturated solution (2 x 5 mL), and brine (5 mL), and dried under anhydrous Na₂SO₄. The solvent was removed under vacuum and the residue purified via silica gel chromatography with EtOAc and then 5% MeOH in EtOAc. Yield: 80%, white solid. ¹H NMR (200 MHz, CDCl₃) δ 7.42 (d, *J* = 8.5 Hz, 2H), 7.28 (d, *J* = 8.5 Hz, 2H), 3.39–3.73 (m, 2H), 2.74–2.99 (m, 2H), 2.33–2.66 (m, 4H), 1.93–2.28 (m, 2H), 1.56–1.85 (m, 6H). Anal. calcd for C₁₅H₂₂ClNO₂: C, 63.48; H, 7.81; Cl, 12.49; N, 4.94; O, 11.28. Found: C, 63.55; H, 7.82; Cl, 12.51; N, 4.95; O, 11.30.

4-(4-chlorophenyl)-1-(4-(4-fluorophenyl)-4-hydroxybutyl)piperidin-4-ol (3)

To a solution of haloperidol (1.33 mmol, 500 mg) in EtOH (50 mL), NaBH₄ was added at 0 °C. The mixture was stirred at rt for 12 h and quenched with 20 mL water. The mixture has been evaporated to remove EtOH and the residue diluted with saturated Na₂CO₃ solution and extracted with CH₂Cl₂. The combined organic layers were dried over anhydrous Na₂SO₄, filtered, and evaporated to dryness. Yield: 97%, white solid. ¹H NMR (200 MHz, CDCl₃) δ 7.21–7.57 (m, 6H), 6.93–7.07 (m, 2H),

4.58–4.70 (m, 1H), 3.03 (d, $J = 11.07$ Hz, 1H), 2.75–2.91 (m, 1H), 2.39–2.71 (m, 4H), 2.09–2.33 (m, 2H), 1.58–2.05 (m, 6H). Anal. calcd for $C_{21}H_{25}ClFNO_2$: C, 66.75; H, 6.67; Cl, 9.38; F, 5.03; N, 3.71; O, 8.47. Found: C, 66.88; H, 6.68; Cl, 9.40; F, 5.04; N, 3.72; O, 8.49.

General procedure for the synthesis of compounds 4–7

To a solution of 4-carbamothioylbenzoic acid or 4-carbamoylbenzoic acid (1.01 mmol) in DMF (5 mL), HOBT (1.53 mmol, 210 mg), and EDC (1.52 mmol, 290 mg) were added. After stirring for 20 min, the appropriate amine or alcohol (2.02 mmol) has been added and the resulting mixture was stirred at rt for 5 h. After the reaction was complete, it was dissolved in EtOAc (20 mL), washed with H_2O (2 x 10 mL), and brine (5 mL), and dried under anhydrous Na_2SO_4 . The solvent was removed under vacuum and the residue purified via silica gel chromatography to provide the desired product.

4-(4-(4-chlorophenyl)-4-hydroxypiperidin-1-yl)-1-(4-fluorophenyl)butyl 4-carbamothioylbenzoate (4a)

The compound has been prepared using **1a** (1.01 mmol, 183 mg) and **3** as alcohol (2.02 mmol, 763 mg). The residue was purified with 5% EtOH in CH_3Cl . Yield: 65%, yellow solid. 1H NMR (500 MHz, $CDCl_3$) δ 8.07 (d, $J = 8.3$ Hz, 2H), 7.90 (d, $J = 8.3$ Hz, 2H), 7.76 (br. s., 1H), 7.37–7.45 (m, 4H), 7.30–7.36 (m, 2H), 7.06 (t, $J = 8.8$ Hz, 1H), 6.00 (t, $J = 6.8$ Hz, 1H), 2.84 (br. s., 2H), 2.52 (d, $J = 7.8$ Hz, 4H), 2.06–2.27 (m, 4H), 1.53–2.05 (m, 4H). ^{13}C NMR (200 MHz, $DMSO-d_6$) δ 199.2, 164.5, 147.7, 143.8, 142.9, 131.3, 129.0, 128.4, 128.0, 127.6, 126.7, 125.0, 123.3, 118.5, 115.6, 115.1, 110.4, 88.9, 75.5, 68.5, 48.4. Anal. calcd for $C_{29}H_{30}ClFN_2O_3S$: C, 64.37; H, 5.59; Cl, 6.55; F, 3.51; N, 5.18; O, 8.87; S, 5.93. Found: C, 64.53; H, 5.61; Cl, 6.54; F, 3.52; N, 5.19; O, 8.89; S, 5.94.

4-(4-(4-chlorophenyl)-4-hydroxypiperidin-1-yl)-1-(4-fluorophenyl)butyl 4-carbamoylbenzoate (4b)

The compound has been prepared using 4-carbamoylbenzoic acid (1.01 mmol, 167 mg) and **3** (2.02 mmol, 763 mg). The residue was purified with 5% MeOH in CH_2Cl_2 and then 5% of 3% $NH_4OH/MeOH$ solution in CH_2Cl_2 . Yield: 60%, white solid. 1H NMR (200 MHz, $DMSO-d_6$) δ 8.17 (s, 1H), 8.05–8.12 (m, 2H), 7.96–8.04 (m, 2H), 7.61 (s, 1H), 7.42–7.58 (m, 4H), 7.30–7.41 (m, 2H), 7.21 (t, $J = 8.8$ Hz, 2H), 5.91–6.06 (m, 1H), 4.77–5.01 (m, 1H), 2.55 (br. s., 2H), 2.18–2.44 (m, 4H), 1.73–2.15 (m, 4H), 1.38–1.66 (m, 4H). ^{13}C NMR (200 MHz, $DMSO-d_6$) δ 167.1, 164.6, 149.2, 138.8, 136.8, 132.1, 130.7, 129.2, 128.6, 128.6, 127.9, 127.7, 126.9, 115.5, 115.1, 99.8, 69.6, 49.2. Anal. calcd for $C_{29}H_{30}ClFN_2O_4$: C, 66.34; H, 5.76; Cl, 6.75; F, 3.62; N, 5.34; O, 12.19. Found: C, 66.47; H, 5.77; Cl, 6.76; F, 3.63; N, 5.35; O, 12.21.

4-(4-(4-chlorophenyl)-4-hydroxypiperidin-1-yl)butyl 4-carbamothioylbenzoate (5a)

The compound has been prepared using **1a** (1.01 mmol, 183 mg) and **2** as alcohol (2.02 mmol, 573 mg). The residue was purified with 5% EtOH in CH_3Cl . Yield: 65%, yellow solid. 1H NMR (200 MHz, $DMSO-d_6$) δ 10.10 (br. s., 1H), 9.69 (br. s., 1H), 7.79–8.28 (m, 4H), 7.15–7.65 (m, 4H), 4.88 (s, 1H), 4.32 (t, $J = 6.0$ Hz, 2H), 2.65 (d, $J = 10.1$ Hz, 3H), 2.18–2.45 (m, 4H), 1.39–2.03 (m, 8H). ^{13}C NMR (200 MHz, $DMSO-d_6$) δ 200.2, 167.7, 146.6, 131.7, 128.4, 127.9, 127.1, 126.4, 67.5, 66.3, 56.9, 55.4, 33.5, 21.2, 20.5. Anal. calcd for $C_{23}H_{27}ClN_2O_3S$: C, 61.80; H, 6.09; Cl, 7.93; N, 6.27; O, 10.74; S, 7.17. Found: C, 61.91; H, 6.10; Cl, 7.95; N, 6.28; O, 10.75; S, 7.18.

4-(4-(4-chlorophenyl)-4-hydroxypiperidin-1-yl)butyl 4-carbamoylbenzoate (5b)

The compound has been prepared using 4-carbamoylbenzoic acid (1.01 mmol, 167 mg) and **2** (2.02 mmol, 573 mg). The residue was purified with 5% MeOH in CH₂Cl₂. Yield: 80%, white solid. ¹H NMR (200 MHz, DMSO-d₆) δ 8.17 (s, 1H), 7.90–8.09 (m, 8H), 7.59 (br. s., 1H), 4.23–4.42 (m, 4H), 3.28–3.49 (m, 4H), 1.53–1.91 (m, 4H), 1.27–1.45 (m, 2H), 1.01–1.20 (m, 2H). ¹³C NMR (200 MHz, DMSO-d₆) δ 167.0, 165.3, 149.2, 138.4, 132.1, 130.7, 129.2, 127.8, 126.7, 69.6, 49.1, 29.0, 23.0. Anal. calcd for C₂₃H₂₇ClN₂O₄: C, 64.11; H, 6.32; Cl, 8.23; N, 6.50; O, 14.85. Found: C, 64.24; H, 6.33; Cl, 8.25; N, 6.49; O, 14.82.

4-(4-benzylpiperazine-1-carbonyl)benzothioamide (6a)

The compound has been prepared using **1a** (1.01 mmol, 183 mg) and 1-benzylpiperazine (2.02 mmol, 356 mg). The residue was purified with 2–4% EtOH in CH₂Cl₂. Yield: 64%, yellow solid. ¹H NMR (200 MHz, DMSO-d₆) δ 10.00 (br. s., 1H), 9.60 (br. s., 1H), 7.90 (d, *J* = 8.2 Hz, 2H), 7.41 (d, *J* = 8.2 Hz, 2H), 7.20–7.36 (m, 5H), 3.62 (br. s., 2H), 3.50 (s, 2H), 3.31 (br. s, 2H), 2.36 (d, *J* = 1.6 Hz, 4H). ¹³C NMR (200 MHz, DMSO-d₆) δ 199.3, 168.2, 140.2, 138.3, 128.9, 128.2, 127.4, 127.0, 126.5, 61.8, 22.6. Anal. calcd for C₁₉H₂₁N₃OS: C, 67.23; H, 6.24; N, 12.38; O, 4.71; S, 9.44. Found: C, 67.36; H, 6.25; N, 12.40; O, 4.72; S, 9.46.

4-(4-benzylpiperazine-1-carbonyl)benzamide (6b)

The compound has been prepared using 4-carbamoylbenzoic acid (1.01 mmol, 167 mg) and 1-benzylpiperazine (2.02 mmol, 356 mg). The residue was purified with 2–4% EtOH in CH₂Cl₂. Yield: 71%, white solid. ¹H NMR (200 MHz, DMSO-d₆) δ 8.05 (br. s., 1H), 7.85–7.97 (m, 2H), 7.40–7.50 (m, 3H), 7.20–7.37 (m, 5H), 3.62 (br.s., 2H), 3.50 (s, 2H), 3.25–3.41 (m, 4H), 2.37 (d, *J* = 4.3 Hz, 2H). ¹³C NMR (200 MHz, DMSO-d₆) δ 168.3, 167.2, 138.5, 137.8, 135.0, 128.9, 128.2, 127.6, 126.8, 61.8. Anal. calcd for C₁₉H₂₁N₃O₂: C, 70.57; H, 6.55; N, 12.99; O, 9.89. Found: C, 70.71; H, 6.56; N, 13.01; O, 9.91.

N-(1-benzylpiperidin-4-yl)-4-carbamothioylbenzamide (7a)

The compound has been prepared using **1a** (1.01 mmol, 183 mg) and 1-benzylpiperidin-4-amine (2.02 mmol, 384 mg). The residue was purified with 4% MeOH in CH₂Cl₂. Yield: 50%, yellow solid. ¹H NMR (200 MHz, DMSO-d₆) δ 10.00 (br. s., 1H), 9.61 (br. s., 1H), 8.36 (d, *J* = 7.4 Hz, 1H), 7.76–8.03 (m, 4H), 7.14–7.44 (m, 5H), 3.75 (br. s., 1H), 3.46 (br. s., 2H), 2.82 (d, *J* = 9.8 Hz, 2H), 2.01 (t, *J* = 10.9 Hz, 2H), 1.46–1.88 (m, 4H). ¹³C NMR (200 MHz, DMSO-d₆) δ 199.3, 164.9, 141.4, 136.7, 128.8, 128.2, 127.1, 126.8, 52.2, 31.5. Anal. calcd for C₂₀H₂₃N₃OS: C, 67.96; H, 6.56; N, 11.89; O, 4.53; S, 9.07. Found: C, 68.09; H, 6.57; N, 11.91; O, 4.52; S, 9.09.

N-(1-benzylpiperidin-4-yl)terephthalamide (7b)

The compound has been prepared using 4-carbamoylbenzoic acid (1.01 mmol, 167 mg) and 1-benzylpiperidin-4-amine (2.02 mmol, 384 mg). The product is purified by precipitation in EtOAc. Yield: 63%, white solid. ¹H NMR (200 MHz, DMSO-d₆) δ 8.37 (d, *J* = 7.4 Hz, 1H), 8.09 (s, 1H), 7.83–8.01 (m, 4H), 7.50 (s, 1H), 7.18–7.41 (m, 5H), 3.77 (d, *J* = 7.0 Hz, 1H), 3.46 (s, 2H), 2.69–2.91 (m, 2H), 1.89–2.12 (m, 2H), 1.43–1.86 (m, 4H). ¹³C NMR (200 MHz, DMSO-d₆) δ 167.2, 165.0, 138.6, 137.0, 136.3, 128.7, 128.1, 127.3, 127.1, 126.8, 62.1, 52.2, 31.4. Anal. calcd for C₂₀H₂₃N₃O₂: C, 71.19; H, 6.87; N, 12.45; O, 9.48. Found: C, 71.33; H, 6.88; N, 12.42; O, 9.49.

Radioligand binding assays. *Materials.* Brain and liver homogenates for σ₁R and σ₂R receptor binding assays were prepared from male Dunkin-Hartley guinea pigs and Sprague Dawley rats,

respectively (ENVIGO RMS S.R.L., Udine, Italy). Animals (200–250 g) were euthanized with CO₂ in a euthanasia chamber and sacrificed by decapitation. Guinea pig brains without cerebellum (~2.5 g each) and rat livers (~7 g each) were kept on dry ice and stored at -80 °C. [³H](+)-Pentazocine (26.9 Ci/mmol) and [³H]1,3-di-o-tolylguanidine ([³H]DTG, 35.5 Ci/mmol) were purchased from PerkinElmer (Zaventem, Belgium). Ultima Gold MV Scintillation cocktail was from PerkinElmer (Milan, Italy). All the other materials were obtained from Merck Life Science S.r.l. (Milan, Italy). The test compound solutions were prepared by dissolving approximately 10 μmol of test compound in DMSO so that a 10 mM stock solution was obtained. The required test concentrations for the assay (from 10⁻⁵ to 10⁻¹¹ M) have been prepared by diluting the DMSO stock solution with the respective assay buffer. All experiments were performed using ultrapure water obtained with a Millipore Milli-Q Reference Ultrapure Water Purification System. All the laboratory glassware was first washed with 6 M HCl water solution and then rinsed with ultrapure water.

Preparation of membrane homogenates from pig brain. Fresh guinea pig brain cortices (~25 g) were homogenized in two portions with 10 volumes of ice-cold Tris (50 mM, pH 7.4) containing 0.32 M sucrose with a Potter-Elvehjem glass homogenizer. The suspension was centrifuged at 1,030 × g for 10 min at 4 °C. The supernatant was separated and centrifuged at 41,200 × g for 20 min at 4 °C. The obtained pellet was suspended with 3 volumes of ice-cold Tris (50 mM, pH 7.4), incubated at rt for 15 min and centrifuged at 41,200 × g for 15 min at 4 °C. The final pellet was resuspended with ~2 volumes of ice-cold Tris buffer, and frozen at -80 °C in ~1 mL portions containing about 5 mg protein/mL [15, 16].

Preparation of membrane homogenates from rat liver. Rat livers (~21 g) were cut into small pieces with a scalpel and homogenized in two portions with 6 volumes of cold 0.32 M sucrose with a Potter-Elvehjem glass homogenizer. The suspension was centrifuged at 1,030 × g for 10 min at 4 °C. The supernatant was separated and centrifuged at 31,100 × g for 20 min at 4 °C. The pellet was resuspended with 6 volumes of ice-cold Tris buffer (50 mM, pH 8) and incubated at rt for 30 min. Then, the suspension was centrifuged at 31,100 × g for 20 min at 4 °C. The final pellet was resuspended with 6 volumes of ice-cold Tris buffer and stored at -80 °C in ~1 mL portions containing about 6 mg protein/mL [15, 16].

Protein determination. The protein concentration was determined by the method of Bradford. The Bradford solution was prepared by dissolving 10 mg of Coomassie Brilliant Blue G 250 in 5 mL of 95% ethanol. To this solution, 10 mL of 85% phosphoric acid were added and the mixture was stirred and filled to a total volume of 100 mL with ultrapure water. The calibration was carried out with bovine serum albumin as a standard at different concentrations. In a 96-well plate, 30 μL of the calibration solution or 30 μL of the membrane receptor preparation were mixed with 240 μL of the Bradford solution, respectively. After 5 min of incubation at rt, the UV absorbance was measured at λ=595 nm using a microplate spectrophotometer reader (Synergy HT, BioTek).

σ₁R Ligand Binding Assays. In vitro σ₁R ligand binding assays were carried out in Tris buffer (50 mM, pH 7.4) for 150 min at 37 °C. The thawed membrane preparation of guinea pig brain cortex (250 μg/sample) was incubated with increasing concentrations of test compounds and [³H](+)-pentazocine (2 nM) in a final volume of 0.5 mL. The K_d value of [³H](+)-pentazocine was 2.9 nM. Unlabeled (+)-pentazocine (10 μM) was used to measure non-specific binding. Bound and free radioligand were separated by fast filtration under reduced pressure using a Millipore filter apparatus through Whatman GF/6 glass fiber filters, which were presoaked in a 0.5% poly(ethyleneimine) water solution for 120 min. Each filter paper was rinsed three times with 3 mL ice-cold Tris buffer (50 mM, pH 7.4), dried

at rt, and incubated overnight with 3 mL scintillation cocktail into pony vials. The bound radioactivity has been determined using a liquid scintillation counter (Beckman LS 6500).

σ_2R Ligand Binding Assays. In vitro σ_2R ligand binding assays were carried out in Tris buffer (50 mM, pH 8.0) for 120 min at rt. The thawed membrane preparation of rat liver (250 $\mu\text{g}/\text{sample}$) was incubated with increasing concentrations of test compounds and [^3H]DTG (2 nM) in the presence of (+)-pentazocine (5 μM) as σ_1R masking agent in a final volume of 0.5 mL. The K_d value of [^3H]DTG was 17.9 nM. Non-specific binding was evaluated with unlabeled DTG (10 μM). Bound and free radioligand were separated by fast filtration under reduced pressure using a Millipore filter apparatus through Whatman GF/6 glass fiber filters, which were presoaked in a 0.5% poly(ethyleneimine) water solution for 120 min. Each filter paper was rinsed three times with 3 mL ice-cold Tris buffer (10 mM, pH 8), dried at rt, and incubated overnight with 3 mL scintillation cocktail into pony vials. The bound radioactivity has been determined using a liquid scintillation counter (Beckman LS 6500).

Data analysis. The K_i -values were calculated with the program GraphPad Prism[®] 5.0 (GraphPad Software, San Diego, CA, USA). The K_i -values are given as mean value \pm SD from at least two independent experiments performed in duplicate.

Fluorescence analysis for H₂S determination. H₂S generation was measured using WSP-1 at a final concentration of 100 μM [17]. A 10 mM solution of the appropriate compound in DMSO was diluted with PBS (10 mM, pH 7.4) containing 1 mM cetrimonium bromide to give the desired final concentration of 100 or 250 μM . The calibration was carried out with NaHS as a standard at different concentrations. In a 96-well plate, 70 μL of the calibration solution or 70 μL of the tested compound were mixed with 140 μL of WSP1 stock solution and diluted at a final volume of 280 μL with the same buffer. After 30 and 60 min of incubation in the dark at rt, the fluorescence signal was recorded at $\lambda=476$ nm using a microplate spectrophotometer reader (Synergy HT, BioTek).

In vivo pharmacology. *Experimental animals.* Experiments were performed in female WT-CD1 (Charles River, Barcelona, Spain) mice weighing 25 to 30 g. Mice were acclimated in our animal facilities for at least 1 week before testing and were housed in a room under controlled environmental conditions: 12/12 h day/night cycle, constant temperature (22 ± 2 °C), air replacement every 20 min, and they were fed a standard laboratory diet (Harlan Teklad Research Diet, Madison, WI, USA) and tap water ad libitum until the beginning of the experiments. Behavioral test was conducted during the light phase (from 9.00 to 15.00), and randomly throughout the oestrous cycle. Animal care was in accordance with institutional (Research Ethics Committee of the University of Granada, Spain), regional (Junta de Andalucía, Spain) and international standards (European Communities Council Directive 2010/63).

Drugs and drug administration. The experimental compounds, whose synthesis is described above, were dissolved in 5% dimethyl sulfoxide (DMSO; Merck KGaA, Darnstadt, Germany) in physiological sterile saline (0.9% NaCl). As selective σ_1R drugs, we used the σ_1R antagonist BD-1063 (1-[2-(3,4-dichlorophenyl)ethyl]-4-methylpiperazine dihydrochloride) and the σ_1R agonist PRE-084 (2-(4-morpholinethyl)-1-phenyl cyclohexane carboxylate hydrochloride) (both provided by Tocris Cookson, Bristol, UK). Both σ_1R drugs were dissolved in physiological sterile saline. Drug solutions were prepared immediately before the start of the experiments and injected subcutaneously (s.c.) in a volume of 5 ml/kg into the interscapular area. H₂S donors or their controls were injected 30 min before the administration of capsaicin, used as the chemical algogen. When we studied the effects of the association of BD-1063 with **1a** or **1b**, BD-1063 solution was administered immediately before

the other drug. To test for the effects of PRE-084 on the antiallodynia induced by the other drugs, it was administered 5 min before the later. When the effect of the association of several drugs was assessed, each injection was performed in different areas of the interscapular zone to avoid mixture of the drug solutions and any physicochemical interaction between them. Capsaicin (Sigma-Aldrich Química S.A.) was dissolved in 1% DMSO in physiological sterile saline to a concentration of 0.05 µg/µL (i.e., 1 µg per mouse). Capsaicin solution was injected intraplantarly (i.pl.) into the right hind paw proximate to the heel, in a volume of 20 µL using a 1710 TLL Hamilton microsyringe (Teknokroma, Barcelona, Spain) with a 30^{1/2}-gauge needle. Control animals were injected with the same volume of the vehicle of capsaicin.

Evaluation of capsaicin-induced secondary mechanical hypersensitivity. Animals were placed for 2 h in individual black-walled test compartments. The test compartments were situated on an elevated mesh-bottomed platform with a 0.5-cm² grid to provide access to the ventral surface of the hind paws. In all experiments, punctate mechanical stimulation was applied with a Dynamic Plantar Aesthesiometer (Ugo Basile, Varese, Italy) 15 min after the administration of capsaicin or saline (i.e., 45 min after the injection of the experimental drug). Briefly, a non-flexible filament (0.5 mm diameter) was electronically driven into the ventral side of the right hind paw (which was previously injected with capsaicin or vehicle) at least 5 mm away from the site of the injection towards the fingers. The intensity of the stimulation was fixed at 0.5 g force, as described previously (Entrena et al., 2009). When a paw withdrawal response occurred, the stimulus was automatically terminated, and the response latency was automatically recorded. The filament was applied three times, separated by intervals of 0.5 min, and the mean value of the three trials was considered the withdrawal latency time of the animal. The degree of effect of drugs on mechanical hypersensitivity induced by capsaicin was calculated as: % reduction in mechanical hypersensitivity = [(LTD - LTS)/(CT - LTS)] x 100, where LTD is latency time in drug-treated animals, LTS is latency time in solvent-treated animals, and CT is the cutoff time (50 s).

REFERENCES

- [1] J. Mao, M.S. Gold, M.M. Backonja, Combination drug therapy for chronic pain: a call for more clinical studies, *The journal of pain*, 12 (2011) 157-166.
- [2] I. Gilron, T.S. Jensen, A.H. Dickenson, Combination pharmacotherapy for management of chronic pain: from bench to bedside, *The Lancet. Neurology*, 12 (2013) 1084-1095.
- [3] R. González-Cano, Á. Montilla-García, M.C. Ruiz-Cantero, I. Bravo-Caparrós, M. Tejada, F.R. Nieto, E.J. Cobos, The search for translational pain outcomes to refine analgesic development: Where did we come from and where are we going?, *Neuroscience and biobehavioral reviews*, 113 (2020) 238-261.
- [4] P.K. Moore, M. Bhatia, S. Moochhala, Hydrogen sulfide: from the smell of the past to the mediator of the future?, *Trends in pharmacological sciences*, 24 (2003) 609-611.
- [5] M. Bhatia, J. Sidhapuriwala, S.M. Moochhala, P.K. Moore, Hydrogen sulphide is a mediator of carrageenan-induced hindpaw oedema in the rat, *British journal of pharmacology*, 145 (2005) 141-144.
- [6] A. Kawabata, T. Ishiki, K. Nagasawa, S. Yoshida, Y. Maeda, T. Takahashi, F. Sekiguchi, T. Wada, S. Ichida, H. Nishikawa, Hydrogen sulfide as a novel nociceptive messenger, *Pain*, 132 (2007) 74-81.

- [7] T.M. Cunha, D. Dal-Secco, W.A. Verri, Jr., A.T. Guerrero, G.R. Souza, S.M. Vieira, C.M. Lotufo, A.F. Neto, S.H. Ferreira, F.Q. Cunha, Dual role of hydrogen sulfide in mechanical inflammatory hypernociception, *European journal of pharmacology*, 590 (2008) 127-135.
- [8] E. Distrutti, S. Cipriani, B. Renga, A. Mencarelli, M. Migliorati, S. Cianetti, S. Fiorucci, Hydrogen sulphide induces micro opioid receptor-dependent analgesia in a rodent model of visceral pain, *Molecular pain*, 6 (2010) 36.
- [9] N. Cenac, M. Castro, C. Desormeaux, P. Colin, M. Sie, M. Ranger, N. Vergnolle, A novel orally administered trimebutine compound (GIC-1001) is anti-nociceptive and features peripheral opioid agonistic activity and Hydrogen Sulphide-releasing capacity in mice, *European journal of pain* (London, England), 20 (2016) 723-730.
- [10] J.Q. Lin, H.Q. Luo, C.Z. Lin, J.Z. Chen, X.Z. Lin, Sodium hydrosulfide relieves neuropathic pain in chronic constriction injured rats, *Evidence-based complementary and alternative medicine : eCAM*, 2014 (2014) 514898.
- [11] L. Di Cesare Mannelli, E. Lucarini, L. Micheli, I. Mosca, P. Ambrosino, M.V. Soldovieri, A. Martelli, L. Testai, M. Taglialatela, V. Calderone, C. Ghelardini, Effects of natural and synthetic isothiocyanate-based H₂S-releasers against chemotherapy-induced neuropathic pain: Role of Kv7 potassium channels, *Neuropharmacology*, 121 (2017) 49-59.
- [12] M. Merlos, L. Romero, D. Zamanillo, C. Plata-Salamán, J.M. Vela, Sigma-1 Receptor and Pain, *Handbook of experimental pharmacology*, 244 (2017) 131-161.
- [13] M.C. Ruiz-Cantero, R. González-Cano, M. Tejada, M. Santos-Caballero, G. Perazzoli, F.R. Nieto, E.J. Cobos, Sigma-1 receptor: A drug target for the modulation of neuroimmune and neuroglial interactions during chronic pain, *Pharmacological research*, 163 (2021) 105339.
- [14] C.M. Cendán, J.M. Pujalte, E. Portillo-Salido, L. Montoliu, J.M. Baeyens, Formalin-induced pain is reduced in sigma(1) receptor knockout mice, *European journal of pharmacology*, 511 (2005) 73-74.
- [15] J.M. Entrena, E.J. Cobos, F.R. Nieto, C.M. Cendán, G. Gris, E. Del Pozo, D. Zamanillo, J.M. Baeyens, Sigma-1 receptors are essential for capsaicin-induced mechanical hypersensitivity: studies with selective sigma-1 ligands and sigma-1 knockout mice, *Pain*, 143 (2009) 252-261.
- [16] B. de la Puente, X. Nadal, E. Portillo-Salido, R. Sánchez-Arroyos, S. Ovalle, G. Palacios, A. Muro, L. Romero, J.M. Entrena, J.M. Baeyens, J.A. López-García, R. Maldonado, D. Zamanillo, J.M. Vela, Sigma-1 receptors regulate activity-induced spinal sensitization and neuropathic pain after peripheral nerve injury, *Pain*, 145 (2009) 294-303.
- [17] C.J. Woolf, Central sensitization: implications for the diagnosis and treatment of pain, *Pain*, 152 (2011) S2-S15.
- [18] K.M. Park, M.B. Max, E. Robinovitz, R.H. Gracely, G.J. Bennett, Effects of intravenous ketamine, alfentanil, or placebo on pain, pinprick hyperalgesia, and allodynia produced by intradermal capsaicin in human subjects, *Pain*, 63 (1995) 163-172.
- [19] C. Sánchez-Fernández, Á. Montilla-García, R. González-Cano, F.R. Nieto, L. Romero, A. Artacho-Cordón, R. Montes, B. Fernández-Pastor, M. Merlos, J.M. Baeyens, J.M. Entrena, E.J. Cobos, Modulation of peripheral μ -opioid analgesia by σ 1 receptors, *The Journal of pharmacology and experimental therapeutics*, 348 (2014) 32-45.
- [20] I. Bravo-Caparrós, G. Perazzoli, S. Yeste, D. Cikes, J.M. Baeyens, E.J. Cobos, F.R. Nieto, Sigma-1 Receptor Inhibition Reduces Neuropathic Pain Induced by Partial Sciatic Nerve Transection

- in Mice by Opioid-Dependent and -Independent Mechanisms, *Frontiers in pharmacology*, 10 (2019) 613.
- [21] D. Zampieri, S. Fortuna, A. Calabretti, M. Romano, R. Menegazzi, D. Schepmann, B. Wunsch, M.G. Mamolo, Synthesis, Cytotoxicity Evaluation, and Computational Insights of Novel 1,4-Diazepane-Based Sigma Ligands, *ACS medicinal chemistry letters*, 11 (2020) 651-656.
- [22] E. Amata, A. Rescifina, O. Prezzavento, E. Arena, M. Dichiara, V. Pittalà, Á. Montilla-García, F. Punzo, P. Merino, E.J. Cobos, A. Marrazzo, (+)-Methyl (1R,2S)-2-[[4-(4-Chlorophenyl)-4-hydroxypiperidin-1-yl]methyl]-1-phenylcyclopropanecarboxylate [(+)-MR200] Derivatives as Potent and Selective Sigma Receptor Ligands: Stereochemistry and Pharmacological Properties, *Journal of medicinal chemistry*, 61 (2018) 372-384.
- [23] E. Amata, M. Dichiara, D. Gentile, A. Marrazzo, R. Turnaturi, E. Arena, A. La Mantia, B.R. Tomasello, R. Acquaviva, C. Di Giacomo, A. Rescifina, O. Prezzavento, Sigma Receptor Ligands Carrying a Nitric Oxide Donor Nitrate Moiety: Synthesis, In Silico, and Biological Evaluation, *ACS medicinal chemistry letters*, 11 (2020) 889-894.
- [24] E. Amata, M. Dichiara, E. Arena, V. Pittalà, V. Pistarà, V. Cardile, A.C.E. Graziano, A. Fraix, A. Marrazzo, S. Sortino, O. Prezzavento, Novel Sigma Receptor Ligand-Nitric Oxide Photodonors: Molecular Hybrids for Double-Targeted Antiproliferative Effect, *Journal of medicinal chemistry*, 60 (2017) 9531-9544.
- [25] C. Liu, J. Pan, S. Li, Y. Zhao, L.Y. Wu, C.E. Berkman, A.R. Whorton, M. Xian, Capture and visualization of hydrogen sulfide by a fluorescent probe, *Angewandte Chemie (International ed. in English)*, 50 (2011) 10327-10329.

Tuning Properties for Blood-Brain Barrier Permeation: A Statistics-Based Analysis

Maria Dichiara, Benedetto Amata, Rita Turnaturi, Agostino Marrazzo, and Emanuele Amata*

Department of Drug Sciences, Medicinal Chemistry Section, Università degli Studi di Catania, Viale Andrea Doria 6, 95125 Catania, Italy

ACS Chemical Neuroscience

Received: October 7, 2019; Accepted: December 3, 2019

ABSTRACT: In the effort to define a set of rules useful in tuning the properties for a successful blood-brain barrier (BBB) permeation, we statistically analyzed a set of 328 compounds and correlated their experimental in vivo logBB with a series of computed descriptors. Contingency tables were constructed, observed and expected distributions were calculated, and chi-square (χ^2) distributions were evaluated. This allowed to point out a significant dependence of certain physicochemical properties in influencing the BBB permeation. Of over 15 computed descriptors, 9 resulted to be particularly important showing highly significant χ^2 distribution: polar surface area ($\chi^2 = 66.79$; $p = 1.08 \times 10^{-13}$), nitrogen and oxygen count ($\chi^2 = 51.17$; $p = 2.06 \times 10^{-10}$), logP ($\chi^2 = 47.38$; $p = 1.27 \times 10^{-9}$), nitrogen count ($\chi^2 = 38.29$; $p = 9.77 \times 10^{-8}$), logD ($\chi^2 = 36.80$; $p = 36.80$), oxygen count ($\chi^2 = 35.83$; $p = 3.13 \times 10^{-7}$), ionization state ($\chi^2 = 33.02$, $p = 3.19 \times 10^{-7}$), hydrogen bond acceptors ($\chi^2 = 30.80$; $p = 3.36 \times 10^{-6}$), and hydrogen bond donors ($\chi^2 = 29.29$; $p = 6.81 \times 10^{-6}$). Other parameters describing the mass and size of the molecules (molecular weight: 11.18; $p = 2.46 \times 10^{-2}$) resulted in being not significant since the population within the observed and expected distribution was similar. Depending on the combination of the significant descriptors, we set a three cases probabilistic scenario (BBB⁺, BBB⁻, BBB⁺/BBB⁻) that would prospectively be used to tune properties for BBB permeation.

KEYWORDS: *BBB permeability, logBB, physicochemical properties, contingency table, chi-square statistics, CNS drug*

Author Contributions

E.A. was responsible for the study design, analysis and interpretation of the data. M.D. and A.M. were responsible for the acquisition of data. E.A. and B.A. were responsible for the graphics design. E.A. and M.D. discussed the results and wrote the manuscript. All authors have participated in the writing refinement and given approval to the final version of the manuscript.

*Corresponding Author

Emanuele Amata (eamata@unict.it)

Acknowledgement

This work was supported by the Italian MIUR, PRIN 2017, Code: 201744BN5T. All the authors gratefully acknowledge Dr. Giovanni Nastasi for his helpful support.

INTRODUCTION

According to the American Neurological Association (ANA), hundreds of million Americans suffer from at least one neurological disease, with headache and epilepsy at the top of the list, followed by sleep disorders, strokes, and dementia. Many of these disorders have an incidence that increases significantly over the age of 65 years with a global annual cost beyond 800 billion dollars [1]. Furthermore, the brain is a common site of metastases in 10–30% of adults with cancer [2]. The brain is the most complex organ in the human body equipped with a sophisticated protection system needed for maintaining the homeostasis and physiological environment. A key player in this finely regulated equilibrium is the blood-brain barrier (BBB), a restricted gateway allowing specific nutrients and hormones to selectively permeate. This protection system hinders the development of central nervous system (CNS) active molecules, and the standard pharmacokinetic parameters such as oral bioavailability and plasma concentration are not sufficient to evaluate drug exposure and time course in the brain [3]. A fine interplay between passive membrane permeability and active transport processes is also determinant for brain entry [4]. Certain drugs freely diffuse through the BBB; nevertheless, the presence of some efflux transport systems in the brain microvasculature, such as the P-glycoprotein (P-gp) and the multidrug resistance-associated protein family (MRP), leads to their immediate extrusion from brain [5,6]. Furthermore, the lack of a completely satisfying in vitro model of the BBB strongly prevents drug discovery and development. Experiments with brain capillary or immortalized endothelial cells are impaired from sufficiently restrictive tight junctions, whereas permeability screening assays using noncerebral cell lines, such as the intestine Caco-2 and kidney MDCK cell lines, be qualitatively poor when compared with BBB endothelial cells [7]. Non-cell-based methods are also available, and these include parallel artificial permeability assay (PAMPA) [8] and separation methods like high-performance liquid chromatography and capillary electrophoresis [9,10]. Nevertheless, PAMPA lacks in reproducing active influx and/or efflux transport mechanisms and some metabolic transformations, while separation methods, relying on the adjusted relationship between their output results and BBB permeation, may well be considered as predictive methods [11]. An index of BBB permeability is represented by the logBB ($\log K_{p,brain}$), the logarithm of the ratio of the concentration of a drug in the brain and in the blood measured at the steady state:

$$\log BB = \log \frac{C_{brain}}{C_{blood}}$$

Lately, there has been a growing acceptance that just the unbound portion of the total drug ($K_{p,uu,brain}$), is free to diffuse across biological barriers and tissues, thus governing, more significantly than logBB, the overall BBB permeation and CNS drug activity [12]. However, at the state of the art, the output results of both methods are employed and beneficial for understanding the magnitude of BBB permeation and to some extent the CNS active dose [13–20]. Over the years, a number of researchers has developed methods to define the properties for a successful BBB permeation, using different starting data sets that inevitably led to different conclusions [21]. Selected studies have considered population distribution or variation in minimum, maximum, and mean of certain parameters of CNS and non-CNS compounds. Other studies are based on more complex algorithms or quantitative structure-property relationship analysis [22]. In 2012, Ghose et al. reported the plain distribution of a number of physicochemical properties and chemical structural profiles of 626 non-CNS and 317 CNS oral marketed drugs [23]. Using a restricted set of six physicochemical parameters, Wager et al.

realized an algorithm to optimize the druglike properties of CNS candidates [24,25]. Based on a structure-property analysis derived from multiple ADMET assays, Gleeson has identified molecular weight and logP as important parameters in determining CNS penetration [26]. In a study conducted by Mahar Doan et al., the in vitro permeability and P-gp mediated efflux have been evaluated for 93 structurally diverse marketed CNS and non-CNS drugs [27]. Similarly, Desai et al. developed an in silico tool based on a P-gp substrate assay on over 2000 compounds [28]. All these are excellent examples of studies conducted with the aim to better understand and classify the properties required for a drug to better accumulate in the CNS, always providing new understanding and hints.

In the present work, we were interested in defining a simple set of rules that would prospectively be used for the design or identification of compounds able or not to cross the BBB. In our analysis, a number of marketed drugs and organic compounds of general interest having experimental in vivo BBB permeation data, expressed as logBB, value were included. For each compound a series of computed descriptors has been calculated in order to observe which of them significantly influences the BBB permeation. For this purpose, 2×5 contingency tables were constructed for each descriptor, considering five descriptor domains or range of values with respect to two populations of compounds, BBB permeable (BBB^+) and BBB not-permeable (BBB^-). Observed and expected distributions were calculated, and percent deviations were measured. Conditional probabilities, fold enrichments, and a chi-square (χ^2) contingency table test with Yates correction were performed to evaluate the statistical significance of the χ^2 distribution [29]. The output of these contingency tables together with the χ^2 statistic provided evidence of a significant association or dependence of certain physicochemical properties evaluated, while it excluded others such as the molecular weight (MW). In other words, BBB^+ and BBB^- compounds show variation in the population distribution for some of the descriptors and there are significant differences between expected and observed populations.

RESULTS AND DISCUSSION

For the construction of the data set, we combined different scholarly journal published data sets. The literature was scanned and articles were selected whether they contained information over chemical compounds ability in crossing the BBB expressed as logBB. The first collection consisted of 415 compounds from Li et al. [30], 380 compounds from Muehlbacher et al. [31], 57 compounds from Liu et al. [32], and 207 compounds from Abraham et al. [33] for a total of 1059 compounds. However, several compounds were reported multiple times, even within the same article, with similar or identical logBB values. Duplicates were removed, a match between reported SMILES, nomenclature, and depicted structures was performed, and erroneous information was corrected. Argon, krypton, neon, thoron, and xenon have been removed from the data set together with nitrous oxide, carbon disulfide, nitrogen, water, methane, and sulfur hexafluoride [31]. Vinblastine, Cyclosporin A, Cefotetan, and Bromocriptine were removed as well, since their descriptors were widely outside range. Fifteen isomers have also been identified and one of the couple removed. Geometrical isomers and tautomers (e.g., clonidine, didanosine) were also checked, and one was removed from the set. For the latest cases in the event that compounds had different logBB values, an average has been considered. For compounds whose logBB was taken multiple times, the one maintained in the data set was the most recently published. After this first round, we ended up with 559 unique compounds. From this set, we wanted to select only those compounds for which an experimental in vivo logBB value has been reported.

For the determination of in vivo experimental logBB, mice are administered with a subcutaneous dose of drug and, after the reach of equilibrium, the drug concentration is measured in the brain and in the blood using a chromatographic method. In some cases, radiolabeled chemical compounds are administered and the radioactivity in the brain or blood is measured with a liquid scintillation counter. Therefore, from this data set, we did not consider those molecules for which logBB values have not been given, determined with in vitro procedures or for which the predicted value was reported [30, 33, 34]. These efforts led to a data set of 342 compounds. From this set, we also wanted to exclude known substrates of P-gp, one of the major transport systems acting at the BBB. Indeed, P-gp substrates, generally lipophilic xenobiotics, can cross cell membranes but are immediately pumped back into the cerebral blood by P-gp. Therefore, searching for substrates of P-gp within our data set, we decided to exclude known substrates of P-gp, obtaining a final data set of 328 compounds [35–44]. These 328 compounds present experimental logBB values, calculated with the chromatographic or scintillation methods, ranging from -2.15 to $+1.64$ (logBB mean $+0.04$), with 182 logBB values positive or equal to zero and 146 negative (Table S1). For each compound a series of descriptors was computed with JChem for excel provided by ChemAxon (17.4.300.1589). A total of 15 descriptors have been computed, including logP, logD[pH7.4] (logD), polar surface area (PSA), atom count (AC), heavy atom count (HAC), molecular weight (MW), rotatable bond count (RBC), hydrogen bond acceptors (HBA), hydrogen bond donors (HBD), ring count (RC), ionization state (IS), nitrogen count (NC), oxygen count (OC), nitrogen and oxygen count (NOC), and molar refractivity (MR). The data set was split into BBB permeable (BBB⁺, logBB > 0.0, BB ratio >1.0) and BBB nonpermeable (BBB⁻, logBB < 0.0, BB ratio <1.0). This let to separate compounds based on their higher accumulation inside or outside the CNS. Compounds tagged as BBB⁺ were 174, compounds with BB ratio equal to 1, thus excluded, were 8, while compounds with BBB⁻ features were 146 for a total of 328 compounds. We decided to bin descriptors in five groups which gave a large enough sample to provide a statistically valid analysis as reported in Table 1.

Table 1. Descriptor Ranges.

Descriptor Range				
logP<0	0≤logP<1.5	1.5≤logP<3.0	3.0≤logP<4.5	logP≥4.5
logD<0	0≤logD<1.5	1.5≤logD<3.0	3.0≤logD<4.5	logD≥4.5
0<PSA<25	25≤PSA<50	50≤PSA<75	75≤PSA<100	PSA≥100
AC<15	15≤AC<25	25≤AC<35	35≤AC<45	AC≥45
HAC<7	7≤HAC<14	14≤HAC<21	21≤HAC<28	HAC≥28
MW<100	100≤MW<200	200≤MW<300	300≤MW<400	MW≥400
RBC<1	1≤RBC≤2	3≤RBC≤4	5≤RBC≤6	RBC≥7
HBA=0	HBA=1	HBA=2	HBA=3	HBA≥4
HBD=0	HBD=1	HBD=2	HBD=3	HBD≥4
RC=0	RC=1	RC=2	RC=3	RC≥4
IS=Neutral Apolar	IS=Neutral Polar	IS=Acid	IS=Basic	
NC=0	NC=1	NC=2	NC=3	NC≥4
OC=0	OC=1	OC=2	OC=3	OC≥4
NOC<1	NOC=2	NOC=3	NOC=4	NOC≥5
MR<30	30≤MR<60	60≤MR<90	90≤MR<120	MR≥120

The IS was split in four groups that correspond to apolar neutral, polar neutral, acid, and basic compounds. Two zwitterions have been found in the set, and these have been included in the polar neutral group since as a unique group was too small. Maximum, minimum, and mean of the values for the selected descriptors are reported in Table S2. At this stage, for each descriptor, a 2×5 contingency table with four degrees of freedom was constructed, observed and expected distributions in the ranges were calculated, and percent deviations were measured. Conditional probabilities and fold enrichments were thus calculated, and a χ^2 contingency table test with Yates correction was performed to evaluate the statistical significance of the χ^2 distribution. The enrichment of a contingency table was considered significant when its χ^2 test p value was <0.01 .

Descriptors scored by enrichment and their respective p values are reported in Table 2. Over 15 descriptors, 6 resulted in being not significant; that means their distribution within the five descriptor ranges and the two BBB groups (BBB⁺ and BBB⁻) does not show significant variation. In other words, compounds having BBB⁺ and BBB⁻ features share similar distribution for these six descriptors and there are no significant differences between expected and observed populations.

Table 2. Descriptors scored by enrichment and statistical significance.

Descriptor	Chi-Squared Test	p value	p
PSA	66.79	1.08×10^{-13}	<0.01
NOC	51.17	2.06×10^{-10}	<0.01
logP	47.38	1.27×10^{-9}	<0.01
NC	38.29	9.77×10^{-8}	<0.01
logD	36.80	1.98×10^{-7}	<0.01
OC	35.83	3.13×10^{-7}	<0.01
IS	33.02	3.19×10^{-7}	<0.01
HBA	30.80	3.36×10^{-6}	<0.01
HBD	29.29	6.81×10^{-6}	<0.01
MW	11.18	2.46×10^{-2}	-
RC	6.61	1.58×10^{-1}	-
MR	6.01	1.99×10^{-1}	-
HAC	5.68	2.24×10^{-1}	-
AC	5.48	2.42×10^{-1}	-
RBC	4.05	4.00×10^{-1}	-

AC ($\chi^2 = 5.48$; $p = 2.42 \times 10^{-1}$) and HAC ($\chi^2 = 5.68$, $p = 2.24 \times 10^{-1}$) are descriptors whose χ^2 distribution between the BBB⁺ and BBB⁻ groups has not given significant variation. Within the five ranges evaluated, the observed distribution is similar to the expected distribution and there are no quadrants with enriched distribution (Figures S1 and S2). Other not significant descriptors are RC ($\chi^2 = 6.61$; $p = 1.58 \times 10^{-1}$), RBC ($\chi^2 = 4.05$; $p = 4.00 \times 10^{-1}$), and MR ($\chi^2 = 6.01$; $p = 1.99 \times 10^{-1}$) where a random distribution and a poor enrichment within the quadrants have been observed (Figure S3–5). The whole interpretation is that these descriptors do not significantly affect the BBB permeability by themselves, and it is not necessary to evaluate their influence in defining whether or not a compound permeate the BBB.

MW ($\chi^2 = 11.18$; $p = 2.46 \times 10^{-2}$) has been found to be a nonessential parameter by itself for having a better BBB permeation (Figure 1). Indeed, MW falls in the not-significant group of descriptors; that

means the population within the 10 quadrants does not provide sufficient variation for correlating MW with a BBB⁺/BBB⁻ variation. MW provides a low variation of its fold enrichments that resulted in being not significant according to the χ^2 test. Thus, MW by itself is not a descriptor that could help in designing or defining molecules that better accumulate in the CNS. Overall, the four descriptors here used for describing the mass and size of the molecules, that is, AC, HAC, MW, and MR, work similarly having a not-significant distribution as measured in the four contingency tables and in the performed χ^2 tests. This means that there are no enrichments within the 10 considered quadrants and that observed and expected population distribution is similar. For all the not-significant descriptors, other considered ranges have given similar results (data not shown).

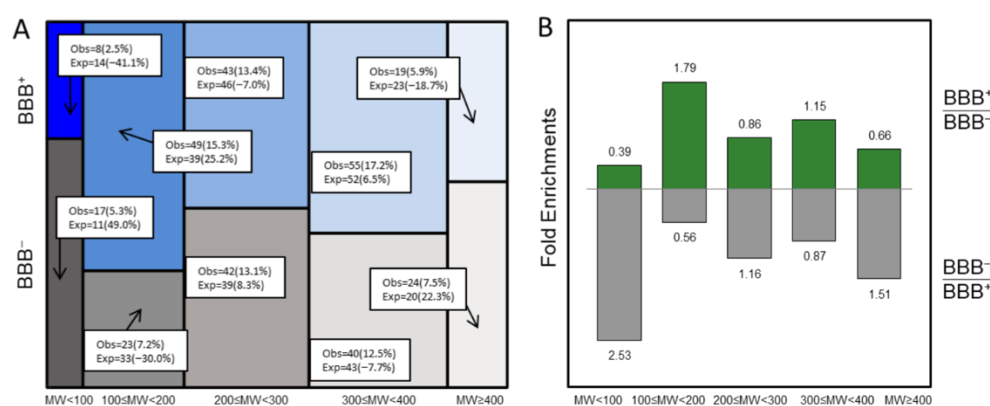


Figure 1. Observed distribution represented as mosaic plot of compounds BBB⁺ (blue) and BBB⁻ (gray) for the MW ranges. White boxes indicate the number of observed (obs) compounds and its relative percent respect the total set and the expected (exp) number of compounds with the percent deviation in parenthesis (Panel A). Fold enrichments for MW (Panel B).

With regard to logP ($\chi^2 = 47.38$, $p = 1.27 \times 10^{-9}$) and logD ($\chi^2 = 36.80$, $p = 1.98 \times 10^{-7}$), significant differences are found with respect to fold enrichment of certain quadrants. Results show that a logP < 1.5 is detrimental for reaching the CNS. Indeed, the population $0 \leq \log P < 1.5$ is composed of 71 compounds and is represented in BBB⁺ by 21 observed versus 39 expected compounds (-45.6% deviation) and in BBB⁻ by 50 observed versus 32 expected compounds (+54.4% deviation). Having a molecule with logP < 0, it points out toward a clear inability of it to properly accumulate inside the CNS since the BBB⁻/BBB⁺ enrichment is 11.92 times [BBB⁺ 2 observed *versus* 12 expected (-83.3% deviation); BBB⁻ 20 observed *versus* 10 expected (+99.3% deviation)]. This trend is inverted for logP values above 1.5, where BBB⁺/BBB⁻ fold enrichment of 1.33, 2.15 and 1.99 has been found for the ranges $1.5 \leq \log P < 3$, $3 \leq \log P < 4.5$, and $\log P \geq 4.5$, respectively (Figure 2). It can be stated that a molecule with logP < 1.5 will probably not cross the BBB; while for logP ≥ 1.5 , there are more chances that the designed molecule will better accumulate within the CNS.

LogD provides similar observations (Figure 2). In particular, the three quadrants BBB⁺/BBB⁻ $1.5 \leq \log D < 3$, BBB⁺/BBB⁻ $3 \leq \log D < 4.5$, and BBB⁺/BBB⁻ $\log D \geq 4.5$ show fold enrichments of 1.80, 1.85, and 6.71, respectively. LogD < 1.5 points out toward a clear reduced ability of molecules to cross the BBB since the BBB⁻/BBB⁺ fold enrichment is 1.71 times with 53 observed compounds in the BBB⁻ (expected 41, +29.1% deviation) *versus* 37 in the BBB⁺ group (expected 49, -24.4% deviation). Similarly to logP, for this descriptor, there is a linear improvement of the fold enrichment moving from low to high logD values with positive BBB⁺/BBB⁻ enrichment for logD ≥ 1.5 .

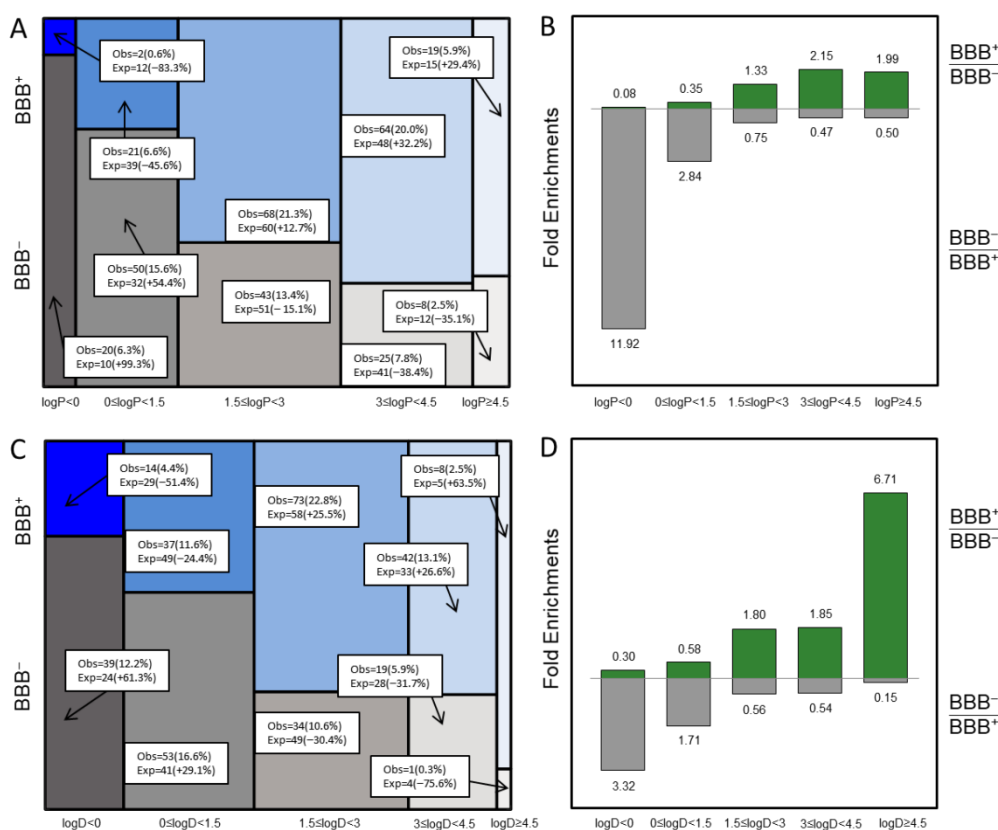


Figure 2. Observed distribution represented as mosaic plot of compounds BBB⁺ (blue) and BBB⁻ (gray) for logP (panel A) and logD (panel C) ranges. White boxes indicate the number of observed (obs) compounds and its relative percent respect the total set and the expected (exp) number of compounds with the percent deviation in parenthesis. Fold enrichments for logP (panel B) and logD (Panel D).

NC ($\chi^2 = 38.29$, $p = 9.77 \times 10^{-8}$) and OC ($\chi^2 = 35.83$, $p = 3.13 \times 10^{-7}$) show important effects on the ability of a molecule to cross the BBB having both descriptors a highly significant distribution within the tables (Figure 3). According to the χ^2 test, NC should be kept between 0 and 1, since at these values the number of BBB⁻ compounds is underrepresented while compounds BBB⁺ are overrepresented. As can be seen in Figure 3, for NC = 0, a BBB⁺/BBB⁻ fold enrichment of 1.50 is found, with 50 observed compounds in the BBB⁺ versus the 42 expected (+17.9% deviation), while in the BBB⁻ group we observe 28 compounds with 36 expected (-21.3% deviation). For NC = 1, a BBB⁺/BBB⁻ fold enrichment of 2.58 is found. We observe 40 compounds in the BBB⁺ set with 29 compounds expected (+38.8% deviation), and 13 compounds in the BBB⁻ group with 24 compounds expected (-46.2% deviation). That means there is a higher probability that a molecule with NC = 0–1 is in the BBB⁺ group. Compounds with NC = 2 show a similar distribution between BBB⁺ and BBB⁻; thus, NC = 2 does not discriminate. For these quadrants, we found a similar observed versus expected distribution [BBB⁺ 55 observed compounds versus 52 expected compounds (+5.4% deviation); BBB⁻ 41 observed compounds versus 44 expected compounds (-6.4% deviation)], and a BBB⁺/BBB⁻ fold enrichment of 1.13 times. At the same time molecules with a higher number of NC (NC = 3) have a higher probability of being in the BBB⁻ group having a BBB⁻/BBB⁺ fold enrichment of 1.31 times. For NC ≥ 4 (BBB⁻/BBB⁺ fold enrichment = 5.56) it was observed a significant deviation of -67.5% for the BBB⁺ group with 28 expected compounds and 9 observed compounds. Conversely the BBB⁻

group is over-represented with a +80.5% deviation having observed 42 compounds in this quadrant against the expected 23 compounds. It can be summarized that a $NC \geq 3$ would result in a compound with a higher probability of being BBB^- . If we reduce NC to 2, the probability of being BBB^+ or BBB^- is similar, while if we set a value below 2 ($NC = 0-1$) there is a higher probability that the molecule would better permeate the BBB.

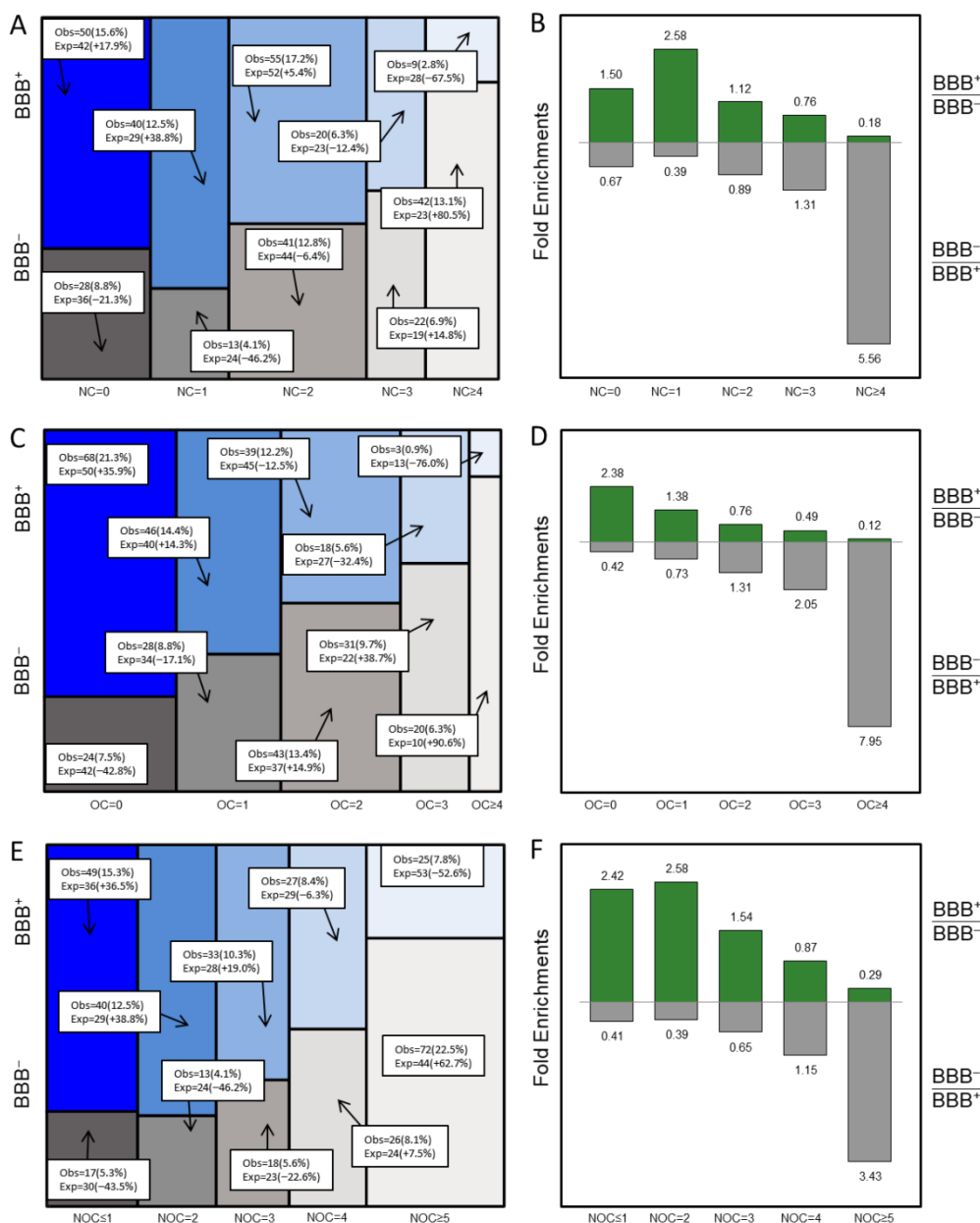


Figure 3. Observed distribution represented as mosaic plot of compounds BBB^+ (blue) and BBB^- (gray) for NC (panel A), OC (panel C), and NOC (panel E) ranges. White boxes indicate the number of observed (obs) compounds and its relative percent respect the total set and the expected (exp) number of compounds with the percent deviation in parenthesis. Fold enrichments for NC (panel B), OC (panel D), and NOC (panel F).

More restrictions are found for the OC having $OC = 0$ $BBB^+/BBB^- = 2.38$ and $OC = 1$ $BBB^+/BBB^- = 1.38$, while $OC = 2$ $BBB^+/BBB^- = 0.76$, $OC = 3$ $BBB^+/BBB^- = 0.49$, and for $OC \geq 4$ $BBB^+/BBB^- = 0.12$ (Figure 3). For $OC = 0$, we observe 68 compounds in BBB^+ versus 50 expected (+35.9%

deviation) and 24 compounds in BBB^- versus 42 expected (-42.8% deviation). For $\text{OC} = 1$, the population is composed by 46 compounds in BBB^+ versus 40 expected (+14.3% deviation) and 28 compounds in BBB^- versus 34 expected (-17.1% deviation). For $\text{OC} = 2$, there are 39 compounds in BBB^+ versus 45 expected (-12.5% deviation) and 43 compounds in BBB^- versus 37 expected (+14.9% deviation). For this last group, while the plain distribution is similar (39 versus 37 observed compounds), according to the contingency table and χ^2 distribution, the probability points out toward compounds mostly accumulated in the BBB^- with fold enrichment $\text{BBB}^-/\text{BBB}^+$ of 1.31 times. If the OC is higher than or equal to 4, we observe 3 compounds in BBB^+ versus 13 expected (-76.0% deviation) and 20 compounds versus 10 expected (+90.6% deviation) in BBB^- .

Based on these results, we were interested in evaluating the optimal nitrogen and oxygen count (NOC). To accomplish this, we summed NC and OC , built a contingency table, and performed a χ^2 test. The NOC has been grouped in $\text{NOC} \leq 1$, $\text{NOC} = 2$, $\text{NOC} = 3$, $\text{NOC} = 4$, and $\text{NOC} \geq 5$, which gave a good distribution within the groups (Figure 3). For NOC , an enrichment of 51.17 and a $p = 2.06 \times 10^{-10}$ were found. This parameter provides a wide enrichment and a high level of probability, meaning that, as already anticipated by the NC and OC analysis, this is a descriptor particularly important for the accumulation of a drug in the CNS with high fold enrichments [$\text{NOC} \leq 1$ $\text{BBB}^+/\text{BBB}^- = 2.42$, $\text{NOC} = 2$ $\text{BBB}^+/\text{BBB}^- = 2.58$, $\text{NOC} = 3$ $\text{BBB}^+/\text{BBB}^- = 1.54$, while $\text{NOC} = 4$ $\text{BBB}^+/\text{BBB}^- = 0.87$ and for $\text{NOC} \geq 5$ $\text{BBB}^+/\text{BBB}^- = 0.29$]. The $\text{NOC} \leq 1$ population was composed by 49 compounds in BBB^+ versus 36 expected (+36.5% deviation) and 17 compounds versus 30 expected (-43.5% deviation) in BBB^- . A similar trend is found for $\text{NOC} = 2$ and $\text{NOC} = 3$. In the $\text{NOC} = 4$ range, a similar probability of being BBB^+ and BBB^- was observed. Finally, for $\text{NOC} \geq 5$, we observe 25 compounds versus 53 expected (-52.6% deviation) in BBB^+ and 72 compounds versus 44 expected (+62.7% deviation) in BBB^- . NC and OC should be kept as low as possible in designing new molecules that have to cross the BBB ; it is preferred to keep $\text{NC} \leq 2$ and $\text{OC} \leq 1$. At the same time, NOC should be kept ≤ 3 in order to have an improved accumulation of the compound in the CNS , although for $\text{NOC} = 4$, a similar probability of being BBB^+ and BBB^- was observed.

HBA ($\chi^2 = 30.80$, $p = 3.36 \times 10^{-6}$) and HBD ($\chi^2 = 29.29$, $p = 6.81 \times 10^{-6}$) have been shown to be fundamental for the ability of a molecule to cross the BBB (Figure 4). Fold enrichments clearly show optimal values for BBB^+ at $\text{HBA} \leq 2$ [$\text{HBA} = 0$ ($\text{BBB}^+/\text{BBB}^- = 3.24$), $\text{HBA} = 1$ ($\text{BBB}^+/\text{BBB}^- = 2.04$), and $\text{HBA} = 2$ ($\text{BBB}^+/\text{BBB}^- = 1.31$), while no significant enrichment is observed for $\text{HBA} = 3$ ($\text{BBB}^+/\text{BBB}^- = 0.94$). For $\text{HBA} \geq 4$, the discrimination between BBB^+ and BBB^- is marked. Indeed, a $\text{BBB}^+/\text{BBB}^-$ fold enrichment of 0.40 was observed, meaning that molecules in this range have a high probability to not cross the BBB .

A different trend is found for HBD (Figure 4). Regarding this parameter, in order to have an optimal $\text{BBB}^+/\text{BBB}^-$, the selection of the number of donor atom is limited. Indeed, just for $\text{HBD} = 0$, the molecule properly accumulates inside the CNS having a $\text{BBB}^+/\text{BBB}^-$ of 1.88. For $\text{HBD} = 1$, the distribution is neutral with a $\text{BBB}^+/\text{BBB}^-$ fold enrichment of 1.13, while once the HBD is brought to a value of 2 the probability of a molecule to not cross the BBB is higher with the ratio of $\text{BBB}^+/\text{BBB}^-$ being equal to 0.48. While $\text{HBD} \geq 3$ clearly points toward molecules that are not able to cross the BBB with a $\text{BBB}^-/\text{BBB}^+$ fold enrichment of 5.36 for $\text{HBD} = 3$ and 10.73 for $\text{HBD} \geq 4$. Overall, for these two descriptors, while there is some space with HBA being a count of two not detrimental for the ability of a molecule to cross the BBB , the HBD must be kept ≤ 1 in order to have a molecule that cross the BBB otherwise the probability for it to do not cross is high.

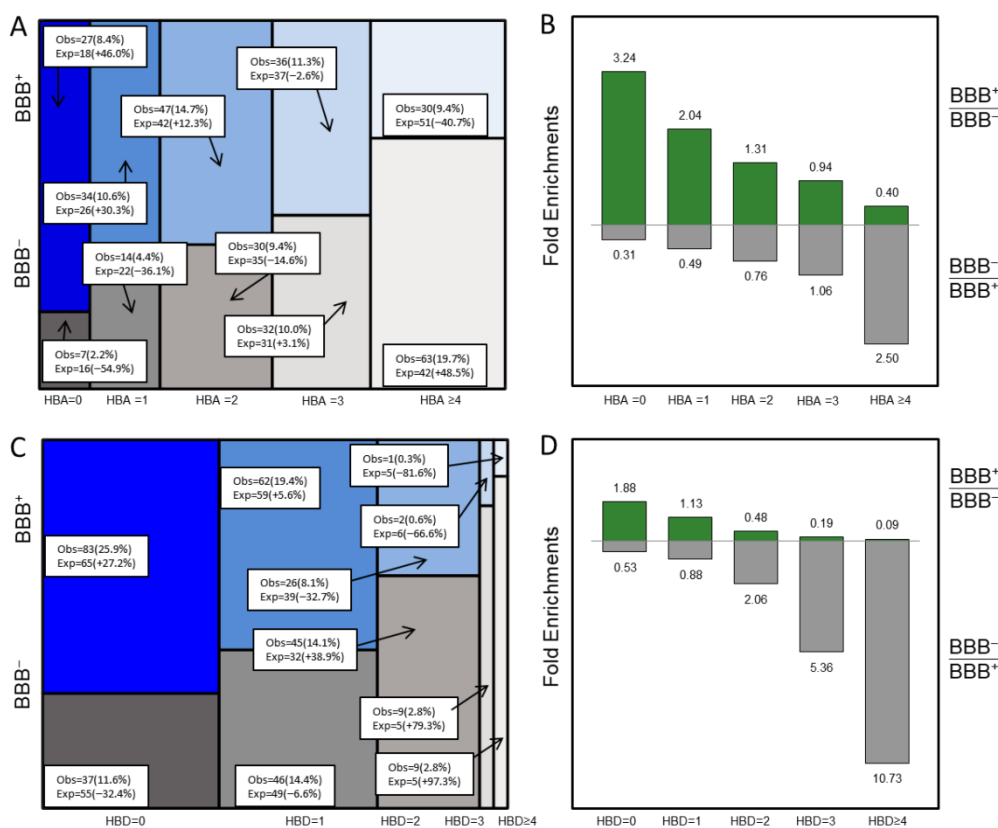


Figure 4. Observed distribution represented as mosaic plot of compounds BBB^+ (blue) and BBB^- (gray) for HBA (panel A) and HBD (panel C) ranges. White boxes indicate the number of observed (obs) compounds and its relative percent respect the total set and the expected (exp) number of compounds with the percent deviation in parenthesis. Fold enrichments for HBA (panel B) and HBD (Panel D).

The IS ($\chi^2 = 33.02$; $p = 3.19 \times 10^{-7}$) has shown significant variation within the eight quadrants considered; that means that the IS is an essential parameter in determining compounds able to cross the BBB (Figure 5). Compounds have been binned in four groups, and of these the neutral apolar and basic compounds have been shown to be over-represented in the BBB^+ group [apolar neutral 42 compounds observed in BBB^+ versus 30 expected (+37.9% deviation) and 14 compounds observed in BBB^- versus 26 expected (-45.2% deviation); basic 88 compounds observed in BBB^+ versus 76 expected (+15.6% deviation) and 52 compounds observed in BBB^- versus 64 expected (-18.6% deviation)]. At the same time, acid and neutral polar compounds that also include two zwitterions have been shown to be more enriched in the BBB^- group with a BBB^-/BBB^+ fold enrichment of 1.86 for neutral polar and 15.49 for acid compounds. For example, an observed acid compound in the BBB^+ is 1 versus 8 expected (-86.9% deviation), while observed acid compounds in the BBB^- are 13 versus 6 expected (+103.5% deviation). This descriptor provided high variation within the eight subgroups and thus it is recommended to consider neutral polar and acid compounds as having lower probability of crossing the BBB with respect to basic and neutral apolar compounds that show higher probabilities to permeate the BBB.

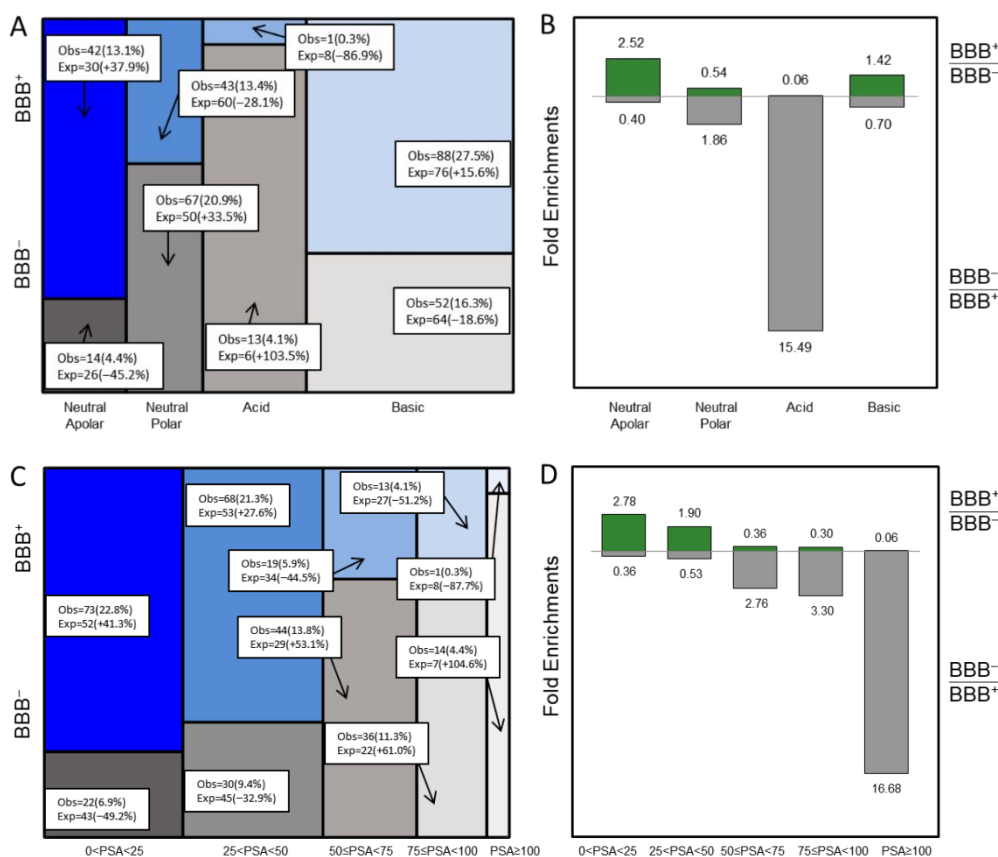


Figure 5. Observed distribution represented as mosaic plot of compounds BBB⁺ (blue) and BBB⁻ (gray) for IS (panel A) and PSA (panel C) ranges. White boxes indicate the number of observed (obs) compounds and its relative percent respect the total set and the expected (exp) number of compounds with the percent deviation in parenthesis. Fold enrichments for IS (panel B) and PSA (Panel D).

Finally, PSA (Figure 5) has proved to be the most significant descriptor within the series with $\chi^2 = 66.79$ and $p = 1.08 \times 10^{-13}$. For the quadrant BBB⁺/0 < PSA < 25, a fold enrichment of 2.78 times with respect to BBB⁻/0 < PSA < 30 has been found. For BBB⁺, we observed 73 compounds *versus* 52 expected (+41.3% deviation), while for BBB⁻ 22 compounds were observed against 43 expected (-49.2% deviation). This trend is maintained in the group $25 \leq \text{PSA} < 50$ (BBB⁺/BBB⁻ fold enrichment 1.90), with 68 observed compounds *versus* 53 expected in BBB⁺ (+27.6% deviation) and 30 observed compounds *versus* 45 expected (-32.9% deviation) in BBB⁻.

The tendency is inverted in quadrants representing higher values of PSA ($50 \leq \text{PSA} < 75$; $75 \leq \text{PSA} < 100$; $\text{PSA} \geq 100$), which are total prerogative of molecules that do not cross the BBB. In particular, for $50 \leq \text{PSA} < 75$ over a total population of 63 compounds, 19 are observed in the BBB⁺ *versus* 34 expected (-44.5% deviation) and 44 observed *versus* 29 expected in the BBB⁻ population (+43.1% deviation), as well as a fold enrichment of 2.73 times (BBB⁻/BBB⁺). Similar observation can be summarized for the quadrant $75 \leq \text{PSA} < 100$. The last range, $\text{PSA} \geq 100$, shows a BBB⁻/BBB⁺ fold enrichment of 16.68, with a +104.6% deviation for observed BBB⁻ compounds *versus* a deviation of -87.7% for BBB⁺ compounds. For this descriptor, overall a value below 50 is optimal for improving the probability of reaching a desirable accumulation of the drug inside the CNS. At this stage, we were interested in setting cumulative rules that could prospectively help in the design or to define molecules with higher or lower probability to permeate the BBB. A general summary of the descriptor probabilistic ranges is given in Table 3.

Table 3. Probabilistic scenarios.

Descriptor Range ^a				
logP<0	0≤logP<1.5	1.5≤logP<3.0	3.0≤logP<4.5	logP≥4.5
logD<0	0≤logD<1.5	1.5≤logD<3.0	3.0≤logD<4.5	logD≥4.5
0<PSA<25	25≤PSA<50	50≤PSA<75	75≤PSA<100	PSA≥100
IS=Neutral Apolar	IS=Neutral Polar	IS=Acid	IS=Basic	
HBA=0	HBA=1	HBA=2	HBA=3	HBA≥4
HBD=0	HBD=1	HBD=2	HBD=3	HBD≥4
NC=0	NC=1	NC=2	NC=3	NC≥4
OC=0	OC=1	OC=2	OC=3	OC≥4
NOC<1	NOC=2	NOC=3	NOC=4	NOC≥5

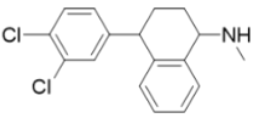
^ared cells indicate BBB⁻ scenario;

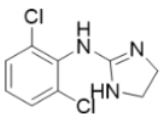
yellow cells indicate BBB⁺/BBB⁻ scenario;

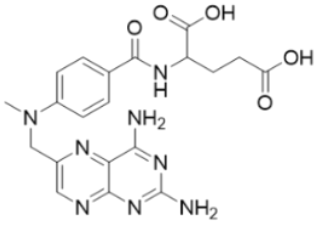
green cells indicate BBB⁺ scenario.

We consider only those descriptors that have shown a significant χ^2 distribution. To this purpose, three different probabilistic scenarios have been identified, BBB⁺, BBB⁺/BBB⁻, and BBB⁻. This classification thus contemplates a scenario, BBB⁺, where there is a higher probability for the molecule of crossing the BBB (BBB⁺/BBB⁻ fold enrichment ≥ 1.33); BBB⁺/BBB⁻, where the probability for the two BBB groups is similar (BBB⁺/BBB⁻ fold enrichment < 1.33 ; BBB⁻/BBB⁺ fold enrichment < 1.33), meaning that compounds having descriptors falling in this range have similar probabilities of being BBB⁺ or BBB⁻; and a BBB⁻ scenario, where the probability of permeating the BBB is low (BBB⁻/BBB⁺ fold enrichment ≥ 1.33). The not-significant computed descriptors may be considered as BBB⁺/BBB⁻. Indeed, for them, the population did not show any statistically significant difference between BBB⁺ and BBB⁻. These descriptors could eventually be taken into consideration although their contribution is limited.

Table 4. Distribution of descriptor values for three representative compounds.







Sertraline				Clonidine				Methotrexate			
logP	logD	PSA	HBA	logP	logD	PSA	HBA	logP	logD	PSA	HBA
5.15	3.02	16.61	1	2.49	1.66	38.03	3	-0.24	-6.56	216.20	12
HBD	NC	OC	NOC	HBD	NC	OC	NOC	HBD	NC	OC	NOC
1	1	0	1	2	3	0	3	5	8	5	13
IS				IS				IS			
Basic				Basic				Acid			
logBB=1.6				logBB=0.11				logBB=-1.51			

As a representative example, sertraline is a compound with good descriptor distribution and with a logBB value of +1.6. Over the nine significant descriptors, sertraline shows eight descriptors in BBB⁺

and one in BBB⁺/BBB⁻. Clonidine, with a logBB value of +0.11, shows six descriptors in BBB⁺, two in BBB⁺/BBB⁻, and one in BBB⁻. Methotrexate has a BBB⁻ distribution for the nine descriptors. Indeed, methotrexate with a logBB value of -1.51 is a compound with very low ability to cross the BBB (Table 4).

CONCLUSION

The purpose of this work was to create a simple set of rules that could prospectively support the development and identification of CNS, non-CNS, or mixed drugs. We statistically analyzed a set of 328 compounds and correlated their logBB with common computed descriptors. The work has contemplated the use of contingency tables and χ^2 distributions for evaluating if there were significant variations in the properties of the BBB⁺ and BBB⁻ populations. Over the computed descriptors, nine were significant for the ability of a molecule to cross the BBB, while six were shown to not influence the BBB permeation. The work has allowed us to define a set of rules that would eventually be used to tune the properties for BBB permeation. We set a three case probabilistic scenario depending on the combination of multiple descriptors. Based on the data analysis, the suggested ranges should be considered as optimal values to be approached with respect to stringent cutoffs that have to be strictly followed. Indeed, the distribution inside and outside the CNS is an equilibrium process resulting from a number of different variables.

METHODS

A 2 × 5 contingency table was constructed, crossing BBB “positive/negative” by the mean of logBB (BBB⁺, logBB >0.0; BBB⁻, logBB <0.0) with a descriptor binned in five ranges (I–V) (Figure 6).

		Descriptor (A ^s)*					
		Range ^I (A ^I)	Range ^{II} (A ^{II})	Range ^{III} (A ^{III})	Range ^{IV} (A ^{IV})	Range ^V (A ^V)	
logBB (A ^r)*	BBB ⁺ (A ⁺) (>cutoff)	BBB ⁺ Range ^I Number of BBB ⁺ compounds with descriptor value in Range ^I (A ^{I+})	BBB ⁺ Range ^{II} Number of BBB ⁺ compounds with descriptor value in Range ^{II} (A ^{II+})	BBB ⁺ Range ^{III} Number of BBB ⁺ compounds with descriptor value in Range ^{III} (A ^{III+})	BBB ⁺ Range ^{IV} Number of BBB ⁺ compounds with descriptor value in Range ^{IV} (A ^{IV+})	BBB ⁺ Range ^V Number of BBB ⁺ compounds with descriptor value in Range ^V (A ^{V+})	$\sum_s A^{s+}$
	BBB ⁻ (A ⁻) (<cutoff)	BBB ⁻ Range ^I Number of BBB ⁻ compounds with descriptor value in Range ^I (A ^{I-})	BBB ⁻ Range ^{II} Number of BBB ⁻ compounds with descriptor value in Range ^{II} (A ^{II-})	BBB ⁻ Range ^{III} Number of BBB ⁻ compounds with descriptor value in Range ^{III} (A ^{III-})	BBB ⁻ Range ^{IV} Number of BBB ⁻ compounds with descriptor value in Range ^{IV} (A ^{IV-})	BBB ⁻ Range ^V Number of BBB ⁻ compounds with descriptor value in Range ^V (A ^{V-})	$\sum_s A^{s-}$
		$\sum_r A^{I+}$	$\sum_r A^{II+}$	$\sum_r A^{III+}$	$\sum_r A^{IV+}$	$\sum_r A^{V+}$	$\sum_{s,r} A^{sr}$

*where s labels the ranges (I–V) and r the BBB groups (BBB⁺ or BBB⁻)

Figure 6. Example of 2×5 contingency table.

From these tables, the expected distribution was calculated for each quadrant as reported below:

$$Expected\ distribution\ (A^{sr}) = \frac{\sum_l A^{sl} \cdot \sum_s A^{sr}}{\sum_{s,r} A^{sr}}$$

where s labels the ranges (I–V) and r represents the BBB groups (BBB⁺ or BBB⁻). Percent deviations between observed and expected distribution were calculated with the following formula:

$$Percent\ Deviation\ (A^{sr}) = \frac{Obs\ A^{(sr)} - Exp\ A^{(sr)}}{Exp\ A^{(sr)}} \cdot 100$$

where s labels the ranges (I–V) and r represents the BBB groups (BBB⁺ or BBB⁻).

Conditional probabilities have been calculated as reported below:

$$pct^{sr} = \frac{A^{sr}}{\sum_{s,r} A^{sr}}$$

where s labels the ranges (I–V) and r the BBB groups (BBB⁺ or BBB⁻).

Finally, 2-fold enrichments were calculated for each descriptor range as ratio of the two conditional probabilities:

$$\left(\frac{BBB^+}{BBB^-}\right) fold\ enrichment^{s+} = \frac{pct^{s+}}{pct^{s-}}$$

$$\left(\frac{BBB^-}{BBB^+}\right) fold\ enrichment^{s-} = \frac{pct^{s-}}{pct^{s+}}$$

where s labels the ranges (I–V).

p Values (χ^2 test) with Yates correction were calculated using R version 3.3.3 (2017-03-06). Mosaic plots have been generated using implemented functions of MATLAB (version R2018b) [45].

REFERENCES

- [1] Gooch, C. L., Pracht, E., and Borenstein, A. R. (2017) The burden of neurological disease in the United States: A summary report and call to action. *Ann. Neurol.* 81, 479–484.
- [2] Achrol, A. S., Rennert, R. C., Anders, C., Soffiotti, R., Ahluwalia, M. S., Nayak, L., Peters, S., Arvold, N. D., Harsh, G. R., Steeg, P. S., and Chang, S. D. (2019) Brain metastases. *Nat. Rev. Dis. Primers* 5, 5.
- [3] Di, L., Rong, H., and Feng, B. (2013) Demystifying brain penetration in central nervous system drug discovery. *Miniperspective. J. Med. Chem.* 56, 2–12.
- [4] Hitchcock, S. A., and Pennington, L. D. (2006) Structure-brain exposure relationships. *J. Med. Chem.* 49, 7559–83.
- [5] Kushihara, H., and Sugiyama, Y. (2005) Active efflux across the blood-brain barrier: role of the solute carrier family. *NeuroRx* 2, 73–85.
- [6] Hitchcock, S. A. (2012) Structural modifications that alter the Pglycoprotein efflux properties of compounds. *J. Med. Chem.* 55, 4877–95.
- [7] Cecchelli, R., Berezowski, V., Lundquist, S., Culot, M., Renftel, M., Dehouck, M. P., and Fenart, L. (2007) Modelling of the bloodbrain barrier in drug discovery and development. *Nat. Rev. Drug Discovery* 6, 650–61.
- [8] Mensch, J., Melis, A., Mackie, C., Verreck, G., Brewster, M. E., and Augustijns, P. (2010) Evaluation of various PAMPA models to identify the most discriminating method for the prediction of BBB permeability. *Eur. J. Pharm. Biopharm.* 74, 495–502.
- [9] Ciura, K., and Dziomba, S. (2020) Application of separation methods for in vitro prediction of blood-brain barrier permeability - The state of the art. *J. Pharm. Biomed. Anal.* 177, 112891.
- [10] Espada, A., and Molina-Martin, M. (2012) Capillary electrophoresis and small molecule drug discovery: a perfect match? *Drug Discovery Today* 17, 396–404.
- [11] Naik, P., and Cucullo, L. (2012) In vitro blood-brain barrier models: current and perspective technologies. *J. Pharm. Sci.* 101, 1337–54.
- [12] Reichel, A. Integrated Approach to Optimizing CNS Penetration in Drug Discovery: From the Old to the New Paradigm and Assessment of Drug-Transporter Interactions. In *Drug Delivery to the*

Brain: Physiological Concepts, Methodologies and Approaches; Hammarlund-Udenaes, M., de Lange, E. C. M., and Thorne, R. G., Eds.; Springer New York: New York, 2014; pp 339–374.

[13] Rabal, O., Sánchez-Arias, J. A., Cuadrado-Tejedor, M., de Miguel, I., Pérez-González, M., García-Barroso, C., Ugarte, A., Estella-Hermoso de Mendoza, A., Sáez, E., Espelosin, M., Ursua, S., Haizhong, T., Wei, W., Musheng, X., Garcia-Osta, A., and Oyarzabal, J. (2016) Design, Synthesis, and Biological Evaluation of First-in-Class Dual Acting Histone Deacetylases (HDACs) and Phosphodiesterase 5 (PDE5) Inhibitors for the Treatment of Alzheimer's Disease. *J. Med. Chem.* 59, 8967–9004.

[14] Fiorito, J., Vendome, J., Saeed, F., Staniszewski, A., Zhang, H., Yan, S., Deng, S. X., Arancio, O., and Landry, D. W. (2017) Identification of a Novel 1,2,3,4-Tetrahydrobenzo[b][1,6]-naphthyridine Analogue as a Potent Phosphodiesterase 5 Inhibitor with Improved Aqueous Solubility for the Treatment of Alzheimer's Disease. *J. Med. Chem.* 60, 8858–8875.

[15] Frantz, M. C., Pellissier, L. P., Pflimlin, E., Loison, S., Gandía, J., Marsol, C., Durroux, T., Mouillac, B., Becker, J. A. J., Le Merrer, J., Valencia, C., Villa, P., Bonnet, D., and Hibert, M. (2018) LIT-001, the First Nonpeptide Oxytocin Receptor Agonist that Improves Social Interaction in a Mouse Model of Autism. *J. Med. Chem.* 61, 8670–8692.

[16] Sánchez-Arias, J. A., Rabal, O., Cuadrado-Tejedor, M., de Miguel, I., Pérez-González, M., Ugarte, A., Sáez, E., Espelosin, M., Ursua, S., Haizhong, T., Wei, W., Musheng, X., Garcia-Osta, A., and Oyarzabal, J. (2017) Impact of Scaffold Exploration on Novel Dual-Acting Histone Deacetylases and Phosphodiesterase 5 Inhibitors for the Treatment of Alzheimer's Disease. *ACS Chem. Neurosci.* 8, 638–661.

[17] Han, J., Lee, H. J., Kim, K. Y., Lee, S. J. C., Suh, J. M., Cho, J., Chae, J., and Lim, M. H. (2018) Tuning Structures and Properties for Developing Novel Chemical Tools toward Distinct Pathogenic Elements in Alzheimer's Disease. *ACS Chem. Neurosci.* 9, 800–808.

[18] Rabal, O., Sánchez-Arias, J. A., Cuadrado-Tejedor, M., de Miguel, I., Pérez-González, M., García-Barroso, C., Ugarte, A., Estella-Hermoso de Mendoza, A., Sáez, E., Espelosin, M., Ursua, S., Haizhong, T., Wei, W., Musheng, X., Garcia-Osta, A., and Oyarzabal, J. (2019) Discovery of in Vivo Chemical Probes for Treating Alzheimer's Disease: Dual Phosphodiesterase 5 (PDE5) and Class I Histone Deacetylase Selective Inhibitors. *ACS Chem. Neurosci.* 10, 1765–1782.

[19] Rook, J. M., Abe, M., Cho, H. P., Nance, K. D., Luscombe, V. B., Adams, J. J., Dickerson, J. W., Remke, D. H., Garcia-Barrantes, P. M., Engers, D. W., Engers, J. L., Chang, S., Foster, J. J., Blobaum, A. L., Niswender, C. M., Jones, C. K., Conn, P. J., and Lindsley, C. W. (2017) Diverse Effects on M1 Signaling and Adverse Effect Liability within a Series of M1 Ago-PAMs. *ACS Chem. Neurosci.* 8, 866–883.

[20] Reed, C. W., Yohn, S. E., Washecheck, J. P., Roenfan, H. F., Qitalig, M. C., Luscombe, V. B., Jenkins, M. T., Rodriguez, A. L., Engers, D. W., Blobaum, A. L., Conn, P. J., Niswender, C. M., and Lindsley, C. W. (2019) Discovery of an Orally Bioavailable and Central Nervous System (CNS) Penetrant mGlu7 Negative Allosteric Modulator (NAM) in Vivo Tool Compound: N-(2-(1H-1,2,4-triazol-1-yl)-5-(trifluoromethoxy)phenyl)-4-(cyclopropylmethoxy)-3-methoxybenzamide (VU6012962). *J. Med. Chem.* 62, 1690–1695.

[21] Pajouhesh, H., and Lenz, G. R. (2005) Medicinal chemical properties of successful central nervous system drugs. *NeuroRx* 2, 541–53.

- [22] Fan, Y., Unwalla, R., Denny, R. A., Di, L., Kerns, E. H., Diller, D. J., and Humblet, C. (2010) Insights for predicting blood-brain barrier penetration of CNS targeted molecules using QSPR approaches. *J. Chem. Inf. Model.* 50, 1123–33.
- [23] Ghose, A. K., Herbertz, T., Hudkins, R. L., Dorsey, B. D., and Mallamo, J. P. (2012) Knowledge-Based, Central Nervous System (CNS) Lead Selection and Lead Optimization for CNS Drug Discovery. *ACS Chem. Neurosci.* 3, 50–68.
- [24] Wager, T. T., Hou, X., Verhoest, P. R., and Villalobos, A. (2010) Moving beyond rules: the development of a central nervous system multiparameter optimization (CNS MPO) approach to enable alignment of druglike properties. *ACS Chem. Neurosci.* 1, 435–49.
- [25] Wager, T. T., Hou, X., Verhoest, P. R., and Villalobos, A. (2016) Central Nervous System Multiparameter Optimization Desirability: Application in Drug Discovery. *ACS Chem. Neurosci.* 7, 767–75.
- [26] Gleeson, M. P. (2008) Generation of a set of simple, interpretable ADMET rules of thumb. *J. Med. Chem.* 51, 817–34.
- [27] Mahar Doan, K. M., Humphreys, J. E., Webster, L. O., Wring, S. A., Shampine, L. J., Serabjit-Singh, C. J., Adkison, K. K., and Polli, J. W. (2002) Passive permeability and P-glycoprotein-mediated efflux differentiate central nervous system (CNS) and non-CNS marketed drugs. *J. Pharmacol. Exp. Ther.* 303, 1029–37.
- [28] Desai, P. V., Sawada, G. A., Watson, I. A., and Raub, T. J. (2013) Integration of in silico and in vitro tools for scaffold optimization during drug discovery: predicting P-glycoprotein efflux. *Mol. Pharmaceutics* 10, 1249–61.
- [29] Amata, E., Xi, H., Colmenarejo, G., Gonzalez-Diaz, R., Cordon-Obras, C., Berlanga, M., Manzano, P., Erath, J., Roncal, N. E., Lee, P. J., Leed, S. E., Rodriguez, A., Sciotti, R. J., Navarro, M., and Pollastri, M. P. (2016) Identification of “Preferred” Human Kinase Inhibitors for Sleeping Sickness Lead Discovery. Are Some Kinases Better than Others for Inhibitor Repurposing? *ACS Infect. Dis.* 2, 180–186.
- [30] Li, H., Yap, C. W., Ung, C. Y., Xue, Y., Cao, Z. W., and Chen, Y. Z. (2005) Effect of selection of molecular descriptors on the prediction of blood-brain barrier penetrating and nonpenetrating agents by statistical learning methods. *J. Chem. Inf. Model.* 45, 1376–84.
- [31] Muehlbacher, M., Spitzer, G. M., Liedl, K. R., and Kornhuber, J. (2011) Qualitative prediction of blood-brain barrier permeability on a large and refined dataset. *J. Comput.-Aided Mol. Des.* 25, 1095–106.
- [32] Liu, R., Sun, H., and So, S. S. (2001) Development of quantitative structure-property relationship models for early ADME evaluation in drug discovery. 2. Blood-brain barrier penetration. *J. Chem. Inf. Model.* 41, 1623–32.
- [33] Abraham, M. H., Ibrahim, A., Zhao, Y., and Acree, W. E., Jr. (2006) A data base for partition of volatile organic compounds and drugs from blood/plasma/serum to brain, and an LFER analysis of the data. *J. Pharm. Sci.* 95, 2091–100.
- [34] Crivori, P., Cruciani, G., Carrupt, P. A., and Testa, B. (2000) Predicting blood-brain barrier permeation from three-dimensional molecular structure. *J. Med. Chem.* 43, 2204–16.
- [35] Bendayan, R., Lee, G., and Bendayan, M. (2002) Functional expression and localization of P-glycoprotein at the blood brain barrier. *Microsc. Res. Tech.* 57, 365–80.
- [36] Kim, R. B. (2002) Drugs as P-glycoprotein substrates, inhibitors, and inducers. *Drug Metab. Rev.* 34, 47–54.

- [37] Doran, A., Obach, R. S., Smith, B. J., Hosea, N. A., Becker, S., Callegari, E., Chen, C., Chen, X., Choo, E., Cianfrogna, J., Cox, L. M., Gibbs, J. P., Gibbs, M. A., Hatch, H., Hop, C. E., Kasman, I. N., Laperle, J., Liu, J., Liu, X., Logman, M., Maclin, D., Nedza, F. M., Nelson, F., Olson, E., Rahematpura, S., Raunig, D., Rogers, S., Schmidt, K., Spracklin, D. K., Szewc, M., Troutman, M., Tseng, E., Tu, M., Van Deusen, J. W., Venkatakrisnan, K., Walens, G., Wang, E. Q., Wong, D., Yasgar, A. S., and Zhang, C. (2005) The impact of P-glycoprotein on the disposition of drugs targeted for indications of the central nervous system: evaluation using the MDR1A/1B knockout mouse model. *Drug Metab. Dispos.* 33, 165–74.
- [38] Matsuzaki, J., Yamamoto, C., Miyama, T., Takanaga, H., Matsuo, H., Ishizuka, H., Kawahara, Y., Kuwano, M., Naito, M., Tsuruo, T., and Sawada, Y. (1999) Contribution of P-glycoprotein to bunitrolol efflux across blood-brain barrier. *Biopharm. Drug Dispos.* 20, 85–90.
- [39] El Ela, A. A., Hartter, S., Schmitt, U., Hiemke, C., Spahn-Langguth, H., and Langguth, P. (2004) Identification of P-glycoprotein substrates and inhibitors among psychoactive compounds—implications for pharmacokinetics of selected substrates. *J. Pharm. Pharmacol.* 56, 967–75.
- [40] Park, J., Zhang, Y., Vykhodtseva, N., Jolesz, F. A., and McDannold, N. J. (2012) The kinetics of blood brain barrier permeability and targeted doxorubicin delivery into brain induced by focused ultrasound. *J. Controlled Release* 162, 134–42.
- [41] Edwards, J. E., Alcorn, J., Savolainen, J., Anderson, B. D., and McNamara, P. J. (2005) Role of P-glycoprotein in distribution of nelfinavir across the blood-mammary tissue barrier and blood-brain barrier. *Antimicrob. Agents Chemother.* 49, 1626–8.
- [42] Toornvliet, R., van Berckel, B. N., Luurtsema, G., Lubberink, M., Geldof, A. A., Bosch, T. M., Oerlemans, R., Lammertsma, A. A., and Franssen, E. J. (2006) Effect of age on functional P-glycoprotein in the blood-brain barrier measured by use of (R)-[(11)C]verapamil and positron emission tomography. *Clin. Pharmacol. Ther.* 79, 540–8.
- [43] Kirn, R. B., Wandel, C., Leake, B., Cvetkovic, M., Fromm, M. F., Dempsey, P. J., Roden, M. M., Belas, F., Chaudhary, A. K., Roden, D. M., Wood, A. J., and Wilkinson, G. R. (1999) Interrelationship between substrates and inhibitors of human CYP3A and P-glycoprotein. *Pharm. Res.* 16, 408–14.
- [44] Lobell, M., Molnar, L., and Keseru, G. M. (2003) Recent advances in the prediction of blood-brain partitioning from molecular structure. *J. Pharm. Sci.* 92, 360–70.
- [45] MATLAB; Matrix Laboratory. <http://www.mathworks.com/products/matlab/>.

Design, synthesis and preclinical evaluation of novel sigma receptors ligands

Spirocyclic and diazabicyclo scaffolds have gained increasing interest in the development of bioactive compounds and contribute to a variety of approved drugs and drug candidates, since the introduction of such moieties in a molecule grant peculiar spatial arrangement that may influence important parameters such as potency, selectivity and the physicochemical properties [149-151]. In the effort to identify classes of σ R ligands with high affinity and selectivity, novel ligands have been developed. The general structure is reported in Figure 1, where the central core has been flanked with hydrophobic groups at a certain distance to the central basic amine being this a common structural requirement of potent σ R ligands as identified by previous works.

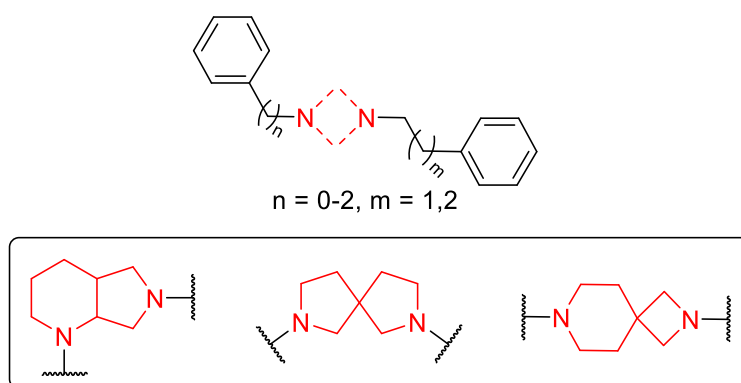


Figure 1. General structure of σ R ligands.

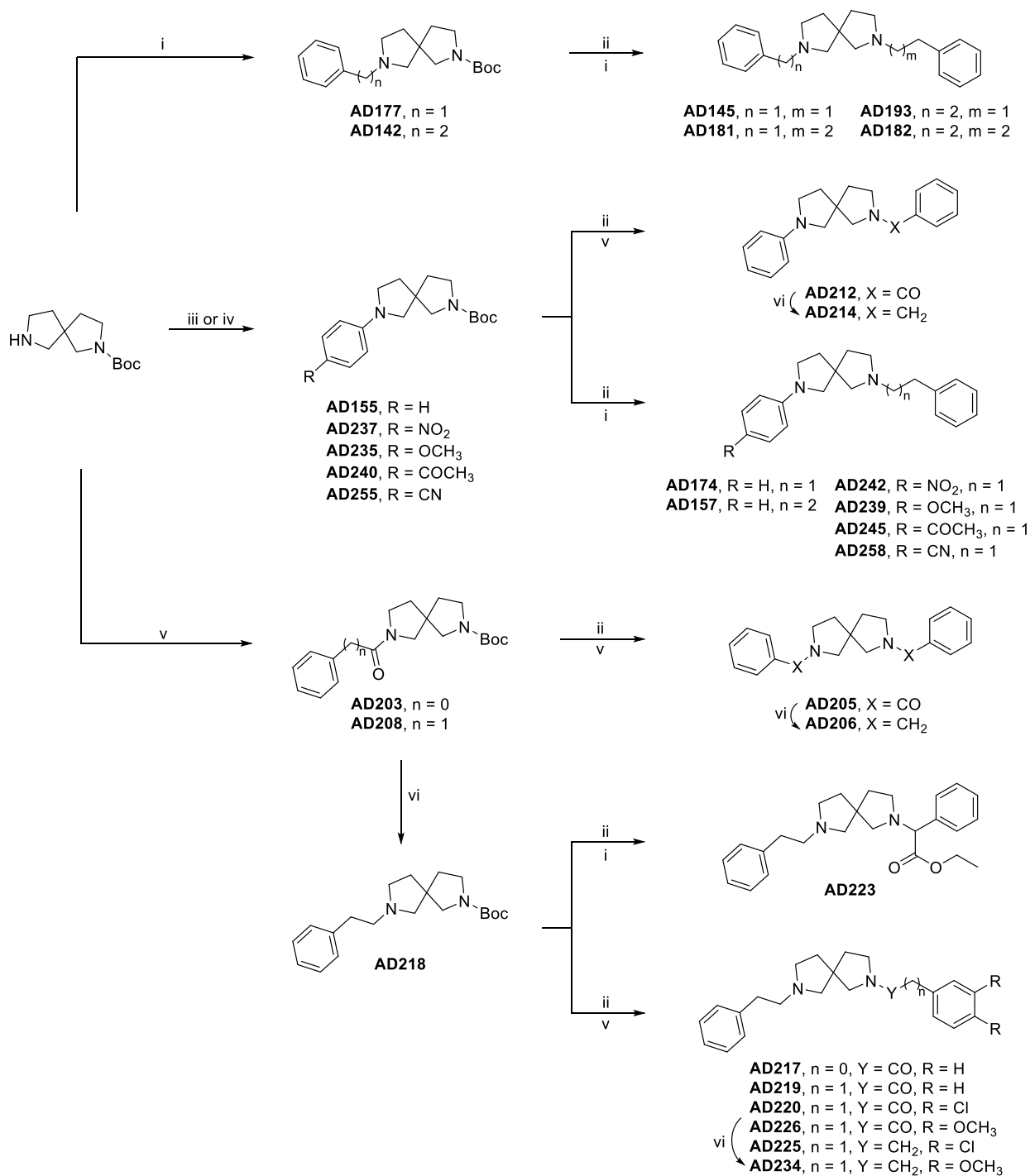
In a first attempt, the focus was on the amino moiety scaffold to understand, by keeping the same substituents, how the affinity and selectivity profile would change over σ Rs. After having understood basic structure-affinity relationships (SAfiR), the focus was moved on the variation of the substituent at only one of the two nitrogen atoms. The affinities for σ_1 R and σ_2 R of the synthesized compounds were determined through radioligand binding assays. Relationships between ligand structure and σ_1 R and σ_2 R affinities as well as σ_1 R/ σ_2 R selectivity are discussed.

SYNTHESIS

The first series of target compounds was synthesized according to the steps illustrated in Scheme 1. Starting from commercially available *tert*-butyl 2,7-diazaspiro[4.4]nonane-2-carboxylate, intermediates **AD177** and **AD142** have been obtained by alkylation with either benzyl bromide or (2-bromoethyl)benzene, respectively. Both intermediates were then deprotected with TFA, followed by alkylation with (2-bromoethyl)benzene or 1-bromo-3-phenylpropane to give the corresponding final compounds **AD145**, **AD181**, **AD193**, and **AD182** (Scheme 1). Intermediates **AD155**, **AD237**, **AD235**, and **AD240** have been obtained via Buchwald–Hartwig amination with appropriate *p*-iodobenzene substituent, whereas compound **AD255** has been synthesized through nucleophilic aromatic substitution with *p*-chlorobenzonitrile. After *N*-Boc deprotection, all the intermediates underwent acylation or alkylation reaction. Intermediate **AD155** was converted into the amide derivative **AD212**, through nucleophilic acyl substitution with benzoyl chloride, which was then reduced to amine **AD214** with LiAlH_4 . Conversely, derivatives **AD237**, **AD235**, **AD240**, and **AD255** have been employed in alkyl substitution reactions to give corresponding final derivatives **AD174**, **AD157**, **AD242**, **AD239**, **AD245** and **AD258**. Intermediates **AD203** and **AD208** have been obtained from reaction with opportune acyl chloride. After *N*-Boc deprotection, **AD203** underwent

nucleophilic acyl substitution with benzoyl chloride to give amide **AD205** which was then reduced to amine **AD206**.

Scheme 1. Synthetic Strategy for the Preparation of Target Compounds.

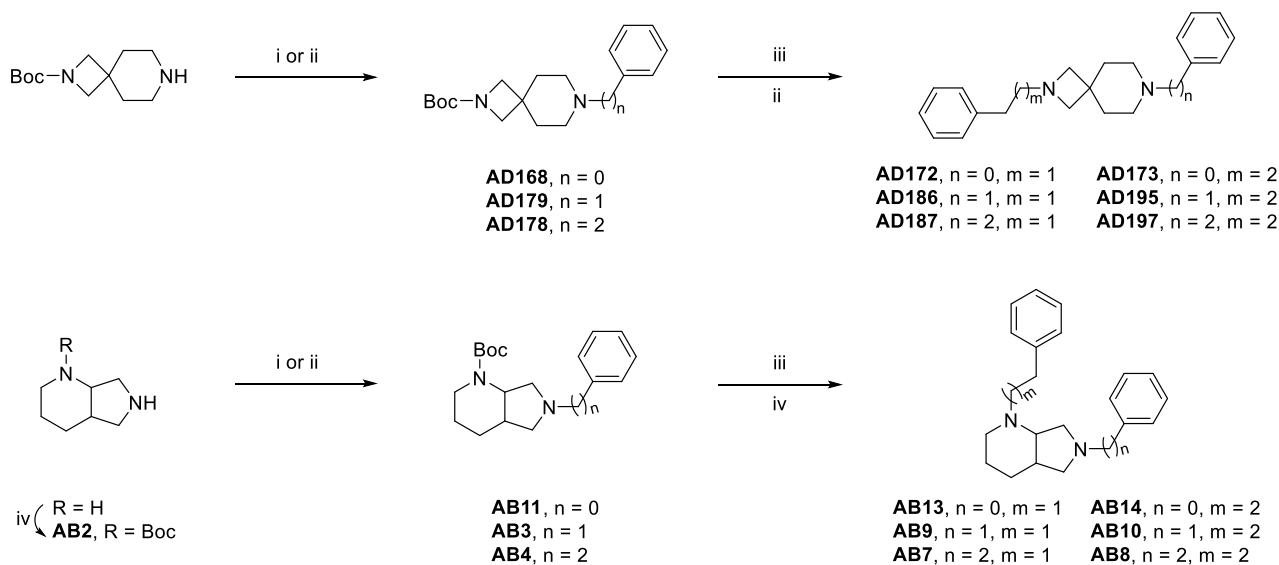


Reagents and conditions: (i) alkyl bromide, K_2CO_3 , ACN, $60\text{ }^\circ\text{C}$, on; (ii) TFA, CH_2Cl_2 , rt, 4h; (iii) *p*-iodobenzene derivative, $Pd_2(dba)_3$, SPhos, *t*-BuOK, toluene, $100\text{ }^\circ\text{C}$, on (iv) *p*-chlorobenzonitrile, K_2CO_3 , DMSO, $120\text{ }^\circ\text{C}$, on; (v) acyl chloride, TEA, CH_2Cl_2 , rt, 2h; (vi) $LiAlH_4$, THF, rt, N_2 .

Following amide group reduction of **AD208**, the corresponding amine derivative **AD218** has been deprotected and used in alkyl substitution to give **AD223**, in acyl substitution to give **AD219**, and in

coupling reactions for obtaining **AD220** and **AD226**. These latter underwent further reduction with LiAlH_4 to give amines **AD225** and **AD234**.

Scheme 2. Synthetic Strategy for the Preparation of Target Compounds.



Reagents and conditions: (i) iodobenzene, $\text{Pd}_2(\text{dba})_3$, SPhos, *t*-BuOK, toluene, 100 °C, on; (ii) alkyl bromide, K_2CO_3 , ACN, 50 °C, on; (iii) TFA, CH_2Cl_2 , rt, 4h; (iv) Boc_2O , CH_2Cl_2 , rt, on.

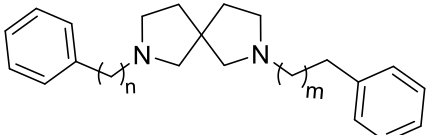
According to the steps illustrated in Scheme 2, intermediates **AD168** and **AB11** have been obtained via Buchwald–Hartwig amination with iodobenzene. For compound **AB11**, the commercially available (*S,S*)-2,8-diazabicyclo[4,3,0]nonane has been previously *N*-protected with Boc anhydride give the amine **AB2**. Alkylation with either benzyl bromide or (2-bromoethyl)benzene of the same starting materials gave intermediates **AD179**, **AD178**, **AB3** and **AB4**. All the intermediates were deprotected with TFA, followed by alkylation with (2-bromoethyl)benzene or 1-bromo-3-phenylpropane to give the corresponding final compounds. The purity of compounds has been evaluated by ^1H and ^{13}C NMR spectroscopy.

AFFINITY EVALUATION

All the 2,7-diazaspiro[4.4]nonane derivatives showed very high $\sigma_1\text{R}$ affinity, with K_i values ranging from 1.8 to 11 nM. Regarding $\sigma_2\text{R}$ affinity, the molecules behaved differently based on substituents (Table 1). In the first three compounds (**AD214**, **AD174** and **AD157**) bearing a plain phenyl ring directly joined to the spirocyclic moiety, therefore having only one nitrogen able to accept a proton and to give ionic interaction with the targets, we observed a 15 times selectivity for $\sigma_1\text{R}$ over $\sigma_2\text{R}$ for compound **AD174**, with $K_i\sigma_1\text{R}$ of 6.5 and $K_i\sigma_2\text{R}$ of 95 nM ($K_i\sigma_2\text{R}/K_i\sigma_1\text{R}=14.6$). The benzyl derivative **AD214** demonstrated a slightly lower affinity at $\sigma_1\text{R}$ and a higher affinity for the $\sigma_2\text{R}$ reducing the gap of affinity respect to **AD174** ($K_i\sigma_1\text{R}$ of 10 and $K_i\sigma_2\text{R}$ of 40 nM; $K_i\sigma_2\text{R}/K_i\sigma_1\text{R}=4$). **AD157**, with a phenpropyl group, shares a similar profile with respect to **AD174** although with a slightly worsening of both affinity and selectivity ($K_i\sigma_1\text{R}$ of 8.6 and $K_i\sigma_2\text{R}$ of 85 nM; $K_i\sigma_2\text{R}/K_i\sigma_1\text{R}=9.9$). The reinstatement of two basic nitrogens given by the substitution with a benzyl group gives the symmetric compound **AD206**, and derivatives **AD145** and **AD193**, with two of them showing higher affinity at $\sigma_1\text{R}$ with respect to **AD174** together with an improvement of the affinity for the $\sigma_2\text{R}$ and a sequential reduction of selectivity. Indeed, compound **AD206** and **AD145** have $K_i\sigma_1\text{R}$ of 1.8 ad 2.5

nM and $K_i\sigma_2R$ of 14 and 20 nM, respectively. For compound **AD193** we have measured similar potency against both receptor subtypes with $K_i\sigma_1R$ of 11 nM and $K_i\sigma_2R$ of 12 nM. The last modification made resulted in the symmetric compound **AD181** and derivative **AD182** bearing a phenethyl group. The elongation to three-carbon chain as in **AD182** has provided a reduction in affinity for both subtypes (**AD181** $K_i\sigma_1R=2.1$ and $K_i\sigma_2R=13$ nM; $K_i\sigma_2R/K_i\sigma_1R=6.2$; **AD182** $K_i\sigma_1R=11$ and $K_i\sigma_2R=18$ nM; $K_i\sigma_2R/K_i\sigma_1R=1.6$). It must be noted that compound **AD193**, having a phenethyl and a benzyl group belongs also to this subset of compounds and it shares a similar profile with respect to **AD182** (**AD193** $K_i\sigma_1R=11$ and $K_i\sigma_2R=12$ nM; $K_i\sigma_2R/K_i\sigma_1R=1.1$).

Table 1. Affinities for 2,7-diazaspiro[4.4]nonane derivatives.



Compound	n	m	K_i (nM) \pm SD ^a		$K_i\sigma_2R/K_i\sigma_1$
			σ_1R	σ_2R	
AD214	0	0	10 \pm 1.4	40 \pm 4.4	4.0
AD174	0	1	6.5 \pm 0.9	95 \pm 9.5	14.6
AD157	0	2	8.6 \pm 1.4	85 \pm 13	9.9
AD206	1	0	1.8 \pm 0.4	14 \pm 1.6	7.8
AD145	1	1	2.5 \pm 0.4	20 \pm 3.1	8.0
AD193	1	2	11 \pm 2.0	12 \pm 2.3	1.1
AD181	2	1	2.1 \pm 0.4	13 \pm 2.2	6.2
AD182	2	2	11 \pm 1.4	18 \pm 3.4	1.6
(+)-Pentazocine			4.3 \pm 0.5	1465 \pm 224	
DTG			124 \pm 19	18 \pm 1	
Haloperidol			2.6 \pm 0.4	77 \pm 18	
BD1063			13.7 \pm 2.7	204 \pm 31	

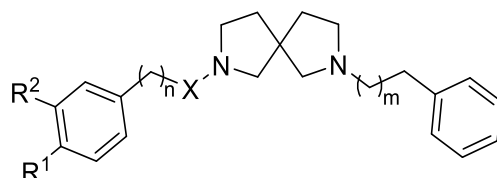
^aEach value is the mean \pm SD of at least two experiments performed in duplicate

Overall, the best compounds in term of σ_1R affinity are those bearing a benzyl or phenethyl substituent on both side of the molecule. Nevertheless, compound **AD174** has emerged to show a high affinity for σ_1R together with a moderate selectivity for the σ_2R .

From this first round, modification of **AD145**, **AD174**, and **AD181** have been designed and developed in order to better understand the influence of nitrogen and of the chain length regarding affinity and selectivity (Table 2). **AD174** derivatives, compounds **AD258**, **AD242**, **AD239**, and **AD245** have been designed to add further binding opportunity with the targets and to dig around selectivity. Compound **AD258**, with a *p*-CN-phenyl group, has shown high affinity for both receptors with K_i values below 4 nM ($K_i\sigma_1R$ of 3.5 nM and $K_i\sigma_2R$ of 2.6 nM). The introduction of a nitro group in the para position has provided an affinity improvement for both σR with $K_i\sigma_1R$ of 0.76 nM and $K_i\sigma_2R$ of 12 nM. Compound **AD242** shows a slightly better selectivity ($K_i\sigma_2R/K_i\sigma_1R=15.8$) if compared with the parent compound **AD174**, but a ten-fold higher affinity for both targets (**AD174** $K_i\sigma_1R=6.5$, $K_i\sigma_2R=95$ nM, $K_i\sigma_2R/K_i\sigma_1R=14.6$). Notably, compound **AD242** is the only compound in the series having affinity

for σ_1R below 1 nM. Compound **AD245** having a *p*-CH₃CO-phenyl group showed a similar $K_i\sigma_1R$ with respect to **AD258** ($K_i\sigma_1R=3$ nM) and a slightly lower affinity for σ_2R ($K_i\sigma_2R=10$ nM). Compound **AD239** bearing a *p*-CH₃O-phenyl group, is the worse binder of the series with K_i for both receptor in the 10 nM range. The modification made have given products with outstanding affinity for σ_1R together with improved affinity for the σ_2R , thus providing compounds with peculiar affinity profile.

Table 2. K_i values over σ_1R and σ_2R for 2,7-diazaspiro[4.4]nonane derivatives.



Compound	R ¹	R ²	X	n	m	K_i (nM) \pm SD ^a		$K_i\sigma_2R/K_i\sigma_1R$
						σ_1R	σ_2R	
AD258	CN	H	-	0	1	3.5 \pm 0.7	2.6 \pm 0.6	0.7
AD242	NO ₂	H	-	0	1	0.76 \pm 0.17	12 \pm 2.9	15.8
AD245	COCH ₃	H	-	0	1	3.0 \pm 0.46	10 \pm 1.7	3.3
AD239	OCH ₃	H	-	0	1	6.2 \pm 1.8	12 \pm 1.2	1.9
AD217	H	H	CO	0	1	209 \pm 18	57 \pm 3.3	0.3
AD223	H	H	CHCOOCH ₂ CH ₃	0	1	63 \pm 8	4.1 \pm 0.4	0.07
AD219	H	H	CO	1	1	79 \pm 3.8	99 \pm 16	1.3
AD220	Cl	Cl	CO	1	1	7.5 \pm 1.0	24 \pm 3.6	3.2
AD225	Cl	Cl	CH ₂	1	1	4.2 \pm 0.8	11 \pm 2.1	2.6
AD226	OCH ₃	OCH ₃	CO	1	1	435 \pm 35	736 \pm 267	1.7
AD234	OCH ₃	OCH ₃	CH ₂	1	1	25 \pm 5.3	23 \pm 3.5	0.9

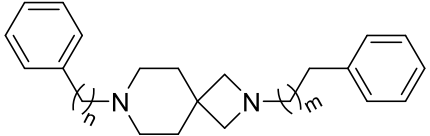
^aEach value is the mean \pm SD of three experiments performed in duplicate.

Variations of **AD145** as in compounds **AD217** and **AD223** determined an inversion of σR profile with preferential affinity for σ_2R as compared to σ_1R . However, the presence of the amide function in compound **AD217** reduces the affinity on both subtypes with K_i values of 209 nM for σ_1R and 57 nM for σ_2R . Unexpectedly, the presence of an ethyl phenylalaninate group as in **AD223** determined a very low nanomolar affinity for σ_2R with K_i of 4.1 nM with respect to σ_1R subtype (K_i 63 nM). Modification of **AD181** with an amide function resulted in **AD219** with reduced affinity on both subtypes similarly to **AD217**. The presence of the chlorine substituents, in position 3 and 4 of the aromatic ring, as in **AD220** takes back to low nanomolar affinity without significant selectivity ($K_i\sigma_1R=7.5$ and $K_i\sigma_2R=24$ nM; $K_i\sigma_2R/K_i\sigma_1R=3.2$). The corresponding amine derivative **AD225** showed an improvement of affinity for both subtypes ($K_i\sigma_1R=4.2$ and $K_i\sigma_2R=11$ nM; $K_i\sigma_2R/K_i\sigma_1R=2.6$). The presence of two methoxy groups as in **AD226** shifted the affinity toward negligible K_i values ($K_i\sigma_1R=435$ and $K_i\sigma_2R=736$). The reduction of the amide function into the corresponding amine derivative **AD234** restored a two-digit nM affinity for both subtypes with K_i values of 25 and 23 nM for σ_1R and σ_2R , respectively.

The 2,7-diazaspiro[3.5]nonane derivatives have revealed a range of different K_i values for σ_1R (Table 3). In particular, compounds containing two basic nitrogen showed low nanomolar K_i for σ_1R with

values of 2.7 and 3.5 nM for **AD186** and **AD187**, respectively, and six to ten times selectivity over σ_2R . **AD172** bearing the phenyl ring directly joined to the nitrogen atom and *N*-phenethyl group on the other side lost affinity over both receptors ($K_i\sigma_1R=28$ and $K_i\sigma_2R=77$ nM, $K_i\sigma_2R/K_i\sigma_1R=2.8$). Similar profile has been shown for compound **AD173** having analogue structure but a three-carbon chain on the basic nitrogen ($K_i\sigma_1R=34$ and $K_i\sigma_2R=51$ nM, $K_i\sigma_2R/K_i\sigma_1R=1.5$). The reinstatement of basic nitrogen as in **AD195** brought back σ_1R affinity to low nanomolar values ($K_i\sigma_1R=7.2$ nM) and four-times selectivity over σ_2R ($K_i\sigma_2R=31$ nM, $K_i\sigma_2R/K_i\sigma_1R=4.3$). Further elongation of carbon chain on both nitrogen atoms as in compound **AD197** determined a decrease of affinity on both subtypes * $K_i\sigma_1R=126$ and $K_i\sigma_2R=149$ nM, $K_i\sigma_2R/K_i\sigma_1R=1.2$).

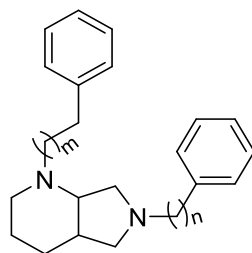
Table 3. Affinities for 2,7-diazaspiro[3.5]nonane derivatives.



Compound	n	m	K_i (nM) \pm SD ^a		$K_i\sigma_2R/K_i\sigma_1R$
			σ_1R	σ_2R	
AD172	0	1	28 \pm 2.0	77 \pm 12	2.8
AD186	1	1	2.7 \pm 0.3	27 \pm 5.3	10
AD187	2	1	3.5 \pm 0.3	22 \pm 2.5	6.3
AD173	0	2	34 \pm 7.7	51 \pm 5.0	1.5
AD195	1	2	7.2 \pm 0.5	31 \pm 5.4	4.3
AD197	2	2	126 \pm 22.3	149 \pm 27	1.2

^aEach value is the mean \pm SD of at least two experiments performed in duplicate.

In the series of octahydro-1*H*-pyrrolo[3,4-*b*]pyridine, all the compounds showed a general loss of affinity on both receptors (Table 4). The only exception is **AB9** with K_i of 10 for σ_1R and more than 15-times of selectivity over σ_2R ($K_i\sigma_2R=165$ nM, $K_i\sigma_2R/K_i\sigma_1R=16.5$). Also **AB10** showed low double-digit $K_i\sigma_1R$ value (19 nM), but reduced selectivity over σ_2R (K_i 126 nM, $K_i\sigma_2R/K_i\sigma_1R=6.6$). **AB13** bearing a *N*-phenethyl substituent and a phenyl ring on the other nitrogen, has a decreased affinity for σ_1R (K_i 505 nM), but an inverted selectivity over σ_2R (K_i 279 nM). The increased σ_2R affinity has also been maintained in compound **AB7** with a K_i value of 114 nM, although the σ_1R affinity (1726 nM) is reduced. Compound **AB14** showed a mixed affinity with respect to both receptor subtypes ($K_i\sigma_1R=108$, $K_i\sigma_2R=91$ nM, $K_i\sigma_2R/K_i\sigma_1R=0.8$). The elongation of the two carbon chains as in **AB8** brought to negligible affinity, although a slightly σ_1R preferential affinity seems to be restored ($K_i\sigma_1R=710$, $K_i\sigma_2R=1026$ nM, $K_i\sigma_2R/K_i\sigma_1R=1.4$).

Table 4. Affinities for octahydro-1*H*-pyrrolo[3,4-*b*]pyridine derivatives.

Compound	n	m	K_i (nM) \pm SD ^a		$K_i\sigma_2R/K_i\sigma_1R$
			σ_1R	σ_2R	
AB13	0	1	505 \pm 88	279 \pm 83	0.6
AB9	1	1	10 \pm 1.6	165 \pm 36.3	16.5
AB7	2	1	1726 \pm 403	114 \pm 15	0.07
AB14	0	2	108 \pm 31	91 \pm 5.8	0.8
AB10	1	2	19 \pm 2.6	126 \pm 19	6.6
AB8	2	2	710 \pm 150.5	1026 \pm 200	1.4

^aEach value is the mean \pm SD of at least two experiments performed in duplicate.

CONCLUSION

Overall, the 2,7-diazaspiro[4.4]nonane moiety has provided compounds with optimal features for the σR recognition allowing to achieve high affinity and a certain selectivity with respect to both receptor subtypes. Three compounds, **AD174**, **AD223**, **AD242** emerged as σ_1R or σ_2R high affinity ligands with selectivity in the 15 times range. In the other hand, compounds **AD258** resulted as a mixed high affinity ligand for both receptor subtypes. Based on these findings, we decided to further investigate the effects of **AD242** and **AD223** in additional in vitro and in vivo models. Particularly, the σ_1R high affinity ligand **AD242** is undergoing evaluation for its σ_1R agonist/antagonist functional profile and efficacy in an in vivo model of capsaicin-induced mechanical hypersensitivity. While the σ_2R high affinity ligand **AD223** is being investigated for its pharmacological effects on the viability of epithelial healthy and malignant cells and for functional profile by modulating intracellular Ca^{2+} levels in human SK-N-SH neuroblastoma cells.

As regard the 2,7-diazaspiro[3.5]nonane and octahydro-1*H*-pyrrolo[3,4-*b*]pyridine series, further SAR studies are in progress in order to complete the series and to define a precise set of SAR.

Discovery, affinity maturation and multimerization of small molecule ligands against human Tyrosinase and Tyrosinase-Related Protein 1

Marco Catalano,^{†a} Gabriele Bassi,^{†a} Giulia Rotondi,^{a,b} Lyna Khettabi,^{c,d} Maria Dichiara,^a Patrizia Murer,^a Jörg Scheuermann,^a Montserrat Soler-Lopez,^c Dario Neri^{*a}

^a Department of Chemistry and Applied Biosciences, Swiss Federal Institute of Technology (ETH Zürich), Vladimir-Prelog-Weg 4, CH-8093 Zürich, Switzerland

^b Dipartimento di Chimica e Tecnologie del Farmaco, Sapienza University of Rome, P.le A. Moro 5, 00185 Rome, Italy

^c Structural Biology Group, European Synchrotron Radiation Facility, 71 Avenue des Martyrs, 38000 Grenoble, France

^d CNRS, DCM, Université Grenoble Alpes, 38000 Grenoble, France

RSC Medicinal Chemistry

Received: September 10, 2020; Accepted: October 28, 2020

ABSTRACT: Human tyrosinase (hTYR) and tyrosinase-related protein 1 (hTYRP1) are closely-related enzymes involved in the synthesis of melanin, which are selectively expressed in melanocytes and, in a pathological context, in melanoma lesions. We used a previously described tyrosinase inhibitor (ThiamidolTM) and DNA-encoded library technology for the discovery of novel hTYR and hTYRP1 ligands, that could be used as vehicles for melanoma targeting. Performing *de novo* selections with DNA-encoded libraries, we discovered novel ligands capable of binding to both hTYR and hTYRP1. More potent ligands were obtained by multimerizing ThiamidolTM moieties, leading to homotetrameric structures that avidly bound to melanoma cells, as revealed by flow cytometry. These findings suggest that melanoma lesions may, in the future, be targeted not only by monoclonal antibody reagents but also by small organic ligands.

*Corresponding Author

Dario Neri (neri@pharma.ethz.ch)

Contributions

M.C. and D.N. designed the project and the experiments. M.S.L. and L.K. provided recombinant human hTYR and hTYRP1. G.B. synthesized GB-DEL library and performed DEL-screening. M.C. and J.S. evaluated HTS data. M.C. and G.B. performed on-DNA synthesis and measurements. M.C., G.R. and M.D. synthesized off-DNA compounds. M.C. and G.R. performed binding and activity assays. M.C., G.R. and P.M. performed FACS analysis. All authors gave approval to the final version of the manuscript.

INTRODUCTION

The majority of conventional cytotoxic agents used for cancer therapy do not preferentially localize to neoplastic lesions [1,2]. This pharmacokinetic limitation contributes to undesired toxicity and prevents dose escalation to therapeutic regimens, that would be needed in order to achieve a durable therapeutic benefit.

One avenue for improving the therapeutic index of chemotherapeutic agents consists in coupling them to monoclonal antibodies, serving as selective delivery vehicles. There has been a substantial interest in the development of antibody-drug conjugates (ADCs) for the therapy of cancer [3–6]. Nine products [MylotargTM, AdcetrisTM, KadcylaTM, BesponsaTM, PolivyTM, PadcevTM, TrodelvyTM, EnhertuTM, BlenrepTM] have gained marketing authorization for the treatment of different types of malignancies and various other ADCs are currently being tested in clinical trials [7,8]. However, the development of ADC products can be problematic, due to high costs-of-goods and to off-target toxicity, which can be severe [9,10]. It is widely recognized that the therapeutic index of ADCs is typically much higher in rodent models of cancer compared to the situation in humans, but the reasons for these discrepancies are still not fully understood [11–13]. The tumor-homing properties of anticancer antibodies are often better in mice compared to patients, which is due (in part) to the fact that highly vascularized and rapidly growing tumors are typically used in the experimental setting [14,15]. Small organic ligands have been proposed as an alternative to antibodies for the delivery of cytotoxics to tumors [16–18]. Small molecule-drug conjugates (SMDCs) can be produced inexpensively and in large quantities. Moreover, a recent comparative analysis of the two platforms has shown that SMDCs may accumulate more efficiently and more homogeneously in tumors compared to ADCs (which are typically confined to the perivascular space) [19,20], since small molecules extravasate more rapidly than antibodies [21,22]. Interestingly, in a side-by-side comparison, ADCs and SMDCs exhibited a comparable performance in mouse models of cancer, even though the tumor uptake of the SMDC products was clearly superior [19].

Until recently, the development of SMDCs has been limited by the availability of small organic ligands, specific to tumor-associated antigens. Folate derivatives, somatostatin analogues, as well as synthetic ligands to prostate-specific membrane antigen (PSMA) and carbonic anhydrase IX (CAIX), represent some of the small ligands, which have been shown to efficiently target tumors both in mouse models of cancer [23–27] and in patients [28–32]. Further developments in the SMDC field will crucially rely on the availability of improved discovery technologies for small organic ligands [16]. DNA-encoded chemical libraries (DELs) are collections of organic molecules, individually coupled to distinctive DNA fragments serving as amplifiable identification barcodes [33,34]. DELs can be conveniently synthesized by split&pool techniques, thus allowing the facile creation of libraries containing millions of compounds [35]. Alternatively, the discovery of small binding peptides has been facilitated by the display on filamentous phage of chemically-modified bicyclic peptides [36,37] or by ribosome display of cyclic peptides, containing unnatural amino acids [38]. The applications of these technologies for SMDC development have recently been reported [39–43].

Human tyrosinase (hTYR) and tyrosinase-related protein 1 (hTYRP1) are closely-related enzymes, which are abundantly expressed in melanosomes and on the surface of melanoma cells [44,45]. They are involved in the biosynthesis of melanin and are detectable in a very limited set of healthy tissues, such as skin, eyes and hairs [46,47]. We hypothesized that ligands specific to hTYR and/or hTYRP1 could be ideally suited for tumor-targeting applications. TA99 is a monoclonal antibody specific to hTYRP1, which has been shown to selectively target melanoma and melanocytes in vivo [48]. We

assumed that a small organic ligand, specific to hTYR or hTYRP1, might represent a valid alternative to TA99 for melanoma targeting applications.

In this article, we explored the possibility to generate hTYR and hTYRP1 ligands, that could be used for the selective recognition of melanoma cells. Our work was inspired by the recent discovery of ThiamidolTM (Beiersdorf AG) as a tyrosinase inhibitor selective for the human version of the enzyme, leading to a product which has been approved for the treatment of irregular pigmentation of the skin [49–52]. We studied whether a chemical modification of ThiamidolTM could be used for the selective delivery of chemical moieties to melanoma cells. We found that oligomerization of ThiamidolTM with dendrimeric scaffolds allowed the generation of novel multivalent ligands, capable of avid binding to melanoma cells. Moreover, we performed DEL selections against immobilized hTYRP1 and hTYR, yielding to novel chemotypes that are selectively enriched against both enzymes.

RESULTS AND DISCUSSION

Binding properties of ThiamidolTM derivatives to hTYR and hTYRP1. The structure of hTYRP1 has been elucidated by X-ray crystallography [53] and has revealed the presence of a catalytic pocket, which could accommodate certain organic ligands, bearing structural analogies to tyrosine, the physiological substrate for melanin biosynthesis [Figure 1a]. Pure preparations of recombinant hTYR and hTYRP1 were used in our studies, as revealed by size-exclusion chromatography and SDS-PAGE analysis [Figure 1b].

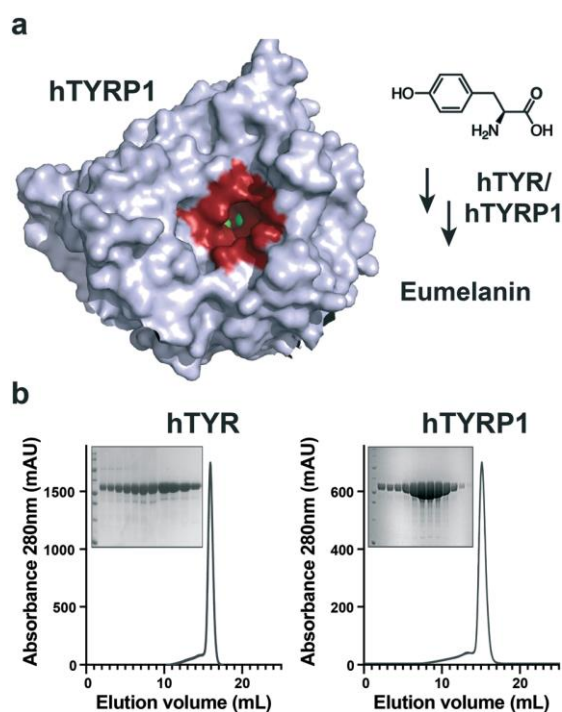


Figure 1. Human tyrosinase (hTYR) and tyrosinase-related protein 1 (hTYRP1) are melanoma associated antigens that present favorable ligandability properties. a) Tyrosine is converted in eumelanin through the interaction with metal ions placed within the active site (depicted in red); b) chromatographic elution profiles of purified intra melanosomal human hTYR and hTYRP1 proteins. In the insets, SDS-PAGE gels showing the purity of the eluted fractions in the peak volume. The first lane contains the MW marker, confirming the expected size of the proteins (PDB: 5M8P).

We synthesized a terminal alkyne derivative of ThiamidolTM, which could be suitable for Cu-catalyzed azide-alkyne cycloaddition (CuAAC) coupling to azide-containing structures [Figure 2]. The inhibitory potency of ThiamidolTM and ThiamidolTM-alkyne was tested against human tyrosinase, using an enzymatic assay based on the production of L-DOPA and its subsequent conversion into a coloured adduct [53,54]. The experimental IC₅₀ values for the two compounds were 2.2 μM and 5.6 μM, respectively [Figure 2]. These values are in keeping with previous measurements, performed on a series of thiazolyl-resorcinol variants [50].

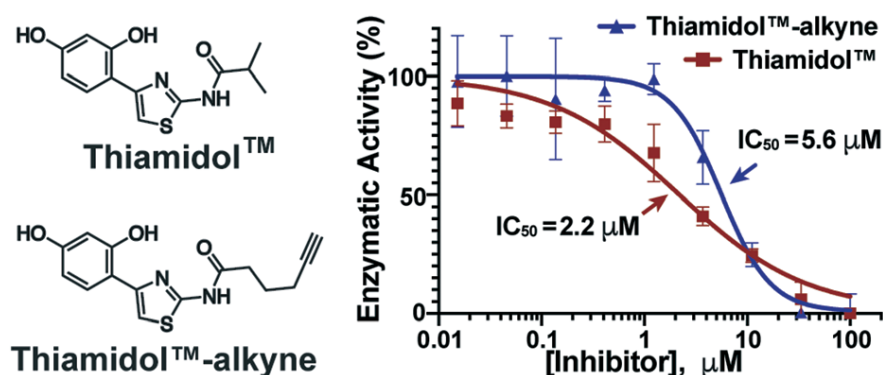


Figure 2. A known hTYR inhibitor (ThiamidolTM) was modified with a derivatizable handle for later modifications. The new ThiamidolTM alkyne derivative retains the inhibitory capacity of the parent compound in presence of human hTYR.

Discovery of novel hTYR and hTYR_{P1} binders from DEL libraries. In order to perform DEL selections against hTYR and hTYR_{P1}, the two enzymes were chemically biotinylated and used in affinity capture procedures on streptavidin-coated magnetic beads. We screened a DEL library recently described by our laboratory (termed GB-DEL) [55], featuring the use of glutamic acid analogues for the combinatorial display of two sets of building blocks [Figure 3a]. The library contained 366'600 encoded compounds.

Decoding of the library after capture on “empty” streptavidin-based supports using high-throughput DNA sequencing [Figure 3b] revealed a homogeneous distribution of compounds, without striking enrichments of individual molecules [55]. By contrast, selections performed on biotinylated hTYR or hTYR_{P1} on streptavidin-coated magnetic beads revealed a characteristic enrichment of “lines” of compounds, which in DEL technology is typically indicative of preferential binding by the corresponding building blocks [Figure 3c,d].

In particular, we observed an enrichment for building blocks A19, A26 and B389, whose structures are depicted in Figure 3e. They all include tri-alkylated amine moieties in the chemical structure, resembling chemical features showed by previously described melanoma-targeting agents [56,57]. The simultaneous selection of these building blocks on both hTYR and hTYR_{P1} may reflect the conservation of the active site of the two enzymes, in spite of the fact that total amino acid sequence homology was only 40% [58]. The compounds were resynthesized as fluorescein conjugates and tested for binding in fluorescence polarization, exhibiting binding potency in the micromolar concentration range [Supplementary Figure S1]. Scarce binding affinities were also detected upon enzymatic assay in the presence of hTYR [Supplementary Figures S2 and S3].

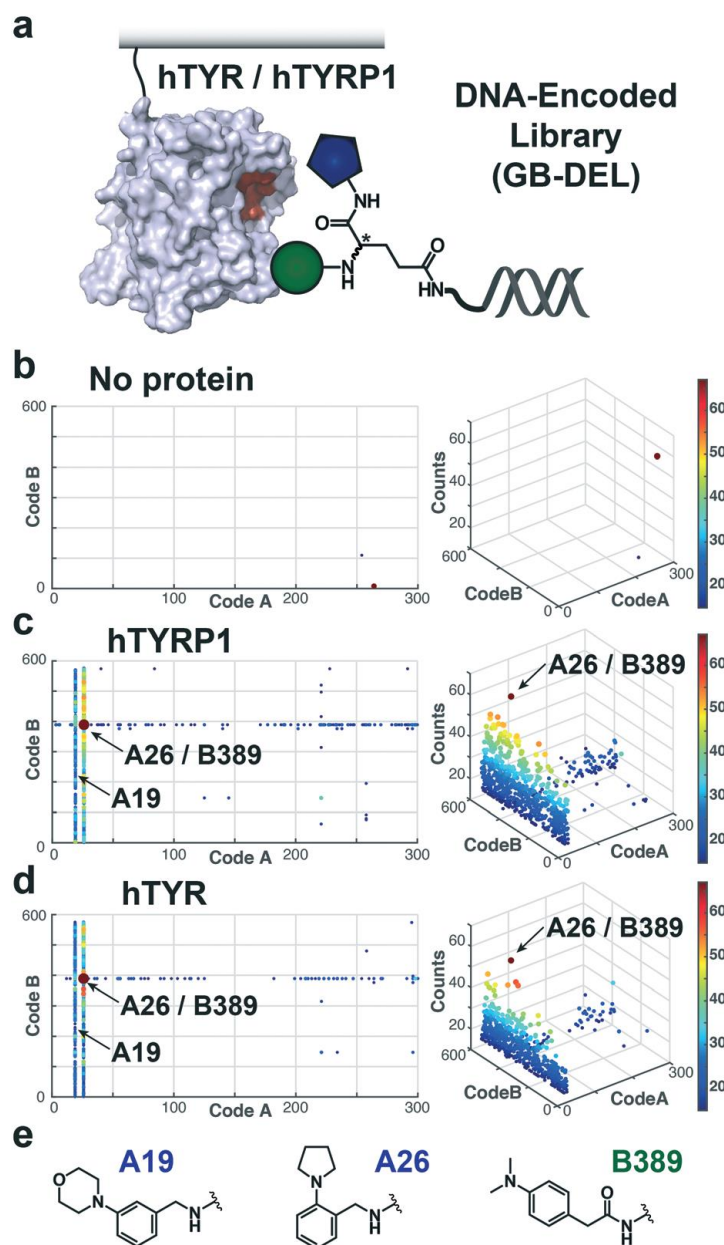


Figure 3. Discovery of novel binding fragments for hTYR and hTYR1 through DNA-encoded library (GB-DEL). a) A single-pharmacophore DEL, based on a racemic glutamic acid scaffold, was screened in presence of immobilized hTYR and hTYR1 proteins; b–d) bi- and tri-dimensional plots of the resulting selections fingerprints after incubation with streptavidin coated beads, hTYR1 and hTYR are reported. Selections against hTYR and hTYR1 displayed A26/B389 as the most enriched combination of building blocks; e) the chemical structures of the enriched fragments are reported, whose binding affinities were evaluated through fluorescence polarization measurements in presence of hTYR1 [Fig. S1†].

We also performed DEL selections in encoded self-assembling chemical (ESAC) library format, pairing the GB-DEL library with a complementary DNA strand, equipped with a Thiamidol™ moiety [Figure 4a]. Also in this case, a characteristic enrichment of lines of compounds was observed, that corresponded to building blocks A221, B147 and B443 [Figure 4b,c]. Bidentate ligands were produced and tested on a fluoresceinated DNA scaffold using previously described procedures

[59–61]. Surprisingly, the combination of Thiamidol™ with A221/B147 and A221/B443 did not substantially improve binding performance in fluorescence polarization studies [Figure 4d].

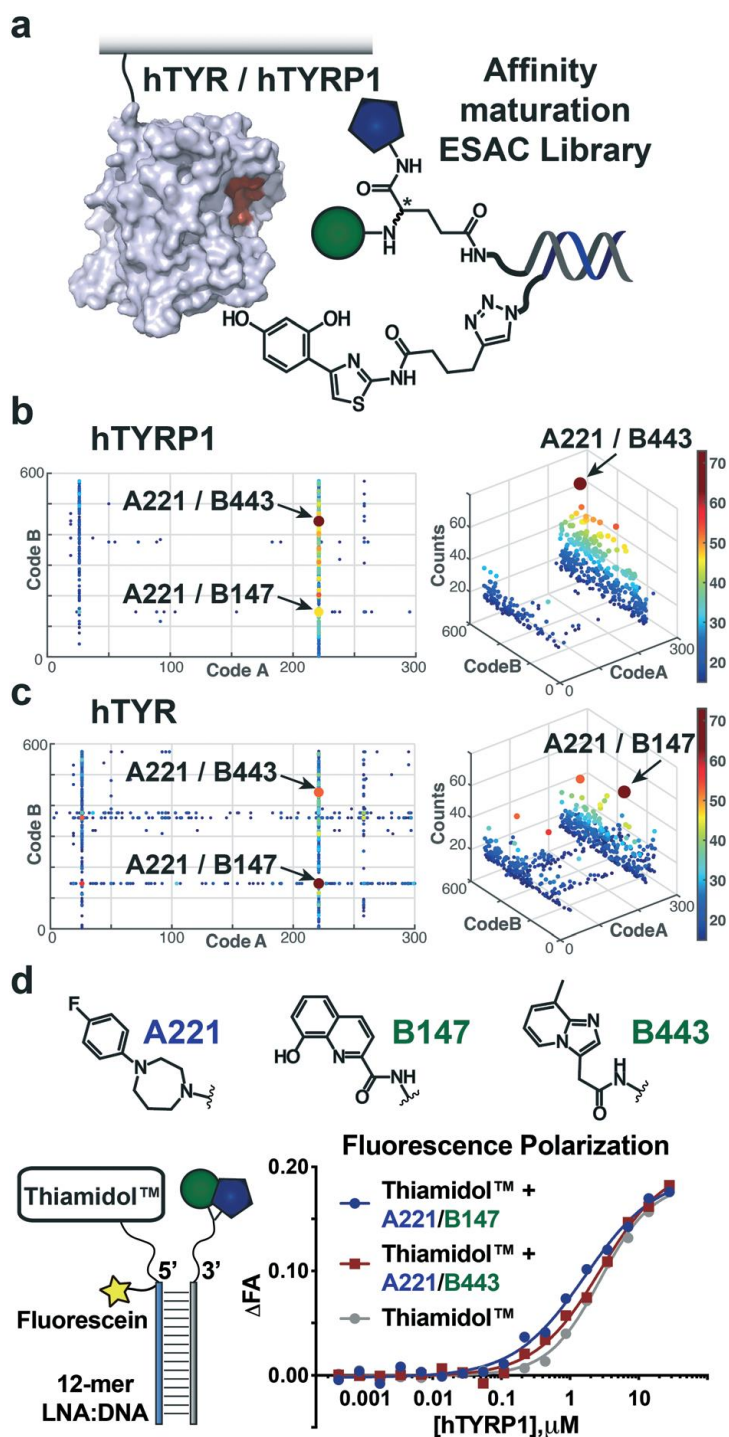


Figure 4. ESAC-based affinity maturation of Thiamidol™ ligand. a) The single-stranded GB-DEL library was paired with a complementary DNA fragment displaying a Thiamidol™ derivative and screened in presence of hTYR and hTYRP1; b and c) decoding plots of the selection experiment delineate fragments particularly enriched upon incubation with hTYRP1 and hTYR; d) DNA-linked fragments were paired to fluoresceinated LNA scaffolds presenting a Thiamidol™ derivative. Binding affinities towards hTYRP1 were measured through fluorescence polarization.

Targeting melanoma cells with oligomeric derivatives of Thiamidol™ Ligands for transmembrane antigens can be constructed on multimeric scaffolds to achieve better targeting performance, by means of avidity. Avid interactions can improve the total affinity of multimeric ligands, yielding to longer residency time on cancer cells and therefore better anticancer outcomes [62,63].

We conjugated the alkyne derivative of Thiamidol™ (Thiamidol™-alkyne) on azide-containing scaffolds, obtaining monomeric, dimeric and tetrameric structures [Figure 5]. The peptidic scaffold included a charged aminoacidic triad (Asp-Arg-Asp) to improve solubility and to confine the ligand in the extracellular space. The terminal cysteine was found particularly convenient, enabling the easy conjugation of Fluorescein-5-Maleimide reagent.

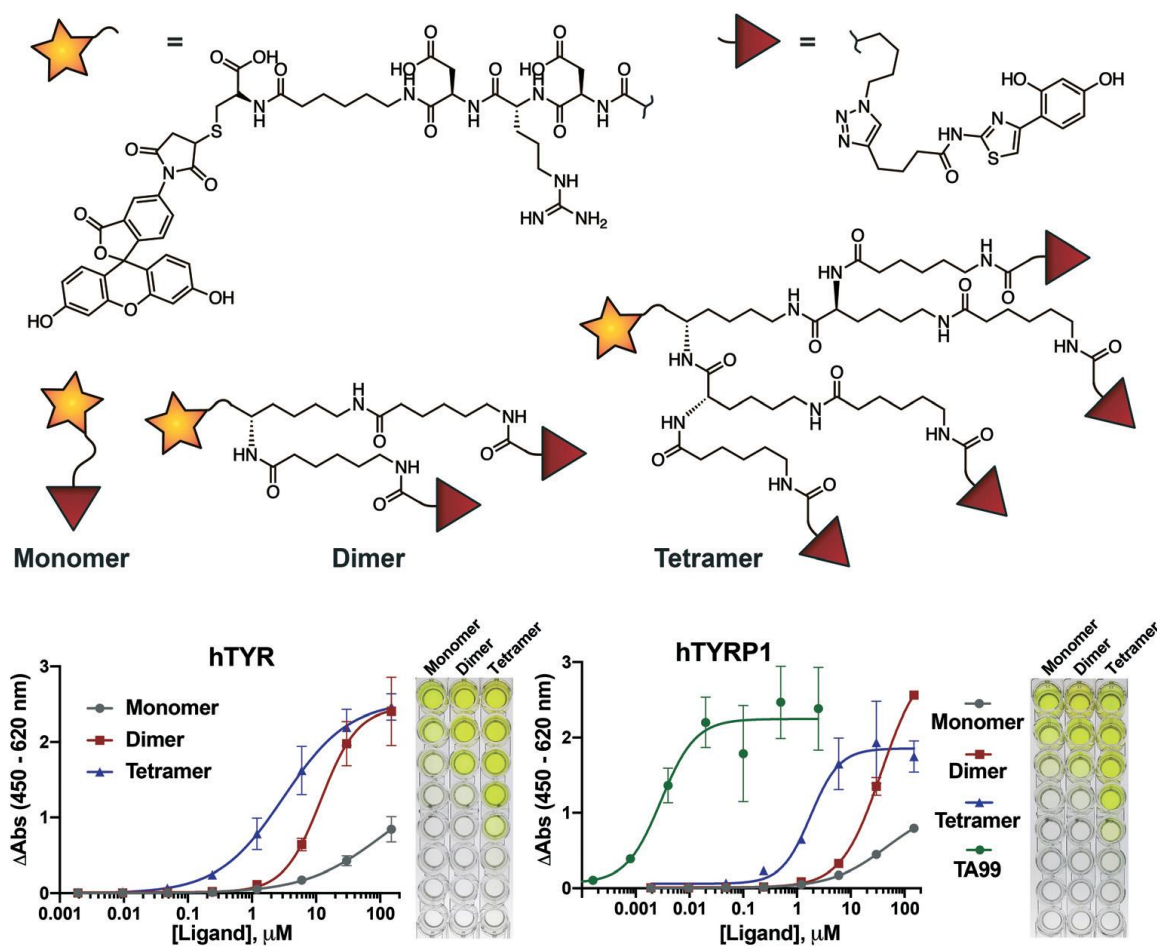


Figure 5. Thiamidol™ alkyne was conjugated to multimeric scaffolds in order to achieve ligands with different binding avidities. The peptidic linker composed by the triad Asp-Arg-Asp was conjugated to fluorescein and to Thiamidol™ derivative through three scaffolds with different valences (i.e., monomeric, dimeric and tetrameric). Binding affinities of monomer, dimer and tetramer were evaluated through ELISA assay on hTYR and hTYRP1 coated microtiter wells.

We measured the affinity in solution of oligomeric Thiamidol™- based ligands using a recently described ELISA assay on hTYR and hTYRP1 coated wells [64]. Both dimeric and tetrameric ligands significantly improved the affinity towards hTYR and hTYRP1, in comparison to an analogue monomeric structure [Figure 5]. The tetrameric structure yielded to the strongest binding interaction with both proteins, reaching single-digit micromolar affinity. However, this affinity is yet ca. 1000-

fold worse/lower than the anti-TYRP1 antibody (TA99), which reacts to both human and murine antigen [65].

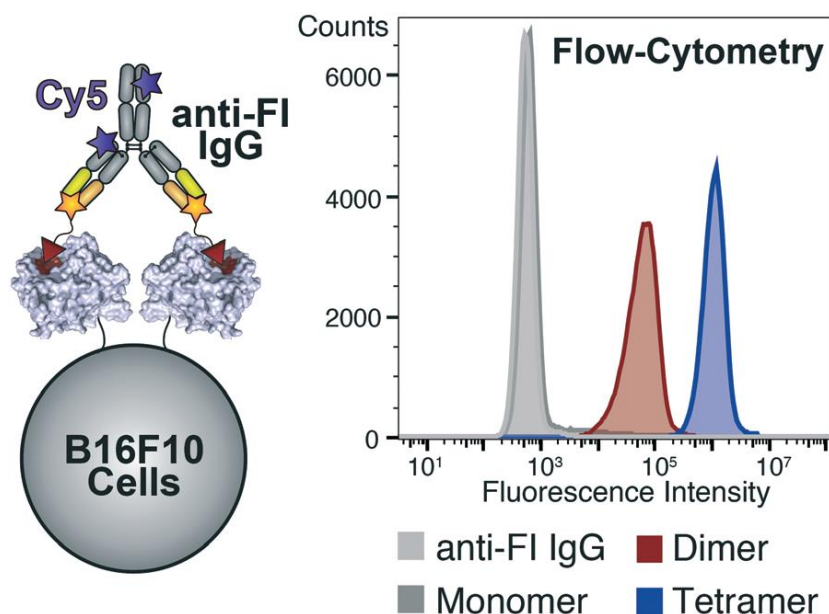


Figure 6. Binding properties of Thiamidol™ based fluorescein-labelled ligands were evaluated in presence of B16F10 melanoma cells. Cells were incubated with a fixed concentration of ligands (1 μ M) and the residual binding was detected by flow-cytometry. An anti-fluorescein antibody labelled with Cy5-dye was employed to enhance signal intensity and reduce autofluorescence background.

We further validated ligands' binding properties in presence of melanoma cells, expressing hTYR and hTYRP1 proteins (i.e., B16F10). Melanoma cells were incubated with fluorescein-labelled ligands, washed from non-binding excess and stained with an anti-fluorescein antibody labelled with Cy5-fluorophore [Figure 6]. The fluorescence signal was detected by flow-cytometry, clearly indicating the Tetramer as the best binding ligand on B16F10 cells compared to the analogue Dimer and Monomer.

DISCUSSION

The development of high affinity small molecule ligands for the human version of tyrosinase and tyrosinase-related protein 1 may result to novel targeting agents for the treatment of melanoma. Here we presented the use of DEL-technology for the discovery of such ligands, yielding to selective enrichment of fragments in the presence of both hTYR and hTYRP1. Additionally, the single-stranded version of a DEL-library (GBDEL) was employed for the affinity maturation of Thiamidol™, obtaining also in this case promising fingerprints. Surprisingly, a significant discrepancy between screening results and binding affinities was detected, highlighting the necessity of DEL-selection experiments that better recapitulate the strength of the molecular interaction with sequence enrichment. We also investigated the use of multimeric Thiamidol™ derivatives to stabilize the binding interaction between the inhibitor and its cognate proteins (hTYR and hTYRP1). Although the tetrameric structure displayed ca. 100-fold affinity enhancement compared to the analogue monomeric ligand, yet the strength of the interaction remains much weaker compared to the one of the TA99 antibody. Furthermore, the conjugation of second moieties to Thiamidol™ resulted in an apparent loss of binding affinity, which may impair further developments of Thiamidol™-based

conjugates. This work represents a starting point for the development of higher affinity organic ligands of hTYR and/or hTYRP1 that can eventually become a novel targeted treatment against melanoma.

CONCLUSION

Collectively, our study suggests that ThiamidolTM derivatives (or more in general hTYR and hTYRP1 binders) may be considered for pharmacodelivery strategies against melanoma. Similar to antibodies, multivalence plays a role in strengthening binding interactions against protein targets, expressed at high density on tumor cells. We anticipate that SMDCs directed against hTYR and/or hTYRP1 may be particularly suited for the treatment of melanoma, as the cognate antigens exhibit an extremely restricted pattern of expression in normal tissues, mainly confined to few melanocyte cells in the skin [47,66]. A radiolabelled derivative of an anti-melanin antibody has previously been proposed for melanoma treatment [67,68] but, to the best of our knowledge, anti-melanoma ADC products have not yet been developed. Intact antibodies to hTYRP1 may be suitable for prevention of metastatic spread [66,69], but are not sufficiently potent for the eradication of established melanoma lesions. The discovery of more potent ligands specific to the human version of tyrosinase and tyrosinase-related protein 1 will be crucially important for the development of efficacious SMDC therapeutics [70].

Conflicts of interest

The authors declare the following competing financial interest(s): D.N. is a cofounder and shareholder of Philochem AG.

Acknowledgements

The authors gratefully acknowledge financial support from ETH Zürich, the Swiss National Science Foundation (Grant Nr. 310030B_182003/1) and European Research Council (ERC) under the European Union's Horizon 2020 research and innovation program (grant agreement 670603). L.K. acknowledges funding support from the IDEX University Grenoble Alpes project (ANR-15-IDEX-02) under grant agreement C7H-ID17-P22-COSMRH

REFERENCES

- [1] A. A. M. van der Veldt, N. H. Hendrikse, E. F. Smit, M. P. J. Mooijer, A. Y. Rijnders, W. R. Gerritsen, J. J. M. van der Hoeven, A. D. Windhorst, A. A. Lammertsma and M. Lubberink, *Eur. J. Nucl. Med. Mol. Imaging*, 2010, 37, 1950–1958.
- [2] A. A. M. van der Veldt, M. Lubberink, R. H. J. Mathijssen, W. J. Loos, G. J. M. Herder, H. N. Greuter, E. F. I. Comans, H. B. Rutten, J. Eriksson, A. D. Windhorst, N. H. Hendrikse, P. E. Postmus, E. F. Smit and A. A. Lammertsma, *Clin. Cancer Res.*, 2013, 19, 4163–4173.
- [3] A. Beck, L. Goetsch, C. Dumontet and N. Corvaia, *Nat. Rev. Drug Discov.*, 2017, 16, 315–337.
- [4] A. Thomas, B. A. Teicher and R. Hassan, *Lancet Oncol.*, 2016, 17, e254–e262.
- [5] M. J. Birrer, K. N. Moore, I. Betella and R. C. Bates, *JNCI J. Natl. Cancer Inst.*, 2019, 111, 538–549.
- [6] C. H. Chau, P. S. Steeg and W. D. Figg, *Lancet*, 2019, 394, 793–804.
- [7] P. Zhao, Y. Zhang, W. Li, C. Jeanty, G. Xiang and Y. Dong, *Acta Pharm. Sin. B*, DOI:10.1016/j.apsb.2020.04.012.

- [8] A. Bardia, I. A. Mayer, L. T. Vahdat, S. M. Tolaney, S. J. Isakoff, J. R. Diamond, J. O'Shaughnessy, R. L. Moroose, A. D. Santin, V. G. Abramson, N. C. Shah, H. S. Rugo, D. M. Goldenberg, A. M. Sweidan, R. Iannone, S. Washkowitz, R. M. Sharkey, W. A. Wegener and K. Kalinsky, *N. Engl. J. Med.*, 2019, 380, 741–751.
- [9] R. S. Zolot, S. Basu and R. P. Million, *Nat. Rev. Drug Discov.*, 2013, 12, 259–260.
- [10] A. W. Tolcher, *Ann. Oncol.*, 2016, 27, 2168–2172.
- [11] E. Khera and G. M. Thurber, *BioDrugs*, 2018, 32, 465–480.
- [12] S. Coats, M. Williams, B. Kebble, R. Dixit, L. Tseng, N.-S. Yao, D. A. Tice and J.-C. Soria, *Clin. Cancer Res.*, 2019, 25, 5441–5448.
- [13] M. Vankemmelbeke and L. Durrant, *Ther. Deliv.*, 2016, 7, 141–144.
- [14] M. de Jong and T. Maina, *J. Nucl. Med.*, 2010, 51, 501–504.
- [15] C.-P. Day, G. Merlino and T. Van Dyke, *Cell*, 2015, 163, 39–53.
- [16] N. Krall, J. Scheuermann and D. Neri, *Angew. Chemie Int. Ed.*, 2013, 52, 1384–1402.
- [17] M. Srinivasarao, C. V Galliford and P. S. Low, *Nat Rev Drug Discov*, 2015, 14, 203–219.
- [18] M. Srinivasarao and P. S. Low, *Chem. Rev.*, 2017, 117, 12133–12164.
- [19] S. Cazzamalli, A. Dal Corso, F. Widmayer and D. Neri, *J Am Chem Soc*, 2018, 140, 1617–1621.
- [20] M. S. Dennis, H. Jin, D. Dugger, R. Yang, L. McFarland, A. Ogasawara, S. Williams, M. J. Cole, S. Ross and R. Schwall, *Cancer Res.*, 2007, 67, 254–261.
- [21] G. M. Thurber and R. Weissleder, *PLoS One*, 2011, 6, e24696.
- [22] G. M. Thurber and R. Weissleder, *Mol. Imaging Biol.*, 2011, 13, 623–632.
- [23] C. J. Mathias, S. Wang, D. J. Waters, J. J. Turek, P. S. Low and M. A. Green, *J. Nucl. Med.*, 1998, 39, 1579–85.
- [24] M. de Jong, R. Valkema, F. Jamar, L. K. Kvols, D. J. Kwekkeboom, W. A. P. Breeman, W. H. Bakker, C. Smith, S. Pauwels and E. P. Krenning, *Semin. Nucl. Med.*, 2002, 32, 133–140.
- [25] M. Ginj, H. Zhang, B. Waser, R. Cescato, D. Wild, X. Wang, J. Erchegyi, J. Rivier, H. R. Macke and J. C. Reubi, *Proc. Natl. Acad. Sci.*, 2006, 103, 16436–16441.
- [26] S. M. Hillier, K. P. Maresca, G. Lu, R. D. Merkin, J. C. Marquis, C. N. Zimmerman, W. C. Eckelman, J. L. Joyal and J. W. Babich, *J. Nucl. Med.*, 2013, 54, 1369–1376.
- [27] N. Krall, F. Pretto, W. Decurtins, G. J. Bernardes, C. T. Supuran and D. Neri, *Angew Chem Int Ed Engl*, 2014, 53, 4231–4235.
- [28] G. M. van Dam, G. Themelis, L. M. A. Crane, N. J. Harlaar, R. G. Pleijhuis, W. Kelder, A. Sarantopoulos, J. S. de Jong, H. J. G. Arts, A. G. J. van der Zee, J. Bart, P. S. Low and V. Ntziachristos, *Nat. Med.*, 2011, 17, 1315–1319.
- [29] P. S. Low, W. A. Henne and D. D. Doorneweerd, *Acc. Chem. Res.*, 2008, 41, 120–129.
- [30] Y. Xia, C. Zeng, Y. Zhao, X. Zhang, Z. Li and Y. Chen, *EJNMMI Res.*, 2020, 10, 36.
- [31] J. A. Barrett, R. E. Coleman, S. J. Goldsmith, S. Vallabhajosula, N. A. Petry, S. Cho, T. Armor, J. B. Stubbs, K. P. Maresca, M. G. Stabin, J. L. Joyal, W. C. Eckelman and J. W. Babich, *J. Nucl. Med.*, 2013, 54, 380–387.
- [32] O. C. Kulterer, S. Pfaff, W. Wadsak, N. Garstka, M. Remzi, C. Vraka, L. Nics, F. Bootz, S. Cazzamalli, N. Krall, D. Neri and A. R. Haug, *J. Nucl. Med.*, 2020, jnumed.120.245530.
- [33] R. A. Goodnow, C. E. Dumelin and A. D. Keefe, *Nat. Rev. Drug Discov.*, 2017, 16, 131–147.
- [34] N. Favalli, G. Bassi, J. Scheuermann and D. Neri, *FEBS Lett.*, 2018, 592, 2168–2180.
- [35] D. Neri and R. A. Lerner, *Annu Rev Biochem*, 2018, 87, 479–502.
- [36] S. Chen and C. Heinis, 2015, pp. 119–137.

- [37] C. A. Rhodes and D. Pei, *Chem. - A Eur. J.*, 2017, 23, 12690–12703.
- [38] J. Ottil, L. Leder, J. V Schaefer and C. E. Dumelin, *Molecules*, 2019, 24, 1629.
- [39] M. Wichert, N. Krall, W. Decurtins, R. M. Franzini, F. Pretto, P. Schneider, D. Neri and J. Scheuermann, *Nat Chem*, 2015, 7, 241–249.
- [40] S. Cazzamalli, B. Ziffels, F. Widmayer, P. Murer, G. Pellegrini, F. Pretto, S. Wulhfard and D. Neri, *Clin Cancer Res*, 2018, 24, 3656–3667.
- [41] G. E. Mudd, A. Brown, L. Chen, K. van Rietschoten, S. Watcham, D. P. Teufel, S. Pavan, R. Lani, P. Huxley and G. S. Bennett, *J. Med. Chem.*, 2020, 63, 4107–4116.
- [42] K. Iwasaki, Y. Goto, T. Katoh, T. Yamashita, S. Kaneko and H. Suga, *J. Mol. Evol.*, 2015, 81, 210–217.
- [43] P. Hoppenz, S. Els-Heindl and A. G. Beck-Sickinger, *Front. Chem.*, DOI:10.3389/fchem.2020.00571.
- [44] S. D’Mello, G. Finlay, B. Baguley and M. Askarian-Amiri, *Int. J. Mol. Sci.*, 2016, 17, 1144.
- [45] A. N. Houghton, M. Eisinger, A. P. Albino, J. G. Cairncross and L. J. Old, *J. Exp. Med.*, 1982, 156, 1755–1766.
- [46] X. Lai, H. J. Wichers, M. Soler-Lopez and B. W. Dijkstra, *Chem. - A Eur. J.*, 2018, 24, 47–55.
- [47] M. Uhlen, L. Fagerberg, B. M. Hallstrom, C. Lindskog, P. Oksvold, A. Mardinoglu, A. Sivertsson, C. Kampf, E. Sjostedt, A. Asplund, I. Olsson, K. Edlund, E. Lundberg, S. Navani, C. A.-K. Szigyarto, J. Odeberg, D. Djureinovic, J. O. Takanen, S. Hober, T. Alm, P.-H. Edqvist, H. Berling, H. Tegel, J. Mulder, J. Rockberg, P. Nilsson, J. M. Schwenk, M. Hamsten, K. von Feilitzen, M. Forsberg, L. Persson, F. Johansson, M. Zwahlen, G. von Heijne, J. Nielsen and F. Ponten, *Science (80-.)*, 2015, 347, 1260419–1260419.
- [48] Y. M. Saenger, Y. Li, K. C. Chiou, B. Chan, G. Rizzuto, S. L. Terzulli, T. Merghoub, A. N. Houghton and J. D. Wolchok, *Cancer Res.*, 2008, 68, 9884–9891.
- [49] T. Mann, W. Gerwat, J. Batzer, K. Eggers, C. Scherner, H. Wenck, F. Stab, V. J. Hearing, K. H. Rohm and L. Kolbe, *J Invest Dermatol*, 2018, 138, 1601–1608.
- [50] T. Mann, C. Scherner, K.-H. Röhm and L. Kolbe, *Int. J. Mol. Sci.*, 2018, 19, 690.
- [51] C. Arrowitz, A. M. Schoelermann, T. Mann, L. I. Jiang, T. Weber and L. Kolbe, *J. Invest. Dermatol.*, 2019, 139, 1691-1698.e6.
- [52] W. G. Philipp-Dormston, A. Vila Echagüe, S. H. Pérez Damonte, J. Riedel, A. Filbry, K. Warnke, C. Lofrano, D. Roggenkamp and G. Nippel, *Int. J. Cosmet. Sci.*, 2020, 42, 377–387.
- [53] X. Lai, H. J. Wichers, M. Soler-Lopez and B. W. Dijkstra, *Angew Chem Int Ed Engl*, 2017, 56, 9812–9815.
- [54] A. J. WINDER and H. HARRIS, *Eur. J. Biochem.*, 1991, 198, 317–326.
- [55] G. Bassi, N. Favalli, M. Vuk, M. Catalano, A. Martinelli, A. Trenner, A. Porro, S. Yang, C. L. Tham, M. Moroglu, W. W. Yue, S. J. Conway, P. K. Vogt, A. A. Sartori, J. Scheuermann and D. Neri, *Adv. Sci.*, , DOI:10.1002/advs.202001970.
- [56] J. Zhou, W. Shi, L. Li, Q. Gong, X. Wu, X. Li and H. Ma, *Anal. Chem.*, 2016, 88, 4557–4564.
- [57] W. Mier, C. Kratochwil, J. C. Hassel, F. L. Giesel, B. Beijer, J. W. Babich, M. Friebe, M. Eisenhut, A. Enk and U. Haberkorn, *J. Nucl. Med.*, 2014, 55, 9–14.
- [58] X. Lai, H. J. Wichers, M. Soler-Lopez and B. W. Dijkstra, *Chemistry (Easton)*, 2018, 24, 47–55.
- [59] G. Zimmermann, Y. Li, U. Rieder, M. Mattarella, D. Neri and J. Scheuermann, *Chembiochem*, 2017, 18, 853–857.

- [60] A. Dal Corso, M. Catalano, A. Schmid, J. Scheuermann and D. Neri, *Angew. Chemie Int. Ed.*, 2018, 57, 17178–17182.
- [61] M. Catalano, M. Moroglu, P. Balbi, F. Mazzieri, J. Clayton, K. H. Andrews, M. Bigatti, J. Scheuermann, S. J. Conway and D. Neri, *ChemMedChem*, 2020, cmdc.202000528.
- [62] A. Pina, M. Kadri, D. Arosio, A. Dal Corso, J. Coll, C. Gennari and D. Boturyn, *Chem. – A Eur. J.*, 2020, 26, 7492–7496.
- [63] A. Borbély, F. Thoreau, E. Figueras, M. Kadri, J. Coll, D. Boturyn and N. Sewald, *Chem. – A Eur. J.*, 2020, 26, 2602–2605.
- [64] M. Catalano, S. Oehler, L. Prati, N. Favalli, G. Bassi, J. Scheuermann and D. Neri, *Anal. Chem.*, 2020, 92, 10822–10829.
- [65] S. Vijayasaradhi, B. Bouchard and A. N. Houghton, *J. Exp. Med.*, 1990, 171, 1375–1380.
- [66] P. Murer, J. D. Kiefer, L. Plüss, M. Matasci, S. L. Blümich, M. Stringhini and D. Neri, *J. Invest. Dermatol.*, 2019, 139, 1339–1348.
- [67] J. D. Nosanchuk, A. Jeyakumar, A. Ray, E. Revskaya, Z. Jiang, R. A. Bryan, K. J. H. Allen, R. Jiao, M. E. Malo, B. L. Gómez, A. Morgenstern, F. Bruchertseifer, D. Rickles, G. B. Thornton, A. Bowen, A. Casadevall and E. Dadachova, *Sci. Rep.*, 2018, 8, 5466.
- [68] M. Klein, M. Lotem, T. Peretz, S. T. Zwas, S. Mizrahi, Y. Liberman, R. Chisin, J. Schachter, I. G. Ron, G. Iosilevsky, J. A. Kennedy, E. Revskaya, A. W. de Kater, E. Banaga, V. Klutzaritz, N. Friedmann, E. Galun, G. L. DeNardo, S. J. DeNardo, A. Casadevall, E. Dadachova and G. B. Thornton, *J. Skin Cancer*, 2013, 2013, 1–8.
- [69] F. Nimmerjahn, *Science (80-.)*, 2005, 310, 1510–1512.
- [70] B. Roulier, B. Pérès and R. Haudecoeur, *J. Med. Chem.*, 2020, acs.jmedchem.0c00994.

5. Discussion

In the present PhD thesis, new small molecules for therapeutic purposes have been investigated. The project consisted of four parts: (1) synthesis and preclinical evaluation of σ R ligands hybridized with H₂S- or NO- donors; (2) development of novel classes of selective σ R ligands with optimal affinity and selectivity; (3) generation of a statistical tool to support the identification of CNS, non-CNS or mixed drugs; (4) investigation for hTYR and hTYRP1 ligands for the selective recognition of melanoma cells.

Part 1: Development of sigma receptor ligands for cancer treatment and analgesia

The modulation of NO and H₂S levels might be useful in therapy, however due their reactive and unstable gaseous nature, the controlled and localized generation or administration of these gas to biological sites is greatly limited. For this reason, NO and H₂S donors are preferred since these agents are stable chemical compounds able to release gas under certain chemical or enzymatical conditions. At this regard, organic compounds bearing a nitrate function, or a thioamide moiety have been reported for being able to release adequate amounts of these gases. Moreover, in light of the ability of σ_1 R to modulate neuropathic pain and to have a target-dependent antiproliferative and antiangiogenic effect, their activity could be significantly enhanced in combination with H₂S- or NO-releasing moieties. The purpose was to obtain improved synergistic properties when compared to σ_1 R antagonists or gas-donor alone. To this extent, the first purpose of the project was the development and preclinical evaluation of selective σ R ligands endowed with specific functional profile and hybridized with H₂S- or NO-donors for the management of pain condition or for the treatment of cancer, respectively. The activity of the σ R ligands has been combined with the peculiar ability to generate H₂S or NO, thus obtaining a synergistic effect.

By the use of radioligand binding assays, K_i values for the receptor-ligand interaction have been determined by measuring the ability of increasing concentrations of a non-radioactive competitor to compete with the binding of a radioactively labeled compound.

Particularly, the NO- σ R hybrid compound **15** (Figure 14) was able to induce a marked loss of viability in both MCF-7 and Caco-2 cell lines, showing a σ_1 R antagonist/ σ_2 R agonist functional profile. Indeed, when incubated with (+)-pentazocine or AC927, the loss of cell viability induced by **15** alone has been fully restored. As confirmation, the negative control cognate derivatives lacking the nitrate function were not able to reduce MCF-7 viability, thus sustaining a possible synergistic effect between the σ Rs and the NO-mediated events in the treatment of neoplastic disorders.

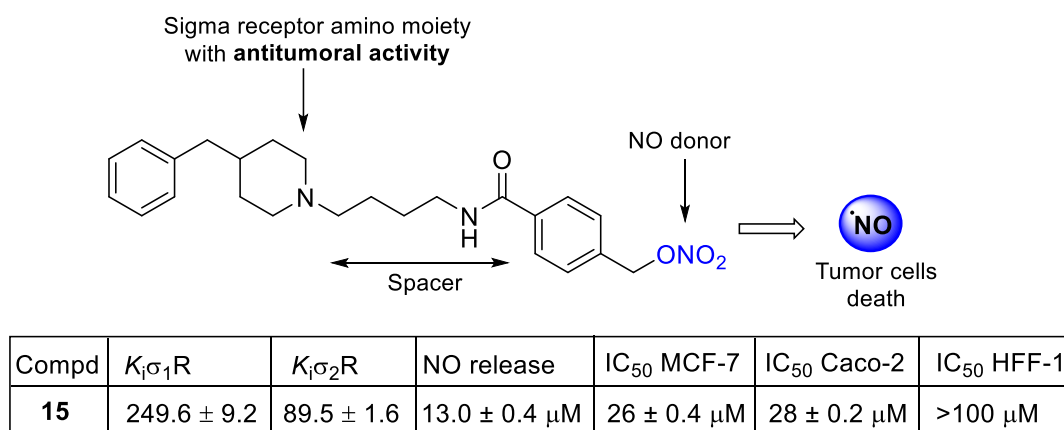


Figure 14. Structure and biological profile of compound **15**.

As regards the hybrid derivatives able to release H₂S, compound **7a** has emerged as a valuable compound in an in vivo model of capsaicin-induced mechanical hypersensitivity (Figure 15). The acute effects of the drug have been evaluated by its s.c. administration 30 min prior to capsaicin injection. On the contrary, the homologous derivative **7b** lacking the thioamide function had only a minimal analgesic effect, highlighting the clear role of the H₂S moiety in contributing to the analgesic effect. Moreover, when co-administered together with the σ_1R agonist PRE-084, a reversion of analgesia supports the synergistic effect between the σ Rs and the H₂S mediated events.

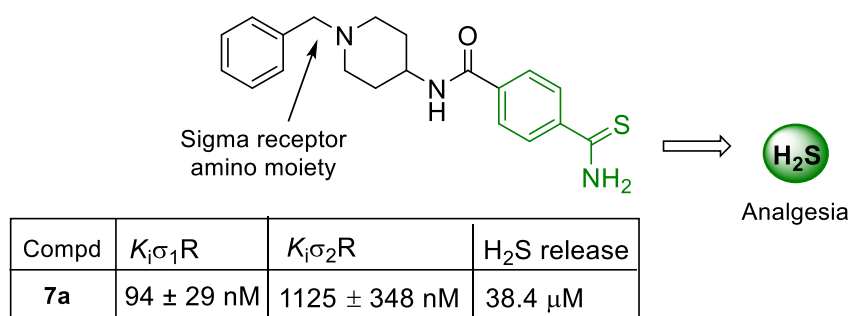


Figure 15. Structure and biological profile of compound **7a**.

Overall, in the cases reported above the combination of H₂S/NO donor and σ Rs ligands provided compounds with beneficial synergistic effects and a precise balanced activity between the two components.

Part 2: Design, synthesis and preclinical evaluation of novel sigma receptors ligands

Another series of compounds was developed with the aim to identify pure σ Rs ligands for their use as such. Thus, σ R ligands with high affinity and selectivity have been obtained based on standard SAfiR approach. First, new candidate ligands have been synthesized and submitted to in vitro radioligand binding assays, then based on the obtained affinity and selectivity values, modification

have been planned and new compounds evaluated. From a first round, compounds **AD145** and **AD174** showed very low single digit nanomolar affinity for σ_1R , with a selectivity over σ_2R ranging from 8-fold for **AD145**, to more than 14-fold for **AD174** (Figure 16). Particularly, unexpected results have been obtained by adding an ethyl ester group as in **AD223** which determined an inversion of σR profile with respect to the parent compound **AD145**. The introduction of a nitro group in the *para* position of compound **AD174** has provided an affinity improvement for both σR and slightly better selectivity. Notably, compound **AD242** is the only compound in the series having affinity for σ_1R below 1 nM. The presence of a *p*-cyano-group as in **AD258** improved the affinity for both subtypes.

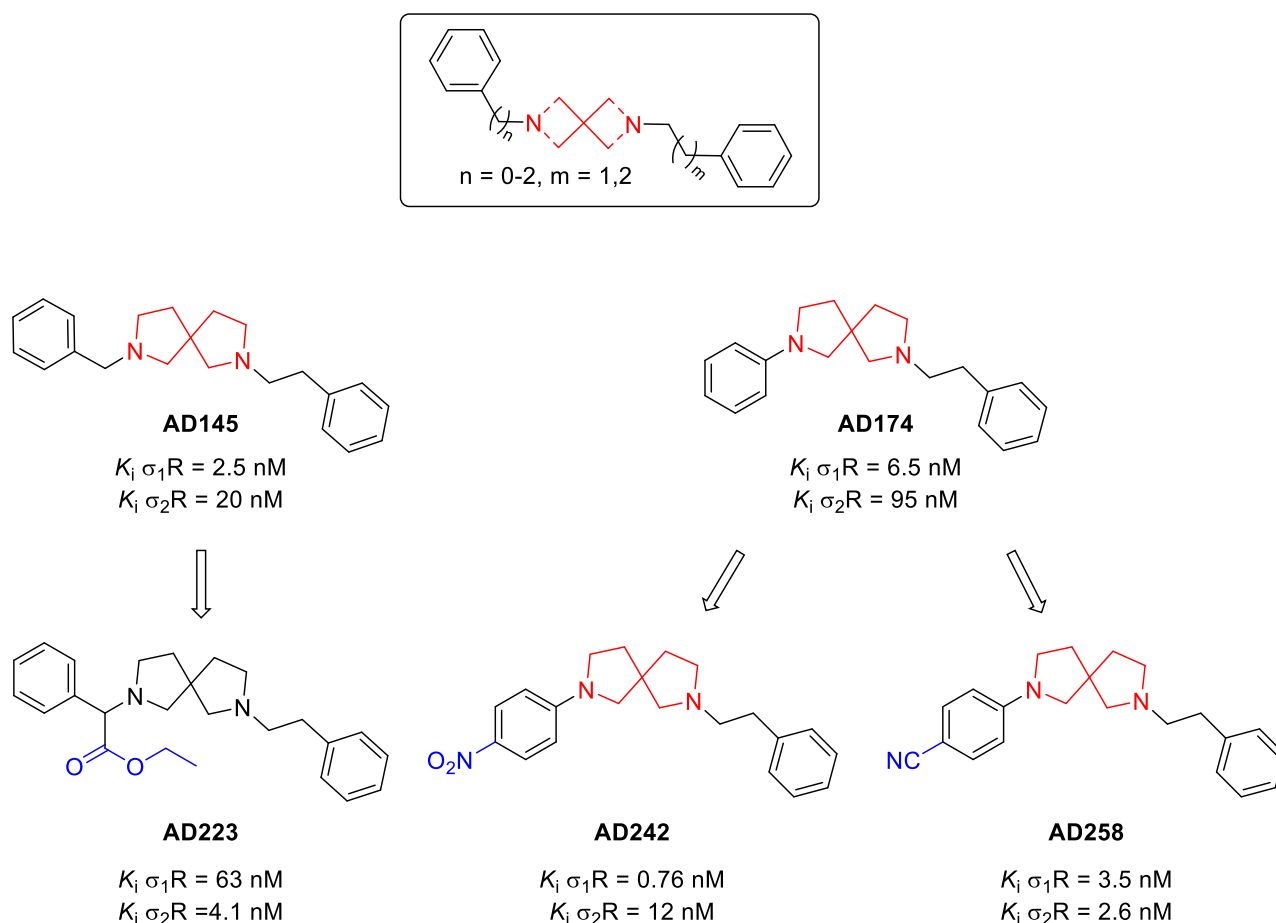


Figure 16. Affinity and selectivity profile for some identified σR ligands.

Overall, these results lead to define a set of chemical modifications that would allow control over the σR s affinity and selectivity profile in the perspective of obtaining selective σR ligands. Further studies are in progress to investigate the effects of these molecules in additional *in vitro* and *in vivo* models.

Part 3: Statistical tool in supporting the identification of BBB crossing parameters

To support the identification of parameters for BBB crossing, useful for those chemical entities grounding their therapeutic value on the effects in the CNS, a statistical tool has been developed allowing to define a set of rules that would prospectively be used to tune the properties of in house synthesized ligands (Figure 17). Indeed, the distribution inside and outside the CNS is an equilibrium process resulting from a number of different variables. Thus, depending on the combination of multiple descriptors, a three cases probabilistic scenario has been set where the suggested ranges should be considered as optimal values to be approached. In particular, **AD214** and **AD225** are compounds with good descriptors distribution. Over the nine significant descriptors, they show seven descriptors in BBB⁺ and two in BBB⁺/BBB⁻. Whereas compound **AD223** shows five descriptors in BBB⁺, and four in BBB⁺/BBB⁻.

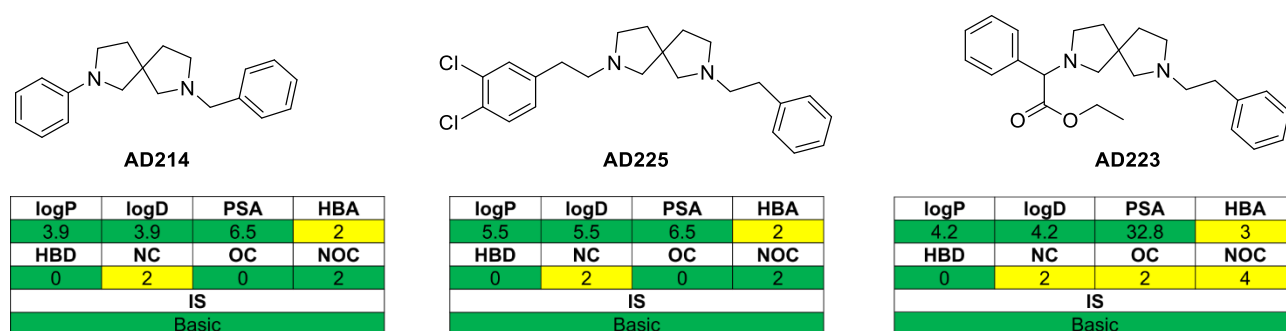


Figure 17. Distribution of descriptor values for three representative compounds.

Part 4: Small molecule ligands against human Tyrosinases

The last stage of this PhD thesis was addressed to the finding of hTYR and hTYRP1 ligands for the selective recognition of melanoma cells in order to specifically deliver cytotoxic compounds to the tumor site. This goal has been pursued either via screening of large libraries of ligands or improving already known binders reported in literature.

The first step of the project was the affinity evaluation of known tyrosinase inhibitors, synthesized as fluorophore-conjugates, by fluorescence polarization (FP) assay. Thus, four fluorescein-conjugated compounds have been initially synthesized (Figure 18). To achieve better targeting performance, the use of multimeric derivatives has been also investigated and trimeric derivatives of mimosine and kojic acids synthesized. Compounds have been incubated with a dilution series of the recombinant protein TYRP1 and FP gave K_d values in the range of 10–20 μ M. Thus, the interest was moved to Thiamidol™, a potent inhibitor of hTYR in clinical trials, and an alkyne derivative was synthesized and tested. Also in this case, the oligomerization of Thiamidol with dendrimeric scaffolds has been undertaken allowing the generation of multivalent ligands with improved affinity towards hTYR and hTYRP1 with respect to the monomeric ligand.

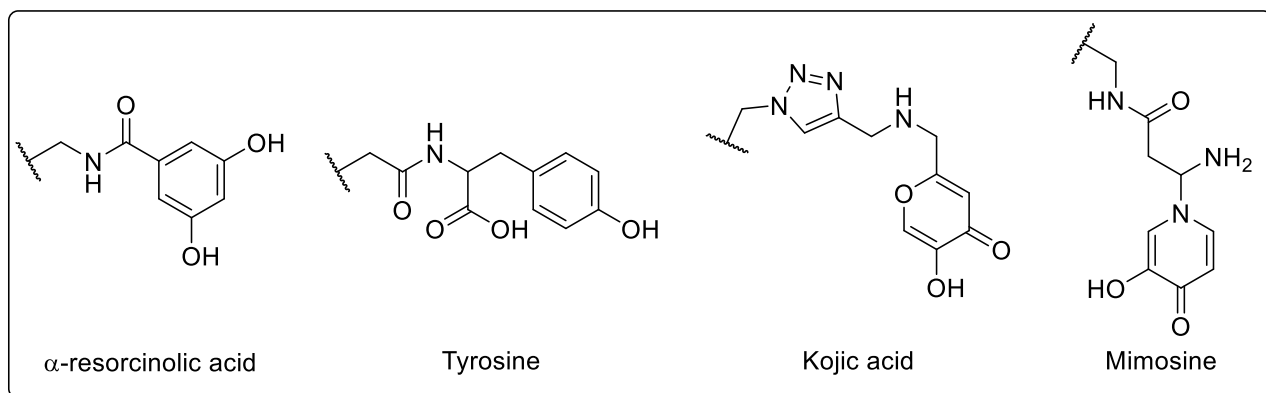
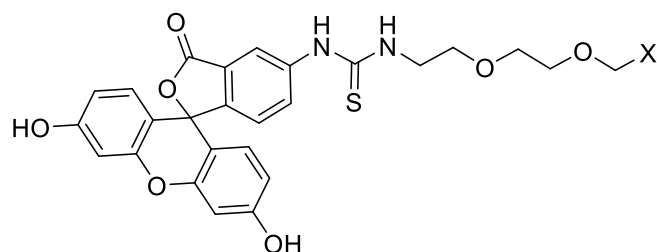


Figure 18. Structures of known tyrosinase inhibitors fluorophore-conjugates.

In addition, starting from different pre-existing dual-pharmacophore DECLs bearing different chemical structures at the two extremities of complementary DNA strands, affinity-based selections over hTYRP1 and hTYR were performed. Best results have been obtained with the GB-DEL library containing 366,600 members, revealing a characteristic enrichment for few building blocks for both hTYR and hTYRP1, highlighting how the active site of the two enzymes is highly conserved. The individual compounds identified have been then synthesized as fluorophore-conjugates and submitted to FP assay, exhibiting binding potency in the micromolar range.

Although more specific and potent ligands for the targeted treatment of melanoma have to be discovered, this work represents a starting point for the development of organic ligands of hTYR and/or hTYRP1 since, particularly in the case of TYRP1, no ligands are currently available.

Concluding remarks

The work presented in this thesis took part in the perspective to identify new small molecules for therapeutic purposes. The PhD project was mainly carried out by focusing on σ R, exploiting their involvement in different pathological states.

Several competences and techniques have been merged and deepened, including different ligand design approaches, strategies for ligand discovery, chemical compounds preparation and affinity evaluation through fluorescence polarization and radioligand binding assays.

The compounds identified and synthesized throughout the PhD project have been submitted for additional biological and pharmacological characterization providing promising ligands with beneficial effects for the treatment of pain or for targeted cancer therapy.

Supplementary Information

Sigma Receptor Ligands Carrying a Nitric Oxide Donor Nitrate Moiety: Synthesis, In-Silico, and Biological Evaluation

Emanuele Amata,^{†,§,*} Maria Dichiara,^{†,§} Davide Gentile,[‡] Agostino Marrazzo,[†] Rita Turnaturi,[†] Emanuela Arena,[†] Alfonsina La Mantia,^{||} Barbara Rita Tomasello,^{||} Rosaria Acquaviva,^{||} Claudia Di Giacomo,^{||} Antonio Rescifina,[‡] Orazio Prezzavento^{†,*}

[†]Department of Drug Sciences, Medicinal Chemistry Section, University of Catania, Viale A. Doria, 95125 Catania, Italy.

[‡]Department of Drug Sciences, Organic Chemistry Section, University of Catania, Viale A. Doria, 95125 Catania, Italy.

^{||}Department of Drug Sciences, Biochemistry Section, University of Catania, Viale A. Doria, 95125 Catania, Italy.

Corresponding Authors:

*E.A.: phone, (+39) 0957384102; email, eamata@unict.it

*O.P.: phone, (+39) 3396392909; email, prezzave@unict.it

Author Contributions:

[§]E.A. and M.D. contributed equally.

EXPERIMENTAL SECTION

Table of contents	
Chemistry	S2
General details	S2
Synthesis of compounds 5–8	S2
Synthesis of compounds 9–20	S3
Synthesis of compounds 23a and 23b	S6
Computational procedures	S6
Molecular docking	S6
Molecular optimization	S7
Molecular dynamics simulations	S8
Molecular dynamics simulations study and trajectories analysis of compound 18	S8
Biological evaluation	S10
Radioligand binding assays	S10
Detection of Nitrite: Griess Reaction	S11
Cell culture	S11
Cell viability	S11
Western Blot Analysis	S12
NMR spectra	S13
References	S20

Chemistry

General details

Reagent grade chemicals were purchased from Sigma-Aldrich (St. Louis, MO, USA) or Merck (Darmstadt, Germany) and were used without further purification. All reactions involving air-sensitive reagents were performed under N₂ in oven-dried glassware using the syringe-septum cap technique. Flash chromatography purification was performed on a Merck silica gel 60 (40–63 μm; 230–400 mesh) stationary phase. Nuclear magnetic resonance spectra (¹H NMR recorded at 200 and 500 MHz) were obtained on VARIAN INOVA spectrometers using CDCl₃, DMSO-*d*₆, or CD₃OD. TMS was used as an internal standard. Chemical shifts (δ) are given in parts per million (ppm) and coupling constants (*J*) in Hertz (Hz). The following abbreviations are used to designate the multiplicities: s = singlet, d = doublet, t = triplet, q = quartet, quint = quintet, m = multiplet, br = broad. The purity of all tested compounds, whether synthesized or purchased, reached at least 95% as determined by microanalysis (C, H, N) that was performed on a Carlo Erba instrument model E1110; all the results agreed within ± 0.4% of the theoretical values. Reactions were monitored by thin-layer chromatography (TLC) performed on 250 μm silica gel Merck 60 F₂₅₄ coated aluminum plates; the spots were visualized by UV light or iodine chamber. UV-Vis absorption spectra were recorded with a Jasco V-560 spectrophotometer. Compound nomenclatures were generated with ChemBioDraw Ultra version 16.0.0.82.

General procedure for the synthesis of compounds 5–8

To a solution of the appropriate halomethyl acid derivative (2.93 mmol) in CH₃CN, AgNO₃ (11.72 mmol, 1.99 g) was added, and the reaction mixture was stirred at rt in the dark. The precipitate (silver halide) was filtered off, and the residue triturated. The solvent was evaporated, and the product used as is without any further purification.

4-((nitrooxy)methyl)benzoic acid (**5**)

The compound has been prepared using 4-(chloromethyl)benzoic acid (2.93 mmol, 0.50 g). Stirring was continued over 4 h at rt in the dark. The AgCl precipitate was filtered off, and the solvent evaporated. The crude product was triturated with CHCl₃ (10 mL) and filtered to remove the unreacted AgNO₃ and AgCl. Yield: 80%, white solid. ¹H NMR (200 MHz, CDCl₃) δ 8.09 (d, *J* = 8.1 Hz, 2H), 7.53 (d, *J* = 8.2 Hz, 2H), 5.51 (s, 2H).

3-((nitrooxy)methyl)benzoic acid (**6**)

The compound has been prepared using 3-(chloromethyl)benzoic acid (2.93 mmol, 0.50 g). Stirring was continued over 4 h at rt in the dark. The AgCl precipitate was filtered, and the solvent evaporated. The crude product was triturated with CHCl₃ (10 mL) and filtered to remove the unreacted AgNO₃ and AgCl. Yield: 76%, white solid. ¹H NMR (200 MHz, CDCl₃) δ 8.14–8.17 (m, 2H), 7.67 (d, *J* = 7.8 Hz, 1H), 7.49–7.58 (m, 1H), 5.49 (s, 2H).

2-(4-((nitrooxy)methyl)phenyl)acetic acid (**7**)

The compound has been prepared using 2-(4-(bromomethyl)phenyl)acetic acid (1.96 mmol, 0.45 g) and the reaction mixture was stirred at rt in the dark for 2 days. The AgBr precipitate was filtered off, and the residue triturated with brine and extracted with EtOAc. Yield: 75%, white solid. ¹H NMR (200 MHz, CDCl₃) δ 7.29–7.44 (m, 4H), 5.42 (s, 2H), 3.68 (s, 2H).

2-(3-((nitrooxy)methyl)phenyl)acetic acid (**8**)

The compound has been prepared using 2-(3-(bromomethyl)phenyl)acetic acid (1.96 mmol, 0.45 g) and the reaction mixture was stirred at rt in the dark for 2 days. The AgBr precipitate was filtered off, and the residue triturated with brine and extracted with EtOAc. Yield: 70%, white solid. ¹H NMR (200 MHz, CDCl₃) δ 6.76–8.02 (m, 4H), 5.42 (s, 2H), 3.68 (s, 2H).

General procedure for the synthesis of compounds 9–20

To a solution of the appropriate nitrooxy-substituted benzoic acid derivative **5–8** (1.01 mmol) in CH₃CN (5 mL), HOBT (1.53 mmol, 0.21 g), and EDC (1.52 mmol, 0.29 g) were added. After stirring for 20 min, the appropriate substituted amine (2.02 mmol) has been added and the resulting mixture was stirred at rt for 5 h. After the reaction was complete, the solvent was evaporated to dryness and the crude solubilized in CH₂Cl₂ (20 mL), washed with H₂O (2 x 10 mL), and brine (5 mL), and dried under anhydrous Na₂SO₄. The solvent was removed under vacuum and the residue was purified via silica gel chromatography (10% MeOH in EtOAc and then 10% MeOH + 3% NH₄OH in EtOAc) to provide the desired product.

3-((2-(4-benzylpiperidin-1-yl)ethyl)carbamoyl)benzyl nitrate (**9**)

The compound has been prepared using 3-((nitrooxy)methyl)benzoic acid (1.01 mmol, 0.20 g) and 4-(4-benzylpiperidin-1-yl)butan-1-amine (2.02 mmol, 0.44 g). Yield: 73%, white solid. ¹H NMR (200 MHz, CDCl₃) δ 7.92 (ddd, *J* = 0.98, 2.83, 5.56 Hz, 2H), 7.78 (dd, *J* = 1.56, 7.42 Hz, 1H), 7.19–7.50 (m, 6H), 7.10 (br. s, 1H), 5.53 (s, 2H), 3.51 (d, *J* = 5.85 Hz, 2H), 2.93 (d, *J* = 11.71 Hz, 2H), 2.45–2.61 (m, 7H), 1.95–2.01 (m, 2H), 1.60–1.69 (m, 2H). ¹³C NMR (200 MHz, CDCl₃) δ 166.41, 143.23, 140.41, 136.10, 129.86, 129.04, 128.15, 127.45, 125.84, 124.56, 120.08, 81.60, 56.46, 53.58, 43.05, 37.83, 36.45, 32.13. Anal. calcd for C₂₂H₂₇N₃O₄: C, 66.48; H, 6.85; N, 10.57; O, 16.10. Found: C, 66.35; H, 6.86; N, 10.59; O, 16.14.

3-((3-(4-benzylpiperidin-1-yl)propyl)carbamoyl)benzyl nitrate (**10**)

The compound has been prepared using 3-((nitrooxy)methyl)benzoic acid (1.01 mmol, 0.20 g) and 3-(4-benzylpiperidin-1-yl)propan-1-amine (2.02 mmol, 0.47 g). Yield: 70%, white solid. ¹H NMR (200 MHz, CDCl₃) δ 8.60 (br. s., 1H), 7.91–8.10 (m, 3H), 7.16–7.42 (m, 6H), 5.56 (s, 2H), 3.50–3.71 (m, 4H), 2.96–3.12 (m, 2H), 2.63 (d, *J* = 6.64 Hz, 2H), 2.20 (d, *J* = 5.85 Hz, 2H), 1.71–2.02 (m, 4H), 1.19–1.33 (m, 1H). ¹³C NMR (200 MHz, CDCl₃) δ 166.91, 138.80, 136.32, 134.61, 129.79, 128.90, 128.52, 127.96, 126.45, 124.58, 120.02, 81.67, 40.39, 36.92, 36.26, 23.24, 22.67, 17.59. Anal. calcd for C₂₃H₂₉N₃O₄: C, 67.13; H, 7.10; N, 10.21; O, 15.55. Found: C, 66.97; H, 7.08; N, 10.23; O, 15.57.

3-((4-(4-benzylpiperidin-1-yl)butyl)carbamoyl)benzyl nitrate (**11**)

The compound has been prepared using 3-((nitrooxy)methyl)benzoic acid (1.01 mmol, 0.20 g) and 4-(4-benzylpiperidin-1-yl)butan-1-amine (2.02 mmol, 0.50 g). Yield: 75%, white solid. ¹H NMR (200 MHz, CDCl₃) δ 7.97 (dd, *J* = 0.98, 8.00 Hz, 1H), 7.72–7.88 (m, 2H), 7.16–7.55 (m, 6H), 6.97 (br. s., 1H), 5.58 (s, 2H), 2.89 (d, *J* = 11.32 Hz, 2H), 2.47 (d, *J* = 6.64 Hz, 2H), 2.34 (t, *J* = 6.44 Hz, 2H), 1.84 (t, *J* = 11.71 Hz, 3H), 1.50–1.72 (m, 7H), 1.09–1.35 (m, 3H). ¹³C NMR 166.85, 140.46, 135.70, 133.38, 132.36, 128.99, 128.09, 125.73, 124.58, 119.96, 108.60, 81.88, 58.16, 53.80, 43.02, 39.90, 37.74, 31.84, 27.33, 24.49. Anal. calcd for C₂₄H₃₁N₃O₄: C, 67.74; H, 7.34; N, 9.88; O, 15.04. Found: C, 67.61; H, 7.35; N, 9.86; O, 15.06.

3-((5-(4-benzylpiperidin-1-yl)pentyl)carbamoyl)benzyl nitrate (**12**)

The compound has been prepared using 3-((nitrooxy)methyl)benzoic acid (1.01 mmol, 0.20 g) and 5-(4-benzylpiperidin-1-yl)pentan-1-amine (2.02 mmol, 0.53 g). Yield: 79%, white solid. ¹H NMR (500 MHz, CDCl₃) δ 7.97 (d, *J* = 8.31 Hz, 1H), 7.36–7.41 (m, 1H), 7.30–7.35 (m, 1H), 7.24–7.29 (m, 3H), 7.16–7.20 (m, 1H), 7.13 (d, *J* = 7.34 Hz, 2H), 6.19 (br. s., 1H), 5.58 (s, 2H), 3.40–3.46 (m, 2H), 2.89 (d, *J* = 11.74 Hz, 2H), 2.53 (d, *J* = 6.85 Hz, 2H), 2.27–2.33 (m, 2H), 1.80–1.88 (m, 2H), 1.59–1.67 (m, 4H), 1.46–1.58 (m, 3H), 1.23–1.44 (m, 4H). ¹³C NMR (500 MHz, CDCl₃) δ 166.66, 143.15, 140.44, 135.36, 132.43, 129.00, 128.08, 125.72, 124.59, 119.92, 81.86, 58.56, 53.58, 42.96, 39.88, 37.71, 31.66, 29.22, 26.24, 24.79. Anal. calcd for C₂₅H₃₃N₃O₄: C, 68.31; H, 7.57; N, 9.56; O, 14.56. Found: C, 68.44; H, 7.56; N, 9.54; O, 14.59.

4-((2-(4-benzylpiperidin-1-yl)ethyl)carbamoyl)benzyl nitrate (**13**)

The compound has been prepared using 4-((nitrooxy)methyl)benzoic acid (1.01 mmol, 0.20 g) and 4-(4-benzylpiperidin-1-yl)butan-1-amine (2.02 mmol, 0.44 g). Yield: 75%, white solid. ¹H NMR (500 MHz, CDCl₃) δ 7.77 (d, *J* = 7.8 Hz, 2H), 7.48 (d, *J* = 8.3 Hz, 2H), 7.25–7.42 (m, 5H), 7.01 (br. s., 1H), 5.59 (s, 2H), 3.52 (q, *J* = 5.7 Hz, 2H), 2.92 (d, *J* = 11.2 Hz, 2H), 2.54–2.62 (m, 4H), 1.96–2.04 (m, 2H), 1.68 (d, *J* = 13.2 Hz, 2H), 1.57 (ddt, *J* = 14.9, 7.5, 3.7 Hz, 1H), 1.24–1.35 (m, 2H). ¹³C NMR (200 MHz, CDCl₃) δ 166.43, 143.25, 140.43, 136.12, 129.88, 128.17, 127.68, 125.84, 120.08, 81.60, 56.46, 53.58, 43.05, 37.83, 36.45, 32.13. Anal. calcd for C₂₂H₂₇N₃O₄: C, 66.48; H, 6.85; N, 10.57; O, 16.10. Found: C, 66.31; H, 6.86; N, 10.59; O, 16.06.

4-((3-(4-benzylpiperidin-1-yl)propyl)carbamoyl)benzyl nitrate (**14**)

The compound has been prepared using 4-((nitrooxy)methyl)benzoic acid (1.01 mmol, 0.20 g) and 3-(4-benzylpiperidin-1-yl)propan-1-amine (2.02 mmol, 0.47 g). Yield: 70%, white solid. ¹H NMR (500 MHz, CDCl₃) δ 8.53 (br. s., 1H), 7.27–7.41 (m, 5H), 7.25 (d, *J* = 7.2 Hz, 2H), 7.07 (d, *J* = 6.8 Hz, 2H), 5.61 (s, 2H), 3.53–3.61 (m, 2H), 3.01 (d, *J* = 11.7 Hz, 2H), 2.53–2.58 (m, 2H), 2.49 (d, *J* = 7.3 Hz, 2H), 1.92 (t, *J* = 11.5 Hz, 2H), 1.80 (dt, *J* = 11.7, 5.9 Hz, 4H), 1.67 (d, *J* = 12.2 Hz, 2H), 1.56 ppm (ddt, *J* = 15.0, 7.4, 3.7 Hz, 1H). ¹³C NMR (200 MHz, CDCl₃) δ 166.46, 145.17, 143.25, 140.18, 132.40, 128.94, 128.20, 125.88, 124.53, 81.98, 58.5, 54.0, 43.1, 41.0, 38.80, 32.1, 24.08. Anal. calcd for C₂₃H₂₉N₃O₄: C, 67.13; H, 7.10; N, 10.21; O, 15.55. Found: C, 66.86; H, 7.04; N, 10.24; O, 15.58.

4-((4-(4-benzylpiperidin-1-yl)butyl)carbamoyl)benzyl nitrate (**15**)

The compound has been prepared using 4-((nitrooxy)methyl)benzoic acid (1.01 mmol, 0.20 g) and 4-(4-benzylpiperidin-1-yl)butan-1-amine (2.02 mmol, 0.50 g). Yield: 80%, white solid. ¹H NMR (200 MHz, CDCl₃) δ 7.75 (d, *J* = 8.20 Hz, 2H), 7.46 (d, *J* = 7.81 Hz, 2H), 7.07–7.40 (m, 5H), 6.98 (br. s., 1H), 5.59 (s, 2H), 3.37–3.54 (m, 2H), 2.81–3.00 (m, 2H), 2.48 (d, *J* = 6.64 Hz, 2H), 2.36 (t, *J* = 6.64 Hz, 2H), 1.85 (t, *J* = 10.93 Hz, 2H), 1.40–1.74 (m, 7H), 1.09–1.34 (m, 2H). ¹³C NMR (200 MHz, CDCl₃) δ 166.88, 142.42, 136.22, 133.83, 129.85, 129.04, 128.18, 127.57, 124.59, 81.63, 65.76, 53.80, 49.78, 42.36, 38.24, 37.68, 31.74, 26.10. Anal. calcd for C₂₄H₃₁N₃O₄: C, 67.74; H, 7.34; N, 9.88; O, 15.04. Found: C, 67.89; H, 7.36; N, 9.85; O, 15.06.

4-((5-(4-benzylpiperidin-1-yl)pentyl)carbamoyl)benzyl nitrate (**16**)

The compound has been prepared using 4-((nitrooxy)methyl)benzoic acid (1.01 mmol, 0.20 g) and 5-(4-benzylpiperidin-1-yl)pentan-1-amine (2.02 mmol, 0.53 g). Yield: 83%, white solid. ¹H NMR (500 MHz, CDCl₃) δ 7.77 (d, *J* = 7.83 Hz, 1H), 7.50 (d, *J* = 7.83 Hz, 1H), 7.39–7.43 (m, 1H), 7.30–7.34 (m, 1H), 7.24–7.29 (m, 3H), 7.12 (d, *J* = 6.85 Hz, 2H), 6.23 (br. s., 1H), 5.57 (s, 2H), 3.43

(q, $J = 6.85$ Hz, 2H), 2.92–2.97 (m, 2H), 2.52 (d, $J = 7.34$ Hz, 2H), 2.33–2.38 (m, 2H), 1.80 (t, $J = 11.25$ Hz, 2H), 1.49–1.68 (m, 7H), 1.32–1.44 (m, 4H). ^{13}C NMR (200 MHz, CDCl_3) 166.63, 140.60, 136.18, 135.93, 129.88, 129.07, 128.12, 127.37, 125.76, 81.54, 58.76, 53.93, 43.13, 39.98, 37.87, 31.97, 29.42, 26.55, 24.93. Anal. calcd for $\text{C}_{25}\text{H}_{33}\text{N}_3\text{O}_4$: C, 68.31; H, 7.57; N, 9.56; O, 14.56. Found: C, 68.3; H, 7.55; N, 9.58; O, 14.59.

3-((1-benzylpiperidin-4-yl)carbamoyl)benzyl nitrate (**17**)

The compound has been prepared using 3-((nitrooxy)methyl)benzoic acid (1.01 mmol, 0.20 g) and 4-amino-benzylpiperidine (2.02 mmol, 0.38 g). Yield: 79%, white solid. ^1H NMR (200 MHz, CDCl_3) δ 7.97 (dd, $J = 1.76, 7.22$ Hz, 1H), 7.68–7.80 (m, 2H), 7.21–7.88 (m, 6H), 5.90 (d, $J = 7.81$ Hz, 1H), 5.57 (s, 2H), 3.87–4.11 (m, 3H), 3.53 (s, 2H), 2.87 (d, $J = 12.10$ Hz, 2H), 2.17 (t, $J = 11.51$ Hz, 2H), 2.00 (d, $J = 11.71$ Hz, 2H), 1.45–1.68 (m, 2H). ^{13}C NMR (200 MHz, CDCl_3) δ 165.99, 143.26, 138.19, 135.47, 129.12, 128.25, 127.10, 124.63, 81.86, 63.02, 52.27, 47.24, 32.21. Anal. calcd for $\text{C}_{20}\text{H}_{23}\text{N}_3\text{O}_4$: C, 65.03; H, 6.28; N, 11.37; O, 17.32. Found: C, 65.16; H, 6.29; N, 11.34; O, 17.35.

3-(2-((1-benzylpiperidin-4-yl)amino)-2-oxoethyl)benzyl nitrate (**18**)

The compound has been prepared using 2-(3-((nitrooxy)methyl)phenyl)acetic acid (1.01 mmol, 0.21 g) and 4-amino-benzylpiperidine (2.02 mmol, 0.38 g). Yield: 81%, white solid. ^1H NMR (200 MHz, CDCl_3) δ 7.18–7.45 (m, 9H), 5.50 (s, 2H), 3.64–3.89 (m, 1H), 3.45 (s, 2H), 2.75 (d, $J = 11.71$ Hz, 2H), 1.98–2.17 (m, 2H), 1.83 (d, $J = 12.10$ Hz, 2H), 1.23–1.49 (m, 2H). ^{13}C NMR (200 MHz, CDCl_3) δ 169.51, 143.23, 138.30, 136.74, 130.52, 129.75, 129.03, 127.02, 124.50, 120.08, 81.97, 62.96, 52.11, 46.60, 43.54, 32.02. Anal. calcd for $\text{C}_{21}\text{H}_{25}\text{N}_3\text{O}_4$: C, 65.78; H, 6.57; N, 10.96; O, 16.69. Found: C, 65.94; H, 6.58; N, 10.92; O, 16.74.

4-((1-benzylpiperidin-4-yl)carbamoyl)benzyl nitrate (**19**)

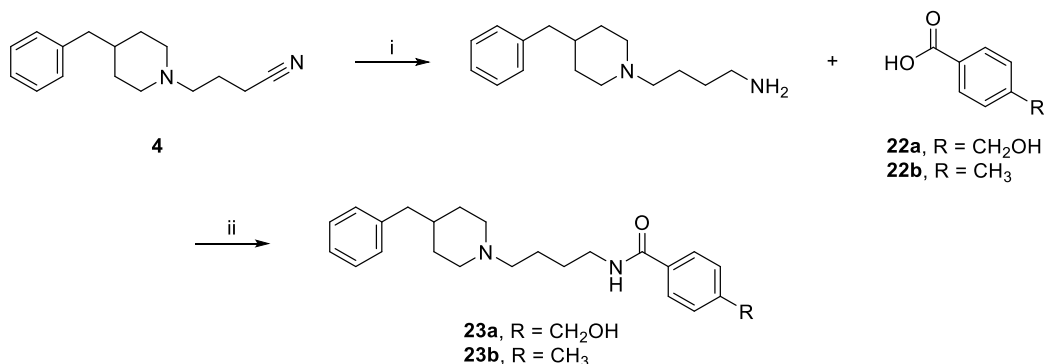
The compound has been prepared using 3-((nitrooxy)methyl)benzoic acid (1.01 mmol, 0.20 g) and 4-amino-benzylpiperidine (2.02 mmol, 0.38 g). Yield: 75%, white solid. ^1H NMR (200 MHz, CDCl_3) δ 7.72 (d, $J = 8.31$ Hz, 2H), 7.45 (d, $J = 8.20$ Hz, 2H), 7.22–7.41 (m, 5H), 5.97 (d, $J = 7.81$ Hz, 1H), 5.58 (s, 2H), 3.88–4.16 (m, 1H), 3.52 (s, 2H), 2.86 (d, $J = 12.49$ Hz, 2H), 2.17 (t, $J = 11.71$ Hz, 2H), 2.02 (d, $J = 12.49$ Hz, 2H), 1.45–1.67 (m, 2H). ^{13}C NMR (200 MHz, CDCl_3) δ 165.98, 143.27, 138.07, 129.90, 129.14, 128.26, 127.37, 124.60, 81.50, 63.02, 52.25, 47.18, 32.20. Anal. calcd for $\text{C}_{20}\text{H}_{23}\text{N}_3\text{O}_4$: C, 65.03; H, 6.28; N, 11.37; O, 17.32. Found: C, 64.88; H, 6.26; N, 11.39; O, 17.27.

4-(2-((1-benzylpiperidin-4-yl)amino)-2-oxoethyl)benzyl nitrate (**20**)

The compound has been prepared using 4-((nitrooxy)methyl)phenylacetic acid (1.01 mmol, 0.21 g) and 4-amino-benzylpiperidine (2.02 mmol, 0.38 g). Yield: 79%, white solid. ^1H NMR (200 MHz, CDCl_3) δ 7.92–8.01 (m, 1H), 7.18–7.45 (m, 8H), 5.53 (s, 2H), 5.15 (d, $J = 8.20$ Hz, 1H), 3.66–3.89 (m, 1H), 3.42–3.56 (m, 4H), 2.75 (d, $J = 12.10$ Hz, 2H), 2.07 (dt, $J = 2.54, 11.61$ Hz, 2H), 1.80 (d, $J = 12.10$ Hz, 2H), 1.17–1.40 (m, 2H). ^{13}C NMR (200 MHz, CDCl_3) δ 169.53, 138.33, 136.76, 132.11, 130.52, 129.75, 129.03, 128.20, 127.89, 81.97, 62.98, 52.13, 46.62, 43.56, 32.04. Anal. calcd for $\text{C}_{21}\text{H}_{25}\text{N}_3\text{O}_4$: C, 65.78; H, 6.57; N, 10.96; O, 16.69. Found: C, 65.94; H, 6.55; N, 10.98; O, 16.71.

General procedure for the synthesis of compounds 23a and 23b

Scheme S1. Synthetic strategy for the preparation of compounds 23a and 23b



Reagents and conditions: (i) LiAlH₄, THF, rt, N₂; (ii) EDC, HOBT, CH₃CN, rt, on.

To a solution of the appropriate benzoic acid derivative **22a** or **22b** (0.46 mmol) in CH₃CN (5 mL), HOBT (0.69 mmol, 0.09 g), and EDC (0.69 mmol, 0.13 g) were added. After stirring for 20 min, appropriate amine (0.92 mmol, 226 mg) has been added, and the resulting mixture was stirred at rt overnight. After the reaction was complete, the solvent was evaporated to dryness and the crude dissolved in CH₂Cl₂ (20 mL), washed with H₂O (2 x 10 mL), brine (5 mL), and dried under anhydrous Na₂SO₄. The solvent was removed under vacuum, and the residue was purified via silica gel chromatography (10% MeOH in EtOAc) to provide the desired product.

N-(4-(4-benzylpiperidin-1-yl)butyl)-4-(hydroxymethyl)benzamide (**23a**)

The compound has been prepared using 4-(hydroxymethyl)benzoic acid (**a**, 0.46 mmol, 0.07 g). Yield: 49%, white solid. ¹H NMR (200 MHz, CDCl₃) δ 8.13 (br. s., 1H), 7.87 (d, *J*=7.4 Hz, 2H), 7.17–7.36 (m, 5H), 7.10 (d, *J*=7.8 Hz, 2H), 4.63 (br. s., 2H), 3.28–3.62 (m, 4H), 2.91 (br. s., 2H), 2.45–2.74 (m, 4H), 1.51–1.97 (m, 8H), 1.21 (t, *J*=7.0 Hz, 2H). ¹³C NMR (200 MHz, CDCl₃) δ 167.79, 145.22, 138.98, 132.49, 129.32, 123.09, 65.82, 57.67, 42.58, 34.81, 26.16. Anal. calcd for C₂₄H₃₂N₂O₂: C, 75.75; H, 8.48; N, 7.36; O, 8.41. Found: C, 75.91; H, 8.43; N, 7.35; O, 8.44.

N-(4-(4-benzylpiperidin-1-yl)butyl)-4-methylbenzamide (**23b**)

The compound has been prepared using 4-methylbenzoic acid (**b**, 0.44 mmol, 0.06 g). Yield: 60%, white solid. ¹H NMR (200 MHz, CDCl₃) δ 7.88 (d, *J*=8.2 Hz, 2H), 7.61 (t, *J*=5.9 Hz, 1H), 7.20–7.39 (m, 5H), 7.10–7.19 (m, 2H), 3.39–3.60 (m, 4H), 2.91–3.04 (m, 2H), 2.48–2.69 (m, 4H), 2.41 (s, 3H), 1.66–2.06 (m, 9H). ¹³C NMR (200 MHz, CDCl₃) δ 167.60, 141.64, 138.92, 131.17, 129.02, 128.88, 128.43, 127.26, 126.33, 52.68, 41.79, 37.73, 28.81, 26.10, 20.75. Anal. calcd for C₂₄H₃₂N₂O: C, 79.08; H, 8.85; N, 7.68; O, 4.39. Found: C, 79.21; H, 8.81; N, 7.65; O, 4.40.

Computational procedures

Molecular docking. Flexible ligands docking experiments were performed employing AutoDock 4.2.6 software implemented in YASARA (v. 19.5.5, YASARA Biosciences GmbH, Vienna, Austria) [1,2] using the crystal structure of the human σ₁ receptor model bound to PD144418 (PDB 5HK1) retrieved from the PDB_REDO Data Bank as a fully optimized one, and the Lamarckian genetic algorithm (LGA). The maps were generated by the program AutoGrid (4.2.6) with a spacing of 0.375 Å and dimensions that encompass all atoms extending 5 Å from the surface of the structure of the

crystallized ligands. All the parameters were inserted at their default settings as previously reported. In the docking tab, the macromolecule and ligand are selected, and GA parameters set as $ga_runs = 100$, $ga_pop_size = 150$, $ga_num_evals = 25000000$, $ga_num_generations = 27000$, $ga_elitism = 1$, $ga_mutation_rate = 0.02$, $ga_crossover_rate = 0.8$, $ga_crossover_mode = two\ points$, $ga_cauchy_alpha = 0.0$, $ga_cauchy_beta = 1.0$, number of generations for picking worst individual = 10. Since no water molecules are directly involved in complex stabilization, they were not considered in the docking process. All protein amino acid residues were kept rigid whereas all single bonds of ligands were treated as fully flexible. Docking for the σ_2 receptor was performed using the homology model of the σ_2 receptor previously built by the same authors maintaining the same parameters as described above [3].

Table S1. Calculated Binding Energies (kcal/mol) and Binding Constants K_i (nM) for the Binding Sites of σ_1 and σ_2 Receptors for Compounds **9–20**.

Compound	Calcd ΔG_{σ_1}	Calcd $K_i_{\sigma_1}$	Exp $K_i_{\sigma_1}$	Calcd ΔG_{σ_2}	Calcd $K_i_{\sigma_2}$	Exp $K_i_{\sigma_2}$
9	-9.96	49.61	49	-8.81	345.91	330
10	-9.83	61.79	64	-9.68	79.60	93
11	-9.20	179.20	148	-9.49	109.71	75
12	-10.27	29.39	50	-9.19	182.08	142
13	-9.77	68.38	89	-7.58	2760.6	2673
14	-9.13	201.50	145	-8.89	302.20	230
15	-9.03	238.57	250	-9.33	143.75	89
16	-10.18	34.22	93	-9.69	78.30	70
17	-10.34	26.11	24	-11.74	2.46	19
18	-11.23	5.81	19	-8.75	382.79	320
19	-10.73	13.52	22	-9.03	238.57	270
20	-9.14	198.13	170	-7.68	2331.71	2514
Haloperidol	-10.9	10.14	2.5	-10.34	30.92	16

Docked poses analysis in σ_2 receptor. Compounds with similar aliphatic linker length in the series (**11** and **16**) show interactions comparable with that observed in the σ_1 receptor pocket. In fact, compound **16**, the most active of the **9–16** series ($K_{i\sigma_2}$ of 70 nM) forms a salt bridge with the Asp29 residue utilizing the pyridinium proton and a hydrogen bond with the Asp56, while the benzyl portion in position 4 to the piperidine ring shows hydrophobic interactions with the residues Val33, Leu26, Leu78, and π - π interaction with Pro79 (Figure S1).

The good affinity of compound **17** with the σ_2 receptor ($K_{i\sigma_2}$ of 19 nM) is due to both the double hydrogen bond and the cation- π interaction between receptor and ligand. In fact, the pyridinium proton forms a salt bridge with Asp29 while the amidic hydrogen forms a hydrogen bond with Asp56; the nitrate group is stabilized by the cation- π interaction with the Phe71 and Pro113 residues (Figure S1).

Molecular optimization. The semi-empirical calculations were performed using the parameterized model number 6 Hamiltonian [4] as implemented in MOPAC package [5] (MOPAC2016 v. 18.151, Stewart Computational Chemistry, Colorado Springs, Colorado, USA).

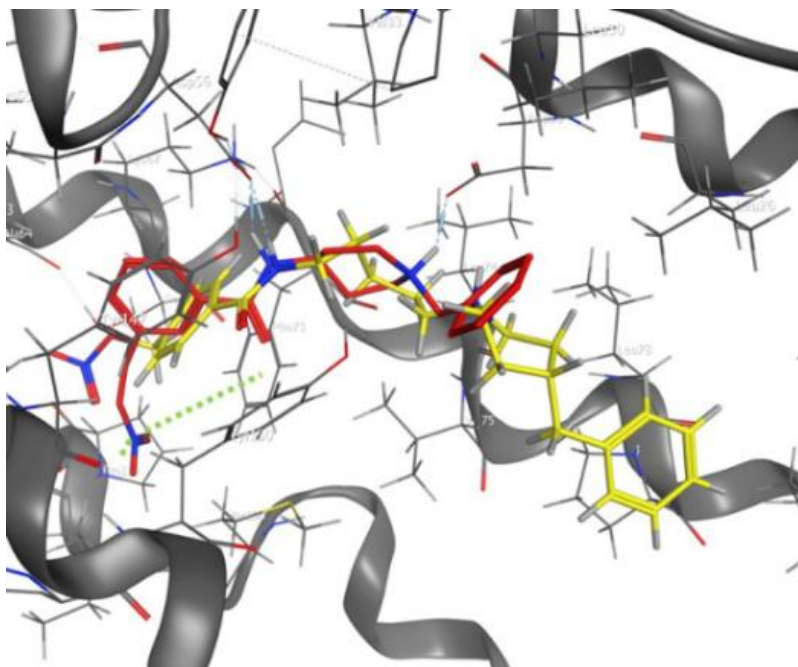


Figure S1. 3D-structures of **16** (yellow) and **17** (red) bound to the σ_2 receptor, showing the salt bridge and the cation- π (green dotted line) interactions, and the hydrogen bonds with Asp29 and Asp56 (blue dotted line).

Molecular dynamics simulations. The MD simulations of the mature human σ_1 receptor/ligand were performed with the YASARA Structure package (19.11.5) [1]. A periodic simulation cell with boundaries extending 8 Å from the surface of the complex was employed. The box was filled with water molecules, with a maximum sum of all bumps water of 1.0 Å, and a density of 0.997 g/mL. YASARA's pK_a utility used to assign pK_a values at pH 7.4 [6], and system charges was neutralized with NaCl (0.9% by mass). Water molecules were deleted to readjust the solvent density to 0.997 g/mL. The final system dimensions were approximately 70 × 70 × 90 Å [3].

The ligand force field parameters were generated with the AutoSMILES utility, employs semiempirical AM1 geometry optimization. Moreover, the assignment of charges, by the assignment of the AM1BCC atom and bond types with refinement using the RESP charges, and finally the assignments of general AMBER force field atom types. Optimization of the hydrogen bonds network of the various enzyme-ligand complexes was obtained using the method established by Hooft et al. [7]. This model allowed us to address ambiguities arising from multiple side-chain conformations and protonation states that are not well resolved in the electron density. Short MD simulation was run on the solvent only.

The entire system was then energy minimized using first a steepest descent minimization to remove conformational stress, followed by a simulated annealing minimization until convergence (<0.01 kcal/mol Å). The MD simulation was then initiated, using the NPT ensemble at 298 K, and integration time steps for intramolecular and intermolecular forces every 1.25 fs and 2.5 fs, respectively. Finally, short 10 ns MD simulations were conducted for the assessment of the correct pose, and a final MD simulation of 100 ns was performed. The conformations of each system were recorded every 100 ps.

Molecular dynamics simulations study and trajectories analysis of compound 18. Before executing the 100 ns MD simulation, it was performed a short MD one (10 ns) to identify the most stable pose. As shown in Figure S2a, compound **18** shows a bidentate interaction between the piperidinium proton

(due to the formation of the salt bridge) and the amidic hydrogen with the Glu172 residue. The ligand is placed inside the pocket, orienting the benzyl group along the bottom side of the receptor and the nitrate group toward the upper.

After 100 ns of MD simulation, it is interesting to note that the ligand maintains the salt bridge with the Glu172 residue, and a new hydrogen bond bridge is established, favored by a water molecule between the Glu172 and Asp126 residues and the amidic hydrogen. Furthermore, the His154 residue maintains a cation- π interaction with the nitrate group, further stabilizing the laying of the ligand inside the receptor. After 100 ns of MD simulation, the distance between the nitrate group and the residue His154 decreases by 0.49 Å (from 3.80 Å to 3.31 Å) while the distance between the pyridinium and Glu172 proton decreases by 0.88 Å (from 2.56 Å to 1.68 Å) (Figure S2b).

The redocking of compound **18**, using the pose after 100 ns MD simulation, resulted in a calculated K_i value of 15 nM, which is in excellent agreement with the experimental one (19 nM).

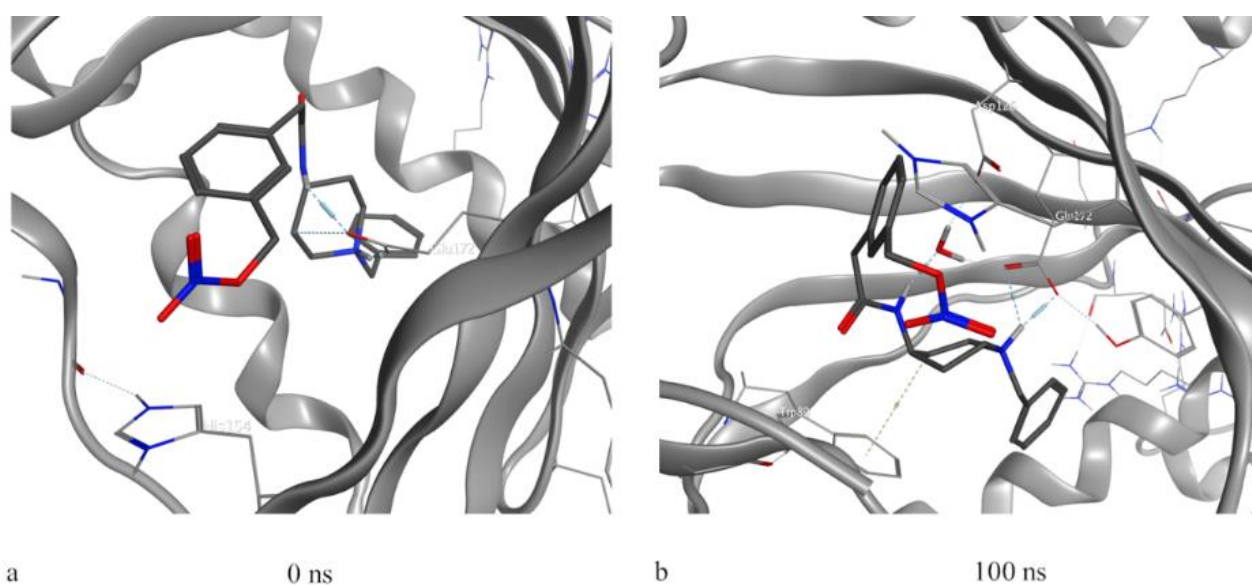


Figure S2. Poses of compound **18** bound to the σ_1 receptor at 0 ns (a) and 100 ns (b) of MD simulation, showing salt bridge interaction with Glu172 (blue dotted line) and extensive hydrophobic contacts with other binding pocket residues.

The overall RMSD for the protein system appeared to have reached equilibrium after 13 ns with slight inflation at 36 ns, while the stabilization of the ligand after 8 ns. The binding energy of the ligand undergoes a slight increase after 58 ns, remaining overall stable throughout the MD simulation. (Figure S3).

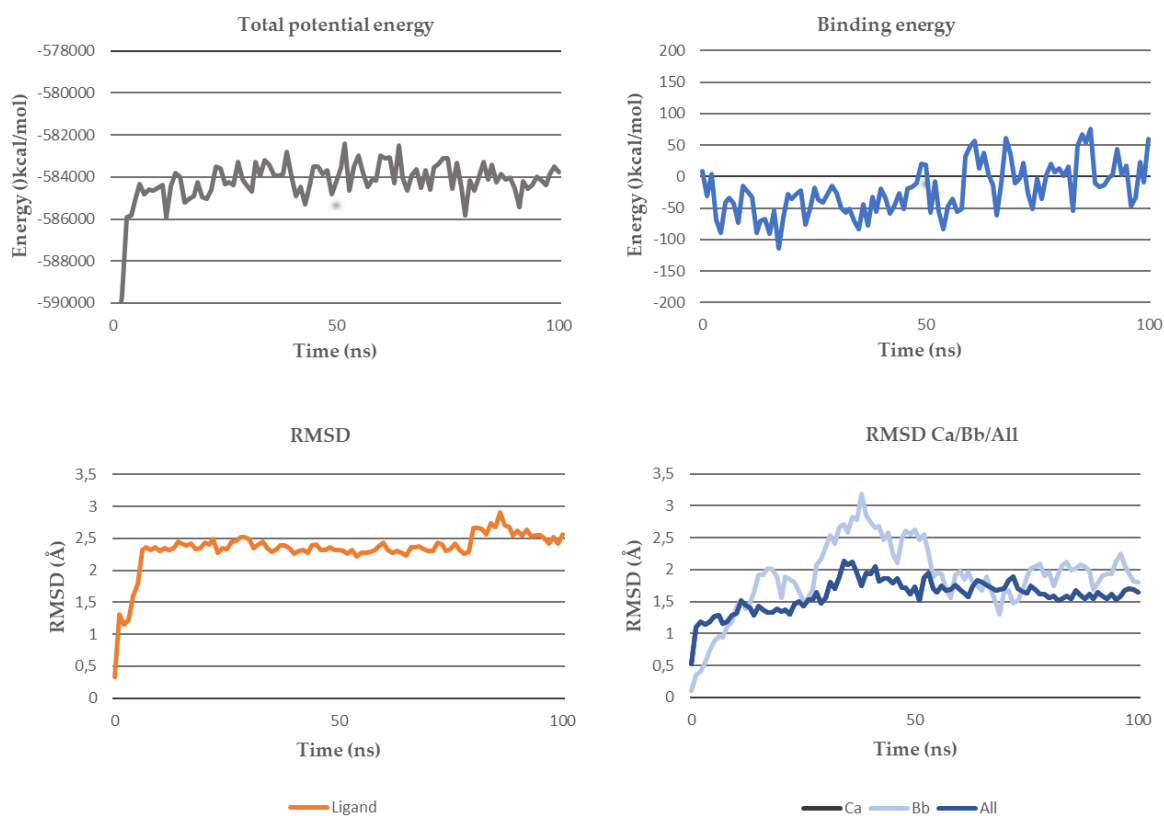


Figure S3. Total potential energy of the system (up-left), binding energy of the ligand (up-right), RMSD ligand after superposition on the receptor (down-left), and RMSDs from the starting protein structure (down-right) of σ_2 receptor and its complex with compound **18**.

Biological evaluation

Radioligand binding assays. In vitro σ_1 ligand binding assays were carried out in Tris-HCl buffer (50 mmol/L, pH 7.4) for 150 min at 37 °C by incubating the guinea pig brain membrane homogenates (500 $\mu\text{g}/\text{sample}$) with [^3H]-(+)-pentazocine (3 nM) and increasing concentrations (from 10^{-5} to 10^{-11} M) of the tested compound in a final volume of 1 mL. Haloperidol (10 μM) was employed to measure non-specific binding. Bound and free radioligand were divided by fast filtration under reduced pressure using a Millipore filter apparatus through Whatman GF/B glass fiber filters, which were presoaked for 1 h in a 0.5% poly(ethyleneimine) solution. Filters were washed with the same ice-cold buffer (2×4 mL), air-dried, and then soaked in 4 mL of Ultima Gold MV Scintillation cocktail. The amount of bound radioactivity on the filters was measured using a liquid scintillation counter Beckman LS6500 [8]. For in vitro σ_2 binding assays, the membranes (360 $\mu\text{g}/\text{sample}$) were incubated with 3 nM [^3H]-1,3-di-o-tolylguanidine ([^3H]-DTG) in the presence of the σ_1 masking agent (+)-SKF10,047 (400 nM) at rt for 120 min in 0.5 mL final volume of binding buffer (50 mmol/L Tris-HCl, pH 8.0). Non-specific binding was evaluated with unlabeled DTG (5 μM). Assays were terminated by adding ice-cold 10 mM Tris-HCl washing buffer (pH 8.0), and each sample was filtered through Whatman GF/B glass fiber filters, presoaked for 1 h in a 0.5% poly(ethyleneimine) solution. Then, filters were washed with ice-cold buffer (2×4 mL), and the amount of bound radioactivity was determined by liquid scintillation counting as described above [9]. Results are expressed as inhibition constants (K_i values) and calculated using GraphPad Prism (GraphPad Software, San Diego, CA, USA).

Detection of Nitrite: Griess Reaction. The method is based on the reaction of diazocoupling of nitrite with the Griess reagent [10]. A 10 mM solution of the appropriate compound in DMSO was diluted with Tris-HCl (50 mM, pH 7.4). The final concentration of the compounds was 100 μ M. After incubation for 30 min at 37 °C, 500 μ L of each compound were incubated for 30 min at 25° C in phosphate buffer (50 mM pH 7.4) with NADPH (50 μ M) and nitrate reductase (60 mU). To remove the excess of NADPH, which could interfere with the Griess reagent, samples were then treated with pyruvate (5 mM) and lactic dehydrogenase (1U). After 10 minutes, 500 μ L of Griess reagent was added to the reaction mixture. After 10 min at rt, the absorbance was measured spectrophotometrically at $\lambda=540$ nm; calibration was obtained using known amounts of KNO₂ (0.1 to 20 μ M). The yields of nitrite are expressed as NO₂⁻ (μ M); the experiments were performed in triplicate. Data are expressed as the mean \pm SD [11].

Cell culture. The human epithelial colorectal adenocarcinoma cell line (CaCo-2) was provided by ATCC cell bank (Rockville, MD, USA), and routinely maintained in DMEM (Gibco BRL, Life Technologies) supplemented with 10% fetal calf serum, 1% sodium pyruvate, 1% L-glutamine solution, and 1% streptomycin/penicillin. The human breast adenocarcinoma cell line (MCF-7) was obtained from the American Type Culture Collection (Rockville, MD, USA) and maintained in Dulbecco's modified Eagle's medium (DMEM) containing 10% fetal calf serum, 100 U/mL penicillin, and 100 μ g/mL streptomycin (Sigma–Aldrich, Italy). The human immortalized cell lines of dermal fibroblasts (HFF-1) provided by ATCC (Manassas, VA, USA) were suspended in Dulbecco's modified essential medium (GIBCO BRL, Life Technologies) supplemented with 10% heat-inactivated fetal calf serum, 1.0 mM sodium pyruvate, 2.0 mM l-glutamine, streptomycin (50 μ g/mL) and penicillin (50 U/mL). Cell lines were cultured in a humidified atmosphere of 5% CO₂/95% air at 37 °C. Cells from semi-confluent cultures were detached using 0.5% trypsin/0.2% EDTA and seeded in complete medium. Individual wells of a 96-well tissue culture microtiter plate (Falcon; Becton-Dickinson) were seeded with complete media containing cells in exponential growth at an initial density of 10×10^3 cells per flat-bottomed well (200 μ L per microwell). The plates were incubated at 37 °C in a humidified 5% CO₂ incubator for 24 h before the experiments. The cells were treated for 24 h with different concentrations (5, 10, 25, 35, 50, 75, or 100 μ M) of the compound solutions previously dissolved in the minimum amount of DMSO and diluted with the medium; the plates were incubated at 37 °C.

Cell viability. Cell viability was assessed by 3-(4,5-dimethylthiazol-2-yl)-2,5-diphenyltetrazolium bromide (MTT) assay, which is based on the conversion of a substrate containing a tetrazolium ring into the spectrophotometrically detectable formazan by mitochondrial dehydrogenases [12]. Cells were seeded in 96-well plates at 8×10^3 cells/well to obtain optimal cell density throughout the experiment. After treatment of cells with test compounds for 24 h, the MTT solution (0.5%, 20 μ L) was added to each well. Following incubation at 37 °C for 3 h, the supernatant was removed and replaced with 100 μ L of DMSO to solubilize formazan crystals. The optical density of each sample in the well was then measured with a microplate spectrophotometer reader (Digital and Analog Systems, Rome, Italy) at $\lambda=550$ nm, and cell viability calculated as percentage respect to untreated controls. Each experiment in quadruplicate wells was repeated at least two times, and the mean \pm SD for each value was calculated. IC₅₀ values have been calculated with GraphPad Prism 5 for Windows using a nonlinear fit transform sigmoidal dose-response (variable slope).

Western Blot Analysis. MCF-7 cells were harvested using cell lysis buffer; cell lysates were collected for Western blot analysis as previously described [13]. The membranes were incubated with the primary antibody against σ_1 receptor, purchased from Thermo Fisher Scientific (Waltham, MA USA). The complex protein–primary antibody was detected using secondary horseradish peroxidase-conjugated anti-rabbit, and the chemiluminescence signal was captured using the Gel Logic 2200 Imaging System.

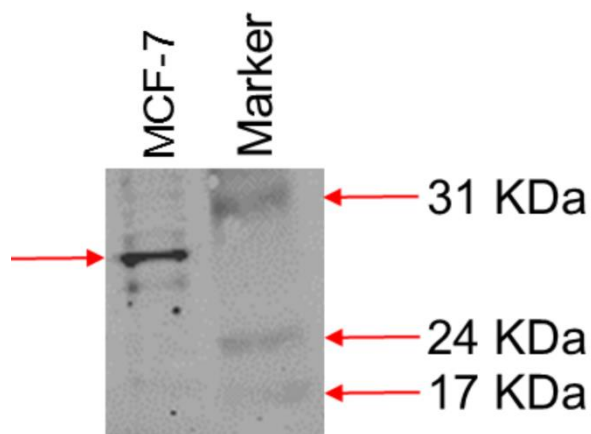
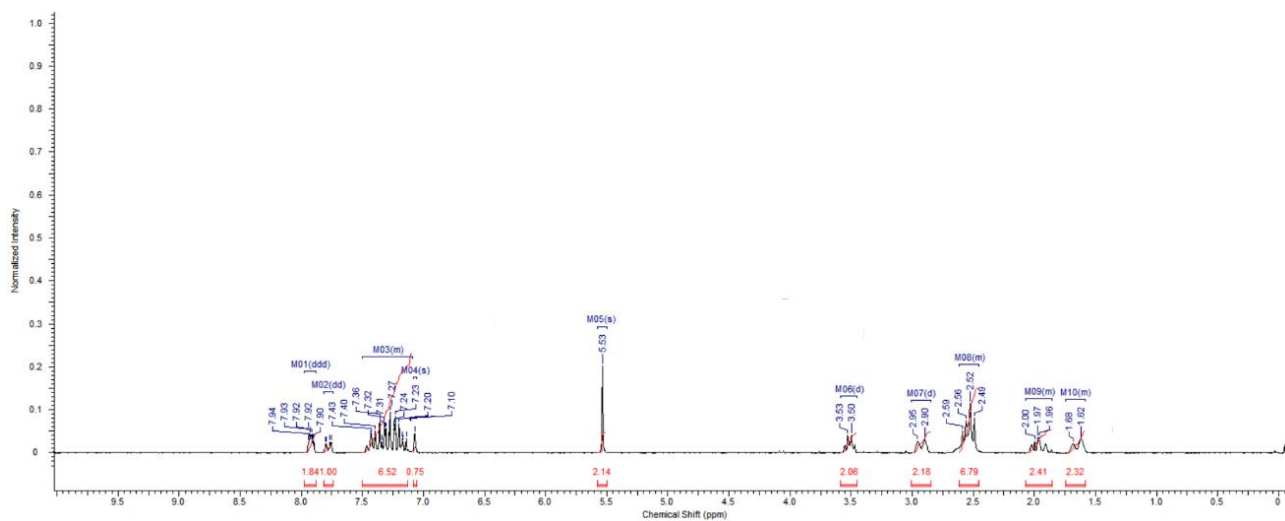
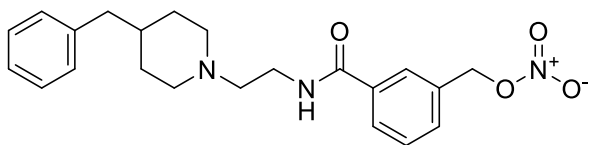


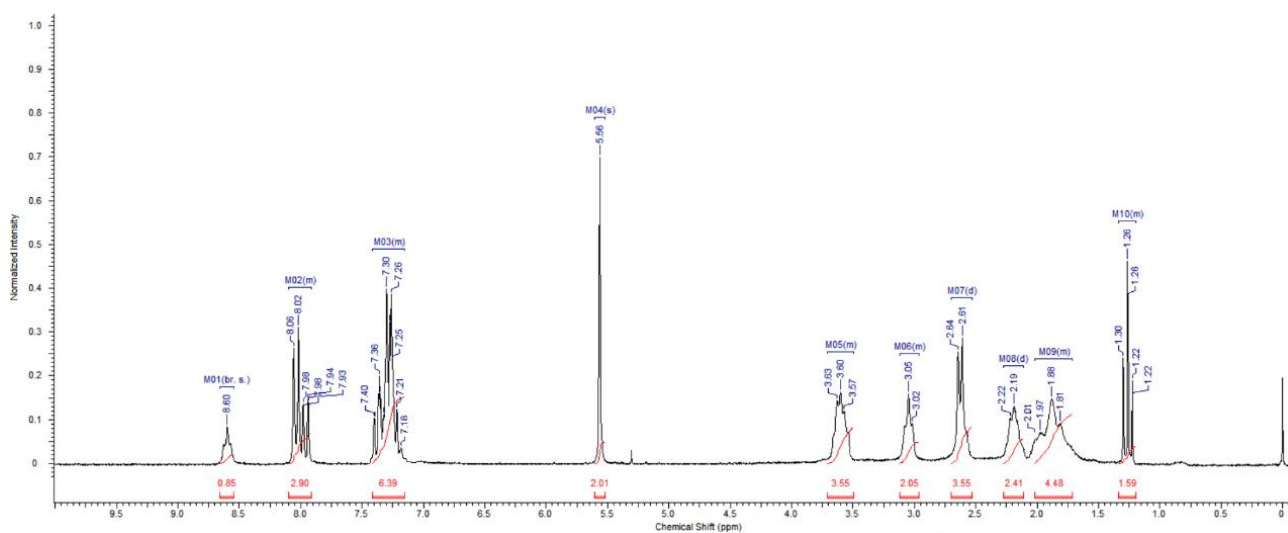
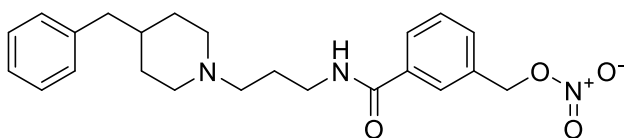
Figure S4: Representative immunoblotting image of σ_1 receptor detected in MCF-7 cells line by specific primary antibody (Thermo Fisher Scientific, PA5-30372).

^1H NMR spectra in CDCl_3

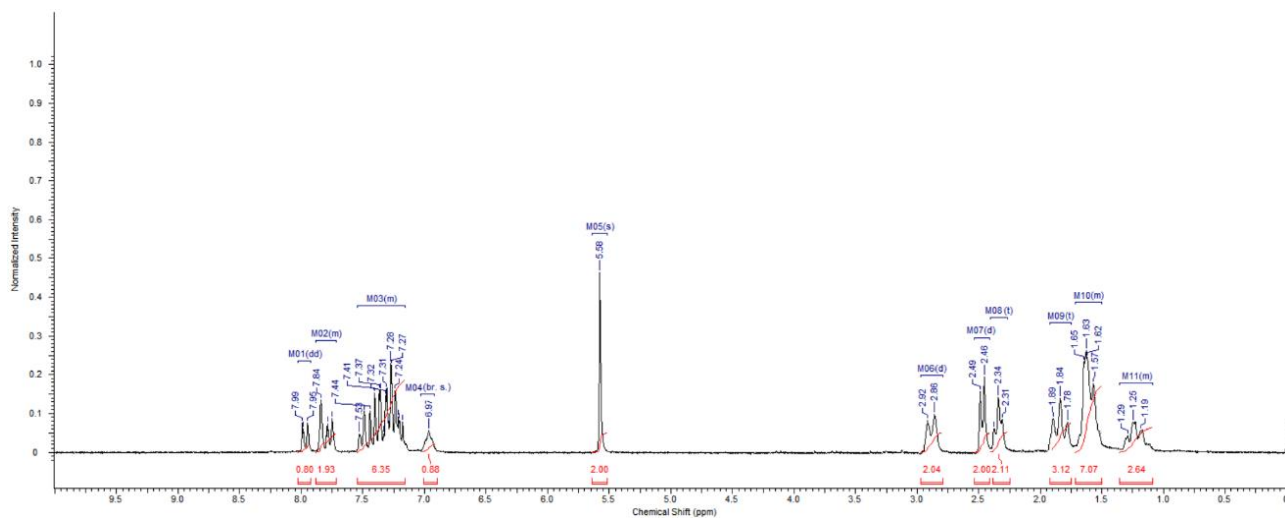
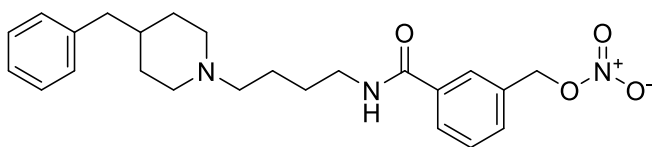
3-((2-(4-Benzylpiperidin-1-yl)ethyl)carbamoyl)benzyl nitrate (**9**)



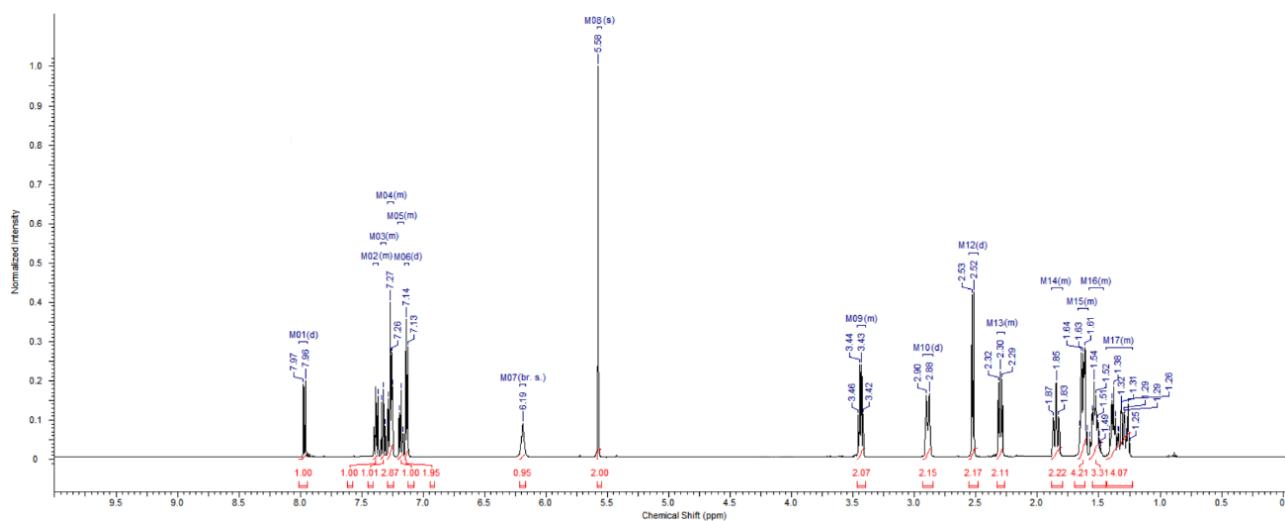
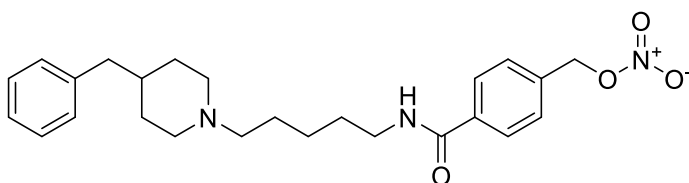
3-((3-(4-Benzylpiperidin-1-yl)propyl)carbamoyl)benzyl nitrate (**10**)



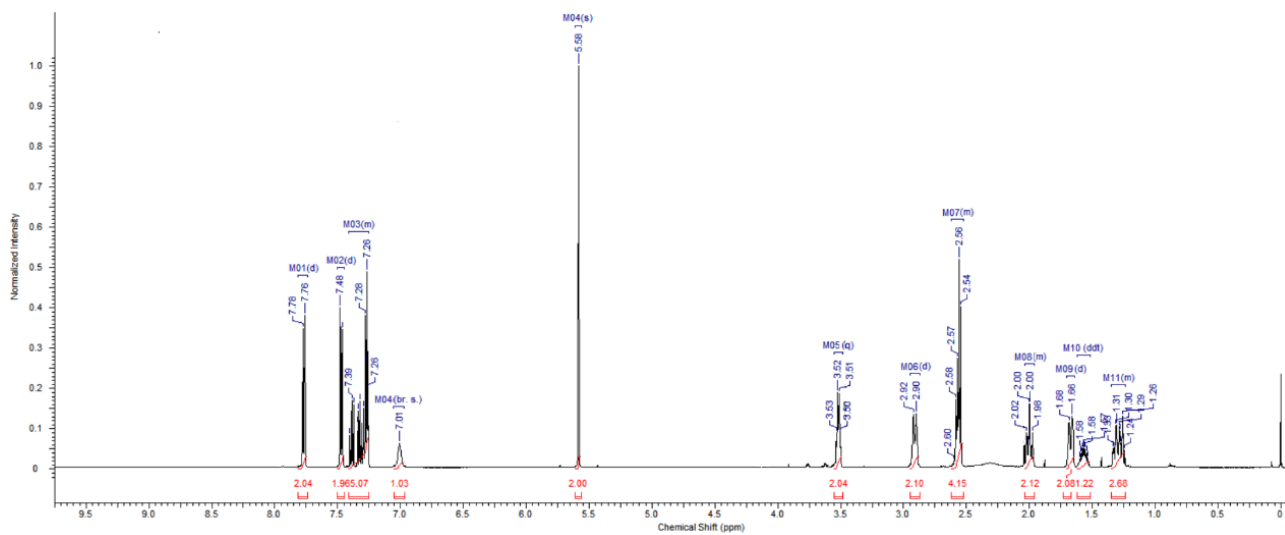
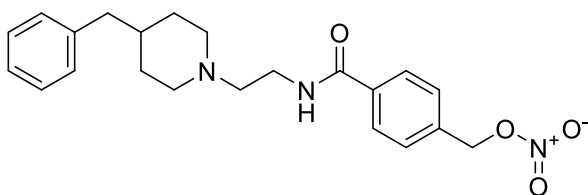
3-((4-(4-Benzylpiperidin-1-yl)butyl)carbamoyl)benzyl nitrate (**11**)



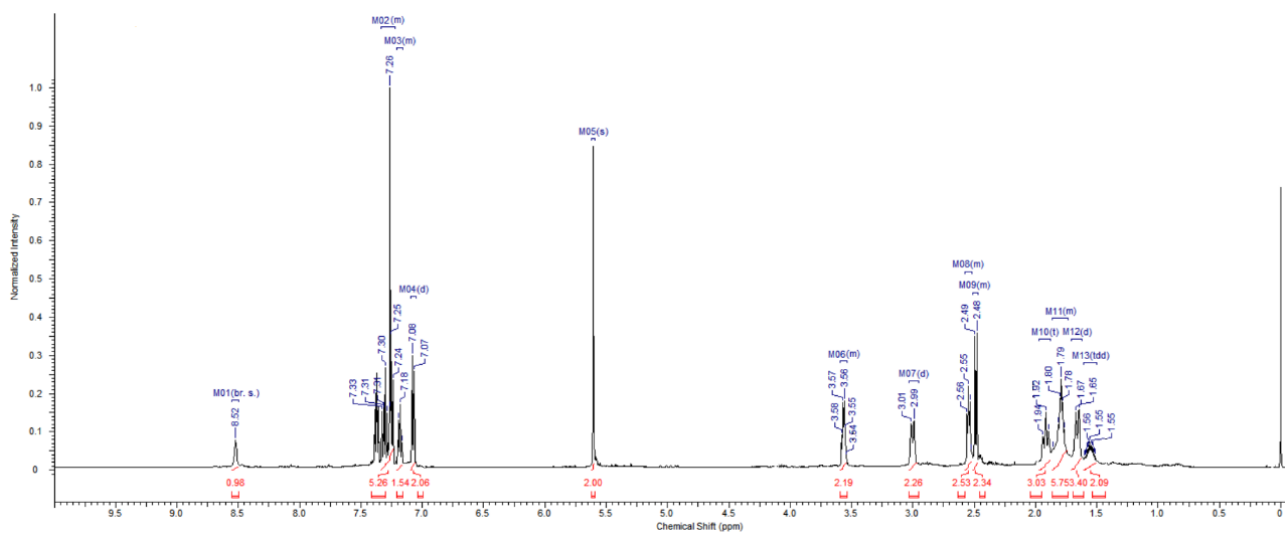
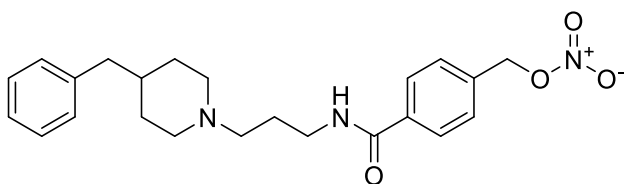
4-((5-(4-Benzylpiperidin-1-yl)pentyl)carbamoyl)benzyl nitrate (**12**)



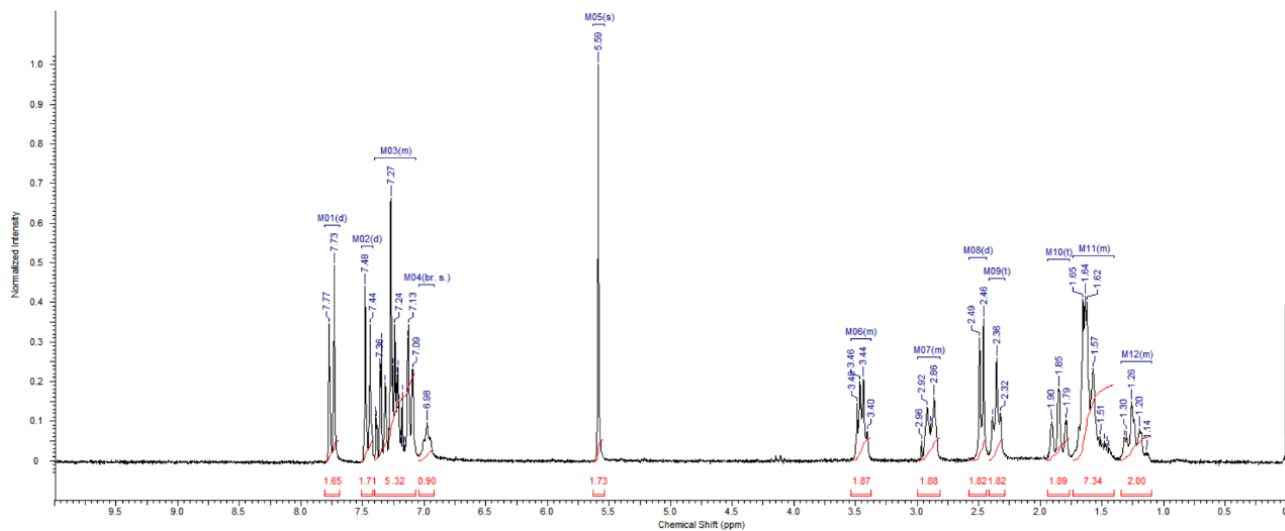
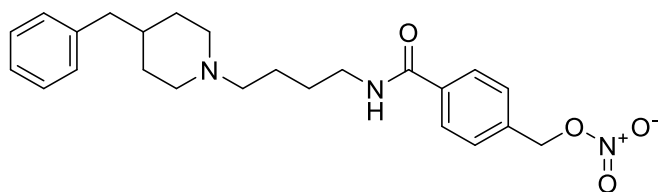
4-((2-(4-Benzylpiperidin-1-yl)ethyl)carbamoyl)benzyl nitrate (**13**)



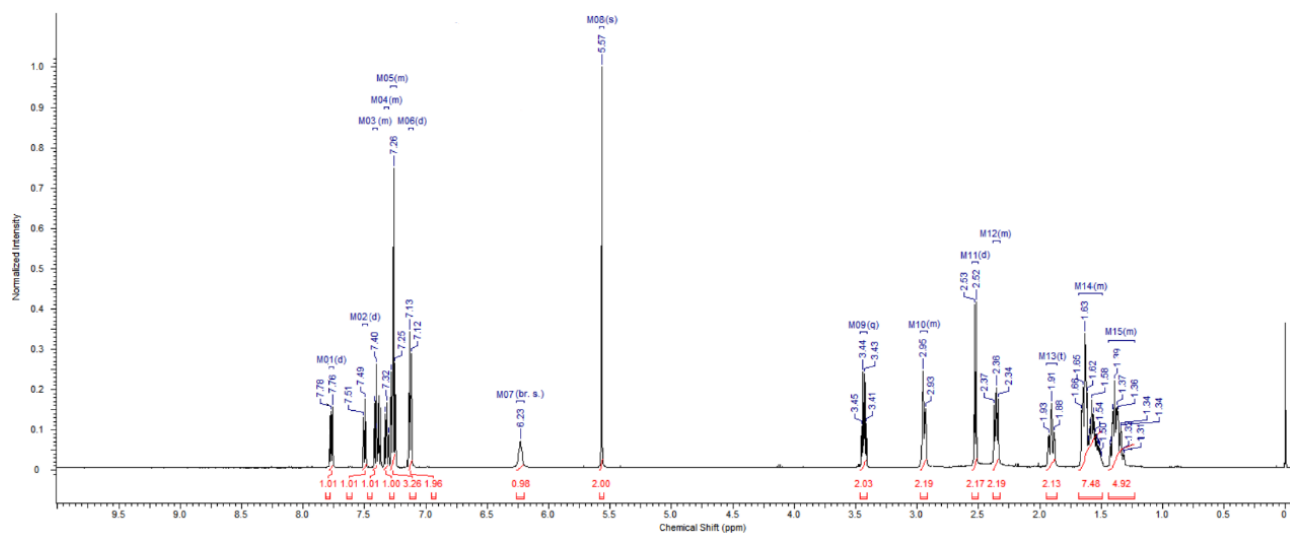
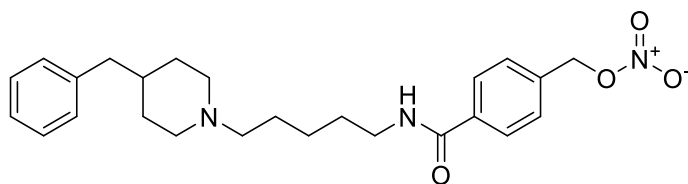
4-((3-(4-Benzylpiperidin-1-yl)propyl)carbamoyl)benzyl nitrate (**14**)



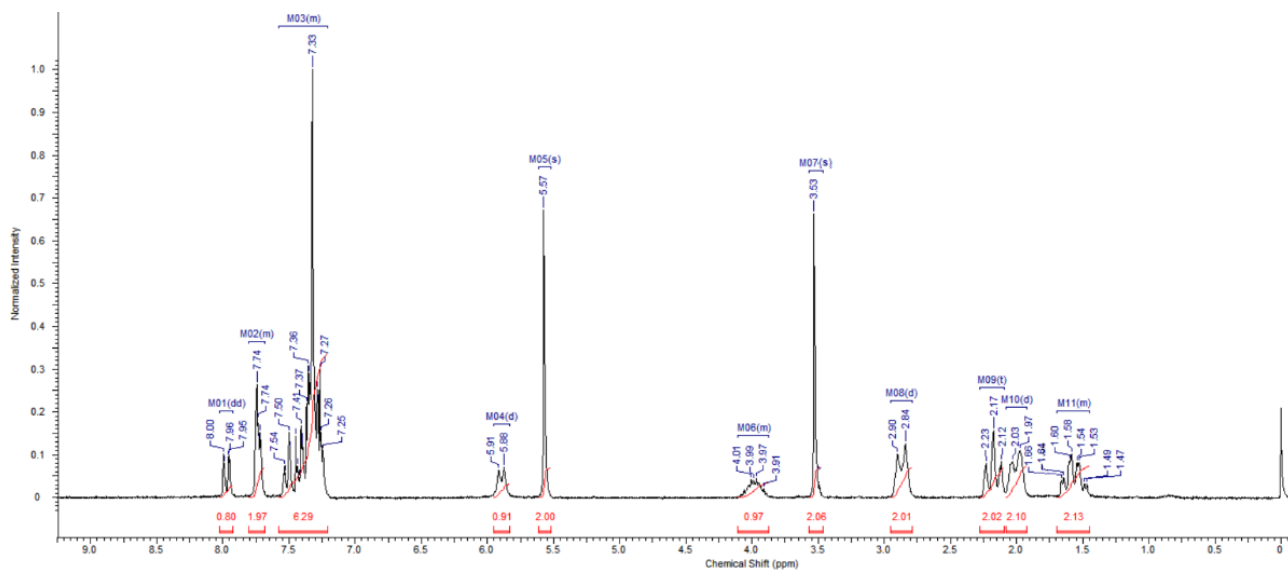
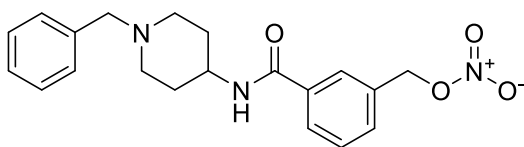
4-((4-Benzylpiperidin-1-yl)butyl)carbamoyl)benzyl nitrate (**15**)



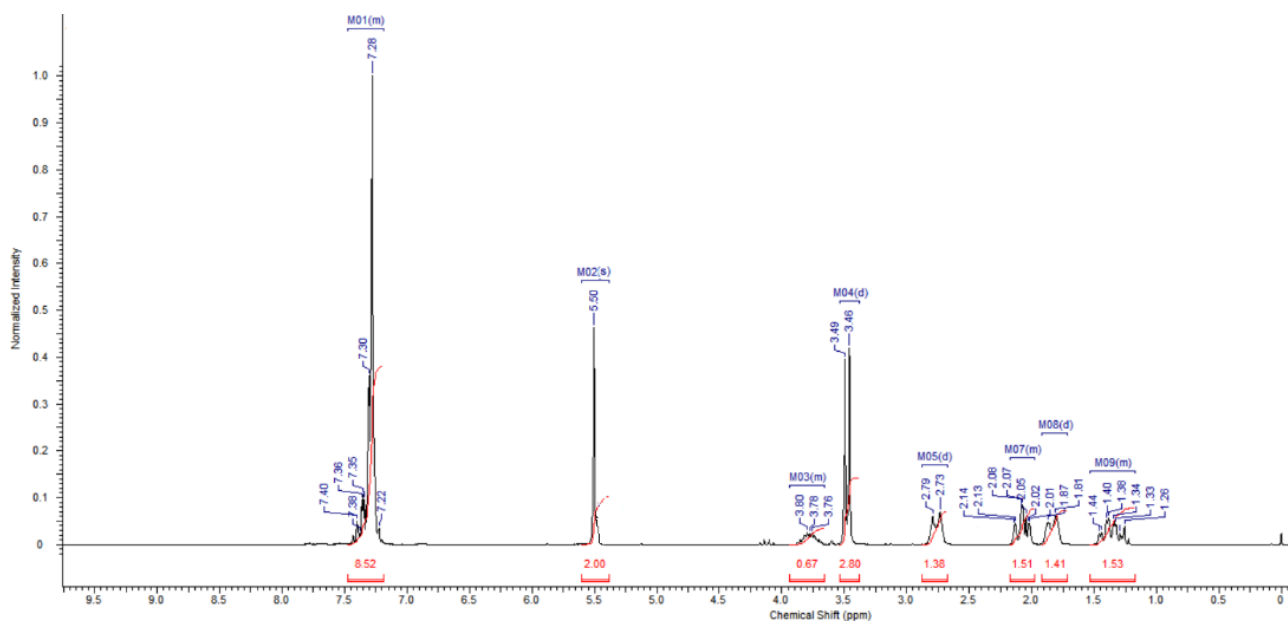
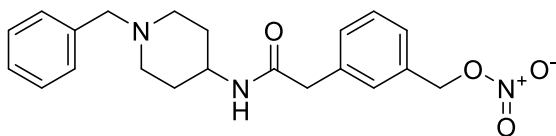
4-((5-(4-Benzylpiperidin-1-yl)pentyl)carbamoyl)benzyl nitrate (**16**)



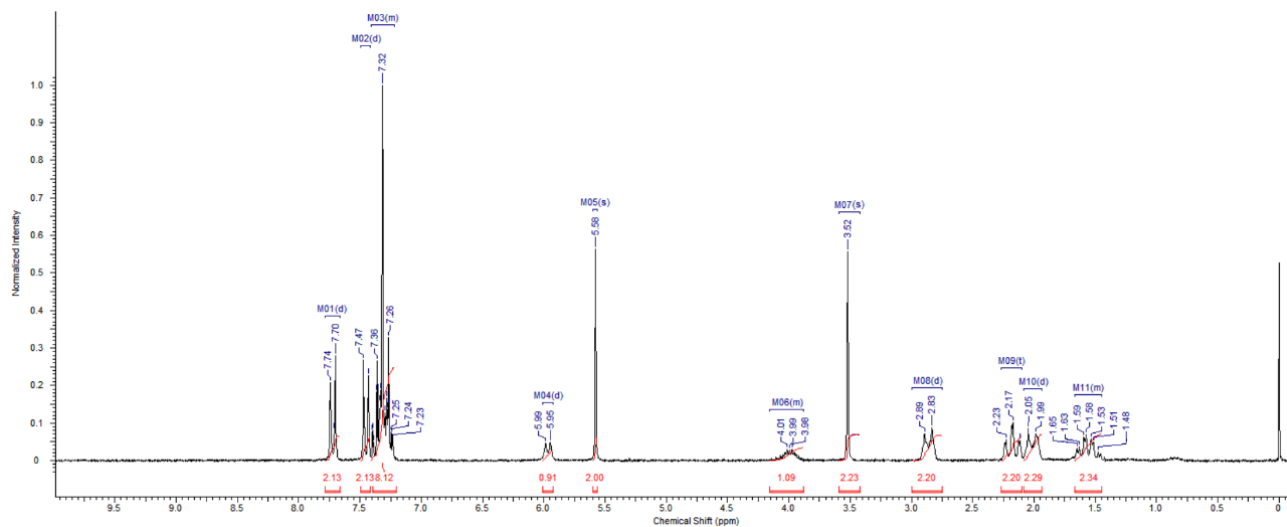
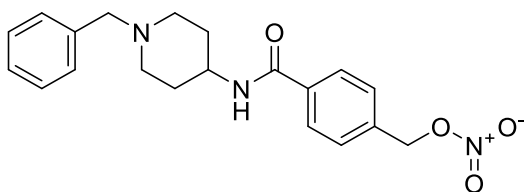
3-((1-Benzylpiperidin-4-yl)carbamoyl)benzyl nitrate (**17**)



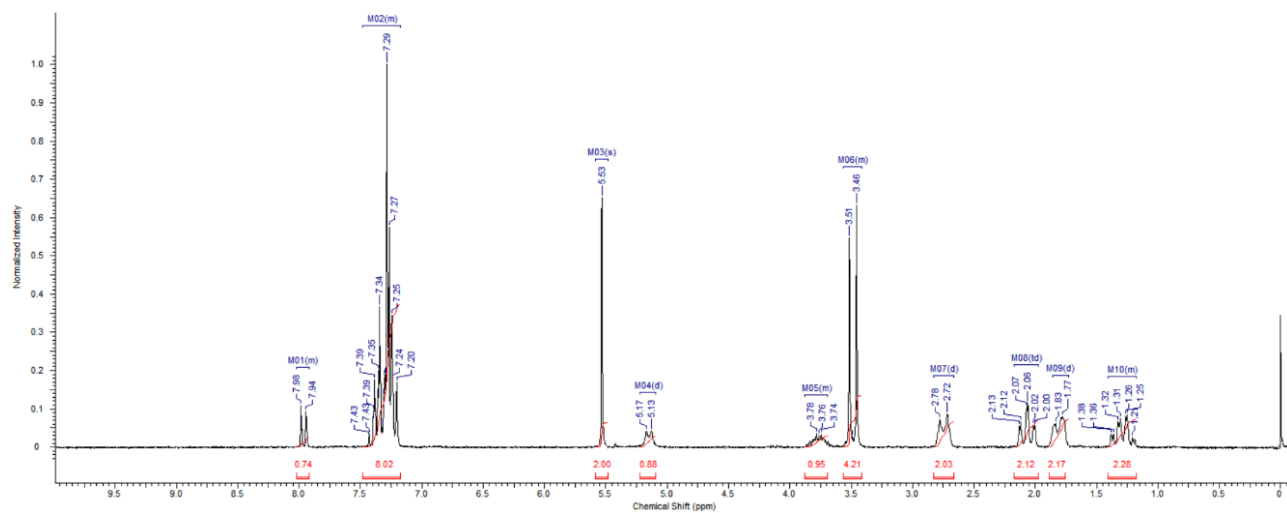
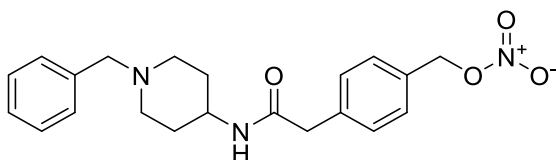
3-(2-((1-Benzylpiperidin-4-yl)amino)-2-oxoethyl)benzyl nitrate (**18**)



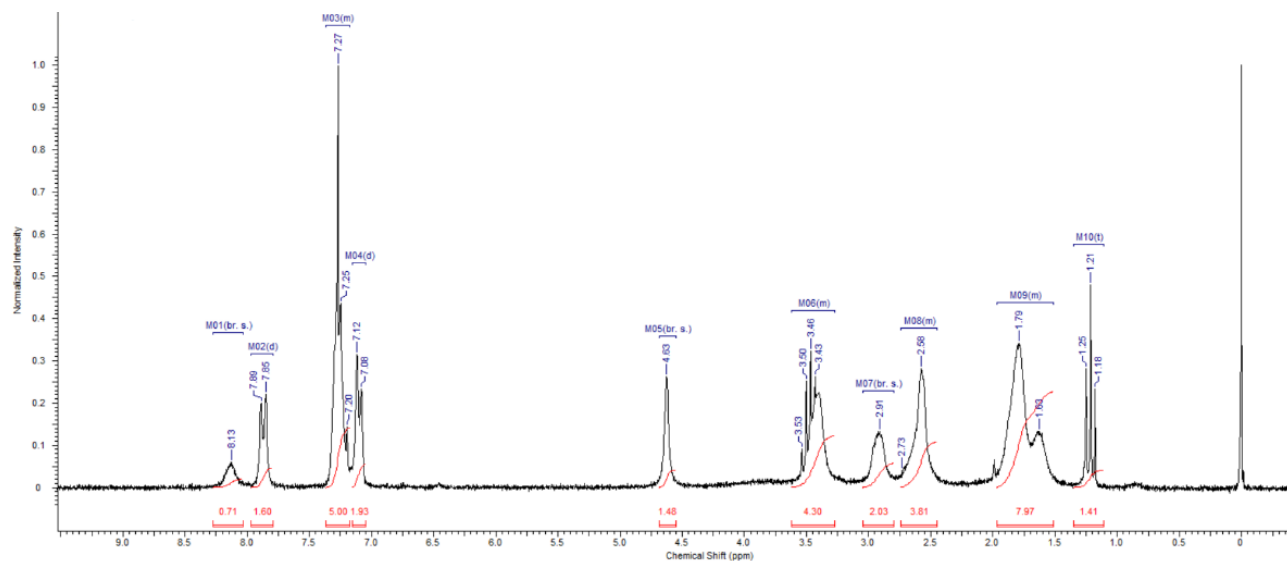
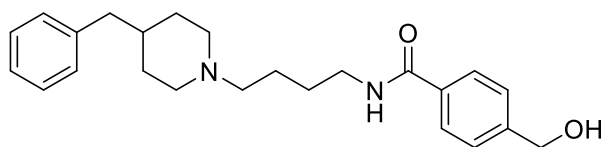
4-((1-Benzylpiperidin-4-yl)carbamoyl)benzyl nitrate (**19**)



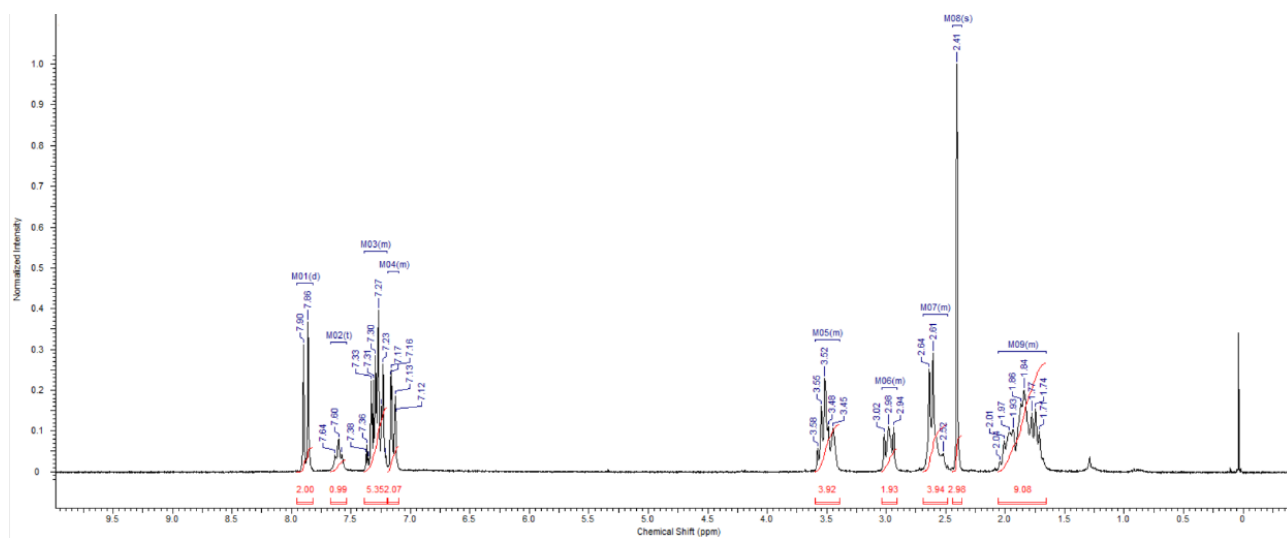
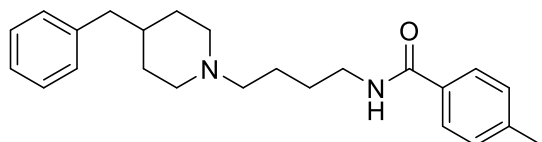
4-(2-((1-Benzylpiperidin-4-yl)amino)-2-oxoethyl)benzyl nitrate (**20**)



N-(4-(4-Benzylpiperidin-1-yl)butyl)-4-(hydroxymethyl)benzamide (**23a**)



N-(4-(4-Benzylpiperidin-1-yl)butyl)-4-methylbenzamide (**23b**)



References

- [1] Krieger, E.; Koraimann, G.; Vriend, G., Increasing the precision of comparative models with YASARA NOVA--a self-parameterizing force field. *Proteins* 2002, 47, 393-402.
- [2] Krieger, E.; Vriend, G., YASARA View - molecular graphics for all devices - from smartphones to workstations. *Bioinformatics* 2014, 30, 2981-2982.
- [3] Floresta, G.; Amata, E.; Barbaraci, C.; Gentile, D.; Turnaturi, R.; Marrazzo, A.; Rescifina, A., A Structure- and Ligand-Based Virtual Screening of a Database of "Small" Marine Natural Products for the Identification of "Blue" Sigma-2 Receptor Ligands. *Mar. Drugs* 2018, 16.
- [4] Stewart, J. J., Optimization of parameters for semiempirical methods V: modification of NDDO approximations and application to 70 elements. *J. Mol. Model* 2007, 13, 1173-1213.
- [5] Stewart, J. J. P., MOPAC2016. 2017.
- [6] Krieger, E.; Nielsen, J. E.; Spronk, C. A.; Vriend, G., Fast empirical pKa prediction by Ewald summation. *J. Mol. Graph. Model* 2006, 25, 481-486.
- [7] Krieger, E.; Dunbrack, R. L., Jr.; Hooft, R. W.; Krieger, B., Assignment of protonation states in proteins and ligands: combining pKa prediction with hydrogen bonding network optimization. *Methods Mol. Biol.* 2012, 819, 405-421.
- [8] DeHaven-Hudkins, D. L.; Fleissner, L. C.; Ford-Rice, F. Y., Characterization of the binding of [3H](+)-pentazocine to sigma recognition sites in guinea pig brain. *Eur. J. Pharmacol.* 1992, 227, 371-378.
- [9] Mach, R. H.; Smith, C. R.; Childers, S. R., Ibogaine possesses a selective affinity for sigma 2 receptors. *Life Sci.* 1995, 57, P157-62.
- [10] Griess, P., Bemerkungen zu der abhandlung der H.H. Weselsky und Benedikt "Ueber einige azoverbindungen". *Ber. Dtsch. Chem. Ges.* 1879, 12.
- [11] Amata, E.; Dichiara, M.; Arena, E.; Pittalà, V.; Pistarà, V.; Cardile, V.; Graziano, A. C. E.; Fraix, A.; A., M.; Sortino, S.; Prezzavento, O., Novel sigma receptors ligands-nitric oxide photodonor: molecular hybrids for double-targeted antiproliferative effect. *J. Med. Chem.* 2017, 60, 9531-9544.
- [12] Acquaviva, R.; Sorrenti, V.; Santangelo, R.; Cardile, V.; Tomasello, B.; Malfa, G.; Vanella, L.; Amodeo, A.; Genovese, C.; Mastrojeni, S.; Pugliese, M.; Ragusa, M.; Di Giacomo, C., Effects of an extract of *Celtis aetnensis* (Tornab.) Strobl twigs on human colon cancer cell cultures. *Oncol. Rep.* 2016, 36, 2298-2304.
- [13] Malfa, G. A.; Tomasello, B.; Acquaviva, R.; Genovese, C.; La Mantia, A.; Cammarata, F. P.; Ragusa, M.; Renis, M.; Di Giacomo, C., *Betula etnensis* Raf. (Betulaceae) Extract Induced HO-1 Expression and Ferroptosis Cell Death in Human Colon Cancer Cells. *Int. J. Mol. Sci.* 2019, 20, E2723.

Synthesis and preclinical evaluation of novel H₂S-donor sigma receptor hybrids for the management of pain

Maria Dichiara, Antonia Artacho-Cordón, Agostino Marrazzo, Enrique J Cobos,* and Emanuele Amata*

^a Department of Drug and Health Sciences, Medicinal Chemistry section, University of Catania, Viale Andrea Doria, 95125 Catania, Italy

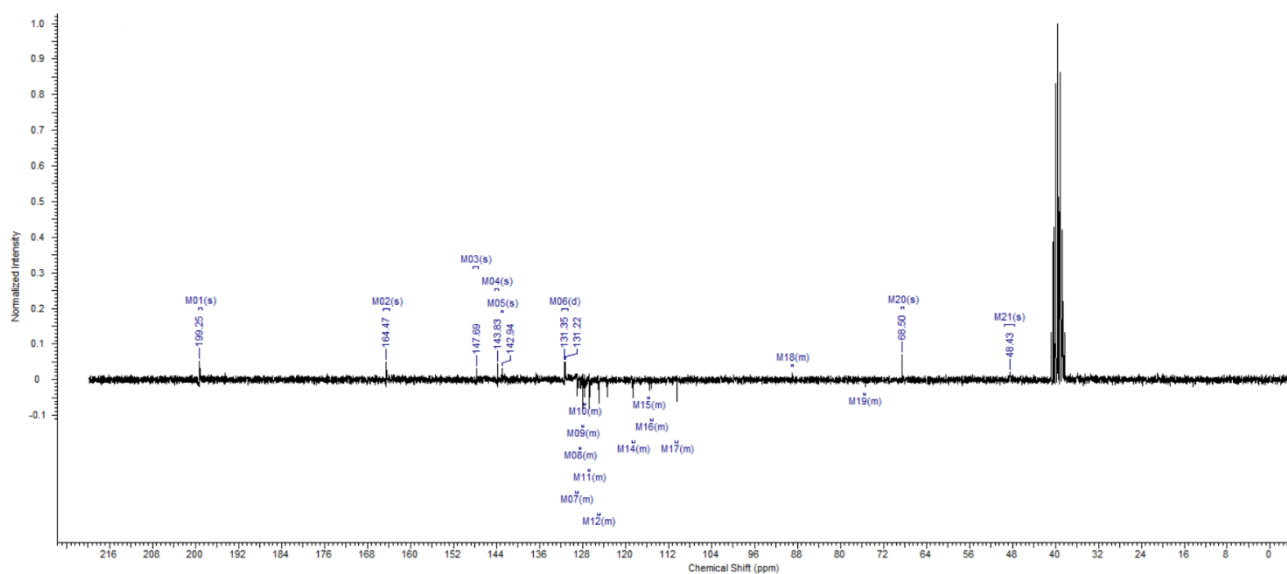
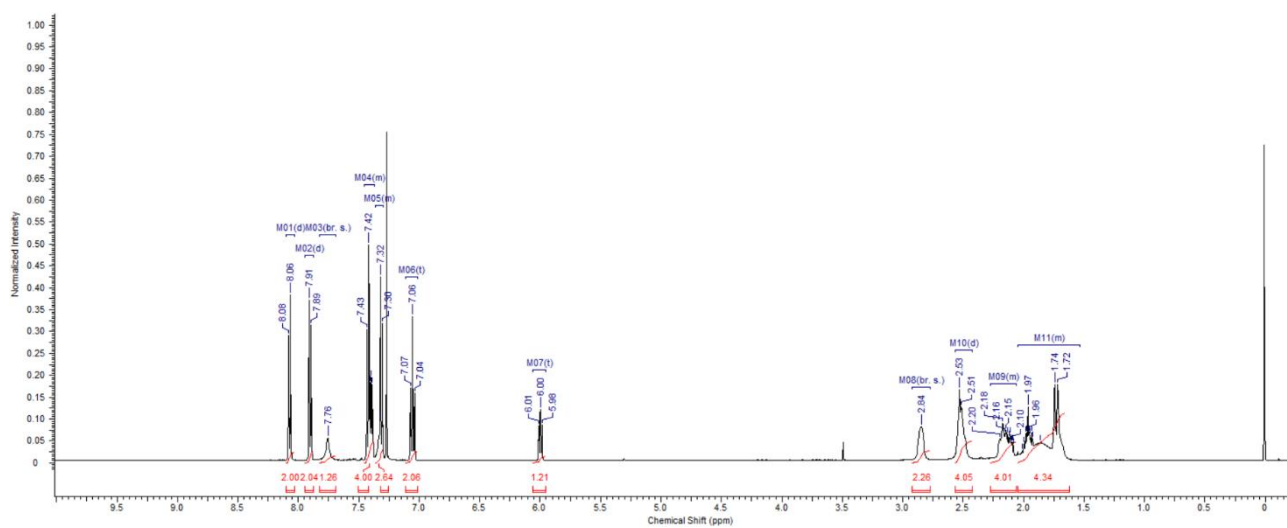
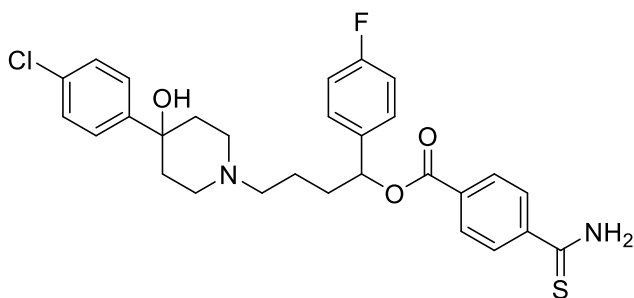
^b Department of Pharmacology, Faculty of Medicine and Institute of Neuroscience, Biomedical Research Center, University of Granada, Parque Tecnológico de Ciencias de la Salud, 18100 Armilla, Granada, Spain

EXPERIMENTAL SECTION

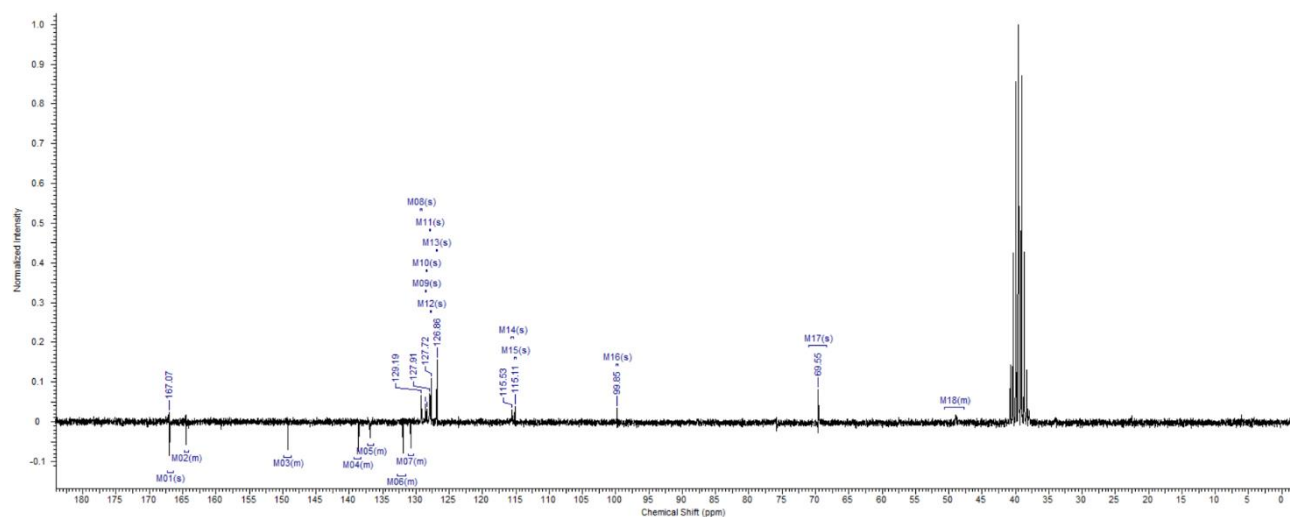
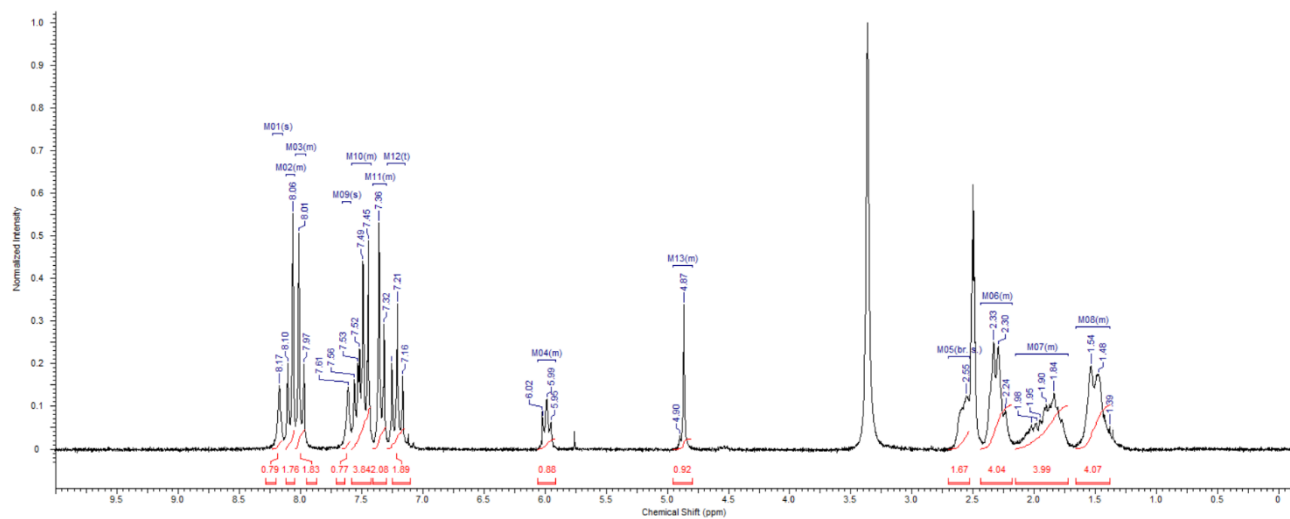
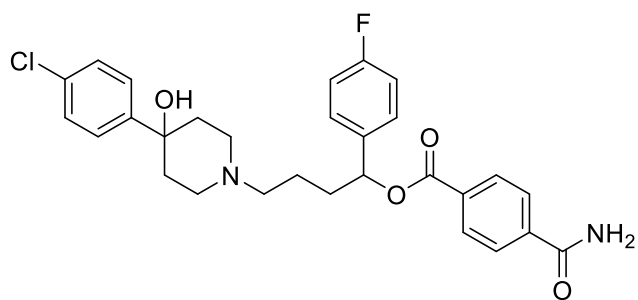
Table of contents	
NMR spectra	S22
Chemistry	S30
In vivo pharmacology	S30

^1H and ^{13}C NMR spectra in DMSO-d_6

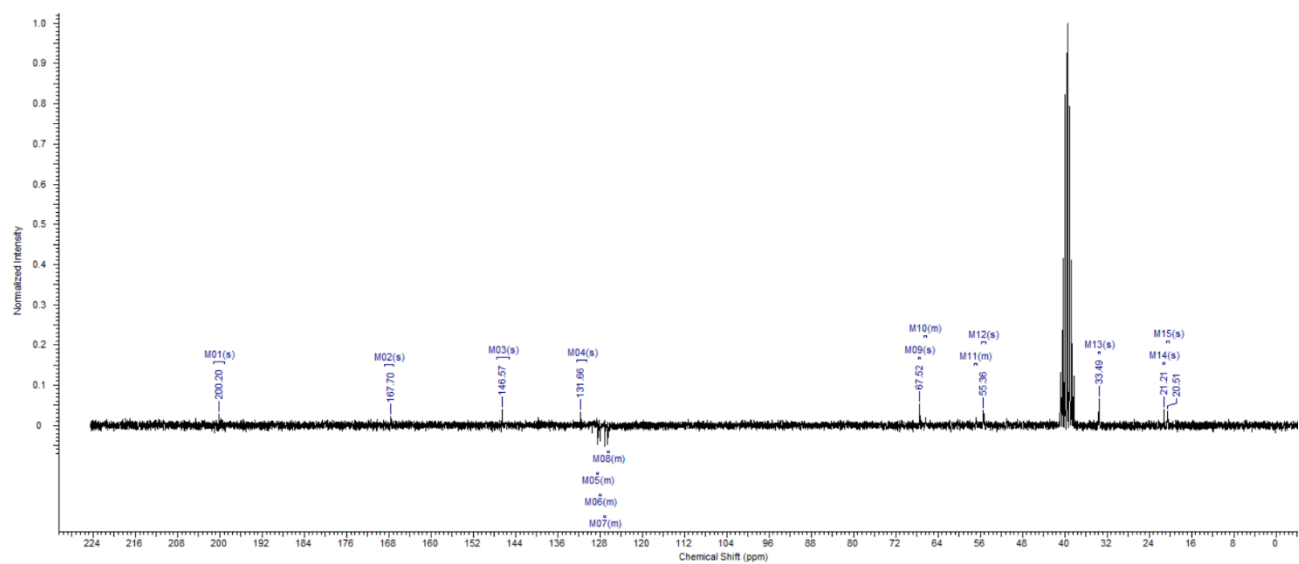
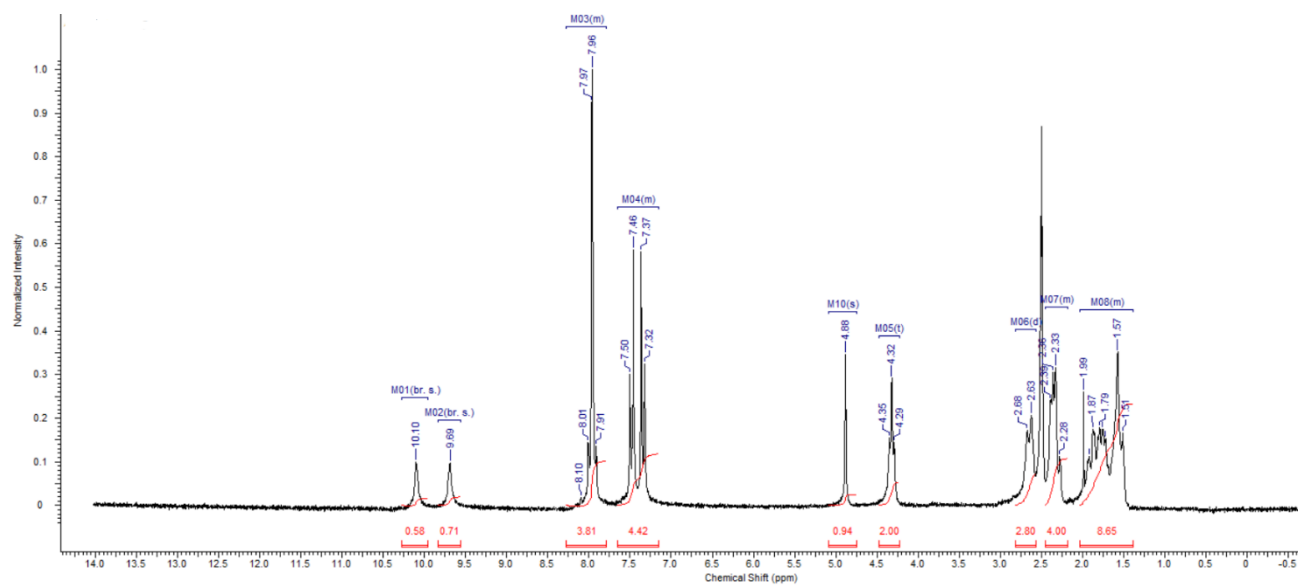
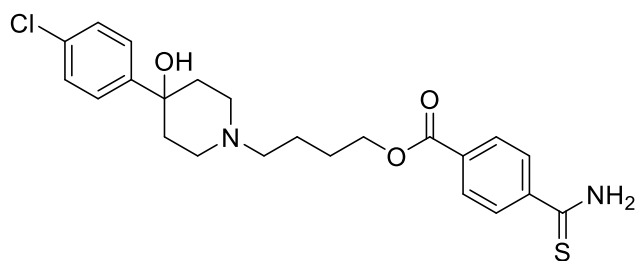
4-(4-(4-Chlorophenyl)-4-hydroxypiperidin-1-yl)-1-(4-fluorophenyl)butyl 4-carbamothioylbenzoate (**4a**)



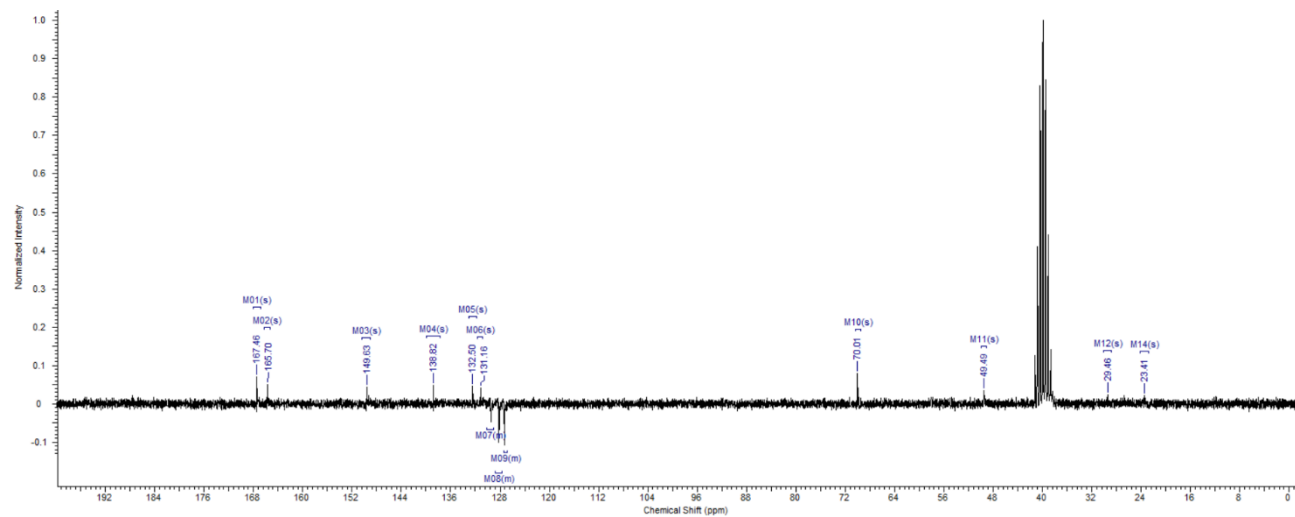
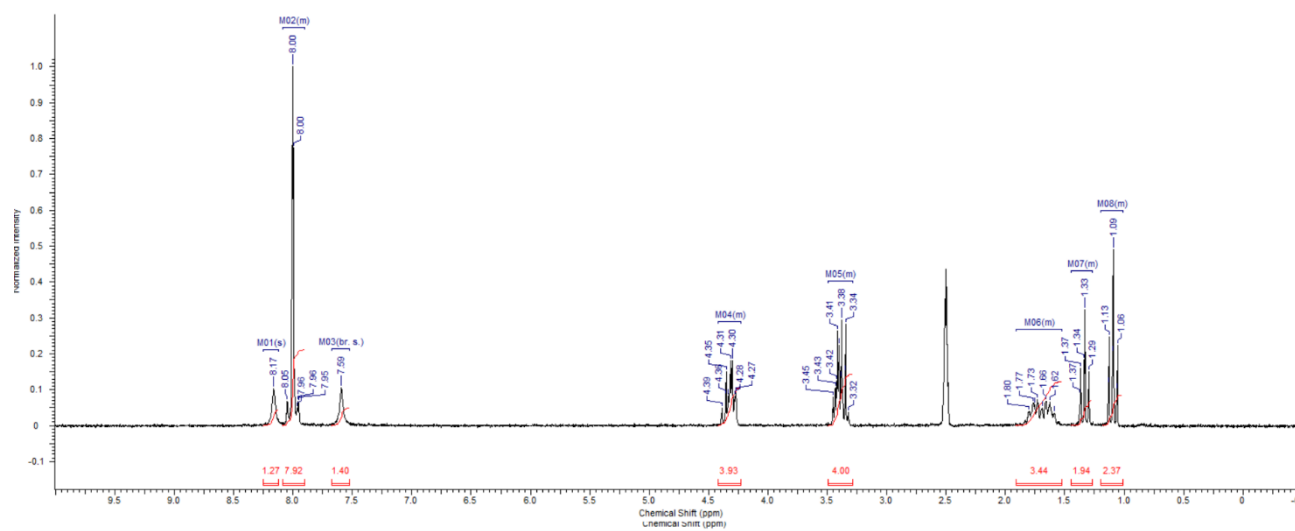
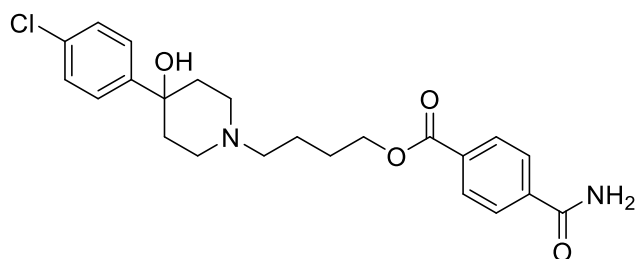
4-(4-(4-Chlorophenyl)-4-hydroxypiperidin-1-yl)-1-(4-fluorophenyl)butyl 4-carbamoylbenzoate (**4b**)



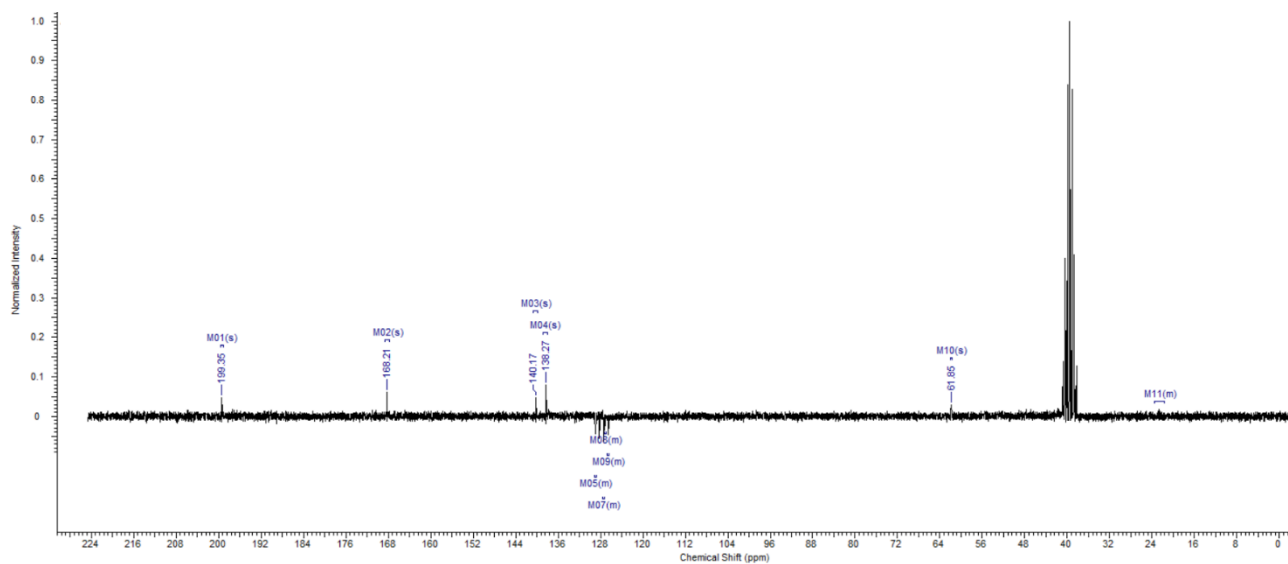
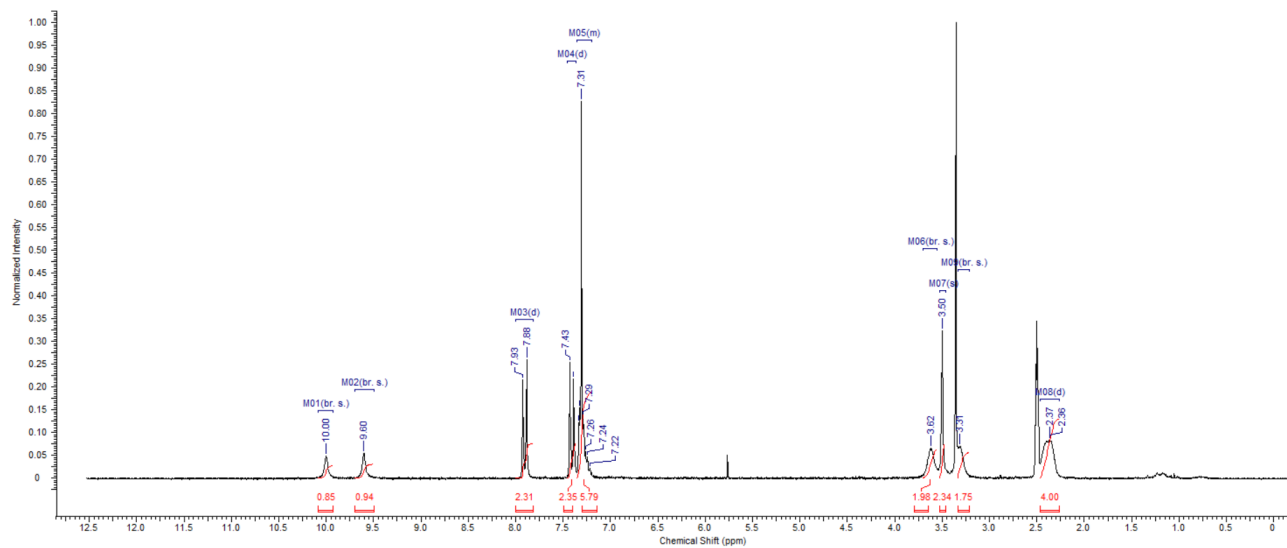
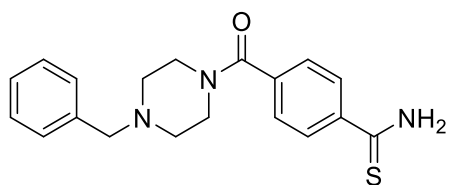
4-(4-(4-Chlorophenyl)-4-hydroxypiperidin-1-yl)butyl 4-carbamothioylbenzoate (**5a**)



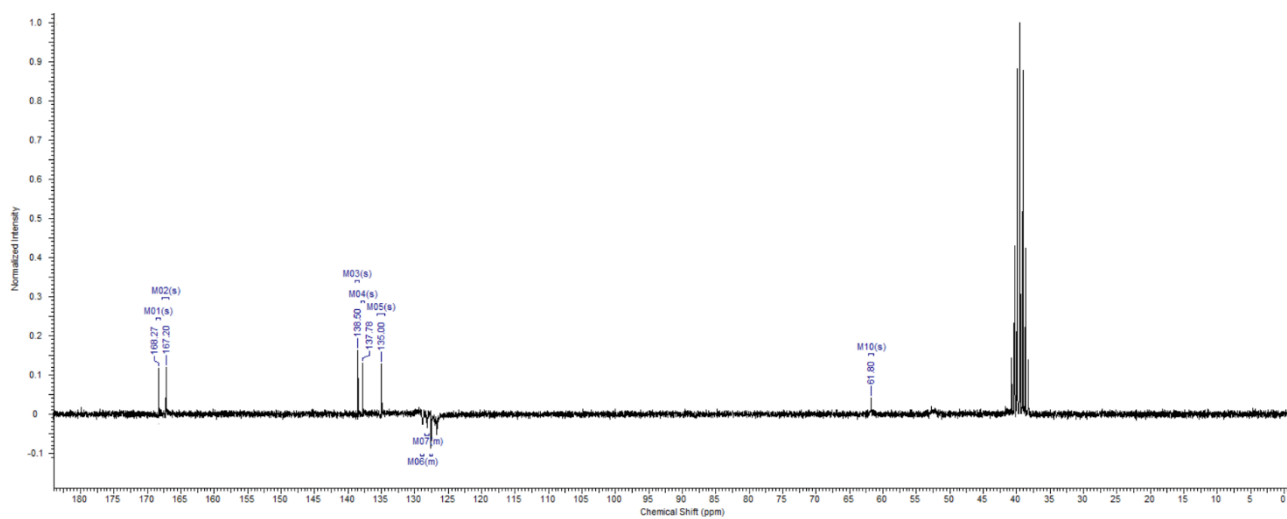
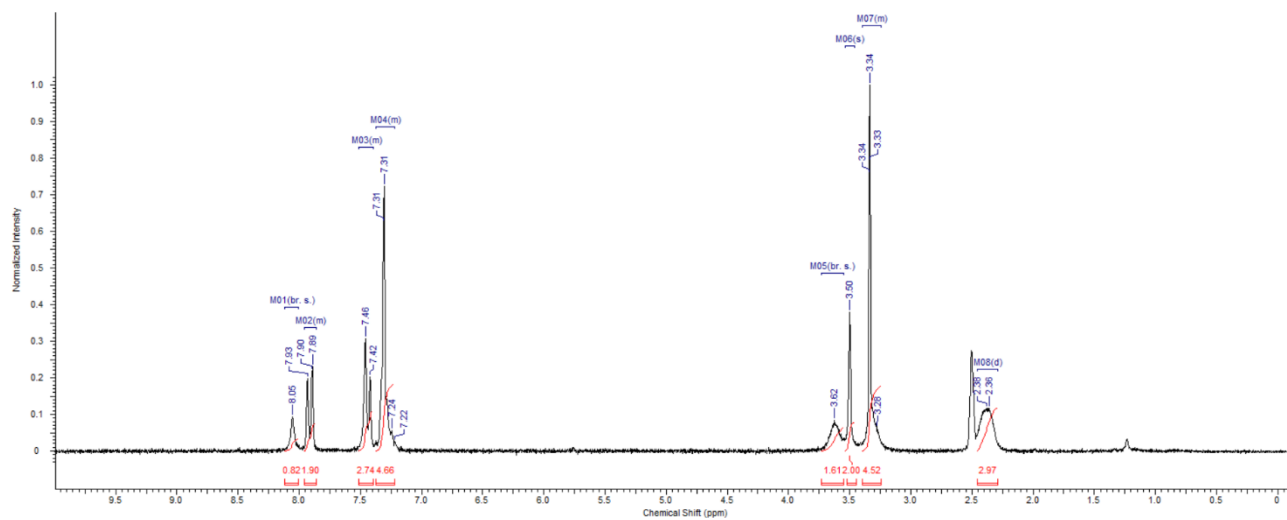
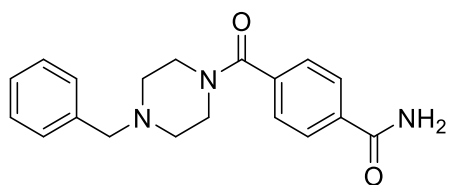
4-(4-(4-Chlorophenyl)-4-hydroxypiperidin-1-yl)butyl 4-carbamoylbenzoate (**5b**)



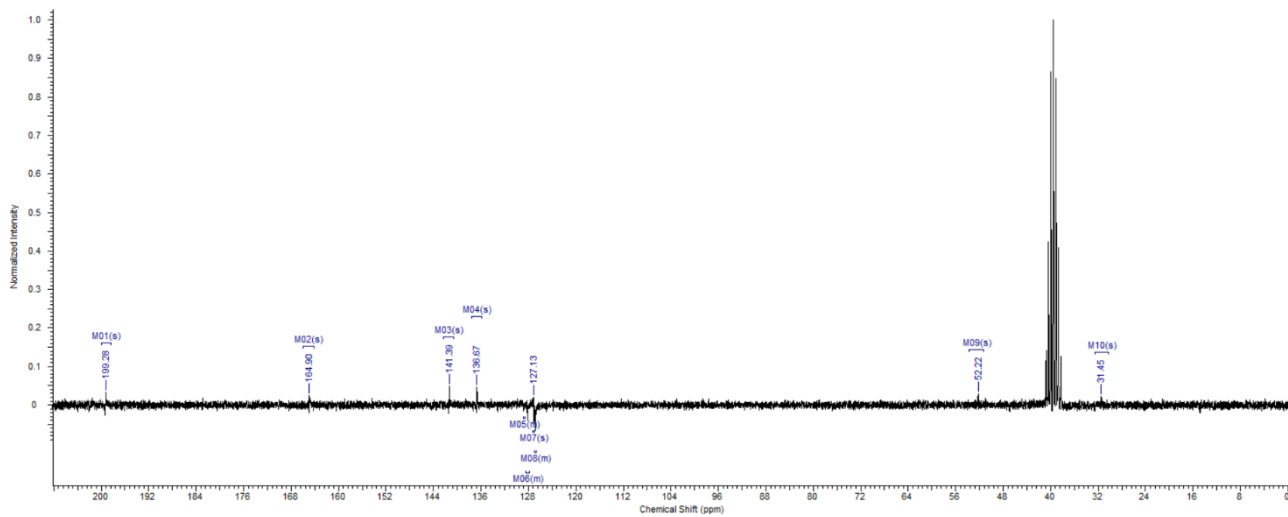
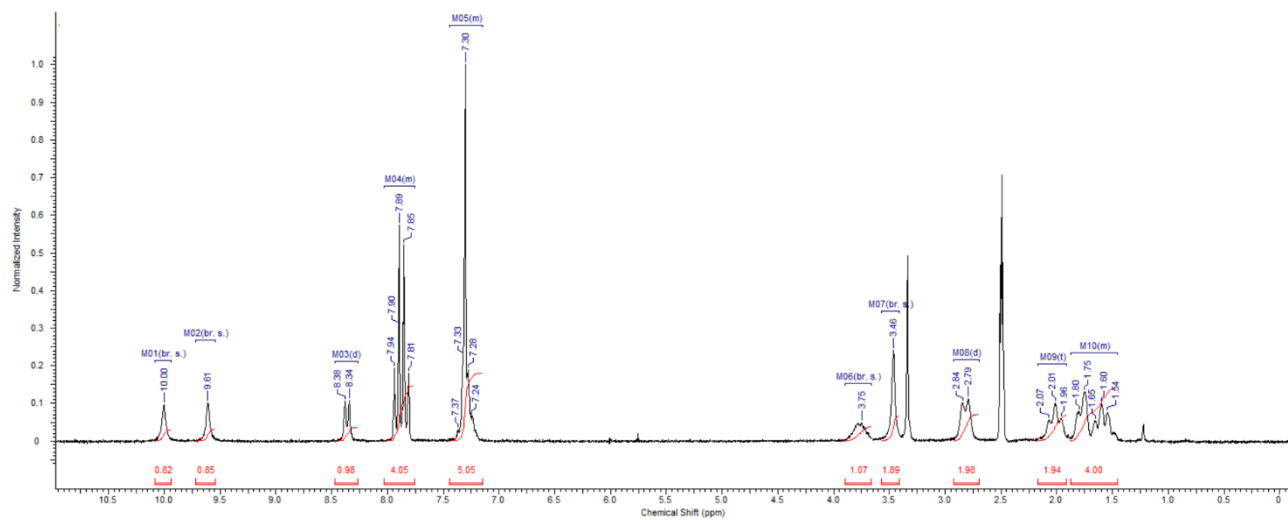
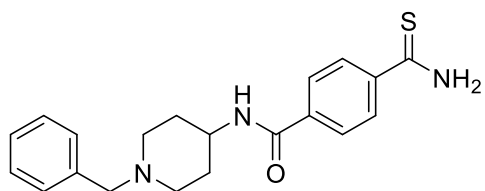
4-(4-Benzylpiperazine-1-carbonyl)benzothioamide (**6a**)



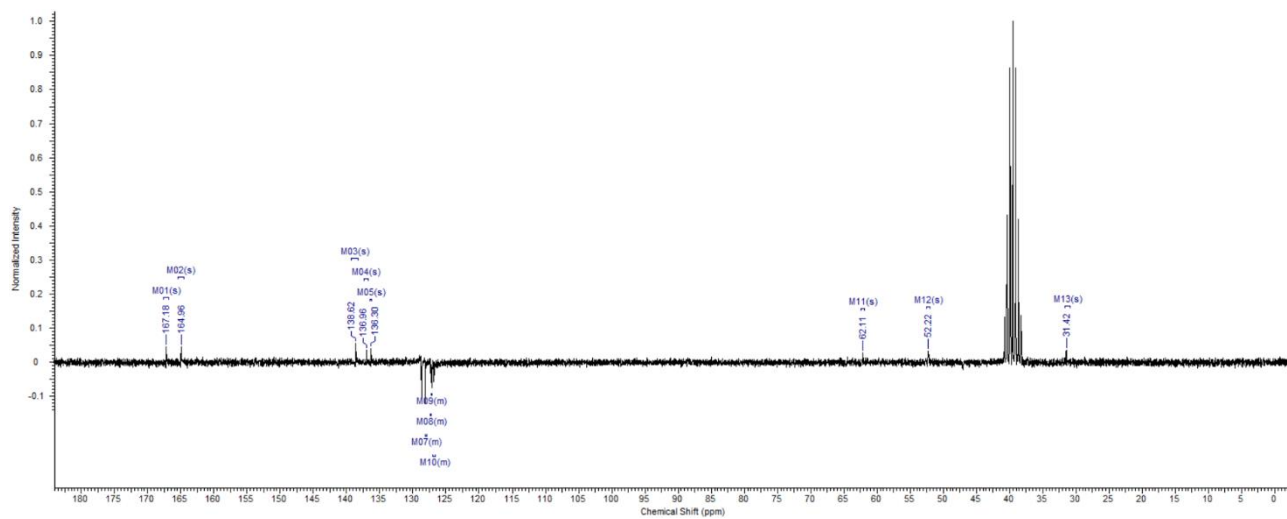
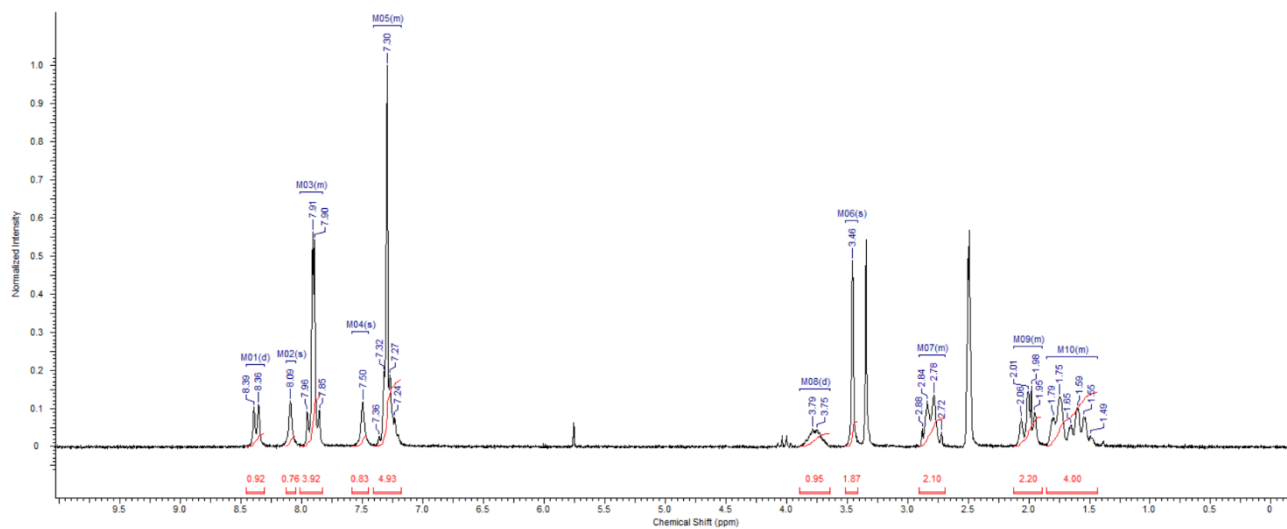
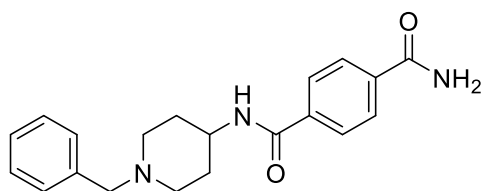
4-(4-Benzylpiperazine-1-carbonyl)benzamide (**6b**)



N-(1-Benzylpiperidin-4-yl)-4-carbamothioylbenzamide (**7a**)

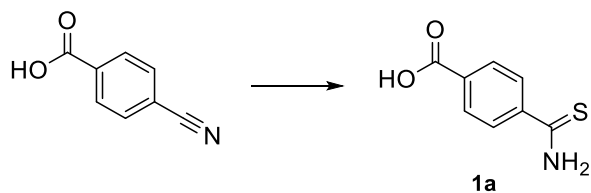


N-(1-Benzylpiperidin-4-yl)terephthalamide (**7b**)



Chemistry

Scheme S1. Synthetic Strategy for the Preparation of Compound **1a**.



Reagents and conditions: P₄S₁₀, EtOH, 100 °C, 5 h.

In vivo pharmacology

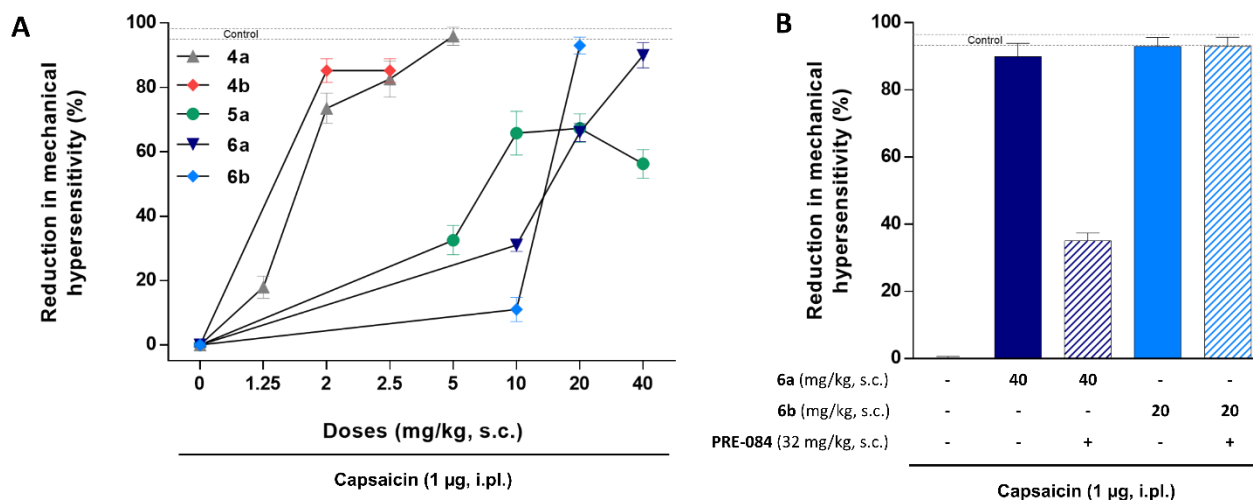


Figure S1. A) Dose dependency of the antinociceptive effects of the subcutaneous (s.c.) administration of **4a**, **4b**, **5a**, **6a** and **6b** in mice. B) Effects of **6a** and **6b** alone and in combination with the σ_1 R agonist PRE-084.

Tuning Properties for Blood–Brain Barrier Permeation: A Statistics-Based Analysis

Maria Dichiara, Benedetto Amata, Rita Turnaturi, Agostino Marrazzo, Emanuele Amata*

Department of Drug Sciences, Medicinal Chemistry Section, University of Catania, Viale A. Doria 6, 95125 Catania, Italy

*Corresponding author: Emanuele Amata, E-mail address: eamata@unict.it

Table of contents	
Figure S1. Atom count (AC)	S32
Figure S2. Heavy atom count (HAC)	S32
Figure S3. Ring count (RC)	S32
Figure S4. Rotatable bond count (RBC)	S33
Figure S5. Molar refractivity (MR)	S33
Table S1. Dataset with experimental log BB values	S33
Table S2. Descriptors values maximum, minimum and mean	S43
References	S44

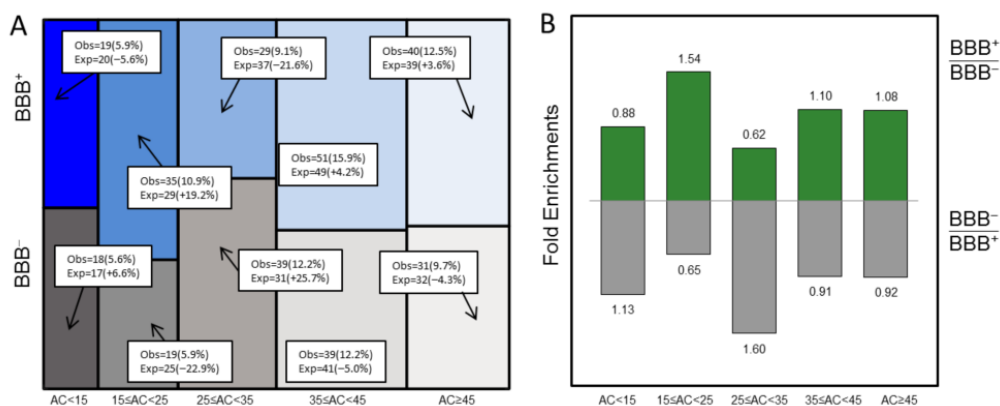


Figure S1. Observed distribution represented as mosaic plot of compounds BBB⁺ (blue) and BBB⁻ (gray) for the AC ranges. White boxes indicate the number of observed (obs) compounds and the relative percent with respect to the total set and the expected (exp) number of compounds with the percent deviation in parentheses (A). Fold enrichments for AC (B).

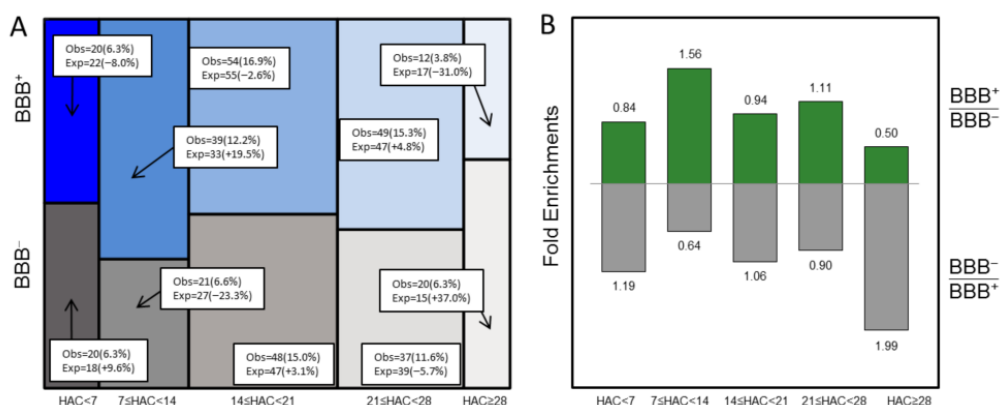


Figure S2. Observed distribution represented as mosaic plot of compounds BBB⁺ (blue) and BBB⁻ (gray) for the HAC ranges. White boxes indicate the number of observed (obs) compounds and the relative percent with respect to the total set and the expected (exp) number of compounds with the percent deviation in parentheses (A). Fold enrichments for HAC (B).

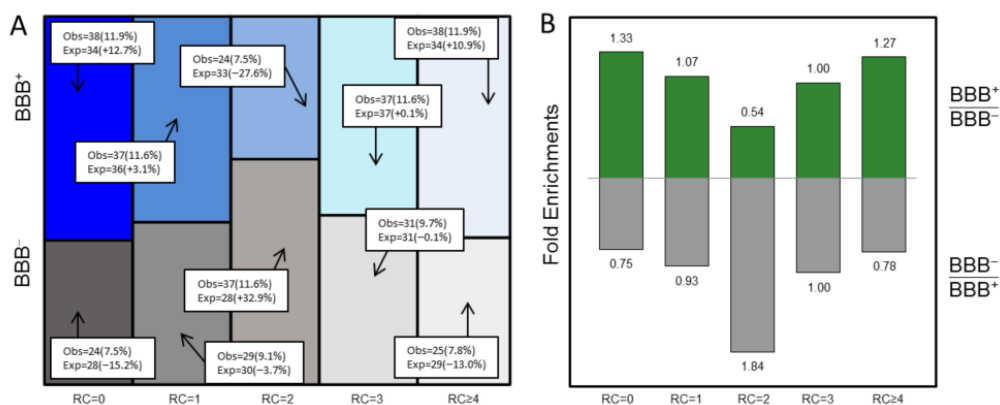


Figure S3. Observed distribution represented as mosaic plot of compounds BBB⁺ (blue) and BBB⁻ (gray) for the RC ranges. White boxes indicate the number of observed (obs) compounds and the relative percent with respect to the total set and the expected (exp) number of compounds with the percent deviation in parentheses (A). Fold enrichments for RC (B).

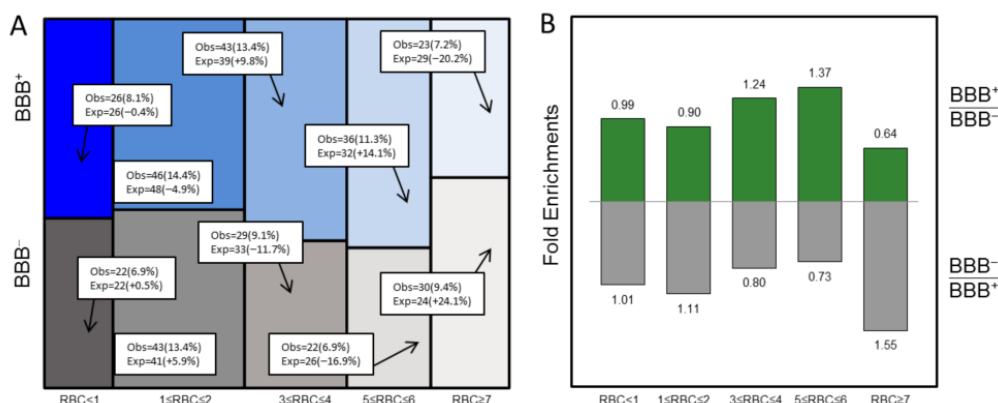


Figure S4. Observed distribution represented as mosaic plot of compounds BBB⁺ (blue) and BBB⁻ (gray) for the RBC ranges. White boxes indicate the number of observed (obs) compounds and the relative percent with respect to the total set and the expected (exp) number of compounds with the percent deviation in parentheses (A). Fold enrichments for RBC (B).

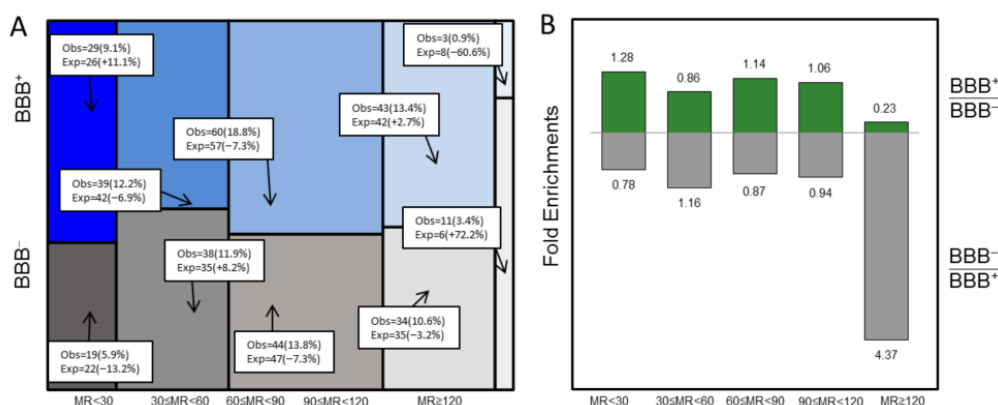


Figure S5. Observed distribution represented as mosaic plot of compounds BBB⁺ (blue) and BBB⁻ (gray) for the MR ranges. White boxes indicate the number of observed (obs) compounds and the relative percent with respect to the total set and the expected (exp) number of compounds with the percent deviation in parentheses (A). Fold enrichments for MR (B).

Table S1. Dataset with experimentally obtained log BB values.

SMILES	ID Original Article	logBB	Reference
FC(F)(F)C1=C(Cl)N=C(C=C1)N1CCNCC1	Org 12962; CHEBI: 568657	1.64	(1,2)
CNC1CCC(C2=CC(Cl)=C(Cl)C=C2)C2=C1C=CC=C2	Sertraline	1.6	(2)
OCCN1CCN(CCCN2C3=CC(=CC=C3SC3=C2C=C3)C(F)(F)F)CC1	Fluphenazine	1.51	(2,3)
CN1CCN(CCCN2C3=CC(=CC=C3SC3=C2C=CC=C3)C(F)(F)F)CC1	Trifluoperazine	1.44	(2,3)
CN(C)CCCN1C2=CC(=CC=C2SC2=C1C=CC=C2)C(F)(F)F	Trifluopromazine	1.44	(2)
CC(NC(C)(C)C)C(=O)C1=CC(Cl)=CC=C1	Bupropion	1.4	(2)
OC1(CCN(CCCC(=O)C2=CC=C(F)C=C2)CC1)C1=CC=C(Br)C=C1	Bromperidol	1.38	(2,3)
CCC(C)N1CCN(CC1)C1=CC=C(I)C=C1	1-Isobutyl-4-(4-iodophenyl)piperazine	1.38	(4)
CNCCCN1C2=CC(Cl)=CC=C2SC2=C1C=CC=C2	Nor-1-chlorpromazine	1.37	(2,3)

<chem>OC1(CCN(CCCC(=O)C2=CC=C(F)C=C2)CC1)C1=CC=C(Cl)C=C1</chem>	Haloperidol	1.34	(2,3)
<chem>CN(C)CCOC(C1=CC=CC=C1)C1=CC=CC=C1</chem>	Diphenhydramine	1.26	(2,5)
<chem>CN(C)CCCN1C2=CC=CC=C2SC2=C1C=CC=C2</chem>	Promazine	1.23	(1,2)
<chem>CCC1=CC=CC(N\C(C)=N\C2=CC(CC)=CC=C2)=C1</chem>	9-C17	1.2	(6)
<chem>COCCC1=CC=C(OCC(O)CNC(C)C)C=C1</chem>	Metoprolol	1.15	(2)
<chem>O=C(CCC1CCN(CC2=CC=CC=C2)CC1)C1=CC2=C(CCCCN2)C=C1</chem>	Zanapezil	1.14	(2)
<chem>I\C=C\CN1CCC(COC2=CC=C(C=C2)C#N)CC1</chem>	I-4-(4-cyanophenoxymethylpiperidineniodoall yl)	1.13	(4)
<chem>CNC(C)CC1CCCCC1</chem>	Propylhexedrine	1.08	(2)
<chem>CN(C)CCCN1C2=CC(Cl)=CC=C2SC2=C1C=CC=C2</chem>	Chlorpromazine	1.06	(1,2)
<chem>CN1CCC2C(C1)C1=CC=CC=C1OC1=CC=C(Cl)C=C21</chem>	7-K06	1.06	(7)
<chem>NCCCN1C2=CC=CC=C2CCC2=CC=CC=C12</chem>	Desmethyldesipramine	1.06	(2,3)
<chem>CN1CC2C(C1)C1=C(OC3=CC=CC=C23)C=CC(Cl)=C1</chem>	Org 5222	1.03	(1,2)
<chem>CCCCCN1CCN(CC1)C1=CC=C(I)C=C1</chem>	CHEBI: 287982	1.01	(2)
<chem>CCC(C)CC</chem>	3-methylpentane	1.01	(2,3,8)
<chem>CC(C)(C)OC(=O)CCCC1=CC=C(C=C1)N(CCCl)CCCl</chem>	Tertbutylchlorambucil	1	(2,9)
<chem>CN1CCC2(C)C1N(C)C1=CC=C(OC(=O)NC3=CC=CC=C3)C=C21</chem>	Phenserine	1	(1,2)
<chem>CNCCCN1C2=C(CCC3=C1C=CC=C3)C=CC=C2</chem>	Desipramine	1.00	(4)
<chem>CN1CCN2C(C1)C1=CC=CC=C1CC1=CC=CC=C21</chem>	Mianserin	0.99	(1,4)
<chem>IC1=C(CN2CCCCC2)C=C(CN2CCCCC2)C=C1</chem>	CHEBI: 385616	0.98	(2)
<chem>NCCCN1C2=CC(Cl)=CC=C2SC2=C1C=CC=C2</chem>	Nor-2-chlorpromazine	0.97	(2,3)
<chem>CNC(C)CC1=CC=CC=C1</chem>	Methamphetamine	0.93	(2)
<chem>CC(N)CC1=CC=CC=C1</chem>	Amfetamine	0.93	(2)
<chem>CC1CCCC1</chem>	Methylcyclopentane	0.93	(2,3,8)
<chem>CC\C=C(\C1=CC=CC=C1)C1=CC=C(OCCN(C)C)C=C1)C1=CC=CC=C1</chem>	Tamoxifen	0.92	(2)
<chem>C1CCCCC1</chem>	Cyclohexane	0.92	(2,3)
<chem>COC1=C(OC)C=C2C(=O)C(CC3CCN(CC4=CC=CC=C4)CC3)CC2=C1</chem>	Donepezil	0.89	(2)
<chem>CN(C)CCC=C1C2=CC=CC=C2CCC2=CC=CC=C12</chem>	Amitriptyline	0.89	(1,2,4)
<chem>CCN(C)C(=O)OC1=CC(=CC=C1)C(C)N(C)C</chem>	Rivastigmine	0.88	(2)
<chem>OC(CCN1CCCCC1)(C1CC2CC1C=C2)C1=CC=CC=C1</chem>	Biperiden	0.85	(2)
<chem>CCCC(=O)C1=CC=C2SC3=C(C=CC=C3)N(CCCN3CCN(C)CC3)C2=C1</chem>	Butaperazine. tyrylen	0.83	(2)
<chem>CN(C)CCCN1C2=CC=CC=C2CCC2=CC=CC=C12</chem>	8; Imipramine	0.83	(1,2,4)
<chem>CN1CCC2(O)C(C1)C1=CC=CC(C)=C1OC1=CC=C21</chem>	Beloxepin (Org4428)	0.82	(1,4)
<chem>CCCCCCC</chem>	Heptane	0.81	(2,3,8)

CCCCCC	n-Hexane	0.8	(2,3,8)
COC(C)C(=N)OCCN)C1=CC=C(C=C1)C(F)(F)F	Fluvoxamine	0.79	(2)
CN1CCN(CC1)C1=C2C=C(C)SC2=NC2=CC=CC=C2N1	Olanzapine	0.78	(2)
CCCCC	Pentane	0.76	(2,3,8)
CSC1=CC=C2SC3=C(C=CC=C3)N(CCC3CCCCN3)C2=C1	Northioridazine	0.75	(2,3)
CC1=NN=C2CN=C(C3=CC(Cl)=CC=C3N12)C1=C(Cl)C=CC=C1	Triazolam	0.74	(2,3)
CNCCC(OC1=CC=C(C=C1)C(F)(F)F)C1=CC=CC=C1	Fluoxetine	0.72	(2)
C(CNC1=NC=CC=C1)COC1=CC(CN2CCCC2)=CC=C1	36; CHEBI: 338033	0.69	(2,10)
CCCCCCCC	Octane	0.69	(2)
CC1N(CCC2=C1C=CC=C2)C1=NC(NC2=CC=C(F)C=C2)=NC(C)=C1C	MP 005-942-485	0.68	(2)
CCCCCCCCC	Decane	0.67	(2)
C1CNC2=C(C1)C=CC=C2	Kusol	0.67	(2)
CC(C)(C)C1=CC=C(C=C1)C(O)CCCN1CCC(CC1)C(O)(C1=CC=CC=C1)C1=CC=CC=C1	Terfenadine	0.64	(2,5)
CCC(C)NC1=CC(NC(C)CC)=C(I)C=C1	4-Iodo-N,N'-isopropyl-m-xylenediamine	0.64	(2)
CN(C)CCOC(C)(C1=CC=CC=C1)C1=NC=CC=C1	Doxylamine	0.64	(2)
CC(C)NCC(O)COC1=CC=CC2=CC=CC=C12	Propranolol	0.64	(3)
OC(C1CCCCN1)C1=CC(=NC2=C(C=CC=C12)C(F)(F)F)C(F)(F)F	Mefloquine	0.63	(2,4,5)
CC(C)C1=CC=CC(C(C)C)=C1O	Propofol	0.63	(2)
OC1N=C(C2=CC=CC=C2)C2=CC(Cl)=CC=C2NC1=O	Oxazepam	0.61	(1,2)
COC1=C(OC2CCCC2)C=C(C=C1)C1CNC(=O)C1	Rolipram	0.61	(2)
COC(=O)C1C2CCC(CC1OC(=O)C1=CC=CC=C1)N2C	Cocaine	0.6	(2)
CCC(=O)N(C1CCN(CCC2=CC=CC=C2)CC1)C1=C(C=CC=C1)	Fentanyl	0.59	(2)
C1CCN(CC1)C1(CCCCC1)C1=CC=CC=C1	Phencyclidine	0.58	(2)
CC(C)Br	2-Bromopropane	0.56	(2)
COC1=CC=C2CC3[C@@H]4C=C[C@H](O)[C@@H]5OC1=C2C45CCN3C	Codeine	0.55	(1,2)
CC(C)CCOC(C)=O	Isopentyl acetate	0.55	(2)
CN(C)C1=C(SC2=C(N)C=C(CCF)C=C2)C=CC=C1	AFE	0.55	(4)
CCCOC(=O)C1=CC=C(N)C=C1	Risocaine	0.54	(2)
CNCCCNC1C2=CC=CC=C2CCC2=C1C=CC(O)=C2	2-Hydroxydesipramine	0.53	(2)
CN1CCN2C(C1)C1=CC=CC=C1CC1=CC=CN=C21	Mirtazapine	0.53	(1,2)
CN1C2=CC=C(Cl)C=C2C(=NCC1=O)C1=CC=CC=C1	Diazepam	0.52	(2,3)
CC1=CC=CC2=C1OC1=CC=CC=C1C1(O)CCNCC21	CID 22154175	0.52	(2)
CCCCCCCCC	n-Nonane	0.52	(2)

<chem>CC1C2CC3=CC=C(O)C=C3[C@]1(C)CCN2CC=C(C)C</chem>	Pentazocine	0.51	(2)
<chem>C1C1=CC=C2NC(=O)CN=C(C3=CC=CC=C3)C2=C1</chem>	Desmethyldiazepam	0.5	(4)
<chem>O=C1CC2(CCCC2)CC(=O)N1CCCCN1CCN(CC1)C1=NC=CC=N1</chem>	Buspirone	0.49	(2)
<chem>COC1=CC=C(CN(CCN(C)C)C2=NC=CC=C2)C=C1</chem>	7; Mepyramine; pyrilamine	0.49	(1,2,8)
<chem>CCC(O)N(C)C(=O)C1=CC2=CC=CC=C2C(=N1)C1=C(C1)C=CC=C1</chem>	PK 11195	0.48	(2)
<chem>CN1CN(C2=CC=CC=C2)C2(CCN(CCCC(=O)C3=C(C=C(F)C=C3)CC2)C1=O</chem>	N-Methylspiroperidol	0.46	(2)
<chem>CC(C)COC(C)=O</chem>	Isobutyl acetate	0.45	(2)
<chem>C(CNC1=NC=CS1)COC1=CC(CN2CCCCC2)=CC=C1</chem>	37; CHEBI: 338961	0.44	(2,8,10)
<chem>OC1N=C(C2=CC(Cl)=CC=C2NC1=O)C1=C(Cl)C=CC=C1</chem>	Lorazepam	0.44	(2)
<chem>CCCCOC(=O)C1=CC=C(N)C=C1</chem>	Butamben	0.42	(2)
<chem>FC(F)OC(Cl)C(F)(F)F</chem>	Isoflurane	0.42	(2,3,8)
<chem>NCCC1=NC=CS1</chem>	Y-G16; 24959	0.42	(2,3,11)
<chem>CC1CC2=C(CCC(=O)C2)C2CCC3(C)C(CCC3(O)C#C)C12</chem>	Tibolone	0.4	(1,2)
<chem>CC(Cl)(Cl)Cl</chem>	Methylchloroform	0.4	(2,3,8)
<chem>CCCCCOC(C)=O</chem>	Pentyl acetate	0.4	(2)
<chem>CC(C)OC(C)=O</chem>	Isopropyl acetate	0.4	(2)
<chem>OCCOCCN1CCN(CC1)C(C1=CC=CC=C1)C1=CC=C(C1)C=C1</chem>	Hydroxyzine	0.39	(1,2)
<chem>COC1=CC2=C(OCC2)C(CNC2CCCNC2C2=CC=C(C=C2)=C1</chem>	9-C15	0.39	(6)
<chem>CC(C)NCC(O)COC1=CC=C(CCOCC2CC2)C=C1</chem>	Betaxolol	0.39	(2)
<chem>C1C1=CC=C2OC3=CC=CC=C3C3CNCCC3C2=C1</chem>	7-K10	0.39	(7)
<chem>C1C1=CC=C2OC3=CC=CC=C3C3CNCC3C2=C1</chem>	Org30526	0.39	(1)
<chem>CN1CCCC1C1=CC=CN=C1</chem>	Nicotine	0.38	(2)
<chem>C1C(Cl)=C(Cl)Cl</chem>	Perchloroethylene	0.37	(2)
<chem>CC1=C(C)C=CC=C1</chem>	Xylene	0.37	(2,3)
<chem>CC1=CC=CC=C1</chem>	Toluene	0.37	(2,3,8)
<chem>C1=CC=CC=C1</chem>	Benzene	0.37	(2)
<chem>CC1=NC=C2CN=C(C3=CC(Cl)=CC=C3N12)C1=C(F)C=CC=C1</chem>	Midazolam	0.36	(1)
<chem>CCCCCCC1(CC)C(=O)NC(=O)NC1=O</chem>	Ortal	0.36	(2)
<chem>CN1C2=C(C=C(Cl)C=C2)N(C2=CC=CC=C2)C(=O)CC1=O</chem>	Clobazam	0.35	(2,3)
<chem>C1C1=CC2=C(NC(=O)CC(=O)N2C2=CC=CC=C2)C=C1</chem>	Desmethylclobazam; norclobazam; nordiazepam	0.35	(2)
<chem>FC(F)(F)CC(Cl)Br</chem>	MP 001-772-915	0.35	(2)
<chem>FC(F)(F)C(Cl)Br</chem>	Halothane	0.35	(2,3,8)
<chem>CCN(CC)CC(=O)NC1=C(C)C=CC=C1C</chem>	Lidocaine	0.34	(2)
<chem>CC(C)NCC(O)COC1=CC(C)=CC=C1</chem>	Toliprolol	0.34	(2)

<chem>CICCC(CI)(CI)CI</chem>	1,1,1,2-Tetrachloroethane	0.33	(2)
<chem>COC1=C2OC3CC(O)C=CC3CCN(C)CC(C=C1)=C23</chem>	Galanthamine	0.32	(2)
<chem>C1CNC(C1)C1=CC=CN=C1</chem>	Nornicotine	0.32	(2)
<chem>CCCCN1CC2CC3=CC(OC)=C(OC)C=C3C2C1</chem>	AR 1D9859	0.31	(2)
<chem>C=C</chem>	Ethylene (ethene)	0.31	(4)
<chem>CCC(NC(=O)C1=C(C)C(=NC2=CC=CC=C12)C1=C(C=CC=C1)C1=CC=CC=C1</chem>	3-Methyl-2-phenyl-N-(1-phenylpropyl)-quinoline-4-carboxamide	0.30	(2)
<chem>CCCN1CC(CSC)CC2C1CC1=CNC3=CC=CC2=C13</chem>	Pergolide	0.3	(2)
<chem>FCOC(C(F)(F)F)C(F)(F)F</chem>	Sevoflurane	0.3	(2)
<chem>NC1=NC(N)=C(N=N1)C1=C(Cl)C(Cl)=CC=C1</chem>	Lamotrigine	0.29	(2)
<chem>CIC(CI)CI</chem>	Trichloromethane	0.29	(2,3)
<chem>CCCCOC(C)=O</chem>	Butyl acetate	0.28	(2)
<chem>FC(Br)C(F)(F)F</chem>	Tefluranum	0.27	(2,3)
<chem>CCOC(=O)C1=CC=C(N)C=C1</chem>	Benzocaine	0.27	(2)
<chem>CCCBBr</chem>	N-Propylbromide	0.27	(2)
<chem>FC1=CC=C(C=C1)C(=O)CCCN1CCC2(CC1)N(CN(C2=O)C1=CC=CC=C1</chem>	Spiperone	0.26	(2)
<chem>CCCN(CCC)CCC1=C2CC(=O)NC2=CC=C1</chem>	Ropinirole; SKF101468	0.25	(2,3)
<chem>COC(F)(F)C(Cl)Cl</chem>	Methoxyflurane	0.25	(2,3)
<chem>CSC1=CC=C2SC3=C(C=CC=C3)N(CCC3CCCCN3C)C2=C1</chem>	Thioridazine	0.24	(2)
<chem>CCCCCCCCC1(CC)C(=O)NC(=O)NC1=O</chem>	5-Octyl-5-ethyl barbituric acid	0.24	(2)
<chem>FC(F)OC(F)(F)C(F)Cl</chem>	Enflurane	0.24	(2,3,8)
<chem>CN1C2CC(CC1C1OC21)OC(=O)C(CO)C1=CC=CC=C1</chem>	Scopolamine	0.23	(2)
<chem>C1=CC2=CC=C3C=CC=C4C=CC(=C1)C2=C34</chem>	Pyrene	0.23	(2)
<chem>C(CNC1=NC2=C(O1)C=CC=C2)COC1=CC(CN2CC(CCC2)=CC=C1</chem>	42; CHEBI: 339055	0.22	(2,10)
<chem>CCOC(C)(C)C</chem>	tert-Butylethylether	0.22	(2)
<chem>CCCC(C)C1(CC=C)C(=O)NC(=O)NC1=O</chem>	Secobarbital	0.2	(2)
<chem>CCCCCO</chem>	1-Pentanol	0.2	(2)
<chem>CCCCC1(CC)C(=O)NC(=O)NC1=O</chem>	Butethal	0.19	(2)
<chem>CN1CCCCC1CCN1C2=CC(=CC=C2)SC2=C1C=CC=C2)S(C)(=O)=O</chem>	Sulforidazine	0.18	(2,3)
<chem>NC1=C(I)C=C(C=C1)C1=NC2=CC=C(O)C=C2S1</chem>	CID 10451635	0.18	(2)
<chem>FC(F)(F)C1=CC=C(Cl)C=C1</chem>	4-Chlorobenzotrifluoride	0.17	(2)
<chem>CCC(C)(C)OC</chem>	tert-Amylmethylether	0.17	(2)
<chem>FC(F)(F)C1=CC(=NC(Cl)=C1)N1CCN(CCCCN2CC(C2=O)CC1</chem>	7-K08	0.16	(7)
<chem>FC(F)(F)C1=CC(=NC=C1)N1CCN(CCCCN2CCCC2=O)CC1</chem>	Org13011; CHEBI: 568728	0.16	(2,3)
<chem>CIC1=CC(Cl)=C(NC2=NCCN2)C=C1</chem>	ST 363	0.16	(2)
<chem>CC1=CC(C)=C(C)C=C1</chem>	Pseudocumene	0.16	(2)

<chem>C(CNC1=NC2=CC=CC=C2S1)COC1=CC(CN2CCC(CC2)=CC=C1</chem>	Zolantidine; 41	0.14	(1,2,8)
<chem>FC(F)(F)COC=C</chem>	Fluorene	0.13	(2,3,8)
<chem>C=COC(C)COC=C</chem>	1,4-Divinylxybutane	0.12	(2)
<chem>CCCOC(C)=O</chem>	Propyl acetate	0.12	(2)
<chem>NCCN1N=CC2=C1C=C(CI)C(CI)=C2</chem>	9-C7	0.11	(6)
<chem>CIC1=CC=CC(CI)=C1NC1=NCCN1</chem>	Clonidine	0.11	(1,2,4)
<chem>FC(F)OC(F)C(F)(F)F</chem>	Suprane	0.11	(2)
<chem>CC(C)(C)O</chem>	tert-Butylalcohol	0.11	(2)
<chem>C1CC1</chem>	Cyclopropane	0.11	(3,4)
<chem>CN1C(=O)NC(=O)C(C)(C1=O)C1=CCCCC1</chem>	Hexobarbital	0.1	(2,3)
<chem>OC(=O)C1=C(O)C=CC(O)=C1</chem>	Gentisic acid	0.09	(2)
<chem>CCCCC1(CC)C(=O)NC(=O)NC1=O</chem>	5-Pentyl-5-ethyl barbituric acid	0.09	(4)
<chem>CCCC1(CC)C(=O)NC(=O)NC1=O</chem>	5-Propyl-5-ethyl barbituric acid	0.09	(4)
<chem>CN(C\C=C\C#CC(C)(C)C)CC1=CC=CC2=CC=CC=C12</chem>	Terbinafine	0.08	(2)
<chem>CCCC(C)C1(CC)C(=O)NC(=O)NC1=O</chem>	Pentobarbital	0.08	(1,2)
<chem>FC(F)(F)CCl</chem>	111-Trifluoro-2-chloroethane	0.08	(2,3,8)
<chem>CNC(=O)OC1=CC=C2N(C)C3N(C)CCC3(C)C2=C1</chem>	Physostigmine	0.079	(1,2)
<chem>FC1=CC=C(C=C1)C(=O)CCCN1CCC2(CC1)N(CN(C2=O)C1=CC=C(Br)C=C1</chem>	p-bromospiperone	0.07	(2)
<chem>CCC(C)(C)O</chem>	Amylene hydrate	0.07	(2)
<chem>CN1C2=CC=C(C=C2C(=NCC1=O)C1=C(F)C=CC=C1)[N+](=O)[O-]=O</chem>	Flunitrazepam	0.06	(2,3)
<chem>CN1C=NC2=C1C(=O)N(C)C(=O)N2</chem>	Paraxanthine	0.06	(2,3)
<chem>CCN(CC)CCOC(=O)C1=CC=C(N)C=C1</chem>	procaine	0.05	(2)
<chem>CC(C)(C)[N+](=O)[O-]=C\C1=CC=CC=C1</chem>	CID 10313352	0.05	(2)
<chem>CC1=NN=C2CN=C(C3=CC=CC=C3)C3=CC(CI)=CC=C3N12</chem>	Alprazolam	0.044	(1,2)
<chem>CCC(O)(CC(N)=O)C1=CC=CC=C1</chem>	3-Hydroxy-3-phenylpentamide	0.04	(2)
<chem>CCC(C)CO</chem>	sec-butylcarbinol	0.04	(2)
<chem>CCC1(CCC(C)C)C(=O)NC(=O)NC1=O</chem>	Amobarbital	0.04	(2,3)
<chem>CCCCCCCC1(CC)C(=O)NC(=O)NC1=O</chem>	5-Ethyl-5-heptyl-1.3-diazinane-2.4.6-trione	0.02	(2)
<chem>CO</chem>	Methanol	0.02	(2)
<chem>CC(C)(C)NCC(O)COC1=CC=CC2=C1CCC(=O)N2</chem>	Carteolol	0.01	(2)
<chem>CC1=CC=NC2=C1NC(=O)C1=CC=CN=C1N2C1CC1</chem>	Nevirapine	0	(1,2)
<chem>NC(CC=C)C1=C(C=CC=C1)C1=NOC2=C1C=CC=C2</chem>	CID 9861160	0	(2)
<chem>CN1CCC23CCCCC2C1CC1=C3C=C(O)C=C1</chem>	Levorphanol	0	(2)
<chem>NC(=O)N1C2=CC=CC=C2C=CC2=CC=CC=C12</chem>	Carbamazepine	0	(1,2)
<chem>CN(C)C1=C(C)N(C)N(C1=O)C1=CC=CC=C1</chem>	Aminopyrine	0	(2,3)
<chem>CCOC(C)=O</chem>	Ethyl acetate	0	(2)

CCOCC	Diethylether	0	(2,3,8)
C=COC=C	Divinylether	0	(3)
CCCN1CN(C2=CC=C(Br)C=C2)C2(CCN(CCCC(=O)C3=CC=C(F)C=C3)CC2)C1=O	BPSP	-0.01	(4)
OC(COCF)CN1C=CN=C1[N+](O-)=O	Misonidazolefluoro (Fluoromisonidazole)	-0.01	(4)
OC(F)CN1C=CN=C1[N+](O-)=O	Fluoromisonidazole	-0.01	(2)
CCCC(C)=O	2-Pentanone	-0.01	(2)
CC1=C(CCN2CCC(CC2)C2=NOC3=C2C=CC(F)=C3)C(=O)N2CCCCC2=N1	Risperidone	-0.02	(1,2)
OCCCCO1=CC(CN2CCCCC2)=CC=C1	34; CHEBI: 338140	-0.02	(2,8,10)
CCCCO	1-Butanol	-0.02	(2)
C1CCN2N=NN=C2CC1	Pentyletetrazol	-0.03	(2)
O=C1NC(=O)C(N1)(C1=CC=CC=C1)C1=CC=CC=C1	Phenytoin	-0.04	(2,3)
CC1=CSC(N=C(N)N)=N1	2	-0.04	(2,8,10,12)
Cl\C=C/Cl	cis-Dichloroethylene	-0.045	(2)
BrC1=CC=C2C3CNCC(C3)CN2C1=O	3-Bromocytisine	-0.05	(2)
CN1N(C(=O)C=C1C)C1=CC=C(F)C=C1	4-Fluoroantipyrine	-0.05	(2)
CN1C=NC2=C1C(=O)N(C)C(=O)N2C	Caffeine	-0.05	(1,2)
CCOC1=C(C=CC=C1)C(N)=O	Ethenzamide	-0.05	(2)
CN1C2CCC1CC(C2)OC(=O)C(CO)C1=CC=CC=C1	Atropine	-0.06	(2)
CCC#CC(C)C1(CC=C)C(=O)NC(=O)N(C)C1=O	Methohexital	-0.06	(2)
CN(C)CCC1=NC=CC=C1	Y-G15; 24593	-0.06	(2,8,11)
CC=C	propene	-0.06	(2)
OCC1=NC=C2CN=C(C3=CC(Cl)=CC=C3N12)C1=C(F)C=CC=C1	1-hydroxymidazolam	-0.07	(2,3)
CCC1(C(=O)NCNC1=O)C1=CC=CC=C1	Primidone	-0.07	(2)
CCC(C)=O	Butanone	-0.08	(2,3)
CC(C)(C)OC(=O)C1=C2C3CCCN3C(=O)C3=C(Br)C=CC=C3N2C=N1	Bretazenil	-0.09	(2,3)
CC(F)OC(=O)C1=C2CN(C)C(=O)C3=C(C=CC(F)=C3)N2C=N1	FFMZ	-0.09	(4)
CN1N(C(=O)C=C1C)C1=CC=CC=C1	Antipyrine	-0.097	(1,2)
CN1N(C(=O)C(I)=C1C)C1=CC=CC=C1	Iodophenazone	-0.1	(2)
ClCC(Cl)Cl	Vinyltrichloride	-0.1	(2)
ClCCl	Dichloromethane; methylenechloride	-0.11	(2,3)
[O-][N+](=O)C1=C(NCCSCC2=NC=CC=C2)NC=C1CC1=CC=CC=C1	17; CHEBI: 337303	-0.12	(2,8,10)
CC(C)(C1=CC=C(O)C=C1)C1=CC=C(O)C=C1	Bisphenol A	-0.12	(2)
NC1=C2C=CC=CC2=NC2=C1CCCC2	Tacrine	-0.12	(2)
CC(C)NCCCOC1=CC(CN2CCCCC2)=CC=C1		-0.13	(8)
COC(C)=O	Methylacetate	-0.13	(2)

<chem>CCOC(=O)C1=C2CN(CCF)C(=O)C3=C(C=CC(F)=C3)N2C=N1</chem>	Fluoroethylflumazenil	-0.14	(2)
<chem>CC(C)NCC(O)COC1=C2C=CNC2=CC=C1</chem>	Pindolol	-0.14	(2)
<chem>CCCC(C)C1(CC)C(=O)NC(=S)NC1=O</chem>	Thiopental	-0.14	(2,3)
<chem>CCC1(CC)C(=O)NC(=O)NC1=O</chem>	Barbital	-0.14	(2)
<chem>C1CCCl</chem>	1,2-Dichloroethane	-0.14	(2)
<chem>NC(N)=O</chem>	Urea	-0.14	(2)
<chem>CCCC(=O)NC1=CC(C(C)=O)=C(OCC(O)CNC(C)C)C=C1</chem>	Acebutolol	-0.15	(2)
<chem>OC1=CC=C(C=C1)C1=COC2=CC(O)=CC=C2C1=O</chem>	Daidzein	-0.15	(2)
<chem>CCCO</chem>	1-Propanol	-0.15	(2,3,8)
<chem>CC(C)O</chem>	2-Propanol	-0.15	(2,8,9)
<chem>CC(C)=O</chem>	Acetone; propanone	-0.15	(2,3,8)
<chem>S=C(NC1CCCCC1)N1CCC(CC1)C1=CNC=N1</chem>	Thioperamide; 25324	-0.16	(2,11,12)
<chem>CN1CCC23C4OC5=C2C(CC1C3C=CC4O)=CC=C5O</chem>	Morphine	-0.16	(2,3)
<chem>CCO</chem>	Ethanol	-0.16	(2,3,8)
<chem>[O-][N+](=O)C1=NC=CN1CCCCCCCCF</chem>	MOLI001285	-0.17	(2)
<chem>CC(C)CO</chem>	Isobutanol	-0.17	(2,3)
<chem>C=CC=C</chem>	Divinyl	-0.17	(2)
<chem>NC(N)=NC1=NC(=CS1)C1=CC=CC=C1</chem>	19	-0.18	(2,8)
<chem>CC(C)CC1=CC=C(C=C1)C(C)C(O)=O</chem>	Ibuprofen	-0.18	(1,2)
<chem>CN1C(CCC1=O)C1=CC=CN=C1</chem>	Cotinine	-0.22	(2)
<chem>CCC1(C)C(=O)NC(=O)NC1=O</chem>	NSC 30403	-0.22	(2)
<chem>CCCC(CCC)C(O)=O</chem>	Valproic acid	-0.22	(1)
<chem>CC(C)NCC(O)COC1=C(CC=C)C=CC=C1</chem>	Alprenolol	-0.23	(2)
<chem>OCC#C</chem>	2-Propyn-1-ol	-0.23	(2)
<chem>O=C(NCCCOC1=CC(CN2CCCCC2)=CC=C1)C1=C C=CC=C1</chem>	31	-0.24	(8,10)
<chem>[O-][N+](=O)C1=NC=CN1CCCF</chem>	MOLI001288	-0.24	(2)
<chem>CN1CC2=C(N=CN2C2=C(SC=C2)C1=O)C(=O)OC(C)(C)C</chem>	RO19-4603	-0.25	(2,3)
<chem>CN1CN(C2=CC=CC=C2)C2(CCN(CCCC(=O)C3=C SC(I)=C3)CC2)C1=O</chem>	I-1	-0.25	(4)
<chem>CC1NC(=O)C2(CCCC2)NC1=O</chem>	Alaptide	-0.26	(2)
<chem>CN(C)CC1=CC=C(O1)C1=CC=CC(NC2=C(C=CN2)[N+](O-)=O)=C1</chem>	26	-0.27	(10)
<chem>NC(=N)SCCF</chem>	2-(2-Fluoro-ethyl)-isothiourea	-0.27	(2)
<chem>CN(C)CC1=CC(=NC=C1)C1=CC=CC(NC2=C(C=C N2)[N+](O-)=O)=C1</chem>	29	-0.28	(10)
<chem>CC(C)NCC(O)C1=CC=C(NS(C)(=O)=O)C=C1</chem>	Sotalol	-0.28	(2)
<chem>CN1C=NC2=C1C(=O)NC(=O)N2C</chem>	Theobromine	-0.28	(2)
<chem>CC(Cl)Cl</chem>	Ethylidene chloride	-0.28	(2)

<chem>CCOC(=O)C1=C2CN(C)C(=O)C3=CC(F)=CC=C3N2C=N1</chem>	Flumazenil	-0.29	(2,3)
<chem>CN1C2=C(N=CN2)C(=O)N(C)C1=O</chem>	Theophylline	-0.29	(1)
<chem>CC(C)C1=NC(=NO1)C1=C2CN(C)C(=O)C3=C(C=CC=C3Cl)N2C=N1</chem>	CHEBI 218555	-0.3	(2)
<chem>CC1=NC=C2C(O)N=C(C3=CC(Cl)=CC=C3N12)C1=C(F)C=CC=C1</chem>	4-Hydroxymidazolam	-0.3	(2,3)
<chem>CC12CCC3C(CCC4=CC(O)=CC=C34)C1CC(F)C2O</chem>	16a-Fluoroestradiol	-0.30	(2)
<chem>CNCCC1=NC=CC=C1</chem>	24228; Y-G14; Betahistine	-0.3	(2,3,11)
<chem>CC(=O)NC1=CC=C(O)C=C1</chem>	Acetaminophen	-0.31	(2,3)
<chem>NC(=O)N1C2=CC=CC=C2C2OC2C2=CC=CC=C12</chem>	Carbamazepine epoxide	-0.34	(2,9)
<chem>NC(=O)N1C2=CC=CC=C2C2CC2C2=CC=CC=C12</chem>	CBZ-EPO	-0.34	(4)
<chem>CN1CCCC1CCN1C2=CC(=CC=C2S)C2=C1C=CC=C2)S(C)=O</chem>	Mesoridazine	-0.36	(2,3)
<chem>CC(C)(C)[N+](=[O-])=C/C1=CC=[N+](=[O-])C=C1</chem>	alpha-(4-Pyridyl-1-oxide)-N-tert-butyl nitron	-0.38	(2)
<chem>C=CC#N</chem>	Acrylonitrile	-0.40	(2)
<chem>CCN1CN(C2=CC=C(Br)C=C2)C2(CCN(CCCC(=O)C3=CC=C(F)C=C3)CC2)C1=O</chem>	BESP	-0.43	(4)
<chem>CCCN(CCC)CCC1=C2CC(=O)NC2=C(O)C=C1</chem>	Gen48; 7-hydroxy ropinirole; SKF89124	-0.43	(1-3)
<chem>OC(=O)CNC(=O)C1=C(O)C=CC=C1</chem>	Salicylic acid	-0.44	(2,3)
<chem>OCC1COC2=C(C=CC=C2O1)N1CCN(CCN(C=O)C2=CC=C(F)C=C2)CC1</chem>	Flesinoxan	-0.45	(2)
<chem>CC(=O)NCCCOC1=CC(CN2CCCCC2)=CC=C1</chem>	30; CHEBI: 338581	-0.46	(2,10)
<chem>CN(C)C(=O)CC1=C(N=C2C=CC(C)=CN12)C1=CC=C(C)C=C1</chem>	Zolpidem	-0.48	(2)
<chem>CN(C)CCCN1C2=CC=CC=C2S(=O)C2=C1C=CC=C2</chem>	Phenothiazine	-0.48	(2)
<chem>CC1=CN(C2OC(CO)C=C2)C(=O)NC1=O</chem>	Stavudine	-0.48	(2)
<chem>C\C(\C=C\C1=C(C)CCCC1(C)C)=C/C=C/C(/C)=C/C(O)=O</chem>	Tretinoin	-0.49	(2)
<chem>CC(=O)OC1=C(C=CC=C1)C(O)=O</chem>	Aspirin	-0.5	(1,2)
<chem>CCCCC1C(=O)N(N(C1=O)C1=CC=CC=C1)C1=CC=CC=C1</chem>	Phenylbutazone	-0.52	(2,3)
<chem>C1CCNC(=O)N(CCC1)N=O</chem>	Carmustine (BCNU)	-0.52	(1,2)
<chem>CN1CN(C2=CC=C(Br)C=C2)C2(CCN(CCCC(=O)C3=CC=C(F)C=C3)CC2)C1=O</chem>	BMSP	-0.55	(4)
<chem>CC(C)CN(CC(O)C(C1=CC=CC=C1)NC(=O)OC1COC1)S(=O)(=O)C1=CC=C(N)C=C1</chem>	Amprenavir	-0.56	(2)
<chem>CC1=CN(C2CC(F)C(CO)O2)C(=O)NC1=O</chem>	Alovudine	-0.59	(2)
<chem>CSC(N)=N</chem>	S-Methyl-isothiourea	-0.6	(2)
<chem>NC(=O)C(C1CCN(CCC2=CC3=C(OCC3)C=C2)C1)(C1=CC=CC=C1)C1=CC=CC=C1</chem>	Darifenacin	-0.62	(2)
<chem>COC1=C(OC)C=C(CCNCCCC(C#N)(C(C)C)C2=CC(OC)=C(OC)C=C2)C=C1</chem>	Norverapamil	-0.64	(2)
<chem>[O-][N+](=O)C1=C(NCCSCC2=NC=CC=C2)NC=C1</chem>	16; CHEBI: 339092	-0.66	(2,8,10)
<chem>CCN1C=C(C(O)=O)C(=O)C2=CC=C(C)N=C12</chem>	Nalidixic acid	-0.66	(2)
<chem>CC1=C(CCN2CCC(CC2)C2=NOC3=C2C=CC(F)=C3)C(=O)N2CCCC(O)C2=N1</chem>	Paliperidone	-0.67	(2)

<chem>[O-][N+](=O)C1=C(NCCSCC2=NC=CC=C2Br)NC=C1</chem>	15; CHEBI: 339093	-0.67	(2,8)
<chem>NC(=O)C1=NN(N=C1)C1OC(CO)C(O)C1O</chem>	Ribavirin	-0.67	(2)
<chem>CN1N=C(C(=O)NC2CC3CCCC(C2)N3C)C2=C1C=CC=C2</chem>	Granisetron	-0.69	(2)
<chem>COC1=C(OC)C=C(CCN(C)CCCC(C#N)(C(C)C)C2=CC(OC)=C(OC)C=C2)C=C1</chem>	Verapamil	-0.70	(2)
<chem>CC1=CN(C2CC(N=[N+]=[N-])C(CO)O2)C(=O)NC1=O</chem>	Zidovudine	-0.72	(4)
<chem>CN(C)CC1=CC=C(CSCCNC2=C(C(CC3=CC=CC=C3)=CN2)[N+](O)=O)O1</chem>	25; BBcpd60; CHEBI: 338035	-0.73	(2,8,12)
<chem>CN(C)CC1=CC=C(O1)SCCNC1=C(C(CC2=CC=CC=C2)=CN1)[N+](O)=O</chem>	BBCPD60	-0.73	(4)
<chem>CC(C)(C)NC(=O)C1CN(CC2=CC=CN=C2)CCN1C(C(O)CC(CC1=CC=CC=C1)C(=O)NC1C(O)CC2=CC=CC=C12</chem>	Indinavir	-0.74	(2,3)
<chem>NC(CC1=CC(O)=C(O)C=C1)C(O)=O</chem>	Levodopa	-0.78	(2,5)
<chem>COC1=CC=C2NC(=NC2=C1)S(=O)CC1=NC=C(C)C(OC)=C1C</chem>	Omeprazole	-0.82	(2)
<chem>CN\C(NCCSCC1=CSC(NC(N)=N)=N1)=N/C#N</chem>	10; 38508; Tiotidine	-0.82	(1,2,11)
<chem>NC1=NC2=C(N=CN2COCCO)C(=O)N1</chem>	Acyclovir	-0.84	(2)
<chem>CN(C)CC1=CC=C(CSCCNC2=C(C=CN2)[N+](O)=O)O1</chem>		-1.04	(8)
<chem>CN(C)CC1=CC=C(CSCCNC2=NC(=O)C(CC3=CC=C(C)N=C3)=CN2)O1</chem>	5; 38480; Lupitidine	-1.06	(1,2,8,11)
<chem>O=C1C=CC=C2C3CNCC(C3)CN12</chem>	Cytisine	-1.09	(2)
<chem>OC(=O)C1=C(O)C=CC=C1</chem>	Salicylic acid	-1.1	(1,2)
<chem>CN(C)CC1=CC=C(O1)SCCNC1=C(C=CN1)[N+](O)=O</chem>	BBCPD17	-1.12	(4)
<chem>CC(C)(C)NCC(O)C1=CC(CO)=C(O)C=C1</chem>	Salbutamol	-1.14	(2,5)
<chem>NC(N)=NC1=NC(=CS1)C1=CC(N)=CC=C1</chem>	20; CHEBI: 338063	-1.15	(2,8,11)
<chem>CN(C)C1=NC=CC(=C1)C1=NNC(N)=N1</chem>	12; BBcpd10	-1.17	(2,11)
<chem>NC1=NC(=O)N(C=C1)C1CCC(CO)O1</chem>	Zalcitabine	-1.18	(2)
<chem>OCC1=NN=C2CN=C(C3=CC=CC=C3)C3=C(C=CC(CI)=C3)N12</chem>	alpha-Hydroxyalprazolam	-1.23	(2)
<chem>CN\C(NCCSCC1=CC=C(CN(C)C)O1)=C/[N+](O)=O</chem>	Ranitidine	-1.23	(8,9)
<chem>COC1=CC=C2N(C(=O)C3=CC=C(CI)C=C3)C(C)=C(CC(O)=O)C2=C1</chem>	Indometacin	-1.26	(1)
<chem>OC(=O)C1=CC=C(C=C1)C1=CC=CC=C1</chem>	4-Carboxybiphenyl	-1.26	(2)
<chem>CN(C)CC1=CC=C(CSCCNC2=NC(=O)C(CC3=CC4=CC=CC=C4C3)=CN2)O1</chem>	4	-1.3	(8,10)
<chem>OCC1CCC(O1)N1C=NC2=C(O)N=CN=C12</chem>	Didanosine	-1.3	(1,2)
<chem>NCCC1=NC(=CS1)C1=CC=CC=C1</chem>	Y-G19; 22767	-1.3	(3)
<chem>CN1CC2=C(N=CN2C2=CC=CC(CI)=C2C1=O)C1=NOC(=N1)C(C)C(O)</chem>	35; Mono-hydroxylated L-663.581	-1.34	(1,3,12)
<chem>CC1(C)C(O)CCC2(C)C1CCC1(C)C2C(=O)C=C2C3CC(C)(CCC3(C)CCC12)C(O)=O</chem>	Enoxolone	-1.4	(2)
<chem>CCCN1C2=C(NC(=N2)C2CCC(=O)C2)C(=O)N(CC(C)C1=O</chem>	Apaxifylline	-1.40	(2)
<chem>NCCC1=CN2C=CC=CC2=N1</chem>	Gen-47; Y-G20	-1.4	(1,3)

<chem>CCC1=C2NC3=C(CCOC3(CC)CC(O)=O)C2=CC=C1</chem>	Etodolac	-1.42	(2)
<chem>CC(C)NCC(O)COC1=CC=C(CC(N)=O)C=C1</chem>	Atenolol	-1.42	(2,3)
<chem>CC1=NN=C2C(O)N=C(C3=CC=CC=C3)C3=C(C=C(C(Cl)=C3)N12</chem>	4-Hydroxyalprazolam	-1.48	(2)
<chem>CN(CC1=CN=C2N=C(N)N=C(N)C2=N1)C1=CC=C(C=C1)C(=O)N[C@@H](CCC(O)=O)C(O)=O</chem>	Methotrexate	-1.51	(2)
<chem>CN\C(NC1=CC=CC(=C1)C1=CSC(N=C(N)N)=N1)=N/C#N</chem>	23; CHEBI: 145922	-1.54	(2,10)
<chem>CC(=O)NC1=CC(=CC=C1)C1=CSC(N=C(N)N)=N1</chem>	22	-1.57	(8,10)
<chem>OCC(O)C(O)C(O)C(O)CO</chem>	D-Mannitol	-1.6	(2)
<chem>OC(=O)CCCC1=CC=C(C=C1)N(CCCl)CCCl</chem>	Chlorambucil	-1.70	(1,2)
<chem>CN1CC2=C(N=CN2C2=CC=CC(Cl)=C2C1=O)C1=NOC(=N1)C(C)(O)CO</chem>	36; Bis-hydroxylated-L-663581	-1.82	(1)
<chem>CC1=CC=C(CC2=CN(CNCCC3=NC=C(Br)C=C3C)=NC2=O)C=N1</chem>	Temelastine	-1.88	(1,2)
<chem>COC1=CC=CN=C1CCCCNC1=NC(=O)C(CC2=CC=C(C)N=C2)=CN1</chem>	3; Icotidine	-2	(1,2,8)
<chem>OC(=O)COCCN1CCN(CC1)C(C1=CC=CC=C1)C1=CC=C(Cl)C=C1</chem>	Cetirizine	-2.15	(2,5)
<chem>CCN\C(NCCSCC1=NC=CC=C1Br)=N/C#N</chem>	13	-2.15	(10)

Table S2. Descriptors values maximum, minimum and mean.

Descriptor	Maximum	Minimum	Mean
LogP	6.48	-3.73	2.34
logD	6.42	-6.56	1.57
PSA	216.20	0	44.00
AC	92	5	33.81
HAC	45	2	17.29
MW	660.36	32.03	267.37
RBC	13	0	3.56
HBA	12	0	2.62
HBD	6	0	0.98
RC	5	0	2.03
NC	8	0	1.88
NO	6	0	1.50
NOC	13	0	3.38
MR	175.89	8.26	70.07

References

- [1] Ooms, F.; Weber, P.; Carrupt, P.A.; Testa, B. A simple model to predict blood-brain barrier permeation from 3D molecular fields. *Biochim. Biophys. Acta* 2002, 1587, 118-125.
- [2] Muehlbacher, M.; Spitzer, G.M.; Liedl, K.R.; Kornhuber, J. Qualitative prediction of blood-brain barrier permeability on a large and refined dataset, *J. Comput.-Aided Mol. Des.* 2011, 25, 1095-1106.
- [3] Platts, J.A.; Abraham, M.H.; Zhao, Y.H.; Hersey, A.; Ijaz, L.; Butina, D. Correlation and prediction of a large blood-brain distribution data set-an LFER study, *Eur. J. Med. Chem.* 2001, 36, 719-730.
- [4] Abraham, M.H.; Ibrahim, A.; Zhao, Y.; Acree, W.E. Jr. A data base for partition of volatile organic compounds and drugs from blood/plasma/serum to brain, and an LFER analysis of the data, *J. Pharm. Sci.* 2006, 95, 2091-2100.
- [5] Crivori, P.; Cruciani, G.; Carrupt, P.A.; Testa, B. Predicting blood-brain barrier permeation from three-dimensional molecular structure, *J. Med. Chem.* 2000, 43, 2204-2216.
- [6] Hou, T.; Xu, X. ADME evaluation in drug discovery. 1. Applications of genetic algorithms to the prediction of blood-brain partitioning of a large set of drugs, *J. Mol. Model.* 2002, 8, 337-349.
- [7] Lobell, M.; Molnar, L.; Keseru, G.M. Recent advances in the prediction of blood-brain partitioning from molecular structure, *J. Pharm. Sci.* 2003, 92, 360-370.
- [8] Liu, R.; Sun, H.; So, S.S. Development of quantitative structure-property relationship models for early ADME evaluation in drug discovery. 2. Blood-brain barrier penetration, *J. Chem. Inf. Model.* 2001, 41, 1623-1632.
- [9] Feher, M.; Sourial, E.; Schmidt, J.M. A simple model for the prediction of blood-brain partitioning, *Int. J. Pharm.* 2000, 201, 239-247.
- [10] Iyer, M.; Mishra, R.; Han, Y.; Hopfinger, A.J. Predicting blood-brain barrier partitioning of organic molecules using membrane-interaction QSAR analysis, *Pharm. Res.* 2002, 19, 1611-1621.
- [11] Luco, J.M. Prediction of the brain-blood distribution of a large set of drugs from structurally derived descriptors using partial least-squares (PLS) modeling, *J. Chem. Inf. Model.* 1999, 39, 396-404.
- [12] Rose, K.; Hall, L.H.; Kier, L.B. Modeling blood-brain barrier partitioning using the electrotopological state, *J. Chem. Inf. Model.* 2002, 42, 651-666.

Design, synthesis and preclinical evaluation of novel sigma receptors ligands

General details

Reagent grade chemicals were purchased from Sigma-Aldrich (St. Louis, MO, USA) or Merck (Darmstadt, Germany) and were used without further purification. All reactions involving air-sensitive reagents were carried out under nitrogen in dried glassware using the syringe-septum cap technique. Flash chromatography purification was performed on a Merck silica gel 60 (40–63 μm ; 230–400 mesh) stationary phase. Nuclear magnetic resonance spectra (^1H NMR recorded at 200 and 500 MHz) were obtained on VARIAN INOVA spectrometers using CDCl_3 , $\text{DMSO}-d_6$ or CD_3OD . TMS was used as an internal standard. Chemical shifts (δ) are given in parts per million (ppm) and coupling constants (J) in Hertz (Hz). The following abbreviations are used to designate the multiplicities: s = singlet, d = doublet, t = triplet, q = quartet, quint = quintet, m = multiplet, br = broad. The purity of all tested compounds, whether synthesized or purchased, reached at least 95% as determined by microanalysis (C, H, N) that was performed on a Carlo Erba instrument model E1110; all the results agreed within $\pm 0.4\%$ of the theoretical values. Reactions were monitored by thin-layer chromatography (TLC) performed on 250 μm silica gel Merck 60 F₂₅₄ coated aluminum plates; the spots were visualized by UV light or iodine chamber. UV-Vis spectra absorption spectra were recorded with a Jasco V-560 spectrophotometer. Compound nomenclatures were generated with ChemBioDraw Ultra version 16.0.0.82.

General Procedure for Buchwald–Hartwig amination (Procedure A)

A mixture of $\text{Pd}_2(\text{dba})_3$ (3 mol %, 11 mg), 2-dicyclohexylphosphino-2',6'-dimethoxybiphenyl (8 mol %, 13 mg) in dry toluene (3 mL) was degassed under N_2 for 30 min into an oven dried sealed vial. Then, *para*-substituted iodobenzene (0.39 mmol), *tert*-butyl 2,7-diazaspiro[nonane-2-carboxylate] or *tert*-butyl octahydro-1H-pyrrolo[3,4-*b*]pyridine-1-carboxylate (**AB2**, 0.39 mmol), and *t*-BuONa (0.55 mmol, 62 mg) were sequentially added and the reaction was stirred on. The reaction mixture was slowly brought to rt, quenched with H_2O (5 mL) and extracted with EtOAc (2 x 10 mL). The organic layer was dried over Na_2SO_4 and concentrated under vacuum. The crude product was purified by flash chromatography on silica gel to afford the desired product.

General Procedure for Amine Preparation (Procedure B)

To a solution of *tert*-butyl 2,7-diazaspiro[nonane-2-carboxylate] or *tert*-butyl octahydro-1H-pyrrolo[3,4-*b*]pyridine-1-carboxylate (**AB2**, 0.44 mmol) in ACN (5 mL), K_2CO_3 (1.32 mmol, 182 mg) and halo-derivative (0.73 mmol) were sequentially added. The reaction was stirred for 3h at rt, then quenched with H_2O (5 mL), and extracted with EtOAc (2 x 10 mL). The organic layer was washed with brine (1 x 5 mL), dried over Na_2SO_4 , filtered, and concentrated under vacuum. The residue was purified via silica gel chromatography to obtain the desired product.

General Procedure for Amine Preparation (Procedure C)

The Boc-protected amine (0.2 mmol) has been stirred with 30% TFA in CH_2Cl_2 (10 mL) at rt for 4h, followed by the removal of the solvents in vacuo. The residue was then dissolved in ACN (5 mL), and K_2CO_3 (0.3 mmol, 41 mg) and alkyl bromide (0.2 mmol) were sequentially added. The reaction has been stirred under reflux on, quenched with H_2O (5 mL) and extracted with EtOAc. The collected organic phases have been washed with brine (1 x 5 mL), dried over Na_2SO_4 and evaporated to dryness.

General Procedure for Amine Preparation (Procedure D)

To a solution of *tert*-butyl 2,7-diazaspiro[4.4]nonane-2-carboxylate (0.44 mmol, 100 mg) in anhydrous CH₂Cl₂ (5 mL), TEA (0.66 mmol, 92.41 μl) and acyl chloride (0.88 mmol) have been added dropwise at 0 °C. The reaction has been stirred for 1 h at rt, then quenched with cold water (5 mL), diluted with CH₂Cl₂ (10 mL) and washed with 5% NH₄Cl (1 x 5 mL), and a saturated solution of NaHCO₃ (1 x 5 mL). The combined organic extracts were dried over anhydrous Na₂SO₄ and concentrated under vacuum. The residue has been purified by flash chromatography.

General Procedure for Amine Preparation (Procedure E)

A mixture of Boc-protected amine (0.30 mmol) with 30% TFA in CH₂Cl₂ (10 mL) has been stirred at rt for 4h, followed by the removal of the solvents in vacuo. The residue was dissolved in fresh anhydrous CH₂Cl₂ (5 mL), and TEA (0.53 mmol, 75 μl) and acyl chloride (0.36 mmol) have been added dropwise at 0 °C. The reaction has been stirred at rt for 2 h and then quenched with H₂O (5 mL), diluted with CH₂Cl₂ (10 mL), washed with 5% NH₄Cl (1 x 5 mL), and then with a saturated solution of NaHCO₃ (1 x 5 mL). The combined organic extracts were dried over anhydrous Na₂SO₄ and concentrated under vacuum. The residue has been purified by flash chromatography to obtain the desired product.

General Procedure for Amide Bond Reduction (Procedure F)

To a solution of amide (0.14 mmol) in THF (10 mL), LiAlH₄ (4M in THF, 0.82 mmol) was added dropwise at -10 °C under N₂ atmosphere. The resulting mixture was stirred for 2 h at appropriate temperature. Then, the reaction was quenched with ice-cold H₂O (1 mL) and 1M NaOH (1 mL) at 0 °C, filtered through Celite and washed with MeOH. The solution was concentrated under reduced pressure and dissolved in EtOAc. The organic phase was dried over anhydrous Na₂SO₄ and concentrated under vacuum. The residue has been purified by flash chromatography.

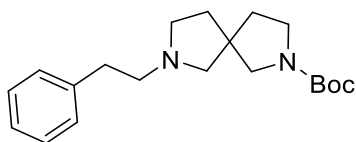
General Procedure for Coupling Reaction (Procedure G)

A mixture of Boc-protected amine (0.31 mmol) with 30% TFA in CH₂Cl₂ (10 mL) has been stirred at rt for 4h, followed by the removal of the solvents in vacuo. In the meanwhile, to a solution of carboxylic acid (0.40 mmol) in ACN (5 mL), EDC (0.46 mmol, 72 mg) and HOBT (0.46 mmol, 63 mg) were added at 0 °C. After 20 min, the previously prepared amine in ACN (2 mL) and DIPEA (0.93 mmol, 162 μL) were added at 0 °C. The reaction has been stirred at rt for 24 h. After reaction was complete, it was diluted with EtOAc (5 mL), washed with H₂O (1 x 5 mL), saturated solution of NaHCO₃ (1 x 5 mL) and brine (1 x 5 mL). The combined organic extracts were dried over anhydrous Na₂SO₄ and concentrated under vacuum. The residue has been purified by flash chromatography.

General Procedure for Oxalate Salts formation (Procedure H)

For all the final compounds, the pure product was dissolved in diethyl ether and a solution of oxalic acid in diethyl ether was added dropwise to obtain the desired product as oxalic acid salt.

***tert*-Butyl 7-phenethyl-2,7-diazaspiro[4.4]nonane-2-carboxylate (AD142)**

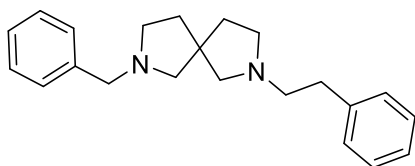


The compound has been prepared using *tert*-butyl 2,7-diazaspiro[4.4]nonane-2-carboxylate (0.44 mmol, 100 mg) and (2-bromoethyl)benzene (0.73 mmol, 99.7 μ L) following Procedure B. The reaction has been left to stir at 50 $^{\circ}$ C on. The residue has been purified with 5% MeOH in EtOAc. Yield: 50%, yellow oil.

Chemical Formula: C₂₀H₃₀N₂O₂ (330.47 g/mol).

¹H NMR (200 MHz, CDCl₃) δ 7.12–7.30 (m, 5H), 3.13–3.52 (m, 5H), 2.57–2.87 (m, 7H), 1.68–1.95 (m, 4H), 1.46 (s, 9H).

2-Benzyl-7-phenethyl-2,7-diazaspiro[4.4]nonane oxalate (AD145)



The compound has been prepared using **AD177** (0.2 mmol, 63 mg) and (2-bromoethyl)benzene (0.2 mmol, 27.3 μ L) following Procedure C and H. The residue was purified by flash chromatography on silica gel eluting with 4% MeOH in CH₂Cl₂. Yield: 25%, orange solid.

Chemical Formula: C₂₂H₂₈N₂·H₂C₂O₄ (410.22 g/mol).

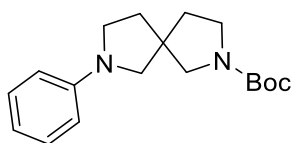
¹H NMR (200 MHz, CDCl₃) δ 7.14–7.48 (m, 10H), 3.76 (s, 2H), 3.10 (br. s., 8H), 2.55–2.93 (free base) (m, 4H), 1.86–2.20 (m, 4H).

¹³C NMR (200 MHz, CDCl₃) δ 137.2, 136.3, 129.2, 128.6, 127.8, 127.0, 64.9, 64.5, 59.5, 57.7, (free base) 53.7, 52.8, 47.7, 37.1, 36.8, 32.9.

Elem. Anal. Anal. calcd: C, 70.22; H, 7.37; N, 6.82.

Found: C, 70.51; H, 7.35; 6.81.

***tert*-Butyl 7-phenyl-2,7-diazaspiro[4.4]nonane-2-carboxylate (AD155)**

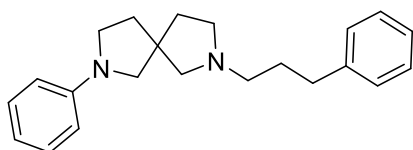


The compound has been prepared using *tert*-butyl 2,7-diazaspiro[4.4]nonane-2-carboxylate (0.39 mmol, 88 mg) and iodobenzene (0.39 mmol, 43.6 μ L) following Procedure A. The reaction was heated to 100 $^{\circ}$ C. The crude product was purified by column chromatography on silica gel using hexane/EtOAc (95:5) as the eluent to afford the desired product. Yield: 82%, brown oil.

Chemical Formula: C₁₈H₂₆N₂O₂ (302.42 g/mol).

¹H NMR (200 MHz, CDCl₃) δ 7.18–7.31 (m, 2H), 6.70 (t, *J* = 7.22 Hz, 1H), 6.55 (d, *J* = 7.99 Hz, 2H), 3.18–3.58 (m, 8H), 1.76–2.09 (m, 4H), 1.47 (s, 9H).

2-Phenyl-7-(3-phenylpropyl)-2,7-diazaspiro[4.4]nonane oxalate (AD157)



The compound has been prepared using **AD155** (0.2 mmol, 60 mg) and (3-bromopropyl)benzene (0.2 mmol, 30.4 μL) following Procedure C and H. The residue was purified by flash chromatography on silica gel eluting with 5% MeOH in CH₂Cl₂. Yield: 25%, brown solid.

Chemical Formula: C₂₂H₂₈N₂·H₂C₂O₄ (410.22 g/mol).

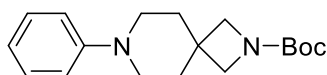
¹H NMR (200 MHz, CDCl₃) δ 7.10–7.39 (m, 7H), 6.63–6.75 (m, 1H), 6.53 (d, *J* = 8.30 Hz, (free base) 2H), 3.21–3.43 (m, 5H), 2.97–3.17 (m, 3H), 2.61–2.85 (m, 5H), 1.91–2.21 (m, 5H).

¹³C NMR (200 MHz, CDCl₃) δ 147.7, 138.8, 129.1, 128.7, 128.3, 126.9, 115.3, 111.3, 64.6, (free base) 60.5, 59.6, 53.9, 48.0, 47.0, 38.0, 36.1, 29.7.

Elem. Anal. Anal. calcd: C, 70.22; H, 7.37; N, 6.82.

Found: C, 70.56; H, 7.38; N, 6.86.

***tert*-Butyl 7-phenyl-2,7-diazaspiro[3.5]nonane-2-carboxylate (AD168)**

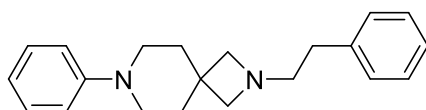


The compound has been prepared using *tert*-butyl 2,7-diazaspiro[3.5]nonane-2-carboxylate (0.39 mmol, 88 mg) and iodobenzene (0.39 mmol, 43.6 μL) following Procedure A. The crude product was purified by column chromatography on silica gel using hexane/EtOAc (90:10) as the eluent to afford the desired product. Yield: 89%, clear solid.

Chemical Formula: C₁₈H₂₆N₂O₂ (302.42 g/mol).

¹H NMR (200 MHz, CDCl₃) δ 7.16–7.33 (m, 2H), 6.76–6.98 (m, 3H), 3.66 (s, 4H), 2.94–3.22 (m, 4H), 1.79–1.91 (m, 4H), 1.45 (s, 9H).

2-Phenethyl-7-phenyl-2,7-diazaspiro[3.5]nonane oxalate (AD172)



The compound has been prepared using **AD168** (0.2 mmol, 60 mg) and (2-bromoethyl)benzene (0.2 mmol, 27.3 μL) following Procedure C and H. The residue was purified by flash chromatography on silica gel eluting with 3% MeOH in CH₂Cl₂. Yield: 30%, yellow solid.

Chemical Formula: C₂₁H₂₆N₂·H₂C₂O₄ (396.20 g/mol).

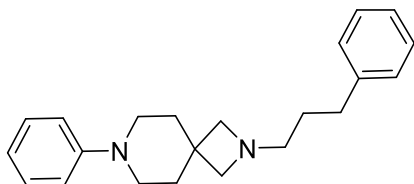
¹H NMR (200 MHz, CDCl₃) δ 7.20–7.41 (m, 7H), 6.79–7.00 (m, 3H), 3.30 (s, 4H), 3.05–3.18 (free base) (m, 4H), 2.72–3.00 (m, 4H), 1.89–2.00 (m, 4H).

¹³C NMR (200 MHz, CDCl₃) δ 150.8, 135.9, 129.1, 127.3, 116.7, 63.3, 60.4, 46.5, 34.6, 29.7, (free base) 21.1, 14.4.

Elem. Anal. Anal. calcd: C, 69.68; H, 7.12; N, 7.07.

Found: C, 69.92; H, 7.17; N, 7.06.

7-Phenyl-2-(3-phenylpropyl)-2,7-diazaspiro[3.5]nonane oxalate (AD173)



The compound has been prepared using **AD168** (0.2 mmol, 60 mg) and (3-bromopropyl)benzene (0.2 mmol, 30.4 μL) following Procedure C and H. The residue was purified by flash chromatography on silica gel eluting with 5% MeOH in CH₂Cl₂. Yield: 30%, brown solid.

Chemical Formula: C₂₂H₂₈N₂·H₂C₂O₄ (410.22 g/mol).

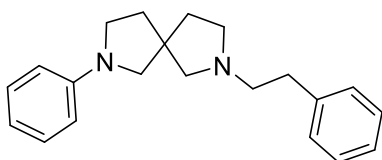
¹H NMR (200 MHz, CDCl₃) δ 7.10–7.45 (m, 7H), 6.78–6.99 (m, 3H), 3.70 (s, 4H), 3.04–3.18 (free base) (m, 4H), 2.92–3.04 (m, 2H), 2.72 (t, *J* = 7.42 Hz, 2H), 1.94–2.15 (m, 6H).

¹³C NMR (200 MHz, CDCl₃) δ 150.9, 139.6, 129.2, 128.7, 128.3, 126.5, 120.2, 116.8, 62.9, (free base) 56.5, 46.7, 35.0, 34.2, 32.6, 26.2.

Elem. Anal. Anal. calcd: C, 70.22; H, 7.37; N, 6.82.

Found: C, 70.56; H, 7.39; N, 6.85.

2-Phenethyl-7-phenyl-2,7-diazaspiro[4.4]nonane oxalate (AD174)



The compound has been prepared using **AD155** (0.2 mmol, 60 mg) and (2-bromoethyl)benzene (0.2 mmol, 27.3 μL) following Procedure C and H. The residue was purified by flash chromatography on silica gel eluting with 1% MeOH in CH₂Cl₂. Yield: 20%, yellow solid.

Chemical Formula: C₂₁H₂₆N₂·C₂H₂O₄ (396.20 g/mol).

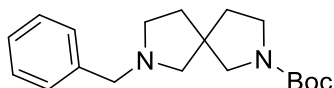
¹H NMR (200 MHz, CDCl₃) δ 7.16–7.53 (m, 7H), 6.71 (t, *J* = 7.42 Hz, 4H), 6.58 (d, *J* = 7.81 Hz, 3H), 3.22–3.48 (m, 4H), 2.57–2.96 (m, 8H), 1.80–2.19 (m, 4H).

¹³C NMR (200 MHz, CDCl₃) δ 147.7, 140.1, 129.2, 128.7, 128.3, 126.1, 115.4, 111.4, 64.8, (free base) 59.6, 58.4, 54.2, 48.0, 47.1, 37.9, 36.0, 35.4

Elem. Anal. Anal. calcd: C, 69.68; H, 7.12; N, 7.07.

Found: C, 69.42; H, 7.11; N, 7.09.

***tert*-Butyl 7-benzyl-2,7-diazaspiro[4.4]nonane-2-carboxylate (AD177)**

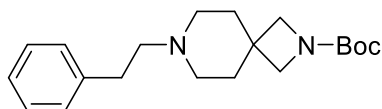


The compound has been prepared using *tert*-butyl 2,7-diazaspiro[4.4]nonane-2-carboxylate (0.44 mmol, 100 mg) and benzylbromide (0.73 mmol, 86.8 μ L) following Procedure B. The residue was purified via silica gel chromatography with hexane/EtOAc (70:30). Yield: 60%, clear oil.

Chemical Formula: C₁₉H₂₈N₂O₂ (316.45 g/mol).

¹H NMR (200 MHz, CDCl₃) δ 7.15–7.35 (m, 5H), 3.57 (s, 2H), 3.07–3.42 (m, 4H), 2.26–2.75 (m, 4H), 1.62–1.95 (m, 4H), 1.34–1.48 (m, 9H).

***tert*-Butyl 7-phenethyl-2,7-diazaspiro[3.5]nonane-2-carboxylate (AD178)**

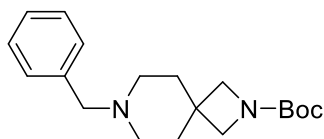


The compound has been prepared using *tert*-butyl 2,7-diazaspiro[3.5]nonane-2-carboxylate (0.44 mmol, 100 mg) and (2-bromoethyl)benzene (0.73 mmol, 134 μ L) following Procedure B. The residue has been purified with 5% MeOH in EtOAc. Yield: 41%, yellow oil.

Chemical Formula: C₂₀H₃₀N₂O₂ (330.47 g/mol).

¹H NMR (200 MHz, CDCl₃) δ 7.13–7.40 (m, 5H), 3.63 (s, 4H), 2.73–2.91 (m, 2H), 2.33–2.65 (m, 6H), 1.80 (t, J = 5.46 Hz, 4H), 1.46 (s, 9H).

***tert*-Butyl 7-benzyl-2,7-diazaspiro[3.5]nonane-2-carboxylate (AD179)**

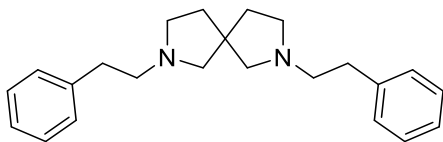


The compound has been prepared using *tert*-butyl 2,7-diazaspiro[3.5]nonane-2-carboxylate (0.44 mmol, 100 mg) and benzylbromide (0.73 mmol, 86.8 μ L) following Procedure B. The residue was purified via silica gel chromatography with 100% EtOAc. Yield: 70%, clear oil.

Chemical Formula: C₁₉H₂₈N₂O₂ (316.45).

¹H NMR (200 MHz, CDCl₃) δ 7.08–7.51 (m, 5H), 3.41–3.72 (m, 6H), 2.40 (br. s., 4H), 1.68–1.98 (m, 4H), 1.36 (s, 9H).

2,7-Diphenethyl-2,7-diazaspiro[4.4]nonane oxalate (AD181)



The compound has been prepared using **AD142** (0.2 mmol, 66 mg) and (2-bromoethyl)benzene (0.2 mmol, 27.3 μ L) following Procedure C and H. The residue has been purified by flash chromatography on silica gel eluting with 3% MeOH in CH_2Cl_2 . Yield: 42%, white solid.

Chemical Formula: $\text{C}_{23}\text{H}_{30}\text{N}_2 \cdot \text{H}_2\text{C}_2\text{O}_4$ (424.24 g/mol).

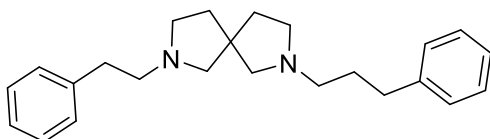
^1H NMR (200 MHz, CDCl_3) δ 7.14–7.43 (m, 10H), 2.57–2.99 (m, 16H), 1.83–2.12 (m, 4H).
(free base)

^{13}C NMR (200 MHz, CDCl_3) δ 139.9, 128.4, 125.8, 67.2, 67.0, 66.8, 58.3, 53.9, 47.6, 38.5,
(free base) 35.1.

Elem. Anal. Anal. calcd: C, 70.73; H, 7.60; N, 6.60.

Found: C, 70.90; H, 7.55; N, 6.58.

2-Phenethyl-7-(3-phenylpropyl)-2,7-diazaspiro[4.4]nonane oxalate (AD182)



The compound has been prepared using **AD142** (0.2 mmol, 66 mg) and (3-bromopropyl)benzene (0.2 mmol, 30.4 μ L) following Procedure C and H. The residue has been purified by flash chromatography on silica gel eluting with 3% MeOH in CH_2Cl_2 . Yield: 39%, light yellow solid.

Chemical Formula: $\text{C}_{24}\text{H}_{32}\text{N}_2 \cdot \text{H}_2\text{C}_2\text{O}_4$ (438.25 g/mol).

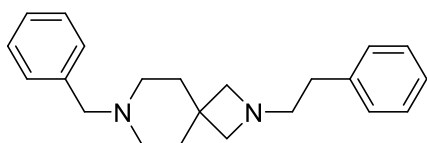
^1H NMR (200 MHz, CDCl_3) δ 7.10–7.47 (m, 10H), 2.58–3.03 (m, 16H), 1.80–2.21 (m, 6H).
(free base)

^{13}C NMR (200 MHz, CDCl_3) δ 141.0, 139.3, 128.6, 128.4, 128.3, 126.3, 126.0, 65.8, 57.9,
(free base) 55.8, 53.6, 47.6, 37.6, 34.6, 33.3, 28.8.

Elem. Anal. Anal. calcd: C, 71.21; H, 7.81; N, 6.39.

Found: C, 71.80; H, 7.82; N, 6.40.

7-Benzyl-2-phenethyl-2,7-diazaspiro[3.5]nonane oxalate (AD186)



The compound has been prepared using **AD179** (0.27 mmol, 80 mg) and 2-bromoethyl)benzene (0.32 mmol, 44 μ L) following Procedure C and H. The residue was purified by flash chromatography on silica gel eluting with 4% MeOH in CH_2Cl_2 . Yield: 30%, white solid.

Chemical Formula: C₂₂H₂₈N₂·H₂C₂O₄ (410.22 g/mol).

¹H NMR (200 MHz, CDCl₃) δ 7.09–7.37 (m, 10H), 3.43 (s, 2H), 3.13 (s, 4H), 2.61–2.89 (m, 4H), 2.31 (br. s., 4H), 1.77 (t, *J* = 5.38 Hz, 4H).

¹³C NMR (200 MHz, CDCl₃) δ 139.1, 138.1, 129.1, 128.5, 128.1, 127.0, 126.3, 64.3, 63.2, 61.0, 50.4, 35.9, 34.2, 33.8.

Elem. Anal. Anal. calcd: C, 70.22; H, 7.37; N, 6.82.
Found: C, 70.53; H, 7.42; N, 6.76.

2,7-Diphenethyl-2,7-diazaspiro[3.5]nonane oxalate (AD187)



The compound has been prepared using **AD178** (0.2 mmol, 66 mg) and (2-bromoethyl)benzene (0.2 mmol, 36.8 μL) following Procedure C and H. The residue was purified by flash chromatography on silica gel eluting with 4% MeOH in CH₂Cl₂. Yield: 25%, white solid.

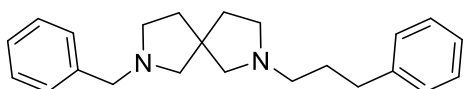
Chemical Formula: C₂₃H₃₀N₂·H₂C₂O₄ (424.24 g/mol).

¹H NMR (200 MHz, CDCl₃) δ 7.11–7.37 (m, 10H), 3.16 (s, 4H), 2.68–2.93 (m, 6H), 2.38–2.63 (m, 6H), 1.85 (t, *J* = 5.53 Hz, 4H).

¹³C NMR (200 MHz, CDCl₃) δ 140.1, 139.2, 128.8, 128.4, 126.3, 126.1, 64.3, 61.2, 60.7, 50.6, 35.9, 34.2, 33.9, 33.6.

Elem. Anal. Anal. calcd: C, 70.73; H, 7.60; N, 6.60.
Found: C, 70.97; H, 7.65; N, 6.59.

2-Benzyl-7-(3-phenylpropyl)-2,7-diazaspiro[4.4]nonane oxalate (AD193)



The compound has been prepared using **AD177** (0.2 mmol, 63 mg) and (3-bromopropyl)benzene (0.2 mmol, 30.4 μL) following Procedure C and H. The residue has been purified by flash chromatography on silica gel eluting with 4% MeOH in CH₂Cl₂. Yield: 37%, yellow solid.

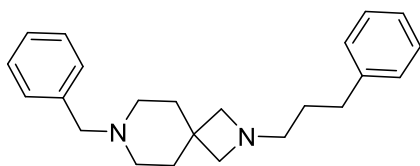
Chemical Formula: C₂₃H₃₀N₂·H₂C₂O₄ (424.24 g/mol).

¹H NMR (200 MHz, CDCl₃) δ 7.04–7.44 (m, 10H), 3.58 (s, 2H), 2.32–2.71 (m, 12H), 1.81 (d, *J* = 6.54 Hz, 6H).

¹³C NMR (200 MHz, CDCl₃) δ 140.9, 139.4, 129.5, 129.2, 129.0, 128.9, 128.0, 126.9, 60.4, 56.5, 56.1, 54.3, 53.5, 48.3, 38.1, 37.7, 33.7.

Elem. Anal. Anal. calcd: C, 70.73; H, 7.60; N, 6.60.
Found: C, 70.69; H, 7.58; N, 6.58.

7-Benzyl-2-(3-phenylpropyl)-2,7-diazaspiro[3.5]nonane oxalate (AD195)



The compound has been prepared using **AD179** (0.2 mmol, 63 mg) and (3-bromopropyl)benzene (0.2 mmol, 30.4 μ L) following Procedure C and H. The residue was purified by flash chromatography on silica gel eluting with 4% MeOH in CH_2Cl_2 . Yield: 35%, yellow solid.

Chemical Formula: $\text{C}_{23}\text{H}_{30}\text{N}_2 \cdot \text{H}_2\text{C}_2\text{O}_4$ (424.24 g/mol).

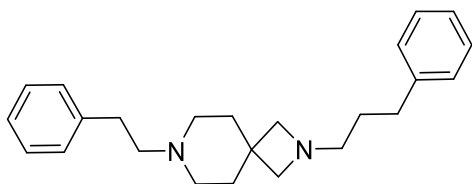
^1H NMR (200 MHz, CDCl_3) δ 7.10–7.50 (m, 10H), 3.80 (s, 2H), 3.70 (s, 2H), 3.48 (s, 2H), (free base) 2.50–3.25 (m, 4H), 2.23–2.48 (m, 4H), 1.89–2.16 (m, 2H), 1.79 (t, $J = 5.42$ Hz, 4H).

^{13}C NMR (200 MHz, CDCl_3) δ 143.2, 138.0, 129.0, 128.5, 128.4, 128.2, 127.1, 63.0, 58.0, (free base) 56.9, 50.3, 47.7, 35.4, 29.7.

Elem. Anal. Anal. calcd: C, 70.73; H, 7.60; N, 6.60.

Found: C, 70.87; H, 7.62; N, 6.58.

7-Phenethyl-2-(3-phenylpropyl)-2,7-diazaspiro[3.5]nonane oxalate (AD197)



The compound has been prepared using **AD178** (0.2 mmol, 66 mg) and (3-bromopropyl)benzene (0.2 mmol, 30.4 μ L) following Procedure C and H. The residue was purified by flash chromatography on silica gel eluting with 5% MeOH in CH_2Cl_2 . Yield: 45%, yellow solid.

Chemical Formula: $\text{C}_{24}\text{H}_{32}\text{N}_2 \cdot \text{H}_2\text{C}_2\text{O}_4$ (438.25 g/mol).

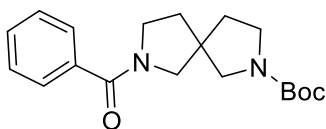
^1H NMR (200 MHz, CDCl_3) δ 7.11–7.39 (m, 10H), 3.78–3.90 (m, 2H), 3.72 (s, 2H), (free base) 2.30–2.91 (m, 12H), 1.71–1.97 (m, 6H).

^{13}C NMR (200 MHz, CDCl_3) δ 141.0, 139.2, 128.6, 128.4, 126.2, 64.4, 60.5, 58.3, 50.4, 35.4, (free base) 35.3, 34.2.

Elem. Anal. Anal. calcd: C, 71.21; H, 7.81; N, 6.39.

Found: C, 71.79; H, 7.87; N, 6.36.

tert-Butyl 7-benzoyl-2,7-diazaspiro[4.4]nonane-2-carboxylate (AD203)

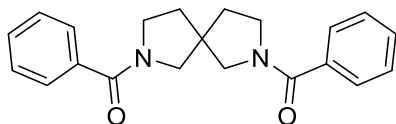


The compound has been prepared using *tert*-butyl 2,7-diazaspiro[4.4]nonane-2-carboxylate (0.44 mmol, 100 mg) and benzoyl chloride (0.88 mmol, 102.1 μ L) following Procedure D. The residue has been purified by flash chromatography with EtOAc/hexane (90:10 to 70:30). Yield: 98%, colorless oil.

Chemical Formula: C₁₉H₂₆N₂O₃ (330.43 g/mol).

¹H NMR (200 MHz, CDCl₃) δ 7.35–7.58 (m, 5H), 3.14–3.85 (m, 8H), 1.72–2.02 (m, 4H), 1.45 (s, 9H).

(2,7-Diazaspiro[4.4]nonane-2,7-diyl)bis(phenylmethanone) (AD205)

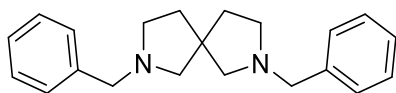


The compound has been prepared using **AD203** (0.30 mmol, 99 mg) and benzoyl chloride (0.36 mmol, 41.8 μ L) following Procedure E. The residue has been purified by flash chromatography with 100% EtOAc. Yield: 76%, colorless oil.

Chemical Formula: C₂₁H₂₂N₂O₂ (334.42 g/mol).

¹H NMR (200 MHz, CDCl₃) δ 7.31–7.66 (m, 10H), 3.20–3.87 (m, 8H), 1.73–2.18 (m, 4H).

2,7-Dibenzyl-2,7-diazaspiro[4.4]nonane oxalate (AD206)



The compound has been prepared using **AD205** (0.14 mmol, 47 mg) following Procedure F and H. The resulting mixture was warmed to 65 °C and stirred for 2 h. The residue has been purified by flash chromatography with 100% CH₂Cl₂ and then with 3% MeOH in CH₂Cl₂. Yield: 83%, white solid.

Chemical Formula: C₂₁H₂₆N₂·H₂C₂O₄ (396.20 g/mol).

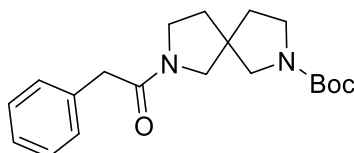
¹H NMR (200 MHz, CDCl₃) δ 7.15–7.36 (m, 10H), 3.59 (s, 4H), 2.36–2.68 (m, 8H), (free base) 1.69–2.00 (m, 4H).

¹³C NMR (200 MHz, CDCl₃) δ 139.1, 128.8, 128.1, 126.8, 67.3, 62.6, 60.5, 53.8, 47.5, 39.3. (free base)

Elem. Anal. Anal. Calcd: C, 69.68; H, 7.12; N, 7.07.

Found: C 69.98; H, 7.17; N, 7.04.

***tert*-Butyl 7-(phenylacetyl)-2,7-diazaspiro[4.4]nonane-2-carboxylate (AD208)**

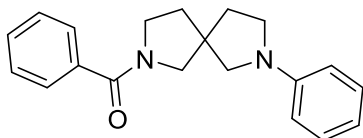


The compound has been prepared using *tert*-butyl 2,7-diazaspiro[4.4]nonane-2-carboxylate (0.44 mmol, 100 mg) and 2-phenylacetyl chloride (0.88 mmol, 116 μ L) following Procedure D. The residue has been purified by flash chromatography with EtOAc/hexane (70:30 to 90:10). Yield: 60%, colorless oil.

Chemical Formula: C₂₀H₂₈N₂O₃ (344.46 g/mol).

¹H NMR (200 MHz, CDCl₃) δ 7.20–7.41 (m, 5H), 3.14–3.71 (m, 10H), 1.61–1.98 (m, 4H), 1.45 (s, 9H).

Phenyl(7-phenyl-2,7-diazaspiro[4.4]nonan-2-yl)methanone (AD212)

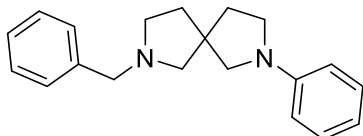


The compound has been prepared using **AD155** (0.3 mmol, 90.7 mg) and benzoyl chloride (0.36 mmol, 42 μ L) following Procedure E. The residue was purified by flash chromatography with hexane/EtOAc (80:20). Yield: 70%, yellow oil.

Chemical Formula: C₂₀H₂₂N₂O (306.41 g/mol).

¹H NMR (200 MHz, CDCl₃) δ 8.05–8.15 (m, 3H), 7.39–7.52 (m, 5H), 7.05–7.23 (m, 2H), 2.84–3.97 (m, 8H), 1.70–2.16 (m, 2H), 0.94–1.45 (m, 2H).

2-Benzyl-7-phenyl-2,7-diazaspiro[4.4]nonane oxalate (AD214)



The compound has been prepared using **AD212** (0.14 mmol, 43 mg) following Procedure F and H. The residue was purified by flash chromatography with hexane/EtOAc (60:40). Yield: 20%, white solid.

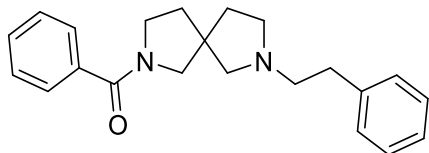
Chemical Formula: C₂₀H₂₄N₂·H₂C₂O₄ (382.19 g/mol).

¹H NMR (200 MHz, CDCl₃) δ (200 MHz, CDCl₃) δ 7.08–7.40 (m, 7H), 6.55–6.68 (m, 1H), (free base) 6.48 (d, *J* = 8.30 Hz, 2H), 3.59 (d, *J* = 1.54 Hz, 2H), 3.23 (quin, *J* = 8.91 Hz, 4H), 2.35–2.76 (m, 4H), 1.68–2.09 (m, 4H).

¹³C NMR (200 MHz, CDCl₃) δ 147.7, 138.8, 129.1, 128.7, 128.3, 126.9, 115.6, 111.3, 64.6, (free base) 60.5, 59.6, 53.9, 48.0, 47.0, 38.0, 36.1.

Elem. Anal. Anal. Calcd: C, 69.09; H, 6.85; N, 7.32.
Found: C, 69.22; H, 6.88; N, 7.27.

(7-Phenethyl-2,7-diazaspiro[4.4]nonan-2-yl)(phenyl)methanone oxalate (AD217)



The compound has been prepared using **AD218** (0.30 mmol, 99 mg) and benzoyl chloride (0.36 mmol, 41.8 μ L) following Procedure E and H. The residue has been purified by flash chromatography with EtOAc/hexane (70:30 to 90:10). Yield: 23%, white solid.

Chemical Formula: $C_{22}H_{26}N_2O \cdot H_2C_2O_4$ (424.20 g/mol).

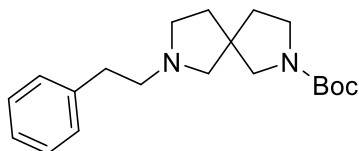
1H NMR (200 MHz, $CDCl_3$) δ 7.09–7.60 (m, 10H), 3.29–3.84 (m, 4H), 2.65–3.13 (m, 6H), (free base) 2.34–2.61 (m, 4H), 1.73–2.19 (m, 4H).

^{13}C NMR (200 MHz, $CDCl_3$) δ 169.8, 138.8, 131.6, 129.6, 128.5, 128.2, 127.9, 127.0, 62.3, (free base) 60.3, 57.8, 53.2, 48.5, 46.7, 45.4, 36.2, 34.5.

Elem. Anal. Anal. Calcd: C, 67.91; H, 6.65; N, 6.60.

Found: C, 68.08; H, 6.68; N, 6.55.

***tert*-Butyl 7-phenethyl-2,7-diazaspiro[4.4]nonane-2-carboxylate (AD218)**

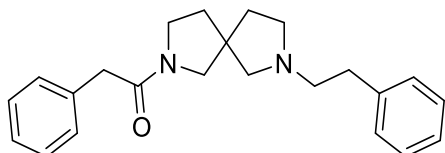


The compound has been prepared using **AD208** (1.74 mmol, 600 mg) following Procedure F. The residue has been purified by flash chromatography with EtOAc/hexane (80:20 to 90:10). Yield: 43%, colorless oil.

Chemical Formula: $C_{20}H_{30}N_2O_2$ (330.47 g/mol).

1H NMR (200 MHz, $CDCl_3$) δ 7.00–7.45 (m, 5H), 3.06–3.54 (m, 4H), 2.40–2.96 (m, 8H), 1.68–2.00 (m, 4H), 1.47 (s, 9H).

1-(7-Phenethyl-2,7-diazaspiro[4.4]nonan-2-yl)-2-phenylethan-1-one oxalate (AD219)



The compound has been prepared using **AD218** (0.30 mmol, 99 mg) and phenylacetyl chloride (0.36 mmol, 47.6 μ L) following Procedure E and H. The residue has been purified by flash chromatography with EtOAc/hexane (70:30 to 90:10). Yield: 37%, light yellow solid.

Chemical Formula: C₂₃H₂₈N₂O·H₂C₂O₄ (438.22 g/mol).

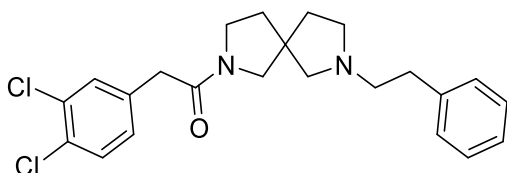
¹H NMR (200 MHz, CDCl₃) δ 7.04–7.44 (m, 10H), 3.39–3.77 (m, 6H), 2.91–3.37 (m, 2H), (free base) 2.83 (d, *J* = 9.76 Hz, 4H), 2.52–2.78 (m, 2H), 1.68–2.15 (m, 4H).

¹³C NMR (200 MHz, CDCl₃) δ 168.9, 139.9, 128.4, 125.8, 67.2, 67.0, 66.8, 58.3, 53.9, 47.6, (free base) 38.5, 35.1.

Elem. Anal. Anal. Calcd: C, 68.47; H, 6.90; N, 6.39.

Found: C, 68.58; H, 6.95; N, 6.34.

2-(3,4-Dichlorophenyl)-1-(7-phenethyl-2,7-diazaspiro[4.4]nonan-2-yl)ethan-1-one oxalate (AD220)



The compound has been prepared using **AD218** (0.31 mmol, 102 mg) and 3,4-dichlorophenylacetic acid (0.40 mmol, 82 mg) following Procedure G and H. The residue has been purified by flash chromatography with 5% MeOH in CH₂Cl₂. Yield: 40%, light yellow solid.

Chemical Formula: C₂₃H₂₆Cl₂N₂O·H₂C₂O₄ (506.14 g/mol).

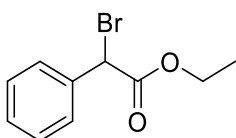
¹H NMR (200 MHz, CDCl₃) δ 6.89–7.39 (m, 8H), 3.31–3.69 (m, 8H), 2.78–3.26 (m, 6H), (free base) 1.77–2.20 (m, 4H).

¹³C NMR (200 MHz, CDCl₃) δ 168.8, 162.8, 162.1, 135.9, 134.6, 134.4, 132.3, 132.2, 131.1, (free base) 130.9, 130.8, 130.3, 128.9, 128.7, 128.5, 127.2, 61.2, 60.9, 57.0, 56.2, 55.4, 53.1, 52.9, 48.3, 46.4, 45.6, 44.8, 40.5, 40.1, 36.3, 34.8, 33.9, 33.4, 31.9.

Elem. Anal. Anal. Calcd: C, 59.18; H, 5.56; N, 5.52.

Found: C, 59.26; H, 5.59; N, 5.49.

Ethyl 2-bromo-2-phenylacetate (AD221)

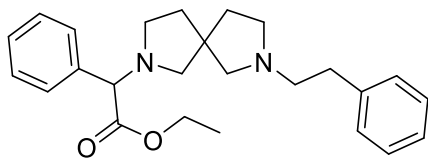


To a solution of 2-bromo-2-phenylacetic acid (2.33 mmol, 500 mg) in EtOH (10 mL), H₂SO₄ (0.2 mmol, 100 μL) was added. The resulting mixture has been stirred for 18 h at 75 °C. After reaction was complete, it was diluted with EtOAc (30 mL) and washed with a saturated solution of NaHCO₃ (1 x 15 mL) and NaCl (1 x 15 mL). The combined organic extracts were dried over anhydrous Na₂SO₄ and concentrated under vacuum. Yield: 83%, colorless oil.

Chemical Formula: C₁₀H₁₁BrO₂ (243.10 g/mol).

¹H NMR (200 MHz, CDCl₃) δ 7.20–7.70 (m, 5H), 5.35 (s, 1H), 4.06–4.41 (m, 2H), 1.10–1.41 (m, 3H).

Ethyl 2-(7-phenethyl-2,7-diazaspiro[4.4]nonan-2-yl)-2-phenethylacetate oxalate (AD-223)



The compound has been prepared using **AD218** (0.80 mmol, 274 mg) and **AD221** (0.89 mmol, 215 mg) following Procedure C and H. The residue was purified by flash chromatography with 2% MeOH in EtOAc. Yield: 10 %, yellow solid.

Chemical Formula: C₂₅H₃₂N₂O₂·H₂C₂O₄ (482.24 g/mol).

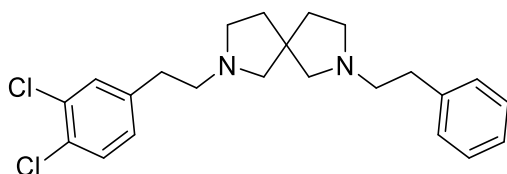
¹H NMR (200 MHz, CDCl₃) δ 7.41–7.56 (m, 2H), 7.06–7.38 (m, 8H), 4.13 (dq, *J* = 4.29, 7.16 (free base) Hz, 2H), 3.99 (s, 1H), 2.39–2.88 (m, 12H), 1.74–2.06 (m, 4H), 1.11–1.34 (m, 3H).

¹³C NMR (200 MHz, CDCl₃) δ 171.5, 139.6, 137.1, 128.6, 128.4, 128.1, 126.1, 73.1, 67.0, (free base) 66.6, 64.8, 60.8, 58.4, 54.0, 53.4, 51.5, 47.3, 38.5, 37.9, 34.8, 14.0.

Exact mass Anal. Calcd: C, 67.20; H, 7.10; N, 5.81.

Found: C, 67.57; H, 7.13; N, 5.85.

2-(3,4-Dichlorophenethyl)-7-phenethyl-2,7-diazaspiro[4.4]nonane oxalate (AD225)



The compound has been prepared using **AD220** (0.14 mmol, 58 mg) following Procedure F and H. The reaction was allowed to warm to r.t. The residue has been purified by flash chromatography with 6% MeOH in CH₂Cl₂. Yield: 33%, white solid.

Chemical Formula: C₂₃H₂₈Cl₂N₂·H₂C₂O₄ (492.16 g/mol).

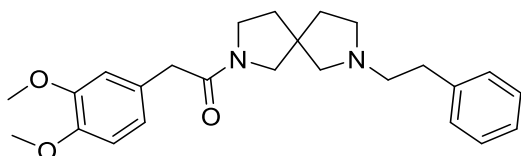
¹H NMR (200 MHz, CDCl₃) δ 7.02–7.48 (m, 8H), 2.50–3.08 (m, 16H), 1.82–2.16 (m, 4H). (free base)

¹³C NMR (200 MHz, CDCl₃) δ 140.5, 139.8, 131.9, 129.9, 128.6, 128.4, 126.1, 67.2, 58.38, (free base) 57.6, 53.9, 47.5, 38.7, 35.1

Elem. Anal. Anal. Calcd: C, 60.86; H, 6.13; N, 5.68.

Found: C, 61.35; H, 6.15; N, 5.65.

2-(3,4-Dimethoxyphenyl)-1-(7-phenethyl-2,7-diazaspiro[4.4]nonan-2-yl)ethan-1-one oxalate (AD226)



The compound has been prepared using **AD218** (0.31 mmol, 102 mg) and 3,4-dimethoxyphenylacetic acid (0.40 mmol, 78 mg) following Procedure G and H. The residue has been purified by flash chromatography with 100% EtOAc. Yield: 25%, white solid.

Chemical Formula: C₂₅H₃₂N₂O₃·H₂C₂O₄ (498.24 g/mol).

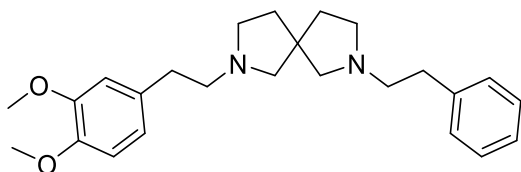
¹H NMR (200 MHz, CDCl₃) δ 7.13–7.44 (m, 5H), 6.75–6.96 (m, 3H), 3.79–3.97 (m, 6H), (free base) 3.21–3.70 (m, 6H), 2.30–3.01 (m, 6H), 1.71–2.02 (m, 6H).

¹³C NMR (200 MHz, CDCl₃) δ 170.0, 148.9, 147.8, 128.6, 128.4, 127.2, 126.1, 121.0, 111.9, (free base) 111.0, 63.9, 58.7, 58.0, 55.8, 53.8, 48.5, 46.6, 45.3, 36.2, 35.5.

Elem. Anal. Anal. Calcd: C, 65.04; H, 6.87; N, 5.62.

Found: C, 65.57; H, 6.91; N, 5.57.

2-(3,4-Dimethoxyphenethyl)-7-phenethyl-2,7-diazaspiro[4.4]nonane oxalate (AD234)



The compound has been prepared using **AD226** (0.14 mmol, 57 mg) following Procedure F and H. The reaction was allowed to warm to r.t. The residue has been purified by flash chromatography with 5% MeOH in CH₂Cl₂. Yield: 37%, white solid.

Chemical Formula: C₂₅H₃₄N₂O₂·H₂C₂O₄ (484.26 g/mol).

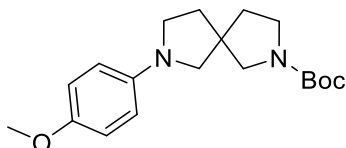
¹H NMR (200 MHz, CDCl₃) δ 7.14–7.38 (m, 5H), 6.67–6.87 (m, 3H), 3.87 (d, *J* = 3.12 Hz, (free base) 6H), 2.53–3.20 (m, 16H), 1.78–2.11 (m, 4H).

¹³C NMR (200 MHz, CDCl₃) δ 148.9, 147.8, 128.6, 128.4, 127.2, 126.1, 121.0, 111.9, 111.0, (free base) 63.9, 58.7, 58.0, 55.8, 53.8, 48.5, 46.6, 45.3, 36.2, 35.5.

Elem. Anal. Anal. Calcd: C, 66.92; H, 7.49; N, 5.78.

Found: C, 67.18; H, 7.51; N, 5.79.

tert-Butyl 7-(4-methoxyphenyl)-2,7-diazaspiro [4.4] nonane-2-carboxylate (AD235)

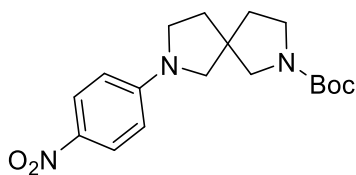


The compound has been prepared using *tert*-butyl 2,7-diazaspiro[4.4]nonane-2-carboxylate (0.47 mmol, 106 mg) and 4-iodoanisole (0.39 mmol, 91 mg) following Procedure A. The reaction mixture was heated to 100 °C. The crude product was purified by flash chromatography using EtOAc/Hex (70:30) to get the desired product. Yield: 51%, orange oil.

Chemical Formula: C₁₉H₂₈N₂O₃ (332.21 g/mol).

¹H NMR (200 MHz, CDCl₃) δ 6.86 (d, *J* = 8.59 Hz, 2H), 6.51 (d, *J* = 8.59 Hz, 2H), 3.77 (s, 3H), 3.10–3.62 (m, 8H), 1.74–2.13 (m, 4H), 1.47 (s, 9H).

***tert*-Butyl 7-(4-nitrophenyl)-2,7-diazaspiro[4.4]nonane-2-carboxylate (AD237)**

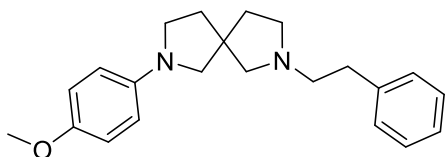


The compound has been prepared using *tert*-butyl 2,7-diazaspiro[4.4]nonane-2-carboxylate (0.47 mmol, 106 mg) and 1-iodo-4-nitrobenzene (0.39 mmol, 97 mg) following Procedure A. The reaction was left stirring at rt. The crude product was purified by flash chromatography using EtOAc/Hex (70:30) to obtain the desired product. Yield: 88%, orange oil.

Chemical Formula: C₁₈H₂₅N₃O₄ (347.18 g/mol).

¹H NMR (200 MHz, CDCl₃) δ 8.11 (d, *J* = 9.37 Hz, 2H), 6.45 (d, *J* = 8.98 Hz, 2H), 3.21–3.67 (m, 8H), 1.75–2.19 (m, 4H), 1.46 (s, 9H).

2-(4-Methoxyphenyl)-7-phenethyl-2,7-diazaspiro[4.4]nonane oxalate (AD239)



The compound has been prepared using **AD235** (0.2 mmol, 66 mg) and 2-bromoethylbenzene (0.2 mmol, 27.3 μL) following Procedure C and H. The reaction has been stirred at 50 °C for 5 h and the crude product purified by flash chromatography using CH₂Cl₂/MeOH 98:2. Yield: 6%, dark solid.

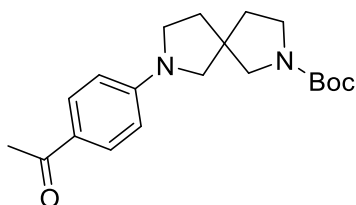
Chemical Formula: C₂₂H₂₈N₂O·H₂C₂O₂ (426.22 g/mol).

¹H NMR (500 MHz, CDCl₃) δ 7.25–7.32 (m, 2H), 7.17–7.23 (m, 3H), 6.85 (d, *J* = 8.80 Hz, 2H), 6.50 (d, *J* = 8.80 Hz, 2H), 3.75 (s, 3H), 3.26–3.35 (m, 3H), 3.19 (d, *J* = 8.80 Hz, 1H), 2.70–2.88 (m, 7H), 2.62 (d, *J* = 8.80 Hz, 1H), 1.82–2.09 (m, 4H).

¹³C NMR (200 MHz, CDCl₃) δ 150.8, 143.0, 139.9, 128.5, 115.0, 112.1, 65.0, 56.0, 54.1, 48.1, 36.1.

Elem. Anal. Anal. Calcd: C, 67.59; H, 7.09; N, 6.57.
Found: C, 67.89; H, 7.11; N, 6.54.

***tert*-Butyl 7 (4-acetylphenyl) -2,7-diazaspiro[4.4]nonane-2-carboxylate (AD240)**

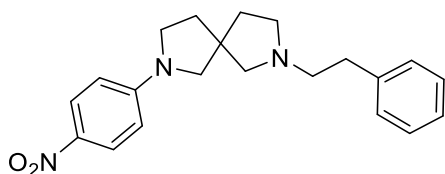


The compound has been prepared using *tert*-butyl 2,7-diazaspiro[4.4]nonane-2-carboxylate (0.47 mmol, 106 mg) and 4-iodoacetophenone (0.39 mmol, 96 mg) following Procedure A. The reaction was left stirring at rt. The crude product was purified by flash chromatography using EtOAc/Hex (70:30) to obtain the desired product. Yield: 76%, orange oil.

Chemical Formula: C₂₀H₂₈N₂O₃ (344.21 g/mol).

¹H NMR (200 MHz, CDCl₃) δ 7.85 (δ, *J* = 8.20 Hz, 2H), 6.48 (δ, *J* = 8.20 Hz, 2H), 3.19 - 3.61 (m, 8H), 2.49 (s, 3H), 1.79 - 2.19 (m, 4H), 1.44 (s, 9H).

2-(4-Nitrophenyl)-7-phenethyl-2,7-diazaspiro[4.4]nonane oxalate (AD242)



The compound has been prepared using **AD237** (0.2 mmol, 69 mg) and (2-bromoethyl)benzene (0.2 mmol, 27.3 μL) following Procedure C and H. The reaction has been stirred at rt for 48 h and the crude product purified by flash chromatography using Hex/EtOAc (70:30 to 30:70). Yield: 55%, yellow solid.

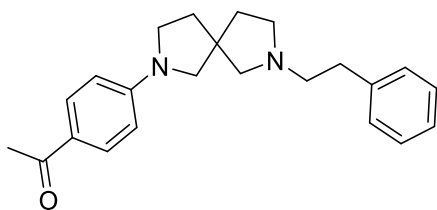
Chemical Formula: C₂₁H₂₅N₃O₂·H₂C₂O₂ (441.19 g/mol).

¹H NMR (500 MHz, CDCl₃) δ 8.00–8.09 (m, 2H), 7.18–7.24 (m, 2H), 7.10–7.16 (m, 3H), (free base) 6.35–6.41 (m, 2H), 3.33–3.45 (m, 3H), 3.24 (d, *J* = 9.78 Hz, 1H), 2.70–2.78 (m, 3H), 2.56–2.67 (m, 4H), 2.46 (d, *J* = 8.80 Hz, 1H), 1.93–2.07 (m, 2H), 1.65–1.87 (m, 2H).

¹³C NMR (200 MHz, CDCl₃) δ 151.8, 140.1, 136.7, 128.5, 126.3, 126.1, 110.3, 64.4, 59.8, (free base) 58.1, 53.8, 48.0, 47.5, 37.4, 35.5.

Elem. Anal. Anal. Calcd: C, 62.57; H, 6.16; N, 9.52.
Found: C, 62.95; H, 6.19; N, 9.49.

1-(7-Phenethyl-2,7-diazaspiro[4.4]nonan-2-yl)ethan-1-one oxalate (AD245)



The compound has been prepared using **AD240** (0.2 mmol, 69 mg) and 2-bromoethylbenzene (0.2 mmol, 27.3 μ L) following Procedure C and H. The reaction has been stirred at 50 °C for 5 h and the crude product purified by flash chromatography using Hex/EtOAc (90:10 to 50:50). Yield: 13%, yellow solid.

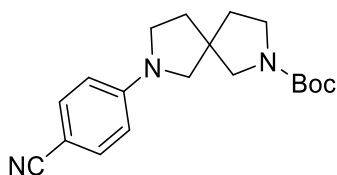
Chemical Formula: $C_{23}H_{28}N_2O \cdot H_2C_2O_4$ (362.18 g/mol).

1H NMR (500 MHz, $CDCl_3$) δ 7.87 (d, $J = 8.80$ Hz, 2H), 7.24–7.32 (m, 2H), 7.17–7.23 (m, 3H), 6.50 (d, $J = 8.80$ Hz, 2H), 3.37–3.48 (m, 3H), 3.29 (d, $J = 9.29$ Hz, 1H), 2.77–2.85 (m, 3H), 2.66–2.76 (m, 4H), 2.56 (d, $J = 9.29$ Hz, 1H), 2.50 (s, 3H), 1.98–2.11 (m, 2H), 1.83–1.96 (m, 2H).

^{13}C NMR (200 MHz, $CDCl_3$) δ 196.3, 150.9, 140.1, 130.4, 128.6, 128.3, 125.0, 110.5, 64.5, 59.5, 58.2, 53.9, 48.0, 47.1, 37.6, 35.7, 35.3, 26.0, 25.9.

Elem. Anal. Anal. Calcd: C, 62.97; H, 7.23; N, 7.73.
Found: C, 63.31; H, 7.28; N, 7.70.

tert-Butyl 7-(4-cyanophenyl)-2,7-diazaspiro[4.4]nonane-2-carboxylate (AD255)

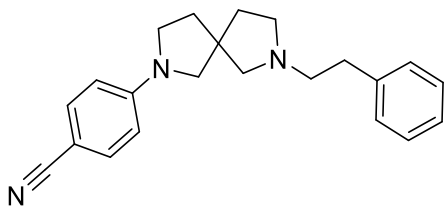


The compound has been prepared using *tert*-butyl 2,7-diazaspiro[4.4]nonane-2-carboxylate (0.66 mmol, 150 mg) and 4-chlorobenzonitrile (0.73 mmol, 100 mg) and DMSO as solvent following Procedure B. The reaction mixture was heated to 120 °C on. The residue was purified via silica gel chromatography using Hex/EtOAc (90:10) to get the desired product. Yield: 56%, white solid.

Chemical Formula: $C_{19}H_{25}N_3O_2$ (327.19 g/mol).

1H NMR (200 MHz, $CDCl_3$) δ 7.46 (d, $J = 8.59$ Hz, 2H), 6.49 (d, $J = 8.20$ Hz, 2H), 3.14–3.58 (m, 8H), 1.81–2.18 (m, 4H), 1.34–1.56 (m, 9H).

4-(7-Phenethyl-2,7-diazaspiro[4.4]nonan-2-yl)benzotrile oxalate (AD258)



The compound has been prepared using **AD255** (0.2 mmol, 65 mg) and 2-bromoethylbenzene (0.2 mmol, 27.3 μ L) following Procedure C and H. The crude product purified by flash chromatography using $\text{CH}_2\text{Cl}_2/\text{MeOH}$ 98:2. Yield: 10%, clear solid.

Chemical Formula: $\text{C}_{22}\text{H}_{25}\text{N}_3 \cdot \text{H}_2\text{C}_2\text{O}_4$ (421.20 g/mol).

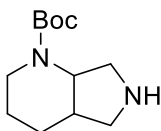
^1H NMR (500 MHz, CDCl_3) δ 7.45 (d, $J = 9.29$ Hz, 2H), 7.25–7.31 (m, 2H), 7.17–7.24 (m, 3H), 6.48 (d, $J = 8.80$ Hz, 2H), 3.33–3.44 (m, 3H), 3.25 (d, $J = 9.29$ Hz, 1H), 2.76–2.84 (m, 3H), 2.63–2.74 (m, 4H), 2.49–2.57 (m, 1H), 1.95–2.11 (m, 2H), 1.81–1.94 (m, 2H).

^{13}C NMR (200 MHz, CDCl_3) δ 149.9, 140.1, 133.6, 128.2, 126.1, 120.9, 111.5, 96.8, 64.5, 59.5, 58.2, 53.9, 48.0, 47.1, 37.5, 35.6.

Elem. Anal. Anal. Calcd: C, 68.39; H, 6.46; N, 9.97.

Found: C, 68.91; H, 6.49; N, 9.91.

tert-Butyl octahydro-1*H*-pyrrolo[3,4-*b*]pyridine-1-carboxylate (AB2)

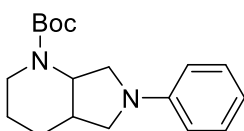


To a solution of (*S,S*)-2,8-diazabicyclo[4,3,0]nonane (7.37 mmol, 902 μ L) in CH_2Cl_2 (30 mL), di-*tert*-butyl dicarbonate (5.89 mmol, 855 μ L) in CH_2Cl_2 (30 mL) was added dropwise at 0 $^\circ\text{C}$. The mixture was left to stir at rt on. The solvent was evaporated to dryness and the obtained residue purified by flash chromatography on silica gel eluting with 10–40% MeOH in CH_2Cl_2 . Yield: 64%, light pink solid.

Chemical Formula: $\text{C}_{12}\text{H}_{22}\text{N}_2\text{O}_2$ (226.32 g/mol).

^1H NMR (200 MHz, CDCl_3) δ 3.20–3.53 (m, 5H), 2.91–3.12 (m, 1H), 2.54–2.78 (m, 2H), 2.11–2.38 (m, 1H), 1.67 (br. s., 3H), 1.44 (s, 9H).

tert-Butyl 6-phenyloctahydro-1*H*-pyrrolo[3,4-*b*]pyridine-1-carboxylate (AB11)



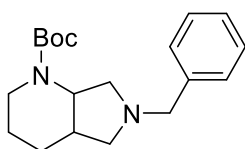
The compound has been prepared using iodobenzene (0.74 mmol, 83 μ L) and **AB2** (0.88 mmol, 200

mg), following Procedure A. The crude product was purified by column chromatography on silica gel with hexane/EtOAc (90:10 to 70:30) as the eluent to afford the desired product. Yield: 89%, brown oil.

Chemical Formula: C₁₈H₂₆N₂O₂ (302.42 g/mol).

¹H NMR (200 MHz, CDCl₃) δ 7.17–7.36 (m, 2H), 6.89–7.00 (m, 2H), 6.75–6.88 (m, 1H), 4.42 (d, *J* = 6.46 Hz, 1H), 3.29–3.50 (m, 4H), 3.12–3.29 (m, 1H), 2.81–3.02 (m, 1H), 2.21–2.43 (m, 1H), 1.51–1.94 (m, 4H), 1.44 (s, 9H).

***tert*-Butyl 6-benzyl octahydro-1*H*-pyrrolo[3,4-*b*]pyridine-1-carboxylate (AB3)**

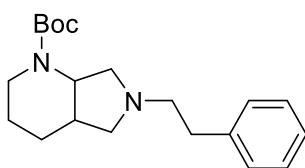


The compound has been prepared using **AB2** (0.88 mmol, 200 mg) and benzylbromide (1.7 mmol, 201 μL) following Procedure B. The residue was purified by flash chromatography on silica gel eluting with 10–20% MeOH in EtOAc to give the title compound. Yield: 90%, yellow oil.

Chemical Formula: C₁₉H₂₈N₂O₂ (316.45 g/mol).

¹H NMR (200 MHz, CDCl₃) δ 7.19–7.40 (m, 5H), 5.25–5.33 (m, 1H), 3.50–3.83 (m, 2H), 3.15–3.45 (m, 4H), 3.06 (br. s., 1H), 2.59 (br. s., 1H), 2.27 (br. s., 2H), 1.51–1.91 (m, 3H), 1.47 (s, 9H).

***tert*-Butyl 6-phenethyl octahydro-1*H*-pyrrolo[3,4-*b*]pyridine-1-carboxylate (AB4)**

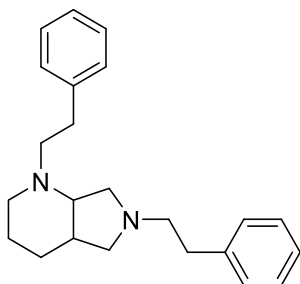


The compound has been prepared using **AB2** (0.88 mmol, 200 mg) and (2-bromoethyl)benzene (1.7 mmol, 229 μL) following Procedure B. The residue was purified by flash chromatography on silica gel eluting with 10–20% MeOH in EtOAc to give the title compound. Yield: 97%, yellow oil.

Chemical Formula: C₂₀H₃₀N₂O₂ (330.47 g/mol).

¹H NMR (200 MHz, CDCl₃) δ 7.06–7.41 (m, 5H), 3.12–3.62 (m, 5H), 2.36–2.93 (m, 6H), 2.24 (br. s., 1H), 1.53–1.95 (m, 4H), 1.46 (s, 9H).

1,6-Diphenethyloctahydro-1*H*-pyrrolo[3,4-*b*]pyridine oxalate (AB7)



The compound has been prepared using **AB4** (0.49 mmol, 160 mg) and (2-bromoethyl)benzene (0.98 mmol, 133 μ L) following Procedure C and H. The obtained residue was purified on silica gel chromatography with 10–20% MeOH in CH_2Cl_2 . Yield: 49%, orange solid.

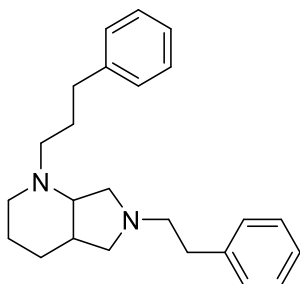
Chemical Formula: $\text{C}_{23}\text{H}_{30}\text{N}_2 \cdot \text{H}_2\text{C}_2\text{O}_4$ (424.24 g/mol).

^1H NMR (200 MHz, CDCl_3) δ 6.83–7.46 (m, 10H), 4.88 (s, 1H), 4.18 (dd, $J = 3.38, 12.60$ Hz, 1H), 3.83–4.05 (m, 1H), 3.41–3.70 (m, 4H), 3.00–3.38 (m, 4H), 2.95 (br. s., 1H), 2.53–2.89 (m, 4H), 2.26–2.46 (m, 1H), 1.87–2.10 (m, 1H), 1.63 (br. s., 2H).

^{13}C NMR (200 MHz, CDCl_3) δ 140.3, 135.2, 135.1, 129.2, 129.0, 128.7, 128.3, 127.6, 127.4, 126.1, 69.1, 65.9, 64.9, 63.2, 62.4, 56.3, 51.3, 36.5, 32.6, 30.3, 29.7, 21.0, 20.2.

Elem. Anal. Anal. Calcd: C, 70.73; H, 7.60; N, 6.60.
Found: C, 70.97; H, 7.66; N, 6.59.

6-Phenethyl-1-(3-phenylpropyl)octahydro-1*H*-pyrrolo[3,4-*b*]pyridine oxalate (AB8)



The compound has been prepared using **AB4** (0.49 mmol, 160 mg) and (3-bromopropyl)benzene (0.74 mmol, 112 μ L) following Procedure C and H. The obtained residue was purified on silica gel chromatography with 10–20 % MeOH in CH_2Cl_2 . Yield: 73%, orange solid.

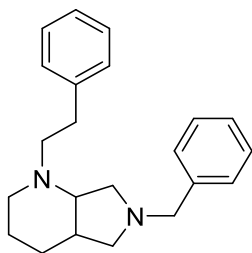
Chemical Formula: $\text{C}_{24}\text{H}_{32}\text{N}_2 \cdot \text{H}_2\text{C}_2\text{O}_4$ (438.25 g/mol).

^1H NMR (200 MHz, CDCl_3) δ 7.11–7.43 (m, 10H), 4.03–4.26 (m, 1H), 3.72–3.97 (m, 1H), 3.22–3.61 (m, 3H), 2.88–3.19 (m, 3H), 2.51–2.86 (m, 4H), 2.45 (t, $J = 7.57$ Hz, 2H), 2.28 (d, $J = 7.22$ Hz, 4H), 1.84–2.08 (m, 2H), 1.41–1.83 (m, 4H).

^{13}C NMR (200 MHz, CDCl_3) δ 140.1, 139.8, 128.8, 128.6, 128.4, 128.2, 126.8, 126.5, 126.3, 68.5, 65.3, 63.2, 62.2, 61.6, 56.0, 51.2, 36.5, 32.0, 31.7, 25.1, 24.9, 21.1, 20.0.

Elem. Anal. Anal. Calcd: C, 71.21; H, 7.81; N, 6.39.
Found: C, 71.79; H, 7.87; N, 6.35.

6-Benzyl-1-phenethyloctahydro-1*H*-pyrrolo[3,4-*b*]pyridine oxalate (AB9)



The compound has been prepared using **AB3** (0.38 mmol, 120 mg) and (2-bromoethyl)benzene (0.75 mmol, 102 μ L) following Procedure C and H. The obtained residue was purified on silica gel chromatography with 0–20% MeOH in CH_2Cl_2 . Yield: 30%, yellow solid.

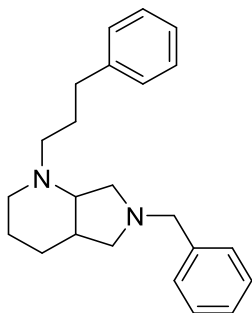
Chemical Formula: $\text{C}_{22}\text{H}_{28}\text{N}_2 \cdot \text{H}_2\text{C}_2\text{O}_4$ (410.22 g/mol).

^1H NMR (200 MHz, CDCl_3) δ 7.11–7.43 (m, 10H), 3.57–3.87 (m, 3H), 3.11–3.45 (m, 7H), (free base) 2.80–3.02 (m, 2H), 2.68 (d, $J = 4.92$ Hz, 1H), 1.92–2.18 (m, 1H), 1.47–1.87 (m, 3H).

^{13}C NMR (200 MHz, CDCl_3) δ 137.6, 136.1, 128.9, 128.6, 128.3, 127.4, 127.2, 105.0, 104.9, (free base) 61.9, 59.3, 57.3, 55.1, 37.8, 32.2, 21.8, 20.7.

Elem. Anal. Anal. Calcd: C, 70.22; H, 7.37; N, 6.82.
Found: C, 70.53; H, 7.38; N, 6.78.

6-Benzyl-1-(3-phenylpropyl)octahydro-1*H*-pyrrolo[3,4-*b*]pyridine oxalate (AB10)



The compound has been prepared using **AB3** (0.38 mmol, 120 mg) and (3-bromopropyl)benzene (0.56 mmol, 85 μ L) following Procedure C and H. The obtained residue was purified on silica gel chromatography with 10–20% MeOH in CH_2Cl_2 . Yield: 16%, yellow solid.

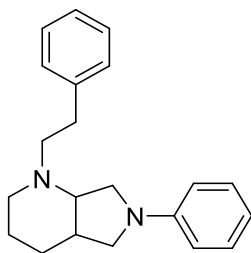
Chemical Formula: $\text{C}_{23}\text{H}_{30}\text{N}_2 \cdot \text{H}_2\text{C}_2\text{O}_4$ (424.24 g/mol).

^1H NMR (200 MHz, CDCl_3) δ 7.08–7.51 (m, 10H), 3.75 (d, $J = 13.8$ Hz, 2H), 3.38–3.62 (m, (free base) 1H), 2.47–3.30 (m, 9H), 1.90–2.31 (m, 3H), 1.42–1.87 (m, 3H).

^{13}C NMR (200 MHz, CDCl_3) δ 139.6, 137.9, 128.7, 128.5, 128.4, 128.3, 127.4, 124.2, 124.0, (free base) 57.3, 54.3, 37.8, 32.7, 22.0, 20.9

Elem. Anal. Anal. Calcd: C, 70.73; H, 7.60; N, 6.60.
Found: C, 71.37; H, 7.65; N, 6.58.

1-Phenethyl-6-phenyloctahydro-1*H*-pyrrolo[3,4-*b*]pyridine oxalate (AB13)



The compound has been prepared using **AB11** (0.35 mmol, 100 mg) and (2-bromoethyl)benzene (0.70 mmol, 94 μ L) following Procedure C and H. The obtained residue was purified on silica gel chromatography with 0–20% MeOH in EtOAc. Yield: 43%, white solid.

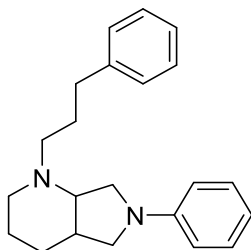
Chemical Formula: C₂₁H₂₆N₂·H₂C₂O₄ (396.20 g/mol).

¹H NMR (200 MHz, CDCl₃) δ 7.12–7.37 (m, 7H), 6.91 (d, J = 8.0 Hz, 2H), 6.78 (t, J = 8.0 Hz, 1H), 4.37 (q, J = 7.7 Hz, 1H), 3.27–3.46 (m, 1H), 2.86–3.11 (m, 3H), 2.68–2.82 (m, 4H), 2.54–2.67 (m, 2H), 2.39 (br. s., 1H), 1.50–2.00 (m, 4H).

¹³C NMR (200 MHz, CDCl₃) δ 150.5, 140.3, 129.1, 128.7, 128.3, 126.0, 118.1, 115.0, 59.0, 58.7, 56.4, 53.0, 44.5, 36.3, 35.4, 26.1, 23.5.

Elem. Anal. Anal. Calcd: C, 69.68; H, 7.12; N, 7.07.
Found: C, 70.09; H, 7.17; N, 7.05.

6-Phenyl-1-(3-phenylpropyl)octahydro-1*H*-pyrrolo[3,4-*b*]pyridine oxalate (AB14)



The compound has been prepared using **AB11** (0.35 mmol, 100 mg) and (3-bromopropyl)benzene (0.52 mmol, 79 μ L) following Procedure C and H. The obtained residue was purified on silica gel chromatography with 0–20% MeOH in EtOAc. Yield: 97%, white solid.

Chemical Formula: C₂₂H₂₈N₂·H₂C₂O₄ (410.22 g/mol).

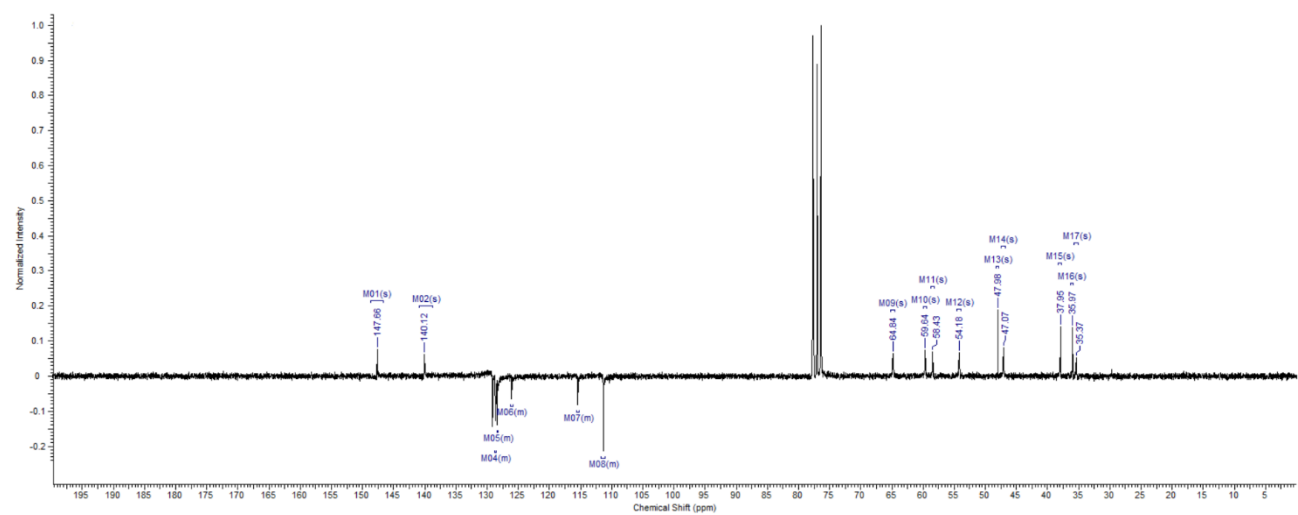
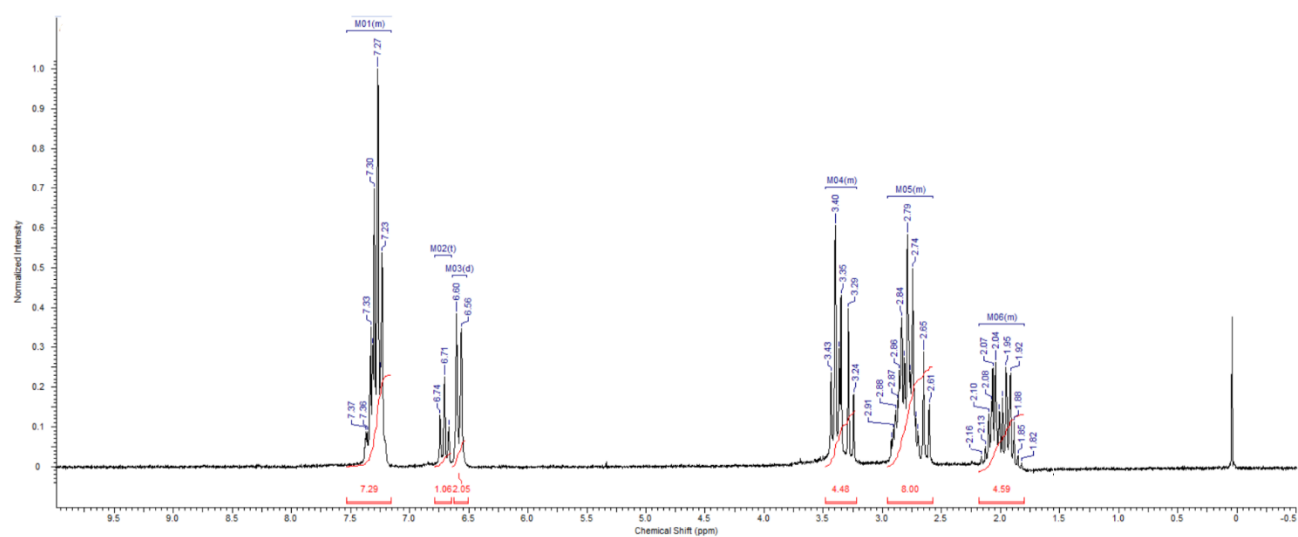
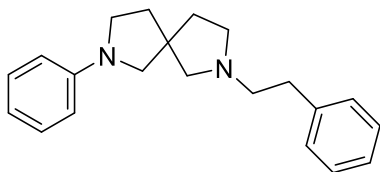
¹H NMR (200 MHz, CDCl₃) δ 7.13–7.37 (m, 7H), 6.93 (d, J = 8.0 Hz, 2H), 6.80 (t, J = 7.2 Hz, 1H), 4.38 (q, J = 7.7 Hz, 1H), 3.32–3.47 (m, 1H), 2.79–3.08 (m, 3H), 2.28–2.72 (m, 7H), 1.54–2.00 (m, 5H).

¹³C NMR (200 MHz, CDCl₃) δ 150.5, 142.2, 129.0, 128.4, 128.2, 125.6, 118.0, 114.9, 58.7, 56.5, 53.1, 44.5, 36.3, 33.6, 30.4, 26.2, 23.5.

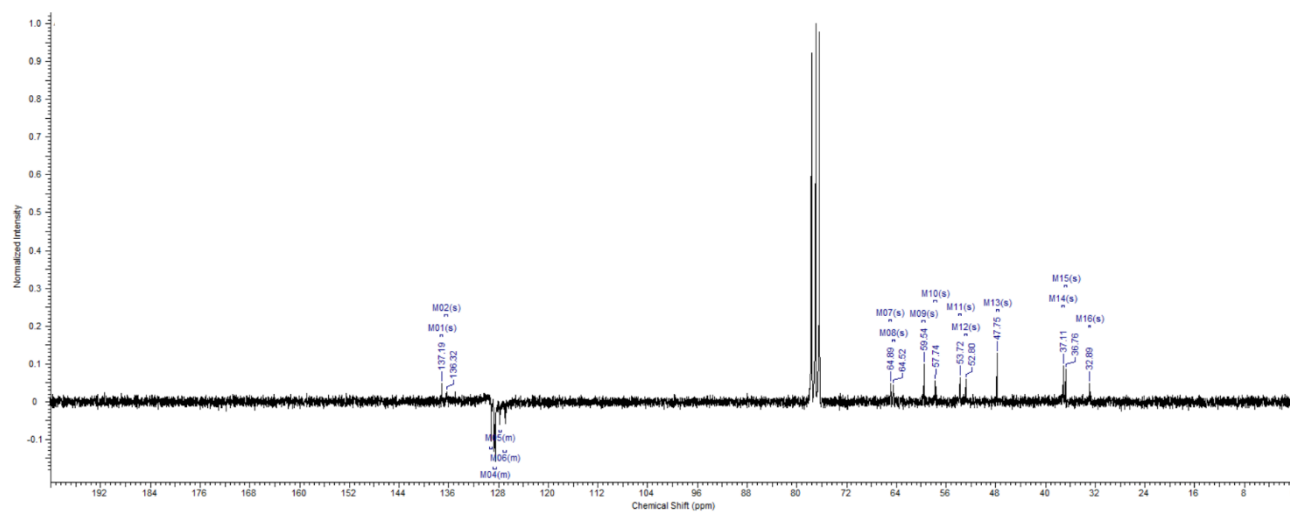
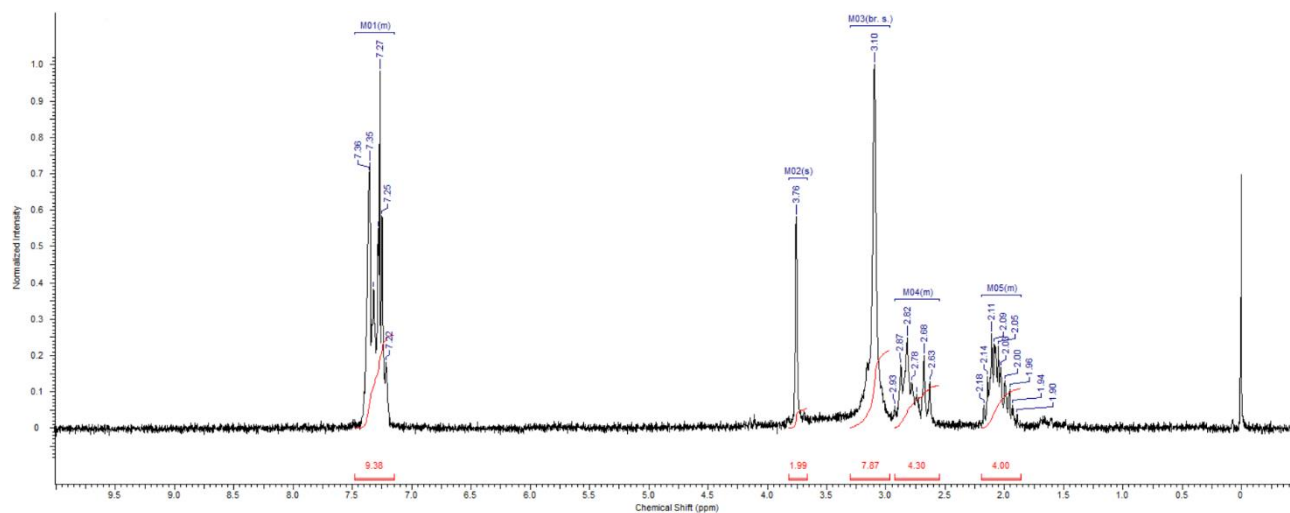
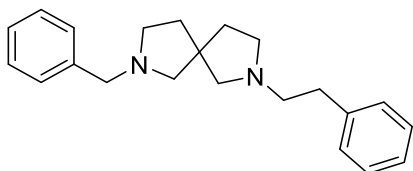
Elem. Anal. Anal. Calcd: C, 70.22; H, 7.37; N, 6.82.
Found: C, 70.53; H, 7.42; N, 6.79.

^1H and ^{13}C NMR-spectra in CDCl_3

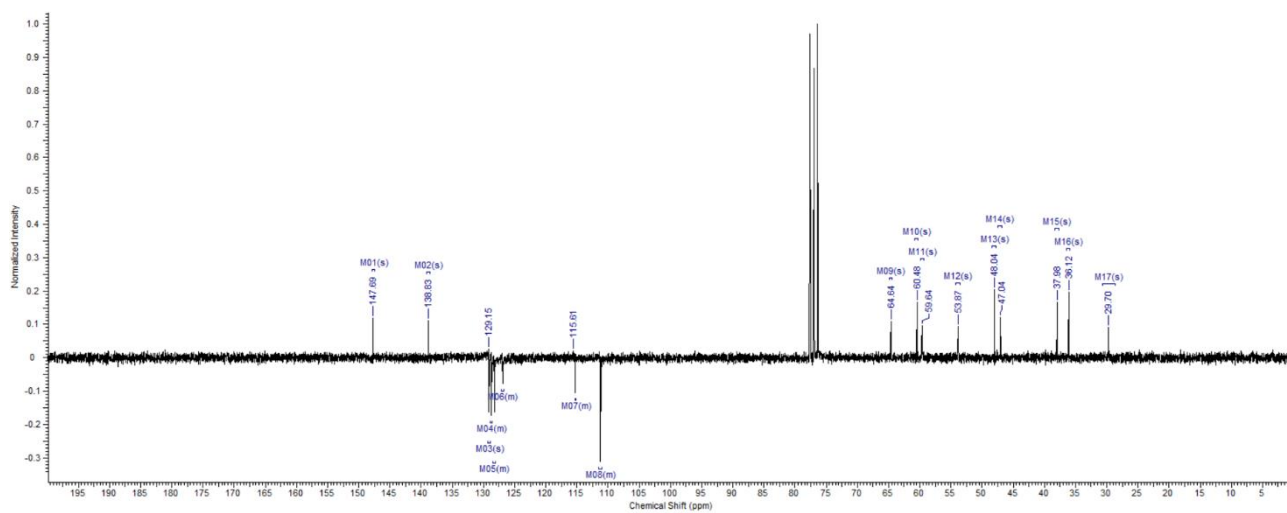
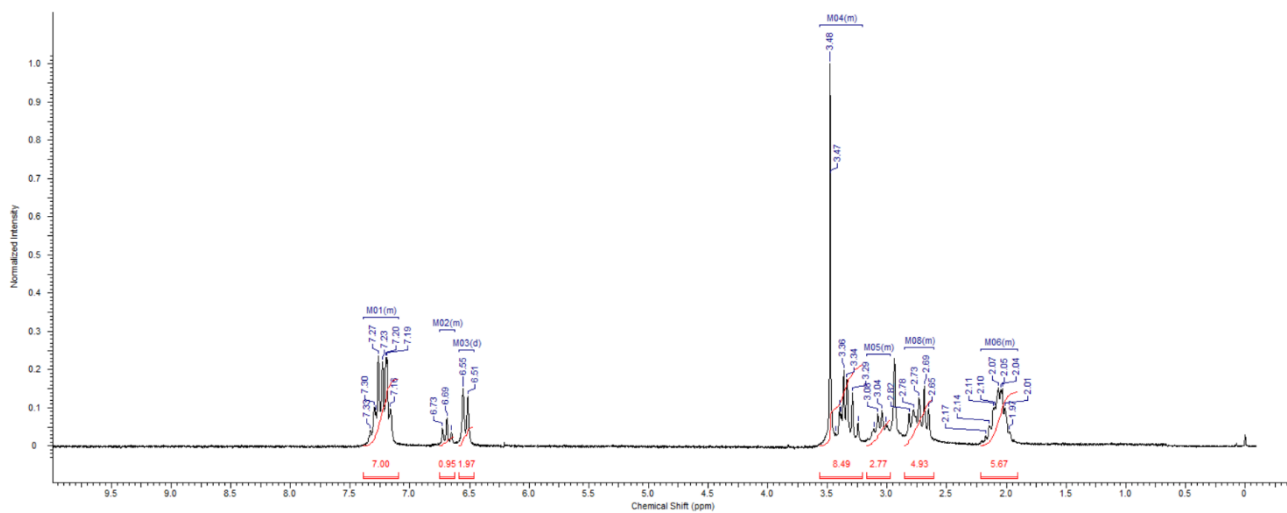
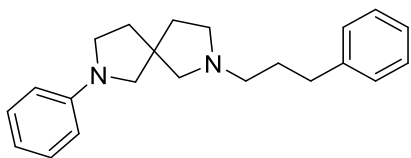
2-Phenethyl-7-phenyl-2,7-diazaspiro[4.4]nonane (AD174)



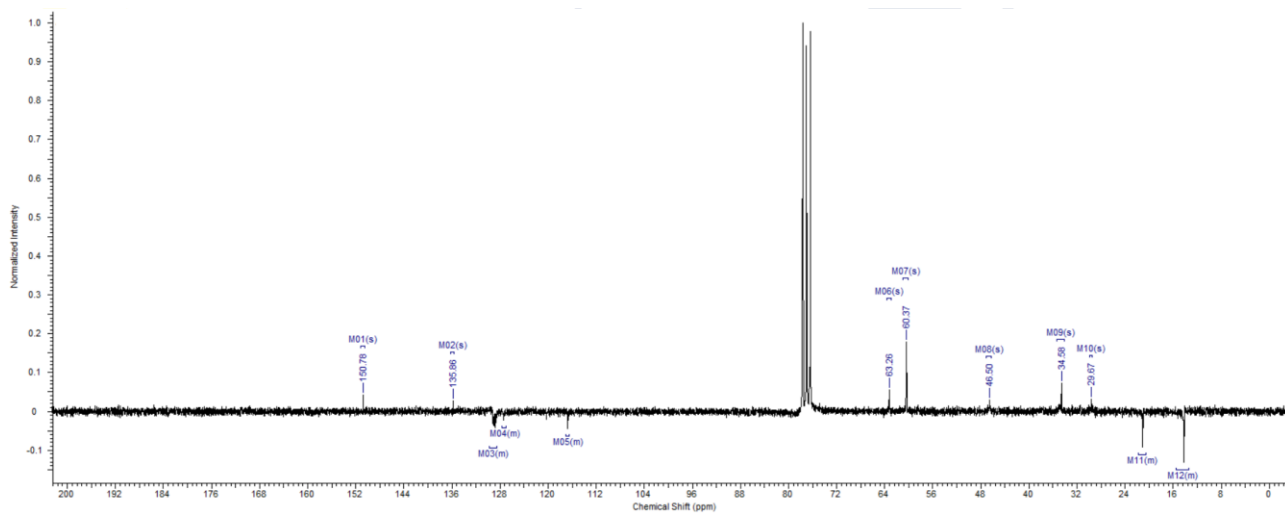
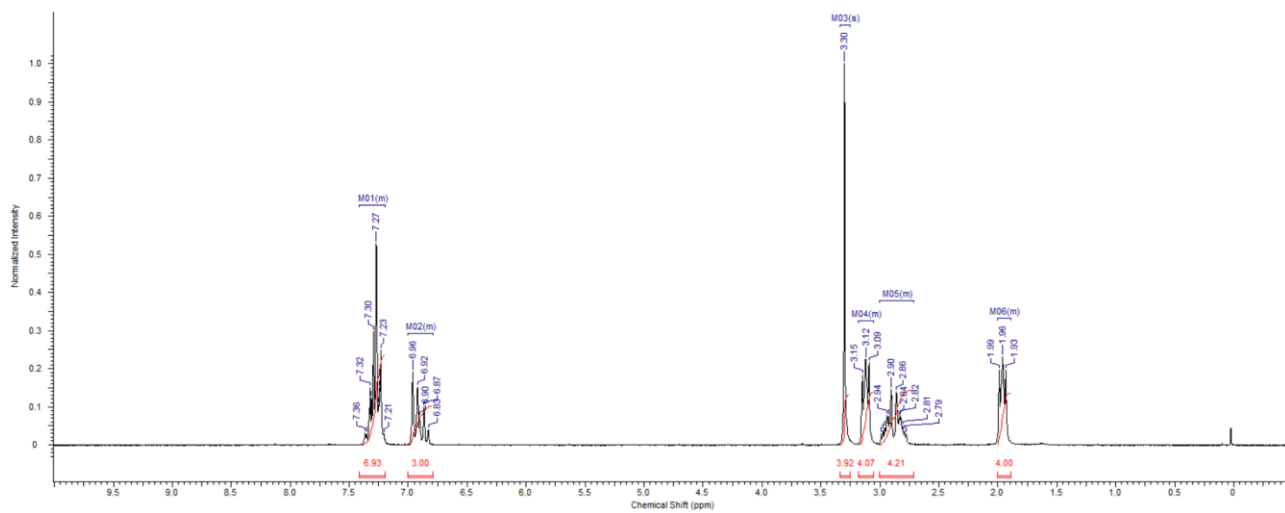
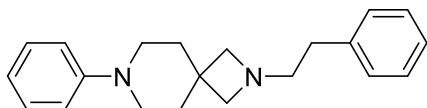
2-Benzyl-7-phenethyl-2,7-diazaspiro[4.4]nonane (AD145)



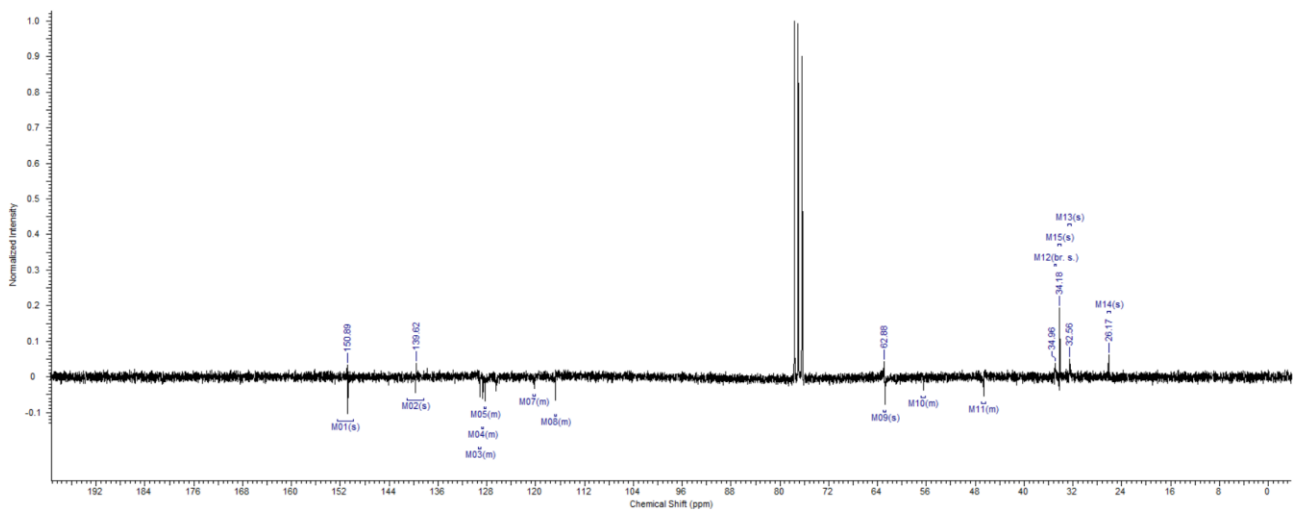
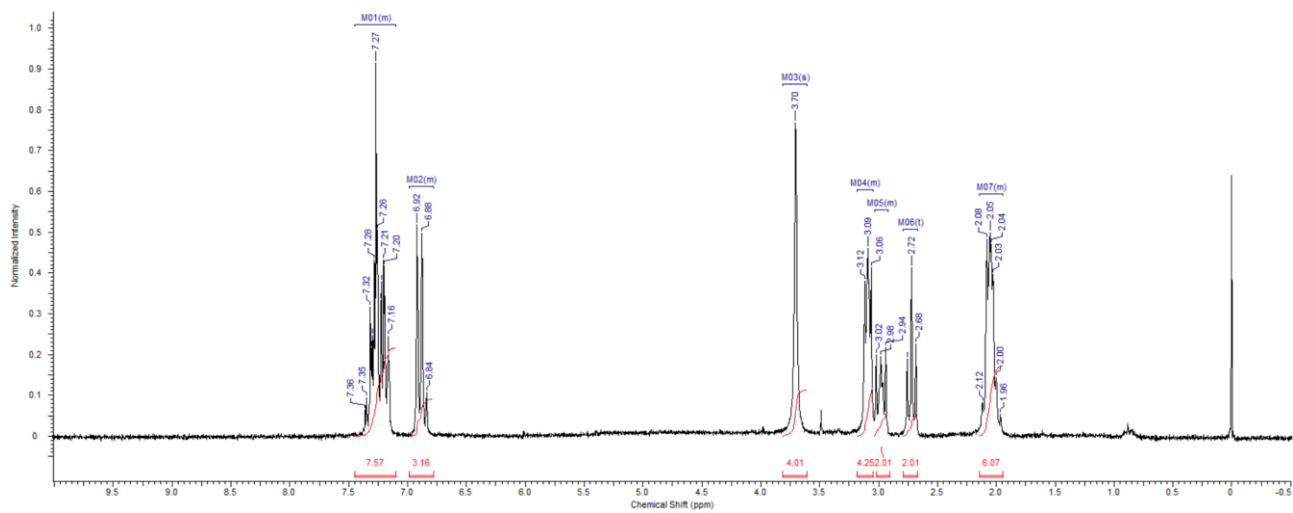
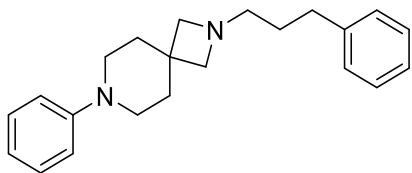
2-Phenyl-7-(3-phenylpropyl)-2,7-diazaspiro[4.4]nonane (AD157)



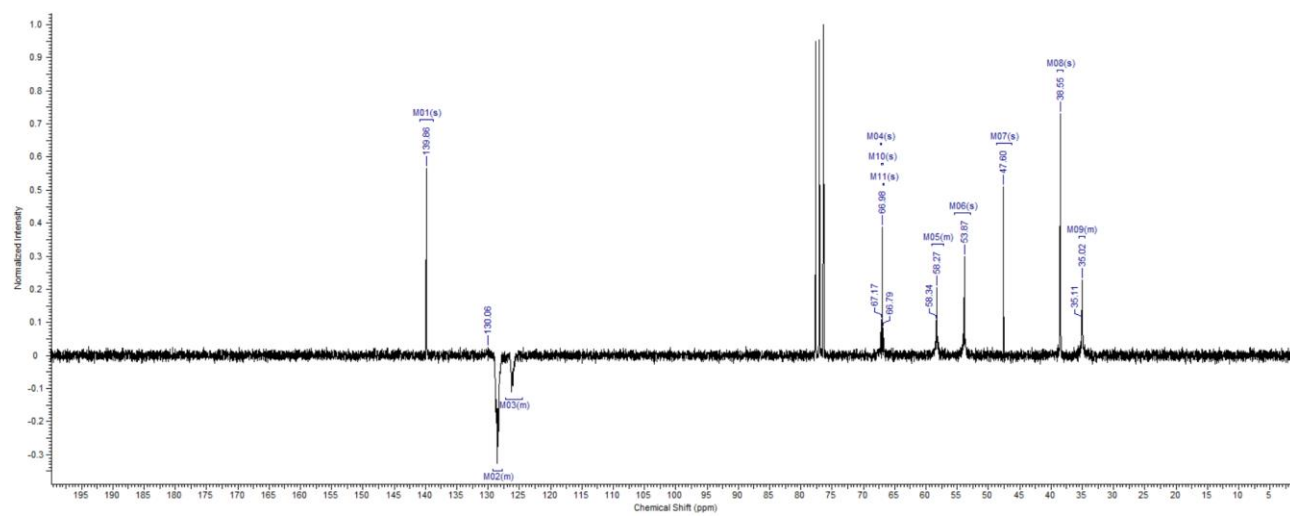
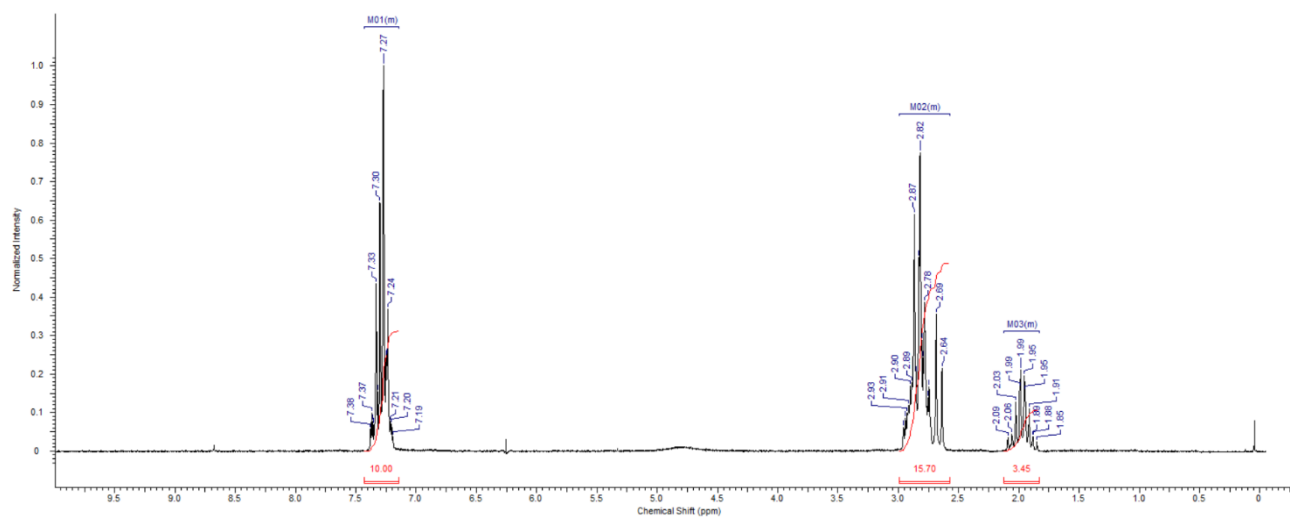
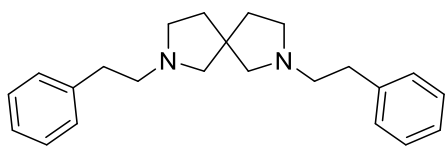
2-Phenethyl-7-phenyl-2,7-diazaspiro[3.5]nonane (AD172)



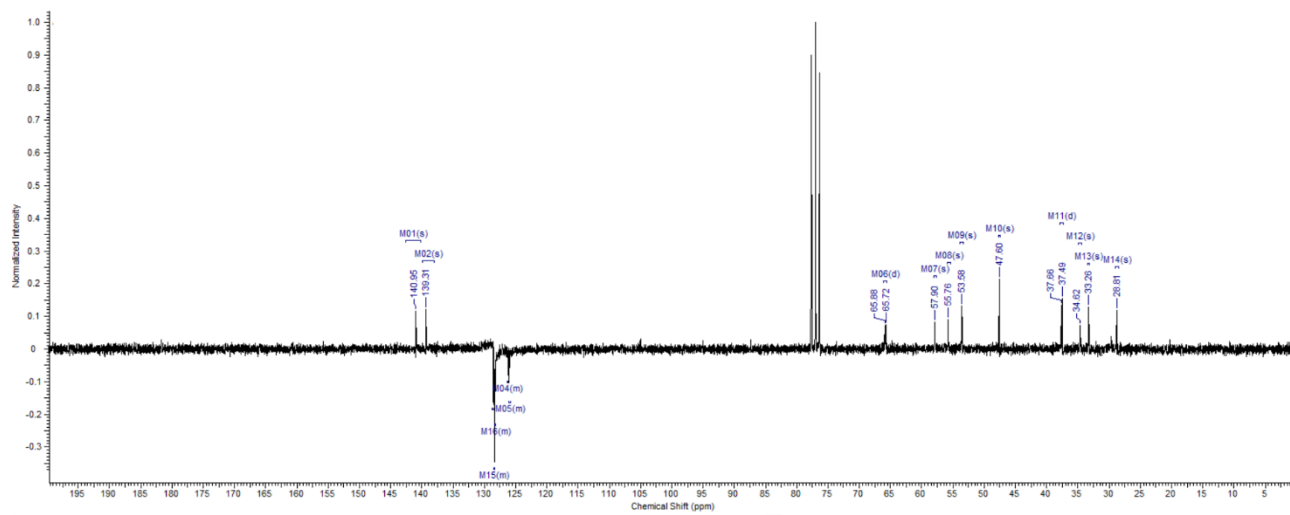
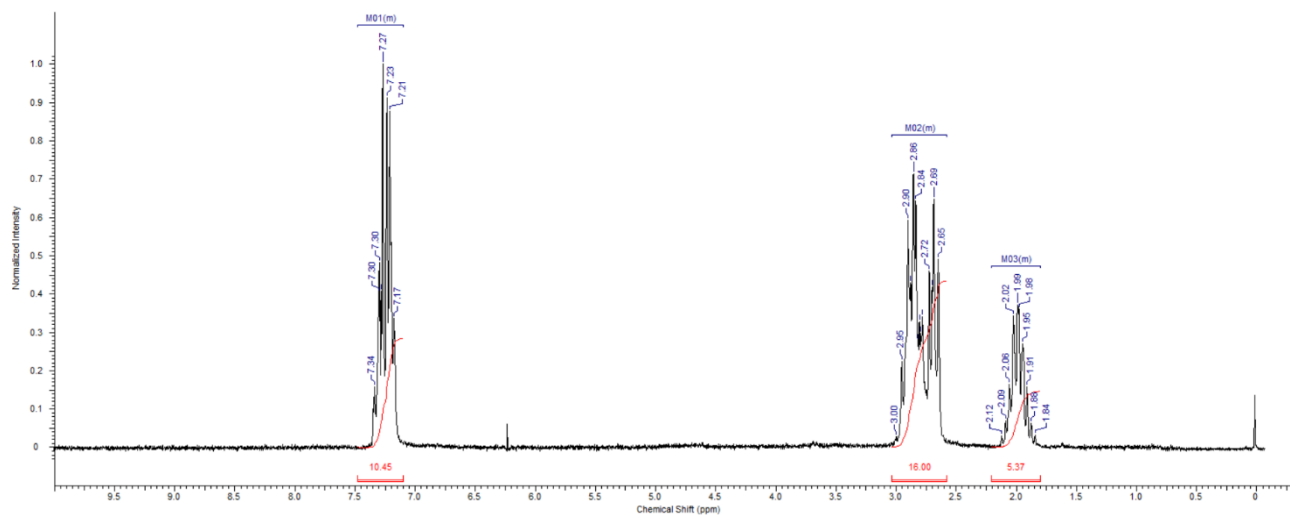
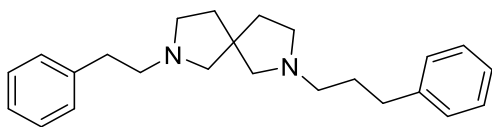
7-Phenyl-2-(3-phenylpropyl)-2,7-diazaspiro[3.5]nonane (AD173)



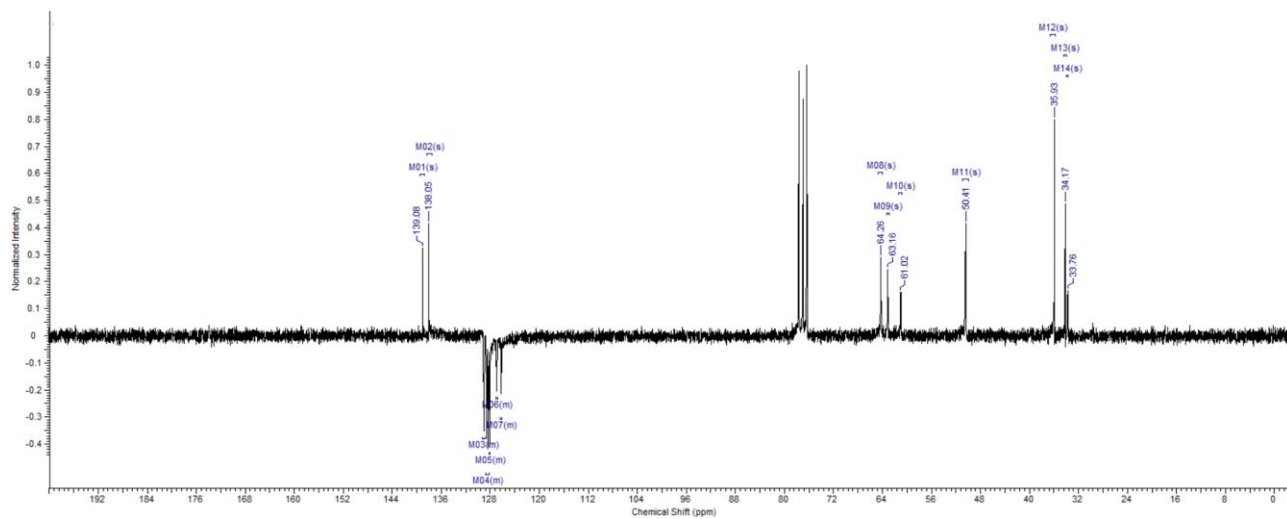
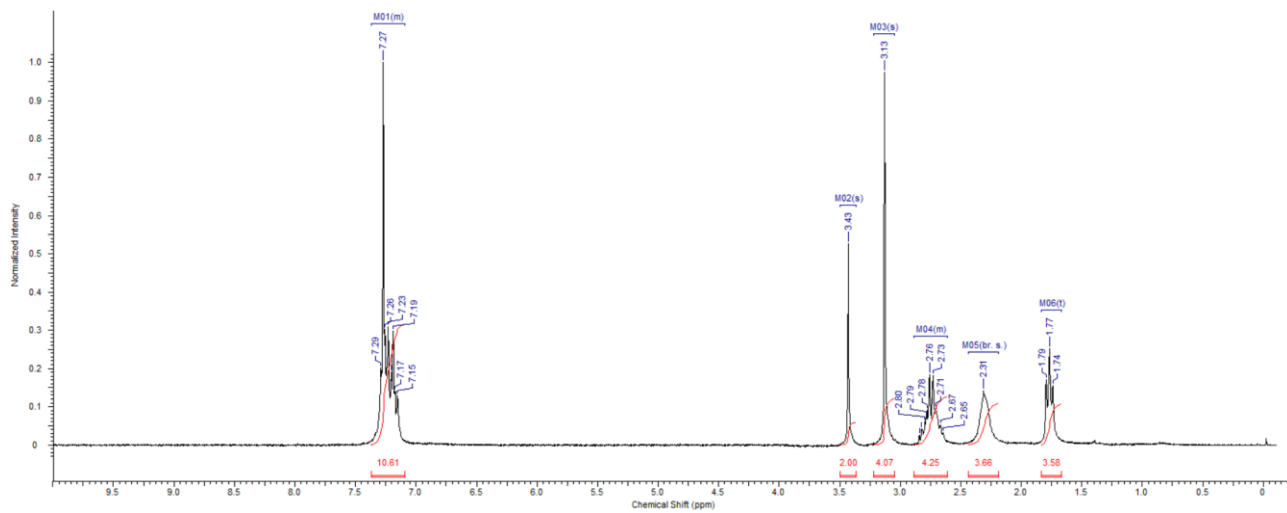
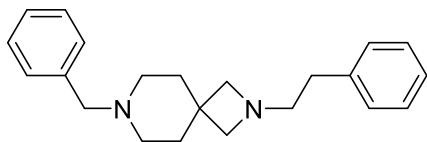
2,7-Diphenethyl-2,7-diazaspiro[4.4]nonane (AD181)



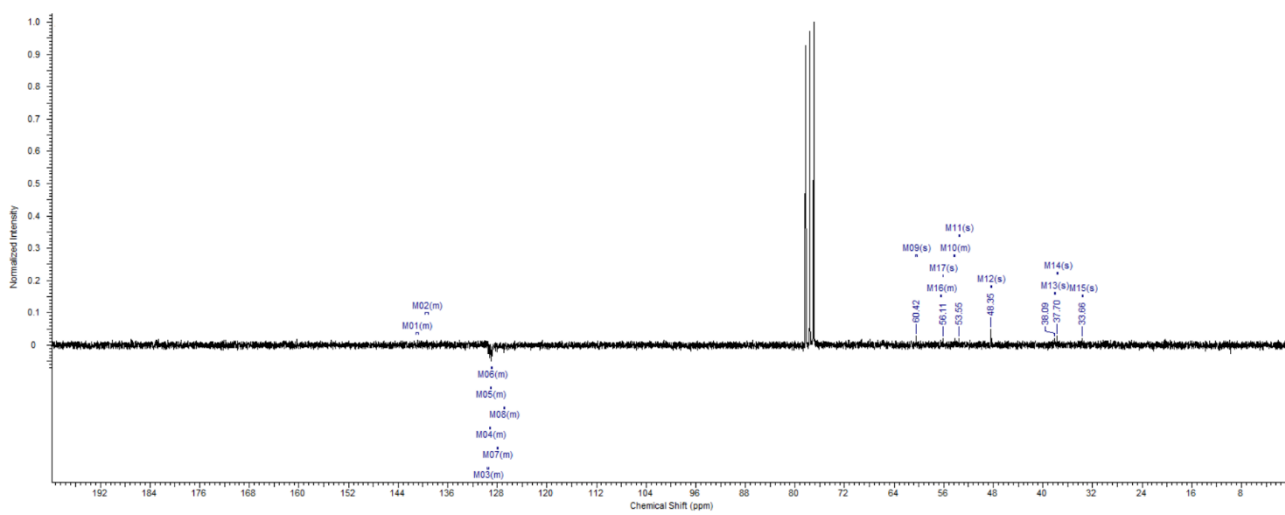
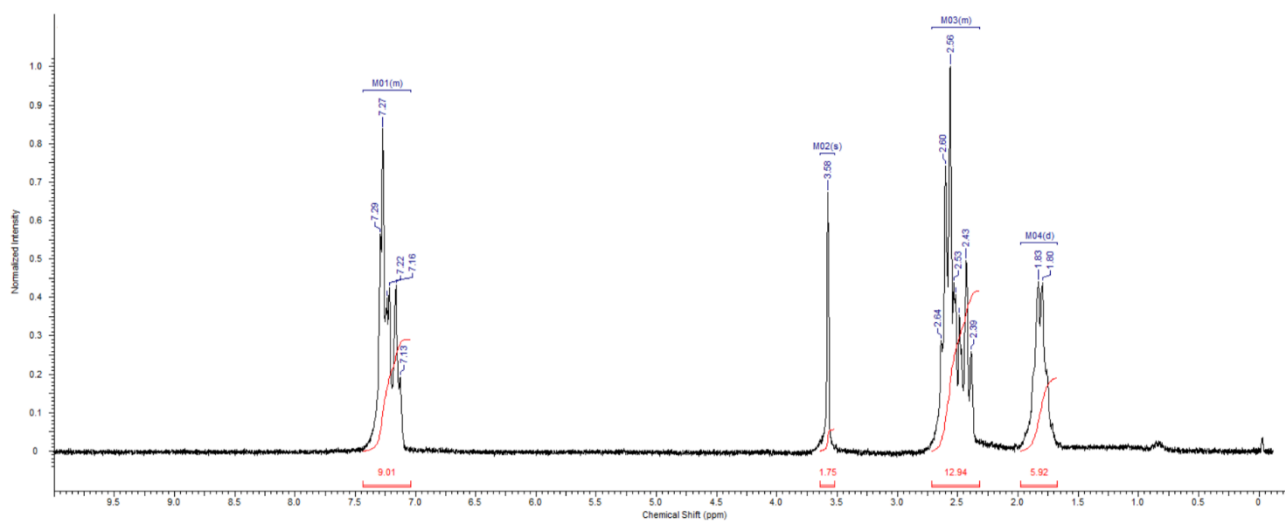
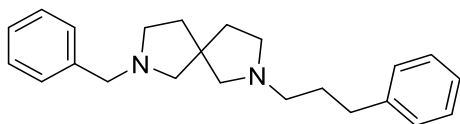
2-Phenethyl-7-(3-phenylpropyl)-2,7-diazaspiro[4.4]nonane (AD182)



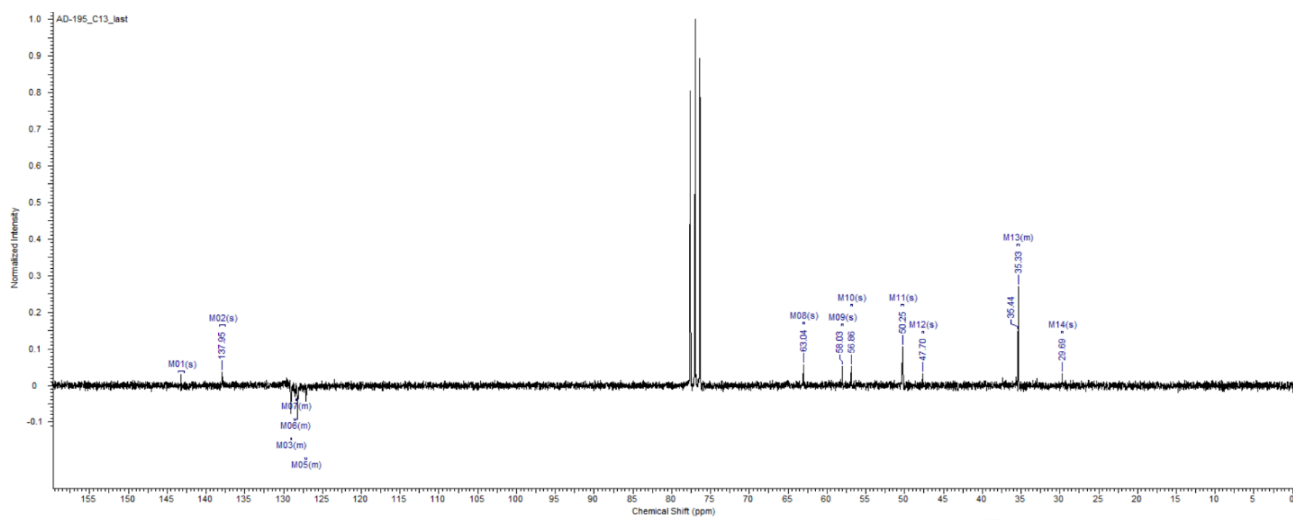
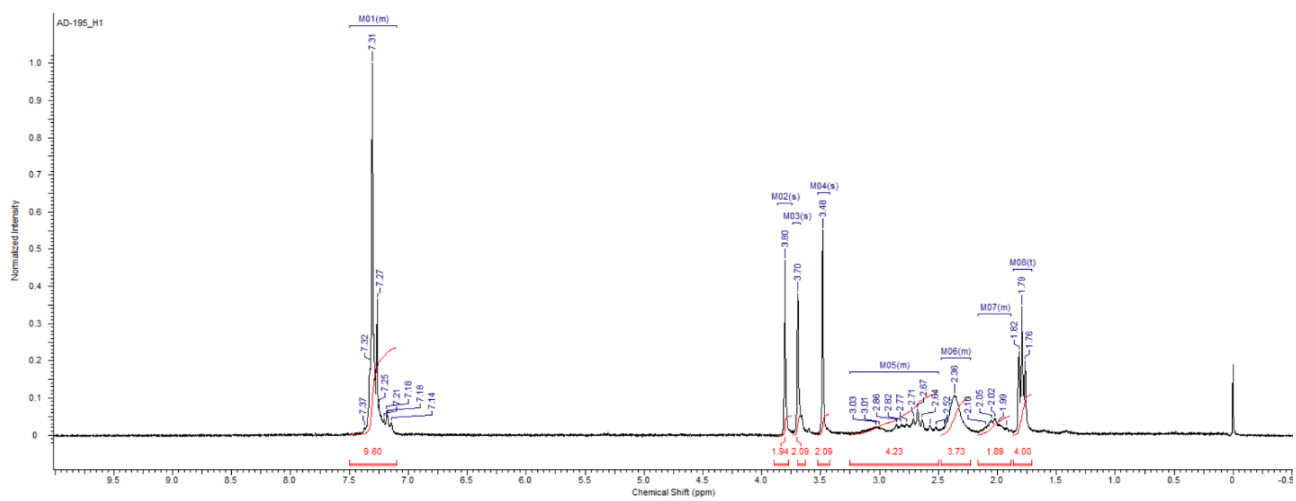
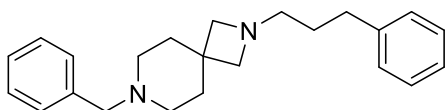
7-Benzyl-2-phenethyl-2,7-diazaspiro[3.5]nonane (AD186)



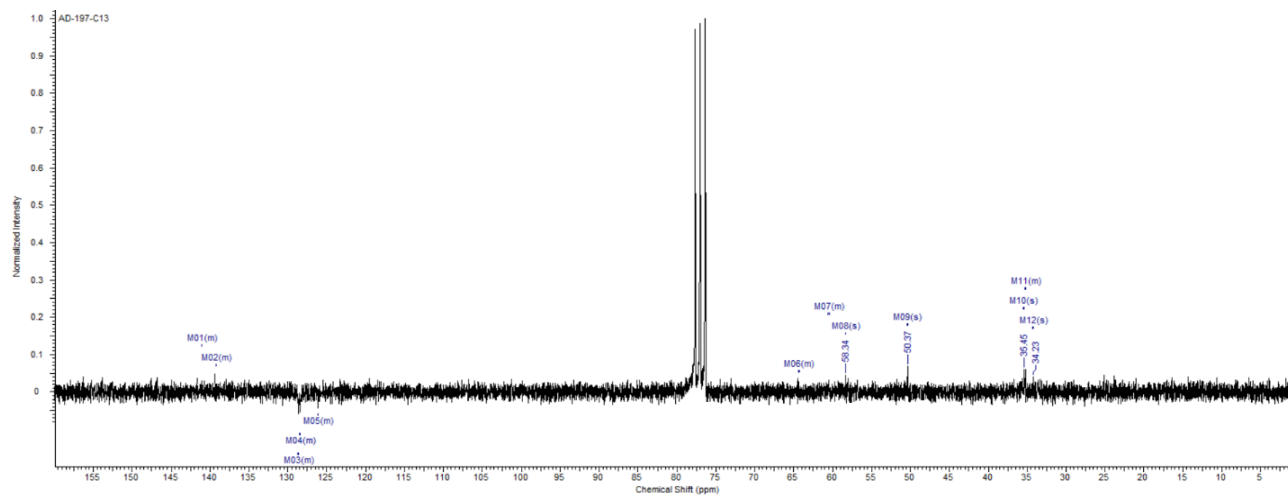
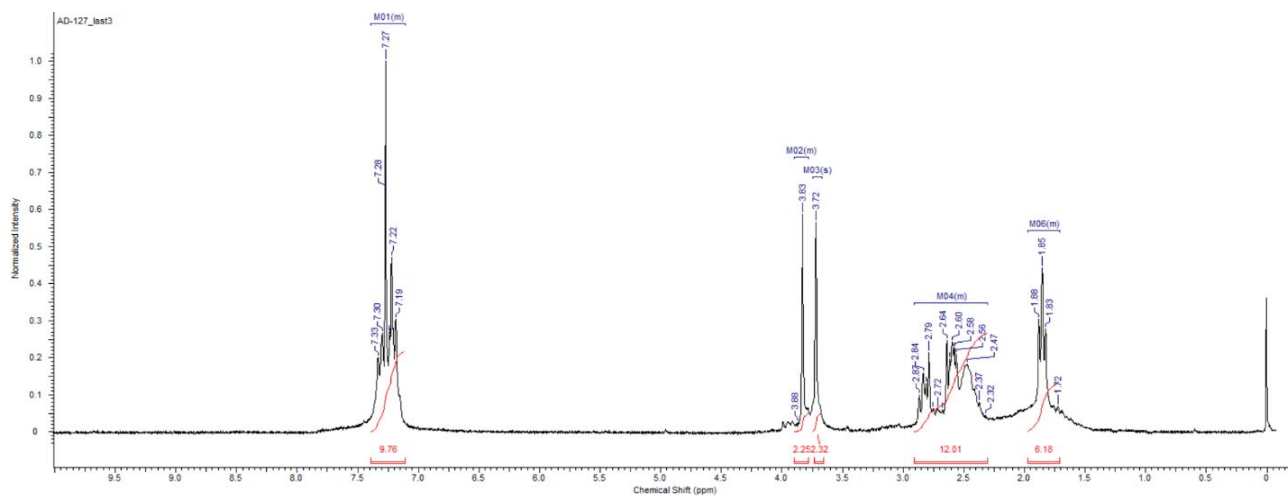
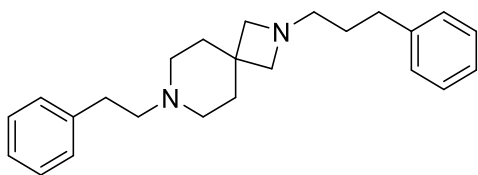
2-Benzyl-7-(3-phenylpropyl)-2,7-diazaspiro[4.4]nonane (AD193)



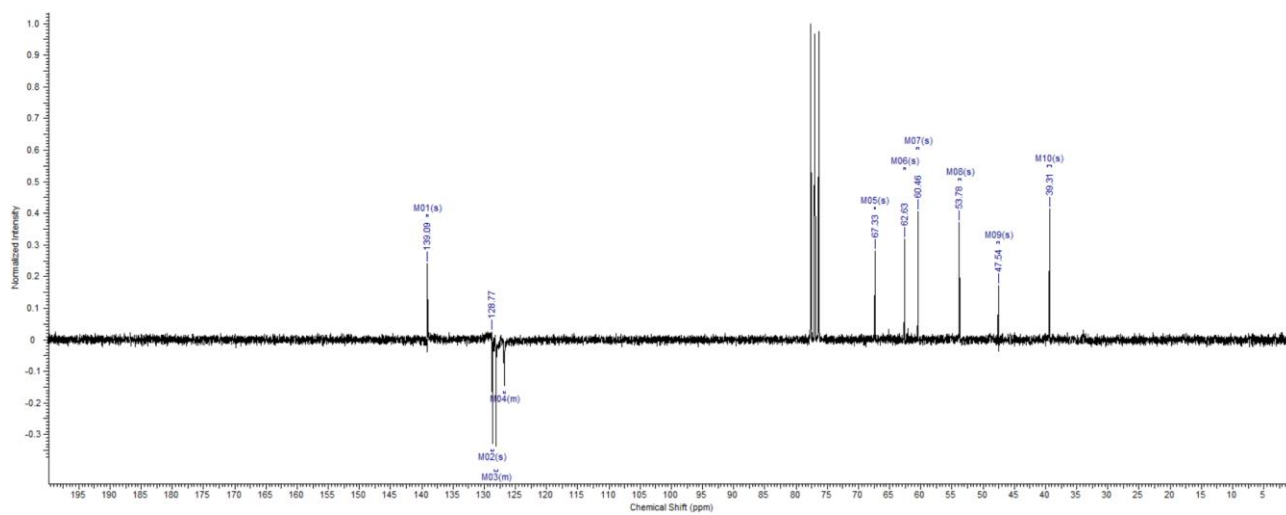
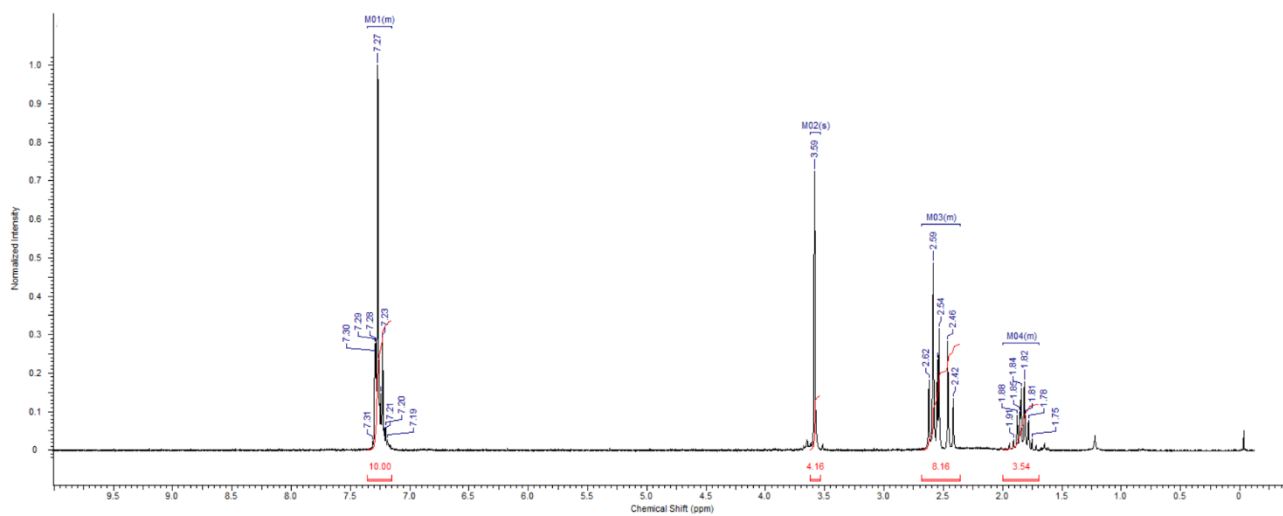
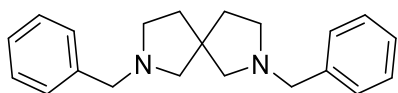
7-Benzyl-2-(3-phenylpropyl)-2,7-diazaspiro[3.5]nonane (AD195)



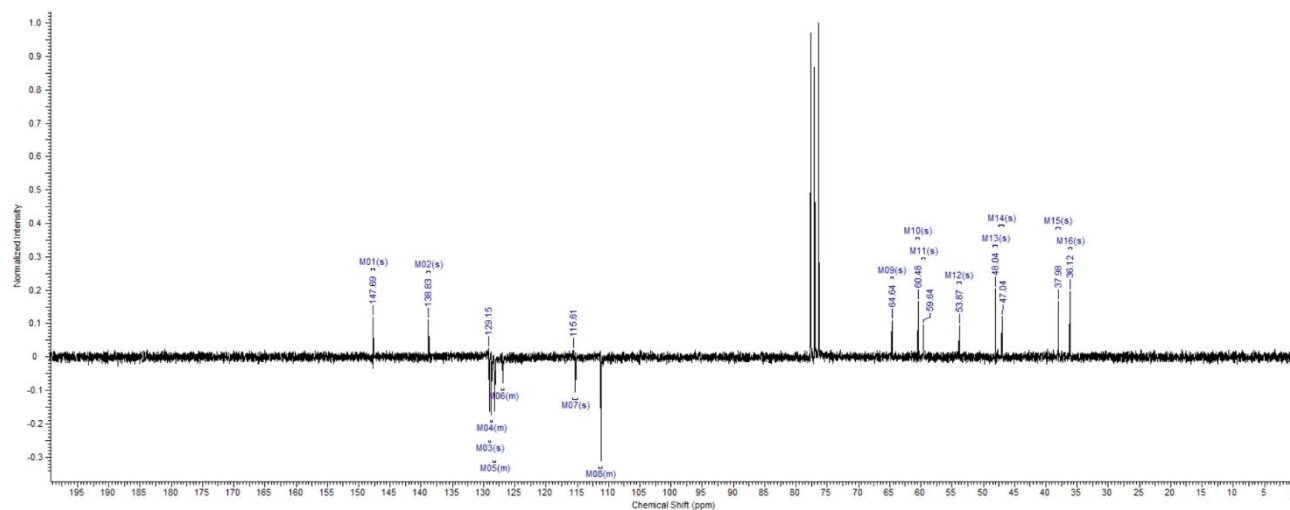
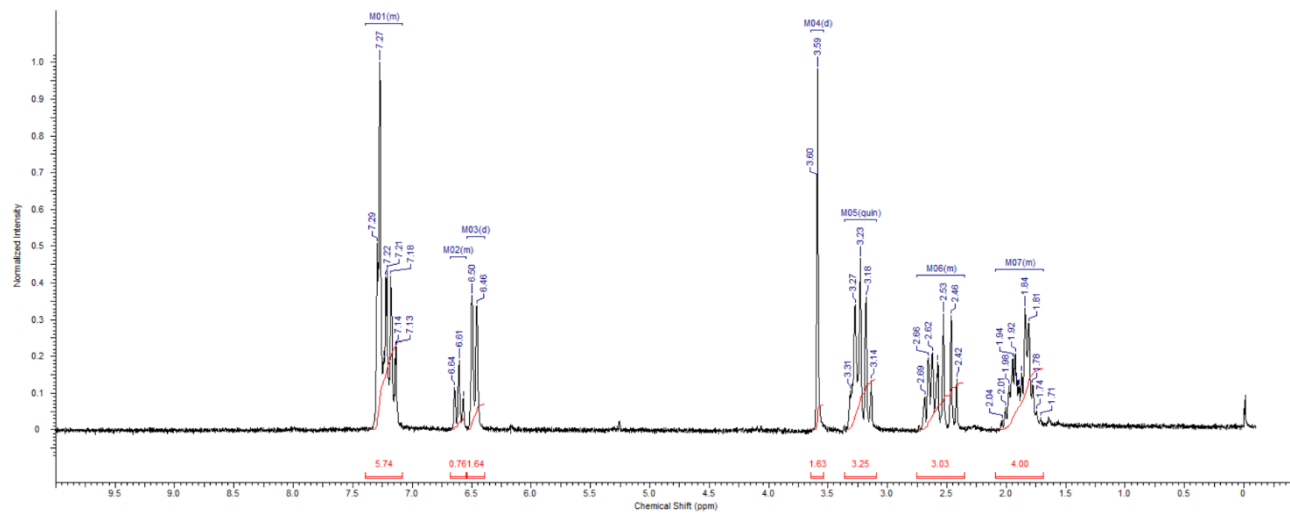
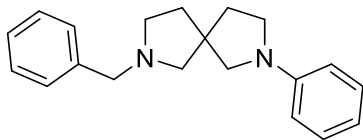
7-Phenethyl-2-(3-phenylpropyl)-2,7-diazaspiro[3.5]nonane (AD197)



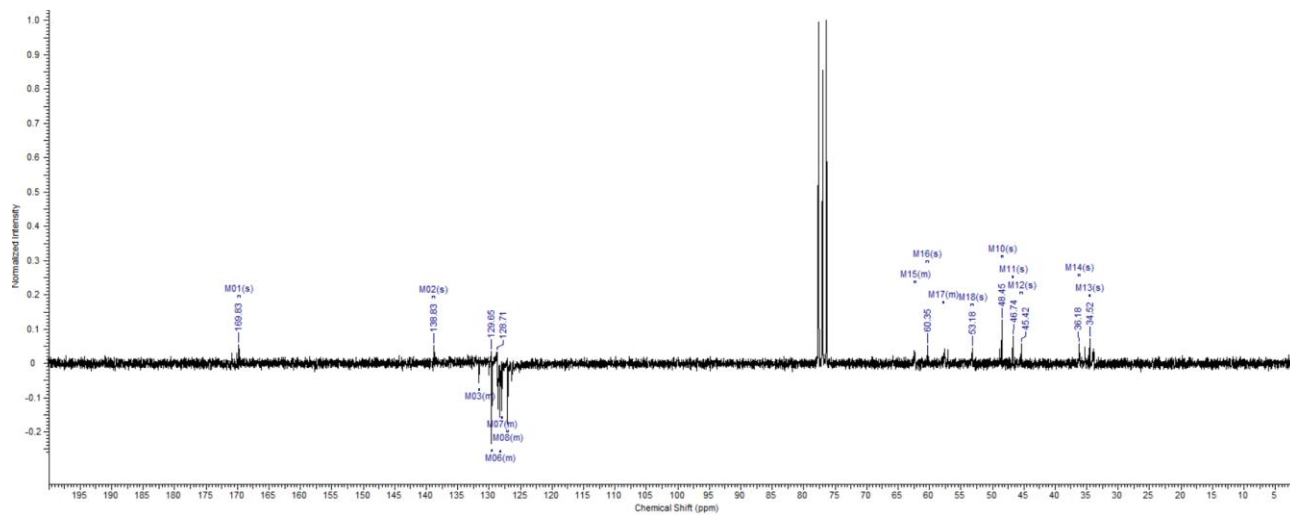
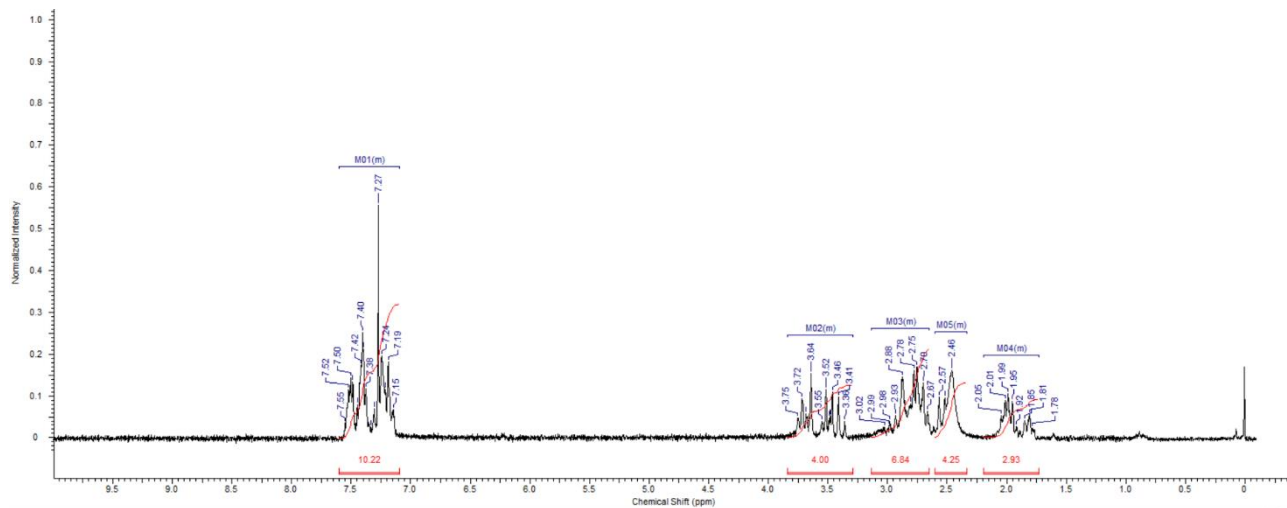
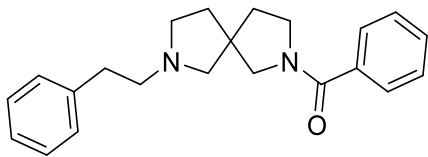
2,7-Dibenzyl-2,7-diazaspiro[4.4]nonane (AD206)



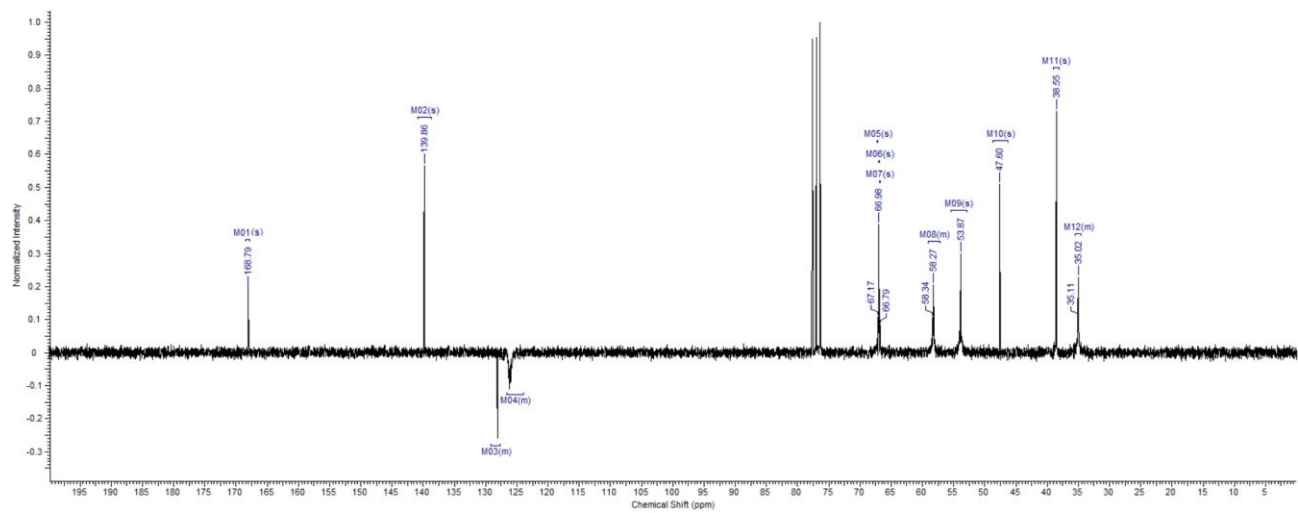
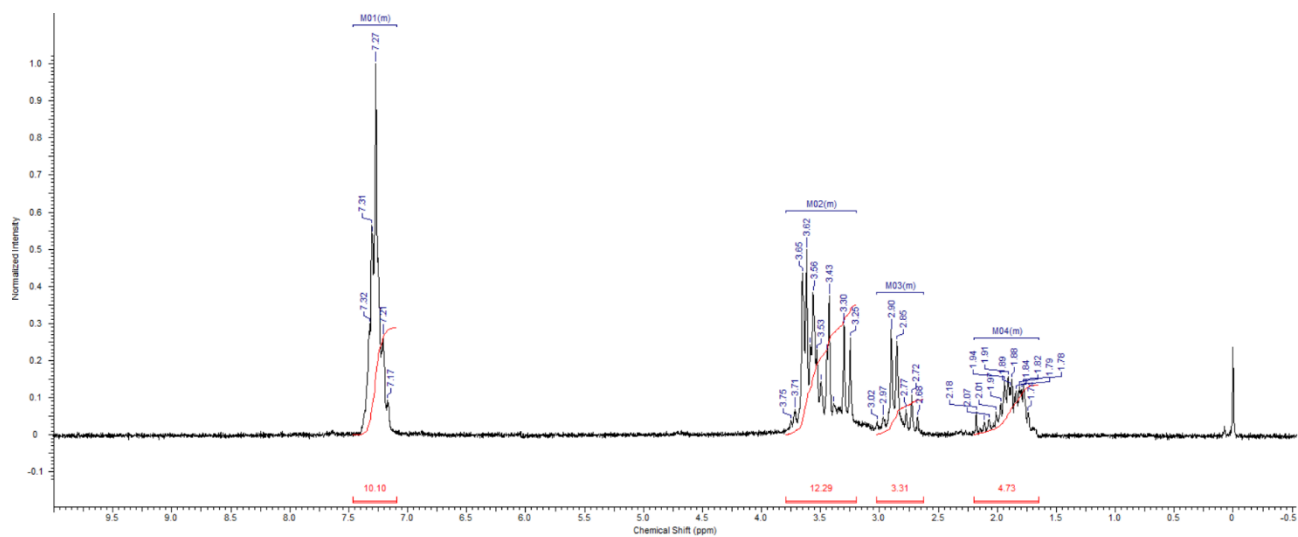
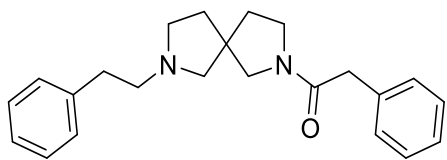
2-Benzyl-7-phenyl-2,7-diazaspiro[4.4]nonane (AD-214)



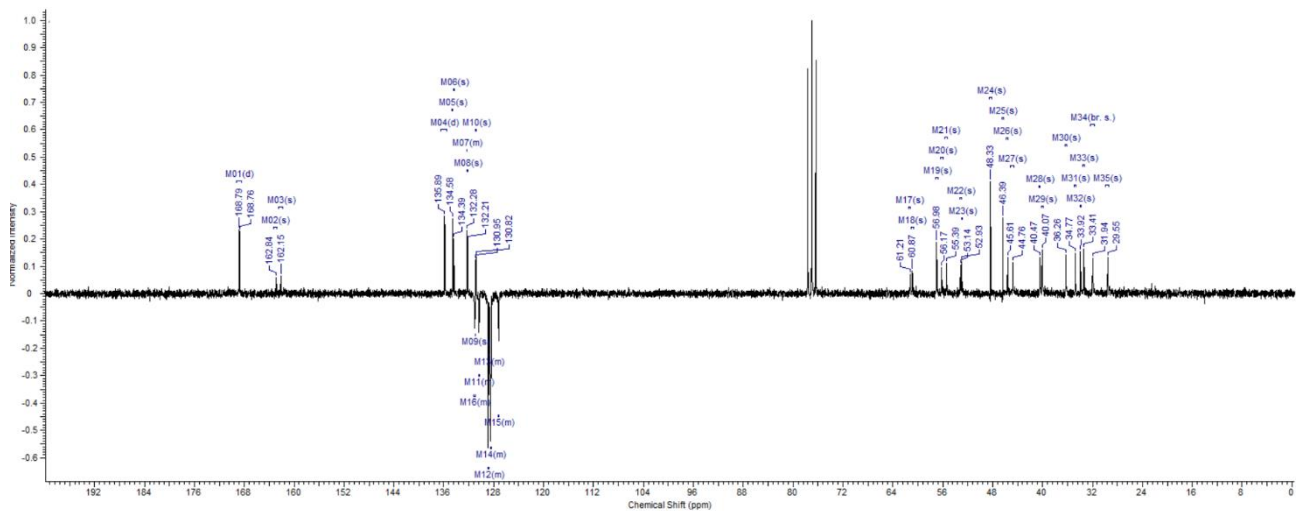
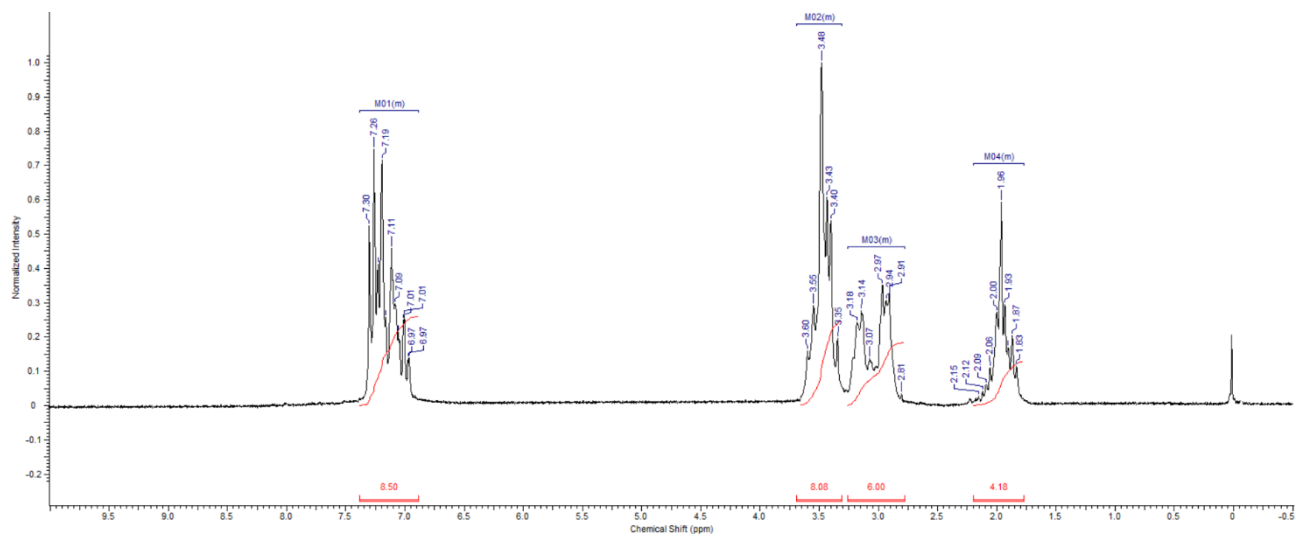
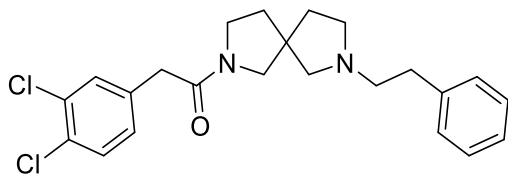
(7-Phenethyl-2,7-diazaspiro[4.4]nonan-2-yl)(phenyl)methanone (AD217)



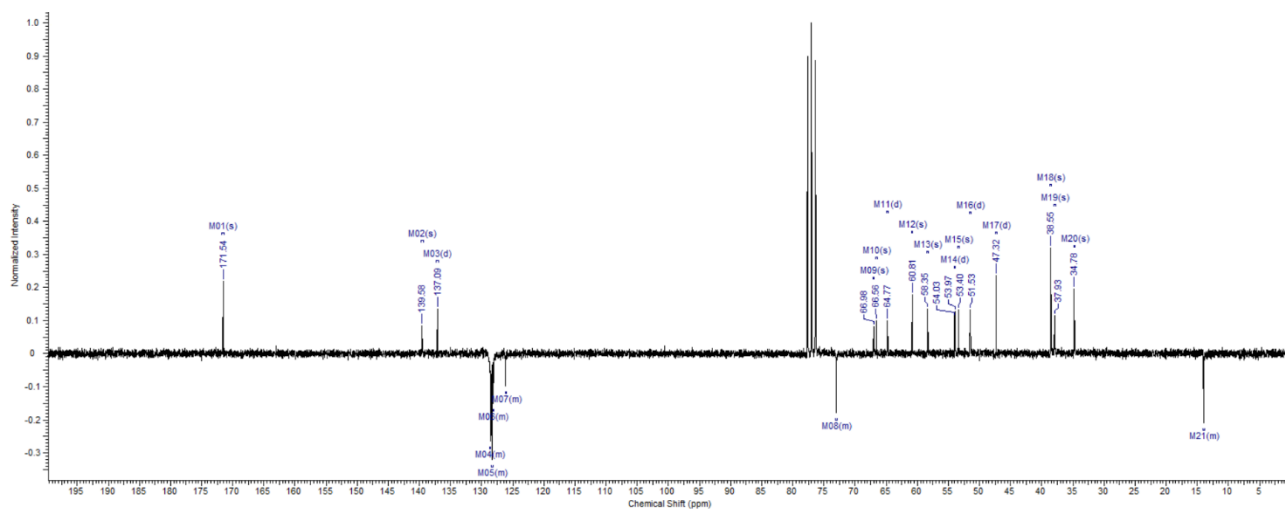
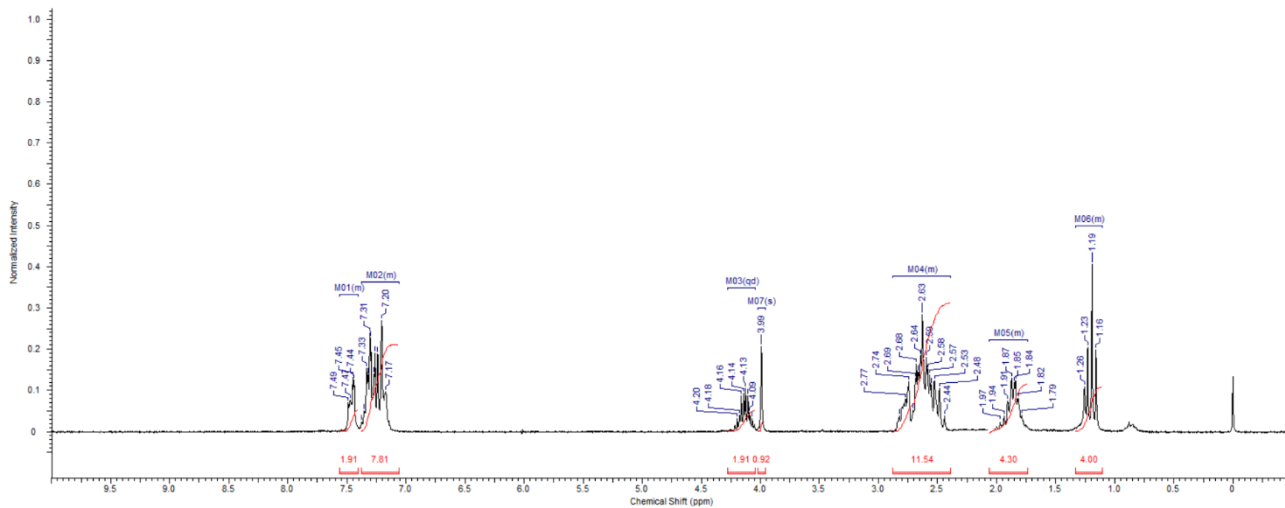
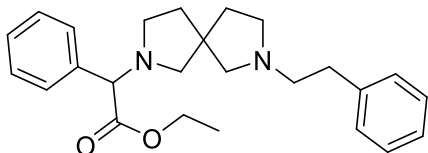
1-(7-Phenethyl-2,7-diazaspiro[4.4]nonan-2-yl)-2-phenylethan-1-one (AD219)



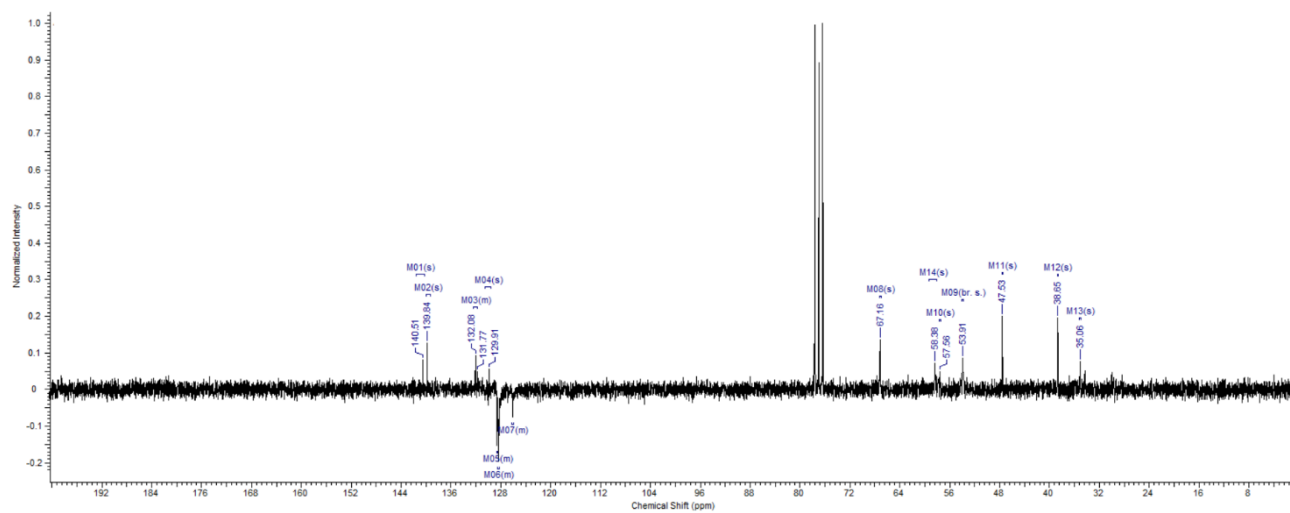
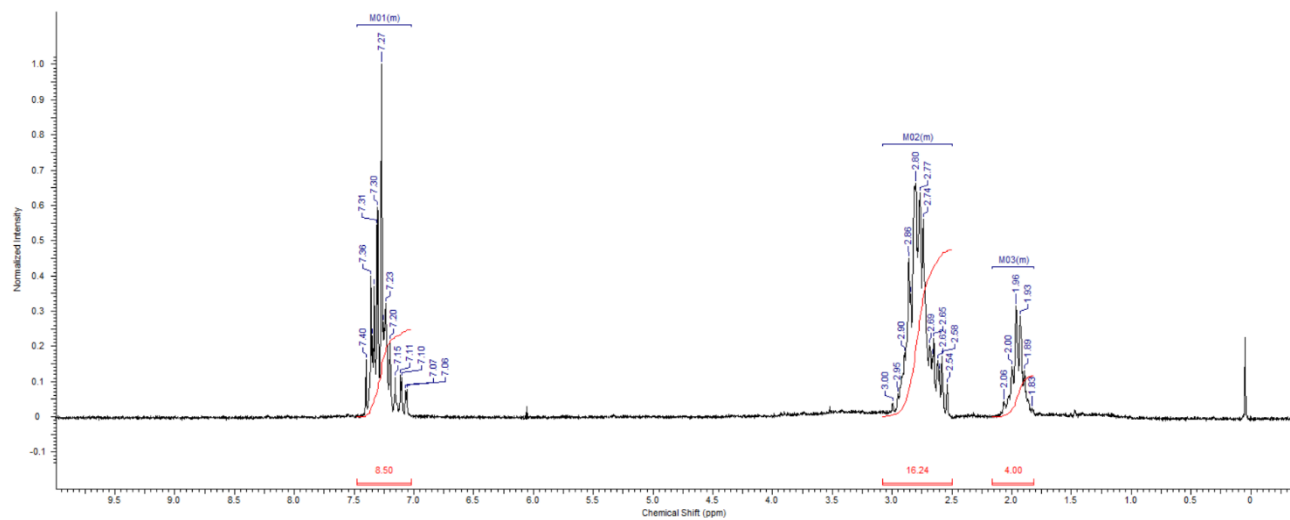
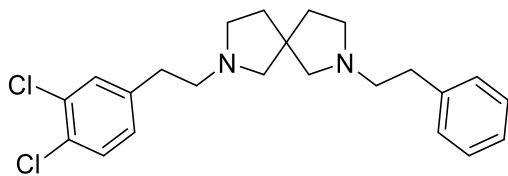
2-(3,4-Dichlorophenyl)-1-(7-phenethyl-2,7-diazaspiro[4.4]nonan-2-yl)ethan-1-one (AD220)



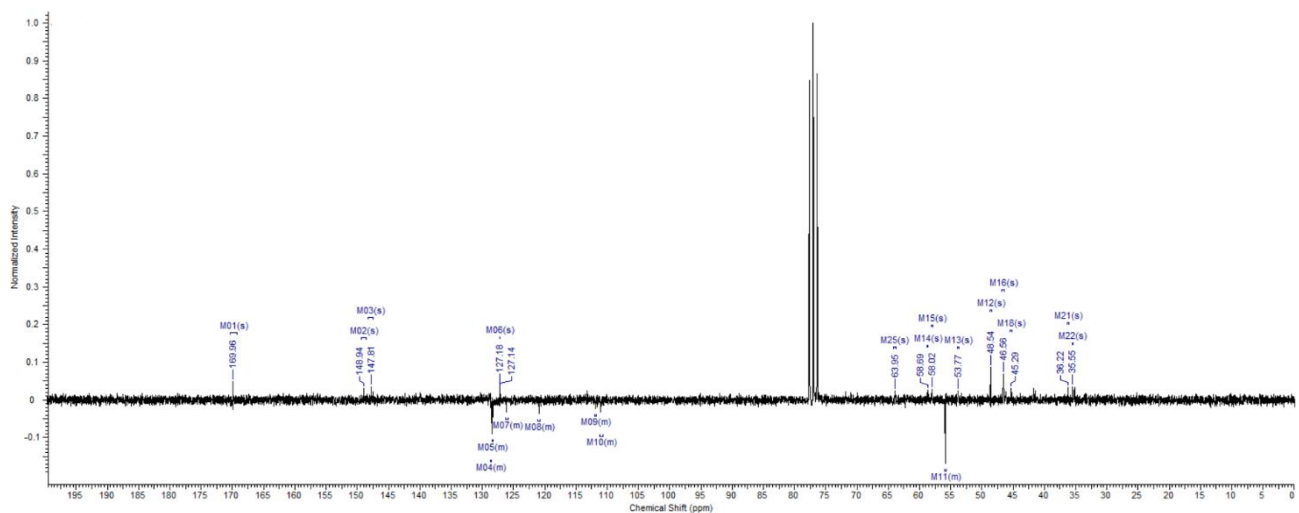
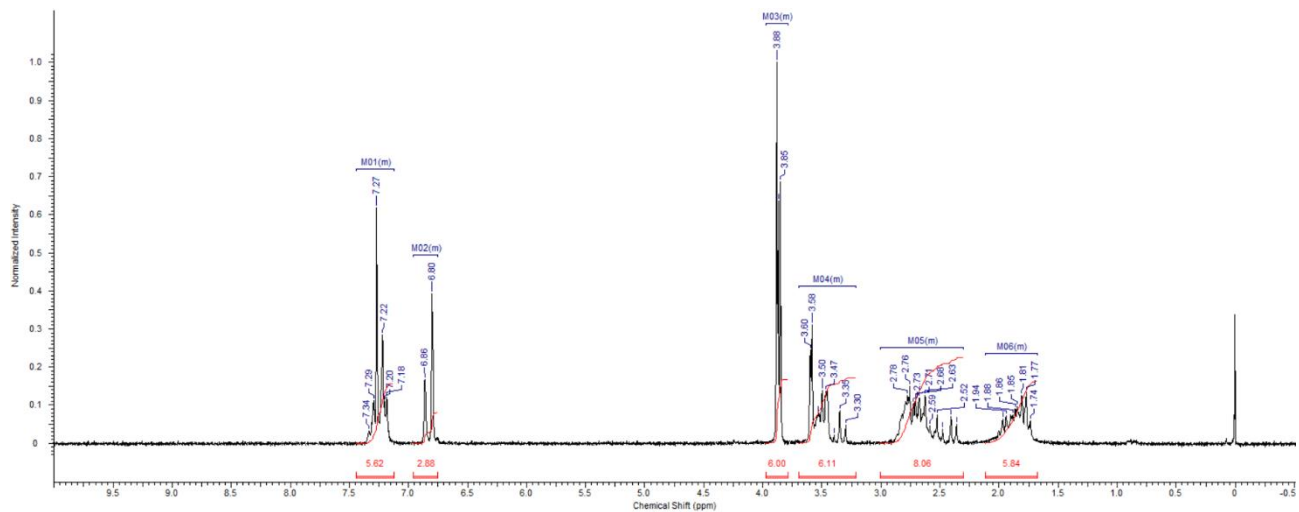
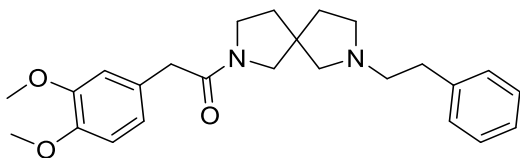
Ethyl 2-(7-phenethyl-2,7-diazaspiro[4.4]nonan-2-yl)-2-phenethylacetate (AD-223)



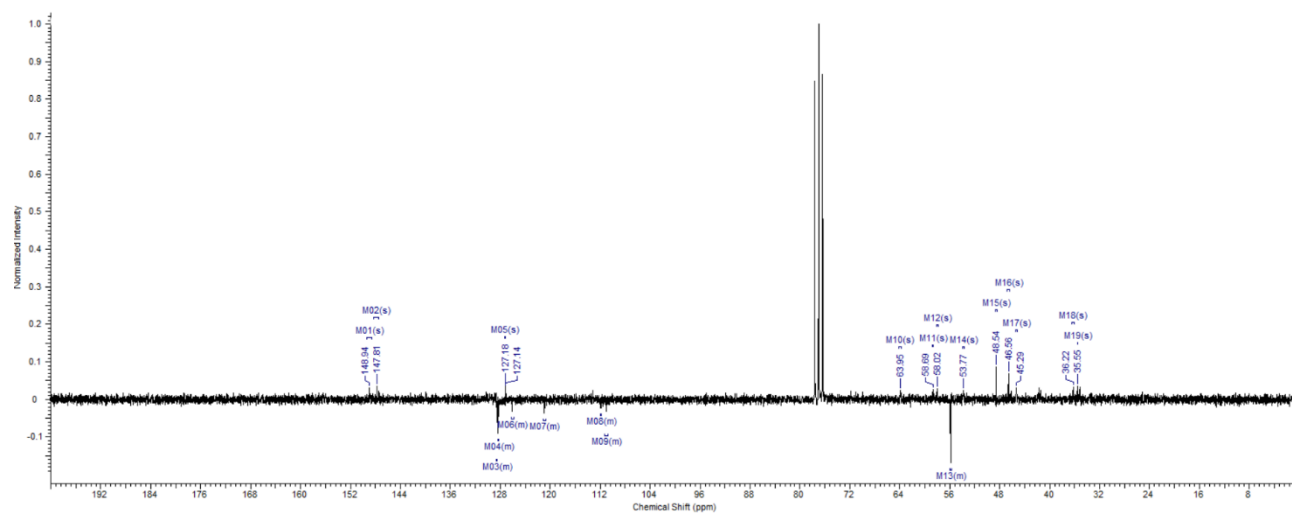
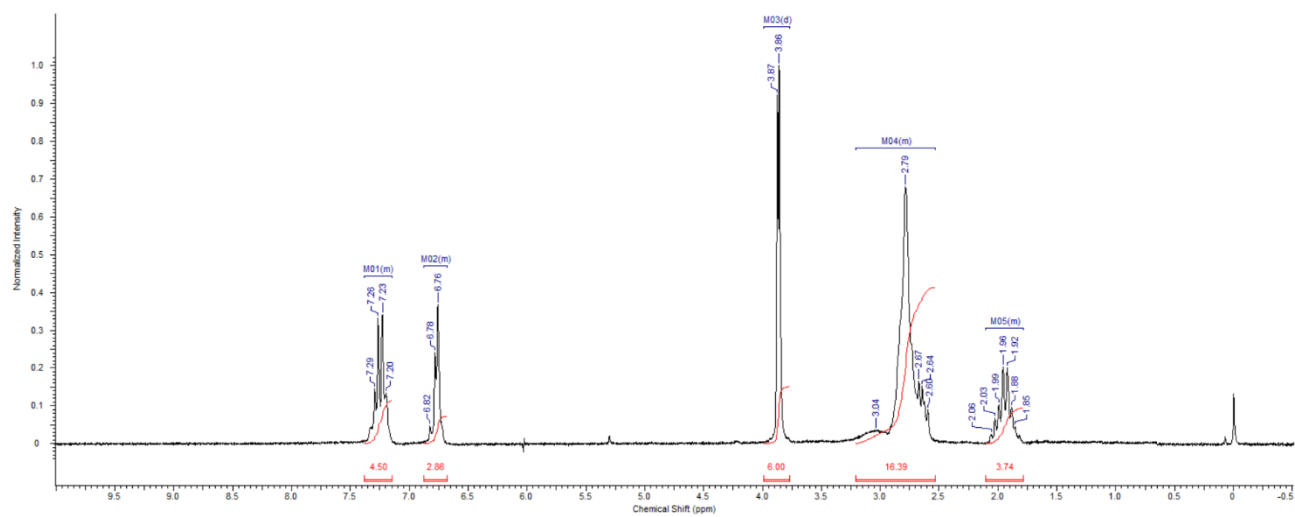
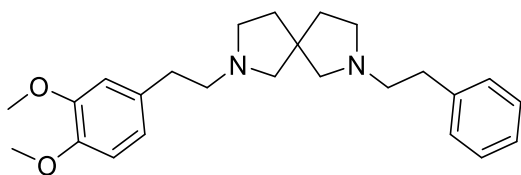
2-(3,4-Dichlorophenethyl)-7-phenethyl-2,7-diazaspiro[4.4]nonane (**AD225**)



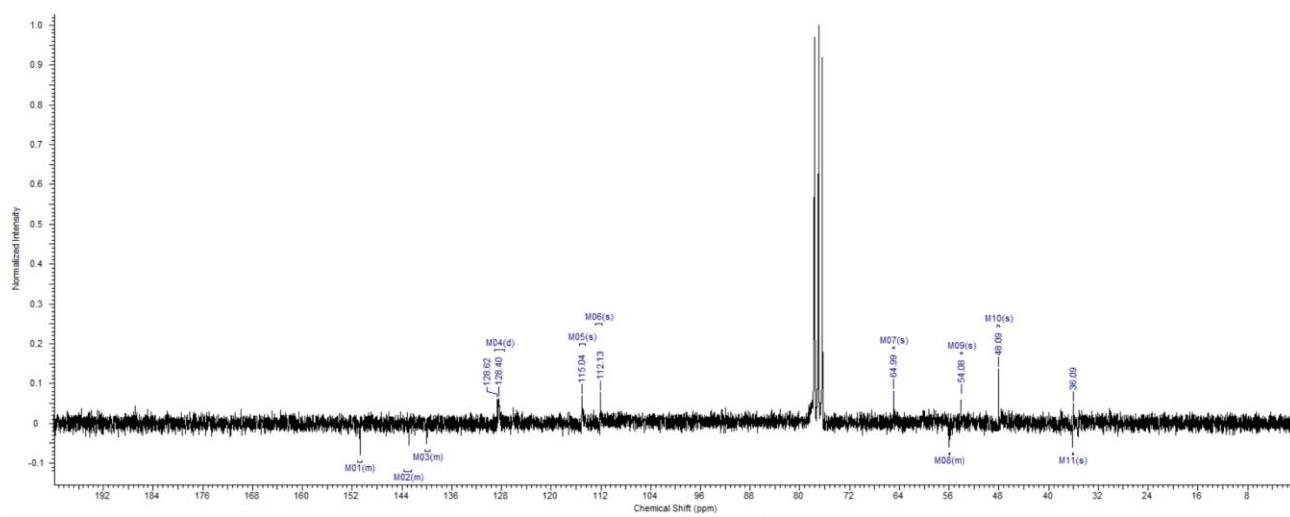
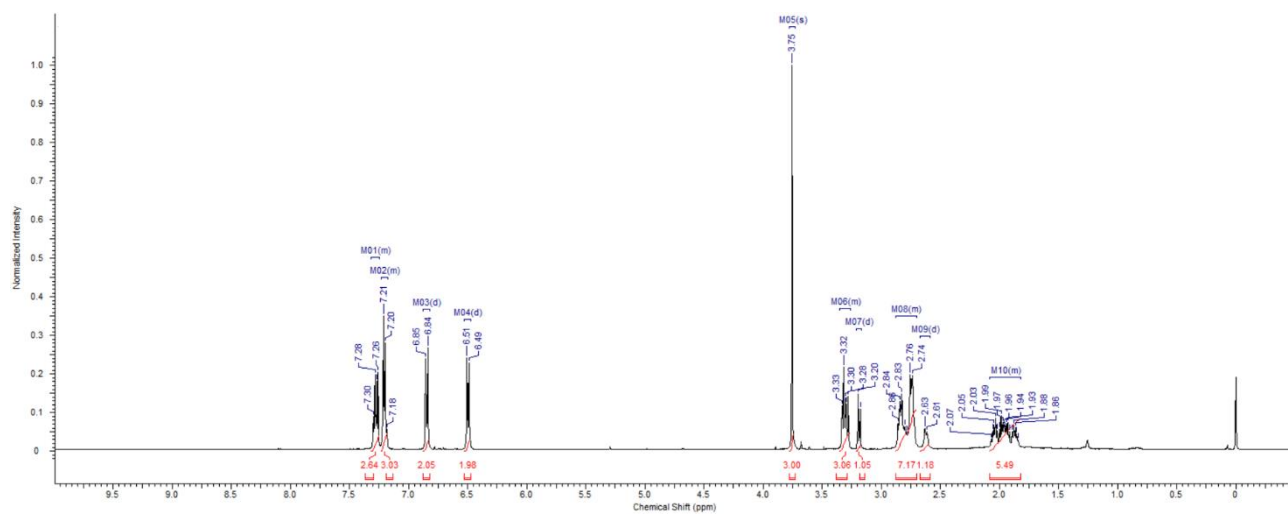
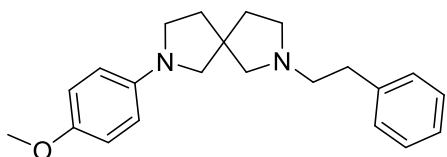
2-(3,4-Dimethoxyphenyl)-1-(7-phenethyl-2,7-diazaspiro[4,4]nonan-2-yl)ethan-1-one (AD226)



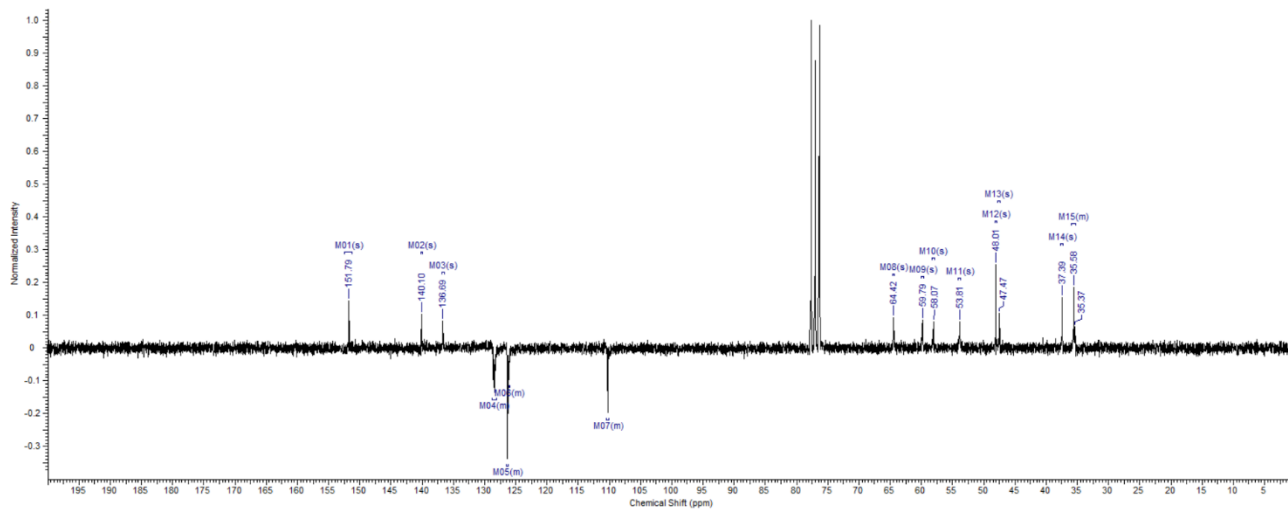
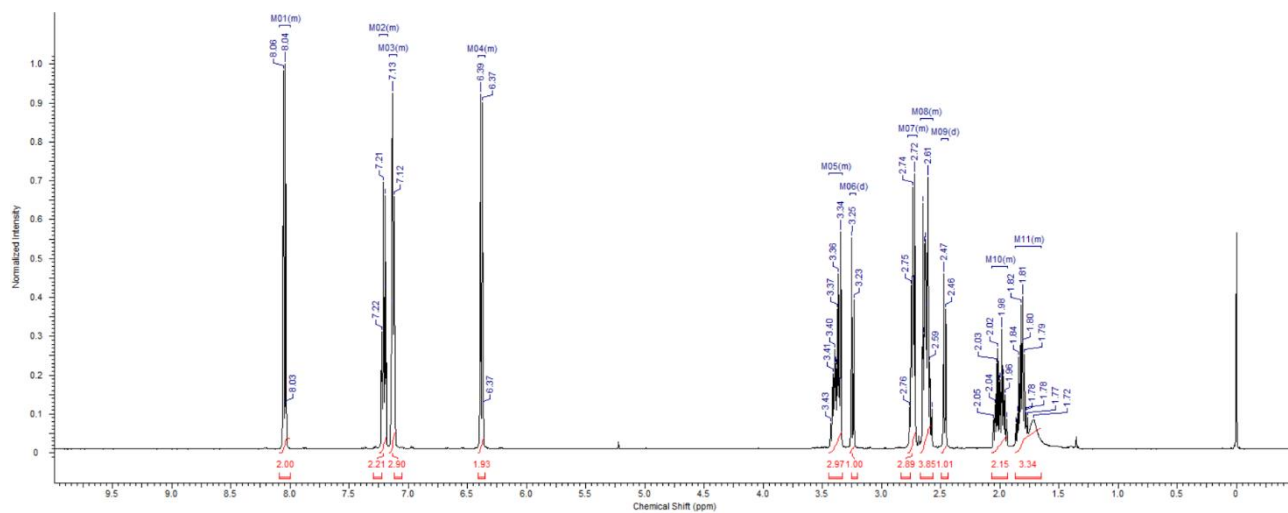
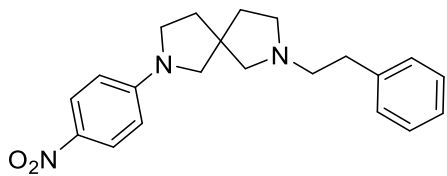
2-(3,4-Dimethoxyphenethyl)-7-phenethyl-2,7-diazaspiro[4,4]nonane (**AD234**)



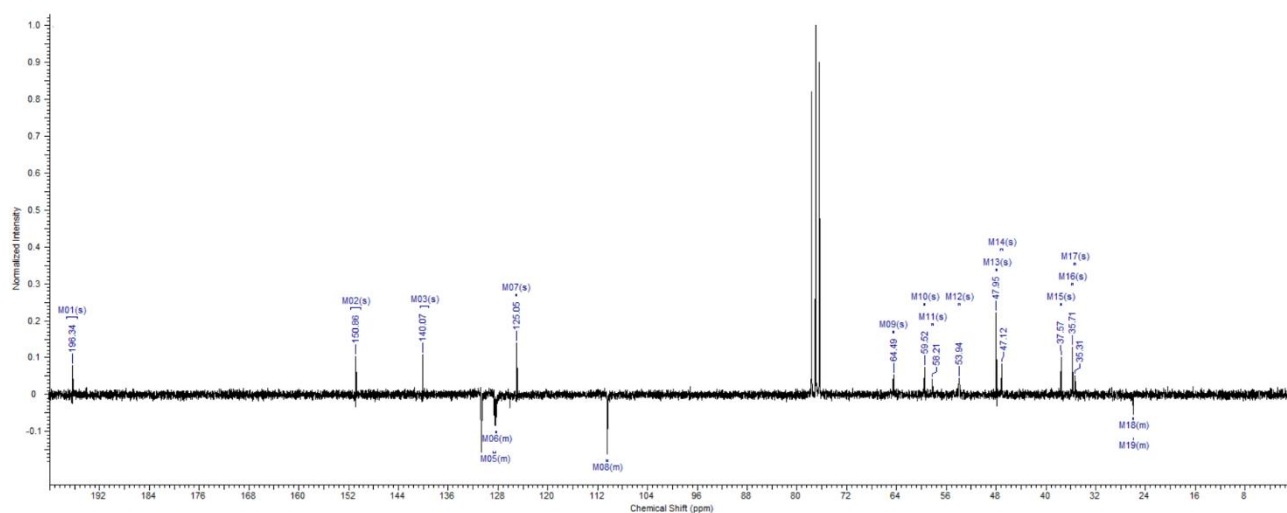
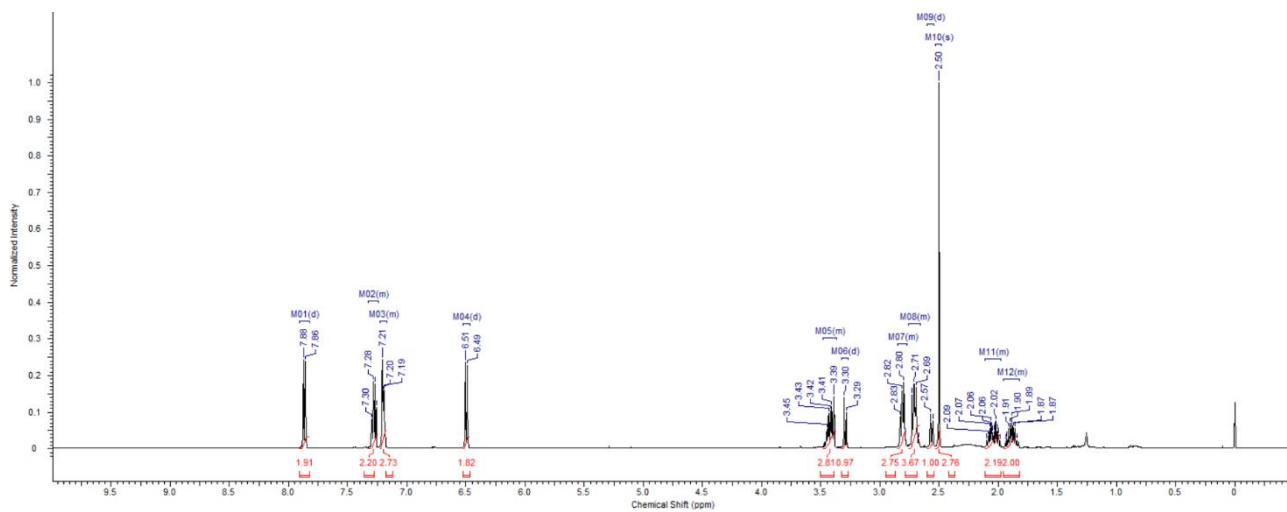
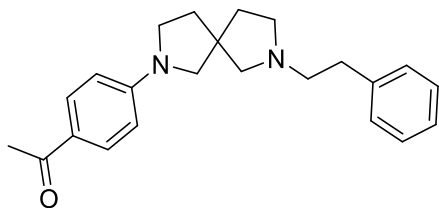
2-(4-Methoxyphenyl)-7-phenethyl-2,7-diazaspiro[4.4]nonane oxalate (AD239)



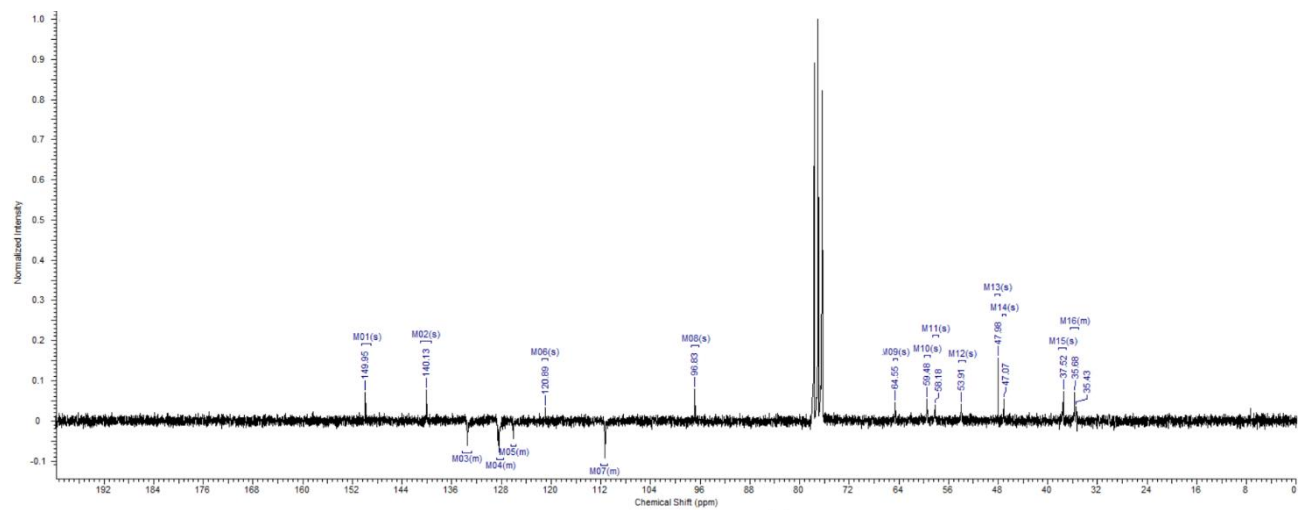
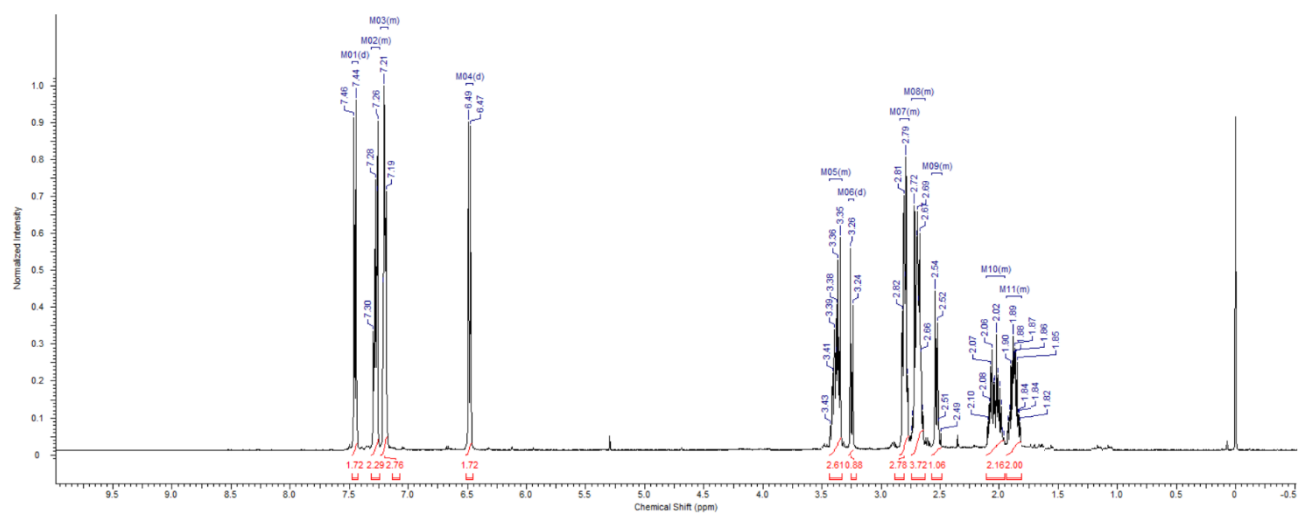
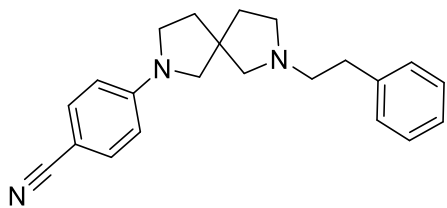
2-(4-Nitrophenyl)-7-phenethyl-2,7-diazaspiro[4.4]nonane (AD242)



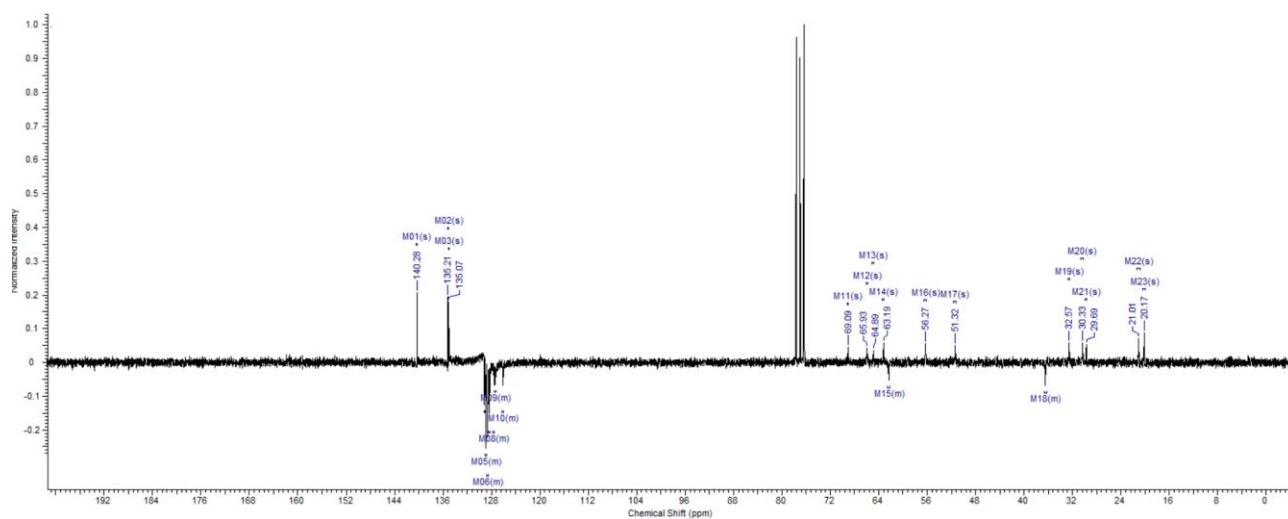
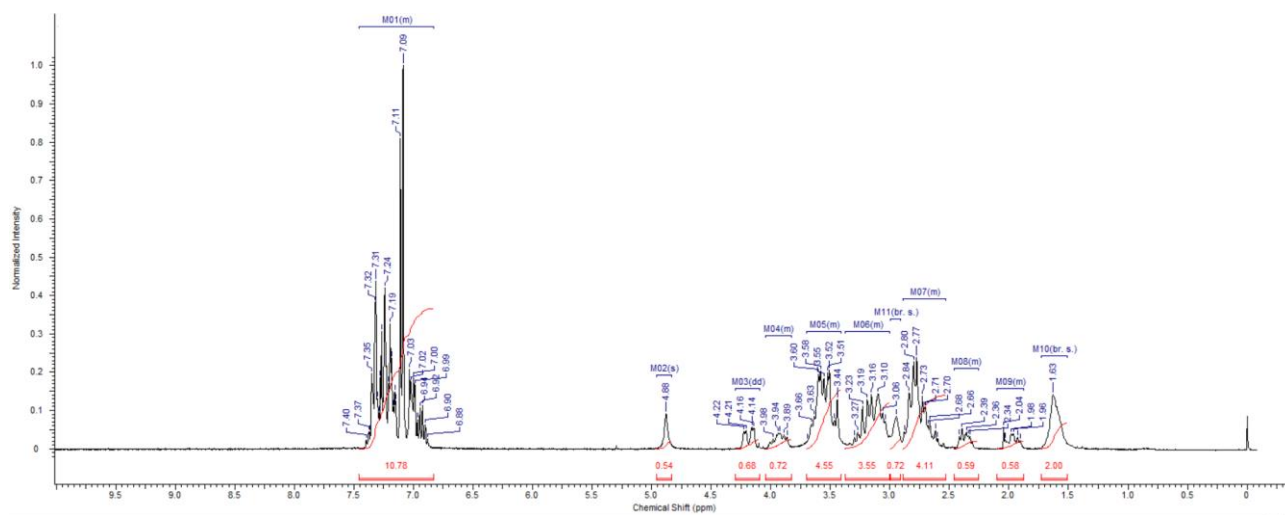
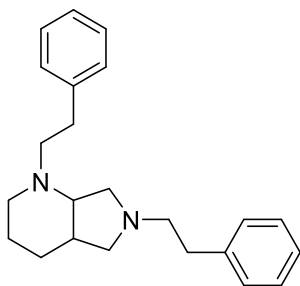
1-(7-Phenethyl-2,7-diazaspiro[4.4]nonan-2-yl)ethan-1-one oxalate (AD245)



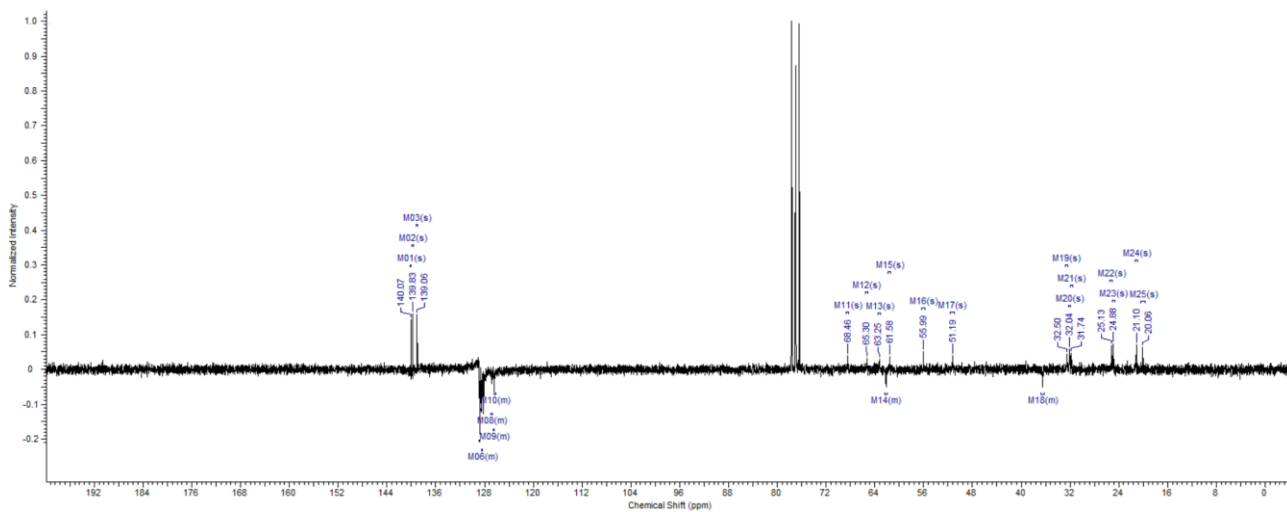
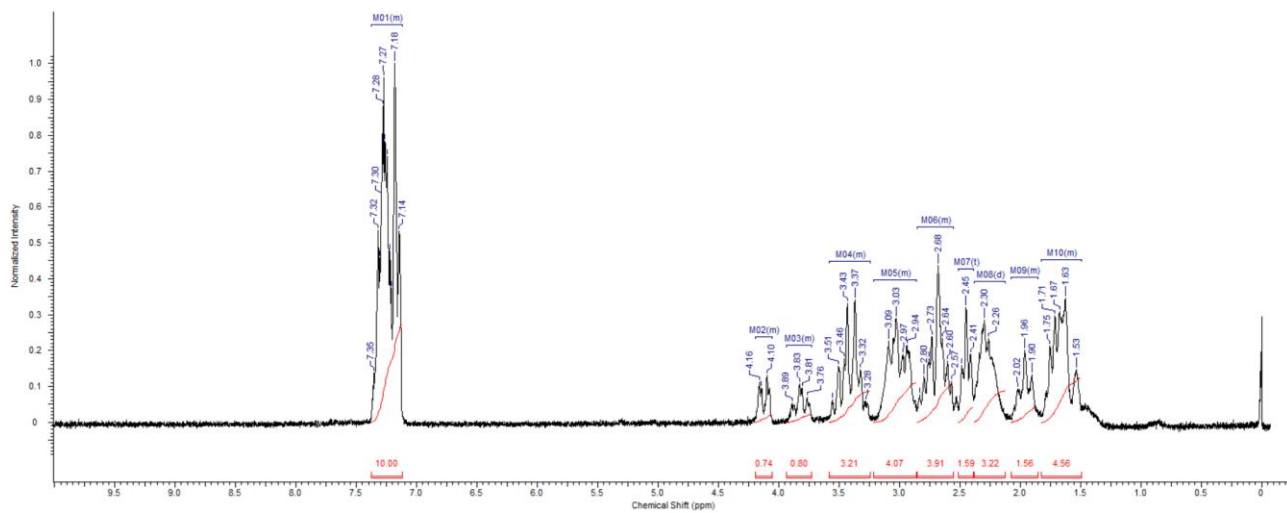
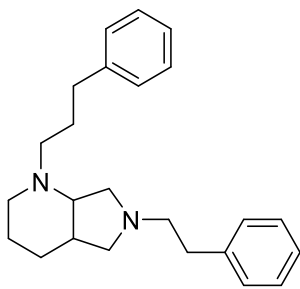
4-(7-Phenethyl-2,7-diazaspiro[4.4]nonan-2-yl)benzonitrile oxalate (AD258)



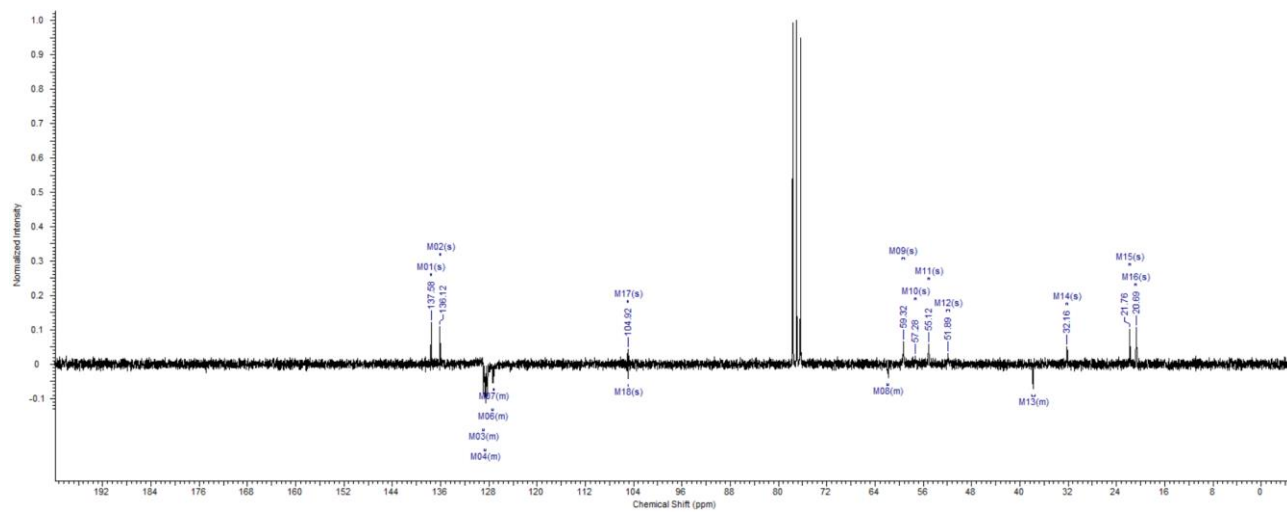
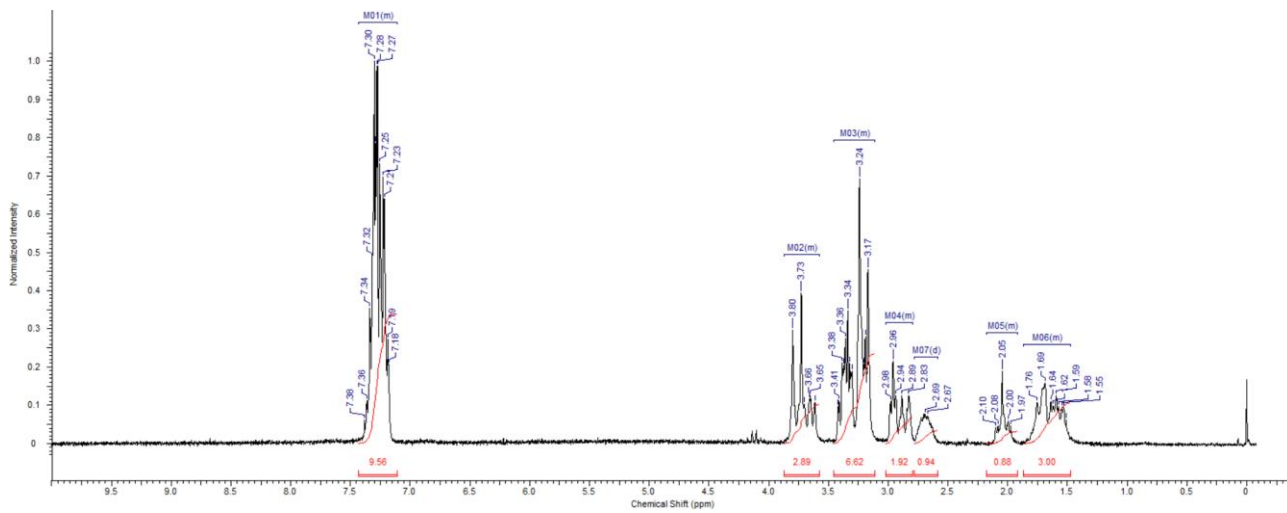
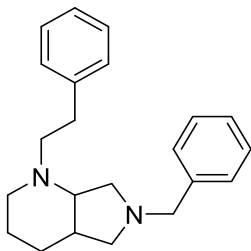
1,6-Diphenethyloctahydro-1*H*-pyrrolo[3,4-*b*]pyridine (AB7)



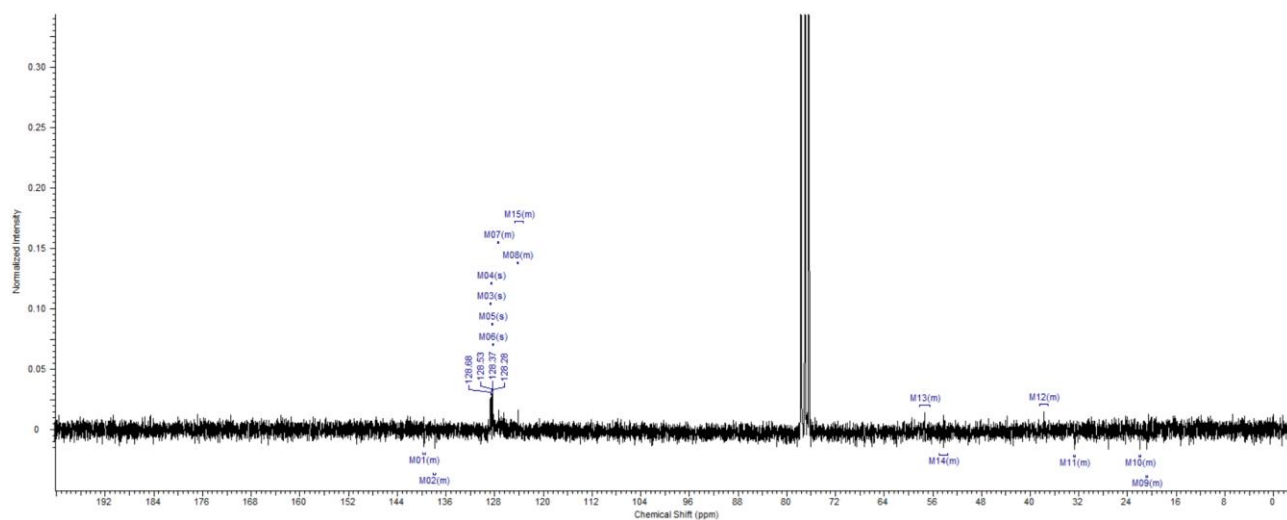
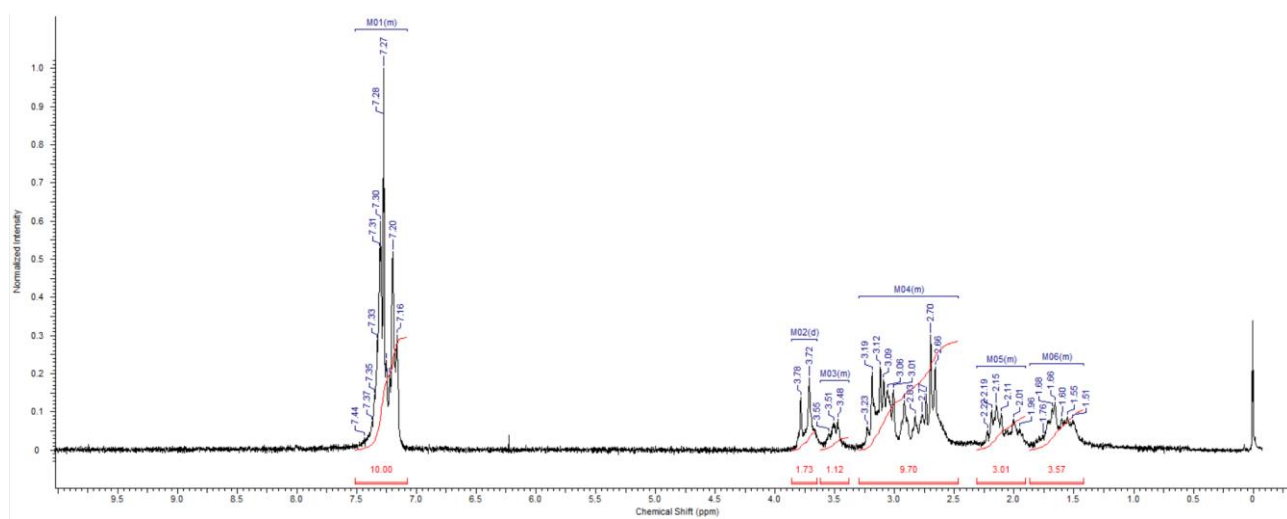
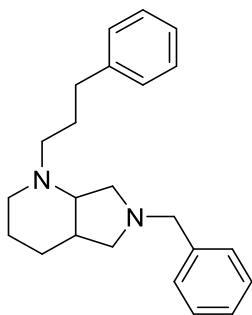
6-Phenethyl-1-(3-phenylpropyl)octahydro-1H-pyrrolo[3,4-b]pyridine (**AB8**)



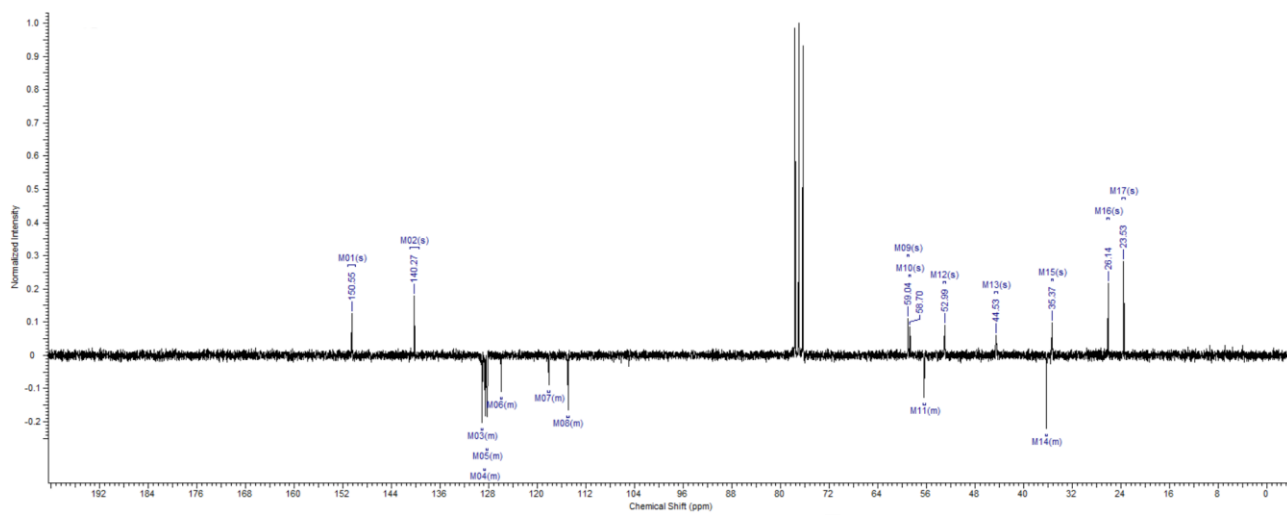
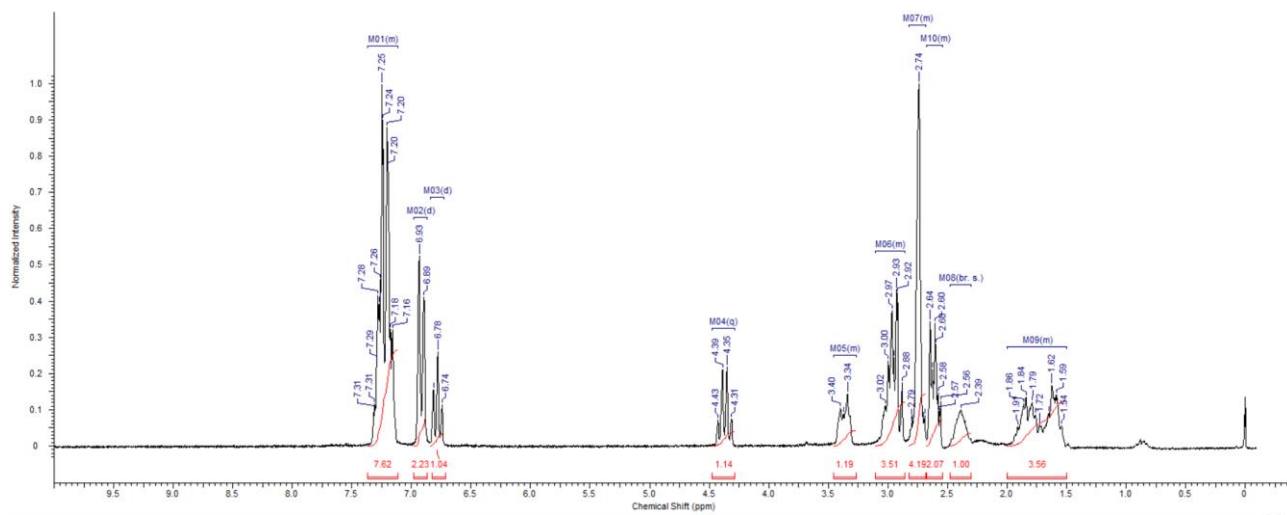
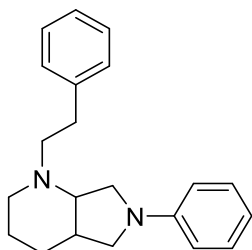
6-Benzyl-1-phenethyloctahydro-1H-pyrrolo[3,4-b]pyridine (AB9)



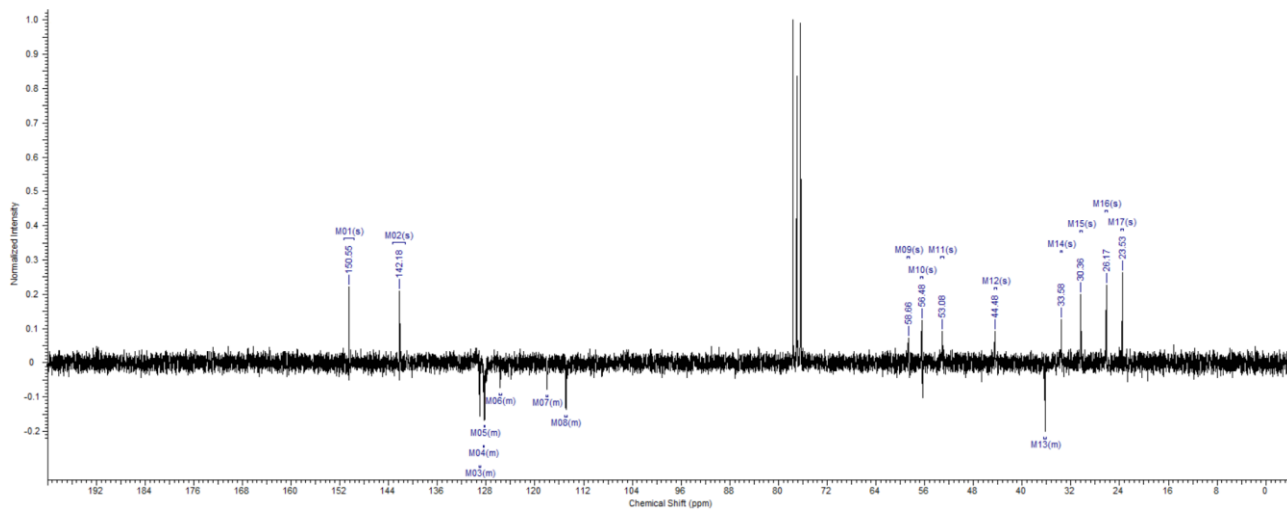
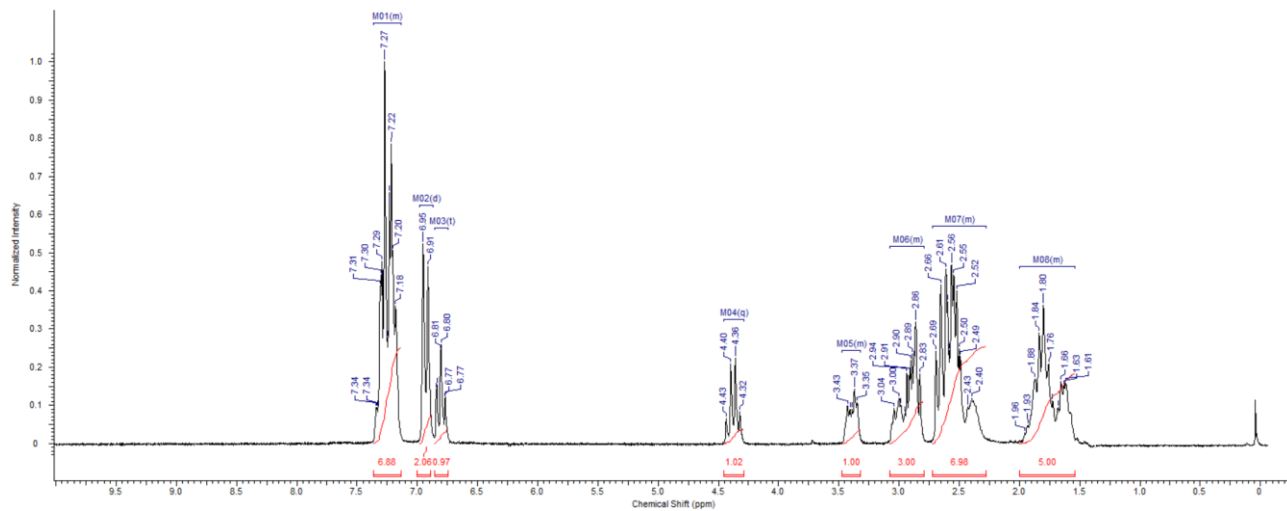
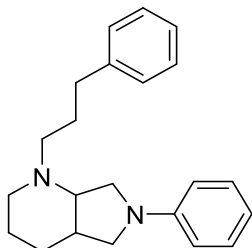
6-Benzyl-1-(3-phenylpropyl)octahydro-1H-pyrrolo[3,4-b]pyridine (AB10)



1-Phenethyl-6-phenyloctahydro-1*H*-pyrrolo[3,4-*b*]pyridine (AB13)



6-Phenyl-1-(3-phenylpropyl)octahydro-1*H*-pyrrolo[3,4-*b*]pyridine (**AB14**)



Discovery and affinity maturation of small molecule ligands against Tyrosinase and Tyrosinase Related Protein 1

Marco Catalano,[†] Gabriele Bassi,[†] Giulia Rotondi, Lyna Khettabi, Maria Dichiara, Patrizia Murer, Jörg Scheuermann, Montserrat Soler-Lopez, and Dario Neri*

Index

General remarks	S100
Reagents	S100
Protein expression.....	S100
Selections	S100
Enzymatic assay	S101
Fluorescence polarization	S101
Fluorescence polarization on-DNA	S101
ELISA	S101
Cell culture	S102
Flow Cytometry	S102
Fluorescence polarization assay A26-B389	S103
TYR-based enzymatic assays	S103
Concentration Inhibitors	S104
Synthesis on-DNA	S105
<i>A12LNA synthetic procedure</i>	<i>S105</i>
<i>B12DNA synthetic procedure</i>	<i>S105</i>
Synthetic procedures	S106
<i>L-Gln-A26-B389</i>	<i>S106</i>
<i>D-Gln-A26-B389</i>	<i>S107</i>
<i>Lys-L-Gln-A26-B389</i>	<i>S108</i>
<i>FI-Lys-L-Gln-A26-B389</i>	<i>S109</i>
<i>Lys-D-Gln-A26-B389</i>	<i>S110</i>
<i>FI-Lys-D-Gln-A26-B389</i>	<i>S111</i>
<i>Hex-5-ynoyl chloride</i>	<i>S111</i>
<i>ThiamidolTM-alkyne</i>	<i>S112</i>
<i>ThiamidolTM</i>	<i>S114</i>
General Procedure on-resin	S115
<i>C-C6-DRD-monomer-ThiamidolTM</i>	<i>S115</i>
<i>Monomer</i>	<i>S116</i>
<i>C-C6-DRD-dimer-ThiamidolTM</i>	<i>S117</i>
<i>Dimer</i>	<i>S118</i>
<i>C-C6-DRD-tetramer-ThiamidolTM</i>	<i>S119</i>
<i>Tetramer</i>	<i>S120</i>
References	S121

General remarks

High-Resolution Mass Spectrometry (HRMS) spectra and analytical Reversed-Phase Ultra Performance Liquid Chromatography (UPLC) were recorded on a Waters Xevo G2-XS QTOF coupled to a Waters Acquity UPLC H-Class System with PDA UV detector, using an ACQUITY UPLC BEH C18 Column, 130 Å, 1.7 µm, 2.1 mm × 50 mm at a flow rate of 0.6 ml/min with linear gradients of solvents A and B (A = Millipore water with 0.1% FA, B = MeCN with 0.1% FA). Preparative reversed-phase highpressure liquid chromatography (RP-HPLC) were performed on a Waters Alliance HT RP-HPLC with PDA UV detector, using a Synergi 4µm, Polar-RP 80Å 10 × 150 mm C18 column at a flow rate of 4 ml/min with linear gradients of solvents A and B (A = Millipore water with 0.1% TFA, B = MeCN with 0.1% TFA). Preparative reversed phase high-pressure liquid chromatography (HPLC) for the LNA conjugates was performed on a Waters Alliance HT RP-HPLC with PDA UV detector, using a Synergi 4 µm, Polar-RP 150 × 10 mm C18 column using a gradient of eluent A (TEAA 100 mM) and eluent B (TEAA 100 mM in 80% ACN). Proton (¹H) nuclear magnetic resonance (NMR) spectra were recorded on a Bruker AV400 (400 MHz). Carbon (¹³C) NMR spectra were recorded on a Bruker AV400 (100 MHz) spectrometer. Shifts are given in ppm using residual solvent as the internal standard. Coupling constants (*J*) are reported in Hz with the following abbreviations used to indicate splitting: s = singlet, d = doublet, t = triplet, dd = doublet of doublets.

Reagents

All compounds and chemical reagents were obtained from Sigma-Aldrich, TCI Europe, Enamine or ABCR, and used without further purification. Peptide grade N,Ndimethylformamide (DMF) for solid phase synthesis was bought from ABCR. Complementary Locked Nucleic Acid (LNA) and DNA starting materials were purchased from LGC Biosearch Technologies. H-Rink amide ChemMatrix[®] resin was purchased from Sigma Aldrich (Cat. Nr. 727768-5G). Fmoc-Lys(Boc)-Wang resin, 200-400mesh was purchased from Bachem (Cat. Nr. 4003241.0005). Fmoc-Cys(Trt)-Wang resin (100-200 mesh, 0.40-1.00 mmol/g) was purchased from Bachem (Cat. Nr. 4028211.0001). 4-(2-aminothiazol-4-yl)benzene-1,3-diol was purchased from Fluorochem (Cat. Nr. 495142-1g).

Protein expression

Overexpression and purification of the human intramelanosomal domain of TYR (residues 19 to 456) and TYRP1 (residues 25 to 471) respectively were done according to already published procedures [1,2]. A final purification step by size exclusion chromatography was carried out using a Superdex 200 10/300 GL column (GE Healthcare) equilibrated with buffer 10 mM Tris-HCl, pH 7.8, 100 mM NaCl. The 0.5 mL elution fractions containing the monomeric pure proteins as shown in **Figure 1b** were subsequently pooled and concentrated using a 30 kDa cut-off Amicon membrane (Merck Millipore, Burlington, Massachusetts, U.S.A.) to a concentration of ≈7.5 mg/mL for TYRP1 and ≈3 mg/ml for TYR, and stored at 193 K.

Selections

Affinity selections were performed with both single (ss) and double stranded (ds) libraries with 10⁷ copies of individual library members for each selection [3]. Selections against TYR/TYRP1 was performed in duplicate. The ss-library and ds-library were diluted to 110 nM in protein-specific buffer, containing also 0.05% tween-20 and 20 µg/mL herring sperm DNA (100 µL). The selections against immobilized protein targets were performed with the automated system King Fisher (Thermo Fisher) as reported by Decurtins et al. [4].

Enzymatic assay

The enzymatic activity of Tyrosinase was measured at 25 °C following already described procedures using L-DOPA as substrate [5–7]. In 384-well microtiter clear plates (Greiner non-binding), a mixture of 1 mM L-DOPA, 4 mM MBTH, 200 nM human Tyrosinase and the inhibitor was prepared (final volume 30 µL in PBS 1% DMSO, pH=6.8). The increase of the absorption at 490-510 nm, due to the formation of the Ldopaquinone-MBTH complex, was recorded using a Spectra Max Paradigm multimode plate reader (Molecular Devices) over 10 minutes. Experiments were performed in duplicates and the values were fitted using Graphpad Prism software. The obtained OD values were plotted as a function of time. Linear regression of the plotted points was performed. IC₅₀ values were calculated fitting the obtained slope as function of the inhibitor concentration.

Fluorescence polarization

The dilution series were done in a non-binding black 384-well microplate (Greiner Bio On.). In a final volume of 30 µL, 50 nM of the fluorescein-conjugated ligand was incubated with a 1:1 dilution series of TYRP1 in PBS pH 7.4. The fluorescence anisotropy was measured on a Spectra Max Paradigm multimode plate reader (Molecular Devices). Experiments were performed in triplicate and the anisotropy values fitted using Graphpad Prism software.

Fluorescence polarization on-DNA

From 1 µM solutions, the A12-LNA and the B12-DNA conjugated complementary strands were annealed in a 1:1.5 ratio in presence of PBS (pH 7.4). The annealing was performed at 65 °C for 4 minutes and then left cooling down at RT for ~0.5 hour. The dilution series were done in a non-binding black 384-well microplate (Greiner Bio On.). In a final volume of 30 µL, 50 nM of the fluorophore-labelled double stranded LNA were incubated with a 1:1 dilution series of TYRP1 in PBS pH 7.4. The fluorescence anisotropy was measured on a Spectra Max Paradigm multimode plate reader (Molecular Devices). Experiments were performed in triplicate and the anisotropy values fitted using Graphpad Prism software.

ELISA

The Enzyme-Linked ImmunoSorbent Assay (ELISA) was performed following already described procedures [8]. Nunc MaxiSorp™ ELISA stripes (ThermoFisher) were incubated over night at 4 °C with 100 µL of 100 nM solution in PBS of protein (i.e., TYR and TYRP1). The supernatant was removed and 200 µL of a 4% solution of Milk powder in PBS (M-PBS) was used as blocking agent for 30-45 minutes. Wells were then washed three times with 200 µL PBS and dried. 50 µL of a pre-made serial dilution of the fluorescein-ligand conjugate was added and incubated for 45 minutes in the dark. Carefully, the supernatant was removed and the wells were quickly washed twice with 200 µL PBS. 100 µL of anti-fluorescein IgG (200 nM) in 2% M-PBS were added and incubated for 45 minutes. The supernatant was removed and wells washed three times with 200 µL PBS. 100 µL of a solution of 1:1000 diluted enzymelinked protein (i.e., proteinA-HRP) in 2% M-PBS was added and incubated for 45 minutes in the dark. The supernatant was removed and wells washed three times with 200 µL of a 0.1% solution of Tween 20 in PBS and three times with PBS. Finally, 60 µL of 3,3',5,5'-tetramethylbenzidine (TMB) was added to each well and left for 10 to 50 seconds at room temperature developing in the dark until formation of a visible intense blue. The reaction was then quenched upon addition of 30 µL of 1 M H₂SO_{4(aq)}. Absorbance at 450 nm and 620 nm were measured with Spectra Max Paradigm multimode plate reader (Molecular Devices) and values were fitted using Graphpad Prism software.

Cell culture

B16F10 melanoma cell line was kindly provided by the group of Michael Detmar (Swiss Federal Institute of Technology, Zurich, Switzerland). Cells were grown according to the manufacturer's protocol.

Flow Cytometry

Adherent B16F10 cells cultured in T-150 flasks were detached with 2 mM EDTA. Resuspended cells were counted, centrifuged, and resuspended in FACS buffer (2 mM EDTA + 0.5% BSA in PBS, filtered solution) to reach a concentration of 2.5 mio/mL. In 96-well plate (Greiner Bio On.), 500.000 cells were incubated with 10 μ M solutions of fluorescein linked ligands in FACS buffer. After 60 minutes, 1x wash was performed and then cells were incubated with Cy5-conjugated anti-Fluorescein IgG (100 nM) for 60 minutes. Cells were 2x washed and sorted by FACS (CytoFLEX, BeckmanCoulter, Brea, CA) and analyzed using FlowJo software (FlowJo, Ashland, OR).

Fluorescence polarization assay A26-B389

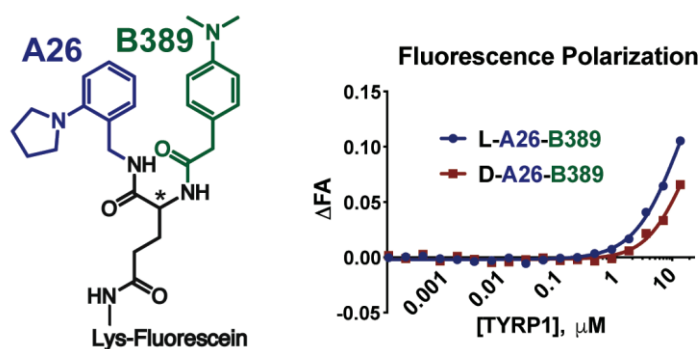


Figure S1. Fluorescence polarization binding assay of FI-Lys-L-Gln-A26-B389 and FI-Lys-D-Gln-A26-B389 in presence of TYRP1. The complete structure and synthetic procedures are described below.

TYR-based enzymatic assays

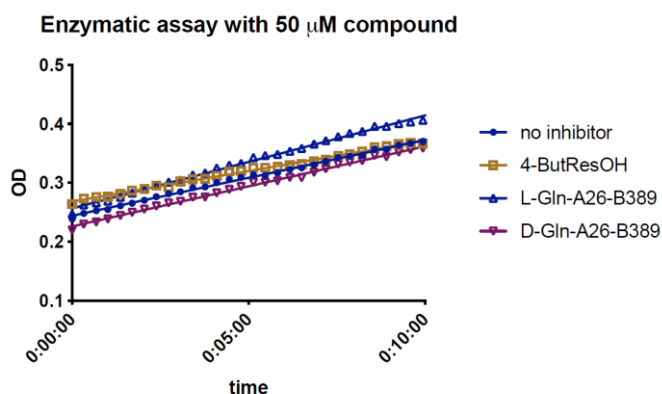


Figure S2. The enzymatic activity of human-TYR was measured with or without inhibitors. 4-butylresorcinol was used as positive control. Inhibitors were incubated at a fixed concentration (50 μM) at pH 6.8.

Enzymatic assay with 50 μM compound

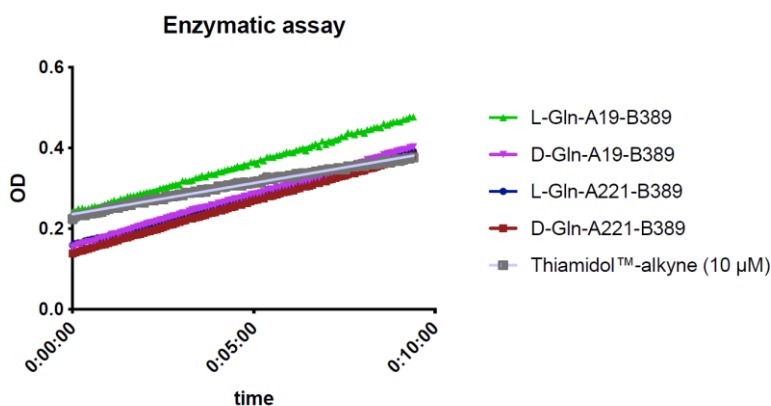


Figure S3. The enzymatic activity of human-TYR was measured in presence of different compounds. Thiamidol™-alkyne was used as positive control. Compounds were incubated at a fixed concentration (50 μM , Thiamidol™-alkyne only 10 μM) at pH 6.8.

Concentration Inhibitors

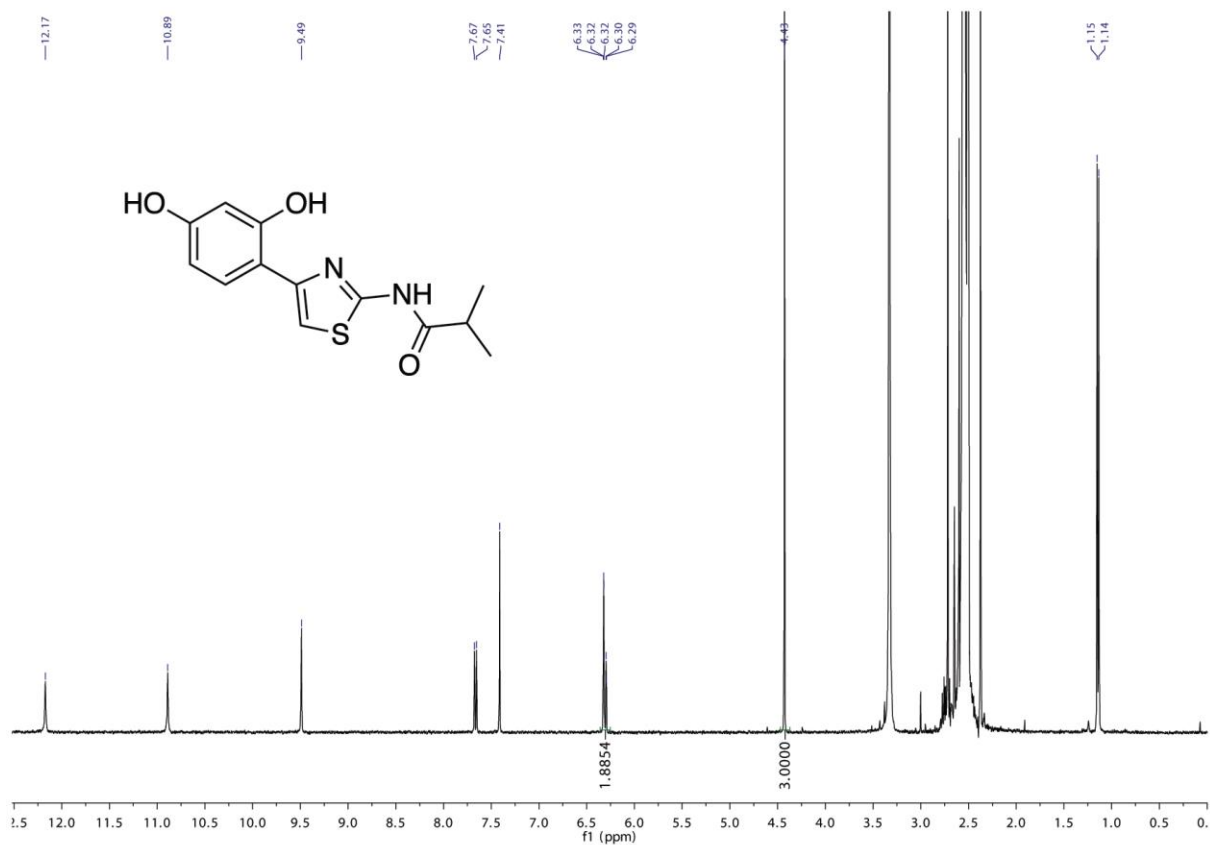
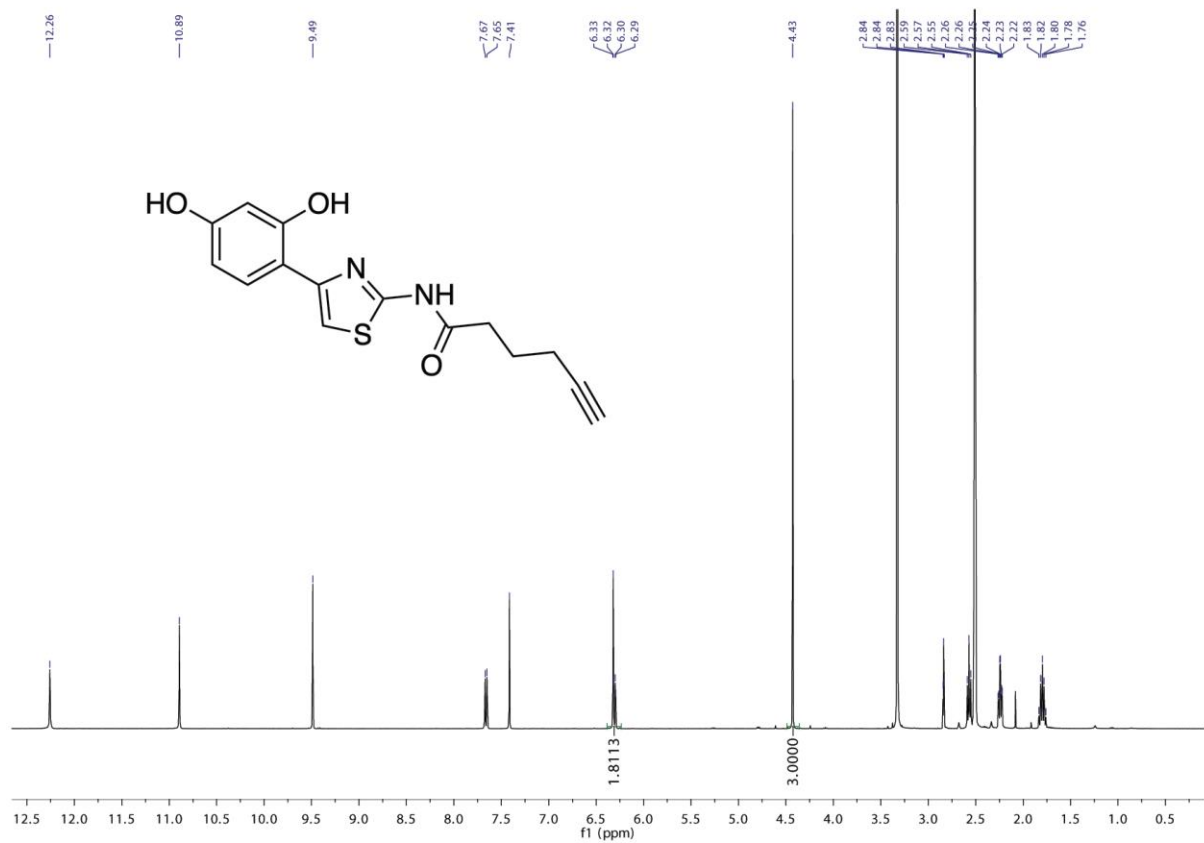


Figure S4. Concentration of Thiamidol™ and Thiamidol™-alkyne was measured *via* NMR in presence of a known concentration of nitromethane (CH₃NO₂, δ 4.43, 3H).

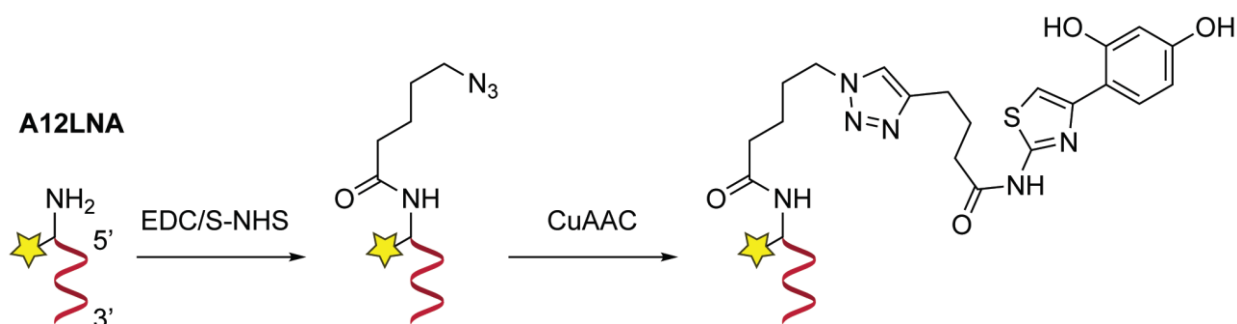
Synthesis on-DNA

Hits compounds selected from affinity maturation 2+1 selections were synthesized and validated on DNA-LNA hybrid. Two complementary oligonucleotides were used:

5' – GGA TGG CTA CTA - 3' AmMC6 (B12-DNA)

3' – CCT ACC GAT GA(dT Fluorescein) - 5' AmMC6 (A12-LNA)

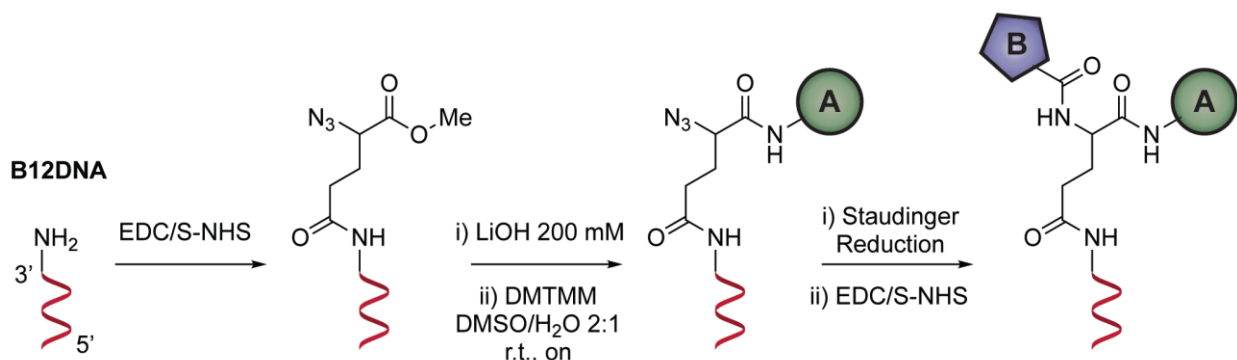
A12LNA synthetic procedure



on-DNA amide bond formation: in a 1.5 mL Eppendorf tube 42 μ L (100 mM DMSO, 85eq.) of the desired carboxylic acid were mixed for 30 minutes with 90 μ L DMSO, 20 μ L (S-NHS 100 mM DMSO/H₂O 2:1, 40eq.), 42 μ L (EDC 100 mM DMSO, 84 eq.). In a separate well 50 μ L DNA (1 nmol/ μ L, 1eq.) in H₂O were mixed with 50 μ L of TEA buffer (100 mM, pH=10). The activated carboxylic acid solution was added to the oligo solution and stirred at room temperature over-night. The reacted DNA was precipitated by adding 30 μ L (NaCl 5 M) and 30 μ L (AcOH/NaAcO- 3 M, pH = 4.7) followed by 900 μ L EtOH absolute. The precipitated DNA was kept at -20 °C for 4hours and centrifuged a 4 °C for 30 mins at 16.1 krpm. The supernatant was discarded and the pellet dried under vacuum.

on-DNA CuAAC click reaction: to 2.5 μ L DNA (0.3 nmol), 30 μ L (Borate buffer pH = 9.5) followed by 2.5 μ L CuSO₄ (5 mM in H₂O, 42 eq) and 10 μ L of the desired alkyne (10 mM in DMSO, 100 eq) were added. The reaction was then started by the addition of 2.5 μ L sodium ascorbate (5 mM in H₂O, 42 eq) and stirred at rt on. The reacted DNA was precipitated by adding 12 μ L 5 M NaCl and 240 μ L EtOH. The precipitated DNA was kept at -20 °C for 4 hours and centrifuged a 4 °C for 30 mins at 16.1 krpm. The supernatant was discarded and the pellet dried under vacuum.

B12DNA synthetic procedure



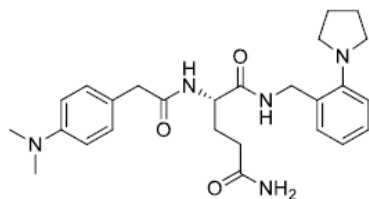
On-DNA methylester deprotection: In a 2 mL Eppendorf tube, DNA (50 nmol) was dissolved in 250 μ L H₂O, 250 μ L LiOH (200 mM) were added and the resulting mixture was stirred at 25 °C for 4 h. The reaction was monitored by LC-MS. After the reaction was completed, LiOH was quenched by adding 16 μ L AcOH (3 M). The reacted DNA was precipitated by adding 50 μ L 5 M NaCl and 1375 μ L EtOH. The precipitated DNA was kept at -20°C for 4 hours and centrifuged at 4°C for 30 mins at 16.1 krpm. The supernatant was discarded and the pellet dried in a speed vacuum machine.

on-DNA Reverse amide bond reactions (acid attached on-DNA): in a 2 mL Eppendorf tube DNA (50 nmol, 1 eq) was dissolved in 40 μ L H₂O. 137 μ L of MOPS buffer (100 mM MOPS, 1 M NaCl, pH= 7.0) was added, followed by 30 μ L of DMTMM (500 mM in MOPS buffer, 300eq). The resulting mixture was stirred at 30 °C for 30 min. 75 μ L (100 mM, 150 eq) of the desired amine was added to the activation solution and stirred at 30 °C for 16 hours. The reacted DNA was precipitated by adding 28 μ L 5 M NaCl and 775 μ L EtOH. The precipitated DNA was kept at -20°C for 4hours and centrifuged at 4°C for 30mins at 16.1 krpm. The supernatant was discarded and the pellet dried in a speed vacuum machine.

on-DNA Staudinger reduction: in a 2 mL Eppendorf tube DNA (1-100 nmol, 1 eq) was dissolved in 100 μ L of TCEP buffer (30 mM TCEP, in 500 mM TRIS*HCl, pH = 7.4). The resulting mixture was stirred at 30 °C for 4 hours. Reaction completion was monitored by LC-MS. The reacted DNA was precipitated by adding 25 μ L 5 M NaCl and 375 μ L EtOH. The precipitated DNA was kept at -20°C for 4hours and centrifuged a 4°C for 30 mins at 16.1 krpm. The supernatant was discarded and the pellet dried under vacuum.

Synthetic procedures

L-Gln-A26-B389

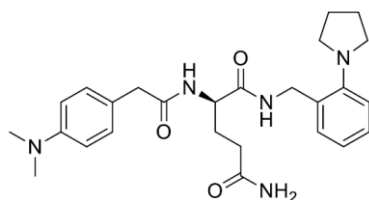


(S)-2-(2-(4-(dimethylamino)phenyl)acetamido)-N1-(2-(pyrrolidin-1-yl)benzyl)pentanediamide: commercially available Rink amide resin (0.02048 g, 0.1 mmol) was swollen in N,N-dimethylformamide (20 mL) for 2 h in a syringe provided with a filter pad. A solution of Fmoc-L-glutamic acid 5-allyl ester (4.0 equiv., 0.4 mmol), DIPEA (4.0 equiv., 0.4 mmol) and HATU (4.0 equiv., 0.4 mmol) in N,Ndimethylformamide (4 mL) was added to the syringe, allowed to react for 16 h and washed with N,N-dimethylformamide (5 \times 4 mL \times 1 min). The O-allyl deprotection was performed using palladium-tetrakis(triphenylphosphine) (Pd(PPh₃)₄, 0.25 equiv., 0.025 mmol) and phenylsilane (PhSiH₃, 24 equiv., 2.4 mmol) in dichloromethane (4 mL) for 2 h. After washing with dichloromethane (5 \times 4 mL \times 1 min) and N,Ndimethylformamide (5 \times 4 mL \times 1 min), a solution of (2-(pyrrolidin-1-yl)phenyl)methanamine (4 equiv., 0.4 mmol), DIPEA (8 equiv., 0.8 mmol) and HATU (4.0 equiv., 0.4 mmol) in N,N-dimethylformamide (4 mL) was added to the syringe and allowed to react for 16 h and washed with N,N-dimethylformamide (5 \times 4 mL \times 1 min). The Fmoc group was removed using a solution of 20% piperidine in N,Ndimethylformamide for 20 min and then washed with N,N-dimethylformamide (5 \times 4 mL \times 1 min). The coupling to the 2-(4-

(dimethylamino)phenyl)acetic (4 equiv., 0.4 mmol) was performed using the same conditions reported before. After washing with *N,N*-dimethylformamide (5 × 4 mL × 1 min) the resin was cleaved using a solution of TFA:TIPS:mqH₂O (95:2.5:2.5, v/v) for 1 h at room temperature. The so-obtained solution was collected in a round-bottom flask, dried under vacuum and purified over a RP HPLC (Synergi RP Polar, 5% MeCN in 0.1% aq. TFA to 80% over 14 min). After lyophilization the final compound was collected as a white solid; ¹H-NMR (400 MHz, DMSO-*d*₆) δ 8.25 (t, *J* = 5.6 Hz, 1H), 8.12 (d, *J* = 8.0 Hz, 1H), 7.31 (s, 1H), 7.22 – 7.14(m, 2H), 7.12 (d, *J* = 8.7 Hz, 2H), 6.98 (d, *J* = 8.0 Hz, 1H), 6.89 (t, *J* = 7.4 Hz, 1H), 6.80 (s, 1H), 6.69 (dd, *J* = 9.2, 2.4 Hz, 2H), 4.31 (d, *J* = 5.7 Hz, 2H), 4.30 – 4.27 (m, 1H), 3.39 (s, 2H), 3.11 (td, *J* = 8.8, 2.6 Hz, 4H), 2.91 – 2.88 (m, 6H), 2.12 (ddd, *J* = 8.1, 6.2, 3.4 Hz, 2H), 1.99 – 1.93 (m, 1H), 1.93 – 1.88 (m, 4H), 1.88 – 1.75 (m, 1H). ¹³C-NMR (101, MHz, DMSO-*d*₆) δ 24.9 (2 × CH₂), 28.5 (CH₂), 32.0 (CH₂), 39.8 (2 × CH₃), 40.8 (CH₂), 41.7 (CH₂), 51.5 (2 × CH₂), 52.9 (CH), 112.9 (2 × Ar), 116.8 (Ar), 120.8 (Ar), 124.3 (Ar), 127.7 (Ar), 128.7 (Ar), 129.8 (Ar), 130.0 (2 × Ar), 148.6 (Ar), 149.6 (Ar), 171.3 (CONH₂), 171.9 (CONH), 174.1 (CONH).

HRMS (ES) calculated for [M+H]⁺ (*m/z*): 466.2813, found 466.2308.

D-Gln-A26-B389

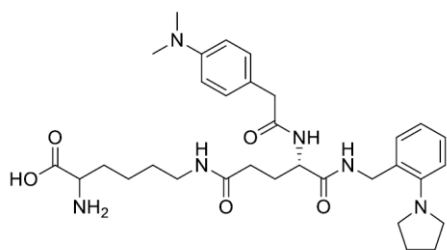


(*R*)-2-(2-(4-(dimethylamino)phenyl)acetamido)-N1-(2-(pyrrolidin-1-yl)benzyl)pentanediamide: commercially available Rink amide resin (0.02048 g, 0.1 mmol) was swollen in *N,N*-dimethylformamide (20 mL) for 2 h in a syringe provided with a filter pad. A solution of Fmoc-D-glutamic acid 5-allyl ester (4.0 equiv., 0.4 mmol), DIPEA (4.0 equiv., 0.4 mmol) and HATU (4.0 equiv., 0.4 mmol) in *N,N*-dimethylformamide (4 mL) was added to the syringe, allowed to react for 16 h and washed with *N,N*-dimethylformamide (5 × 4 mL × 1 min). The *O*-allyl deprotection was performed using palladium-tetrakis(triphenylphosphine) (Pd(PPh₃)₄, 0.25 equiv., 0.025 mmol) and phenylsilane (PhSiH₃, 24 equiv., 2.4 mmol) in dichloromethane (4 mL) for 2 h. After washing with dichloromethane (5 × 4 mL × 1 min) and *N,N*-dimethylformamide (5 × 4 mL × 1 min), a solution of (2-(pyrrolidin-1-yl)phenyl)methanamine (4 equiv., 0.4 mmol), DIPEA (8 equiv., 0.8 mmol) and HATU (4.0 equiv., 0.4 mmol) in *N,N*-dimethylformamide (4 mL) was added to the syringe and allowed to react for 16 h and washed with *N,N*-dimethylformamide (5 × 4 mL × 1 min). The Fmoc group was removed using a solution of 20% piperidine in *N,N*-dimethylformamide for 20 min and then washed with *N,N*-dimethylformamide (5 × 4 mL × 1 min). Thus, the coupling to the 2-(4-(dimethylamino)phenyl)acetic (4 equiv., 0.4 mmol) was performed using the same conditions reported before. After washing with *N,N*-dimethylformamide (5 × 4 mL × 1 min) the resin was cleaved using a solution of TFA:TIPS:mqH₂O (95:2.5:2.5, v/v) for 1 h at room temperature. The so-obtained solution was collected in a round-bottom flask, dried under vacuum and purified over a RP HPLC (Synergi RP Polar, 5% MeCN in 0.1% aq. TFA to 80% over 14 min). After lyophilization the final compound was collected as a white solid; ¹H NMR (400 MHz, DMSO-*d*₆) δ 1.76-1.84 (m, 1H, CH₂), 1.89-1.92 (m, 4H, 2 × CH₂), 1.94-1.99 (m, 1H, CH₂), 2.10-2.15 (m, 2H, CH₂), 2.90 (6, 6H, 2 ×

CH₃), 3.08-3.14 (m, 4H, 2 × CH₂), 3.39 (s, 2H, CH₂), 4.27-4.29 (m, 1H, CH), 4.31 (d, *J* = 5.7 Hz, 2H, CH₂), 6.68-6.71 (m, 2H, Ar), 6.80 (s, 1H, CONH₂), 6.87-6.91 (m, 1H, Ar), 6.97-6.99 (m, 1H, Ar), 7.12 (d, *J* = 8.7 Hz, 2H, Ar), 7.15-7.20 (m, 2H, Ar), 7.31 (s, 1H, CONH₂), 8.12 (d, *J* = 8.0 Hz, 1H, CONH), 8.25 (t, *J* = 5.6 Hz, 1H, CONH); ¹³C NMR (101, MHz, DMSO-*d*₆) δ 24.91 (2 × CH₂), 28.55 (CH₂), 32.00 (CH₂), 39.77 (2 × CH₃), 40.79 (CH₂), 41.69 (CH₂), 51.55 (2 × CH₂), 52.91 (CH), 112.92 (2 × Ar), 116.78 (Ar), 120.85 (Ar), 124.34 (Ar), 127.70 (Ar), 128.74 (Ar), 129.77 (Ar), 129.96 (2 × Ar), 148.64 (Ar), 149.64 (Ar), 171.29 (CONH₂), 171.93 (CONH), 174.11 (CONH).

HRMS (ES) calculated for [M+H]⁺ (*m/z*): 466.2813, found 466.2308.

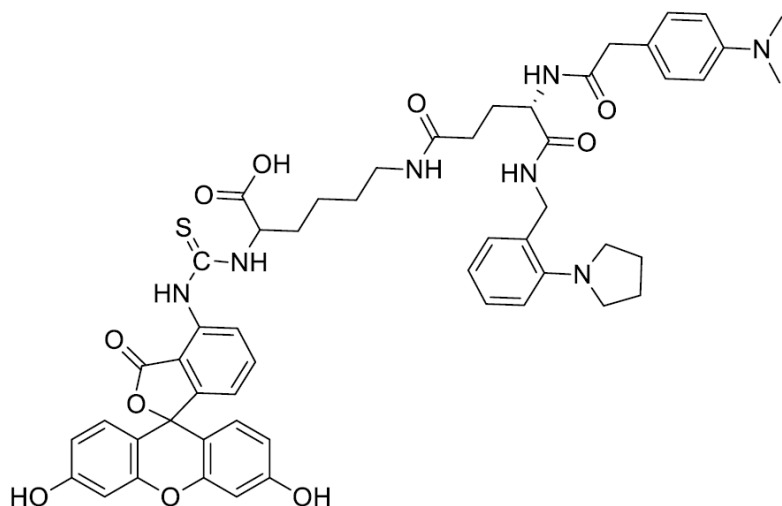
Lys-L-Gln-A26-B389



2-amino-6-((S)-4-(2-(4-(dimethylamino)phenyl)acetamido)-5-oxo-5-((2-(pyrrolidin-1-yl)benzyl)amino)pentanamido)hexanoic acid: commercially available Fmoc-Lys(Boc)-Wang resin (0.25 mmol) was swollen in *N,N*-dimethylformamide (10 mL) for 2 h inside a syringe provided with a filter pad. The Fmoc group was removed using a solution of 20% piperidine in *N,N*-dimethylformamide for 20 min and after washing the resin with *N,N*-dimethylformamide (5 × 10 mL × 1 min), a solution of Fmoc-L-glutamic acid 5-allyl ester (4.0 equiv., 1 mmol), DIPEA (8.0 equiv., 2 mmol) and HATU (4.0 equiv., 1 mmol) in *N,N*-dimethylformamide (10 mL) was added to the syringe, allowed to react for 16 h and washed with *N,N*-dimethylformamide (5 × 10 mL × 1 min). The *O*-allyl deprotection was performed using palladium-tetrakis(triphenylphosphine) (Pd(PPh₃)₄, 0.25 equiv., 0.0625 mmol) and phenylsilane (PhSiH₃, 24 equiv., 6 mmol) in dichloromethane (20 mL) for 2 h. After washing with dichloromethane (5 × 10 mL × 1 min) and *N,N*-dimethylformamide (5 × 10 mL × 1 min) a solution of the (2-(pyrrolidin-1-yl)phenyl)methanamine (4 equiv., 1 mmol), DIPEA (8 equiv., 2 mmol) and HATU (4.0 equiv., 2 mmol) in *N,N*-dimethylformamide (10 mL) was added to the syringe and allowed to react for 16 h. After washing with *N,N*-dimethylformamide (5 × 10 mL × 1 min) the Fmoc group was removed and the coupling to the 2-(4-(dimethylamino)phenyl)acetic acid (4 equiv., 1.0 mmol) was performed using the same conditions reported before. After washing with *N,N*-dimethylformamide (5 × 10 mL × 1 min) the resin was cleaved using a solution of TFA:TIPS:mqH₂O (95:2.5:2.5, *v/v*) for 1 h at room temperature. The so-obtained solution was collected in a round-bottom flask, dried under vacuum and purified over a RP-HPLC (Synergi RP Polar, 5% MeCN in 0.1% aq. TFA to 100% over 14 min). After lyophilization the final compound was collected as a white solid.

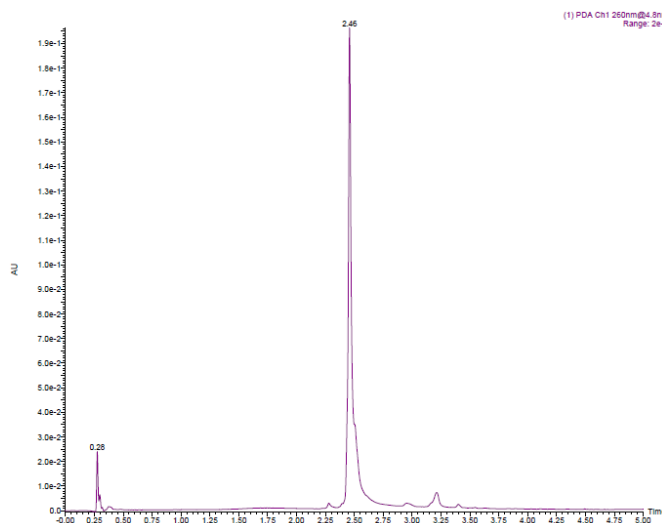
HRMS (ES) calculated for [M+H]⁺ (*m/z*): 595.3603, found 595.3643.

FI-Lys-L-Gln-A26-B389

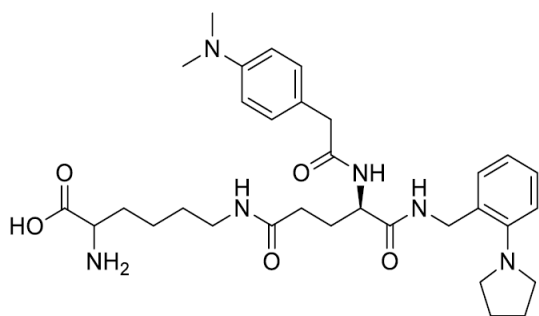


To a solution of Lys-L-Gln-A26-B389 (2.8 mg, 1 equiv.) in dimethyl sulfoxide (100 μ L) was added DIPEA (20 μ L) and a solution of commercially available fluorescein isothiocyanate (3.668 mg, 2.0 equiv.) in dimethyl sulfoxide (100 μ L). After stirring for 30 min in the dark, the reaction was diluted with a solution of DMSO:mqH₂O (1:1 v:v,) and purified over a RP HPLC (Synergi RP Polar, 5% MeCN in 0.1% aq. TFA to 100% over 14 min). The fractions containing the product, identified by mass spectrometry, were collected and then lyophilized to give the title compound as a yellow powder.

HRMS (ES) calculated for [M+H]⁺ (*m/z*): 984.3961, found 984.3460.



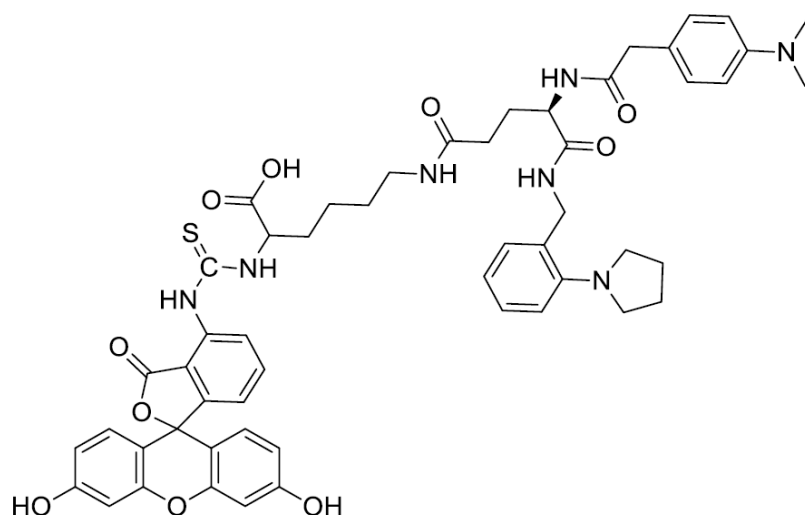
Lys-D-Gln-A26-B389



2-amino-6-((*R*)-4-(2-(4-(dimethylamino)phenyl)acetamido)-5-oxo-5-((2-(pyrrolidin-1-yl)benzyl)amino)pentanamido)hexanoic acid: commercially available Fmoc-LysBoc-Wang resin (0.25 mmol) was swollen in *N,N*-dimethylformamide (10 mL) for 2 h inside a syringe provided with a filter pad. The Fmoc group was removed using a solution of 20% piperidine in *N,N*-dimethylformamide for 20 min and after washing the resin with *N,N*-dimethylformamide (5×10 mL \times 1 min), a solution of Fmoc-D-glutamic acid 5-allyl ester (4.0 equiv., 1 mmol), DIPEA (8.0 equiv., 2 mmol) and HATU (4.0 equiv., 1 mmol) in *N,N*-dimethylformamide (10 mL) was prepared, added to the syringe, allowed to react for 16 h and washed with *N,N*-dimethylformamide (5×10 mL \times 1 min). The *O*-allyl deprotection was performed using palladium-tetrakis(triphenylphosphine) ($\text{Pd}(\text{PPh}_3)_4$) (0.25 equiv., 0.0625 mmol) and phenylsilane (PhSiH_3) (24 equiv., 6 mmol) in dichloromethane (20 mL) for 2 h. After washing with dichloromethane (5×10 mL \times 1 min) and *N,N*-dimethylformamide (5×10 mL \times 1 min) a solution of the (2-(pyrrolidin-1-yl)phenyl)methanamine (4 equiv., 1 mmol), DIPEA (8 equiv., 2 mmol) and HATU (4.0 equiv., 2 mmol) in *N,N*-dimethylformamide (10 mL) was added to the syringe and allowed to react for 16 h. After washing with *N,N*-dimethylformamide (5×10 mL \times 1 min) the Fmoc group was removed and the coupling to the 2-(4-(dimethylamino)phenyl)acetic (4 equiv., 1.0 mmol) performed using the same conditions reported before. After washing with *N,N*-dimethylformamide (5×10 mL \times 1 min) the resin was cleaved using a solution of TFA:TIPS:mqH₂O (95:2.5:2.5, *v/v*) for 1 h at room temperature. The so-obtained solution was collected in a round-bottom flask, dried under vacuum and purified over a reversed-phase HPLC (Synergi RP Polar, 5% MeCN in 0.1% aq. TFA to 100% over 14 min). After lyophilization the final compound was collected as a white solid.

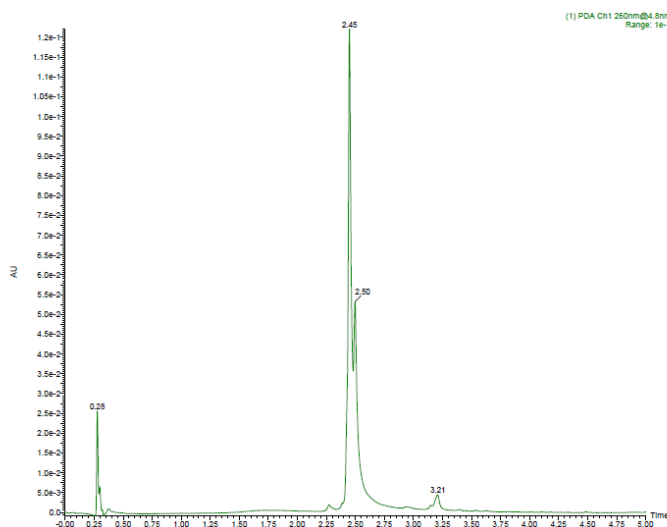
HRMS (ES) calculated for $[\text{M}+\text{H}]^+$ (*m/z*): 595.3603, found 595.3448.

FI-Lys-D-Gln-A26-B389

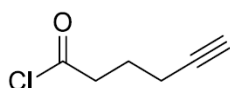


To a solution of Lys-D-Gln-A26-B389 (3.3 mg, 1 equiv.) in dimethyl sulfoxide (100 μ L) was added DIPEA (20 μ L) and a solution of commercially available fluorescein isothiocyanate (4.3210 mg, 2.0 equiv.) in dimethyl sulfoxide (100 μ L). After stirring for 30 min in the dark, the reaction was diluted with a solution of DMSO:mqH₂O (1:1 *v:v*) and purified over a reversed-phase HPLC (Synergi RP Polar, 5% MeCN in 0.1% aq. TFA to 100% over 14 min). The fractions containing the product identified by mass spectrometry, collected and then lyophilized to give the title compound as a yellow powder.

HRMS (ES) calculated for $[M+H]^+$ (m/z): 984.3961, found 984.3598.



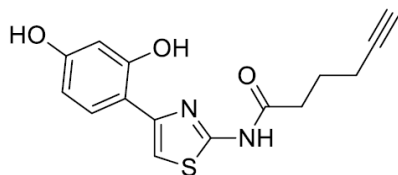
Hex-5-ynoic chloride



To a stirring solution of 5-hexynoic acid (1.0 equiv.) in dichloromethane (0.1 M) and in presence of a catalytic amount of *N,N*-dimethylformamide, a 2.0 M solution of oxalyl chloride in dichloromethane (1.1 equiv.) was added dropwise at 0 $^{\circ}$ C. After 1 h, the reaction was completed, evaporated under

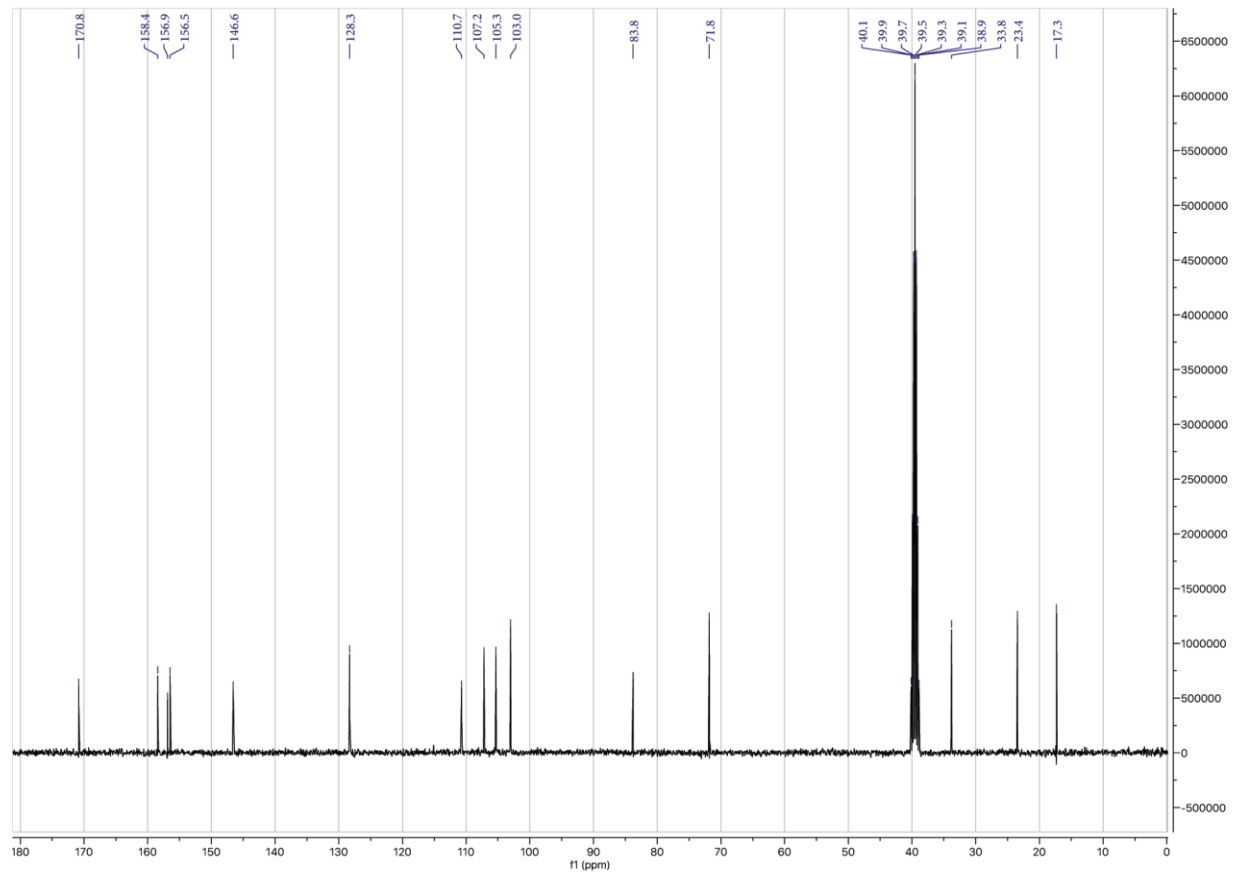
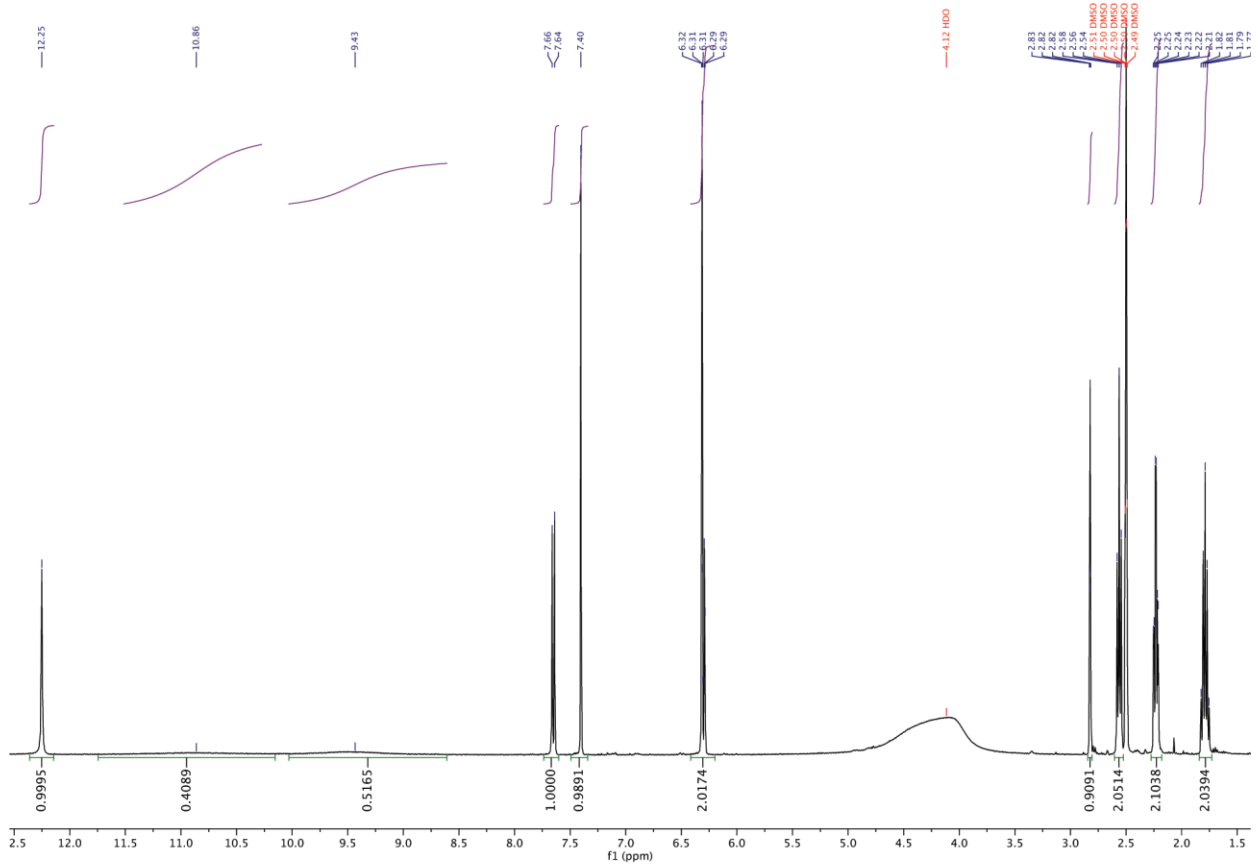
vacuum and the so obtained red precipitate resuspended in a solution of tetrahydrofuran, in presence of a catalytic amount of pyridine.

ThiamidoTM-alkyne

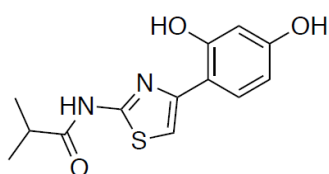


***N*-(4-(2,4-dihydroxyphenyl)thiazol-2-yl)hex-5-ynamide**: to a stirring solution of 4-(2-aminothiazol-4-yl)benzene-1,3-diol (1.0 equiv.) in tetrahydrofuran (0.1 M) the fresh solution of hex-5-ynoyl chloride (from 3.0 to 5.0 equiv. depending on the stability of the chloride) was added dropwise. The reaction was controlled through LC-MS analysis until the formation of a tri-functionalized derivative. After 16 h, the reaction mixture was treated with a 33 % solution of methylamine in absolute ethanol (8 M, 10 equiv.). After 2 h, the reaction was dried under vacuum, resuspended in the proper amount of CH₃CN:mqH₂O and purified over a Purification Systems (2% MeCN in 0.1% aq. TFA over 10 min, 2% MeCN in 0.1% aq. TFA to 70% over 30 min). The fractions containing the product identified by mass spectrometry, were collected and then lyophilized to give the title compound as a white solid; ¹H NMR (400 MHz, DMSO-*d*₆) δ 12.25 (s, 1H), 10.86 (s, 1H), 9.43 (s, 1H), 7.65 (d, *J* = 8.3 Hz, 1H), 7.40 (s, 1H), 6.42 – 6.20 (m, 2H), 2.82 (t, *J* = 2.6 Hz, 1H), 2.56 (t, *J* = 7.4 Hz, 2H), 2.23 (td, *J* = 7.1, 2.7 Hz, 2H), 1.79 (p, *J* = 7.2 Hz, 2H). ¹³C NMR (101 MHz, DMSO) δ 170.6, 158.2, 156.7, 156.2, 146.3, 128.1, 110.5, 107.0, 105.1, 102.8, 83.6, 71.6, 33.6, 23.2, 17.1.

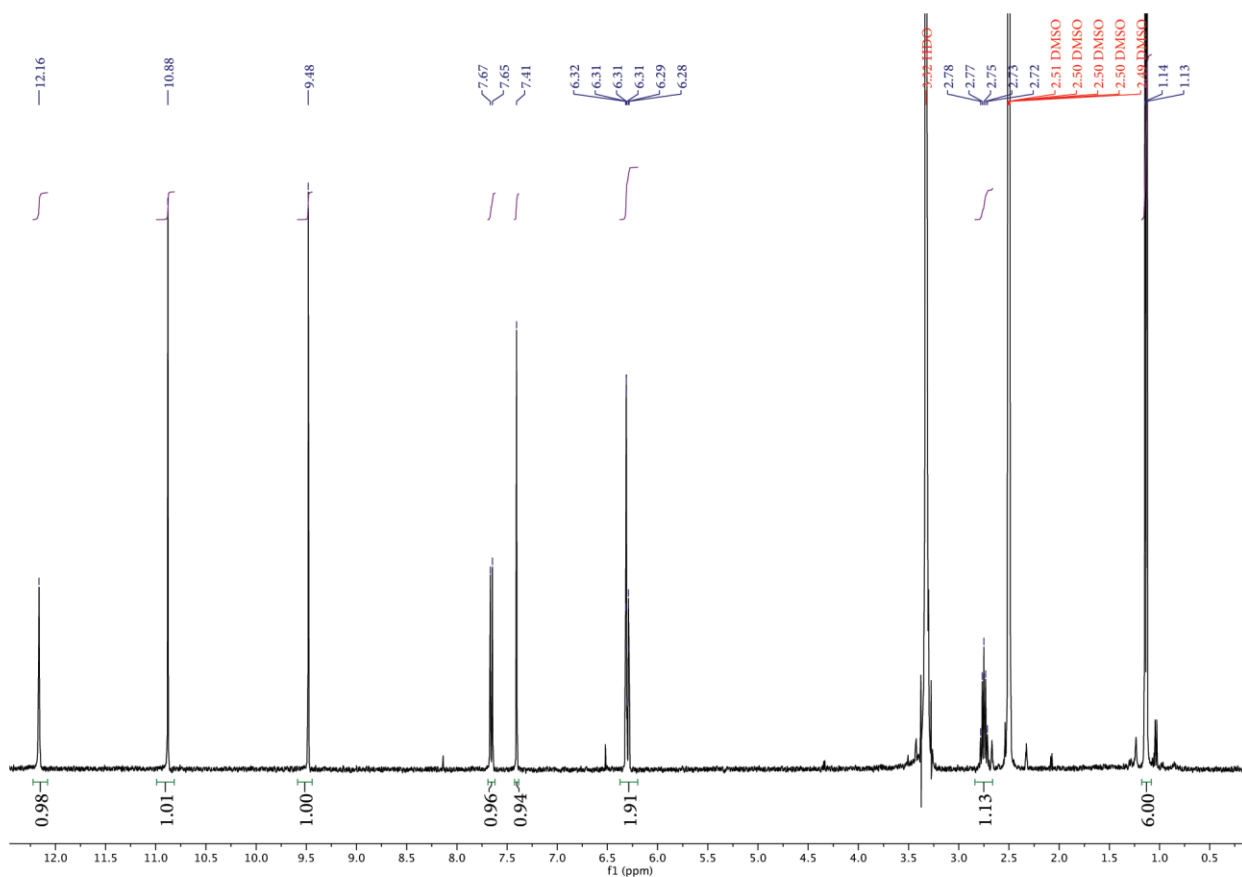
HRMS (ES) calculated for [M+H]⁺ (*m/z*): 303.0803, found 303.0596.



Thiamido™



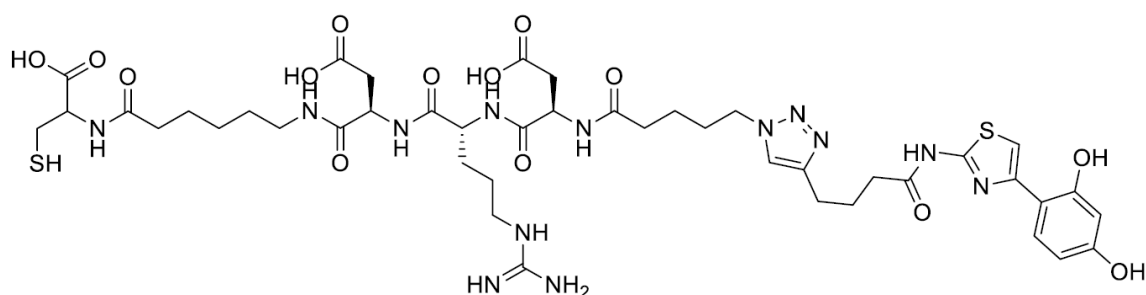
N-(4-(2,4-dihydroxyphenyl)thiazol-2-yl)isobutyramide: to a stirring solution of 4-(2-aminothiazol-4-yl)benzene-1,3-diol (1.0 equiv.) in tetrahydrofuran (0.1 M) the commercially available isobutyryl chloride (5.0 equiv.) was added drop-wise in presence of pyridine (0.1 equiv.). The reaction was controlled through LC-MS analysis until the formation of a tri-functionalized derivative. After 16 h, the reaction mixture was treated with a 33 % solution of methylamine in absolute ethanol (8 M, 10 equiv.). After 2 h, the reaction was dried under vacuum, resuspended in the proper amount of CH₃CN:mqH₂O and purified over a Purification Systems (2% MeCN in 0.1% aq. TFA over 10 min, 2% MeCN in 0.1% aq. TFA to 70% over 30 min). The fractions containing the product identified by mass spectrometry, were collected and then lyophilized to give the title compound as a white solid; ¹H NMR (400 MHz, DMSO-*d*₆) δ 12.16 (s, 1H), 10.88 (s, 1H), 9.48 (s, 1H), 7.66 (d, *J* = 8.3 Hz, 1H), 7.41 (s, 1H), 6.37 – 6.20 (m, 2H), 2.75 (p, *J* = 6.8 Hz, 1H), 1.14 (d, *J* = 6.8 Hz, 6H). NMR data are in full agreement with previously reported values.^[9]



General Procedure on-resin

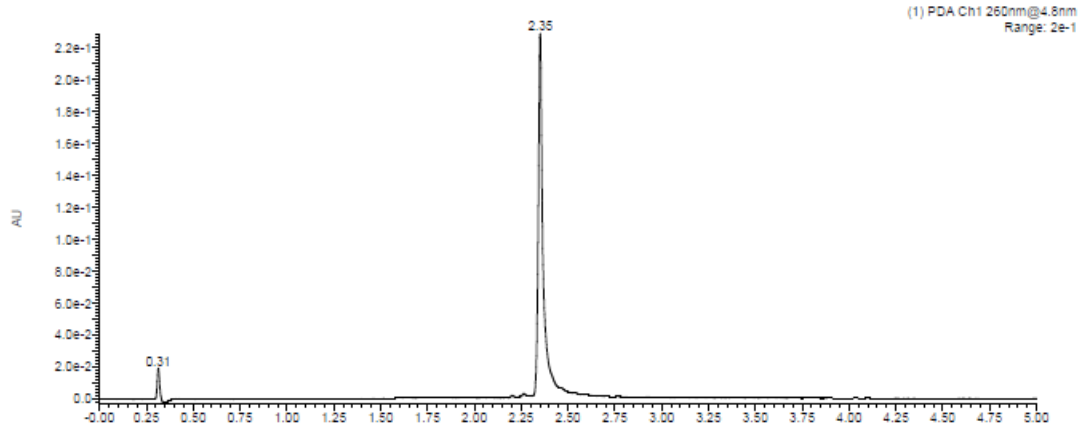
Commercially Fmoc-Cys(Trt) Wang resin (0.7 g, 0.5 mmol) was swollen in *N,N*-dimethylformamide (20 mL) for 1 h inside a syringe provided with a filter pad. The Fmoc group was removed using a solution of 20% piperidine in *N,N*-dimethylformamide for 20 min and then the resin washed with *N,N*-dimethylformamide ($5 \times 20 \text{ mL} \times 1 \text{ min}$). A solution of Fmoc-6-aminocaproic acid (4.0 equiv., 2 mmol), DIPEA (8.0 equiv., 4 mmol) and HATU (4.0 equiv., 2 mmol) in *N,N*-dimethylformamide (20 mL) was prepared, added to the syringe and allowed to react for 2 h. After washing with *N,N*-dimethylformamide ($5 \times 20 \text{ mL} \times 1 \text{ min}$) the Fmoc group was removed using a solution of 20 % piperidine in *N,N*-dimethylformamide. The peptide was extended with Fmoc-Asp(OtBu)-OH, Fmoc-Arg(Pbf)-OH and Fmoc-Asp(OtBu)-OH using the same coupling conditions (HATU/DIPEA equiv.), Fmoc deprotection (20% piperidine in DMF) and washing step as reported before. The resin was split into different parts for the synthesis of the ThiamidolTM-derivatives.

C-C6-DRD-monomer-ThiamidolTM

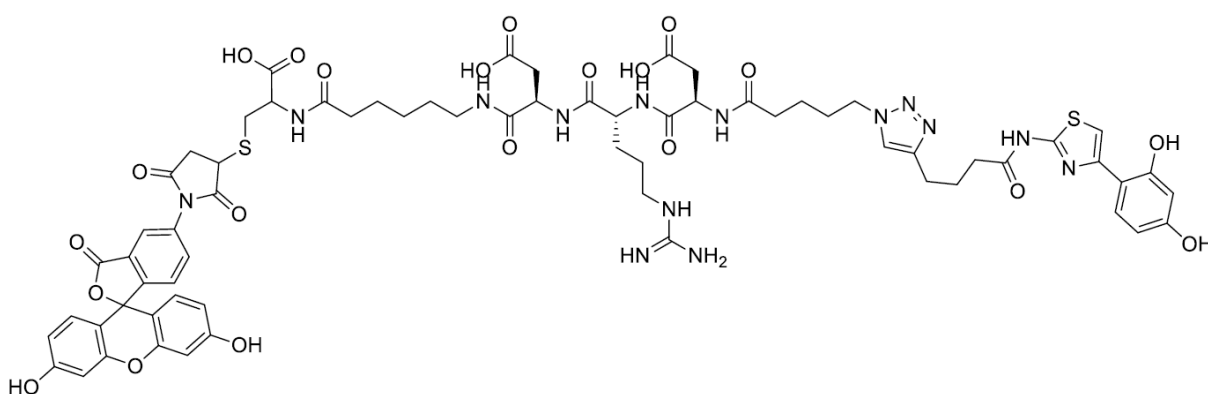


After removing the Fmoc-group, 0.1 mmol of the obtained resin was reacted with a solution of 5-azido pentanoic acid (4 equiv., 0.4 mmol), DIPEA (8.0 equiv., 0.4 mmol) and HATU (4.0 equiv., 0.4 mmol) in *N,N*-dimethylformamide (4 mL) for 2 h. After washing with *N,N*-dimethylformamide ($5 \times 4 \text{ mL} \times 1 \text{ min}$) the Cu-catalysed alkyneazide cycloaddition was performed. The reaction protocol was adjusted from a previously described procedure.^[10] A solution of sodium ascorbate (1 equiv.), 2,6-lutidine (10 equiv.) and DIPEA (10 equiv.) in degassed mqH₂O was added to a solution of CuI (1.0 equiv.) in *N,N*-dimethylformamide. The resulting solution and the alkyne (2.0 equiv.) were added to the resin and allowed to react for 16 h. After washing with *N,N*-dimethylformamide ($5 \times 4 \text{ mL} \times 1 \text{ min}$), 50 mM aq. EDTA solution pH = 8 ($5 \times 4 \text{ mL} \times 1 \text{ min}$), *N,N*-dimethylformamide ($5 \times 4 \text{ mL} \times 1 \text{ min}$) and dichloromethane ($5 \times 4 \text{ mL} \times 1 \text{ min}$), the resin was cleaved using a mixture of TFA (3.30 mL, 82.5 %), *m*-Cresol (200 mL, 5 %), thioanisol (200 mL, 5 %), mq-H₂O (200 mL, 5 %) and TIPS (100 mL, 2.5 %) for 2 h at room temperature and then washed with TFA ($1 \times 1 \text{ mL} \times 1 \text{ min}$). The combined cleavage and washing solutions were added dropwise to ice cold diethyl ether (20 mL), leading to precipitate formation that was collected by centrifugation, washed with ice cold diethyl ether ($3 \times 20 \text{ mL} \times 2 \text{ min}$, 2000 rpm), dried, re-dissolved in mqH₂O:DMSO and treated with Tris(2-carboxyethyl)phosphine hydrochloride (2 equiv.). The solution was injected and purified over a RP-HPLC (Synergi RP Polar, 5% MeCN in 0.1% aq. TFA to 80% over 14 min), the fractions containing the product identified by mass spectrometry collected and then lyophilized to give the title compound as a white solid.

HRMS (ES) calculated for $[M+H]^+$ (m/z): 1048.3980, found 1048.3822.

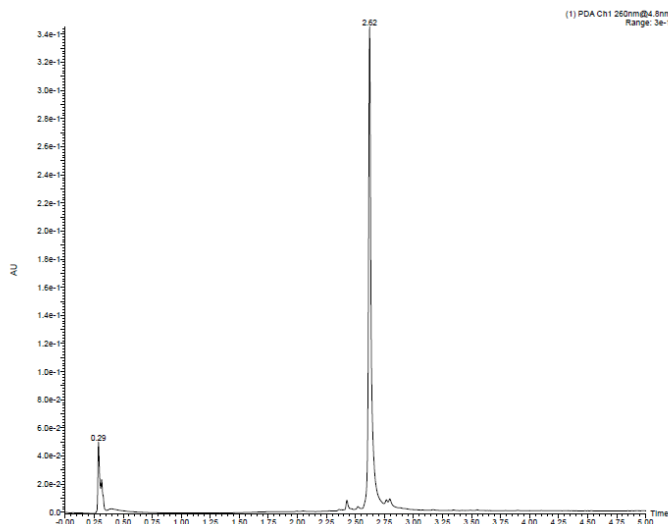


Monomer

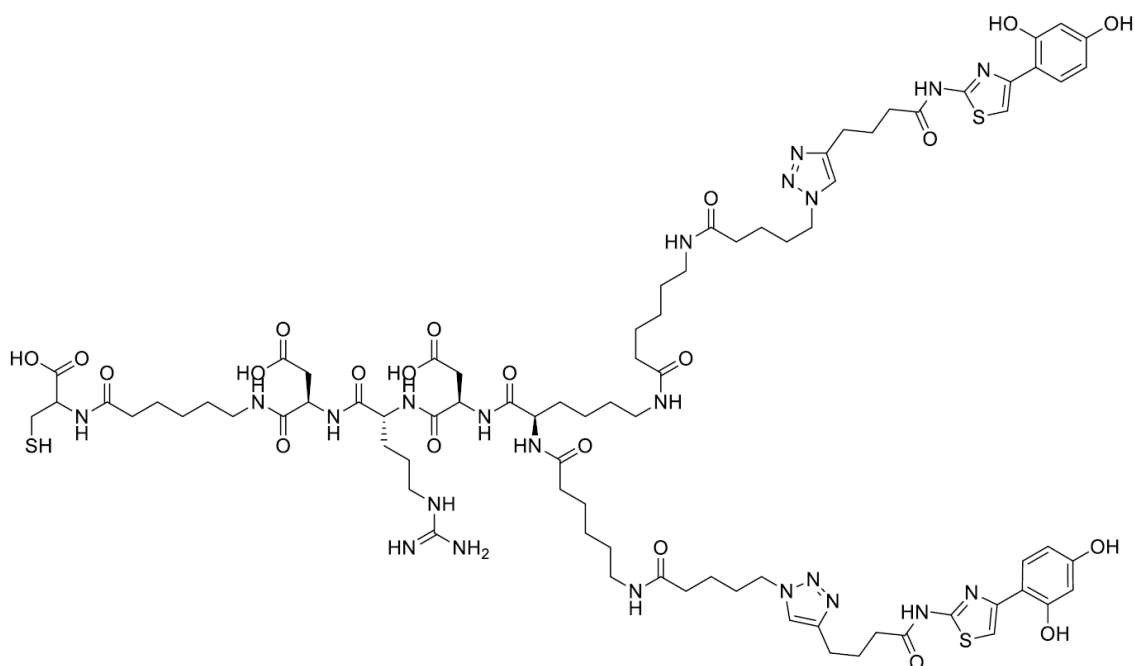


FI-C-C6-DRD-monoThiamidol™: to a solution of C-C6-DRD-monomer-Thiamidol™ (2.0 mg, 1 equiv.) in dimethyl sulfoxide (100 μ L) was added a 0.1 M solution of commercially available fluorescein-5-maleimide (0.81557 mg, 1.0 equiv.) in dimethyl sulfoxide (19.1 μ L). After stirring for 30 min in the dark, the reaction was quenched with the proper volume of DMSO:mqH₂O, injected and purified over a reversed-phase HPLC (Synergi RP Polar, 5% MeCN in 0.1% aq. TFA to 70% over 14 min). The fractions containing the product were identified by mass spectrometry, collected and lyophilized to give the title compound as a yellow solid.

HRMS (ES) calculated for $[M+2H]^+$ (m/z): 1476.4753, found 1476.4056.

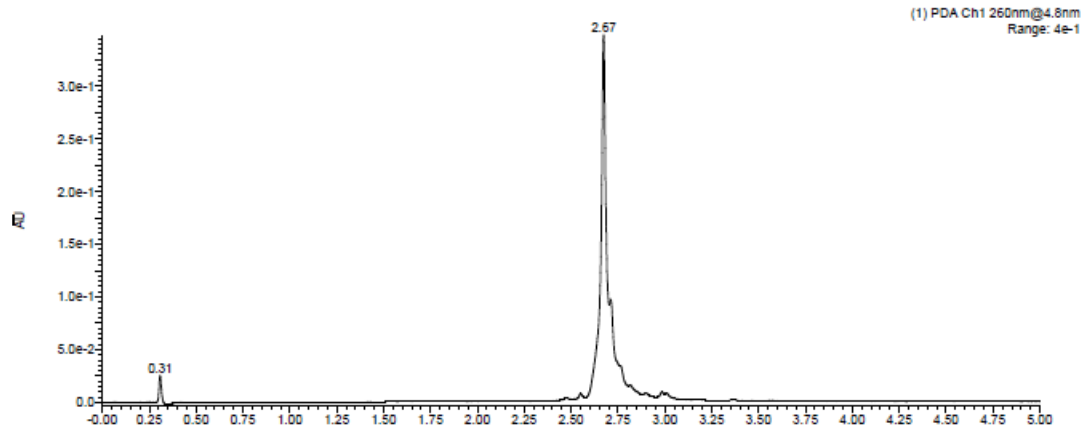


C-C6-DRD-dimer-Thiamidol™

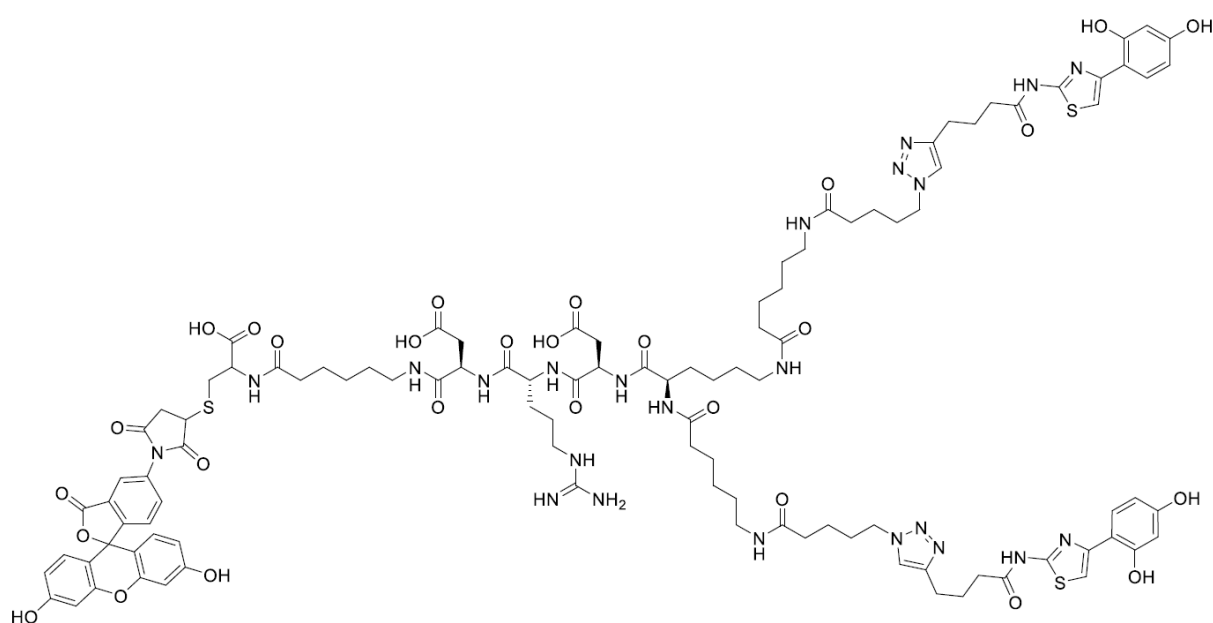


After removing the Fmoc-group, 0.2 mmol of the resin was reacted with a solution of Fmoc-Lys(Fmoc)-OH (4 equiv., 0.8 mmol), DIPEA (8 equiv., 1.6 mmol) and HATU (4.0 equiv, 0.8 mmol) in *N,N*-dimethylformamide (8 mL) for 2 h. After washing with *N,N*-dimethylformamide ($5 \times 8 \text{ mL} \times 1 \text{ min}$) the peptide was extended with Fmoc-6-aminocaproic acid and then capped with 5-azido pentanoic acid fixing the coupling conditions (Fmoc-6-aminocaproic or 5-azido pentanoic and HATU 6 equiv., DIPEA 12 equiv.), using the same Fmoc deprotection conditions (20 % piperidine in DMF) and washing step mentioned before. After the last coupling step, the Cu-catalysed alkyneazide cycloaddition was performed. The reaction protocol was adjusted from a previously described procedure.^[10] A solution of sodium ascorbate (1.5 equiv.), 2,6-lutidine (15 equiv.) and DIPEA (15 equiv.) in degassed mqH₂O was added to a solution of CuI (1.5 equiv.) in *N,N*-dimethylformamide. The resulting solution and the alkyne (3 equiv.) were added to the resin and allowed to react for 16 h. After washing with *N,N*-dimethylformamide ($5 \times 8 \text{ mL} \times 1 \text{ min}$), 50 mM aq. EDTA solution pH = 8 ($5 \times 8 \text{ mL} \times 1 \text{ min}$), *N,N*-dimethylformamide ($5 \times 8 \text{ mL} \times 1 \text{ min}$) and dichloromethane ($5 \times 4 \text{ mL} \times 1 \text{ min}$), the resin was cleaved using a mixture of TFA (6.60 mL, 82.5 %), *m*-Cresol (400 mL, 5 %), thioanisol (400 mL, 5 %), mq-H₂O (400 mL, 5 %) and TIPS (200 mL, 2.5 %) for 2 h at room temperature and washed with TFA ($1 \times 4 \text{ mL} \times 1 \text{ min}$). The combined cleavage and washing solutions were added dropwise to ice cold diethyl ether (40 mL) leading to precipitate formation that was collected by centrifugation, washed again with ice cold diethyl ether ($3 \times 40 \text{ mL} \times 2 \text{ min}$, 2000 rpm), dried, redissolved in mqH₂O:DMSO and treated with Tris(2-carboxyethyl)phosphine hydrochloride (2 equiv.). The solution was injected and purified over a RP HPLC (Synergi RP Polar, 5% MeCN in 0.1% aq. TFA to 80% over 14 min), the fractions containing the product identified by mass spectrometry, collected and lyophilized to give the title compound as a white solid.

HRMS (ES) calculated for $[M+2H]^+$ (m/z): 1830.8004, found 1830.7086.

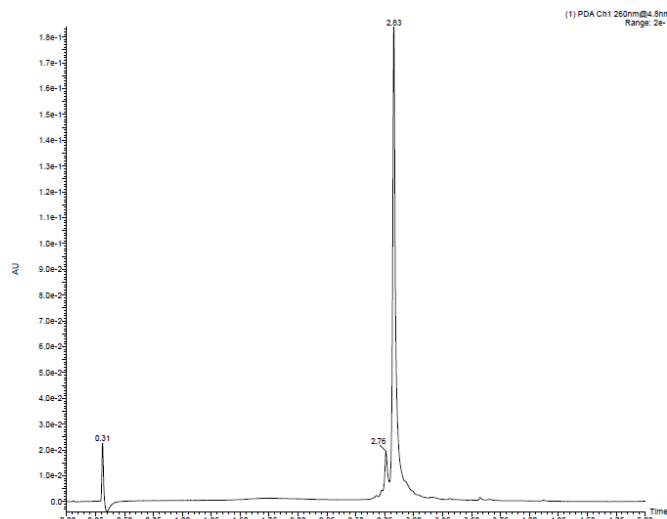


Dimer

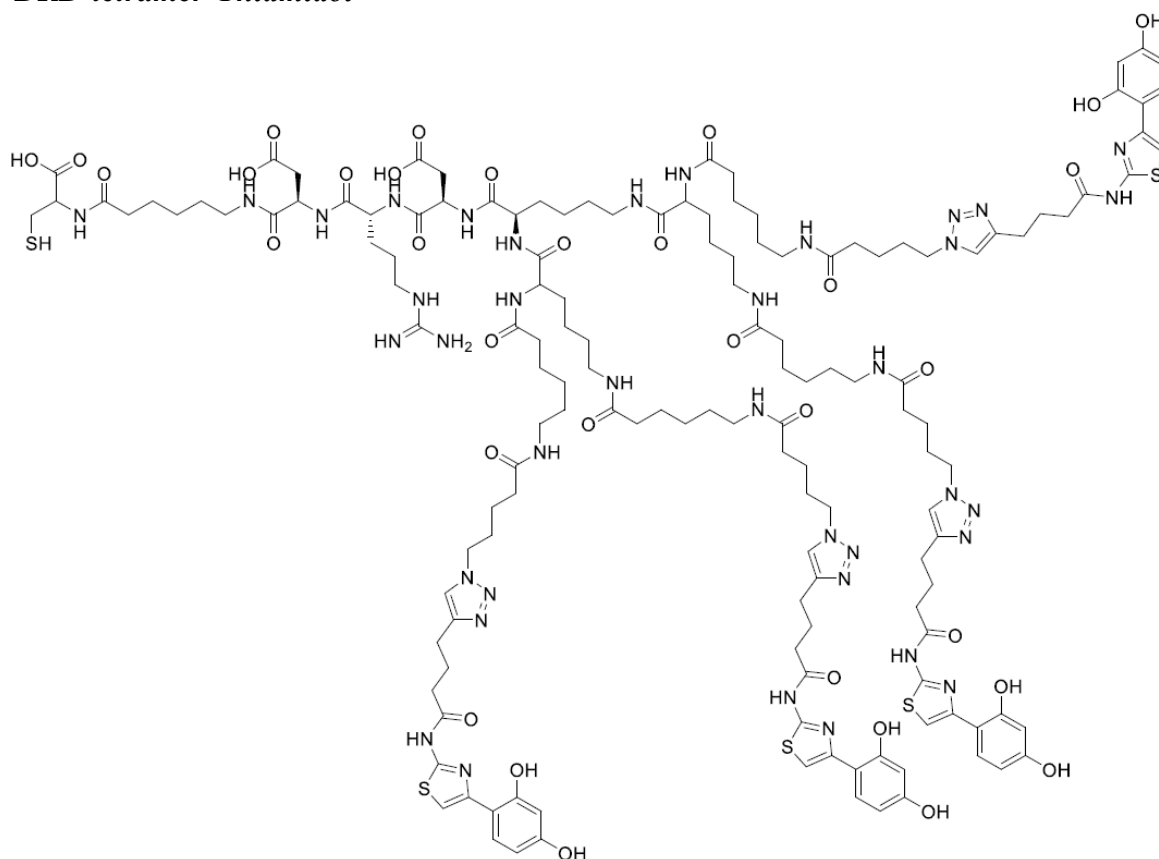


FI-C-C6-DRD-dimerLongThiamidol™: To a solution of the so-obtained compound (3.2 mg, 1 equiv.) in dimethyl sulfoxide (100 μL) was added a 0.1 M solution of commercially available fluorescein-5-maleimide (0.8537 mg, 1.0 equiv.) in dimethyl sulfoxide (20 μL). After stirring for 30 min in the dark, the reaction was quenched with the proper volume of DMSO:mqH₂O, injected and purified over a reversed-phase HPLC (Synergi RP Polar, 5% MeCN in 0.1% aq. TFA to 70% over 14 min). The fractions containing the product were identified by mass spectrometry, collected and lyophilized to give the title compound as a yellow solid.

HRMS (ES) calculated for $[\text{M}+\text{H}]^+$ (m/z): 2257.8651, found 2258.0203.



C-C6-DRD-tetramer-ThiamidolTM

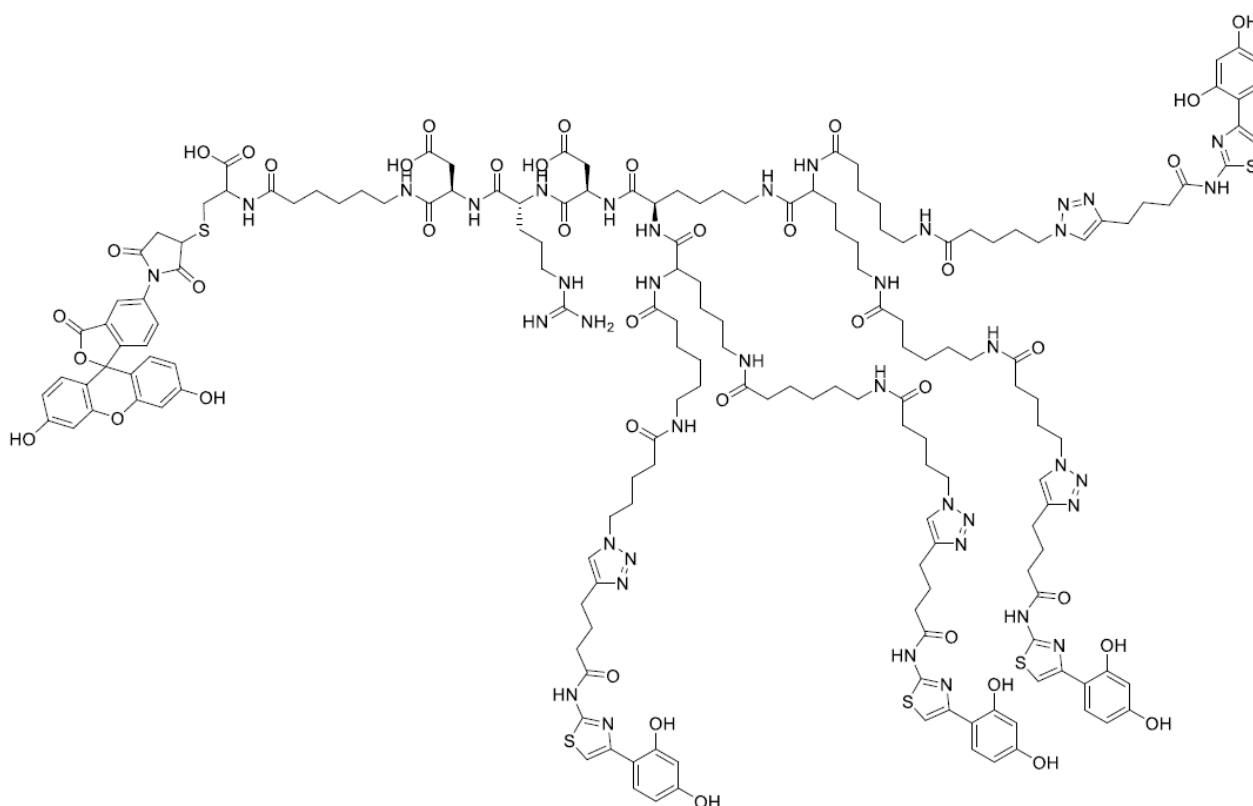


After removing the Fmoc-group, 0.2 mmol of the resin was reacted with a solution of Fmoc-Lys(Fmoc)-OH (4 equiv., 0.8 mmol), DIPEA (8 equiv., 1.6 mmol) and HATU (4.0 equiv, 0.8 mmol) in *N,N*-dimethylformamide (8 mL) for 2 h. After washing with *N,N*-dimethylformamide (5 × 8 mL × 1 min) the peptide was extended with Fmoc-Lys(Fmoc)-OH, Fmoc-6-aminocaproic acid and then capped with 5-azido pentanoic acid fixing the coupling conditions (Fmoc-Lys(Fmoc)-OH and HATU 6 equiv., DIPEA 12 equiv., Fmoc-6-aminocaproic or 5-azido pentanoic and HATU 12 equiv., DIPEA 24 equiv.), using the same Fmoc deprotection conditions (20 % piperidine in DMF) and washing step mentioned before. After the last coupling step, the Cu-catalysed alkyneazide cycloaddition was performed. The reaction protocol was adjusted from a previously described procedure [10]. A solution

of sodium ascorbate (3 equiv.), 2,6-lutidine (30 equiv.) and DIPEA (30 equiv.) in degassed mqH₂O was added to a solution of CuI (3 equiv.) in *N,N*-dimethylformamide. The resulting solution and the alkyne (6 equiv.) were added to the resin and allowed to react for 16 h. After washing with *N,N*-dimethylformamide (5 × 8 mL × 1 min), 50 mM aq. EDTA solution pH = 8 (5 × 8 mL × 1 min), *N,N*-dimethylformamide (5 × 8 mL × 1 min) and dichloromethane (5 × 4 mL × 1 min), the resin was cleaved using a mixture of TFA (6.60 mL, 82.5 %), *m*-Cresol (400 mL, 5 %), thioanisol (400 mL, 5 %), mq-H₂O (400 mL, 5 %) and TIPS (200 mL, 2.5 %) for 2 h at room temperature and washed with TFA (1 × 4 mL × 1 min). The combined cleavage and washing solutions were added dropwise to ice cold diethyl ether (40 mL) leading to precipitate formation that was collected by centrifugation, washed again with ice cold diethyl ether (3 × 40 mL × 2 min, 2000 rpm), dried, redissolved in mqH₂O:DMSO and treated with Tris(2-carboxyethyl)phosphine hydrochloride (2 equiv.). The solution was injected and purified over a RP HPLC (Synergi RP Polar, 5% MeCN in 0.1% aq. TFA to 80% over 14 min), the fractions containing the product identified by mass spectrometry, collected and lyophilized to give the title compound as a white solid.

HRMS (ES) calculated for [M+2H]⁺ (*m/z*): 1584.2132, found 1584.2404.

Tetramer



FI-C-C6-DRD-dimerLongThiamidol™: To a solution of C-C6-DRD-tetramer-Thiamidol™ (4.9 mg, 1 equiv.) in dimethyl sulfoxide (100 μL) was added a 0.1 M solution of commercially available fluorescein-5-maleimide (0.665 mg, 1.0 equiv.) in dimethyl sulfoxide (15.5 μL). After stirring for 30 min in the dark, the reaction was quenched with the proper volume of DMSO:mqH₂O, injected and purified over a reversed-phase HPLC (Synergi RP Polar, 5% MeCN in 0.1% aq. TFA to 70% over

14 min). The fractions containing the product were identified by mass spectrometry, collected and lyophilized to give the title compound as a yellow solid.

HRMS (ES) calculated for $[M+2H]^+$ (m/z):, 1797.7523 found 1798.6615.

References

- [1] X. Lai, M. Soler-Lopez, H. J. Wichers, B. W. Dijkstra, PLoS One 2016, 11, e0161697.
- [2] X. Lai, H. J. Wichers, M. Soler-Lopez, B. W. Dijkstra, Angew Chem Int Ed Engl 2017, 56, 9812–9815.
- [3] G. Bassi, N. Favalli, S. Oehler, A. Martinelli, M. Catalano, J. Scheuermann, D. Neri, Biochem. Biophys. Res. Commun. 2020, DOI 10.1016/j.bbrc.2020.04.035.
- [4] W. Decurtins, M. Wichert, R. M. Franzini, F. Buller, M. A. Stravs, Y. Zhang, D. Neri, J. Scheuermann, Nat. Protoc. 2016, 11, 764–780.
- [5] X. Lai, H. J. Wichers, M. Soler-Lopez, B. W. Dijkstra, Chemistry (Easton). 2018, 24, 47–55.
- [6] A. J. WINDER, H. HARRIS, Eur. J. Biochem. 1991, 198, 317–326.
- [7] J. C. Espín, M. Morales, P. A. García-Ruiz, J. Tudela, F. García-Cánovas, J. Agric. Food Chem. 1997, 45, 1084–1090.
- [8] M. Catalano, S. Oehler, L. Prati, N. Favalli, G. Bassi, J. Scheuermann, D. Neri, Anal. Chem. 2020, 92, 10822–10829.
- [9] T. Mann, C. Scherner, K.-H. Röhm, L. Kolbe, Int. J. Mol. Sci. 2018, 19, 690.
- [10] S. Ingale, P. E. Dawson, Org. Lett. 2011, 13, 2822–2825.

List of papers (2017–2020)

1. Discovery, affinity maturation and multimerization of small molecule ligands against human Tyrosinase and Tyrosinase-Related Protein 1.
Catalano M, Bassi G, Rotondi G, Khettabi L, Dichiarà M, Murer P, Scheuermann J, Soler-Lopez M, Neri D. *RSC Med. Chem.*, 2021, Advance Article. doi: 10.1039/D0MD00310G.
2. Sigma Receptor Ligands Carrying a Nitric Oxide Donor Nitrate Moiety: Synthesis, In Silico, and Biological Evaluation.
Amata E[†], Dichiarà M[†], Gentile D, Marrazzo A, Turnaturi R, Arena E, La Mantia A, Tomasello BR, Acquaviva R, Di Giacomo C, Rescifina A, Prezzavento O. [†]equal contribution
ACS Med Chem Lett. 2020 Apr 9;11(5):889-894. doi: 10.1021/acsmchemlett.9b00661. eCollection 2020 May 14. PMID: 32435401.
3. Novel N-Substituted Benzomorphan-Based Compounds: From MOR-Agonist/DOR-Antagonist to Biased/Unbiased MOR Agonists.
Pasquinucci L, Parenti C, Ruiz-Cantero MC, Georgoussi Z, Pallaki P, Cobos EJ, Amata E, Marrazzo A, Prezzavento O, Arena E, Dichiarà M, Salerno L, Turnaturi R.
ACS Med Chem Lett. 2020 Jan 28;11(5):678-685. doi: 10.1021/acsmchemlett.9b00549. eCollection 2020 May 14. PMID: 32435370.
4. Exploiting the Power of Stereochemistry in Drug Action: 3-[(2S,6S,11S)-8-Hydroxy-6,11-dimethyl-1,4,5,6-tetrahydro-2,6-methano-3-benzazocin-3(2H)-yl]-N-phenylpropanamide as Potent Sigma-1 Receptor Antagonist.
Turnaturi R, Pasquinucci L, Chiechio S, Grasso M, Marrazzo A, Amata E, Dichiarà M, Prezzavento O, Parenti C.
ACS Chem Neurosci. 2020 Apr 1;11(7):999-1005. doi: 10.1021/acscchemneuro.9b00688. Epub 2020 Mar 23. PMID: 32186844.
5. Tuning Properties for Blood-Brain Barrier Permeation: A Statistics-Based Analysis.
Dichiarà M, Amata B, Turnaturi R, Marrazzo A, Amata E.
ACS Chem Neurosci. 2020 Jan 2;11(1):34-44. doi: 10.1021/acscchemneuro.9b00541. Epub 2019 Dec 18. PMID: 31793759.
6. Morphing of Ibogaine: A Successful Attempt into the Search for Sigma-2 Receptor Ligands.
Floresta G, Dichiarà M, Gentile D, Prezzavento O, Marrazzo A, Rescifina A, Amata E.
Int J Mol Sci. 2019 Jan 23;20(3):488. doi: 10.3390/ijms20030488. PMID: 30678129.
7. Targeting heme Oxygenase-1 with hybrid compounds to overcome Imatinib resistance in chronic myeloid leukemia cell lines.
Sorrenti V, Pittalà V, Romeo G, Amata E, Dichiarà M, Marrazzo A, Turnaturi R, Prezzavento O, Barbagallo I, Vanella L, Rescifina A, Floresta G, Tibullo D, Di Raimondo F, Intagliata S, Salerno L.
Eur J Med Chem. 2018 Oct 5;158:937-950. doi: 10.1016/j.ejmech.2018.09.048. Epub 2018 Sep 17. PMID: 30261468.
8. Identification of Potentially Potent Heme Oxygenase-1 Inhibitors through 3D-QSAR Coupled to Scaffold-Hopping Analysis.
Floresta G, Amata E, Dichiarà M, Marrazzo A, Salerno L, Romeo G, Prezzavento O, Pittalà V, Rescifina A.
ChemMedChem. 2018 Jul 6;13(13):1336-1342. doi: 10.1002/cmdc.201800176. Epub 2018 May 29. PMID: 29693778.

List of conference participations (2017–2020)

- Dichiara M., Marrazzo A., Amata E..
CNS permeability parameters determination through a statistical analysis driven approach.
6th Prague-Weizmann Summer School Advances in Drug Discovery, Prague, Czech Republic.
September 2–6, 2019
Poster presentation
- Dichiara M., Acquaviva R., La Mantia A., Di Giacomo C., Arena E., Floresta G., Marrazzo A., Amata E., Prezzavento O..
Development of NO-releasing sigma receptor hybrids as anticancer agents.
MedChem19–Paul Ehrlich Euro-PhD Network & MuTaLig COST Action meeting 2019, Catanzaro.
June 13–15, 2019
Oral communication
- Dichiara M., Barbaraci C., Gentile D., Intagliata S., Pittalà V., Arena E., Fraix A., Farina G., Prezzavento O., Amata E., Marrazzo A..
Design, synthesis, and pharmacological evaluation of NO donor-sigma receptors hybrids for the treatment of cancer.
Italian-Spanish-Portuguese Joint Meeting in Medicinal Chemistry - MedChemSicily2018, Palermo.
July 17–20, 2018
Poster presentation
- Dichiara M., Amata E..
Design and synthesis of H₂S releasing-sigma receptor hybrids for the management of pain.
European School of Medicinal Chemistry (ESMEC) - XXXVIII Advanced Course of Medicinal Chemistry and Seminar for PhD students, Urbino.
July 1–5, 2018
Poster presentation

List of fellowships

- CA15135 grant assigned by the MuTaLig Scientific Commission to attend the BImBS 2019 Training School - BioInformatics meets BioSimulations in protein and DNA studies: from theory to practice. Lugano, October 5–12, 2019.
- Prague-Weizmann School on Drug Discovery fellowship assigned by the Scientific Committee to attend the 6th Prague-Weizmann Summer School Advances in Drug Discovery: Drug discovery and development from basic research through preclinical to clinical phases. Prague, Czech Republic, September 2–6, 2019.
- European School of Medicinal Chemistry (ESMEC) fellowship assigned by the Division of Medicinal Chemistry of the Italian Chemical Society to attend the XXXVIII Advanced Course of Medicinal Chemistry and Seminar for PhD students. Urbino, July 1–5, 2018.